

Functional Characterisation of *Candida glabrata* Open
Reading Frames with no Orthologue in *Saccharomyces
cerevisiae*

Submitted by Lauren Claire Ames to the University of Exeter
as a thesis for the degree of
Doctor of Philosophy in Biological Sciences
In September 2013

This thesis is available for Library use on the understanding that it is copyright
material and that no quotation from the thesis may be published without proper
acknowledgement.

I certify that all material in this thesis which is not my own work has been
identified and that no material has previously been submitted and approved for
the award of a degree by this or any other University.

Signature:

Abstract

Candida glabrata is a significant and increasingly common pathogen of humans yet its mechanism of virulence remains unclear. Comparative genomic studies revealed that *C. glabrata* is more closely related to the non-pathogenic yeast *Saccharomyces cerevisiae* and that both these genomes are distinct from *C. albicans*. In order to explore *C. glabrata* virulence attributes, *C. glabrata* ORFs with no orthologue in *S. cerevisiae* were studied since these ORFs may have accompanied the adaptation of *C. glabrata* to the human host.

Reciprocal best hit searches identified *C. glabrata* ORFs with no *S. cerevisiae* orthologue. A barcoded deletion library targeting 65 *C. glabrata*-specific ORFs was constructed. To functionally characterise the deletion library, mutants were tested for fitness and phenotypically screened to identify gene products required for growth in response to biologically relevant stresses. As such, novel phenotypes associated with the deletion of previously uncharacterised ORFs were uncovered. Mutants were also tested for infection-related properties including biofilm formation, antifungal agent susceptibility and for virulence in a *Drosophila melanogaster* infection model, resulting in the identification of two *C. glabrata*-specific ORFs, *CAGL0K05687g* and *CAGL0H01749g*, which were required for virulence.

Three ORFs with notable phenotypes were taken forward for further characterisation. An adapted genome-wide synthetic genetic interaction approach was used to create genetic interaction networks for *C. glabrata* ORFs over-expressed in *S. cerevisiae*. Genetic interaction analysis of a *C. glabrata* chromatin remodeler *CAGL0D05434g* revealed a role for this ORF in metal ion homeostasis and DNA damage repair. Genetic interaction profiling for an oxidoreductase encoded by *CAGL0K05687g* was used to reveal mechanisms related to transport by which this ORF may be required for virulence.

Acknowledgements

I would like to thank members of the Haynes lab, both past members at Imperial College London and current members at the University of Exeter for their support throughout the past four years. In particular, I would like to thank Dr. Melanie Puttnam for always looking out for me. I would like to thank Prof. Ken Haynes for giving me the opportunity to undertake this PhD, for all his help and advice and for putting up with me when I don't get his jokes.

I would also like to thank Dr. Maxime Huvet (Imperial College London) for his expertise in bioinformatics; Dr. Darren Soanes (University of Exeter) for his assistance with phylogenetic work and Dr Petros Ligoxygakis and Dr. Ilias Kounatidis (University of Oxford) for their help with *Drosophila* work. I would like to thank members of the Kuchler lab for strains, for allowing me to visit their lab and training me in phenotypic screening. In addition, thanks go to Prof. Al Brown (University of Aberdeen) and Dr. Jan Quinn (University of Newcastle) for help and advice.

Lastly I would like to thank my amazing team of helpers, especially during my write up. Massive thanks to Dr. Hsueh-lui "Munchkins" Ho, for being a great transformation partner over the years, regularly keeping me in check and for her wonderful formatting skills. Also massive thanks to Sophie Shaw for making sure I am regularly walked, encouraging bad behaviour and for the endless computer assistance and proof reading. The biggest thanks go to Dr. Jane Usher for taking me under her wing, teaching me everything I know about yeast, regularly feeding me meatballs and all the time spent reading this thesis.

Table of Contents

	Page
Title	1
Declaration	1
Abstract	2
Acknowledgments	3
Table of Contents	4
List of Figures	12
List of Tables	15
List of Abbreviations	17
Chapter 1: Introduction	22
1.1 <i>Candida</i> species: Disease and Epidemiology	22
1.2 The <i>C. glabrata</i> Genome	25
1.2.1 Genetic Plasticity in <i>C. glabrata</i> Clinical Isolates	28
1.2.2 Phenotype Plasticity of <i>C. glabrata</i>	29
1.2.3 <i>C. glabrata</i> has no Apparent Sexual Cycle	29
1.3 The <i>S. cerevisiae</i> Molecular Toolkit	33
1.3.1 <i>S. cerevisiae</i> Deletion Collections and their Applications	35
1.3.1.1 Molecular Barcoding	36
1.3.1.2 Chemical-Genomic Screening	38
1.3.1.3 Haploinsufficiency profiling (HIP)	38
1.3.1.4 <i>S. cerevisiae</i> as a Model for Human Disease Genes and Drug Targets	39
1.3.2 Chemical-Genetic Screening in Clinically-Relevant Organisms	39
1.3.3 Genetic Interactions and the Synthetic Genetic Array (SGA)	40
1.3.3.1 Genetic Interaction Networks as Models for Human Disease	42
1.3.3.2 Genetic Interaction Mapping in Non-Yeast Model Organisms	43

1.3.3.3 Combining Chemical-Genetic & Genetic Interaction Data	43
1.4 <i>C. glabrata</i> Lacks Molecular Tools	44
1.5 Establishment and Development of <i>C. glabrata</i> Infection in the Human Host	45
1.5.1 <i>C. glabrata</i> Adhesion to Host Cells	45
1.5.2 <i>Candida</i> Biofilm Formation	48
1.5.3 Mechanisms of Host Invasion by <i>Candida</i> Species	50
1.6 The Interaction of <i>C. glabrata</i> with Host Immune Cells	51
1.6.1 Immune Defence Mechanisms Against Invading Microorganisms	51
1.6.2 <i>C. glabrata</i> Survives and Replicates within Macrophages	52
1.6.3 The Transcriptional Response of Phagocytosed <i>C. glabrata</i> Cells	56
1.6.4 Oxidative Killing of <i>Candida</i> Species	58
1.6.5 <i>C. glabrata</i> Elicits a Robust Oxidative Stress Response	59
1.6.5.1 Iron Scavenging is Required for Oxidative Stress Resistance and Pathogenicity	61
1.7 Sensing the Host Environment	62
1.8 Evading the Immunological Response	63
1.9 Evolution of Drug Resistance in <i>C. glabrata</i> Isolates	64
1.9.1 Azole Resistance	64
1.9.2 Echinocandin Resistance	67
1.10 Conclusion	68
1.11 Aims of the Study	69
Chapter 2: Materials and Methods	70
2.1 Organisms, Strains and Plasmids	70
2.1.1 Yeast strains	70
2.1.2 Bacterial Strains	73
2.1.3 <i>Drosophila</i> Strains	73

2.1.4 Plasmids	74
2.2 Primers	75
2.3 Storage, Media and Culture of Strains	75
2.3.1 Yeast Media and Culture	75
2.3.2 Bacterial Media and Culture	75
2.3.3 Storage of Yeast and Bacterial Strains	75
2.3.4 <i>Drosophila</i> Media and Growth	75
2.4 General Molecular Techniques	76
2.4.1 Preparation of Competent <i>E. coli</i>	76
2.4.2 <i>E. coli</i> Transformation	76
2.4.3 Isolation of Plasmid DNA from <i>E. coli</i>	76
2.4.4 Extraction of DNA from <i>C. glabrata</i> and <i>S. cerevisiae</i>	77
2.4.5 Resolution of DNA fragments by Gel Electrophoresis	77
2.4.6 Purification of PCR Products from Agarose Gels	78
2.4.7 <i>C. glabrata</i> Transformation by Electroporation	78
2.4.8 Lithium Acetate-mediated Yeast Transformation	79
2.5 Cloning of <i>C. glabrata</i> ORFs using Invitrogen Gateway® Technology	79
2.5.1 Amplification of <i>C. glabrata</i> ORFs	79
2.5.2 Addition of <i>attB</i> Sites onto Amplification Products	79
2.5.3 BP Clonase® Reaction	80
2.5.4 LR Clonase® Reaction	81
Chapter 3: Selection of <i>C. glabrata</i> specific genes for targeted gene deletion	83
3.1 Overview	83
3.2 Materials and Methods	84
3.2.1 Detection of Horizontal Gene Transfer Events between Prokaryotes and <i>C. glabrata</i>	84
3.2.2 Targeted Gene Deletion in <i>C. glabrata</i>	85
3.2.2.1 Amplification of 5' and 3' Ends of the Target ORF	85
3.2.2.2 Amplification of the NAT ^R Cassette	86

3.2.2.3 Fusion PCR of the Deletion Construct	86
3.2.2.4 Precipitation of Fusion Construct	89
3.2.2.5 Verification of <i>C. glabrata</i> Transformants	89
3.3 Results	89
3.3.1 Identification of <i>C. glabrata</i> ORFs with no <i>S. cerevisiae</i> Orthologue	89
3.3.2 Mapping the Chromosomal Location of <i>C. glabrata</i> ORFs with no Orthologue in <i>S. cerevisiae</i>	91
3.3.3 Alternative Approaches for the Identification of <i>C. glabrata</i> ORFs with no Orthologue in <i>S. cerevisiae</i>	93
3.3.4 The Acquisition of Prokaryotic Genes by <i>C. glabrata</i>	94
3.3.5 <i>C. glabrata</i> CAGL0D01210g: Acquisition of a Putative Aspartate Racemase	95
3.3.6 <i>C. glabrata</i> CAGL0K11066g is Highly Similar to Bacterial Acetyl Transferases	98
3.3.7 <i>C. glabrata</i> CAGL0M14091g has Similarity to Prokaryotic NADPH Dehydrogenases	100
3.3.8 Functional Annotation and Selection of <i>C. glabrata</i> -specific Genes for Targeted Gene Deletion	102
3.4 Discussion	107
3.4.1 Identification and Location of <i>C. glabrata</i> ORFs with no Orthologue in <i>S. cerevisiae</i>	107
3.4.2 HGT and the Acquisition of Prokaryotic Genes by <i>C. glabrata</i>	109
3.4.3 Generation of a <i>C. glabrata</i> Deletion Library as a Molecular Tool for the Functional Characterisation of <i>C. glabrata</i> ORFs	111
Chapter 4: Functional characterisation of the <i>C. glabrata</i> deletion library	113
4.1 Overview	113
4.1.1 Deletion Libraries and Chemical-Genetic Screening	
4.1.2 Models of <i>Candida</i> Biofilm Formation and	114

Virulence	
4.1.3 Aims	118
4.2 Materials & Methods	119
4.2.1 Phenotypic Screening	119
4.2.1.1 High-throughput Phenotypic Screening of <i>C. glabrata</i> Mutants	119
4.2.1.2 Serial Dilution of <i>C. glabrata</i> Mutants	119
4.2.2 Growth Analysis of <i>C. glabrata</i> and <i>S. cerevisiae</i> Strains	120
4.2.3 Quantification of <i>C. glabrata</i> Biofilm Formation	120
4.2.4 <i>Drosophila melanogaster</i> Gastrointestinal Infection Model	121
4.3 Results	121
4.3.1 Growth Profiling of <i>C. glabrata</i> Deletion Mutants	121
4.3.2 High-throughput Phenotypic Screening of <i>C. glabrata</i> Deletion Mutants	125
4.3.3 Screening <i>C. glabrata</i> Mutants for Biofilm Formation	133
4.3.4 Virulence Screening of <i>C. glabrata</i> Mutants	136
4.4 Discussion	142
4.4.1 Fitness Analysis of the <i>C. glabrata</i> Deletion Library	142
4.4.2 Phenotypic Screening of the <i>C. glabrata</i> Deletion Library	143
4.4.3 Screening of <i>C. glabrata</i> Deletion Mutants for Biofilm Formation	146
4.4.4 Virulence Screening of <i>C. glabrata</i> deletion mutants	147
Chapter 5: Functional characterisation of <i>CAGL0D05434g</i> and <i>CAGL0K05687g</i>	151
5.1 Overview	151
5.2 Materials and Methods	152
5.2.1 Quantification of <i>C. glabrata</i> Colony Size	152
5.2.2 Synthetic Genetic Interaction Profiling of <i>C.</i>	152

<i>glabrata</i> ORFs	
5.2.2.1 Construction of the SGA Query Strain	153
5.2.2.2 Condensing the <i>S. cerevisiae</i> Deletion Array	153
5.2.2.3 Automated Pinning Steps for the Generation of Double Mutants	153
5.2.2.4 Visualisation of Genetic Interactions	154
5.3 Results	154
5.3.1 Phenotypic Screening of <i>C. glabrata</i> Δ CAGL0D05434g	154
5.3.2 <i>C. glabrata</i> CAGL0D05434g Encodes a Putative HMG box Chromatin Remodeler	159
5.3.3 SGA Analysis of <i>C. glabrata</i> CAGL0D05434g	162
5.3.3.1 Expression of <i>C. glabrata</i> CAGL0D05434g Inhibits Growth in <i>S. cerevisiae</i>	162
5.3.3.2 Expression of <i>C. glabrata</i> CAGL0D05434g Inhibits the Formation of Double Mutants by SGA	164
5.3.3.3 Genetic Interactions for <i>C. glabrata</i> CAGL0D05434g	166
5.3.4 <i>C. glabrata</i> CAGL0D05434g is required for growth in response to DNA damage	172
5.3.5 Genetic Interactions of <i>C. glabrata</i> CAGL0K05687g	174
5.4 Discussion	177
5.4.1 <i>C. glabrata</i> CAGL0D05434g is required for fitness and growth on metal and metalloid compounds	177
5.4.2 <i>C. glabrata</i> CAGL0D05434g Encodes a Putative MATA HMG-box Domain	178
5.4.3 <i>C. glabrata</i> CAGL0D05434g Genetic Interactions	179
5.4.4 <i>C. glabrata</i> CAGL0D05434g – a Role in Meiosis?	179
5.4.5 CAGL0D05434g and the DNA-damage Response	180
5.4.6 Genetic Interaction Mapping of <i>C. glabrata</i>	182

CAGL0K05687g – a Role in Transport?

Chapter 6: Discussion	184
6.1 Overview	184
6.2 Defining <i>C. glabrata</i> ORFs with no Orthologue in <i>S. cerevisiae</i>	186
6.3 The Use of a Non-Mammalian Host for Virulence Studies of <i>C. glabrata</i> Strains	189
6.4 Genetic Interaction Analysis Facilitates the Functional Characterisation of <i>C. glabrata</i> ORFs	191
6.5 Future work	193
6.5.1 Studying the Evolutionary Differences of <i>C. glabrata</i> <i>CAGL0D03850g</i> and <i>S. cerevisiae</i> <i>RSC30</i>	193
6.5.2 Understanding the Role of Horizontal Gene Transfer in <i>C. glabrata</i>	193
6.5.3 Exploiting Barcoded <i>C. glabrata</i> Mutants for Competitive Growth Analysis	194
6.5.4 Further Characterising <i>C. glabrata</i> Fluconazole-Susceptible Mutants	195
6.5.5 Dissecting the Role of Novel Biofilm-Associated ORFs in <i>C. glabrata</i>	195
6.5.6 Validating <i>C. glabrata</i> ORFs Required for Virulence	196
6.5.7 Functional Characterisation of <i>C. glabrata</i> <i>CAGL0D05434g</i>	196
6.6 Conclusion	197
Appendices	199
Appendix 1: List of Oligonucleotides used in this study	199
Appendix 2: Phenotypic Screening Media	219
Appendix 3: <i>C. glabrata</i> ORFs with no orthologue in <i>S. cerevisiae</i>	222
Appendix 4: Functional information for targeted <i>C. glabrata</i> gene deletions	246
Appendix 5: Statistical Analysis of Fitness Profiles	259

Appendix 6: Genetic interactions with <i>C. glabrata</i> <i>CAGL0D05434g</i>	260
Appendix 7: Fitness Measures for <i>C. glabrata</i> Deletion Mutants	270
Appendix 8: Growth profiling of <i>C. glabrata</i> mutants	273
Appendix 9: <i>C. glabrata</i> deletion mutants from the Schwarz Müller <i>et al.</i> , 2013 study with no <i>S. cerevisiae</i> orthologue used in phenotypic screens	306
Appendix 10: Screening <i>C. glabrata</i> deletion mutants for virulence using a <i>Drosophila melanogaster</i> gastrointestinal infection model	308
Appendix 11: Screening <i>C. glabrata</i> deletion mutants for Biofilm Formation	314
Appendix 12: <i>CAGL0K05687g</i> genetic interactions	317
Appendix 13: Schwarz Müller <i>et al.</i> , 2013 paper submitted to PLoS Pathogens.	323
Appendix 14: Verification of fusion constructs and <i>C.</i> <i>glabrata</i> deletion mutants	379
Appendix 15: Plasmid maps of Gateway® vectors	417
Bibliography	422

List of Figures

Figure		Page
1.1	Phylogenetic representation of selected fungal species.	23
1.2	Frequency of <i>Candida</i> species from 364 clinical blood stream isolates in North America.	25
1.3	Phylogeny of <i>Candida</i> and <i>Saccharomyces</i> clade species.	26
1.4	The life cycle of <i>S. cerevisiae</i> .	30
1.5	Competitive growth assays using mixed pools of <i>S. cerevisiae</i> mutants.	37
1.6	The genetic landscape of a cell.	41
1.7	The fungal cell wall.	46
1.8	Comparison of biofilm structures formed by <i>C. albicans</i> and <i>C. glabrata</i> .	49
1.9	<i>C. glabrata</i> interaction with macrophages.	54
1.10	The production of ROS and RNS intermediates by mammalian cells as part of the oxidative burst.	59
1.11	Model of niacin-dependent regulation of sirtuins <i>HST1</i> and <i>SIR2</i> in <i>C. glabrata</i> .	63
2.1	Diagrammatic representation of the BP clonase® reaction.	81
3.1	Targeted gene deletion method in <i>C. glabrata</i> .	88
3.2	Workflow of RBH searches used to identify <i>C. glabrata</i> ORFs with no orthologue in <i>S. cerevisiae</i> .	90
3.3	Chromosomal distribution of <i>C. glabrata</i> ORFs with no orthologue in <i>S. cerevisiae</i> .	92
3.4	Comparison and overlap of <i>C. glabrata</i> ORFs with no orthologue in <i>S. cerevisiae</i> derived from two different bioinformatic approaches.	94
3.5	Maximum likelihood phylogenetic tree for putative <i>C. glabrata</i> aspartate racemase encoded by <i>CAGL0D01210g</i> .	97
3.6	Maximum likelihood tree for <i>C. glabrata</i> <i>CAGL0K11066g</i> .	99
3.7	Maximum likelihood tree for <i>C. glabrata</i> <i>CAGL0M14091g</i> .	101

3.8	Verification of fusion constructs by gel electrophoresis.	103
3.9	PCR checks for the validation of putative <i>C. glabrata</i> Δ CAGL0E06644g transformants.	105
3.10	Functional annotations of deleted <i>C. glabrata</i> ORFs according to InterPro.	106
4.1	Comparison of homologous mammalian TLR4 and <i>D. melanogaster</i> Toll pathway.	117
4.2	Comparison of mammalian TNFR-1 pathway and <i>D. melanogaster</i> IMD pathway.	118
4.3	Growth profile of <i>C. glabrata</i> Δ CAGL0A04565g and parental strain Cg2001 Δ his3.	123
4.4	Fluconazole-sensitive <i>C. glabrata</i> mutants.	129
4.5	Phenotypic screening of <i>C. glabrata</i> Δ CAGL0D03850g isolates and parental strain Cg2001 Δ his3.	130
4.6	Complementation of <i>C. glabrata</i> Δ CAGL0D03850g with putative orthologue <i>S. cerevisiae</i> RSC30.	131
4.7	Phenotypic screening of Δ CAGL0D02750g.	132
4.8	YGOB alignment of <i>C. glabrata</i> CAGL0D02750g.	133
4.9	Biofilm formation by <i>C. glabrata</i> mutants.	135
4.10	A <i>D. melanogaster</i> model of <i>C. glabrata</i> GI infection.	136
4.11	<i>C. glabrata</i> mutants attenuated for virulence in a <i>D. melanogaster</i> model of <i>C. glabrata</i> infection.	138
5.1	Deletion of CAGL0D05434g confers reduced <i>C. glabrata</i> colony size.	156
5.2	Phenotypic screening of Δ CAGL0D05434g.	157
5.3	Growth profile of two <i>C. glabrata</i> Δ CAGL0D05434g isolates A and B compared with the parental strain Cg2001 Δ his3 in YPD.	158
5.4	Multiple sequence alignment of <i>C. glabrata</i> CAGL0D05434g with characterised HMGB proteins HMGB1 & HMGB2 (<i>Homo sapiens</i>) and HMO1 & NHP6A (<i>S. cerevisiae</i>) showing conservation of a DNA-binding HMG-box domain.	160
5.5	Growth profile of <i>S. cerevisiae</i> SGA strains expressing <i>C. glabrata</i> ORF CAGL0D05434g.	164

5.6	Schematic describing the formation of double mutants by SGA.	165
5.7	Genetic interaction maps for SGA query strains <i>S. cerevisiae</i> Δ IME1 “ScdellIME2” and Δ IME2 “ScdellIME2” and <i>S. cerevisiae</i> Δ IME1 and Δ IME2 overexpressing <i>C. glabrata</i> CAGL0D05434g “ScdellIME1 CgD05434” and “ScdellIME2 CgD05434” respectively.	167
5.8	Genetic interaction maps for SGA query strains <i>S. cerevisiae</i> Δ IME1 “ScdellIME1” and <i>S. cerevisiae</i> Δ IME1-D05434 overexpressing <i>C. glabrata</i> CAGL0D05434g “ScdellIME1 CgD05434”.	168
5.9	Genetic interaction maps for SGA query strains <i>S. cerevisiae</i> Δ IME2 “ScdellIME2” and <i>S. cerevisiae</i> Δ IME2 over-expressing <i>C. glabrata</i> CAGL0D05434g “ScdellIME2 CgD05434”.	169
5.10	Phenotypic screening of <i>C. glabrata</i> CAGL0D05434g deletion and overexpression mutants on DNA damage agents hydroxyurea (HU), methyl methanesulfonate (MMS) and UV light.	173
5.11	Genetic interaction maps for SGA query strains KH03-K05687 expressing <i>C. glabrata</i> CAGL0K05687g.	175

List of Tables

Table		Page
1.1	Summarised genome features of sequenced strains of <i>S. cerevisiae</i> S288C, <i>C. glabrata</i> CBS138 and <i>C. albicans</i> SC5314	27
1.2	<i>C. glabrata</i> orthologues of <i>S. cerevisiae</i> genes involved in mating, meiosis and sporulation	32
1.3	Summary outlining the molecular tools available for <i>S. cerevisiae</i> and examples of their applications where they have facilitated genome-wide molecular studies in this organism	34
1.4	Summary of putative GPI-linked adhesin proteins, their subgroups and localisation in <i>C. glabrata</i>	47
1.5	<i>C. glabrata</i> cell surface and cell wall proteins significantly upregulated in a azole-resistant petite mutant	66
1.6	Non-synonymous mutations accompanying the evolution of echinocandin resistance from a <i>C. glabrata</i> clinical isolate	68
2.1	<i>C. glabrata</i> strains used during this study	70
2.2	<i>S. cerevisiae</i> strains used during this study	71
2.3	<i>E. coli</i> strains used during this study	73
2.4	<i>Drosophila</i> strains used during this study	73
2.5	Plasmids used during this study	74
3.1	Summary of <i>C. glabrata</i> ORFs which yield top BLAST hits with prokaryotic sequences.	95
4.1	<i>C. glabrata</i> mutants with altered fitness	124
4.2	Phenotypic screening conditions and the associated functional implications of phenotypes	126
4.3	Chemogenomic screening of the <i>C. glabrata</i> deletion library.	128
4.4	Summary of all phenotypes conferred by deletion of <i>C. glabrata</i> ORFs with no orthologue in <i>S. cerevisiae</i> .	140
5.1	Orthologues of <i>C. glabrata</i> <i>CAGL0D05434g</i> in related yeast species	162

5.2	Significantly enriched GO Biological Process terms amongst <i>S. cerevisiae</i> genes which showed genetic interactions with <i>C. glabrata</i> <i>CAGL0D05434g</i> in SGA screens of query strain Δ <i>Ime1</i> -D0543	171
5.3	Significantly enriched GO terms relating to the molecular function, biological process and cellular component of <i>S. cerevisiae</i> genes which showed genetic interactions with <i>C. glabrata</i> <i>CAGL0K05687g</i> in SGA screens of query strain KH03-K05687	173

Abbreviations

3'	Three prime
5'	Five prime
ABC	ATP-binding cassette
ALS	Agglutinin-like sequence
ANOVA	Analysis of variance
ARS	Autonomously replicating sequence
ATP	Adenosine triphosphate
BaCl ₂	Barium chloride
BLAST	Basic Local Alignment Search Tool
bp	Base pair
BPS	Bathophenanthrolinedisulfonic acid disodium salt hydrate
CaCl ₂ (.2H ₂ O)	Calcium chloride (hydrous)
CdCl ₂	Cadmium chloride
CDS	Coding DNA sequence
CGD	<i>Candida</i> genome database
ChIP-seq	Chromatin immunoprecipitation sequencing
CIN	Chromosome instability
CoCl ₂	Cobalt chloride
CsCl	Caesium chloride
CuCl ₂	Copper chloride
CuSO ₄	Copper sulphate
DNA	Deoxyribonucleic acid
dNTP	Deoxyribonucleotide
Drs	Drosomycin
DRYGIN	Data repository of yeast genetic interactions
DTT	Dithiothreitol
EDTA	Ethylenediaminetetraacetic acid
EM	Electron microscopy
ER	Endoplasmic reticulum
<i>et al.</i>	and others
EtOH	Ethanol
FACS	Fluorescence-activated cell sorting

FeCl ₂	Iron chloride
FMN	Flavin mononucleotide
FRT	Flippase recognition target
FSC	Forward scatter
G418	Geneticin sulphate
g	Grams
GFP	Green fluorescent protein
GI	Gastrointestinal
GM-CSF	Granulocyte-macrophage colony-stimulating factor
GO	Gene ontology
GPD	Glyceraldehyde phosphate dehydrogenase
GPI	Glycosylphosphatidylinositol
GSH	Glutathione
GST	Glutathione S- transferase
g/L	Grams per litre
H ₂ O	Water
H ₂ O ₂	Hydrogen peroxide
HA	Hemagglutinin
HCl	Hydrochloric acid
HGT	Horizontal gene transfer
HIP	Haploinsufficiency profiling
HIV	Human immunodeficiency virus
HMG-box	High mobility group-box
HU	Hydroxyurea
IFN-γ	Interferon gamma
IL-N	Interlukin (where N represents number)
IMD	Immune deficiency
iNOS	Inducible nitric oxide synthase
KanR	Kanamycin resistance
kb	Kilobase
KCl	Potassium chloride
KOH	Potassium hydroxide
L	Litre
LB	Luria broth media
LiCl	Lithium chloride

M	Molar
MAPK	Mitogen-activated protein kinase
MAT	Mating type
Mb	Megabases
MDM	Monocyte-derived macrophage
mg	Milligram
MgCl ₂	Magnesium chloride
mg/ml	Milligram per millilitre
ml	Millilitre
ml/L	Millilitre per litre
mM	Millimolar
MMS	Methyl methanesulfonate
MNase	Micrococcal nuclease
MnCl ₂ (.4H ₂ O)	Manganese chloride (hydrous)
MNT	Mannosyltransferase
MOA	Mechanism of action
MoBY	Molecular barcoded yeast
MOPS	3-(N-morpholino)propanesulfonic acid
Na	Sodium
NaCl	Sodium chloride
NAD ⁺	Nicotinamide adenine dinucleotide
NADPH	Nicotinamide adenine dinucleotide phosphate
NAT	Nourseothricin
NCBI	National center for biotechnology information
NET	Neutrophil extracellular trap
NI	No interaction
nm	Nanometres
OD ₅₅₀	Optical density at 550 nm
OD ₆₀₀	Optical density at 600 nm
ORF	Open reading frame
PAMP	Pathogen-associated molecular pattern
PBS	Phosphate buffered saline
PCR	Polymerase chain reaction
PEG	Polyethylene glycol

pH	Measure of the acidity or alkalinity of a solution (concentration of protons in a solution)
PhyML	Phylogenetic estimation using maximum likelihood
PRR	Pattern recognition receptors
RBH	Reciprocal best hit
RNA	Ribonucleic acid
RNAi	RNA interference
RNase A	Ribonuclease A
RNS	Reactive nitrogen species
ROS	Reactive oxygen species
rpm	Revolutions per minute
RSC	Chromatin structure remodelling complex
RT-PCR	Reverse transcription polymerase chain reaction
S	Suppressor
SAP	Secreted aspartyl protease
SC	Synthetic complete media
SDL	Synthetic dosage lethal
SDS	Sodium dodecyl sulphate
SGA	Synthetic genetic array
SGD	<i>Saccharomyces</i> genome database
SNARE	SNAP receptor protein
SL	Synthetic lethal
SS	Synthetic sick
STM	Signature tagged mutagenesis
TAE	Tris-acetate-EDTA
TAP	Tandem affinity purification
tBOOH	t-Butyl hydroperoxide
TE	Tris-EDTA
TNF- α	Tumour necrosis factor alpha
tRNA	Transfer RNA
TTSS	Type III secretion system
UTR	Untranslated region
UV	Ultraviolet
U/ μ l	Units per microlitre
V	Volts

v-SNARE	Vesicle associated SNARE
v/v	Volume to volume ratio
WGD	Whole genome duplication
w/v	Weight to volume ratio
XTT	2,3-Bis(2-methoxy-4-nitro-5-sulfophenyl)-2 <i>H</i> -tetrazolium-5-carboxanilide
YFP	Yellow fluorescent protein
YGOB	Yeast gene order browser
YPD	Yeast extract peptone media
YPS	GPI-linked aspartyl proteases
ZnCl ₂	Zinc chloride
°C	Degrees Celcius
µg	Micrograms
µg/ml	Micrograms per millilitre
µl	Microlitre
µM	Micromolar

Chapter 1: Introduction

1.1 *Candida* Species: Disease and Epidemiology

The fungal kingdom encompasses a diverse range of microorganisms estimated at 1.5 million species, which employ a plethora of different lifestyles and morphologies. Over 600 fungal species are known to infect humans and present an emerging threat to human health as the causative agents of billions of infections each year (Hawksworth, 2001; Brown *et al.*, 2012; Fisher *et al.*, 2012). Despite this, pathogenic fungi remain less well studied and understood compared to other infectious microorganisms, in particular bacterial pathogens such as *Mycobacterium tuberculosis* or the protist *Plasmodium falciparum*, for example (Brown *et al.*, 2012). In an expanding susceptible population with an increasing life expectancy, fungal infections have emerged as a prominent public health problem (Pfaller & Diekema 2007).

The *Candida* species (Figure 1.1) are of particular interest as a group of significant pathogens of humans and are the fourth most commonly isolated pathogen from blood stream infections (Wisplinghoff *et al.*, 2004; Klotz *et al.*, 2007). Surveillance programmes such as the PATH® Alliance report that *Candida* species are a major cause of invasive fungal infections, accounting for up to 73.4 % of diagnoses. The remainder of infections are attributed to *Aspergillus* species, *Cryptococcus* species, moulds and Mucormycetes (Azie *et al.*, 2012) and similar trends have been noted worldwide (Sifuentes-Osornio *et al.*, 2012; Pfaller & Diekema, 2007).

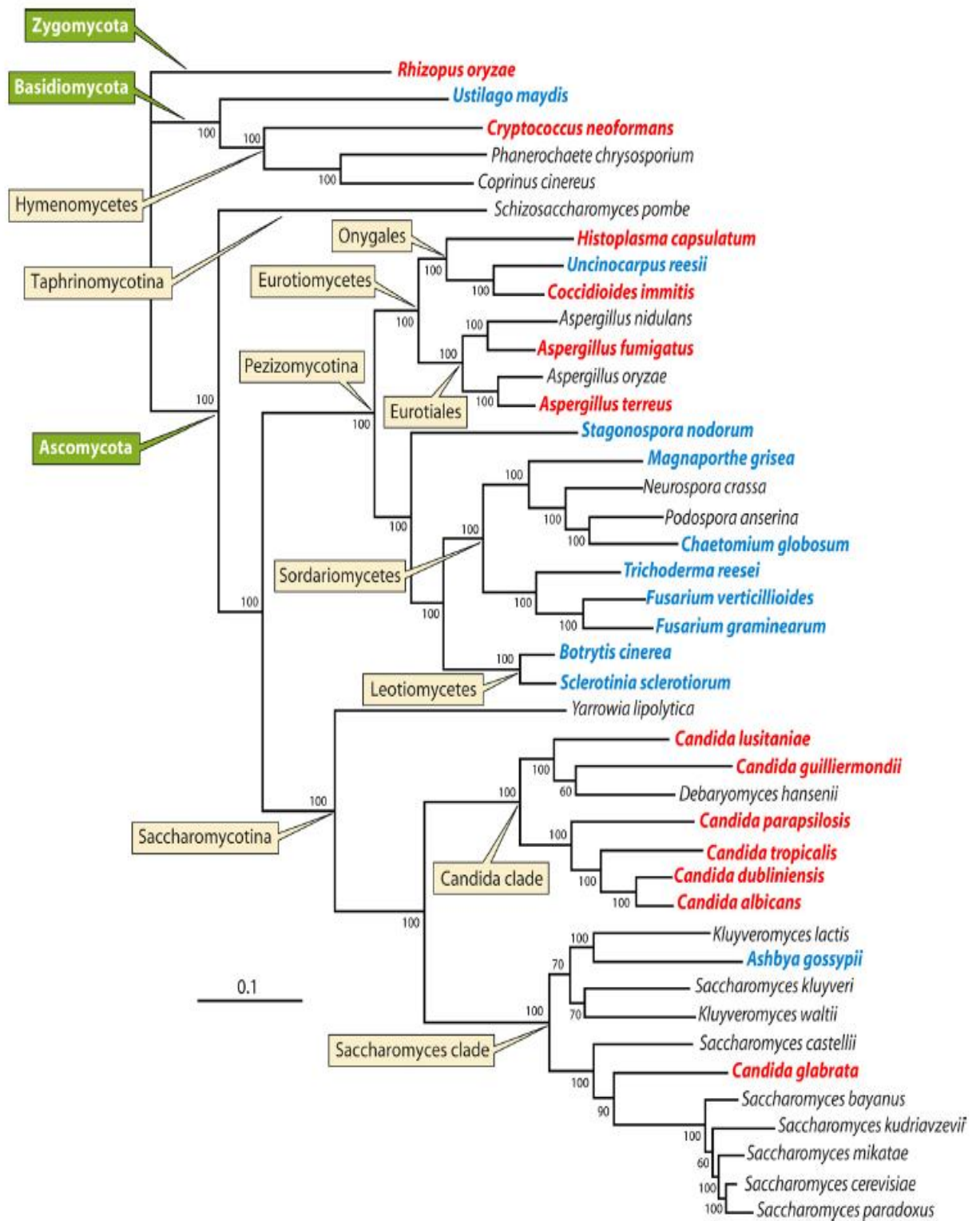


Figure 1.1: Phylogenetic representation of selected fungal species. Species highlighted in blue represent pathogens of plants. Species highlighted in red indicate human pathogens (Butler, 2010).

Candida species are frequently isolated as an asymptomatic commensal from the mucosa of healthy individuals, most commonly colonising the gut, oral or vaginal cavity. Colonisation by *Candida* species can lead to minor superficial infections of the mucosa which are usually cleared by the immune system. However, under certain circumstances colonisation can develop into more serious systemic blood stream infections which are associated with high rates of morbidity and mortality (Fidel *et al.*, 1999; Miramón *et al.*, 2013). A number of predisposing factors such as previous exposure to antifungal drugs, surgical procedures, immunosuppressive therapy, use of central venous catheters and diabetes are linked to the development of systemic *Candida* infections (Almirante *et al.*, 2005; Pfaller *et al.*, 2012). Recurrent oropharyngeal candidiasis is a common problem incurred by patients suffering from immunosuppressive diseases such as HIV (Lin *et al.*, 2009). Reports following the outcomes of patients diagnosed with invasive *Candida* infections estimate mortality rates in the range of 40-75 % (Pfaller & Diekema, 2007; Almirante *et al.*, 2005; Pfaller *et al.*, 2012). The costs of increased length of stay in hospitals, administration of antifungal therapy and diagnostic procedures associated with *Candida* infections cost an estimated \$216-281 in excess medical costs a year in North America (Pfaller & Diekema, 2007; Pelz *et al.*, 2008; Rentz *et al.*, 1998). When it is considered that approximately two thirds of invasive *Candida* infections are hospital acquired (Pfaller *et al.*, 2012), it obviates the need for effective diagnosis, treatment and understanding of *Candida* infections.

Many *Candida* species are able to colonize and establish disease in the human host (Figure 1.1). 97 % of *Candida* infections are attributed to five species: *Candida albicans* (42.1 %), *C. glabrata* (26.7 %), *C. parapsilosis* (15.9 %), *C. tropicalis* (8.7 %) and *C. krusei* (3.4 %) (Pfaller *et al.*, 2012; Figure 1.2). Although *C. albicans* remains the single most frequently isolated *Candida* species, the incidence of infections caused by non-*albicans* *Candida* species is increasing (Pfaller *et al.*, 2012; Horn *et al.*, 2009). *C. glabrata* is currently the second most frequently isolated *Candida* species (Figure 1.2) and its effective treatment is compromised by its innate resistance to the azoles - a major class of antifungal drugs used to treat *Candida* infections and its ability to acquire resistance to the echinocandins (Pfaller & Diekema, 2007; Pfaller *et al.*, 2012; see 1.9).

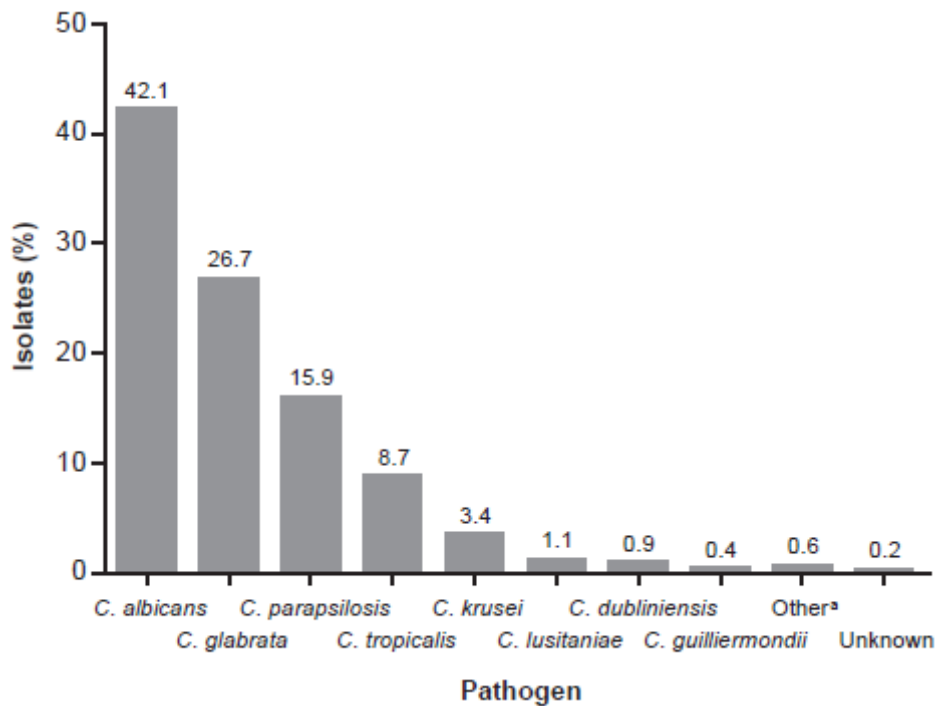


Figure 1.2: Frequency of *Candida* species from 364 clinical blood stream isolates in North America. *C. glabrata* is the second most frequently isolated species causing 26.7 % of all *Candida* infections (Pfaller *et al.*, 2012)

1.2 The *C. glabrata* Genome

Hemiascomycete yeasts have become model organisms for eukaryotic evolutionary and comparative genomic studies and the ease in which they can be genetically manipulated has led to their extensive use in genetic studies. The *C. glabrata* CBS138 genome sequence was published in 2004 simultaneously with the sequences of related species *Kluyveromyces lactis*, *Debaryomyces hansenii* and *Yarrowia lipolytica* as part of the Génolevures consortium (Dujon *et al.*, 2004). Projects such as Génolevures (Sherman *et al.*, 2004; Sherman *et al.*, 2013), YGOB (Byrne & Wolfe, 2005), SGD (yeastgenome.org) and CGD (candidagenome.org) have enabled large scale comparisons of hemiascomycetous yeast genomes.

Although nomenclature and the pathogenic nature of *C. glabrata* has led to its classification with the *Candida* species, comparative genomic analysis revealed that *C. glabrata* is more closely related to the relatively non-pathogenic yeast *S. cerevisiae* (Dujon *et al.*, 2004). The *C. glabrata* genome is unlike those in the *Candida* clade which are distinguishable by a unique translation event whereby

the CUG codon is read (by a special tRNA-Ser) as serine rather than leucine (Santos & Tuite, 1995; Butler *et al.*, 2009). Rather, *C. glabrata* genome features such as genome size and GC content (Table 1.1) much more closely resemble that of *S. cerevisiae* than *C. albicans*, and share 65 % amino acid identity between orthologous proteins. Thus it is postulated that *C. glabrata* and *S. cerevisiae* share a common ancestral lineage and that divergence from this ancestor occurred following a whole genome duplication (WGD) event (Figure 1.3; Dujon *et al.*, 2004; Kellis *et al.*, 2004; Dujon, 2010).

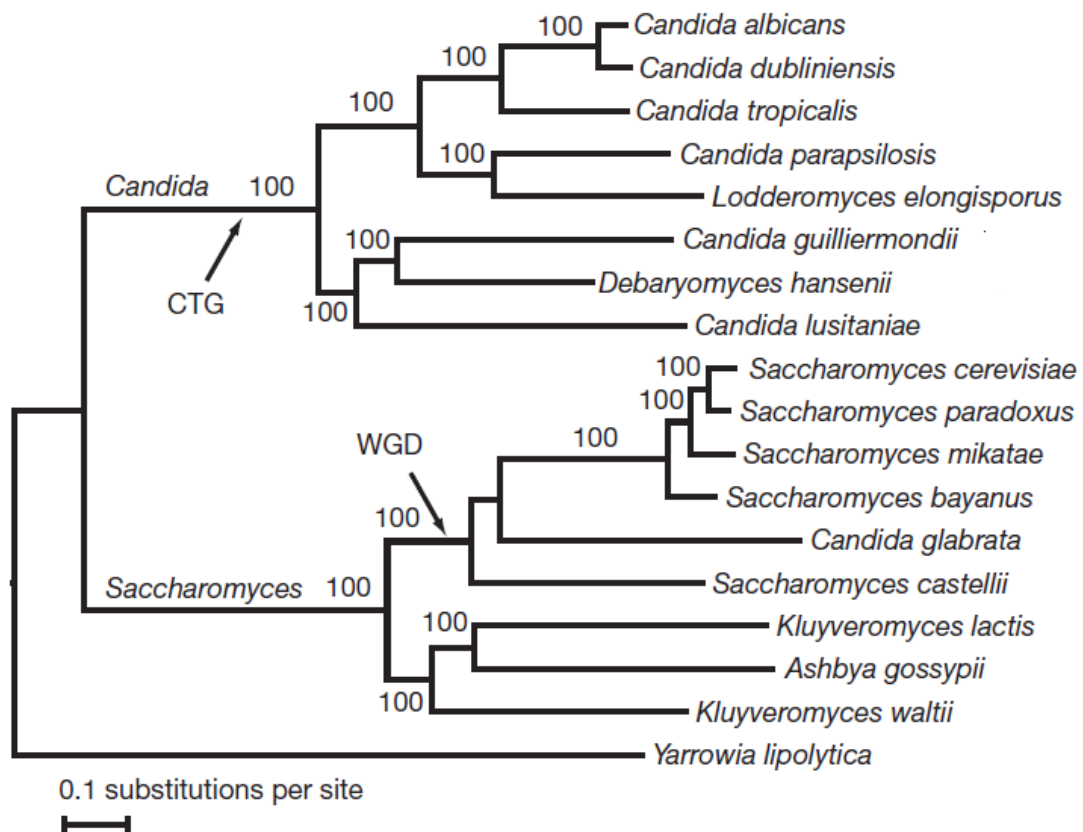


Figure 1.3: Phylogeny of *Candida* and *Saccharomyces* clade species. WGD indicates the occurrence of a whole genome duplication event in an ancestral lineage of *S. cerevisiae* and *C. glabrata*. CTG highlights a switch in the translation of the CUG codon as serine rather than leucine. *C. glabrata* lies in the WGD clade, distinct from the *Candida* clade.

Table 1.1: Summarised genome features of sequenced strains of *S. cerevisiae* S288C, *C. glabrata* CBS138 and *C. albicans* SC5314 (Dujon *et al.*, 2004; Byrne & Wolfe, 2005; Dujon, 2010).

Feature	<i>S. cerevisiae</i>	<i>C. glabrata</i>	<i>C. albicans</i>
Number of chromosomes	16	13	8
Genome size (Mb)	12.1	12.3	14.3
GC Content (%)	38.0	38.8	33.5
Total Coding Sequences (CDS)	5,807	5,283	6,107
Average Gene Density (%)	70.3	65.0	-
Average CDS size (codons)	485	493	489
Ploidy	Haploid	Haploid	Diploid
No. of ohnologue pairs	551	404	-

Duplication of genetic material, such as a WGD event, provides scope for genetic novelty. Genes with new function can arise through gene duplications, a major evolutionary force which can lead to the adaptation of a species to new environments or the development of species-specific traits (Byrne & Wolfe, 2005; Magadum *et al.*, 2013). Duplicated genes may evolve completely novel function (neofunctionalisation) or differentiate by taking on different aspects of the parent gene function (subfunctionalisation) (Magadum *et al.*, 2013). Alternatively, reciprocal loss of duplicated genes can lead to genetic isolation of populations and speciation (Byrne & Wolfe, 2005).

Evidence suggests that post-WGD, the *C. glabrata* genome evolved in a reductive fashion with the frequent loss of genes that remain duplicated in *S. cerevisiae* - characteristic of an emerging pathogen adapting to the novel host niche (Dujon *et al.*, 2004; Byrne & Wolfe, 2005). Fewer blocks of ancestral duplications are found in the *C. glabrata* genome compared to that of *S. cerevisiae*. Hence, there is a lower genetic redundancy in *C. glabrata* and a

reduced number of orthologues, paralogous genes pairs arising from a WGD event (Dujon *et al.*, 2004; Byrne & Wolfe, 2005). Compared with related yeast species studied as part of the Génolevures consortium, genes losses specific to *C. glabrata* include those involved in galactose and phosphate metabolism, cell rescue, defence, virulence and nitrogen and sulphur metabolism (Dujon *et al.*, 2004). Instances where neofunctionalisation has aided adaptation of *C. glabrata* to a host niche lie in the phosphate starvation response where *C. glabrata* does not encode an orthologue of *PHO5*, a phosphate-repressible acid phosphatase, yet has retained both duplications of *PHO2*. Neofunctionalisation of *C. glabrata* *PHO2* lead to functional replacement of *PHO5* with *PHO2*, enabling phosphate-starvation-inducible phosphatase activity in this species (Orkwis *et al.*, 2010).

Expansion of specific gene families can also generate genetic diversity. Uniquely to *C. glabrata*, expansions have occurred in the *YPS* gene cluster (GPI-linked aspartyl proteases) and at the *MNT3* locus. The *C. glabrata* *YPS* gene cluster encodes six additional genes compared with that of *S. cerevisiae* while the *MNT3* *S. cerevisiae* gene, encoding an α -1.3-mannosyltransferase involved in cell wall biogenesis, has eight copies in *C. glabrata* (Dujon, 2010). Expansion of these gene clusters may contribute to *C. glabrata* virulence through restructuring of the cell wall and the *YPS* cluster are important for adaptation and survival in the host and for adhesion to host cells. Similar patterns of gene family expansion have occurred in other pathogenic *Candida* species. In these species, expanded gene families are enriched for function related to the fungal cell wall, cell surface transporters and GPI-linked proteins. These patterns highlight the importance of extracellular activity and the cell wall in virulence (Butler *et al.*, 2009).

1.2.1 Genetic Plasticity in *C. glabrata* Clinical Isolates

Unlike many *Candida* species, blood stream isolates of *C. glabrata* from the same patient can have different karyotypes (Shin *et al.*, 2007). Additional chromosomes comprising large segmental duplications of 120-420 bp have been identified in clinical isolates of *C. glabrata* (Poláková *et al.*, 2009; Ahmad *et al.*, 2013). These segments contain centromeric regions and have acquired telomeric regions but have reduced genetic stability. Alteration of gene dosage in this way could comprise an effective strategy employed by microorganisms to

overcome environmental stresses. Most interestingly, duplicated regions includes virulence-related genes encoding ABC transporters *AUS1* (CAGL0F01419g), *PDH1* (CAGL0F02717g), *CDR1* (CAGL0M01760g), *DHA1* (CAGL0I10384g) and members of the *YPS* cluster and predicted GPI-anchored protein *PLB3* (CAGL0J11770g). As such, increase in gene dosage of genes implicated in drug resistance, virulence and survival in macrophages via new chromosome generation could be a unique strategy employed by *C. glabrata* to adapt to the host environment (Poláková *et al.*, 2009; Ahmad *et al.*, 2013).

1.2.2 Phenotypic Plasticity of *C. glabrata*

Candida species (including *C. glabrata*) are able to undergo phenotypic switching (Lachke *et al.*, 2002; Lan *et al.*, 2002). In *C. glabrata*, a phenotypic switching system has been described in which both lab strains and clinical isolates have been shown to switch between three main phases: white, light brown & dark brown (Lachke *et al.*, 2000). Studies have shown the dark brown phenotype to have a pathogenic advantage as it is better adapted to colonize host organs in a murine infection model (Srikantha *et al.*, 2008). Thus this form of phenotypic plasticity in *C. glabrata* may aid pathogenesis by producing variants that may better survive environmental challenges presented by the host and provide a mechanism for rapid adaptation (Srikantha *et al.*, 2005).

1.2.3 *C. glabrata* has no Apparent Sexual Cycle

To date, all *C. glabrata* clinical isolates have been haploid with no apparent sexual cycle and existing mostly as a clonal population structure (Fidel Jr. *et al.*, 1999; Kaur *et al.*, 2005; Brunke & Hube, 2013). This is contrary to many members of the WGD clade (to which *C. glabrata* belongs) which are able to create genetic diversity through mating and meiotic recombination. In *S. cerevisiae*, upon sensing of pheromone of the opposite mating type, haploid α and a cells form a polarized mating projection (shmoo) in the direction of the partner haploid cell. Upon contact, cells fuse and karyogamy takes place to form an a/α diploid (Merlini *et al.*, 2013). In response to nitrogen starvation, the diploid nuclei undergoes chromosome segregation and meiosis to produce four haploid progeny nuclei which are packaged into spores which are encased by the mother cell to form a tetrad structure (Figure 1.4; Neiman, 2011).

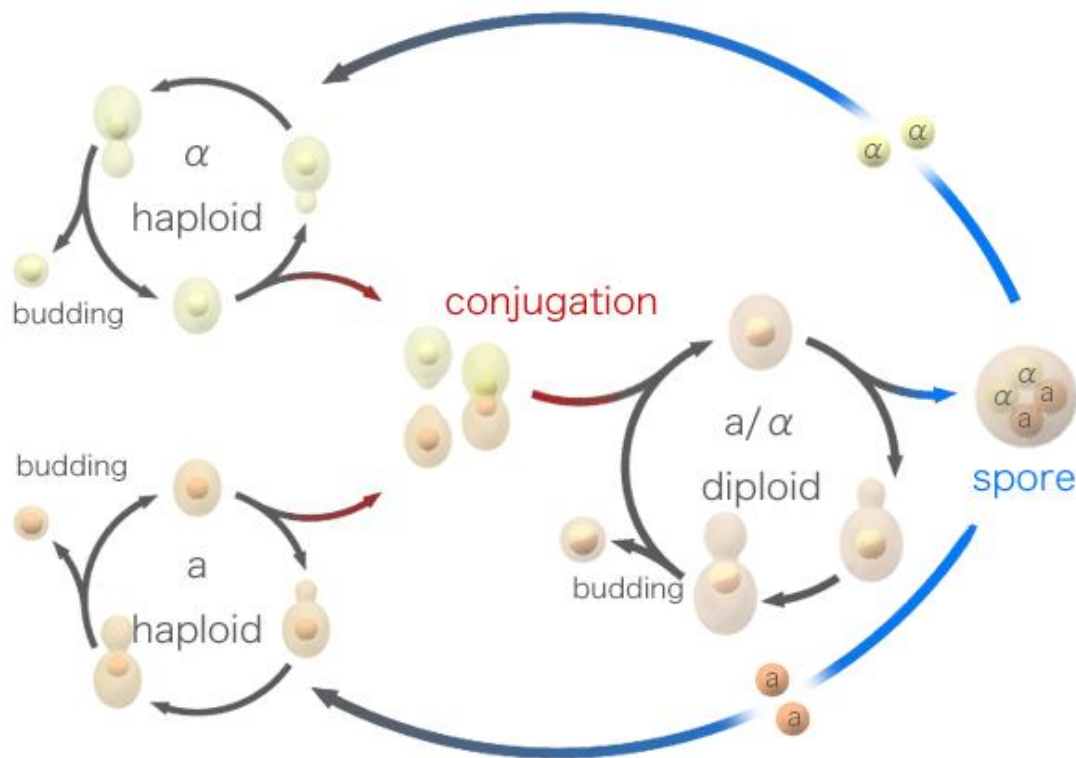


Figure 1.4: The life cycle of *S. cerevisiae* (yeastgenome.org). In response to pheromone from the opposite mating type, haploid a and α cells form mating projections and upon contact, fuse to form a/ α diploid cells. Under nitrogen starvation conditions, diploids undergo meiosis and sporulation forming tetrads which encase four haploid meiotic progeny (spores).

Despite the lack of a sexual cycle, *C. glabrata* is closely related to sexual species *Kluyveromyces delphensis*, *S. cerevisiae* and members of the *Saccharomyces* clade. Although no sexual cycle has been identified, *C. glabrata* does exist in two haploid mating types: MATa (lab strain BG2) and MAT α (lab strain CBS138), both of which (although mostly MATa) have been isolated from colonisation sites of patients (Brockert *et al.*, 2003; Muller *et al.*, 2008; Butler, 2010). As in the case of *S. cerevisiae*, *C. glabrata* MAT loci and the silent MAT-like cassettes, HML α and HMRa, are present (Srikantha *et al.*, 2003; Butler, 2010). Although these homologues encode the same proteins in both species, in *S. cerevisiae* these cassettes are located on the same chromosome. In *C. glabrata*, the MAT and HML-like cassettes are located on chromosome B while the HMR-like cassette is located to chromosome E, which

could signify differences in regulation (Muller *et al.*, 2008). Unlike *S. cerevisiae*, few cases of mating type switching have been observed in *C. glabrata* (Brockert *et al.*, 2003; Butler, 2010).

Further to this, bioinformatic searches identified *C. glabrata* orthologues of numerous genes implicated in the mating and meiosis pathway of *S. cerevisiae*. They encode components of the mating signalling pathway, pheromone synthesis and response and meiosis and sporulation genes (Table 1.2; Wong *et al.*, 2003). Although *C. glabrata* expresses both a- and α -factor receptors, cells of neither mating type show an observable response to pheromone (Muller *et al.*, 2008; Butler, 2010). Since many components of the mating machinery have been retained in *C. glabrata*, it is unknown whether an undiscovered *C. glabrata* sexual cycle exists. Alternatively orthologues of the mating pathway may have emerged new functions as is the case for *STE12* which regulates the response to pheromone in non-pathogenic *S. cerevisiae* yet has a role in virulence in *C. glabrata* (Calcagno *et al.*, 2003).

Table 1.2: *C. glabrata* orthologues of *S. cerevisiae* genes involved in mating, meiosis and sporulation (Wong *et al.*, 2003)

<i>C. glabrata</i> ORF	<i>S. cerevisiae</i> orthologue	Role in <i>S. cerevisiae</i>
<i>CAGLOB02739g</i>	<i>STE11</i>	Mating signalling
<i>CAGLOI03498g</i>	<i>STE7</i>	
<i>CAGLOJ04290g</i>	<i>FUS3</i>	
<i>CAGLOM01254g</i>	<i>STE12</i>	
<i>CAGLOC01919g</i>	<i>MFA2</i>	Pheromone synthesis and response
<i>CAGLOL02651g</i>	<i>STE13</i>	
<i>CAGLOK00363g</i>	<i>STE6</i>	
<i>CAGLOI06138g</i>	<i>FAR1</i>	
<i>CAGLOF05269g</i>	<i>CDC42</i>	
<i>CAGLOH00759g</i>	<i>SGS1</i>	
<i>CAGLOM09042g</i>	<i>IME1</i>	
<i>CAGLOF05357g</i>	<i>UME6</i>	
<i>CAGLOE01683g</i>	<i>MCK1</i>	
<i>CAGLOE03630g</i>	<i>RIM4</i>	
<i>CAGLOG04455g</i>	<i>IME2</i>	

The lack of mating and meiotic recombination in *C. glabrata* is consistent with pathogenic fungal species (including *Candida* species), which have independently limited their sexual cycle and reproduce mitotically perhaps to maximise virulence (Butler, *et al.*, 2009). Although *C. albicans* encodes homologues of key *S. cerevisiae* genes that could support a full sexual cycle, it exists in a mainly asexual lifecycle (Tzung *et al.*, 2001). However, *C. albicans* undergoes a parasexual cycle in which diploid α and a cells conjugate, a process regulated by phenotypic switching, to form a/α tetraploids in which genetic recombination but not full meiosis can take place. Tetraploids undergo subsequent random chromosome loss to produce diploid progeny (although many are aneuploid for certain chromosomes) which contain assorted combinations of the 8 chromosomes (Forche *et al.*, 2008). More recently, a haploid form of *C. albicans* was discovered which has arisen through concerted chromosome loss (Hickman *et al.*, 2013).

1.3 The *S. cerevisiae* Molecular Toolkit

The ease with which *S. cerevisiae* can be genetically manipulated has facilitated the production of a number of molecular tools which have enabled genome-wide studies in this model organism. Large collaborative projects have produced an array of deletion and ORF libraries which have become valuable resources for a plethora of downstream applications (Table 1.3).

Table 1.3: Summary outlining the molecular tools available for *S. cerevisiae* and examples of their applications where they have facilitated genome-wide molecular studies in this organism.

<i>S. cerevisiae</i> tool	Application
<p>ORF libraries:</p> <ul style="list-style-type: none"> • Yeast ORF collection • Yeast YFP Fusion Kinase collection • Yeast TAP-tagged ORFs • Molecular Barcoded Yeast (MoBY) ORF collection • Yeast GST-tagged ORFs • Yeast HA tag collection • Yeast Barcode Collection 	<p>Global analysis of protein glycosylation (Gelperin <i>et al.</i>, 2005)</p> <p>Protein localisation studies (Kumar <i>et al.</i>, 2002; Ma <i>et al.</i>, 2008)</p> <p>Identification of log-phase specific genes (Ghaemmaghami <i>et al.</i>, 2003)</p> <p>Uncovering the genetic basis of drug resistance (Ho <i>et al.</i>, 2009)</p> <p>Over-expression screens (Sopko <i>et al.</i>, 2006)</p> <p>SDL screening (Sopko <i>et al.</i>, 2006)</p> <p>Molecular barcoding (Yan <i>et al.</i>, 2008)</p>
<p>Deletion libraries:</p> <ul style="list-style-type: none"> • Yeast essential collection • Yeast Heterozygous collection • Yeast Homozygous collection • Yeast mata/mata collection 	<p>Functional profiling of the <i>S. cerevisiae</i> genome (Giaever <i>et al.</i>, 2002; Deutschbauer <i>et al.</i>, 2002; Fabrizio <i>et al.</i>, 2010)</p> <p>Global synthetic genetic interaction profiling (Davierwala <i>et al.</i>, 2005; Tong <i>et al.</i>, 2001; Tong <i>et al.</i>, 2005)</p> <p>Haploinsufficiency profiling (Giaever <i>et al.</i>, 1999)</p> <p>Pooled competitive growth assays (Winzeler <i>et al.</i>, 1999)</p> <p>Aneuploidy profiling (Hughes <i>et al.</i>, 2000)</p> <p>Genome-wide screens of human disease genes (Steinmetz <i>et al.</i>, 2002)</p> <p>Drug/small molecule targets and MOA discovery (Hillenmeyer <i>et al.</i>, 2010; dos Santos & Sá-Correia, 2011; Zakrzewska <i>et al.</i>, 2007; Troppens <i>et al.</i>, 2013)</p>

1.3.1 *S. cerevisiae* Deletion Collections and their Applications

The generation and completion of *S. cerevisiae* deletion libraries has greatly facilitated annotation of the genome and made gene deletion studies possible on a genome-wide scale. Although the creation of such libraries is laborious, it offers advantages over forward genetic approaches for genome-scale studies. Firstly, full coverage of the entire genome is ensured as opposed to random mutagenesis methods in which a significantly greater number of mutants than genes must be created in order to achieve saturation of the genome. In addition targeted deletion mutants allow phenotypes to be rapidly linked to known genetic perturbations rather than using sequencing to map mutations in selected random mutants (Pierce *et al.*, 2007). Lastly, deletion libraries provide a lasting resource for community use.

The creation of similar genome-wide deletion libraries in pathogenic fungal species has been hampered by numerous factors. Most notably in some *Candida* species, the obligate diploid state and lack of a complete sexual cycle increases the difficulty and complexity of genetic manipulation and targeted gene deletion efforts (Xu *et al.*, 2007). As such, information gleaned from the *S. cerevisiae* deletion collection has been used extensively as a basis for the generation of testable experimental hypothesis for other eukaryotic organisms.

The largest collection of deletion mutants in a pathogenic fungal species exists in *C. albicans*. Thus far, a homozygous deletion collection covering 11 % of the genome has been generated and successfully used for the study of determinants of dimorphism and for *in vivo* studies in which the synthesis of sphingolipids were associated with virulence (Noble *et al.*, 2010). Such studies have highlighted the need for molecular biology tools in medically relevant fungal pathogens as components of the glucosylceramide biosynthetic pathway, which are required for establishment of disease and proliferation in the murine kidney, are not present in *S. cerevisiae* (Noble *et al.*, 2010).

1.3.1.1 Molecular Barcoding

An attractive alternative to the timely analysis of individual mutants is the use of molecular barcoding to analyse mixed pools of mutants simultaneously. Molecular barcoding was originally developed by Hensel *et al.*, 1995, for the identification of virulence genes in a murine model of typhoid fever. Tagged-transposon mutagenesis was used to create a mixed input pool of *Salmonella typhimurium* mutants which were studied in a murine model of infection. Analysis of barcodes recovered from the murine model identified *inv/spa* genes as novel *S. typhimurium* virulence factors – components of the type III secretion system (TTSS) required for entry into host cells (Hensel *et al.*, 1995; Fàbrega & Vila, 2013).

In the *S. cerevisiae* deletion collections, each mutant is tagged with two unique DNA sequences of 20 base pairs termed a molecular barcode, which allows for individual quantification of each mutant within a mixed population (Mazurkiewicz *et al.*, 2006; Pierce *et al.*, 2007; Delneri, 2010; Figure 1.5). Barcodes are flanked by universal sequences which can be used for amplification of barcodes in one reaction (Delneri, 2010). Detection of barcodes is subsequently performed by hybridisation to a tag microarray (Pierce *et al.*, 2007) or more recently using next generation sequencing (Bar-seq) (Craig *et al.*, 2008). Multiplexing of numerous samples of pooled DNA tags can increase the efficiency, throughput and reduce costs of barcode sequencing (Smith *et al.*, 2010). Molecular barcoding has proven a robust technique for use in competitive growth assays. In these experiments, non-essential deletion mutants (and their associated DNA barcode) with decreased competitive fitness in specific conditions will be depleted from a mixed pool of mutants (Mazurkiewicz *et al.*, 2006). Pooled deletion screening *in vitro* has already yielded numerous applications in the study of gene function, drug target identification and compound mode of action discovery (Pierce *et al.*, 2007, Delneri, 2010). It offers particular advantages for characterising large number of mutants *in vivo* by reducing the number of animals required (Idnurm *et al.*, 2009; Noble *et al.*, 2010).

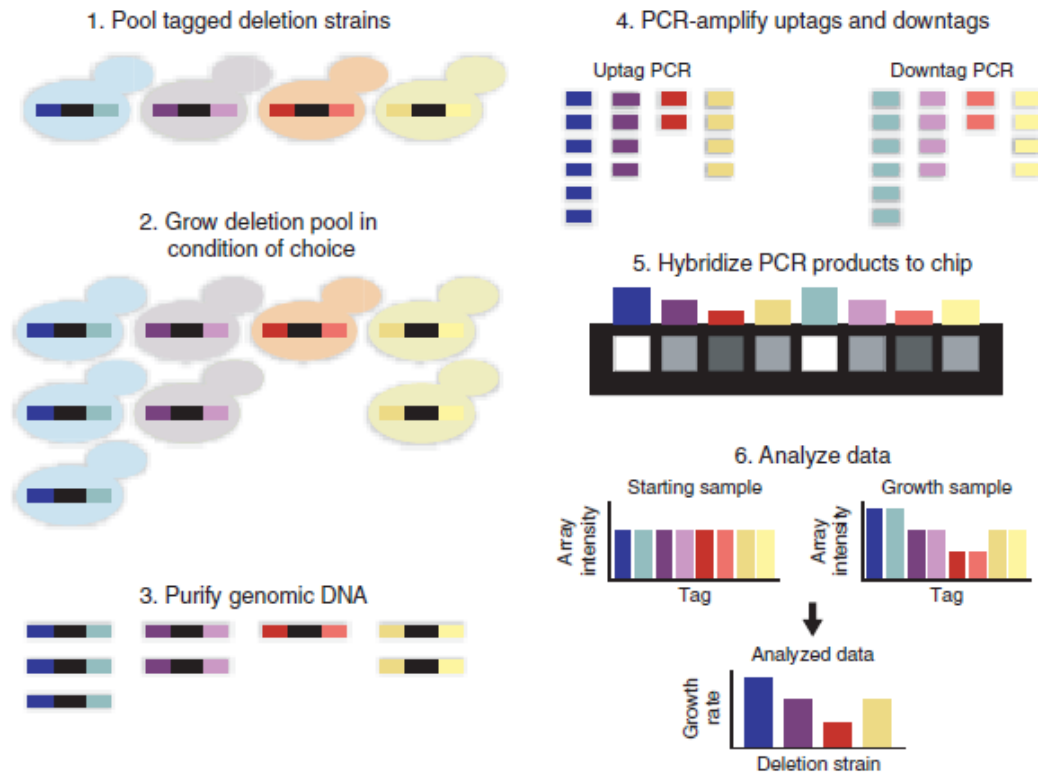


Figure 1.5: Competitive growth assays using mixed pools of *S. cerevisiae* mutants. 1) Mixed pools of *S. cerevisiae* deletion mutants are created whereby each mutant is equally represented. 2) The pool of mutants is grown under a defined stress condition. Mutants which have reduced fitness under a given stress condition will be depleted from the pool (red). Mutants with the greatest fitness will proliferate and become overrepresented within the pool (Blue). 3) DNA is isolated from pooled mutants. 4) PCR (using primers targeting universal sequences flanking the barcodes) is used to amplify barcodes from the DNA of pooled samples. 5) Amplified barcodes are hybridized to a barcode tag array (or alternatively barcodes can be sequences). 6) Tag intensities are used as a representative measure of individual strain fitness under the defined growth condition (Pierce *et al.*, 2007).

Since its first use in *S. typhimurium*, STM has been widely used for the parallel analysis of pooled mutants in both prokaryotic and eukaryotic systems. This includes pathogenic bacterial species *Mycobacterium tuberculosis* (Cox *et al.*, 1999; Blumenthal *et al.*, 2010), *Pseudomonas aeruginosa* (Bianconi *et al.*, 2011) and *E. coli* (Gonzalez *et al.*, 2001; Antão *et al.*, 2009). STM has also proven an effective method for the study of virulence genes in fungal pathogens including *C. albicans* (Noble *et al.*, 2010), *Aspergillus fumigatus* (Brown *et al.*, 2000) and *C. neoformans* (Nelson *et al.*, 2001; Idnurm *et al.*, 2009).

1.3.1.2 Chemical-Genomic Screening

The availability of the *S. cerevisiae* deletion collections has increased the efficiency with which functional relationships between genes and chemical compounds can be uncovered in a systematic and unbiased fashion, enabling the annotation of genes with unknown function (Ho *et al.*, 2011; Andrusiak *et al.*, 2012). Chemical-genomic screening has become a powerful tool in the identification of cellular drug targets and mode of action (MOA) of chemical compounds and bioactive molecules with no prior knowledge of the compound MOA required – a major challenge in the field of drug development (Ho *et al.*, 2011; Andrusiak *et al.*, 2012). As well as bioactive compounds, chemical genomic screening has been used for MOA and cellular target discovery of bacterial secondary metabolites with fungicidal activity (Troppens *et al.*, 2013).

1.3.1.3 Haploinsufficiency profiling (HIP)

Haploinsufficiency occurs when genes dosage is reduced from two to one copy in a diploid organism, resulting in reduced fitness. Given that in a heterozygous mutant a decreased dose of compound target yields increased compound sensitivity, the heterozygous *S. cerevisiae* deletion array allows haploinsufficiency profiling to be performed on a genome-wide scale (Ho *et al.*, 2011). An advantage of HIP is that it allows unbiased profiling of the whole genome, including essential genes which is not possible in haploid or homozygous deletion mutants (Delneri, 2010). However, HIP is not of use if deletion of one copy of the target gene does not confer a drug sensitive phenotype and HIP is only applicable to diploid organisms (Ho *et al.*, 2011).

1.3.1.4 *S. cerevisiae* as a Model for Human Disease Genes and Drug Targets

Twenty eight percent of known human genes implicated in disease have *S. cerevisiae* homologues (Foury, 1997). Thus the yeast deletion collection provides a powerful model for the study of genes associated with disease in mammalian systems. The heterozygous deletion collection has been of particular use for the study of cancers and HIV which are associated with abnormalities in gene copy number (Delneri, 2010).

The deletion collection has also been exploited as a model for the identification of drug targets in mammalian systems. As an example, the collection was successfully used to identify novel secondary targets of nitrogen-containing bisphosphates (drugs for treatment of cancer-induced bone disease) and hence to understand the consequences of exposing cells to such compounds. Competitive growth of pooled mutants in sub-lethal concentrations of nitrogen-containing bisphosphates identified genes involved in DNA damage and cytoskeletal dynamics as putative secondary targets. Candidate yeast targets were further validated in a mammalian breast cancer cell line confirming that DNA damage and disruption of microtubule assembly were indeed involved in the cytotoxic effects of nitrogen containing bisphosphates (Bivi *et al.*, 2009).

1.3.2 Chemical-Genetic Screening in Clinically-Relevant Organisms

Since the success of chemical-genomic screening in the model organism *S. cerevisiae*, molecular tools with applications of chemical-genomic screening are being developed in more clinically relevant pathogenic organisms, since knowledge of *S. cerevisiae* may not always be directly transferable to species with different lifestyles, morphology, genomic organisation or essential genes (Ho *et al.*, 2011; Andrusiak *et al.*, 2012).

Haploinsufficiency profiling in *C. albicans* has successfully been used to examine nutrient- and drug-induced haploinsufficiency in a medically relevant system (Xu *et al.*, 2007; Oh *et al.*, 2010). Through the construction and screening of 3633 tagged heterozygous transposon mutants, a *C. albicans* haploinsufficiency profile was revealed with features distinct from *S. cerevisiae* such as increased emphasis on oxidative metabolism, nutrient sensing and

resistance to oxidative stress, which may be reflective of the *C. albicans* niche. Comparison of drug-induced haploinsufficiency between the two species identified Sec7p as the *C. albicans* target of Brefeldin A – a gene which was not identified in *S. cerevisiae* haploinsufficiency screens (Oh *et al.*, 2010). In a smaller study of 2868 barcoded heterozygous deletion mutants covering 45 % of the *C. albicans* genome haploinsufficiency profiling successfully uncovered known targets of the azoles (*ERG11* and *NCP1*). HIP was further used to uncover the mode of action of unknown chemical compounds as microtubule inhibitors (Xu *et al.*, 2007).

1.3.3 Genetic Interactions and the Synthetic Genetic Array (SGA)

Genome-scale collections of deletion mutants have facilitated the mapping of quantitative genetic interactions throughout the *S. cerevisiae* genome. A genetic interaction arises when the phenotype of a double mutant is not explained by combining the phenotypes of single genetic variants in a multiplicative manner (Dixon *et al.*, 2009). For example, a synthetic lethal interaction occurs when two mutations are individually non-lethal, but combined yield a lethal phenotype (Tong *et al.*, 2001). Genetic interactions tend to occur in genes which function in parallel pathways which can buffer defects in the other, genes functioning within the same pathway or within the same protein complex (Hartman IV *et al.*, 2001; Tong *et al.*, 2001; Dixon *et al.*, 2009). Hence, the study of genetic interactions is a powerful tool for uncovering gene function.

The creation of ordered arrays of non-essential gene deletion collections has opened up the possibility of generating thousands of double mutants simultaneously using the Synthetic Genetic Array platform in which a number of pinning steps are used to facilitate mating, meiotic recombination and selection of haploid double mutants. Analysis of double mutants for positive or negative genetic interactions can subsequently be used to create visual networks of interactions for the chosen query gene (Tong *et al.*, 2001; Tong *et al.*, 2004; Tong *et al.*, 2005). Collections of temperature sensitive conditional alleles or conditional expression alleles of *S. cerevisiae* essential genes has broadened the scope for SGA analysis to also include large scale genetic interaction profiling of essential genes (Davierwala *et al.*, 2005).

Synthetic genetic interaction profiles covering 75 % of the *S. cerevisiae* genome (approximately 5.4 million gene pairs) has yielded the first functional map of the cell (Costanzo *et al.*, 2010; Figure 1.6). The genetic landscape clustered genes based on similar genetic interaction profiles and found genes functioning in similar biological processes and pathways form clusters (Dixon *et al.*, 2009; Costanzo *et al.*, 2010; Figure 1.6). It also revealed that genetic interactions are more likely to occur between genes encoding components of parallel pathways which can buffer or compensate each other – in contrast to physical interactions which are more frequent between genes acting within the same pathway (Dixon *et al.*, 2009). In addition, genetic interactions were enriched amongst genes which confer similar mutant phenotypes, genes encoding proteins with similar cellular localisation patterns, homologous genes and those which encode components of the same protein complex (Tong *et al.*, 2004).

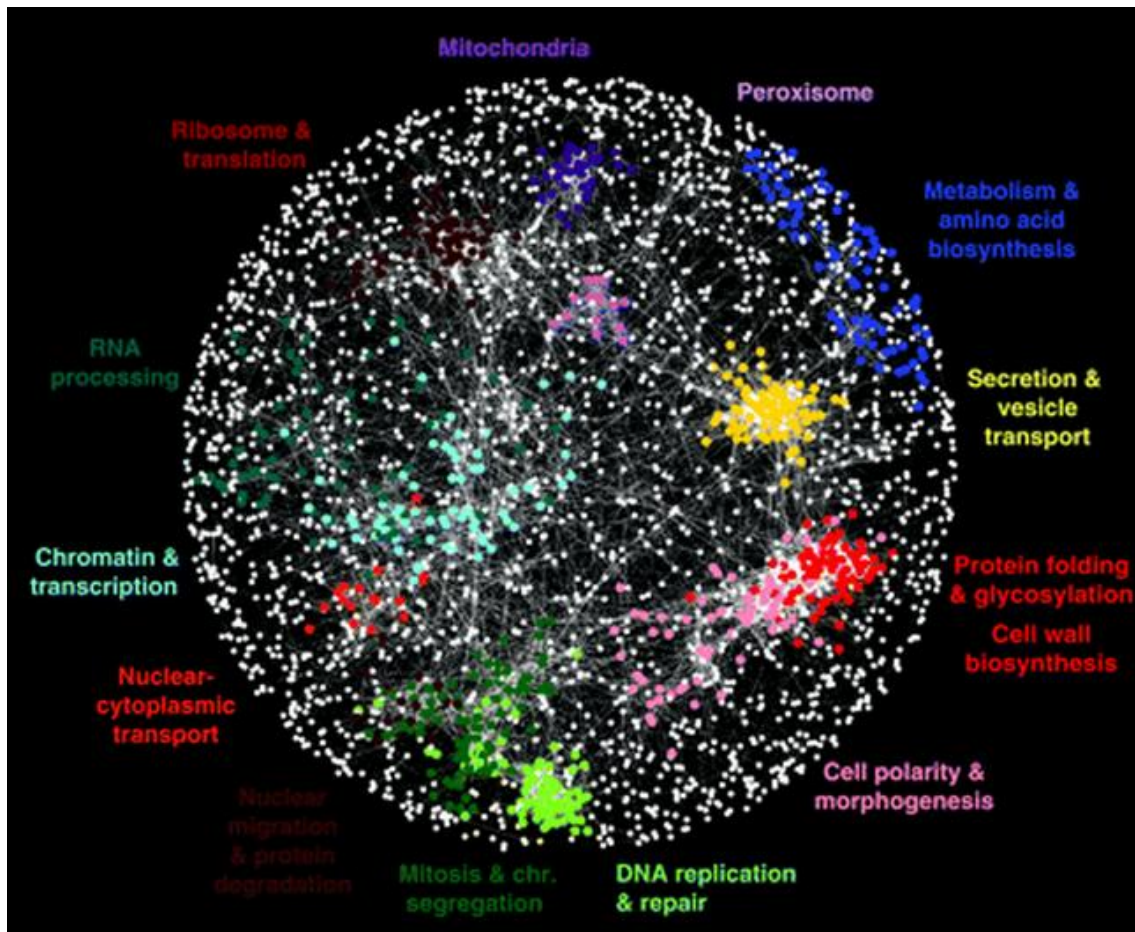


Figure 1.6: The genetic landscape of a cell. Correlation network of ~5.4 million gene pairs in which genes with similar genetic interaction profiles are clustered. Clusters of genes are coloured according to their molecular GO term (Costanzo *et al.*, 2010).

Within the interaction network, individual genes share varying degrees of connectivity. Whilst some genes are poorly connected, others are highly connected and may be strongly clustered. Highly connected and strongly clustered genes which confer a fitness defect when individually deleted are denoted network hubs (Costanzo *et al.*, 2010). Similarly, essential genes are highly connected and the density of genetic interactions in the essential gene network is five times that of the non-essential genetic interaction network, demonstrating the fundamental requirement of these genes for growth (Davierwala *et al.*, 2005; Dixon *et al.*, 2010).

Given that genes with similar function have similar genetic interaction profiles, interaction networks are a useful tool in the characterisation of unknown genes based on their position within clusters of the genetic interaction landscape (Tong *et al.*, 2004). Due to high levels of genetic redundancy in yeast and a high tolerance to deletion of single genes, a large proportion of *S. cerevisiae* ORFs remain uncharacterised following gene deletion studies (Tong *et al.*, 2001). Genetic interaction profiling allows the annotation of such genes. For example uncharacterised *S. cerevisiae* ORF *YMR299C* clusters with components of the dynactin spindle orientation pathway in the genetic landscape. Indeed, further bioinformatic analysis of the encoding protein showed similarity to the mammalian dynein light intermediate chain and deletion of this ORF conferred defects in dynein-dynactin function, consistent with the position of this ORF within the dynactin cluster of the genetic interaction landscape (Tong *et al.*, 2004).

The wealth of genetic interaction data produced has been deposited on the DRYGIN (data repository of yeast genetic interactions), which can be accessed as a community tool for genetic network analysis, visualisation and the integration of other data such as pathway information and physical interaction data (Koh *et al.*, 2010).

1.3.3.1 Genetic Interaction Networks as Models for Human Disease

Genetic interaction networks in yeast can be extrapolated to model networks in other eukaryotic systems. Evolutionarily conserved genetic interaction data was

used to construct a network of CIN (chromosome instability) genes in a cancer cell model, effectively identifying synthetic lethal interactors, such as *FEN1*, which could be potential anticancer drug targets (van Pel *et al.*, 2013).

1.3.3.2 Genetic Interaction Mapping in Non-Yeast Model Organisms

High-throughput genetic interaction profiling has been employed for the study of the genetic landscape in model organisms, although none have yet to achieve the extensive coverage of the *S. cerevisiae* genetic landscape. Genetic interaction mapping in the fission yeast *Schizosaccharomyces pombe* currently covers 50 % of the genome, comprising approximately 1.6 million pairwise interactions (Roguev *et al.*, 2007; Ryan *et al.*, 2012). Smaller scale studies of genetic interactions exist in *Escherichia coli* (Typas *et al.*, 2008), *Drosophila melanogaster* (Horn *et al.*, 2011) and *C. elegans* (Lehner *et al.*, 2006).

Most recently, RNA interference (RNAi) methods in mice fibroblasts has enabled quantitative genetic interaction mapping in mammalian cells from 11,000 pairwise knock-downs. Similarly to the genetic landscape of the yeast cell, the mammalian genetic interaction map highlighted known pathways and genes encoding components of the same protein complex showed correlated genetic interaction profiles (Roguev *et al.*, 2013).

1.3.3.3 Combining Chemical-Genetic & Genetic Interaction Data

Typically SGA data has been generated using colony size measured by automated image analysis software as a phenotypic readout. Whilst this has been successfully used to map the genetic landscape of the cell (Costanzo *et al.*, 2010), it ignores other phenotypes which arise from genetic perturbation. Automated high content screening was used to integrate quantitative morphological phenotypes with genetic interaction data sets in an unbiased, genome-wide fashion (Vizeacoumar *et al.*, 2010). Having introduced GFP-tubulin to the *S. cerevisiae* deletion collection, an automated image acquisition methodology analysed spindle morphogenesis phenotypes in live cells from both single and double mutant arrays. Thus, integration of multiple phenotypic readouts should greatly increase the accuracy with which genetic interaction profiling can define gene function. In this study alone 122 novel genes involved

in spindle formation were identified - some of which would remain undiscovered using fitness as a sole phenotypic measurement (Vizeacoumar *et al.*, 2010).

Integrating chemogenomic and genetic interaction data sets can provide a powerful tool for linking drug targets with their associated pathways. In a study by Parsons *et al.* (2004) chemical genetic interaction profiles of 12 bioactive molecules were overlaid with genetic interaction profiles of target genes resulting in a significant overlap. Clustering analysis revealed the chemical-genetic profiles of bioactive compounds clustered with genetic interaction profiles of known target genes and their associated pathway, providing links between these compounds and their target pathways (Parsons *et al.*, 2004).

1.4 *C. glabrata* Lacks Molecular Tools

Despite the prominence of *C. glabrata* as a pathogen of humans (see 1.5) the study of virulence in this species is hampered by a lack of molecular tools. Unlike *S. cerevisiae*, no genome-wide ORF or deletion collections are available for *C. glabrata*. Recently, the first large-scale deletion library in *C. glabrata* was generated, containing over 700 individually barcoded *C. glabrata* mutants (Schwartzmüller *et al.*, 2013; Appendix 13). However, this collection is mostly biased towards *C. glabrata* ORFs with known orthologues in *S. cerevisiae* that are components of signalling pathways or transcription factors, for example, and may not be of use for the study of *C. glabrata*-specific traits such as virulence. A *C. glabrata* ORF collection is also under construction (personal communication, Dr. Hsueh-lui Ho, University of Exeter) which will greatly facilitate the functional characterisation of *C. glabrata* ORFs in the future. However, to date, no complete deletion or ORF collections are available for the study of *C. glabrata* biology. Much knowledge of *C. glabrata* biology is reliant on the extrapolation of knowledge of orthologous ORFs in *S. cerevisiae*.

Due to the lack of deletion arrays and no apparent sexual cycle, genome-wide genetic interaction studies (such as the SGA platform used for *S. cerevisiae*) are also not applicable to *C. glabrata*. However, it has been shown that ORFs from non-*S. cerevisiae* species can be used in the *S. cerevisiae* SGA system to yield biologically relevant insights into ORFs function. Brown & Madhani, 2012, used an adapted *S. cerevisiae* SGA screen to uncover the molecular function of *C. neoformans* pathogenicity factor Liv7. Similarly, *C. glabrata* ORFs have been

shown to work in the *S. cerevisiae* SGA system (Personal communication, Dr. Jane Usher, University of Exeter).

1.5 Establishment and Development of *C. glabrata* Infection in the Human Host

Despite the significance of *C. glabrata* as a pathogen, the mechanisms by which *C. glabrata* is able to establish disease in the human host remains poorly understood. Since *C. glabrata* shares similar epidemiology and disease symptoms with infections caused by *C. albicans*, it has been assumed that their mechanisms of virulence would be similar also. Yet murine models comparing systemic infection with both species produce strikingly different outcomes. *C. albicans*-infected mice rapidly succumb to infection 3-4 days post infection whereas infection with comparable doses of *C. glabrata* results in chronic but non-fatal infection which leads to only a mild immunological response (Brieland *et al.*, 2001; Jacobsen *et al.*, 2010). The two species also share different life cycles, particularly with regards to morphology and ploidy (Sudbery, 2011; Brunke & Hube, 2013). Regardless of such differences adhesion to host cells, biofilm formation, traversing host barriers and immune evasion are critical for the establishment of infection by both species.

1.5.1 *C. glabrata* Adhesion to Host Cells

Adhesion of *C. glabrata* to host epithelial cells is primarily mediated by constituents of the fungal cell wall and is vital for colonisation and the successful establishment of infection. The ability of pathogenic yeasts such as *C. glabrata* to adhere to abiotic surfaces such as medical devices presents an opportunity to gain access to the blood stream and the internal organs of patients (Verstrepen & Klis, 2006; Brunke & Hube, 2013). Similarly to *C. albicans* and *S. cerevisiae*, the *C. glabrata* cell wall comprises a complex network of β -1,3 glucan, β -1,6 glucan, chitin and an outer layer predominantly consisting of mannoproteins which are at the forefront of the host-pathogen interaction (Figure 1.7; de Groot *et al.*, 2008; El-Kirat-Chatel *et al.*, 2013). Such proteins include glycosylphosphatidylinosol (GPI)-modified cell surface proteins which confer adherence of fungal cells to host and abiotic surfaces. These are linked to β -1,3 glucan in the fungal cell wall via a phosphodiester bridge with β -

1,6 glucan. In *C. albicans*, the ALS (agglutinin-like sequence) adhesin family are a major family of GPI-modified cell wall proteins required for adherence and orthologues are present in most related *Candida* species with the exception of *C. glabrata* (Butler *et al.*, 2009; Zhu & Filler, 2010). *S. cerevisiae* also encodes an array of GPI-anchored adhesins such as the *FLO* gene family which confer cell-cell adhesion (flocculation) and adhesion to abiotic substrates (Verstrepen & Klis, 2006; Soares, 2011).

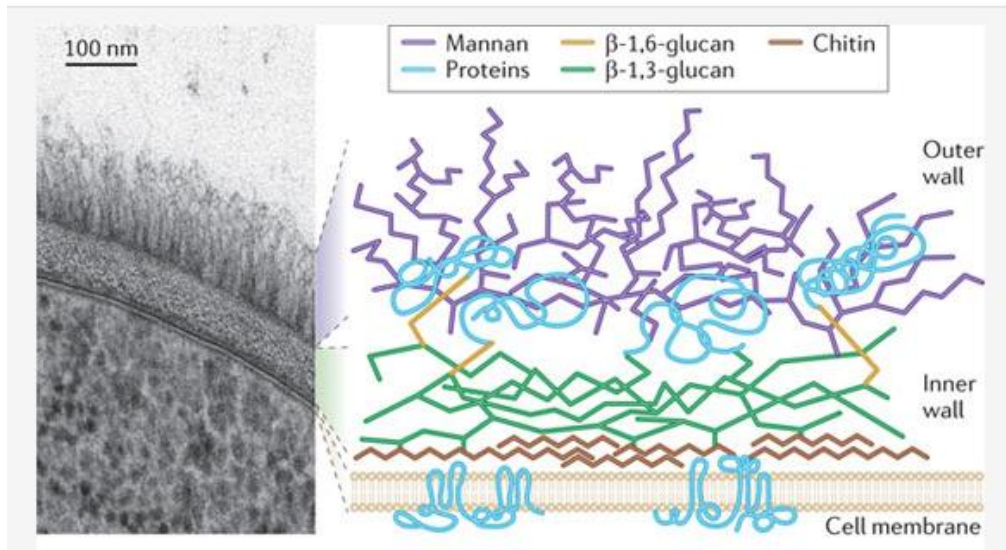


Figure 1.7: Structure of the fungal cell wall. The plasma membrane is surrounded by an inner cell wall layer consisting of β -1,3 glucan, β -1,6 glucan, chitin and an outer layer enriched with mannoproteins. (GPI)-modified cell surface proteins are linked to 1,3- β -glucan in the inner layer of fungal cell wall (Gow *et al.*, 2012).

The *C. glabrata* genome encodes a repertoire of 67 putative adhesin-like glycosylphosphatidylinositol (GPI) – modified cell wall proteins (Table 1.4), many of which are specific to this species (de Groot *et al.*, 2008). Of these, the *EPA* family is the largest containing approximately 17 members (dependent on the isolate). *Epa* proteins contain an N-terminal adhesion domain resembling a Ca^{+} -dependent lectin, a central serine- and threonine-rich domain and a C-terminal anchor which covalently attaches the protein to the fungal cell wall (Frieman *et al.*, 2002). *EPA1* (CAGL0E06644g) is the main adhesin required for epithelial adhesion to *N*-acetyl lactosamine-containing glycoconjugates and its deletion renders *C. glabrata* non-adherent to human epithelial cells (Cormack *et*

al., 1999). Although single deletion of *EPA1* has no direct effect on *C. glabrata* virulence, deletion of multiple *EPA* genes (*EPA1-3*) significantly reduces virulence in a murine model (De Las Penas *et al.*, 2003). Adhesins *Epa6* (*CAGLOC00110g*) and *Epa7* (*CAGLOC05643g*) have a role in *C. glabrata* adherence to epithelial cells yet they have not been fully characterised. It is known that these paralogues of *Epa1* also bind glycans containing a terminal galactose residue although they vary in the specificity and range of glycans they bind to (Gallegos-Garcia *et al.*, 2012; Zupancic *et al.*, 2008). Studies examining *EPA* adhesion domain structure highlighted the importance of calcium-coordinating loops CBL1 and CBL2 in differential ligand binding specificities (Maestre-Reyna *et al.*, 2012).

Table 1.4: Summary of putative GPI-linked adhesin proteins, their subgroups and localisation in *C. glabrata*.

GPI family subgroup	No. Of proteins	No. with subtelomeric localisation
I – Epa family	17	14
II – Pwp family	7	1
III	13	11
IV	3	3
V – includes Awp2 & Awp4	13	12
VI – includes Awp1 & Awp3	7	1
VII	5	2

Similarly to *S. cerevisiae* *FLO* genes, *C. glabrata* *EPA* genes are mainly localised in clusters at subtelomeres (Table 1.4) where their expression is subject to epigenetic silencing by *SIR* complex (De Las Peñas *et al.*, 2003; de Groot *et al.*, 2008; Jandric & Schüller, 2011). The *SIR* complex and its interactors (*SIR2-4*, *RAP* and *RIF1*) achieve epigenetic silencing at the telomeres by enzymatic modification of nucleosomes and subsequent binding to modified nucleosomes forming a silent chromatin structure (Fox & McConnell, 2005; Talbert & Henikoff, 2006). Reduction of *SIR*-dependent silencing and thus

mis-regulation of *EPA* genes by deletion of *SIR* complex components *SIR3* (*CAGL0M00770g*) and *RIF1* (*CAGL0B03399g*) induces a hyper-adherent phenotype of *C. glabrata* cells. *SIR* complex mutants also yield enhanced organ colonisation due to increased expression of adhesins *EPA1*, *EPA6* and *EPA7* which are normally transcriptionally silent (Castano *et al.*, 2005). *EPA* genes are also subject to regulation by mechanisms independent of the silencing machinery. For example, a *cis*-acting negative regulatory element located at the intergenic region of *EPA1* and *EPA2* is known to repress *EPA1* expression (Gallegos-García *et al.*, 2012). Interestingly, within populations of *C. glabrata* cells, *EPA1* expression can be heterogeneous. This variation is mediated at the RNA level and it is hypothesised that the presence of adherent variants masked within a non-adherent population could be an important virulence factor (Halliwell *et al.*, 2012).

To date, the main focus of *C. glabrata* adhesion research has been placed on the *EPA* family whilst other subgroups of putative adhesins have remained relatively uncharacterised (Table 1.4). Some studies have focused on members of the Pwp and Awp family, which have been shown to facilitate adhesion of *C. glabrata* cells to endothelial cells *in vitro* (Weig *et al.*, 2004; de Groot *et al.*, 2008; Desai *et al.*, 2011). Interestingly, many *C. glabrata* adhesin genes have no orthologue in *S. cerevisiae* or *C. albicans* (Desai *et al.*, 2011). Although the role of many of these adhesin-like proteins remains unknown, such a broad repertoire of adhesins in *C. glabrata* could be the key to successful establishment of infection (Weig *et al.*, 2004).

1.5.2 *Candida* Biofilm Formation

Candida species form surface-associated communities, termed biofilms, which acquire phenotypic properties distinct from planktonic cells such as increased tolerance to antifungal drugs and host molecules and increased protection to the host immune response (Silva *et al.*, 2011; Tati *et al.*, 2013). As such, the formation of *Candida* biofilms on host surfaces is an important virulence factor. In addition, the formation of biofilms on abiotic surfaces (such as medical devices) are a major source of bloodstream candidaemia (Francolini & Donelli, 2010).

Biofilm structure, development and its regulation has to date been most comprehensively described in *C. albicans*. *C. albicans* biofilms are formed following the adherence of anchoring yeast cells to a surface and proliferation. A morphological switch to hyphal and pseudohyphal growth ensues forming a complex biofilm network embedded in extracellular matrix (Figure 1.8). From this structure, yeast cells are dispersed which may then go on to seed further sites of colonisation (Nobile *et al.*, 2012). *BCR1*, *TEC1*, *EFG1*, *NDT80*, *ROB1* and *BRG1* are the major transcriptional regulators of biofilm formation in *C. albicans*, putatively regulating 1,061 target genes in a complex interwoven regulatory network, and are required for normal biofilm formation *in vitro* and *in vivo* rat denture and catheter models (Nobile *et al.*, 2012; Lin *et al.*, 2013). The environmental cues that stimulate biofilm growth are unknown, however, it is noted that biofilm formation in *C. albicans* can be stimulated by pheromone (Lin *et al.*, 2013).

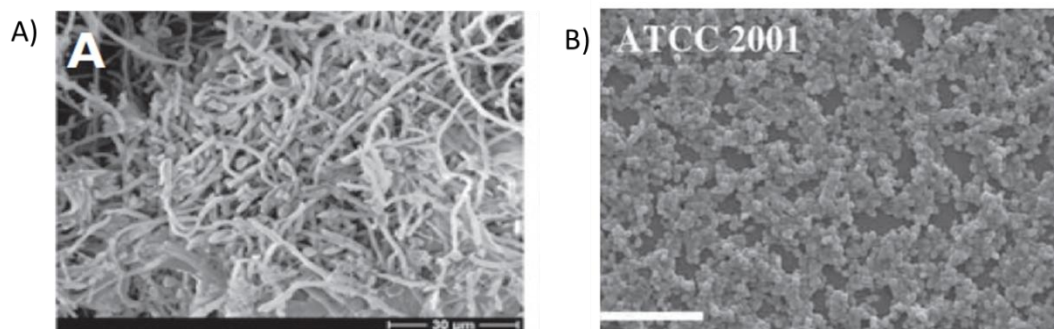


Figure 1.8: Comparison of biofilm structures formed by *C. albicans* and *C. glabrata*. A) Scanning electron microscopy (SEM) of *C. albicans* SC5314 biofilm on a catheter model at 1000x magnification (Nobile *et al.*, 2012) B) SEM image of *C. glabrata* ATCC2001 biofilm formed in SDB at 48 h at 1000x magnification. White bar represents 20 μ M (Silva *et al.*, 2009).

Similarly, *C. glabrata* cells can form biofilm structures on both biotic and abiotic surfaces and acquire distinct drug resistant properties. Consequently, the presence of biofilms in *C. glabrata* infections increase the difficulty in which infections can be controlled and as such is associated with high mortality rates (Silva *et al.*, 2011). However, in stark contrast to biofilms formed by most *Candida* species, *C. glabrata* biofilms exist as communities of surface-attached yeast cells only since *C. glabrata* has no hyphal growth form. Adhered *C. glabrata* yeast cells form compact multilayers or clusters of cells which are

embedded within an extracellular matrix high in protein and carbohydrate (Figure 1.8; Silva *et al.*, 2009).

Attachment of *C. glabrata* yeast cells to biotic or abiotic surfaces to enable biofilm formation is mediated by adhesins. Epa6 is the predominant adhesin required for biofilm formation in *C. glabrata* although the expression of several other Epa and non-Epa adhesins is also upregulated in biofilm forming cells, many of which likely facilitate surface attachment (Kraneveld *et al.*, 2011). The regulatory circuit of biofilm formation is much less well studied in *C. glabrata* compared with *C. albicans*. However *C. glabrata* EPA6 expression is known to be subject to regulation by the kinase Yak1p and the Swi/Snf chromatin remodelling complex via the subtelomeric silencing machinery, Sir4p and Rif1p. EPA6 is also negatively regulated by Cst6p in a Yak1p-independent manner (Iraqi *et al.*, 2005; Riera *et al.*, 2012).

To explore the drug resistant properties acquired by biofilm communities, differential protein expression studies observed that stress response proteins (namely heat and oxidative stress response proteins such as Hsp12p, Trx1p and Pep4p) were upregulated in biofilm-forming *C. glabrata* cells when compared to their planktonic counterpart (Seneviratne *et al.*, 2010). Similar trends of increased oxidative stress response proteins were also reported in *C. albicans* biofilms (Seneviratne *et al.*, 2008). The increased antioxidant capacity and response to stress could contribute to the stress resistant phenotype of *Candida* biofilms (Seneviratne *et al.*, 2010). The role of the exopolymeric matrix encasing the biofilm structure in drug resistance has also been investigated by the treatment of *C. glabrata* biofilms with labelled fluconazole. The study found minimal amounts of labelled fluconazole located in the fungal cell wall or cytoplasm. Most of the labelled fluconazole was located within the β -1,3 glucan matrix and thus it has been proposed that the exopolymeric matrix may contribute to the antifungal resistance of biofilm structures by physically excluding xenobiotics from *C. glabrata* cells (Mitchell *et al.*, 2013).

1.5.3 Mechanisms of Host Invasion by *Candida* Species

Mechanisms of *Candida* host invasion have been best described in *C. albicans* which utilises a morphological switch to gain entry into host epithelial cells. The

active penetration of host cells by *C. albicans* is achieved by anchoring of *C. albicans* cells to the host epithelia (mediated by the Als3 adhesin), the exertion of directed physical pressure by hyphal growth and the secretion of hydrolytic enzymes and other tissue damaging factors (Dalle *et al.*, 2010; Wächtler *et al.*, 2012; Fu *et al.*, 2013). Alternatively, *C. albicans* hyphae can gain entry into host epithelial cells by induced endocytosis in which Als3 (and other cell wall proteins) mediates an interaction with host cadherin, inducing actin cytoskeleton rearrangement and subsequent internalisation of *Candida albicans* hyphae (Phan *et al.*, 2007; Sun *et al.*, 2010; Wächtler *et al.*, 2012; Fu *et al.*, 2013). Post invasion, ALS3 contributes to fungal dissemination by mediating trafficking to the brain, renal cortex and contributes to fungal persistence in the kidney (Fu *et al.*, 2013). Thus, epithelial invasion mechanisms in *C. albicans* are largely dependent on hyphal growth and Als adhesins. Although not truly polymorphic, the morphological switch to filamentous growth forms promotes colonisation and tissue invasion in *C. tropicalis* for example (Silva *et al.*, 2011 C). Similarly to *C. albicans*, *C. parapsilosis* and *C. tropicalis* also encode SAPs (Secreted Aspartyl Proteases) which cause tissue damage and aid host cell invasion (Silva *et al.*, 2009 B; Silva *et al.*, 2011 C).

The mechanism by which *C. glabrata* is able to traverse the host epithelial barrier and access the bloodstream and disseminate to internal organs is unclear. Since *C. glabrata* lacks polymorphism, the mechanisms by which it achieves host invasion must be independent of those employed by *C. albicans*, which relies heavily on a morphological switch to hyphal growth. Despite lacking this virulence attribute, *C. glabrata* is successful in the establishment of blood stream infections and thus must traverse the epithelial barrier by an unknown mechanism. In experimental systems, *C. glabrata* has been shown to enter deep tissues in a chicken embryo model of infection despite lacking a hyphal growth form (Jacobsen *et al.*, 2011). Also in contrast to *C. albicans*, sites of *C. glabrata* colonisation of epithelial cells show significantly lower levels of tissue damage – perhaps a consequence of lacking SAPs (Silva *et al.*, 2011 B).

1.6 The Interaction of *C. glabrata* with Host Immune Cells

1.6.1 Immune Defence Mechanisms Against Invading Microorganisms

Phagocytic cells (macrophages, dendritic cells and neutrophils) of the host innate immune system provide the first response against invading microorganisms and comprise a vital part of the host defence against challenge by *Candida* species. Detection of invading microorganisms is initially achieved by the recognition of pathogen-associated molecular patterns (PAMPs) on the fungal cell wall via a plethora of host pattern recognition receptors (PRRs) (Levitz, 2010; Miramón *et al.*, 2013). For example *C. albicans* α -1,2-mannose cell wall residues and β -glucans are key for fungal recognition by macrophage mannose receptors, Toll-like receptors TLR2 and TLR4 and dectin-1 (Netea *et al.*, 2008; Keppler-Ross *et al.*, 2010; Hall *et al.*, 2013). Although the mechanism by which macrophages recognise *C. glabrata* is less well understood, Epa1 is known to mediate *C. glabrata* recognition and attachment to macrophages by a yet-unidentified receptor (Kuhn & Vyas, 2012). Such interactions between the *Candida* cell wall and the phagocyte triggers the engulfment of the invading cells and subsequent destruction via the phagocytic pathway in which the pathogen-containing phagosome fuses with endosomal vesicles to form the mature phagolysosome (Viera *et al.*, 2002; Miramón *et al.*, 2013). As the phagolysosome matures and becomes increasingly acidified, engulfed *Candida* cells encounter carbon source limitation, nutrient limitation, acidic hydrolases, oxidative killing, reactive nitrogen species and the accumulation of antimicrobial peptides (Roetzer *et al.*, 2010; Rai *et al.*, 2012). Thus the harsh internal environment of the phagolysosome presents *C. glabrata* with a number of challenges which must be overcome for survival. Further to this, the phagocytic cell activates and recruits cells of the adaptive immune system through presentation of antigen and by secretion of cytokines and chemokines.

In addition to phagocytosis, *C. glabrata* cells are subjected to the fungicidal activity of other immune cells. For example, the production of neutrophil extracellular traps (NETs) – structures consisting of chromatin and antimicrobial peptide calprotectin – by neutrophils plays a major part in the innate immune defence against pathogens such as *Candida* species (Urban *et al.*, 2009).

1.6.2 *C. glabrata* Survives and Replicates within Macrophages

Despite these challenges, *C. glabrata* is able to both survive and replicate within the internal macrophage environment (Figure 1.9 A and B; Kaur *et al.*, 2007;

Rai *et al.*, 2012). In a study of *C. glabrata* uptake by human MDMs (monocyte-derived macrophages), the majority of *C. glabrata* cells were rapidly internalised within 3 hours post infection (Seider *et al.*, 2011). Similarly, following 30 minutes incubation with neutrophils, 81 % of *C. glabrata* cells were internalised (Fukuda *et al.*, 2011). Interestingly, the uptake of *C. glabrata* cells by macrophages is more efficient than that of *C. albicans*. Competitive uptake assays revealed a 10-fold preference for the uptake of *C. glabrata* yeast cells over their *C. albicans* counterparts by J774 macrophages (Keppler-Ross *et al.*, 2010). This could be reflective of *C. albicans* immune evasion strategies that are not shared with *C. glabrata*. Post internalisation, *C. glabrata* cells have been shown to replicate inside macrophages. Between 12 and 24-hours post co-incubation with macrophages a 3-fold increase in the number of internalised yeast cells was observed, indicative of intracellular replication (Seider *et al.*, 2011). Similar studies also show evidence for replication of internalised *C. glabrata* cells (Kaur *et al.*, 2007; Rai *et al.*, 2012; Figure 1.9 A). In order for replication to take place, *C. glabrata* cells must employ a number of mechanisms to survive the internal phagosome environment, allowing them to adapt, replicate and ultimately lead to macrophage lysis and escape (Figure 1.9 B; Seider *et al.*, 2011; Rai *et al.*, 2012).

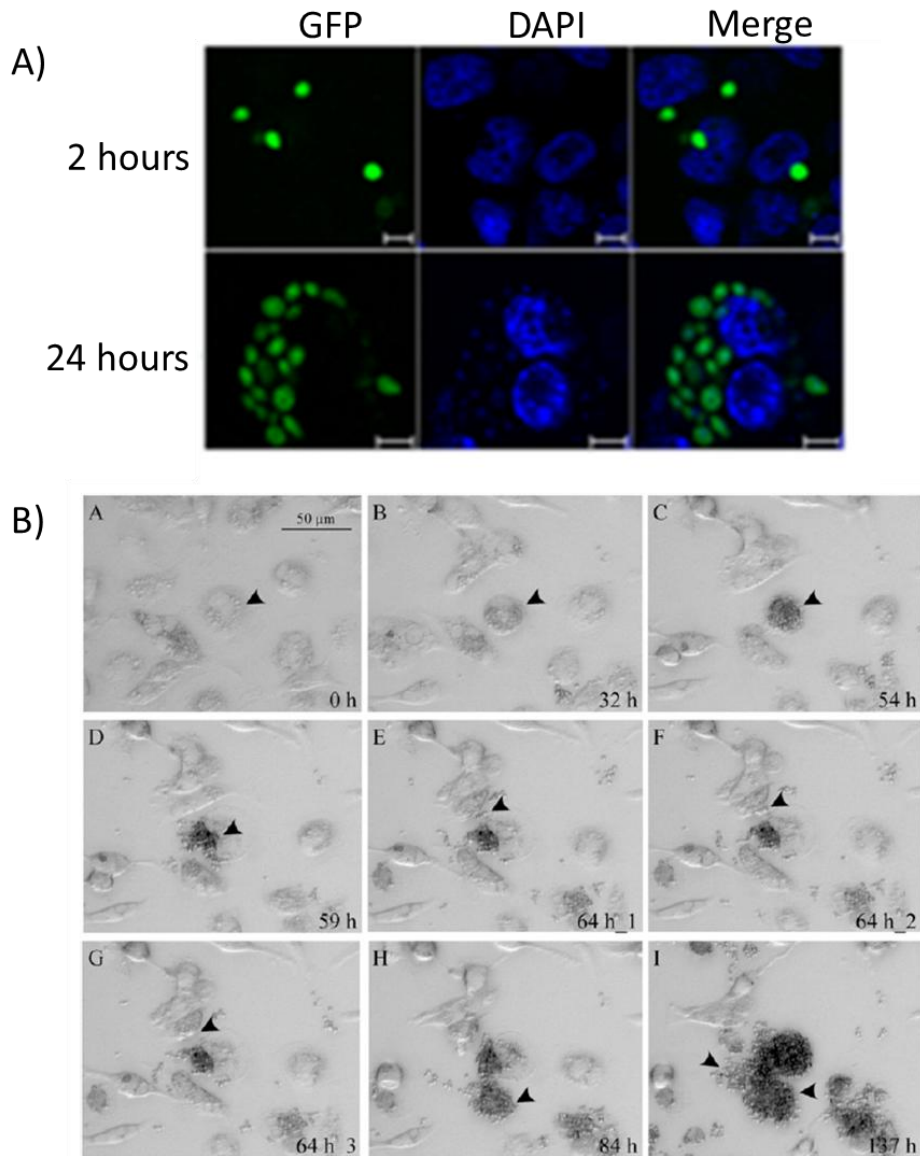


Figure 1.9: *C. glabrata* interaction with macrophages A) *C. glabrata* survives and replicates in differentiated THP-1 cells. Confocal microscopy of GFP-tagged *C. glabrata* cells 2 and 24 hours post infection of THP-1 cells. Nuclei are stained with DAPI. Scale bar represents 5 μm (Rai *et al.*, 2012).

B) *C. glabrata* survives and replicates within macrophages leading to cell macrophage lysis and escape. Time-lapse microscopy of MDMs and phagocytosed *C. glabrata* (black arrows in panels A–C). After three days, MDMs burst (black arrow in panel D) and *C. glabrata* cells were released (black arrows in panels E–G). Escaped *C. glabrata* cells were viable and proliferated in the surrounding media (black arrows in panels H & I). (Seider *et al.*, 2011)

Phagocytosed *C. glabrata* cells cause little cytotoxicity to macrophages and are unable to rapidly escape or induce apoptosis in immune cells. This is in stark contrast to internalised *C. albicans* cells which cause significant levels of damage and killing of macrophages enabling rapid escape as soon as 3 hours post infection (Seider *et al.*, 2011). This escape mechanism depends upon the formation and elongation of hyphae which stretch and pierce the macrophage membrane, ultimately leading to macrophage lysis and killing (McKenzie *et al.*, 2010). In addition, infection of macrophages with *C. albicans* also induces host cell apoptosis, a mechanism used by pathogens for survival (Navarre & Zychlinsky, 2000; Ibata-Ombetta *et al.*, 2003; Seider *et al.*, 2011), by eliciting caspase-3 and -7 activation and causing DNA fragmentation (Sieder *et al.*, 2011). 48 hours post infection, *C. glabrata* caused very low levels of macrophage cytotoxicity (comparable to levels of cytotoxicity reported for macrophage infection with *S. cerevisiae*) most likely due to the lack of hyphae formation (Sieder *et al.*, 2011). *C. glabrata*-infected macrophage damage occurred as late as 3 days post infection, whereby increased fungal load (due to intracellular replication) caused macrophages to tighten and contract leading to cell lysis and the subsequent dissemination of viable *C. glabrata* cells (Sieder *et al.*, 2011; Figure 1.9 B). *C. glabrata* was also unable to induce human macrophage apoptosis. Infection of macrophages with *C. glabrata* failed to elicit caspase-3 or-7 activation nor cause DNA fragmentation (Sieder *et al.*, 2011). As such, the strategies by which *C. albicans* achieves rapid macrophage escape are not shared with *C. glabrata*. Therefore, *C. glabrata* must utilise alternative strategies to survive and escape the macrophage environment.

One such strategy employed by *C. glabrata* for macrophage survival is the manipulation of the phagosome maturation pathway, a mechanism employed by phagocytic cells for the elimination and clearance of invading microorganisms. *C. glabrata* subverts phagosome maturation preventing progression from the late endosomal to the lysosomal stage in which the phagosome would normally fuse with lysosomes, acquiring acid hydrolases (such as cathepsin D) and becoming acidified. *C. glabrata*-containing phagosomes fail to display the lysosomal stage marker cathepsin D and do not undergo normal acidification, thus facilitating survival within the phagosome (Sieder *et al.*, 2011; Rai *et al.*, 2012). Although it is unknown which *C. glabrata* attribute mediates the

modulation of phagosome maturation and acidification, it is likely a cell wall factor and is proposed to be independent of active transcription or translation (Seider *et al.*, 2011).

1.6.3 The Transcriptional Response of Phagocytosed *C. glabrata* Cells

Upon engulfment by phagocytic cells, *C. glabrata* launches a transcriptional response vital for adaptation to the internal phagosome environment. *C. glabrata* chromatin remodelling and histone modification genes *RSC3* (*CAGL0D03850g*), *RTT109* (*CAGL0D05786g*) and *SGS1* (*CAGL0H00759g*) have been shown to play key roles in the regulation of adaptation to the internal macrophage environment and as such are essential for full virulence in *C. glabrata* (Rai *et al.*, 2012).

Similarly to related species *S. cerevisiae* and *C. albicans* (Lorenz & Fink, 2001; Lorenz *et al.*, 2004), substantial reprogramming of *C. glabrata* carbon metabolism, upregulation of the glyoxylate cycle and gluconeogenesis occur upon internalisation of *C. glabrata* cells by both macrophages and neutrophils which may provide scope for adaptation to the glucose-limited environment of the phagosome (Kaur *et al.*, 2007; Rai *et al.*, 2012; Fukuda *et al.*, 2013). Of particular significance is the upregulation of glyoxylate cycle components which have been reported to be required for full virulence in *C. albicans* and other bacteria (Lorenz & Fink, 2001; Lorenz *et al.*, 2004). In agreement with these findings, microscopic observations of peroxisome proliferation in *C. glabrata* support an ongoing adjustment of carbon metabolism which may facilitate utilisation of non-fermentable carbon sources within the phagosome (Roetzer *et al.*, 2010). Phagocytosis also induces the upregulation of *C. glabrata* genes implicated in DNA damage, oxidative stress and the core stress response, most likely in response to damage elicited by ROS in the phagosome (Rai *et al.*, 2012; Fukuda *et al.*, 2013). In particular, expression of the sole *C. glabrata* catalase *CTA1* (*CAGL0K10868g*) is induced in the early stages of internalisation (Roetzer *et al.*, 2010). Similarly to observations in the fungal pathogen *C. neoformans* (Palmer *et al.*, 2008), the upregulation of autophagy-related genes in engulfed *C. glabrata* cells facilitates survival in the nutrient-deprived environment of the phagosome by sequestering and recycling intracellular resources (Roetzer *et al.*, 2011; Fukuda *et al.*, 2013). In particular,

autophagy of peroxisomes mediated by *C. glabrata* *ATG11* (CAGL0H08558g) and *ATG17* (CAGL0J04686g) is beneficial for macrophage survival during phagocytosis (Roetzer *et al.*, 2010; Fukuda *et al.*, 2013). Although autophagy is a less important virulence determinant in filamentous fungi which can actively escape and kill macrophages, it plays a more major role in *C. glabrata* which lacks a rapid strategy for macrophage escape and must survive prolonged nutrient starvation in the phagosome (Roetzer *et al.*, 2010).

The *YPS* genes are significantly upregulated upon *C. glabrata* uptake by both macrophages and neutrophils (Kaur *et al.*, 2007; Bairwa & Kaur, 2011; Fukuda *et al.*, 2013). *C. glabrata* *YPS* genes constitute a cluster of eleven GPI-linked aspartyl proteases, structurally related to *S. cerevisiae* yapsins, which are known to function in cell wall remodelling, cell wall integrity (Miyazaki *et al.*, 2011) and pH homeostasis (Bairwa & Kaur, 2011). *YPS* genes are required for *C. glabrata* macrophage survival and replication as upon deletion of some *YPS* cluster members, *C. glabrata* cells did not replicate and lost viability following macrophage uptake (Kaur *et al.*, 2007). They were also required for virulence in a mouse model of disseminated candidiasis (Kaur *et al.*, 2007). The *YPS* cluster, in particular *YPS1* (CAGL0M04191g), may contribute to *C. glabrata* virulence through the regulation of pH homeostasis (crucial for the maintenance of vital physiological process) under the increased acidity of the phagolysosome (Bairwa & Kaur, 2011). The implication of *YPS1* in cell wall integrity (through its regulation by the cell-wall-related calcineurin-Crz1 pathway) in *C. glabrata* could aid adaptation to various stresses in the phagosome and is postulated to prevent cell lysis at elevated temperatures (Miyazaki *et al.*, 2011). *YPS* genes have also been implicated in immune evasion. Infection of macrophages with *C. glabrata* *YPS* mutants stimulate significantly more nitric oxide production, a marker of macrophage activation, than the parental strain. It is proposed that Yps proteins target GPI-linked cell wall proteins, most notably Epa1, as a substrate for proteolytic processing and thus removing it from the cell wall, perhaps masking *C. glabrata* from immune recognition (Kaur *et al.*, 2007; Kuhn & Vyas, 2012).

1.6.4 Oxidative Killing of *Candida* Species

The oxidative burst and the production of reactive oxygen species (ROS) and reactive nitrogen species (RNS) in the phagosome is a powerful strategy employed for the elimination of phagocytosed microorganisms. Driving the oxidative burst is the NADPH enzyme complex situated in the cytoplasmic and phagosomal membrane, generating superoxide radicals through the transfer of electrons from cytoplasmic NADPH to oxygen. Superoxide radicals are further dismuted to produce hydrogen peroxide – a molecule with strong oxidative properties (Figure 1.10; Fang, 2004; Jandric & Schüller, 2011; Miramón *et al.*, 2013). The production of RNS in the phagocyte is catalysed by iNOS (inducible nitric oxide synthase) which uses molecular oxygen and arginine as substrates to produce nitric oxide. In the presence of superoxide, nitric oxide is converted into peroxynitrite which is subsequently decomposed yielding nitrogen dioxide and hydroxyl radicals (Fang, 2004; Figure 1.10). Although ROS are endogenous by-products of cellular aerobic metabolism in eukaryotes (Gutiérrez-Escobedo *et al.*, 2013), elevated levels of ROS and RNS cause damage to DNA, lipids and proteins and are therefore highly toxic to fungal cells. In this way the production of free radicals contributes to *Candida* killing and is used as a major defence mechanism to clear *Candida* infection (Elahi *et al.*, 2001; Donini *et al.*, 2007). Rai *et al.*, 2012, observed a 7-fold increase of intracellular ROS levels in macrophages incubated with *C. glabrata* compared with non-infected control cells (Rai *et al.*, 2012). The importance of oxidative killing by macrophages has been well exemplified in murine models gp91^{phox-/-} and gp47^{phox-/-} which have a defective phagocyte oxidative capacity. In such models where oxidative killing is impaired, intravenous injection of *C. glabrata* leads to lethal progressive infection within days compared with wild-type mice thus demonstrating the importance for oxidative killing of *C. glabrata* in this model system (Ju *et al.*, 2002; Fukuda *et al.*, 2013). Conversely, similar studies have noted that *Candida* species may possess mechanisms to actively downregulate ROS production by phagocytic cells given that only a minor fraction of engulfed *C. glabrata* cells shows signs of acute oxidative stress whereas most indicated a mild oxidative load (Roetzer *et al.*, 2010; Seider *et al.*, 2011).

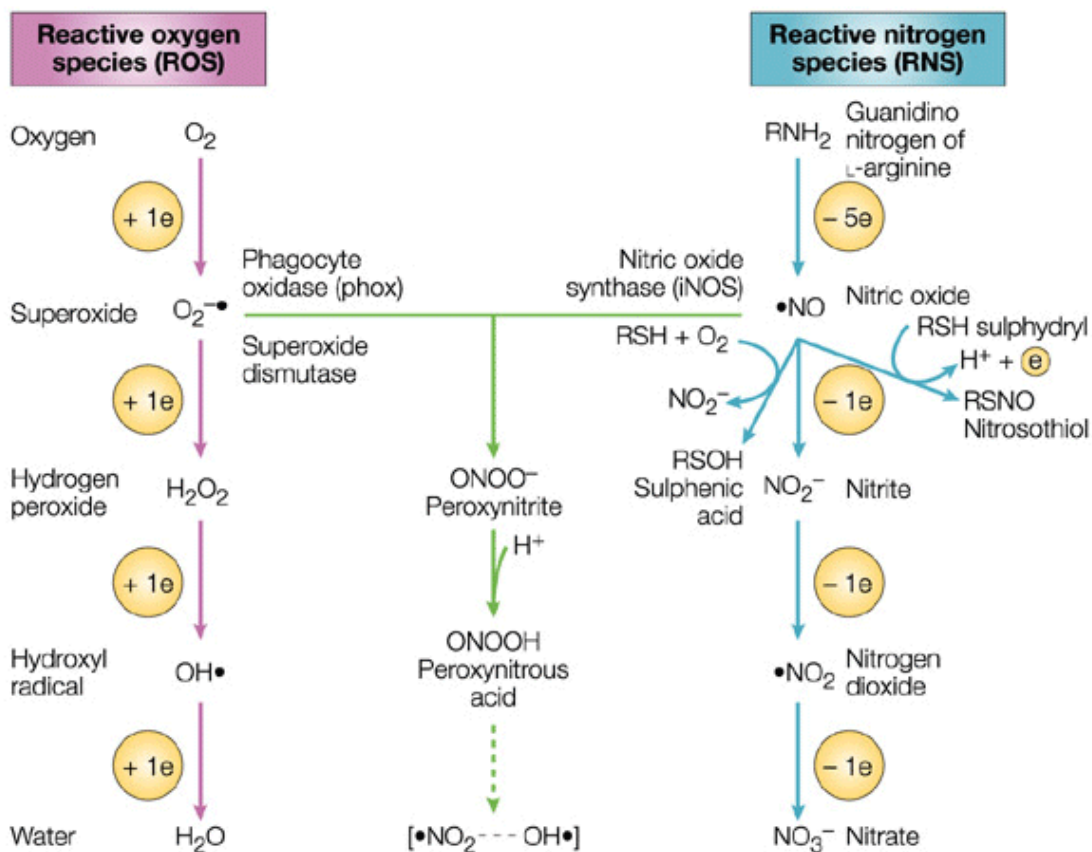


Figure 1.10: The production of ROS and RNS intermediates by mammalian cells as part of the oxidative burst (Fang, 2004). NADPH enzymes drive the conversion of molecular oxygen to superoxide anions. Superoxide is subsequently converted into hydrogen peroxide and hydroxyl radicals, molecules with strong oxidative capacity. The conversion of oxygen and arginine into nitric oxide is catalysed by iNOS. In the presence of superoxide, further RNS are generated such as peroxynitrite.

1.6.5 *C. glabrata* Elicits a Robust Oxidative Stress Response

Pathogenic microbes use multiple strategies to survive oxidative killing. *C. glabrata* is intrinsically more resistant to oxidative stress than *S. cerevisiae* or *C. albicans* (Cuéllar-Cruz *et al.*, 2008; Kaloriti *et al.*, 2012). Expression of catalases, superoxide dismutases and the production of glutathione and thioredoxin serve as strategies to adapt to oxidative stress in *C. glabrata* by the detoxification of ROS (Brown *et al.*, 2009; Jandric & Schüller, 2011; Roetzer *et al.*, 2011).

Upon encountering ROS and glucose starvation in the phagolysosome, expression of *C. glabrata* catalase, *CTA1*, is induced which enzymatically catalyses the conversion of hydrogen peroxide to neutral water and oxygen (Cuéllar-Cruz *et al.*, 2008; Roetzer *et al.*, 2010). Additionally, constitutive expression of a superoxide dismutase, *SOD1* (*CAGLOC04741g*), also contributes to oxidative stress resistance through the conversion of cytotoxic superoxide radicals to hydrogen peroxide and water (Roetzer *et al.*, 2011; Jandric & Schüller, 2011). The antioxidant molecule glutathione is essential in *C. glabrata* under normal conditions due to its role in the assembly of cytoplasmic Fe-S clusters, detoxification of metal ions and for maintaining ROS at physiologically low concentrations (López-Mirabel & Winther, 2008; Yadav *et al.*, 2011; Gutiérrez-Escabedo *et al.*, 2013). However under elevated levels of ROS, glutathione also participates in the oxidative stress response of *C. glabrata* by maintaining redox homeostasis. *C. glabrata* encodes orthologues of GSH biosynthesis genes, *GSH1* (*CAGL0L03630g*) and *GSH2* (*CAGL0F00825g*), yet unlike *S. cerevisiae* does not encode a high affinity plasma membrane glutathione transporter (Yadav *et al.*, 2011) but may uptake glutathione through another unknown transporter since the addition of external GSH increases oxidative stress resistance (Gutiérrez-Escobedo *et al.*, 2013). Components of the thioredoxin antioxidant system, *TRX1* (*CAGL0K00803g*), *TRR1* (*CAGL0I01166g*) and *TSA1* (*CAGL0K06259g*), are also upregulated in response to *C. glabrata* H₂O₂ treatment (Saijo *et al.*, 2010).

Components of the *C. glabrata* oxidative stress response are coordinated by transcription factors *YAP1* (*CAGL0H04631g*) and *SKN7* (*CAGL0F09097g*) (Roetzer *et al.*, 2011) and partially upon transcriptional activators of the core stress response *MSN2* (*CAGL0F05995g*) and *MSN4* (*CAGL0M13189g*) (Cuéllar-Cruz *et al.*, 2008). Yap1p, belonging to a family of basic leucine zipper domain transcription factors, controls the expression of 32 genes involved in oxidative stress resistance in *C. glabrata* (Cuéllar-Cruz *et al.*, 2008) and is required for sustained survival in murine macrophage models (Roetzer *et al.*, 2011). Under oxidative stress, Skn7p is required for the transcriptional induction of components of the thioredoxin system (*TRX1*, *TRR1* and *TSA1*) and catalase (*CTA1*) (Cuéllar-Cruz *et al.*, 2008; Saijo *et al.*, 2010). *SKN7* deletion mutants display reduced virulence in a murine model of disseminated *C. glabrata*

infection (Saijo *et al.*, 2010) thus exemplifying the requirement of an intact oxidative stress response for virulence.

Despite its high tolerance to oxidative stress, studies suggest that *C. glabrata* is able to suppress the oxidative burst elicited by the phagocyte (Seider *et al.*, 2011). Roetzer *et al.*, 2010, observed only a low oxidative load on engulfed *C. glabrata* cells and that only a minor fraction of engulfed cells showed signs of acute oxidative stress (Roetzer *et al.*, 2010).

1.6.5.1 Iron Scavenging is Required for Oxidative Stress Resistance and Pathogenicity

Iron plays a crucial role in the tolerance of oxidative stress as a cofactor in catalase and superoxide dismutase enzymes crucial for the detoxification of ROS (Hood & Skaar, 2012). It is also essential for survival under normal conditions as an integral part of normal cellular biochemistry and its uptake and assimilation is required for virulence in many pathogens of mammals and plants (Eichhorn *et al.*, 2006; Nairz *et al.*, 2010; Albarouki *et al.*, 2013). On the contrary, excess iron can be toxic to cells via induced oxidative damage (Lin *et al.*, 2010) and thus maintenance of iron homeostasis is crucial in iron-fluctuating environments such as the host (Chen *et al.*, 2011). In *C. albicans*, regulators of iron homeostasis (*AFT1* and *AFT2*) are also linked to oxidative stress resistance and pathogenesis-related processes such as surface adhesion and hyphal development (Xu *et al.*, 2013).

As a strategy to eliminate invading microorganisms, macrophages limit iron availability by reducing iron transport, reducing bound iron from the serum and depleting iron from the phagolysosome (Hood & Skaar, 2012). Thus, pathogenic microorganisms must employ mechanisms for iron acquisition in the host niche – in particular during prolonged persistence in the nutrient-limited phagosome. Under iron-limited conditions, bacteria and fungi use siderophores, chelating molecules with high affinity for Fe^{3+} , to scavenge available extracellular iron (Haas, 2003; Schrettl *et al.*, 2004; Fischbach *et al.*, 2006). An endogenous pathway for siderophore biosynthesis is absent in *C. glabrata*. However, *C. glabrata* is able to take up xenosiderophores (siderophores produced by other species) through siderophore transporter *SIT1* (*CAGL0E04092g*) under iron deficient conditions. *SIT1*-mediated uptake of extracellular iron in this manner

contributes to *C. glabrata* survival from macrophage killing (Nevitt & Thiele, 2011).

1.7 Sensing the Host Environment

Upon colonisation of the host, the success of a fungal pathogen relies on its ability to readily adapt to the host niche where it is exposed to changes in osmolarity, pH and temperatures (Jandric & Schüller, 2011). The mammalian host is colonised by a vast number of microorganisms and the acquisition of nutrients in the highly competitive environment is critical for survival and virulence. Adaptation can be achieved through changes in the transcriptional programme, global chromatin remodelling and epigenetic regulation in response to environmental cues.

The response of *C. glabrata* to external niacin limitation experienced in the urinary tract has been well characterised. *C. glabrata* is auxotrophic for NAD⁺ and requires supplementation with NAD⁺ precursors (niacin) for growth. Thus under external niacin limitation, intracellular NAD⁺ levels are reduced which directly affect the activity of sirtuins Sir2 (*CAGL0K01463g*) and Hst1 (*CAGL0C05357g*) which require NAD⁺ as a cofactor for the catalysis of deacetylation reactions. Thus the activity of the *SIR* silencing machinery, of which Sir2 constitutes the main enzymatic component, is reduced under niacin limited conditions leading to subsequent de-repression of the *EPA* adhesin genes which are normally subject to silencing by the SIR complex (Domergue *et al.*, 2005; Ma *et al.*, 2009; Figure 1.11). This is supported by *in vitro* data where *EPA6* expression was induced in *C. glabrata* cells grown in urine thus linking increased adhesion to epithelial cells with niacin limitation (Domergue *et al.*, 2005; Jandric & Schüller, 2011). Similarly, the de-repression of *HST1* targets also occurs under niacin-starvation. Most notably *HST1* repression targets include high affinity niacin transporters *TNA1* (*CAGL0F08371g*), *TNR1* (*CAGL0L13354g*) and *TNR2* (*CAGL0M14113g*) which are mandatory for intracellular NAD⁺ homeostasis and promote growth in niacin-poor conditions such as human urine (Ma *et al.*, 2009; Figure 1.11). Furthermore, *HST1* is also implicated in the regulation of oxidative stress and drug resistance genes which may promote survival in the human host. Loss of *HST1*-mediated transcriptional

silencing increases *C. glabrata* oxidative stress resistance by increased expression of *CTA1* and *MSN4* (Orta-Zavalza *et al.*, 2013; Figure 1.11). Similarly, *HST1*-inactivation leads to the induction of the ABC transporter gene *CDR1* (*CAGL0M01760g*) and the major regulator of drug resistance *PDR1* (*CAGL0A00451g*) conferring azole drug resistance. Interestingly, regulation of stress-resistance genes by the *HST1*-silencing complex seems to be unique to *C. glabrata* as this regulation is not apparent in the non-pathogenic, yet closely related yeast, *S. cerevisiae* (Orta-Zavalza *et al.*, 2013). The regulation of such pathogenesis-promoting factors in response to environmental stimuli may be an adaptation of *C. glabrata* to promote colonization of the human host.

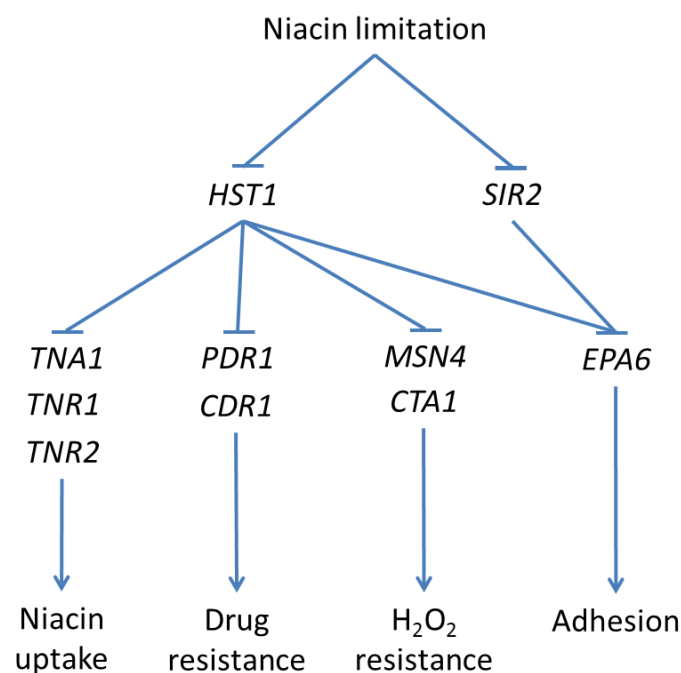


Figure 1.11: Model of niacin-dependent regulation of sirtuins *HST1* and *SIR2* in *C. glabrata*. Under niacin-limiting conditions, activity of sirtuins *HST1* and *SIR2* is reduced, relieving derepression of their targets genes implicated in niacin uptake, drug resistance, stress resistance and adhesion (adapted from Orta-Zavalza *et al.*, 2013).

1.8 Evading the Immunological Response

Infection of macrophages with *C. glabrata* induces a modest inflammatory cytokine cascade compared with infection by *C. albicans* (Seider *et al.*, 2011; Rai *et al.*, 2012). *C. glabrata* failed to elicit a significant pro-inflammatory (TNF- α , IL-1 β , IL-6, IL-8 or IFN- γ) or anti-inflammatory (IL-10) cytokine response in human macrophages *in vitro* – many of which were strongly induced upon

challenge with *C. albicans* or *S. cerevisiae* (Seider *et al.*, 2011). This is in agreement with *in vivo* studies where *C. glabrata* infection induced only a mild immunological response in murine models (Jacobsen *et al.*, 2010). GM-CSF (Granulocyte-Macrophage Colony-Stimulating Factor) is the sole cytokine significantly induced following the interaction of *C. glabrata* with macrophages or epithelial cells (Li & Dongari-Bagtzoglou, 2009; Jacobsen *et al.*, 2010). GM-CSF promotes the activation, proliferation and fungicidal activity of monocytes and neutrophils, providing protection against fungal pathogens such as *C. glabrata* (Quezada *et al.*, 2007; Li & Dongari-Bagtzoglou, 2009; MacCallum *et al.*, 2009).

1.9 Evolution of Drug Resistance in *C. glabrata* Isolates

In relation to other *Candida* species, *C. glabrata* is intrinsically more resistant to the azoles – the main class of antifungal drug used to treat *Candida* infections – and its ability to readily acquire cross resistance to other classes of antifungal drugs is a significant medical problem. A number of clinical studies have reported such isolates of *C. glabrata* with cross-resistance to both azoles and echinocandins. It was recently reported that 11.1 % of fluconazole-resistant clinical *C. glabrata* isolates also had elevated tolerance to echinocandins (Pfaller *et al.*, 2012).

1.9.1 Azole Resistance

The azoles comprise a major class of antifungal drug used to treat *Candida* infections. Azoles exert fungistatic activity against *Candida* species through the targeted inhibition of cytochrome P450-dependent lanosterol demethylase encoded by *ERG11* (*CAGL0E04334g*). Disruption of ergosterol biosynthesis in this manner results in an alteration of cell membrane fluidity, signalling and transport as cells are unable to build or renew membrane sterols (Jandric & Schüller, 2011). Increased expression of drug target Erg11 rescues azole susceptibility in *C. glabrata*. However, tolerance to azole drugs is dependent on extracellular iron availability as iron depletion impairs Erg11 function resulting in increased azole susceptibility (Hosogaya *et al.*, 2013).

C. glabrata *PDR1* (*CAGL0A00451g*), the sole orthologue of *S. cerevisiae* multidrug resistance regulators *PDR1* and *PDR3*, is a major regulator of azole

resistance in *C. glabrata* (Vermitsky & Edlind, 2004). *PDR1* mediates azole resistance through the transcriptional regulation of drug efflux pumps and ATP-binding cassette transporters *CDR1* (*CAGL0M01760g*), *CDR2/PDH1* (*CAGL0F02717g*) and *SNQ2* (*CAGL0I04862g*) and drug:H⁺ antiporter *QDR2* (*CAGL0G08624g*) which actively extrude xenobiotics from the cell (Costa *et al.*, 2013; Thakur *et al.*, 2008). A role for *STB5* (*CAGL0I02552g*) in the negative regulation of these *PDR1* targets has more recently been uncovered (Noble *et al.*, 2013). Similar *PDR1*-mediated mechanisms of azole resistance also exist in related fungal species *S. cerevisiae* and *C. albicans* (Anderson, 2005). Gain of function mutations in *C. glabrata PDR1* occur frequently *in vivo*, activating the expression of its target genes and increasing azole resistance. Activation mutations in *PDR1* are diverse and can fall in locations throughout the protein (including the activation domain, xenobiotic binding domain and the inhibition domain). To exemplify this diversity, a study of *C. glabrata* clinical isolates identified 57 amino acid substitutions in *PDR1* alleles - all of which conferred *PDR1* hypersensitivity and increased azole resistance and increased fitness in a murine infection model (Ferrari *et al.*, 2009). Interestingly, the various *PDR1* gain of function isolates activate differential gene expression patterns with little overlap despite all conferring azole resistance (Ferrari *et al.*, 2011 A). Direct binding of azole or other xenobiotic molecules to Pdr1p can also stimulate the expression of its target genes and can induce drug resistance in both *C. glabrata* and *S. cerevisiae* (Thakur *et al.*, 2008). Therefore gain of function mutations in *PDR1* and enhanced expression of ABC transporters provides a major mechanism for azole resistance in *C. glabrata* (Sanglard *et al.*, 1999; Sanglard *et al.*, 2001; Torelli *et al.*, 2002; Caudle *et al.*, 2011).

Azole resistance in *C. glabrata* also arises in petite mutants which have been isolated directly from patients receiving azole treatment (Bouchara *et al.*, 2000). The petite mutant phenotype has respiratory deficiency due to loss or deletions within mitochondrial DNA which is associated with increased cross resistance to azoles (Brun *et al.*, 2003). In petite mutants, increased *PDR1* expression and the consequential upregulation of ABC transporters contributes to azole resistance yet is independent of point mutations in *PDR1* (Tsai *et al.*, 2006). Transcriptome analysis of the *C. glabrata* petite phenotype revealed mitochondrial dysfunction was accompanied by the upregulation of genes

implicated in multidrug resistance and small molecule transporters (*CDR1*, *CDR2*, *SNQ2*, *YOR1* (*CAGL0G00242g*), *YBT1* (*CAGL0C03289g*) and *YCF1* (*CAGL0L06402g*)) which contribute to the azole-resistant phenotype of petite mutants (Ferrari *et al.*, 2009).

A number of studies have found azole-resistant *C. glabrata* isolates to have altered interaction with the host. Both *PDR1* gain of function mutants and petite mutants had increased fitness in a murine model of systemic infection (Ferrari *et al.*, 2009; Ferrari *et al.*, 2011 B). In the petite mutants, cell wall biogenesis and maintenance genes and cell surface proteins were upregulated (Table 1.5) which could modify the interaction with the host and possibly explain the hypervirulent phenotype of the azole-resistant isolates in *in vivo* infection models (Ferrari *et al.*, 2009; Ferrari *et al.*, 2011 B). Gain of function *PDR1* mutants also showed both positively and negatively modified interaction with host cells. In one instance, increased adherence to epithelial cells yielded increased colonisation efficiency yet reduced adherence to macrophages lead to reduced uptake and successful evasion of phagocytosis (Vale-Silva *et al.*, 2013). Thus the emergence of azole-resistance and the associated increase in virulent properties in *C. glabrata* isolates poses a problem in the treatment of *Candida* infections.

Table 1.5: *C. glabrata* cell surface and cell wall proteins significantly upregulated in an azole-resistant petite mutant (Ferrari *et al.*, 2011 B)

<i>C. glabrata</i> ORF	Gene name	Description
<i>CAGL0E01727g</i>	<i>YPS3</i>	GPI-anchored aspartic protease
<i>CAGL0E01815g</i>	<i>YPS8</i>	GPI-anchored aspartic protease
<i>CAGL0E01837g</i>	<i>YPS9</i>	GPI-anchored aspartic protease
<i>CAGL0E01859g</i>	<i>YPS10</i>	GPI-anchored aspartic protease
<i>CAGL0H05621g</i>	<i>RLM1</i>	Transcription factor, role in cell wall integrity
<i>CAGL0K13002g</i>	<i>AGA1/AED2</i>	GPI-anchored adhesin
<i>CAGL0K13024g</i>	<i>MUC1</i>	GPI-anchored glycoprotein

1.9.2 Echinocandin Resistance

Echinocandins are the most recent class of antifungal drugs to reach clinical approval and have rapid fungicidal activity against *Candida* species by targeting the fungal cell wall through the inhibition of β -1,3-glucan synthesis (Denning, 2002; Walker *et al.*, 2010). The emergence of echinocandin resistance is becoming more frequent, particularly in *C. glabrata* where the prevalence of echinocandin resistance amongst clinical isolates from blood stream infections increased from 4.9 % to 12.3 % from 2001 to 2010, respectively (Alexander *et al.*, 2013). Following treatment with caspofungin, *C. albicans*, *C. parapsilosis* and *C. guilliermondii* exhibit elevated chitin levels which acts as a mechanism to reduce the efficacy of echinocandin drugs (Walker *et al.*, 2008; Walker *et al.*, 2013). Intrinsic echinocandin-tolerance in the *C. parapsilosis* group (including *C. orthopsilosis* and *C. metapsilosis*) is conferred by a naturally occurring amino acid substitution (P660A) in Fks1p (Garcia-Effron *et al.*, 2008). Similarly echinocandin-resistant clinical isolates of *Candida* species, in particular *C. albicans* and *C. krusei* and other fungal species, predominantly encode mutations in the *FKS1* gene encoding β -glucan synthase (Balashov *et al.*, 2006; Kahn *et al.*, 2007; Walker *et al.*, 2010). Although echinocandin resistance can arise following mutations in either *C. glabrata FKS1* (*CAGL0G01034g*) and *FKS2* (*CAGL0K04037g*), point mutations in *FKS2*, the catalytic subunit of 1,3- β -D-glucan synthase, are found twice as frequently as those in *FKS1* (Katiyar *et al.*, 2012). Also in contrast to most *Candida* species, *C. glabrata* isolates do not alter the chitin content of the cell wall following treatment with caspofungin (Walker *et al.*, 2013).

Global analysis of *C. glabrata* mutations underlying the evolution of echinocandin resistance *in vivo* uncovered a sharp increase in echinocandin resistance conferred by an *FKS2* T1987C mutation (Singh-Babak *et al.*, 2012; Table 1.6). Resistance to echinocandins in *C. glabrata* is dependent on heat shock protein *HSP90* and calcineurin, which control the expression of *FKS2* in the presence of caspofungin (Katiyar *et al.*, 2012; Singh-Babak *et al.*, 2012). However, *FKS2* mutations incurred a fitness cost in *C. glabrata* which was alleviated by further evolution, most notably by mutation in *CDC55* (*CAGL0L06182g*). Non-synonymous mutations in eight other genes, previously

not associated with drug resistance, also contributed to echinocandin resistance (Singh-Babak *et al.*, 2012; Table 1.6).

Table 1.6 Non-synonymous mutations accompanying the evolution of echinocandin resistance from a *C. glabrata* clinical isolate (Singh-Babak *et al.*, 2012; yeastgenome.org).

<i>C. glabrata</i> ORF	<i>S. cerevisiae</i> orthologue	Non-synonymous mutation	GO Molecular Function
<i>CAGL0F04631g</i>	<i>MOH1</i>	<i>Y5H</i>	Unknown
<i>CAGL0F04895g</i>	<i>GPH1</i>	<i>H409Y</i>	Glycogen phosphorylase activity
<i>CAGL0K00605g</i>	<i>CDC6</i>	<i>K171E</i>	ATPase activity
<i>CAGL0J08591g</i>	<i>TCB1/2</i>	<i>A1161V</i>	Lipid binding
<i>CAGL0K04037g</i>	<i>FKS2</i>	<i>S663P</i>	1,3-beta-D-glucan synthase activity
<i>CAGL0A04257g</i>	<i>DOT6</i>	<i>K347Stop</i>	Sequence-specific DNA binding
<i>CAGL0J09724g</i>	<i>MRPL11</i>	<i>Y161H</i>	Structural constituent of ribosome
<i>CAGL0B03795g</i>	<i>SUI2</i>	<i>I121M</i>	Translation initiation factor activity
<i>CAGL0L06182g</i>	<i>CDC55</i>	<i>P155S</i>	Protein phosphatase regulator activity

1.10 Conclusion

The generation of genome-wide deletion libraries, ORF collections and the development of SGA technology has provided a powerful tool for uncovering gene function and lead to a greater understanding of the genetic wiring of the cell in the model organism yeast *S. cerevisiae* (Giaever *et al.*, 2002; Costanzo *et al.*, 2010). Such tools in *S. cerevisiae* have proved fundamental in the study of conserved pathways and processes in other eukaryotic systems (Dixon *et al.*, 2009). However, the need for a molecular toolbox to aid further understanding in the biology of pathogenic species such as *C. glabrata* has been recognised.

Comparative genomic studies of yeast genomes identified *C. glabrata* to be more closely related to non-pathogenic yeast *S. cerevisiae* than *C. albicans*. It is hypothesised that *C. glabrata* and *S. cerevisiae* shared a common ancestor and that divergence from this ancestor occurred an estimated 60 million years ago following a whole genome duplication event (Dujon *et al.*, 2004). Since divergence, *C. glabrata* has evolved in a reductive fashion and the adaptation to the host niche has been accompanied by the expansion of gene families associated with cell wall and the loss of a full sexual cycle (Byrne & Wolfe, 2005; Dujon, 2010).

To date, *C. albicans* remains the most well characterised *Candida* species with regards to pathogenesis and adaptation to the host niche. Meanwhile, responses to physiologically relevant stresses have been dissected in the model yeast *S. cerevisiae*. Whilst in many instances extrapolation of knowledge from *C. albicans* and *S. cerevisiae* can yield useful insights to *C. glabrata* biology, it is not necessarily always relevant due to the non-pathogenic nature of *S. cerevisiae* and stark differences in biology (polymorphism, for example) in *C. albicans*. Hence, there is a need to study *C. glabrata* biology as many of its virulence attributes remain poorly understood.

1.11 Aims of the Study

This study aims to create molecular tools for the study of *C. glabrata* virulence attributes. In particular, this study sets out to identify *C. glabrata* ORFs with no orthologue in *S. cerevisiae* which may play a role in virulence. Characterisation of *C. glabrata* ORFs will be achieved through the generation of a deletion library, development of high-throughput phenotypic screening assays and the use of a recently established *Drosophila melanogaster* model of infection. Further, the use of genetic interaction mapping in *S. cerevisiae* as a tool for characterisation of *C. glabrata* ORFs will be explored.

Chapter 2: Materials and Methods

2.1 Organisms, Strains and Plasmids

2.1.1 Yeast strains

Yeast strains used during this study are listed in Table 2.1 and Table 2.2.

Table 2.1: *C. glabrata* strains used during this study.

Strain	Genotype	Origin
ATCC 2001	<i>C. glabrata</i> clinical isolate	ATCC
Cg2001 $\Delta his3$	ATCC 2001 $\Delta his3$	Jacobsen <i>et al.</i> , 2009
Deletion mutants	ATCC 2001 $\Delta geneX::NAT1$	This study (Appendix 4 Table 1)
Cg2001 ΔHTL	ATCC 2001 <i>his3</i> $\Delta::FRT$ <i>leu2</i> $\Delta::FRT$ <i>trp1</i> $\Delta::FRT$	Jacobsen <i>et al.</i> , 2009
Cg2001 $\Delta his3$ p423GPD	Empty Gateway® destination vector pAG423GPD-ccdB transformed into <i>C.</i> <i>glabrata</i> ATCC 2001 $\Delta his3$	This study
Cg2001 $\Delta his3$ p423GPD- D05434	Gateway® destination vector pAG423GPD- ccdB carrying <i>C. glabrata</i> <i>CAGL0D05434g</i> transformed into <i>C.</i> <i>glabrata</i> ATCC 2001 $\Delta his3$	This study
$\Delta CAGL0D03850g$ p423GPD	Empty Gateway® destination vector pAG423GPD-ccdB transformed into <i>C.</i> <i>glabrata</i> Cg2001 $\Delta his3$	This study

	Δ CAGL0D03850g	
Δ CAGL0D03850g p423GPD-ScRSC30	Gateway® destination vector pAG423GPD-ccdB carrying <i>S. cerevisiae</i> RSC30 transformed into <i>C. glabrata</i> Cg2001 Δ his3 Δ CAGL0D03850g	This study

Table 2.2: *S. cerevisiae* strains used during this study.

Strain	Genotype	Origin
BY4741	MATa <i>his3</i> Δ 1 <i>leu2</i> Δ 0 <i>met15</i> Δ 0 <i>ura3</i> Δ 0	Brachmann <i>et al.</i> , 1998
BY4742	MATalpha <i>his3</i> Δ 1 <i>leu2</i> Δ 0 <i>lys2</i> Δ 0 <i>ura3</i> Δ 0	Brachmann <i>et al.</i> , 1998
Haploid deletion collection	MATalpha <i>his3</i> Δ 1 <i>leu2</i> Δ 0 <i>lys2</i> Δ 0 <i>ura3</i> Δ 0 <i>GeneX</i> Δ :: <i>KanMX</i>	Thermo Scientific
Y7092 (SGA starter strain)	MATa <i>can1</i> Δ :: <i>STE2pr-Sp_his5</i> <i>lyp1</i> Δ <i>his3</i> Δ 1 <i>leu2</i> Δ 0 <i>ura3</i> Δ 0 <i>met15</i> Δ 0	Tong <i>et al.</i> , 2005
Y7093-D05434	Y7092 transformed with pAG416GPD-ccdB carrying <i>CAGL0D05434g</i>	This study
Y7094-D05434	Y7092 transformed with pAG426GPD-ccdB carrying <i>CAGL0D05434g</i>	This study
KH01 (SGA starter strain)	MATa <i>his3</i> Δ 1 <i>leu2</i> Δ 0 <i>met15</i> Δ 0 <i>ura3</i> Δ 0	This study
KH02	KH01 transformed with empty pAG416GPD-ccdB destination vector	This study
KH02-D05434	KH01 transformed with	This study

	pAG416GPD-ccdB carrying <i>CAGL0D05434g</i>	
KH03	KH01 transformed with pAG426GPD-ccdB destination vector	This study
KH03-D05434	KH01 transformed with pAG426GPD-ccdB carrying <i>CAGL0D05434g</i>	This study
KH03-K05687	KH01 transformed with pAG426GPD-ccdB carrying <i>CAGL0K05687g</i>	
<i>Δime1</i>	<i>ime1::KanMx;</i> <i>MATA can1Δ::STE2pr-</i> <i>SP-his5 lyp1Δ his3Δ1</i> <i>leu2Δ0 ura3Δ0 met15Δ0</i> <i>LYS2+</i>	Gift from Dr. Jane Usher, University of Exeter
<i>Δime2</i>	<i>ime2::KanMx;</i> <i>MATA can1Δ::STE2pr-</i> <i>SP-his5 lyp1Δ his3Δ1</i> <i>leu2Δ0 ura3Δ0 met15Δ0</i> <i>LYS2+</i>	Gift from Dr. Jane Usher, University of Exeter
<i>Δime1</i> -D05434	<i>Δime1</i> transformed with pAG426GPD-ccdB carrying <i>CAGL0D05434g</i>	This study
<i>Δime2</i> -D05434	<i>Δime2</i> transformed with pAG426GPD-ccdB carrying <i>CAGL0D05434g</i>	This study

2.1.2 Bacterial Strains

Bacterial strains used in the course of this study are listed in Table 2.3.

Table 2.3: *E. coli* strains used during this study.

Strain	Genotype	Origin
DH5 α	<i>fhuA2 lac(del)U169 phoA glnV44 Φ80' lacZ(del)M15 gyrA96 recA1 relA1 endA1 thi-1 hsdR17</i>	Gift received from Dr. Carol Munro, University of Aberdeen
One Shot [®] ccdB Survival [™]	<i>F⁻ mcrA Δ(mrr-hsdRMS-mcrBC) Φ80lacZΔM15 ΔlacX74 recA1 araΔ139 Δ(ara-leu)7697 galU galK rpsL (Str^R) endA1 nupG fhuA::IS2</i>	Life Technologies [™]

2.1.3 *Drosophila* Strains

Drosophila melanogaster strains used in this study are listed in Table 2.4.

Table 2.4: *Drosophila* strains used during this study.

Strain	Genotype	Origin
Dif/Key	Canton ^S Δ dif Δ key	Gift received from Dr. Petros Ligoxygakis, Oxford University
Dros-GFP	w ⁻ Drs-GFP	Gift received from Dr. Petros Ligoxygakis, Oxford University

2.1.4 Plasmids

Details of the plasmids used in the course of this study are listed in Table 2.5. For plasmid maps and features, see Appendix 15.

Table 2.5: Plasmids used during this study.

Plasmid name	Description	Origin
pENTR™221	Gateway® entry vector. Contains <i>attL1</i> and <i>attL2</i> sites for site-specific recombination	Life Technologies™
pAG413GPD-ccdB	Low copy number Gateway® destination vector. Contains constitutive GPD promoter and <i>his3</i> selectable marker.	Addgene
pAG423GPD-ccdB	High copy number Gateway® destination vector. Contains constitutive GPD promoter and <i>his3</i> selectable marker.	Addgene
pAG416GPD-ccdB	Low copy number Gateway® destination vector. Contains constitutive GPD promoter and <i>ura3</i> selectable marker.	Addgene
pAG426GPD-ccdB	High copy number Gateway® destination vector. Contains constitutive GPD promoter and <i>ura3</i> selectable marker.	Addgene

2.2 Primers

For a comprehensive list of primers used in the study, refer to Appendix 1.

2.3 Storage, Media and Culture of Strains

2.3.1 Yeast Media and Culture

Yeast strains were cultured in rich YPD medium (1 % yeast extract, 2 % bacteriological peptone and 2 % glucose). For selection of mutants, YPD was supplemented with nourseothricin (NAT, Werner Bioagents) to a final concentration of 200 µg/ml. Synthetic complete (SC) medium was prepared with 0.67 % yeast nitrogen base without amino acids (Formedium™), 2 % glucose and 0.079 % complete supplement mixture (Formedium™). For auxotrophic selection medium, complete supplement mixture was replaced with the appropriate drop-out mixture supplied by Formedium™ to the concentration recommended by the supplier. All broth cultures were incubated at 30 °C, 180 rpm unless otherwise stated. For solid medium, YPD or SC was supplemented with 2 % agar.

2.3.2 Bacterial Media and Culture

Bacteria were cultured in Luria broth (LB, Formedium™) at 37 °C, 180 rpm. For solid medium, LB was supplemented with 2 % agar. For antibiotic selection, ampicillin or kanamycin were added to the media to a final concentration of 200 µg/ml or 100 µg/ml, respectively.

2.3.3 Storage of Yeast and Bacterial Strains

For long term storage, strains were stored at -80 °C in the appropriate selective medium supplemented with 15 % glycerol.

2.3.4 *Drosophila* Media and Growth

Drosophila strains were incubated at 25 °C in fly bottles containing standard *Drosophila* medium (7.7 g/L agar, 69.2 g/L maize, 8.3 g/L soya, 14.0 g/L yeast extract, 69.2 g/L malt, 19.2 g/L molasses, 30 ml/L Nipagin stock (10 % in ethanol), 5 ml/L propionic acid and 0.34 ml/L orthophosphoric acid). Adult *Drosophila* were allowed to lay eggs for 24 hours at 25 °C and then transferred to a fresh fly bottle. After 5 days, larvae were harvested for infection assays.

2.4 General Molecular Techniques

2.4.1 Preparation of Competent *E. coli*

5 ml LB was inoculated with a single *E. coli* colony and incubated overnight at 37 °C, 180 rpm. The overnight culture was subcultured into 100 ml LB and grown to an OD₅₅₀ of 0.48. Cells were chilled for 5 minutes prior to being harvested by centrifugation at 5000 rpm for 5 minutes at 4 °C. The cell pellet was resuspended in 40 ml chilled Tfb1 solution (30 mM potassium acetate, 100 mM KCl, 10 mM CaCl₂·2H₂O, 50 mM MnCl₂·4H₂O, 15 % glycerol, pH to 5.8 with acetic acid) and chilled on ice for 5 minutes. The cells were harvested at 5000 rpm, 4 °C for 5 minutes and resuspended in 4 ml chilled TfbII solution (10 mM MOPs, 75 mM CaCl₂, 10 mM KCl, 15 % glycerol, adjusted to pH 6.5 using 3 M KOH) and chilled for 15 minutes. Competent cells were dispensed into aliquots, snap frozen in liquid nitrogen or dry ice and stored at -80 °C for later transformation.

2.4.2 *E. coli* Transformation

Competent *E. coli* cells were thawed on ice. 100 ng of plasmid was added to 20 µl competent cells and kept on ice for 30 minutes before being heat shocked at 42 °C for 1 minute. Cells were subsequently chilled on ice for 5 minutes. After the addition of 150 µl LB, cells were incubated for 1 hour at 37 °C, 180 rpm, harvested and plated onto LB agar supplemented with antibiotic.

2.4.3 Isolation of Plasmid DNA from *E. coli*

For the extraction of plasmid DNA from *E. coli* cultures, the GenElute™ HP Plasmid Miniprep Kit (Sigma-Aldrich®) was used. 5 ml of *E. coli* overnight culture was harvested by centrifugation and the cell pellet resuspended in 200 µl Resuspension Solution containing RNase A. 200 µl Lysis Buffer was added to the cell suspension and mixed by gentle inversion, allowing the mixture to become clear. 350 µl Neutralization/Binding Buffer was added to the lysis solution and gently inverted for precipitation of cellular debris. The mixture was centrifuged at 12,000 rpm for 10 minutes. To prepare the Miniprep binding column, 500 µl Column Preparation Solution was added to a column placed inside a microcentrifuge tube and centrifuged for one minute at 12, 000 rpm. The flow through was discarded. Clear supernatant containing plasmid DNA

was transferred to the binding column and centrifuged for 1 minute, discarding flow through. The column was washed with 500 µl Wash Solution 1 and subsequently with 750 µl Wash Solution 2 and the flow through discarded following centrifugation. To elute plasmid DNA, 100 µl Elution Solution was added to the binding column and incubated for 1 minute at room temperature before centrifugation for 1 minute to yield plasmid DNA. DNA was stored at -20 °C.

2.4.4 Extraction of genomic DNA from *C. glabrata* and *S. cerevisiae*

Yeast DNA was isolated using the MasterPure™ Yeast DNA Purification kit (Epicentre®). Briefly, a single yeast colony was transferred into a microcentrifuge tube containing 300 µl Yeast Cell Lysis Solution and resuspended by vortex mixing. The cell solution was incubated for 15 minutes at 65 °C and then on ice for 5 minutes. 150 µl of MPC Protein Precipitation Reagent was added to the lysis solution and mixed by vortex for 10 seconds. Precipitated cellular debris was collected by centrifugation for 10 minutes at 10,000 rpm followed by removal of the DNA-containing supernatant into a fresh microcentrifuge tube, carefully avoiding the cell precipitate. To precipitate DNA, 500 µl was added to the supernatant, mixed by inversion 5 times followed by centrifugation at 10,000 rpm for 10 minutes. After removal of the supernatant, the DNA pellet was washed once with 70 % ethanol, air dried and suspended in 35 µl TE buffer. DNA was stored at -20 °C.

2.4.5 Resolution of DNA fragments by Gel Electrophoresis

Agarose gel consisting of 1 % Agarose in 1 x TAE (4.84 g/L Tris base, 1.14 ml/L glacial acetic acid and 0.37 g/L EDTA) was prepared by heating in a microwave. Once cooled to approximately 50 °C, ethidium bromide was added to the gel mixture to a final concentration of 0.4 µg/ml. After mixing the gel was poured into a gel cast and allowed to set. The gel tank was filled with 1 x TAE buffer ensuring full coverage of the agarose gel. 5 µl of DNA sample mixed with 1 µl DNA loading buffer (30 % (v/v) glycerol, 0.25 % (w/v) bromophenol blue and 0.25 % (w/v) xylene cyanol) were loaded into individual wells of the agarose gel. For standardisation of DNA fragment size, 2.5 µg (5 µl) of 1 kb or 100 bp DNA ladder (New England Biolabs) were loaded onto the gel. Samples were run for

approximately 30 minutes at 80 V. DNA fragments were visualised using in a Syngene G:BOX gel imager.

2.4.6 Purification of PCR Products from Agarose Gels

Purification of PCR products from agarose gels was performed using the GenElute™ Gel Extraction Kit (Sigma-Aldrich®). Briefly, the DNA fragment was excised from the agarose gel, placed in 3 gel volumes of Gel Solubilization Solution and incubated at 50 °C until completely dissolved. To prepare the DNA binding column, 500 µl of Column Preparation Solution was added to a GenElute Binding Column which had been placed inside a 2 ml collection tube. The binding column was centrifuged for 1 minute at 12,000 rpm and the flow-through discarded. Once melted, 1 gel volume of isopropanol was added to the solubilised gel mixture and mixed by inversion. The solubilised gel solution was added to the DNA binding column and centrifuged for 1 minute at 12,000 rpm discarding the flow through liquid. The binding column was washed with 700 µl Wash Solution and centrifuged twice at 12,000 rpm for 1 minute, discarding the flow-through to ensure the removal of excess ethanol. The column was then placed into a fresh collection tube. Lastly, to retrieve DNA from the binding column, 50 µl Elution Solution was added to the column and centrifuged for 1 minute at 12,000 rpm. DNA was stored at -20 °C.

2.4.7 *C. glabrata* Transformation by Electroporation

A single *C. glabrata* colony was used to inoculate 5 ml YPD and grown overnight at 37 °C, 180 rpm. 1 ml of overnight culture was subcultured into a conical flask containing 50 ml YPD and grown for 3 hours to an OD₆₀₀ of 1 – 1.5. Cells were harvested and washed once in 25 ml sterile water and then gently resuspended in 10 ml solution containing 1 x TE (10 mM Tris, 1 mM EDTA, pH 8) and 100 mM lithium acetate and incubated for 30 minutes at 30 °C, 150 rpm. After the addition of 125 µl DTT (2 M stock in ethanol) the cell suspension was incubated for a further hour. Cells were harvested, washed with 25 ml chilled water followed by washing in chilled 1M sorbitol. Where possible competent cells were kept on ice between wash steps. Once washed, the competent cells were resuspended in 550 µl chilled 1 M sorbitol.

For electroporation, 55 µl competent cells were mixed with 6 µl fusion construct or plasmid in a pre-chilled electroporation cuvette. The mixture was electroporated at 1500 V in an Eppendorf Eporator® and transferred into a sterile 1.5 ml centrifuge tube containing 1 ml YPD. After incubation at 30 °C, 180 rpm for 4 hours, cells were harvested and plated onto YPD agar plates supplemented with 200 µg/ml NAT.

2.4.8 Lithium Acetate-mediated Yeast Transformation

An overnight culture from a single yeast colony was grown in YPD at 30 °C, 180 rpm. 1.25 ml of overnight culture was transferred into 25 ml fresh YPD and grown for 4-5 hours at 30 °C, 180 rpm. Cells were harvested and washed twice in 15 ml sterile water and the pellet resuspended in 100 mM lithium acetate. 50 µl of the cell suspension was mixed with 500 µl solution A (40 % (w/v) PEG 3300, 100 mM lithium acetate and 10 mM Tris-HCl pH 7.5), 50 µl carrier DNA (2 mg/ml) and 2 µg plasmid DNA and incubated at 30 °C, 100 rpm for 30 minutes. The mixture was subsequently heatshocked at 42 °C for 15 minutes. The cells were harvested and plated onto YPD agar plates containing the appropriate selection.

2.5 Cloning of *C. glabrata* ORFs using Invitrogen Gateway® Technology

2.5.1 Amplification of *C. glabrata* ORFs

C. glabrata ORFs were amplified by PCR using a forward primer of 5'-AC AAA AAA GCA GGC TTC ATG-3' followed by 27 bp specific to each ORF and a reverse primer of 5'-A CAA GAA AGC TGG GTC-3' followed by 30 bp specific to each ORF but omitting the STOP codon (Appendix 1 Table 5). ORF amplification was achieved using Platinum® *Pfx* DNA polymerase as per the manufacturer's instructions. Amplification product size was verified by gel electrophoresis.

2.5.2 Addition of *attB* Sites onto Amplification Products

Recombination sites from the bacteriophage lambda (*attB* sites) were added onto the flanking ends of amplification products using a second PCR reaction. Primers AttB-For and AttB-Rev were universal for adding *attB* sites onto all amplification products due to homology with primers from the amplification step (Appendix 1 Table 4). Platinum® *Pfx* DNA polymerase was used for PCR

according to the manufacturer's instructions. PCR products were verified by gel electrophoresis.

2.5.3 BP Clonase® Reaction

Amplification products were shuttled into pENTRY vector pDONR™221 (Life Technologies™; Figure 2.1) in a BP Clonase® reaction. 1 µl TE buffer, 0.5 µl pDONR™221 and 1 µl BP Clonase® were mixed on ice. To this reaction, 2 µl of the appropriate *attB* PCR product was added. The mixture was incubated at 25 °C for a minimum of 2 hours, after which the reaction was either stored at -20 °C for future use or directly transformed into *E. coli DH5α* cells. Transformed *E. coli* were plated onto LB Kanamycin to select for clones containing pENTRY vectors carrying the gene of interest.

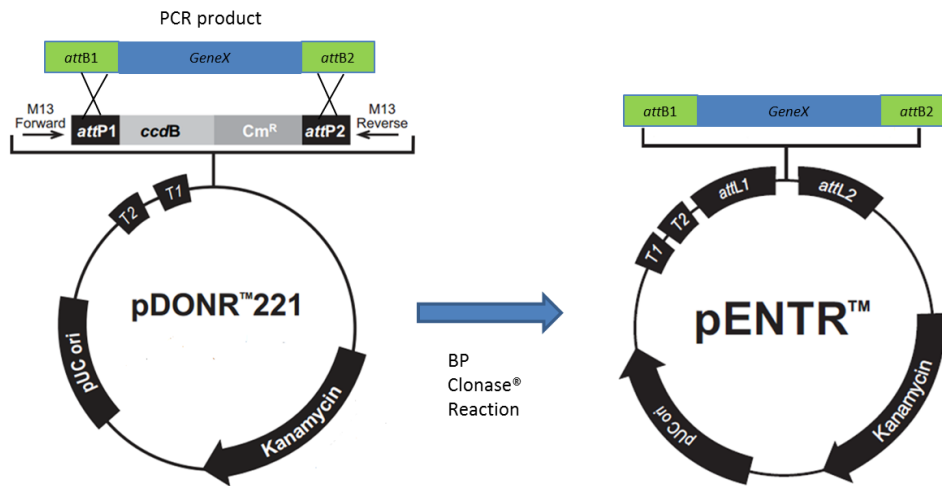


Figure 2.1: Diagrammatic representation of the BP clonase® reaction. During the BP Clonase® reaction, the *attB* sites flanking the ORF of interest (*GeneX*) recombine with *attP* of the pDONR™221 vector, yielding a pENTRY vector containing *GeneX*.

Following transformation, single *E. coli* colonies were picked to inoculate 5 ml LB Kanamycin broth and grown overnight at 37 °C, 180 rpm. Cells from overnight cultures were harvested and plasmid was extracted using the GenElute™ HP Plasmid Miniprep Kit (Sigma; see 2.4.3). Integration of the correct size insertion into the pENTRY vector was verified by PCR amplification using primers M13-For and M13-Rev (Appendix 1 Table 4), which target regions of the vector flanking the insertion. Gel electrophoresis was used to check for correct size amplification product (target ORF size + 253 bp).

2.5.4 LR Clonase® Reaction

To shuttle the target ORF from the pENTRY vector to a chosen destination vector (pDEST), LR clonase® reactions were performed. 0.5 µl of the pENTRY vector were added to a mix of 3 µl TE buffer, 0.5 µl pDEST vector and 1 µl LR clonase® on ice. The reaction was incubated at 25 °C for 2 hours, transformed into *E. coli DH5α* cells and subsequently plated onto LB Ampicillin plates. The remaining LR Clonase® reaction mix was stored at -20 °C. Transformants were selected to inoculate 5 ml LB Ampicillin broth and grown overnight at 37 °C, 180 rpm. Plasmid was extracted from overnight cultures using the GenElute™ HP Plasmid Miniprep Kit (Sigma; see 2.4.3). Correct shuttling of the insert was verified by PCR amplification of the target ORF using primers M13-For and

M13-Rev (See Appendix 1 Table 4). Correct destination vectors were transformed into *C. glabrata* or *S. cerevisiae* (see 2.4.7 and 2.4.8).

Chapter 3: Selection of *C. glabrata* specific genes for targeted gene deletion

3.1 Overview

The high number of sequenced Ascomycete species have made this group of fungi the focus of many comparative genomic studies (Souciet *et al.*, 2000; Dujon *et al.*, 2004; Butler *et al.*, 2009; Moran *et al.*, 2011). Such studies found the pathogenic yeast *C. glabrata* to be more closely related to the non-pathogenic yeast *S. cerevisiae* and that both genomes are distinct from *C. albicans* and other members of the CTG clade (Dujon *et al.*, 2004; Dujon, 2010; Figure 1.3). As yet, *C. glabrata* and its biology with respect to infection has remained poorly explored and much knowledge is inferred from orthologues from *C. albicans* and *S. cerevisiae*.

The completion of full deletion libraries in *S. cerevisiae* has pushed this model organism to the forefront of genome-wide molecular biological studies, greatly accelerating the functional characterisation of genes and pathways, enabling high-throughput non-biased chemical-genetic studies and facilitating the creation of the genetic landscape of the cell through genome-wide genetic interaction studies (Giaever *et al.*, 2002; Costanzo *et al.*, 2010; see 1.3). Following the success of the *S. cerevisiae* deletion project, smaller scale gene deletion collections in *C. albicans* have proven a powerful tool which, for example, has facilitated the understanding of genetic regulation networks underlying biofilm formation – a medically important population structure in this species (Nobile *et al.*, 2012). However, knowledge gained from the well-studied pathogen *C. albicans* is not always applicable or relevant to *C. glabrata* biology due to stark differences in their lifestyles (Brunke & Hube, 2013; see 1.5.1, 1.5.2, 1.5.3). Similarly, whilst *C. glabrata* is closely related to *S. cerevisiae* and shares high levels of protein orthology (Dujon *et al.*, 2004), *S. cerevisiae* is relatively non-pathogenic and generally regarded as safe and thus provides little insight into *C. glabrata* virulence factors. Whilst data generated from these screens can often be extrapolated to yield useful functional information about

orthologues in related species, there is a need for molecular tools for the study of ORFs which are of relevance to pathogenicity in clinically relevant species.

This study aims to gain insight into *C. glabrata* virulence attributes through the generation of molecular tools for the functional characterisation of *C. glabrata* ORFs which may play a role in pathogenicity. Firstly, to address the question of what factors have allowed *C. glabrata* to emerge as a pathogen, yet be so closely related to non-pathogenic yeast species such as *S. cerevisiae*, *C. glabrata* ORFs with no *S. cerevisiae* orthologue needed to be identified. This study hypothesises that *C. glabrata* ORFs with no orthologue in *S. cerevisiae* may be important for *C. glabrata* virulence (Desai *et al.*, 2011). Such ORFs may have emerged since divergence of *C. glabrata* and *S. cerevisiae* from a common ancestor following a whole genome duplication event (Byrne & Wolfe, 2005; see 1.2; Figure 1.3) or alternatively could have been retained in *C. glabrata* and lost from *S. cerevisiae*. Such changes have accompanied the emergence of *C. glabrata* as a human pathogen. Indeed this hypothesis has held true for the *EPA* genes and other *C. glabrata* adhesins which facilitate epithelial and immune-cell attachment in *C. glabrata* (Cormack *et al.*, 1999; Butler *et al.*, 2009; Desai *et al.*, 2011). Therefore a number of bioinformatic approaches were used to identify and functionally annotate *C. glabrata*-specific ORFs. It was also hypothesised that the acquisition of prokaryotic genes by *C. glabrata* could have contributed to the adaptation to a new niche. To further fulfil the aims of this study, a deletion library of selected *C. glabrata* ORFs was generated to provide a molecular tool for the downstream functional characterisation of these ORFs. Thus, functional studies through the exploitation of such a deletion library may reveal *C. glabrata* virulence attributes.

3.2 Materials and Methods

3.2.1 Detection of Horizontal Gene Transfer Events between Prokaryotes and *C. glabrata*

BLASTP searches of the *C. glabrata* proteome were performed against a bespoke database of 4,294,681 proteins from 680 bacterial genomes and 93 fungal genomes to identify *C. glabrata* ORFs with significant similarity (e-value < 1e-5) with bacterial protein sequences (Dr. Darren Soanes, University of

Exeter). Protein sequences for selected *C. glabrata* ORFs were retrieved from CGD (candidagenome.org) and sequences of the top 100 BLASTP hits (blast.ncbi.nlm.nih.gov/) were downloaded. Multiple sequence alignments were performed in ClustalW (genome.jp/tools/clustalw/) employing the Slow/Accurate pairwise alignment and downloaded in PIR format. Multiple sequence alignments were uploaded into Gblocks (molevol.cmima.csic.es/castresana/Gblocks_server.html) for the selection of conserved blocks to be later used for phylogenetic analysis. Selected blocks were subsequently run through ModelGenerator (Keane *et al.*, 2006) to select the optimal amino acid substitution model for phylogenetic analysis. LG substitution models (Le & Gascuel, 2008) were selected for *C. glabrata* ORFs *CAGL0D01210g*, *CAGL0K11066g* and *CAGL0M14091g*. Having converted the GBlocks file to FASTA format using Readseq (ebi.ac.uk/Tools/sfc/readseq/), files were uploaded to the ATCG PhyML 3.0 (Guindon *et al.*, 2010) applying a bootstrap of 100. The resultant estimated maximum tree file downloaded from PhyML was visualised in FigTree (tree.bio.ed.ac.uk/software/figtree/). Identical or duplicated sequences from the same species were removed from the analysis.

3.2.2 Targeted Gene Deletion in *C. glabrata*

3.2.2.1 Amplification of 5' and 3' Ends of the Target ORF

Flanking regions of the target ORF were amplified incorporating ORF-specific barcode sequences and universal U1, U2, D1 and D2 sequences. Barcode sequences from the *S. cerevisiae* deletion collection (Winzeler *et al.*, 1999) were used to tag *C. glabrata* mutants.

For the 5' flanking region, 500 bp upstream of but excluding the start codon was amplified using ORF-specific primers -500-F and -1-NAT-R (Appendix 1 Table 2) to generate the 5' construct (Figure 3.1). Sequences universal to all deletions, regions U1 and U2, allow for amplification of barcodes from all deletion mutants in one reaction. Sequence U2 contains overlaps with that of the NAT^R cassette.

For the 3' flanking region, 500 bp downstream of but excluding the stop codon was amplified using ORF-specific primers +500-R and +1-NAT-F (Appendix 1 Table 2) to generate the 3' construct in (Figure 3.1). Sequences universal to all

deletions, regions D1 and D2 allow for amplification of barcodes from all deletion mutants in one reaction. Sequence D2 contains overlaps with that of the NAT^R cassette.

Up- and down-stream flanking regions were amplified using Green *Taq* DNA polymerase as per manufacturer's instructions in a Techne TC-4000 thermocycler. PCR products were verified by gel electrophoresis. The 500 bp products were excised from the agarose gel, purified (see 2.4.6) and stored at -20 °C.

3.2.2.2 Amplification of the NAT^R Cassette

The NAT^R cassette was amplified from the pCR2.1-SAT plasmid using primers U2-BC-NAT and D2-BC-NAT (Appendix 1 Table 1) to produce a DNA fragment with ends which overlap with the U2 and D2 regions of the 5' and 3' ends respectively. The cassette contains *S. pombe* *TEF1* promoter, *SAT* gene conferring CloneNAT-resistance, and *S. pombe* *TEF1* 3' UTR and FRT (flippase recognition target) sequence for subsequent removal and recycling of the NAT^R cassette as a marker (Figure 3.1). BIO-X-ACTTM short DNA polymerase was used for amplification of the NAT^R cassette as per the manufacturer's instructions. The 1.3 kb NAT^R cassette PCR product was verified by gel electrophoresis, gel purified (see 2.4.6) and stored at -20 °C.

3.2.2.3 Fusion PCR of the Deletion Construct

Flanking 5' and 3' ends of the target ORF and NAT^R cassette were fused in a PCR reaction to produce a fusion deletion cassette (Figure 3.1).

DNA mix per single reaction:

8 µl	2.5 mM ExTaq dNTP mix
1.25 µl	forward primer (-500-F, 50 µM)
1.25 µl	reverse primer (+500-R, 50 µM)
2 µl	5' and 3' UTRs mix (gel purified)
1 µl	NAT ^R cassette (gel purified)
16.5 µl	H ₂ O

The DNA mix was boiled for 10 minutes in a Techne TC-4000 thermocycler to ensure complete DNA denaturation and stored on ice for a minimum of 1 minute.

Added to the DNA mix per single reaction:

10 μ l	10 x ExTaq buffer
4 μ l	25 mM MgCl ₂
2 μ l	2.5 mM ExTaq dNTP mix
0.6 μ l	ExTaq DNA polymerase (Lonza, 5 U/ μ l)
<u>53.4 μl</u>	H ₂ O
100 μl	Final volume

PCRs were replaced in the thermocycler for the following cycle:

Temperature	Time	Cycles
95 °C	30 seconds	3
42 °C	30 seconds	
72 °C	2.5 minutes	
95 °C	30 seconds	30
52 °C	30 seconds	
72 °C	2.5 minutes	
72 °C	10 minutes	1

The fusion construct (~2.3-2.4 kb) was verified by gel electrophoresis.

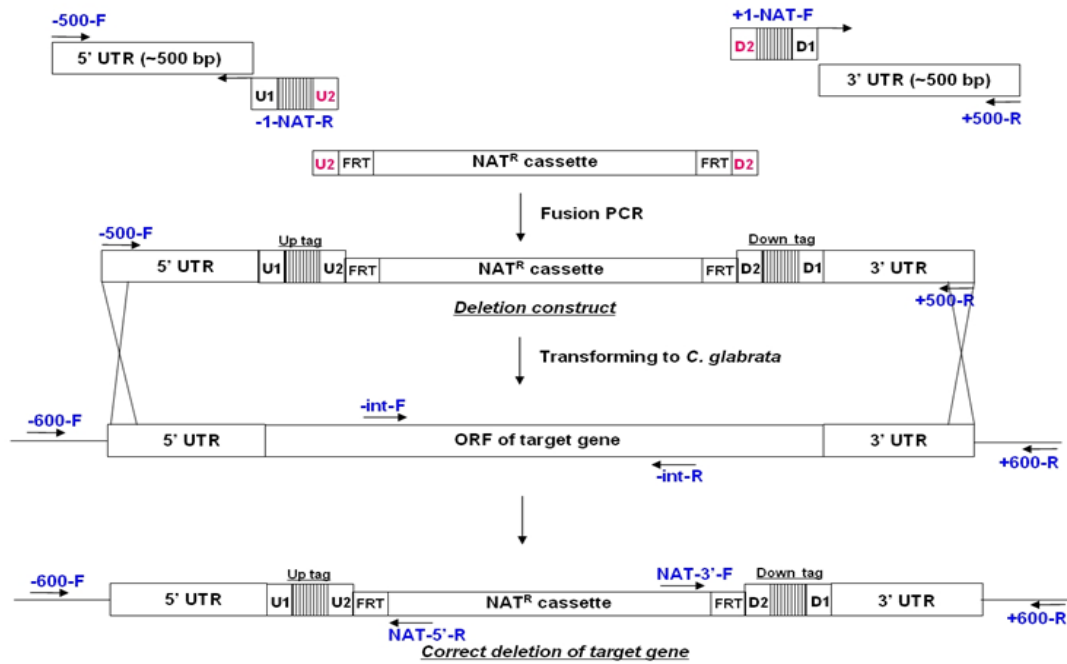


Figure 3.1: Targeted gene deletion method in *C. glabrata* (Dr. Biao Ma, personal communication). Firstly, 5' and 3' ends of the target gene were amplified. The 5' end (500 bp upstream of the start codon) was amplified using ORF specific primers -500-F and -1-NAT-R (Appendix 1 Table 2), incorporating universal sequences U1 and U2 as well as a 20bp unique “Up tag”. The 3' end (500 bp downstream of the stop codon) was amplified using ORF-specific primers +1-NAT-F and +500-R (Appendix 1 Table 2), incorporating universal sequences D1 and D2 as well as a unique 20bp “Down tag”. Secondly, the NAT^R cassette was amplified using primers U2-BC-NAT and D2-BC-NAT (Appendix 1 Table 1), incorporating flanking FRT (flippase recognition targets) sites and U2 and D2 universal sequences. Lastly, a fusion PCR incorporated 5' and 3' ends with the NAT^R cassette using ORF-specific primers -500-F and +500-R (Appendix 1 Table 2) to yield the deletion construct. The deletion construct was transformed into competent *C. glabrata* cells by electroporation. Deletion mutants were verified using three PCR checks. Removal of the target ORF was verified using ORF specific primers int-F and int-R (Appendix 1 Table 3). Insertion of the NAT^R cassette at the correct target locus was verified by amplification of the 5' junction using universal primer NAT-5'-R (Appendix 1 Table 1) and ORF specific primer -600-F (Appendix 1 Table 3). The 3' junction was verified using universal primer NAT-3'-F (Appendix 1 Table 1) and ORF specific primer +600-R (Appendix 1 Table 3).

3.2.2.4 Precipitation of Fusion Construct

10 µl of Na-acetate (3 M, pH 5.2) and 800 µl of ethanol were added to 100 µl of the fusion PCR reaction, mixed and stored at -20°C for a minimum of 1 hour. The mixture was centrifuged at 13,000 rpm for 8 minutes to yield a DNA pellet which was subsequently washed with 1 ml of 70 % ethanol, air-dried, and dissolved in 50 µl of 0.1 x TE (1 mM Tris-HCl, pH 8.5, 0.1 mM EDTA). The DNA solution was directly used for transformation into competent *C. glabrata* Cg2001 $\Delta his3$ cells by electroporation (see 2.4.7).

3.2.2.5 Verification of *C. glabrata* Transformants

C. glabrata transformants were initially verified by colony PCR. Firstly, presence of the target ORF was checked using ORF-specific primers int-F and int-R (Figure 3.1; Figure 3.9 A; Appendix 1 Table 3) which target sequences within the deleted ORF. Secondly, correct integration of the deletion cassette at the target locus was verified using ORF-specific primer -600-F and NAT-5'-R targeting the 5' junction (Figure 3.1; Figure 3.9 B). Primers NAT-3'-F and +600-R were used for verification of the 3' junction (Figure 3.1; Figure 3.9 B). Correct insertion of the deletion cassette yielded a PCR product of 0.9 – 1.2 kb at both junctions. Primers NAT-5'-R and NAT-3'-F (Appendix 1 Table 1) target sequences within the NAT^R cassette whilst +600-R and -600-F are ORF-specific (Appendix 1 Table 1 and 3).

Genomic DNA of transformants yielding PCR products indicative of correct integration of the deletion cassette was extracted and verified using the described PCR reactions.

Where possible, three independent isolates of each deletion strain were collected and stored as glycerol stocks at -80 °C.

3.3 Results

3.3.1 Identification of *C. glabrata* ORFs with no *S. cerevisiae* Orthologue

A bespoke BLAST-based bioinformatic search was used to identify *C. glabrata* ORFs which may have no orthologue in *S. cerevisiae* (Dr. Maxime Huvet, Imperial College London, personal communication). Reciprocal best hit (RBH) searches of the *C. glabrata* proteome (uniprot.org) against that of *S. cerevisiae*

identified 4000 *C. glabrata* proteins with orthologues in *S. cerevisiae* (Figure 3.2). Amongst the remaining 1192 *C. glabrata* proteins with no strict *S. cerevisiae* orthologue, 465 were identified to have putative homologues in *S. cerevisiae* by BLAST search. To increase the stringency of searches, filters were applied at both sequence comparison stages to ensure 30 % sequence identity within a minimum of 50 % of the protein sequence. This approach identified 727 *C. glabrata* proteins which may have no orthologue in *S. cerevisiae* (Figure 3.2; Appendix 3 Table 1).

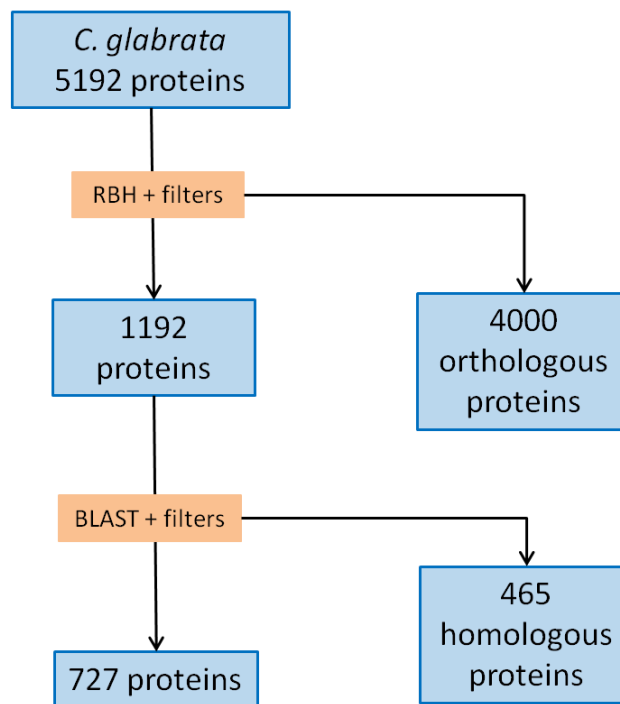


Figure 3.2: Workflow of RBH searches used to identify *C. glabrata* ORFs with no orthologue in *S. cerevisiae*. RBH searches of the *C. glabrata* proteome were performed against that of *S. cerevisiae*. Filters were applied to RBH searches ensuring a minimum of 30 % sequence identity covering a minimum of 50 % of the protein sequence. RBH searches identified 4000 *C. glabrata* ORFs with strict *S. cerevisiae* orthologues. BLAST searches of the remaining 1192 *C. glabrata* ORFs identified *S. cerevisiae* orthologues for 465 ORFs, leaving 727 *C. glabrata* proteins with no orthologue in *S. cerevisiae*.

3.3.2 Mapping the Chromosomal Location of *C. glabrata* ORFs with no Orthologue in *S. cerevisiae*

The location of 727 *C. glabrata* ORFs identified by RBH searches to have no orthologue in *S. cerevisiae* were mapped on the *C. glabrata* chromosomes (Figure 3.3). *C. glabrata*-specific ORFs were distributed throughout all 13 *C. glabrata* chromosomes. Comparison of the proportion of *C. glabrata*-specific ORFs (identified in RBH searches) falling on each chromosome found no significant enrichment of these ORFs on any particular chromosome (Chi-squared, $p=0.997$). However, statistical analysis identified 10 regions in which *C. glabrata* ORFs with no orthologues were statistically clustered compared with the distribution of coding sequences throughout the chromosome (Figure 3.3; Poisson distribution, $p<0.05$). The chromosome B cluster contains putative *C. glabrata* β -mannosyltransferases whilst clusters located on Chromosomes E and J contain putative adhesins. However, clusters of *C. glabrata*-specific ORFs are located at various regions on the chromosomes with no trend towards the centromere or telomere.

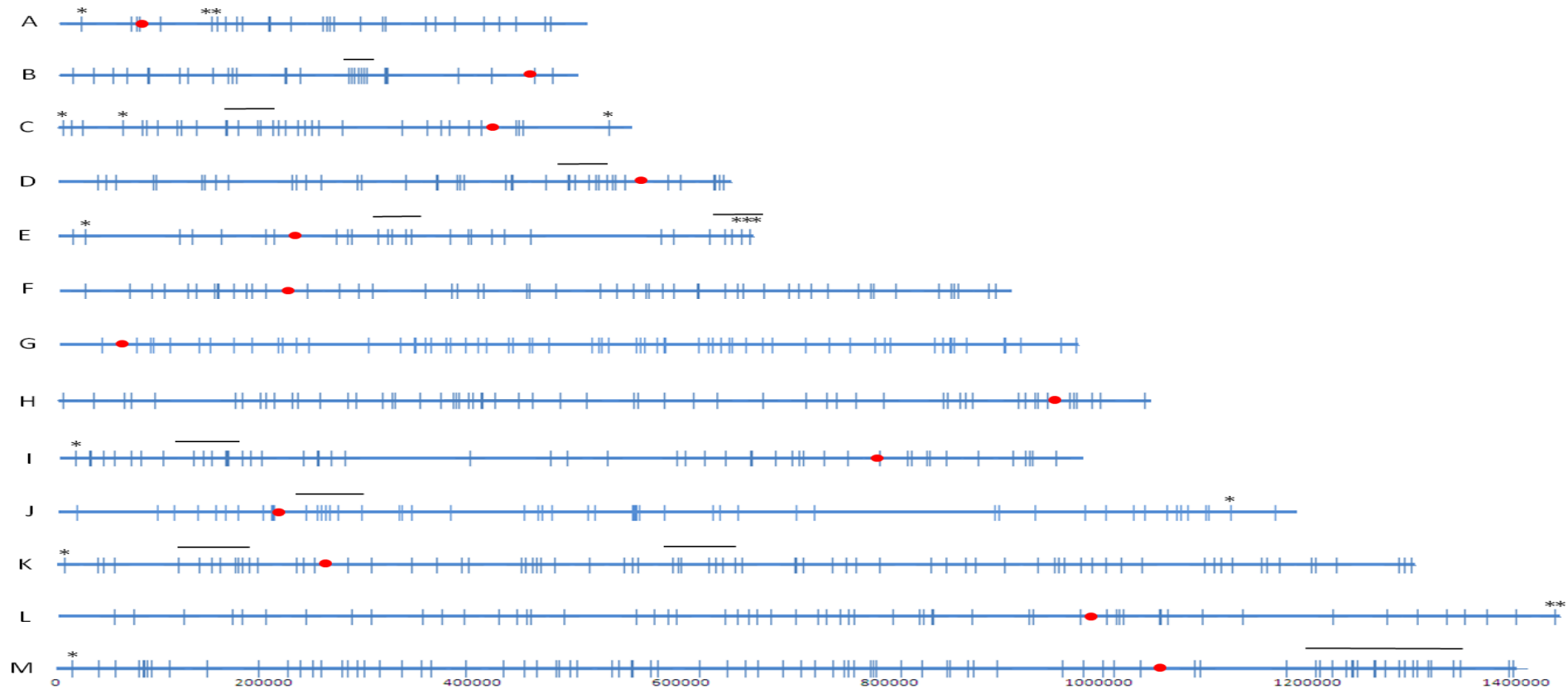


Figure 3.3: Chromosomal distribution of *C. glabrata* ORFs with no orthologue in *S. cerevisiae*. Blue horizontal lines represent *C. glabrata* chromosomes labelled A to M with centromeric locations denoted by a red circle. Vertical blue lines indicate the chromosomal locations of *C. glabrata* ORFs with no *S. cerevisiae* orthologue based on RBH searches (Appendix 3 Table 1). Black asterisks show the location of *C. glabrata* EPA genes identified in RBH searches. Black horizontal lines lie above significant clusters of *C. glabrata*-specific ORFs (poisson distribution, $p < 0.05$).

3.3.3 Alternative Approaches for the Identification of *C. glabrata* ORFs with no Orthologue in *S. cerevisiae*

RBH searches identified a large proportion of *C. glabrata* ORFs, encompassing nearly 14 % of the genome, to have no orthologue in *S. cerevisiae*. Thus additional search criteria were required to generate a more stringent list of *C. glabrata*-specific ORFs.

The Yeast Gene Order Browser (YGOB) was exploited to further investigate whether *C. glabrata* genes identified in RBH searches do, in fact, have an *S. cerevisiae* orthologue. YGOB incorporates annotation of orthologous genes from the literature, annotation from automated BLASTP searches as well as manual editing. Syntenic information regarding *S. cerevisiae* genes and their orthologues can also be visualised (Byrne & Wolfe, 2005). Searches of the entire *C. glabrata* genome using YGOB identified 294 *C. glabrata* ORFs to have no *S. cerevisiae* orthologue (Appendix 3 Table 2), a comparably smaller number than those selected by RBH searches. Of these, 37 *C. glabrata* ORFs have orthologues in other closely related yeasts. For example, *C. glabrata* ORF *CAGL0D05434g* has no *S. cerevisiae* orthologue however orthologues are present in *Vanderwaltozyma polyspora*, *Tetrapisispora phaffii*, *Naumovozyma dairenensis* and *Kluyveromyces lactis*. Comparison of the number of *C. glabrata* genes predicted to have no *S. cerevisiae* orthologue by RBH- and YGOB-based approaches found only 197 ORFs common to both lists (Figure 3.4). YGOB and RBH searches identified 97 and 530 ORFs unique to each list, respectively, highlighting a stark difference between the two approaches (Figure 3.4). Thus, ORFs common to both searches were mostly focused on as *C. glabrata* ORFs with no orthologue in *S. cerevisiae*.

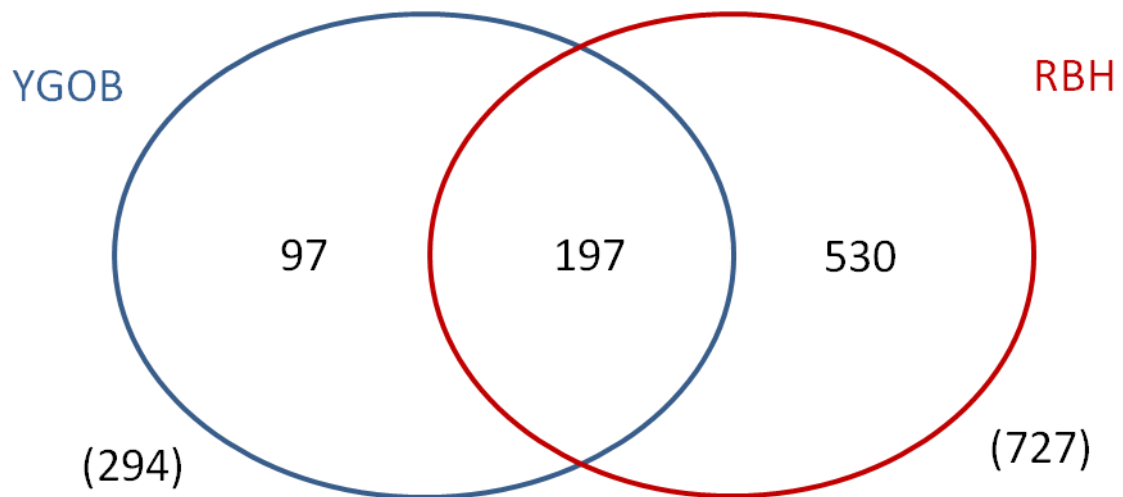


Figure 3.4: Comparison and overlap of *C. glabrata* ORFs with no orthologue in *S. cerevisiae* derived from two different bioinformatic approaches. RBH searches (red) identified 727 ORFs with no *S. cerevisiae* orthologue whilst YGOB identified only 294 ORFs with no *S. cerevisiae* orthologue. Bracketed numbers indicate the total number of *C. glabrata* ORFs identified by each search method.

3.3.4 The Acquisition of Prokaryotic Genes by *C. glabrata*

To assess whether the acquisition of prokaryotic genes by *C. glabrata* may have contributed to its adaptation to the host niche, protein BLAST searches were used to identify *C. glabrata* ORFs which had high similarity to prokaryotic sequences. Initial BLASTP searches against the bespoke database identified four *C. glabrata* ORFs for which the top BLASTP hits (to a maximum e-value of 1e-5) were prokaryotic: *CAGL0D01210g*, *CAGL0E00231g*, *CAGL0M14091g* and *CAGL0K11066g* (Dr Darren Soanes, University of Exeter, personal communication).

Table 3.1: Summary of *C. glabrata* ORFs which yield top BLAST hits with prokaryotic sequences.

<i>C. glabrata</i> ORF	Putative molecular function/domains	Top BLASTP hit species	E- value	No. Bacterial species in top 100 hits
CAGL0D01210g	Aspartate racemase	<i>Zymomonas mobilis</i> subsp. <i>Mobilis</i> (Proteobacteria)	1e-48	99
CAGL0E00231g	Adhesin-like protein	<i>Rickettsia prowazekii</i> (Proteobacteria)	1e-06	-
CAGL0M14091g	Quinone reductase/NADPH dehydrogenase Flavodoxin-like fold	<i>Salinispora arenicola</i> (Actinobacteria)	5e-44	83
CAGL0K11066g	Hexapeptide transferase	<i>Bacteroides vulgatus</i> (Bacteroidetes)	1e-56	93

Putative *C. glabrata* GPI-anchored adhesin CAGL0E00231g was initially identified in BLASTP searches as a candidate for horizontal gene transfer due to its sequence similarity with a protein from the bacterial species *Rickettsia prowazekii* – a member of the Alphaproteobacteria (Table 3.1). However, BLASTP searches yielded only two significant hits (E-value 1e-5) for this protein, the second of which originated from the flagellated protozoan species *Thecamonas trahens*. Further to this, RBH searches did not identify this ORF to be specific to *C. glabrata* and YGOB predicted this ORF to be a pseudogene. Due to this and the lack of significant BLASTP hits in other species, further investigation into the origin of ORF CAGL0E00231g was not pursued.

3.3.5 *C. glabrata* CAGL0D01210g: Acquisition of a Putative Aspartate Racemase

Initial BLASTP searches for *C. glabrata* ORF CAGL0D01210g against the bespoke protein database scored high confidence hits with predominantly prokaryotic protein sequences (Table 3.1). Functional annotations by CGD (candidagenome.org) and Interpro (ebi.ac.uk/interpro) predict CAGL0D01210g

to encode an aspartate racemase – an enzyme catalysing the interconversion of L-aspartate and D-aspartate enantiomers. Both RBH searches and YGOB found *CAGL0D01210g* to have no orthologue in *S. cerevisiae* (Appendix 3 Table 1 and 2). Furthermore, Fungal BLAST searches (yeastgenome.org) did not identify orthologues of *CAGL0D01210g* in other fungal species with the exception of similar proteins in distantly related fungi *Aspergillus terreus* (E-value 7.8e-27) and *Penicillium chrysogenum* (E-value 4.6e-22). Most importantly, no significantly similar sequences were found in the *Candida* or *Saccharomyces* species, bioinformatically confirming this ORF to have no orthologue in closely related species. Maximum likelihood phylogenies found the *C. glabrata* *CAGL0D01210g* encoding protein to be closely related to protein sequences of aspartate racemases from both Gram positive and Gram negative bacteria and also from Archaea. As shown in the phylogeny for *CAGL0D01210g* and related sequences (Figure 3.5), *CAGL0D01210g* was clustered within branches representing proteins from *Lactobacillus coryniformis*, *Oenococcus kitaharae*, *Lactobacillus vaginalis*, *Lactobacillus acidophilus* and *Lactobacillus gigeriorum* – all of which reside in the Firmicute phylum. However branch support in some instances is low, most likely due to the high similarity between protein sequences. *S. cerevisiae* protein sequences most similar to *CAGL0D01210g* (*YGL171W* and *YLL008W*, E-value 0.41 and 0.99 respectively) were used as an out-group, lying distanced from the clusters of bacterial and archaeal protein sequences surrounding that of *C. glabrata* *CAGL0D01210g* with strong branch support (Figure 3.5). Due to the grouping of *C. glabrata* *CAGL0D01210g* with bacterial aspartate racemase protein sequences and the nature in which this group lies distinct from the most similar protein sequences in the close relative yeast *S. cerevisiae*, it could be hypothesised that *C. glabrata* *CAGL0D01210g* originated from bacterial species (most likely from *Lactobacillus* sp. or other Firmicute species). Thus, *C. glabrata* ORF *CAGL0D01210g* may encode an aspartate racemase recently acquired from bacteria by a horizontal gene transfer event due to a lack of orthologues in related yeast species.

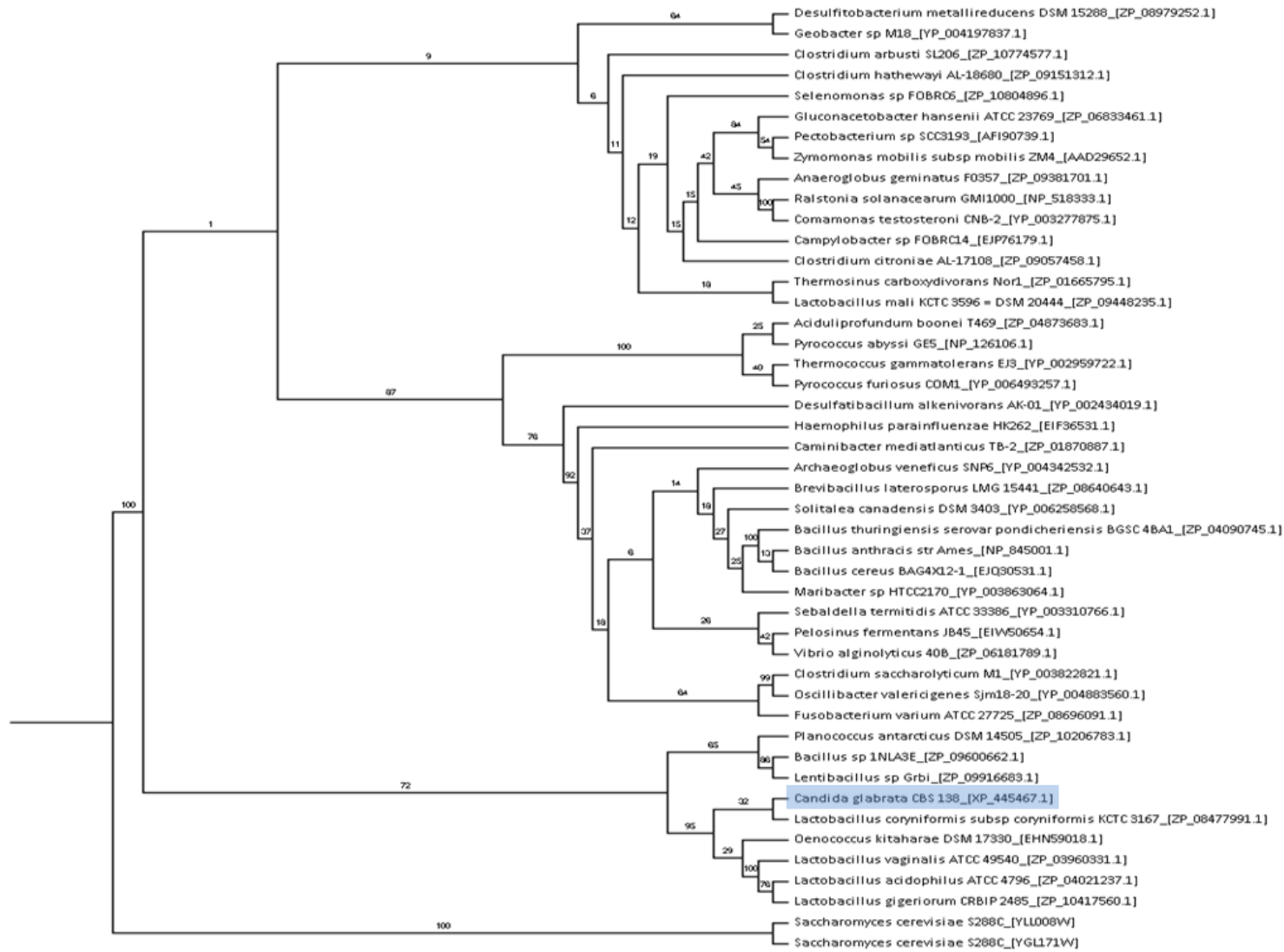


Figure 3.5: Maximum likelihood phylogenetic tree for putative *C. glabrata* aspartate racemase encoded by *CAGL0D01210g* (highlighted in blue). Analysis was performed using 43 representative sequences retrieved from the top 100 BLASTP hits with duplicates and identical sequences removed. Branch labels denote branch support by bootstrap 100 values. Top BLAST hits in *S. cerevisiae* were used as an outgroup. Species within the phylogeny are labelled according to Kingdom or Bacterial Phylum (Red - Firmicutes, Blue - Archaea, Proteobacteria - green, Yellow - Bacteroidetes, Actinobacteria - purple, black - Ascomycete, orange - other)

2.0

3.3.6 *C. glabrata* CAGL0K11066g is Highly Similar to Bacterial Acetyl Transferases

In searches utilising the bespoke database of fungal and bacterial proteins, the *C. glabrata* CAGL0K11066g encoding protein scored significant BLASTP hits with 93 bacterial sequences, namely with proteins encoding bacterial acetyl transferases (Table 3.1). Functional analysis of the *C. glabrata* CAGL0K11066g protein sequence also predicted this protein to have transferase activity (GO:0016740; Appendix 4 Table 1) due to the presence of a Trimeric LpsA-like domain containing a hexapeptide transferase conserved site. However, RBH and YGOB searches did not identify this protein as *C. glabrata*-specific most likely due to similarity to a putative *S. cerevisiae* acetyl transferase encoded by ORF YJL218W. In contrast, phylogenetic analysis showed *C. glabrata* CAGL0K11066g to be more similar to acetyl transferases from bacterial species from the Phyla Firmicutes, Bacteroidetes, Actinobacteria, Proteobacteria and Fusobacteria (Figure 3.6). Similar sequences were also found in Archaea species *Methanobrevibacter ruminantium*. *S. cerevisiae* YJL218W was also included in the analysis but sits outside the cluster of bacterial sequences (which include *C. glabrata*) as an outgroup from which it separated by many branches of the phylogenetic tree. Within the groups of bacterial sequences, *C. glabrata* CAGL0K11066g groups with sequences from the closely related Ascomycete species *Naumovozya castelli* and *N. dairenensis* (Figure 3.6). This analysis provides preliminary evidence for the occurrence of a horizontal gene transfer event from bacteria to an ancestral fungal species prior to the divergence of the three species. However, branch support for the phylogenetic analysis is very low and further validation is required.

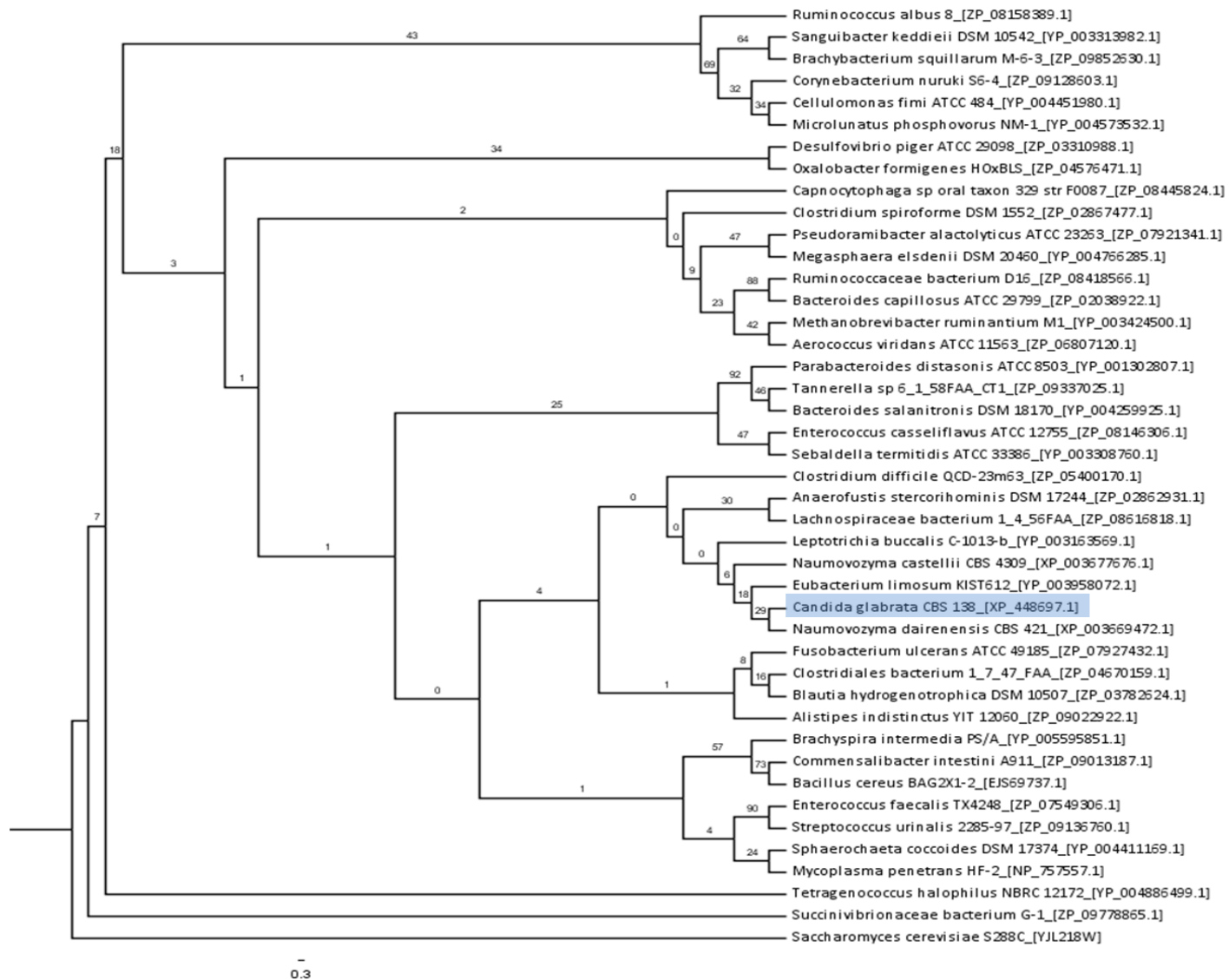


Figure 3.6: Maximum likelihood tree for *C. glabrata* CAGL0K11066g (highlighted in blue) showing phylogenetic relationships with 42 representative protein sequences from BLASTP searches. Identical sequences and duplicates were removed. Branch labels denote bootstrap 100 values. *S. cerevisiae* YJL218W was used as an outgroup. Species within the phylogeny are labelled according to Kingdom or Bacterial Phylum (Red - Firmicutes, Blue - Archaea, Proteobacteria - green, Yellow - Bacteroidetes, Actinobacteria - purple, black - Ascomycete, orange = other)

3.3.7 *C. glabrata* CAGL0M14091g has Similarity to Prokaryotic NADPH Dehydrogenases

Using both RBH and YGOB search criterion, *C. glabrata* CAGL0M14091g was identified to have no orthologue in *S. cerevisiae* (Appendix 3 Tables 1 and 2). The encoding protein encompasses a flavodoxin-like fold and may function as a NADPH dehydrogenase/quinine reductase enzyme (ebi.ac.uk/Interpro; candidagenome.org). BLASTP searches and phylogenetic analysis identified *C. glabrata* CAGL0M14091g to have significant similarity to NADPH dehydrogenase enzymes encoded by both Proteobacteria and Actinobacteria species (Table 3.1; Figure 3.7). In the maximum likelihood phylogeny, *C. glabrata* CAGL0M14091g clusters with three *Vanderwaltozyma polyspora* proteins, two *N. dairenensis* proteins and three *N. castellii* proteins. This cluster of Ascomycetous proteins lies distantly separated to the most similar *S. cerevisiae* protein sequence encoded by YKL225W (Figure 3.7) suggestive of the acquisition of CAGL0M14091g in an ancestral species post divergence from *S. cerevisiae* but prior to the divergence of *C. glabrata*, *V. polyspora*, *N. castellii* and *N. dairenensis*. However, the acquisition of this ORF by a horizontal gene transfer event from bacteria cannot be confirmed due to low branch support in the phylogenetic analysis.

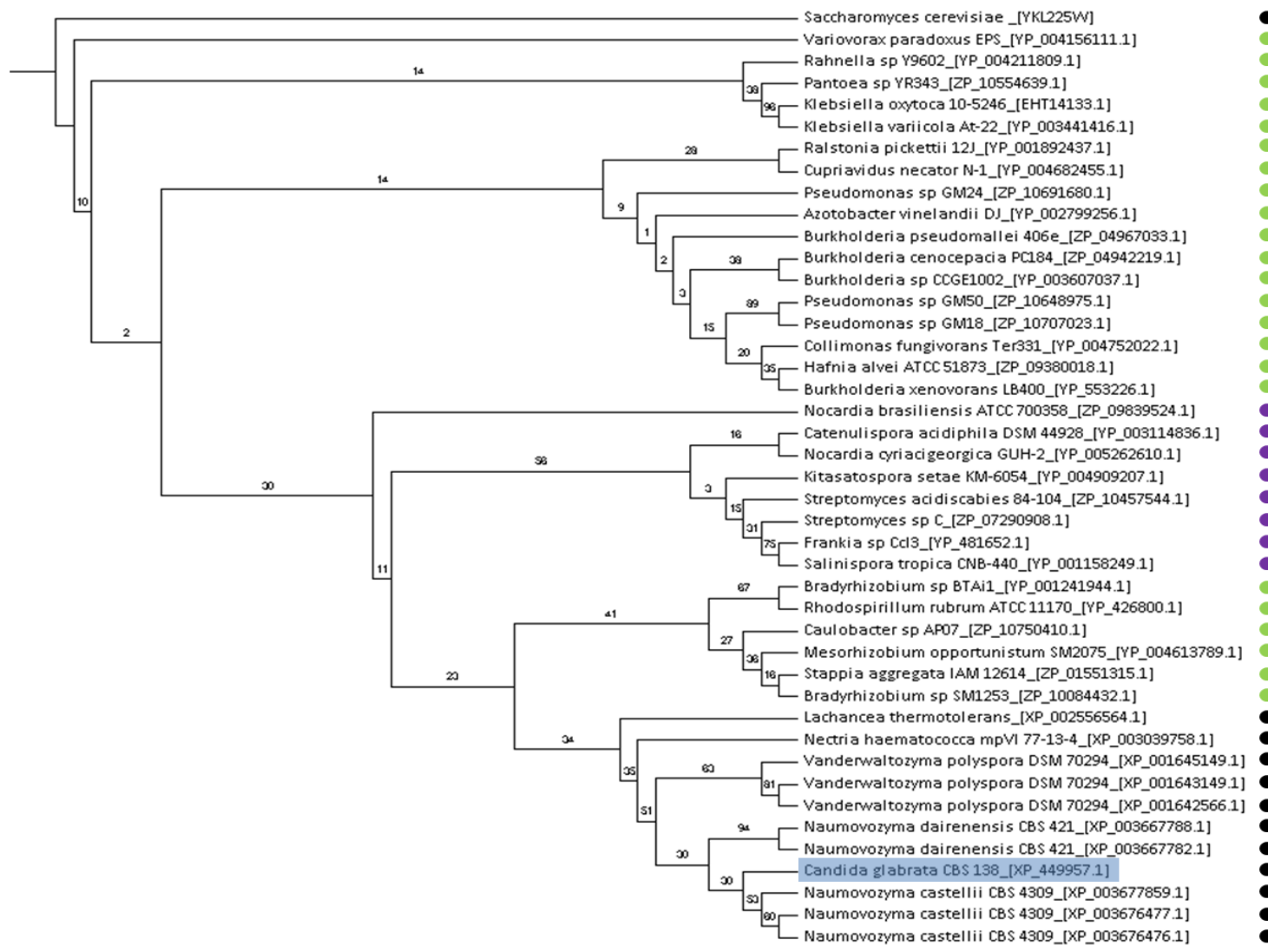


Figure 3.7: Maximum likelihood tree for *C. glabrata* CAGL0M14091g (highlighted in blue) showing phylogenetic relationships with 41 representative protein sequences from BLASTP searches. Identical sequences and duplicates were removed. Branch labels denote bootstrap 100 values. *S. cerevisiae* YKL225W was used as an outgroup. Species within the phylogeny are labelled according to Kingdom or Bacterial Phylum (Red - Firmicutes, Blue - Archaea, Proteobacteria - green, Yellow - Bacteroidetes, Actinobacteria - purple, black - Ascomycete, orange = other)

3.3.8 Functional Annotation and Selection of *C. glabrata*-specific Genes for Targeted Gene Deletion

To prioritise ORFs for deletion, InterPro and InterProScan (ebi.ac.uk/interpro) were used to determine the potential function of selected *C. glabrata* ORFs (Appendix 4 Table 1). Interpro curates predictive models or signatures from multiple databases (such as Pfam, PANTHER and ProDom) against which protein sequences can be searched to yield information on protein families, functional domains and active sites. As such, this tool was used to gain insight into the function and associated GO terms inferred from matching sequences and signatures of *C. glabrata* genes with no *S. cerevisiae* orthologue (Quevillom *et al.*, 2005; Hunter *et al.*, 2012). Accordingly, a prioritised list of *C. glabrata* ORFs as candidates for characterisation was generated taking into account the presence of *S. cerevisiae* orthologues and the presence of functional domains in the encoding protein sequence. *C. glabrata* ORFs which were identified in HGT studies were also targeted for deletion to enable their further characterisation.

Barcoded fusion constructs targeting 100 *C. glabrata* ORFs (Appendix 4 Table 1 and 2) were created using a PCR-based method (see 3.2.2). Fusion cassettes were designed to give deletion mutants a number of features, making them amenable to further downstream applications. FRT (flippase recognition targets) sites flanking the NAT^R cassette allows future removal and recycling of the NAT^R marker for further genetic manipulations (Figure 3.1). Two up- and down-barcode unique to each ORF targeted by the fusion construct were also included for use in downstream pooled growth assays (Figure 3.1; Appendix 1 Table 2). Universal sequences U1, U2, D1 and D2 flanking up- and down-barcode respectively allow the universal amplification of barcode tags in a single reaction (Figure 3.1). Fusion constructs were validated by gel electrophoresis (Figure 3.8; Appendix 14).

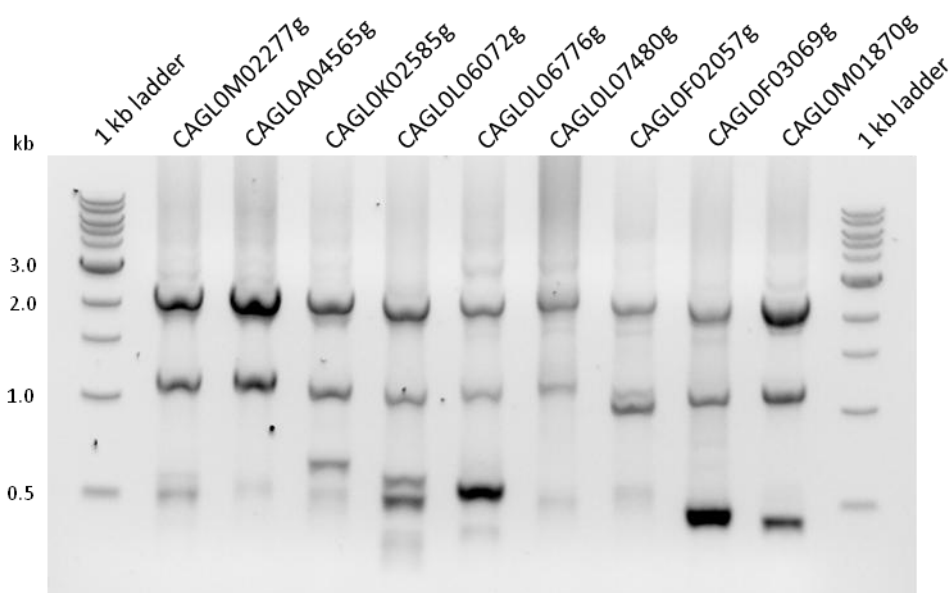


Figure 3.8: Verification of fusion constructs by gel electrophoresis. ORF-specific -500-F and +500-R primers (Appendix 1 Table 2) were added to a PCR reaction permitting the fusion of the NAT^R cassette with homologous regions of ORF-specific 5' and 3' ends. Correct fusion produced a 2.3-2.4 kb amplification product, although several minor bands were also produced. For verification of all fusion constructs, see Appendix 14.

Transformation by electroporation was performed, allowing the deletion construct to integrate into the target locus by homologous recombination. Following transformation into the Cg2001 $\Delta his3$ background, insertion of the fusion construct at the correct locus was verified by three individual PCR reactions. Firstly, absence of the target ORF was verified by PCR using primers homologous to a short region internal of the ORF which yielded an amplification product in the parental Cg2001 $\Delta his3$ strain but not in a correct transformant (Figure 3.9 A; Appendix 14). Secondly, PCR reactions were performed targeting the 5' and 3' junction sites where the fusion construct integrated into the target locus. To validate the 5' junction, a forward primer targeting a region upstream of the homologous recombination site and a reverse primer targeting an internal region of the NAT^R cassette was used (Appendix 1 Table 1 and 2). Similarly to validate the 3' junction, a forward primer targeting a region of the NAT^R cassette

and a reverse primer targeting a region downstream of the site of homologous recombination were used (Appendix 1 Table 1 and 2). For both junction checks, no amplification product was observed in the parental *C. glabrata* 2001 $\Delta his3$ strain whereas amplification products were observed for correct transformants (Figure 3.9 B). Transformants yielding correct amplification products in all three PCR reactions were considered validated deletion mutants. Where transformation by electroporation was not successful, the lithium acetate transformation protocol was used. A total of 35 of the 100 fusion constructs were not successfully transformed using either transformation method (Appendix 4 Table 2). These yielded either no transformants, targeted a region which may lie within an ARS sequence or were not able to be verified by PCR analysis.

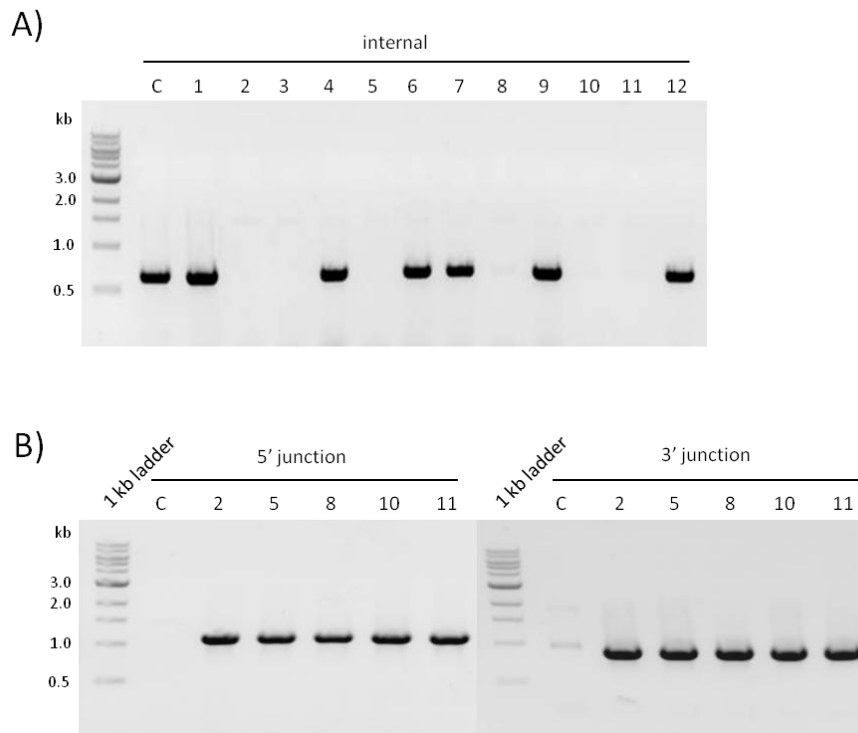


Figure 3.9: PCR checks for the validation of putative *C. glabrata* Δ CAGL0E06644g transformants. A) 12 transformants (labelled 1-12) were checked for the presence of ORF *CAGL0E06644g* using ORF-specific primers E06644 int-F and E06644 int-R (Appendix 1 Table 3), yielding a 600bp product in the parental strain (labelled C) and no product in correct transformants. B) Junction PCR checks were performed on transformants 2, 5, 8, 10, and 11 which passed the internal PCR check. For PCR amplification of the 5' junction, primers E06600-600-F (Appendix 1 Table 3) and NAT-5'-R (Appendix 1 Table 1) were used, yielding a amplification product of 1-1.3 kb in transformants where the fusion construct has integrated at the correct locus. For the 3' junction, primers E06600+600-R (Appendix 1 Table 3) and NAT-3'-F (Appendix 1 Table 1) were used, yielding a 0.9-1.2 kb amplification product in correct transformants. Thus, transformants 2, 5, 8, 10, 11 were deemed verified isolates of *C. glabrata* Δ CAGL0E06644g .

Together, 65 fusion constructs were successfully transformed and verified in *C. glabrata*, forming an individually barcoded library of *C. glabrata*-specific deletion mutants (Appendix 4 Table 1). Where possible, up to three independent isolates of each deletion were retained. Of the 65 ORFs deleted, Interpro predicted functional domains or active sites in 44 of the encoding protein sequences (Figure 3.10; Appendix 4 Table 1). GO Molecular function assignments

predicted 17 of the deleted ORFs to have nucleic acid binding transcription factor activity – the most significantly represented GO function within the deletion library. Other deleted ORFs have protein signature sequences matching domains including kinase, transferase or phosphatase domains (Figure 3.10). However, no predicted functional domains were identified for 22 deleted ORFs.

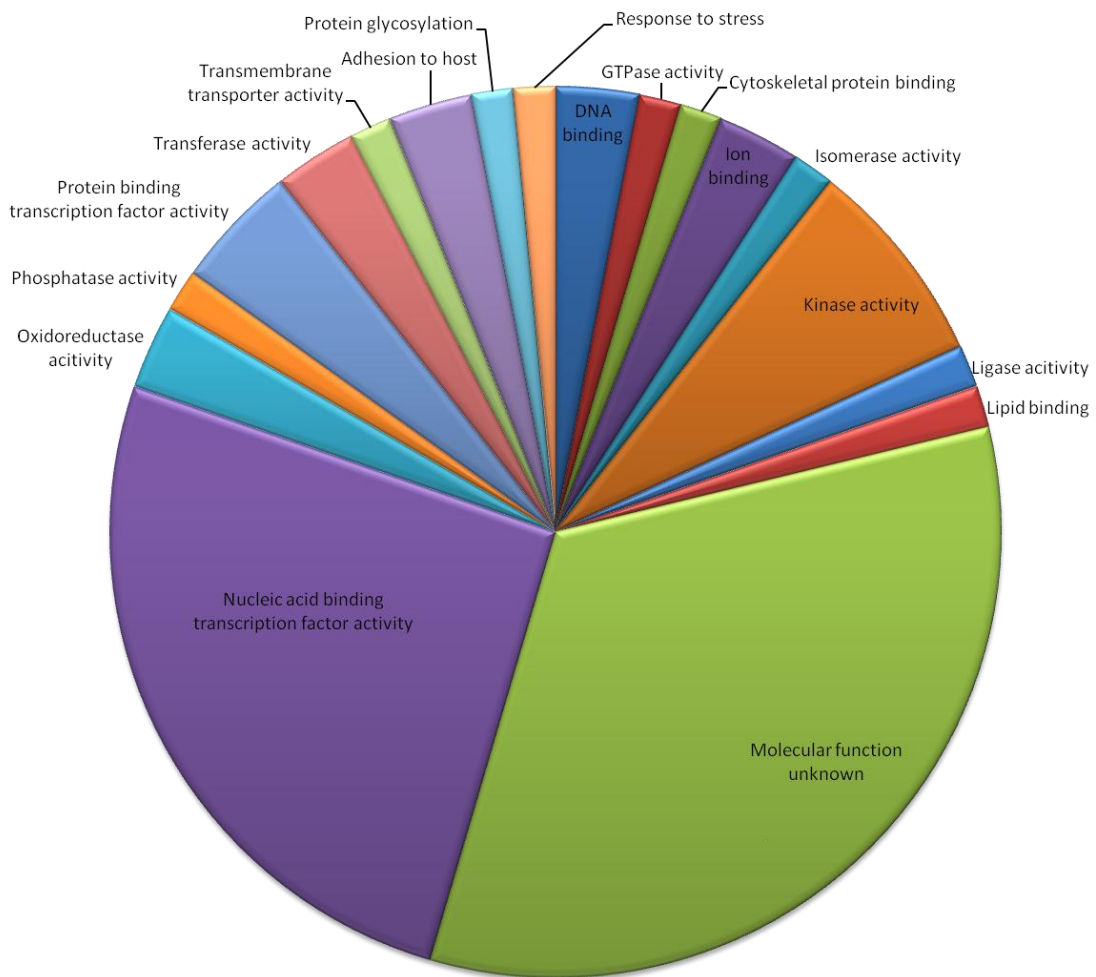


Figure 3.10: Functional annotations of deleted *C. glabrata* ORFs according to InterPro (ebi.ac.uk/interpro). Segments represent GO Molecular function terms assigned by Interpro based on domain matches for 65 *C. glabrata* ORFs successfully targeted for deletion.

3.4 Discussion

3.4.1 Identification and Location of *C. glabrata* ORFs with no Orthologue in *S. cerevisiae*

In order to further elucidate virulence attributes of the pathogenic yeast *C. glabrata*, ORFs with no orthologue in the relatively non-pathogenic yeast *S. cerevisiae* were targeted in this study (see 3.1). Modified RBH-based searches identified 727 *C. glabrata* ORFs which may have no orthologue in *S. cerevisiae* (Appendix 3 Table 1; Personal communication, Dr. Maxime Huvet, Imperial College London). The resultant list was very broad (constituting 14 % of the *C. glabrata* genome) and as such it is likely that many of these ORFs do have an *S. cerevisiae* orthologue. In contrast, searches based on the Yeast Gene Order Browser (<http://ygob.ucd.ie/>) identified 294 *C. glabrata* ORFs which share no orthologue with any *S. cerevisiae* ORF (Appendix 3 Table 2).

However, the two search approaches were validated by the correct inclusion of *C. glabrata* ORFs that are known to have no *S. cerevisiae* orthologue and which play a role in virulence. For example, RBH and YGOB searches identified many of the *EPA* genes and other GPI-anchored proteins (members of the *AWP*, *AED* and *PWP* adhesin gene families) which have been previously implicated in adhesion of *C. glabrata* to host cells, biofilm formation and the establishment of infection (see 1.5.1; Cormack *et al.*, 1999; De Las Penas *et al.*, 2003; Kraneveld *et al.*, 2011; Desai *et al.*, 2011). The search also identified members of the *MNT* gene cluster, which is known to be expanded in *C. glabrata* and encodes a number of α -1,3 mannosyltransferases which are thought to be important for *C. glabrata* virulence due to their role in cell wall biogenesis (Dujon, 2010). YGOB searches identified members of the *YPS* cluster as well as phosphate starvation inducible acid phosphatases (*PMU* genes) which are associated with adaptation and survival in the mammalian host niche (Kaur *et al.*, 2007; Orkwis *et al.*, 2010). Thus the search approaches were validated for the identification of *C. glabrata* ORFs with no *S. cerevisiae* orthologue as a means for exploring *C. glabrata* ORFs which may contribute to virulence.

Despite both search approaches identifying *C. glabrata*-specific genes which are implicated in virulence, both search results yielded different numbers of non-orthologous *C. glabrata* ORFs with RBH searches identifying twice the

number of ORFs identified by YGOB (Figure 3.4). Indeed, many *C. glabrata* ORFs identified by RBH searches have orthologues according to YGOB. Further to this, the two ORF lists have a surprisingly small overlap of 197 genes (Figure 3.4). Large numbers of genes were selected by one search method only – demonstrating the variability between the two methods and highlighting the need for more stringent search methods when defining orthologous gene pairs between two related species. The stark difference in defining *C. glabrata* ORFs with no orthologue in *S. cerevisiae* is likely due to the different search methods, criteria and stringency used by the two approaches. For example, YGOB incorporates annotation of orthologous genes from the literature, annotation from automated BLASTP searches as well as manual editing for comparisons of orthologous genes from related species (ygob.ucd.ie; Byrne & Wolfe, 2005). In contrast, RBH searches relied solely on sequence comparison methods provided by automated BLASTP searches, likely resulting in much less stringent search results compared with that of the YGOB database which curates data from a number of resources. In addition, filters applied in RBH searches likely limited the identification of orthologous gene pairs in *S. cerevisiae* and *C. glabrata*. For example, in instances where conservation of a functional domain only is required to retain orthologous gene function, the filters (30 % sequence identity within a minimum of 50 % of the protein sequence) would have excluded the identification of orthologous ORF due to the conserved domain representing less than 50 % of the protein sequence. As a consequence, RBH search approaches identified many *C. glabrata* ORFs which have an *S. cerevisiae* orthologue to be non-orthologous. However, *C. glabrata* ORFs identified in searches which do have *S. cerevisiae* orthologues may be interesting candidates for study since orthologous genes may not encode the same function and may have undergone functional reassignment over evolutionary time.

During the course of this study, Desai *et al.*, (2011) published work in which they identified 337 *C. glabrata* ORFs with no *S. cerevisiae* orthologue using genome-wide searches based on protein sequences from the Génolevures database (Sherman *et al.*, 2009) and statistical algorithmic consensus clustering methods to compare protein families from the two species (Desai *et al.*, 2011). The number of *C. glabrata* ORFs identified by Desai *et al.*, (2011) much more

closely resembles that of YGOB, suggesting that the true number of *C. glabrata* ORFs with no *S. cerevisiae* orthologues is likely to be between 297 and 337. Through the study of *C. glabrata*-specific ORFs, Desai *et al.*, (2011) continued to identify and characterise two novel *C. glabrata* ORFs which interact and contribute to adhesion of *C. glabrata* cells to human endothelial cells. Thus, this further supports the focus on *C. glabrata* ORFs with no orthologue in *S. cerevisiae* as a valid approach in the search for novel *C. glabrata* virulence attributes.

Chromosomal location mapping of *C. glabrata* ORFs identified to have no *S. cerevisiae* orthologue by RBH searches revealed 10 significant clusters of *C. glabrata*-specific ORFs throughout the genome (Figure 3.3). However the location of clusters showed no trend towards either centromeric or telomeric localisation. This is contrary to a number of studies where it has been observed that virulence-associated genes of various pathogens are often associated with the subtelomere (Horn & Barry, 2005; Duraisingh *et al.*, 2006) as is also the case for *C. glabrata* adhesins (De Las Peñas *et al.*, 2003). In addition, no significant enrichment of the 727 *C. glabrata* ORFs identified by RBH searches were found on any particular chromosome. However, the lack of significant clustering at specific locations in on the chromosome could be an artefact of the broad nature of RBH searches including many *C. glabrata* genes which do have orthologues. Chromosomal location studies of smaller, more stringent lists of *C. glabrata* ORFs may reveal more significant data on the location patterns of *C. glabrata*-specific ORFs throughout the *C. glabrata* genome.

3.4.2 HGT and the Acquisition of Prokaryotic Genes by *C. glabrata*

Sequence comparison searches and phylogenetic analysis identified three possible HGT events from prokaryotes to *C. glabrata*. Analysis detected the putative transfer of an aspartate racemase (*CAGL0D01210g*) from species of the Firmicute phylum (Figure 3.5), an acetyl transferase (*CAGL0K11066g*; Figure 3.6) and an NADPH dehydrogenase (*CAGL0M014091g*) putatively acquired from Proteobacteria or Actinobacteria species (Figure 3.7). Transfer of *CAGL0K11066g* and *CAGL0M014091g* from Prokaryotes may have occurred prior to divergence of *C. glabrata* from closely related *Naumovozyma* species since sequences from these species cluster together in phylogenetic trees

(Figures 3.6 and 3.7) whereas acquisition of *CAGL0D01210g* seems to have occurred solely in *C. glabrata* (Figure 3.5). Although many examples of horizontal gene transfer from prokaryotes to Ascomycetous fungi exist, *C. glabrata* ORFs acquired by HGT as yet remain uncharacterised (Marcet-Houben & Gabaldón, 2010).

The acquisition of prokaryotic genes by fungi has previously been associated with the adaptation to a new host niche. As an example, HGT of an endoglucanase enzyme from rumen bacteria *Fibrobacter succinogenes* to fungi *Orpinomyces joyonii* has enabled the latter species to degrade cellulose and other plant polysaccharides, thus allowing *O. joyonii* to establish a new niche in the rumen of herbivorous animals where cellulose is in abundance as a nutritional source (Garcia-Vallvé et al., 2000). Thus, it is possible that the horizontal gene transfer of prokaryotic ORFs could contribute to the adaptation of *C. glabrata* to a host niche.

Of particular relevance to *C. glabrata* adaptation could be the acquisition of an aspartate racemase (*CAGL0D01210g*) from the Firmicutes, in particular the *Lactobacilli* species. Despite phylogenetic analysis in this work lacking strong statistical support, a large scale study of inter-domain HGT events into fungi from prokaryotes by Marcet-Houben & Gabaldón, 2010, also presented evidence for the horizontal gene transfer of an aspartate racemase (*CAGL0D01210g*) from bacteria to *C. glabrata*. Aspartate racemase enzymes are universal in prokaryotes and archaea. They catalyse the conversion of L-aspartate to D-aspartate which is a constituent in the peptidoglycan layer of the bacterial cell wall (Yoshimura & Esaki, 2003). Although it is unclear what physiological role an aspartate racemase would play in *C. glabrata* (see 4.3.2), the observation of an acquired racemase enzyme is consistent with similar transfer events of racemases from prokaryotes to fungi in the literature. Marcet-Houben & Gabaldón, 2010, identified seven instances of HGT from bacteria to *Fusarium*, *Aspergillus* and *Candida* species involving three racemases which target enantiomers of aspartate, hydantoin and mandelate as substrates. Prior to this, the horizontal transfer of a proline racemase from Proteobacteria to *Candida parapsilosis* was also reported (Fitzpatrick et al., 2008). It has been proposed that aspartate racemases acquired by fungi could detoxify or

assimilate D-isomers of amino acids found in bacterial cell walls or host tissues (Marcet-Houben & Gabaldón, 2010). Indeed, characterisation of an alanine racemase acquired from Proteobacteria by the fission yeast *S. pombe* found that the heterologous expression of this enzyme in *S. cerevisiae* remediated D-alanine toxicity and enabled *S. cerevisiae* to assimilate D-alanine as a sole nitrogen source as is the case in *S. pombe* (Uo *et al.*, 2001). The frequent occurrence of such transfers of bacterial racemase enzymes to fungal species such as *C. glabrata* suggests it could confer a growth advantage in a competitive environment such as the host niche perhaps by reducing the cytotoxicity and allowing the assimilation of D-amino acid isomers encountered in the microflora of the host niche.

It is also unclear what physiological role a putative acetyl transferase (*CAGL0K11066g*) or NADPH dehydrogenase (*CAGL0M014091g*) may have in *C. glabrata* (see 4.3.2). Interestingly, expression of *CAGL0M014091g* was found to be upregulated in an azole-resistant strain of *C. glabrata* (Vermitsky *et al.*, 2006), perhaps linking the acquisition of this ORF to drug resistance. However, further investigation is required to verify that these ORFs were in fact acquired through horizontal gene transfer events. Although outgroups of the most similar *S. cerevisiae* sequences showed these ORFs to be more closely related to bacterial sequences with high confidence, bootstrap support within the branches of bacterial sequences was low in many instances.

3.4.3 Generation of a *C. glabrata* Deletion Library as a Molecular Tool for the Functional Characterisation of *C. glabrata* ORFs

In this work, a deletion library of 65 *C. glabrata* deletion mutants was generated and verified (Appendix 4 Table 1), contributing to an existing collection of 700 *C. glabrata* deletion mutants (Schwartzmüller *et al.*, 2013; Appendix 13). *C. glabrata* ORFs of interest were selected for deletion according to a set of criteria based on bioinformatic search results. ORFs were selected based on their lack of an *S. cerevisiae* orthologue (as identified by RBH and YGOB searches) and functional annotation of the encoding protein (CGD or predicted functional domains using InterProScan). ORFs suspected to have been acquired by HGT were also included. Fusion constructs targeting 100 *C. glabrata* ORFs were constructed, of which 65 were successfully transformed and verified for correct

integration in *C. glabrata* (Appendix 4 Table 1). However, 35 fusion constructs were not successfully transformed into *C. glabrata* (Appendix 4 Table 2). Although it was not further explored it is possible that some ORFs could be essential in *C. glabrata*, although it is unlikely this is true of all 35 ORFs for which constructs were made. Some constructs conferred ARS mutations in *C. glabrata* hence in future work, shortening of the ORF sequence included within the construct could remediate ARS mutations observed.

The methodology chosen to construct the *C. glabrata* deletion library makes it amenable to a number of downstream applications. Similarly to the *S. cerevisiae* mutant collections, the incorporation of unique DNA barcodes into each *C. glabrata* deletion mutant allows each mutant to be detected within a mixed population of strains (see 1.3.1.1). To facilitate the ease with which barcode tags can be retrieved from pools of mutants, the tags were designed to be flanked by sequences universal to all strains to allow the amplification of all barcode tags in one PCR reaction. Molecular barcoding has proven a valuable tool in the *S. cerevisiae* deletion collections (see 1.3.1.1) and has particular implications in virulence screens where the ability to pool mutants greatly reduces the number of animals required. Also, flippase recognition target sites were incorporated into the deletion constructs to allow the removal and recycling of the resistance cassette in further genetic manipulations. Deletion mutants from this study contribute to an existing library of over 700 *C. glabrata* deletion mutants previously constructed by the Haynes lab and collaborating groups (Schwartzmüller *et al.*, 2013; Appendix 13) and provides a lasting community tool for the functional characterisation of *C. glabrata*-specific ORFs (see Chapter 4).

Chapter 4: Functional characterisation of the *C. glabrata* deletion library

4.1 Overview

A *C. glabrata* deletion library of 65 unique gene deletions was constructed (see 3.3.8) to serve as a molecular tool for the study of *C. glabrata* ORFs with no orthologue in *S. cerevisiae*. It was hypothesised that the study of *C. glabrata* ORFs with no orthologue in *S. cerevisiae* may elucidate *C. glabrata* virulence determinants (see 3.1). Thus, a number of assays will be used to functionally characterise *C. glabrata* deletion mutants with particular emphasis on processes relevant to infection.

4.1.1 Deletion Libraries and Chemical-Genetic Screening

Deletion collections have previously provided a powerful tool in the functional annotation of uncharacterised ORFs in the model yeast *S. cerevisiae* (Giaever *et al.*, 2002; Fabrizio *et al.*, 2010; see 1.3.1) and fungal pathogens such as *C. albicans* (Noble *et al.*, 2010) and *C. neoformans* (Liu *et al.*, 2008). Recently, targeted gene deletion and phenotypic screens have proven a successful strategy for characterisation studies in *C. glabrata* (Schwarz Müller *et al.*, 2013; Appendix 13). For fungal pathogens entering the host environment, strain fitness is an important virulence attribute. Altered strain fitness can affect the ability of strains to replicate within the host and influence the physiological robustness of invading pathogens in the diverse host niches they inhabit. In *C. albicans*, for example, homozygous deletion mutants with decreased growth phenotypes such as the $\Delta ssn6/\Delta ssn6$ strain (Homann *et al.*, 2009) have been associated with decreased virulence in a murine model system of infection (Hwang *et al.*, 2003). In *S. cerevisiae*, fitness profiling of the homozygous deletion collection identified gene products important for growth (Giaever *et al.*, 2002). Furthermore in a recent study, fitness scoring of a *C. glabrata* mutant collection identified 71 strains with fitness defects and thus their encoded gene products were required for growth (Schwarz Müller *et al.*, 2013; Appendix 13). However, their effect on virulence is as yet unexplored.

Chemogenomic screens of deletion mutants have been used to uncover the functional relationships between genes and stresses induced by chemicals (Wuster & Babu, 2008). Characterisation of previously unstudied genes can be achieved through phenotypic screening by identifying conditions under which genes are required for growth (see 1.3.1.2). In particular, chemogenomic screening can be used as a tool to identify components of stress response pathways or identify gene products required for survival under conditions relevant to the human host niche. For example genes required for osmotic and oxidative stress adaptation, tolerance to changes in pH, iron limitation or antifungal drug susceptibility (Giaever *et al.*, 2002; Homann *et al.*, 2009). High-throughput phenotypic screening of the *S. cerevisiae* deletion libraries has validated the power of chemogenomic screening in the functional annotation of uncharacterised genes. For example, *S. cerevisiae* deletion mutants of uncharacterised genes *YGR182C*, *GSC1* and *YDL023C* were found to confer osmosensitivity despite no previous association with the osmotic stress response (Giaever *et al.*, 2002). Similarly, chemical-genetic screening of the *C. glabrata* deletion library lead to the identification of osmosensitive *C. glabrata* deletions $\Delta atm1$, $\Delta arb1$, $\Delta kre1$, $\Delta anp1$, $\Delta mps3$ and $\Delta ptr3$ which had not been previously linked to the osmotic stress response in related fungal species (Schwartzmüller *et al.*, 2013; Appendix 13).

4.1.2 Models of *Candida* Biofilm Formation and Virulence

Biofilm formation by *Candida* species has been recognised as an important virulence factor (Silva *et al.*, 2011; see 1.5.2) and in *C. glabrata*, biofilm formation is primarily mediated by members of the Epa family, a family of *C. glabrata* adhesins with no orthologue in *S. cerevisiae* (Kaur *et al.*, 2005). In agreement with the importance of biofilm formation for *C. glabrata* infection, derepression of major biofilm adhesins Epa6 and Epa7 resulted in hypercolonisation of murine kidneys (Castaño *et al.*, 2005). Two previous studies assessed the biofilm-forming ability of *C. glabrata* mutant collections, identifying mutants with both increased and decreased biofilm-forming capacity (Iraqi *et al.*, 2005; Schwartzmüller *et al.*, 2013; Appendix 13). Thus far only few *EPA* adhesins and components of the subtelomeric silencing machinery have been implicated in the regulation of biofilm formation by *C. glabrata*. The role of *C. glabrata* ORFs with no orthologue in *S. cerevisiae* in biofilm formation

remains relatively unexplored. Thus this work aims to increase our understanding of *C. glabrata* ORFs implicated in biofilm formation through screening of a *C. glabrata*-specific deletion library. Indeed, high-throughput screening of *C. albicans* deletion mutants for biofilm formation was highly successful in facilitating our understanding of the underlying regulatory circuitry governing biofilm formation in this species (Nobile *et al.*, 2012).

Various murine models of *C. glabrata* infection have been exploited to study the virulence of *C. glabrata* mutants, facilitating the identification of factors which contribute to pathogenesis. For example, previous studies have implicated *PDR1* (*CAGL0A00451g*), encoding a major regulator of drug resistance; *SKN7* (*CAGL0F09097g*), encoding a regulator of the oxidative stress response; and *YPS* genes in pathogenesis (Kaur *et al.*, 2007; Ferrari *et al.*, 2009; Saijo *et al.*, 2010). However, mammalian host models are restricted to either the study of groups of pooled mutants or the individual study of small numbers of strains. As a consequence, they are not amenable to high throughput screening of individual strains from large deletion collections. Thus, a need for alternative models of *Candida* infection has been recognised. A comprehensive study exploited a chicken embryo model for the study of *C. albicans* and *C. glabrata* infection via the chorio-allantoic membrane, demonstrating the ability of *C. glabrata* to colonise deep tissues despite causing low levels of mortality (Jacobsen *et al.*, 2011). The use of non-mammalian models of infection has also been explored since these hosts are available in large numbers, are less labour intensive and avoid ethical issues surrounding the use of mammalian hosts. Thus these host models are amenable to higher throughput virulence studies of yeast strain collections. *Galleria mellonella* larvae have become an established infection model for pathogenic yeasts such as *Candida* species (Cotter *et al.*, 2000; Brennan *et al.*, 2002). However, infection by injection of *C. glabrata* cells into the larval haemolymph resulted in zero mortality thus eliminating this host as a viable insect model for pathogenicity of *C. glabrata* isolates (Cotter *et al.*, 2000). Recently, *Drosophila melanogaster* was introduced as a model for gastrointestinal infection by *C. albicans*. Infection by feeding or injection of *C. albicans* cells was able to activate systemic immunity via the Toll pathway (Figure 4.1 B) in larvae and induce antimicrobial peptide production (Glittenberg *et al.*, 2011 A). In addition, the ready availability and ease of

working with large sample sizes of *D. melanogaster* larvae increases the suitability of this host for virulence studies of deletion mutant collections. *D. melanogaster* provides a biologically relevant model for mammalian infection due to the presence of two major immune signalling pathways in *D. melanogaster*, the Toll and Immune deficiency (IMD) pathways, which are homologous to mammalian Toll-like receptor and tumour necrosis factor pathways (Figure 4.1 & 4.2; Wang & Ligoxygakis, 2006; Kounatidis & Ligoxygakis, 2012). In agreement, survival measurements of *D. melanogaster* larvae following infection with 15 *C. albicans* mutants correlated well with pathogenicity reports for these isolates in infection models in a murine host (Glittenberg *et al.*, 2011 B), validating *D. melanogaster* as a suitable host for large scale *Candida* virulence studies.

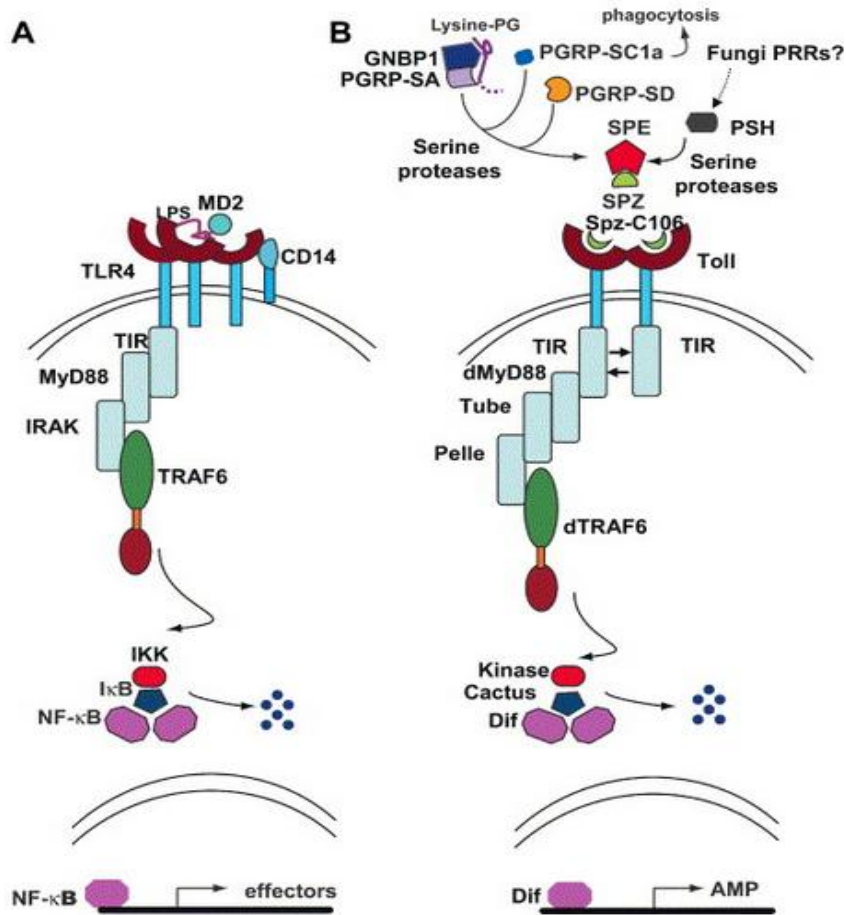


Figure 4.1 Comparison of homologous mammalian TLR4 and *D. melanogaster* Toll pathway (Wang & Ligoxygakis, 2006). A) Presentation of PAMPS (such as LPS) to TLR4 activates interactions between the TLR4 TIR domain and MyD88 and recruitment of IRAK. IRAK interaction with TRAF6 activates the IKK complex which phosphorylates inhibitor IκB. IκB is targeted for degradation leaving NF-κB free to translocate to the nucleus and activate transcription of its targets. B) Activation of Toll-ligand Spaeztle (Spz) is achieved by two protease cascades stimulated by either Gram+ bacterial or fungal PAMPs. Active Spz binds cleaved C-106. Upon interaction with C-106, Toll proteins dimerize and interact with dMyD88 through dimerized TIR domains. dMyD88 recruits Tube which activates Pelle. Pelle signals through dTRAF6 to activate an unknown Cactus kinase. Cactus is phosphorylated and targeted for degradation and Dif translocates to the nucleus activating the transcription of its targets.

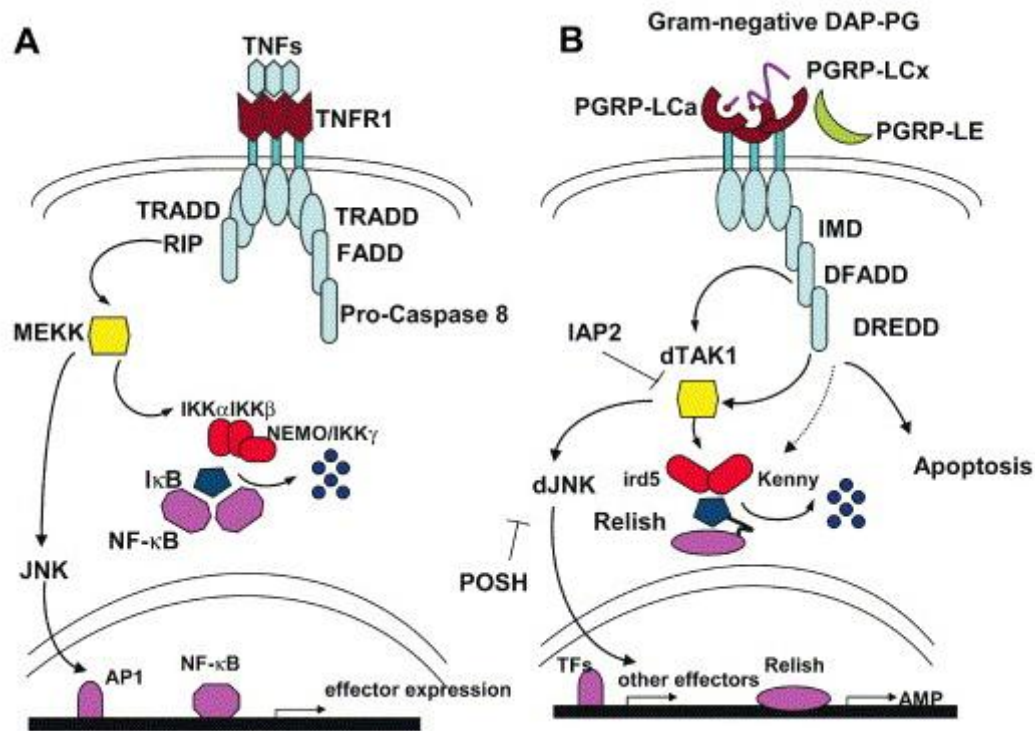


Figure 4.2 Comparison of mammalian TNFR-1 pathway and *D. melanogaster* IMD pathway (Wang & Ligoxygakis, 2006). A) Upon stimulation of TNFR1, TRADD (TNFR-associated death domain) is recruited which forms a signalling complex with RIP (receptor interacting protein) and FADD (Fas-associated death-domain protein). RIP activates MEKK kinase which activates the IKK α , IKK β , IKK γ /NEMO complex leading to the phosphorylation of I κ B. I κ B is targeted for degradation, releasing NF- κ B to translocate to the nucleus and activate its transcriptional targets. B) Recognition of peptidoglycan from Gram negative bacteria results in dimerisation of LC isoforms of peptidoglycan recognition proteins (PGRP). DFADD is recruited to the intracellular domain of PGRP by IMD and interacts with DREDD. DREDD signals through dTAK1 to activate the IKK complex (Ird5 & Kenny (or Key)), releasing inhibition of Relish. Relish translocates to the nucleus to regulate transcription of its target genes.

4.1.3 Aims

- 1) Assess the impact on fitness conferred by deletion of *C. glabrata* ORFs with no orthologue in *S. cerevisiae*.
- 2) Develop a high-throughput phenotypic screening platform to functionally characterise deleted *C. glabrata* ORFs and identify conditions under which ORFs are required for *C. glabrata* growth.

- 3) Investigate the impact of deletion of *C. glabrata* ORFs with no orthologue in *S. cerevisiae* on biofilm formation.
- 4) Utilise a *D. melanogaster* gastrointestinal infection model of *C. glabrata* infection to identify *C. glabrata* deletion mutants with altered virulence.

4.2 Materials & Methods

4.2.1 Phenotypic Screening

4.2.1.1 High-throughput Phenotypic Screening of *C. glabrata* Mutants

C. glabrata mutants were arrayed into a 96-well plate and stored as glycerol stocks at -80 °C. Glycerol stocks were used to inoculate 200 µl YPD NAT in a fresh 96-well plate and grown overnight at 30 °C. Overnight cultures were diluted by a factor of 10 in sterile water and distributed in quadruplicate into a 384 well plate. For example, cells from well A1 of the 96-well overnight were transferred into wells A1, A2, B1 and B2 of the 384-well plate and so forth. Cells were pinned from the 384-well plate onto YPD agar plates containing defined chemical agents (Appendix 2 Table 1) using a ROTOR HDA[®] robot (Singer Instruments) and incubated at 30 °C (unless stated otherwise) for 2-5 days. Images of colonies were acquired in a Syngene G:BOX and analysed for phenotypes. For example, if a mutant showed decreased fitness when grown on a given chemical compared with the YPD control plate, it was noted “sick”. Further, if a deletion was unable to grow on a given chemical but showed no fitness defect on YPD, it was noted “lethal”.

4.2.1.2 Serial Dilution of *C. glabrata* Mutants

The optical density (OD₆₀₀) of *C. glabrata* overnight cultures was measured in a Jenway 7305 spectrophotometer. Cells were then diluted in sterile water to OD₆₀₀ 0.1 (approximately 10⁶ cells per ml). 100 µl of cells were transferred into well A1 of a 96-well plate from which 10 µl were taken and transferred to well A2 containing 90 µl sterile water as such forming a 10-fold dilution. This step was repeated across a further four wells producing six 10-fold serial dilutions of *C. glabrata* cells in water. Using a multichannel pipette, 4 µl of cells were transferred from the 96-well plate and spotted onto YPD agar plates containing defined chemicals and incubated at 30 °C (unless otherwise specified) for 48 hours. Images of serial dilutions were acquired in a Syngene G:BOX and

analysed for phenotypes by comparison of growth to a YPD control and the parental strain.

4.2.2 Growth Analysis of *C. glabrata* and *S. cerevisiae* Strains

The optical density (OD₆₀₀) of *C. glabrata* overnight cultures was measured in a Jenway 7305 spectrophotometer. Accordingly, cells were diluted into fresh YPD broth to OD₆₀₀ 0.1 (approximately 10⁶ cells per ml). 100 µl cells were distributed into a flat bottomed 96-well plate, covered with a sterile transparent film and placed into the VersaMax™ Absorbance Microplate Reader pre-warmed to 30 °C. Optical density (OD₆₀₀) readings were taken at 10 minute intervals over a 48 hour period, with shaking between reads.

Three measures of fitness were taken from *C. glabrata* and *S. cerevisiae* growth profiles. Lag time was measured as the time taken for cultures to reach an OD₆₀₀ of 0.2 following inoculation. Doubling times T_d were calculated according to the following formula, whereby q₁ and q₂ represent OD₆₀₀ measurements at time points t₁ and t₂, respectively, for cells in exponential phase (approximately OD₆₀₀ 0.4 to 0.8):

$$Td = (t_2 - t_1) \times \left(\frac{\log(2)}{\log\left(\frac{q_2}{q_1}\right)} \right)$$

Final density was taken as the OD₆₀₀ of cultures at 24 hours. Statistical analysis of *C. glabrata* growth profiles was performed using ANOVA, followed by Dunnett's test using the following formula whereby M_i denotes the mean of the experimental group, M_c represents the mean of the control group, MSE represents mean square error and nh denotes the harmonic mean:

$$D = \frac{M_i - M_c}{\sqrt{2MSE/nh}}$$

4.2.3 Quantification of *C. glabrata* Biofilm Formation

The ability of *C. glabrata* mutants to form biofilms was quantified using an enzymatic method adapted from Iraqui *et al.* (2005) in which the metabolic activity of cells adhered to a polystyrene plate was quantified by XTT reduction.

C. glabrata cells were grown overnight to stationary phase in SC at 37 °C, 180 rpm. Cells were washed in sterile water and resuspended in SC to OD₆₀₀ of 1. 100 µl of the cell suspension was distributed into individual wells of a flat bottomed 96-well polystyrene plate and incubated at 37 °C for 24 hours. To remove loose cells, the biofilms were washed three times with sterile water and once with PBS. 100 µl XTT-menadione solution (0.5 mg/ml XTT in PBS, 1 µM menadione) was added to each well. After incubation for 1 hour at 37 °C in the dark, XTT reduction was measured in a VersaMax™ Absorbance Microplate Reader at 472 nm.

4.2.4 *Drosophila melanogaster* Gastrointestinal Infection Model

A single *C. glabrata* colony was picked to inoculate 10 ml YPD broth and grown overnight at 30 °C, 180 rpm. Cells were harvested by centrifugation at 3,000 rpm for 5 minutes. 200 µl of *C. glabrata* pellet was transferred into a microcentrifuge tube to which 400 µl mashed banana and 50 5-day-old *Drosophila* larvae were added and mixed. Microcentrifuge tubes were sealed with foam bungs and left for the *Drosophila* to feed for 30 minutes at room temperature. Larvae were then transferred to fresh fly bottles and incubated at 30 °C for 48 hours. Larvae survival counts compared to uninfected larvae were used as a read-out for *C. glabrata* virulence. To assess *Drosophila* Toll pathway activation, GFP expression in Dros-GFP larvae were viewed using a Nikon ECCLIPSE TE2000-U inverted microscope. Virulence assays were performed jointly by Dr. Ilias Kounatidis, University of Oxford, and Lauren Ames, University at Exeter.

4.3 Results

4.3.1 Growth Profiling of *C. glabrata* Deletion Mutants

Following the generation of a *C. glabrata* deletion library (see 3.3.8), fitness profiling was performed on all *C. glabrata* strains to assess the contribution of *C. glabrata* ORFs with no orthologue in *S. cerevisiae* for fitness. Fitness profiles were generated for 64 of 65 *C. glabrata* deletion mutants in YPD broth at 30 °C (Appendix 8 Figures 1-64). Fitness profiles for *CAGL0A03608g* were inconsistent and thus were excluded from the liquid growth study. Where available, two independent isolates of each mutant were tested, yielding a total of 118 fitness profiles for *C. glabrata* mutants. Strain fitness was quantified

using three independent measures taking into account different aspects of the profiles: lag phase, doubling time and maximum density (see 4.2.2). Comparison of measures from fitness profiles identified instances where deletion of a given *C. glabrata* ORF gave rise to either reduced or increased fitness with that of parental strain Cg2001 $\Delta his3$ (Appendix 7 Table 1).

Firstly, the lag phase of *C. glabrata* mutants was measured (see 4.2.2). Deletion of 21 *C. glabrata* ORFs yielded a lag phase significantly increased or reduced compared with that of the parental strain Cg2001 $\Delta his3$ (ANOVA, $p=2.9e-222$). Within this cohort, 14 deletion strains yielded an extended lag phase whilst seven deletion strains showed a reduction in lag (Appendix 7 Table 1). For example, the lag time of *C. glabrata* $\Delta CAGL0D03850g$ isolates were increased up to 75 minutes (Appendix 7 Table 1; Appendix 8 Figure 16), normalised to parental strain controls. In contrast, the lag phase of $\Delta CAGL0G10175g$ isolates was reduced by 107.5 minutes (Appendix 7 Table 1; Appendix 8 Figure 37). Secondly, the doubling time of deletion mutants was measured from cultures in the exponential growth phase (approximately OD_{600} 0.4 to 0.8). A significant increase in doubling time was observed for 11 *C. glabrata* deletion mutants (Table 4.1) normalised to the parental strain (ANOVA, $p=6.8e-240$). However, no deletion strains yielded a reduced doubling time (Appendix 7 Table 1). Lastly, the maximum cell density of saturated *C. glabrata* cultures was measured 24 hours post inoculation. *C. glabrata* $\Delta CAGL0D04565g$ was the sole strain to show a significantly reduced final density (ANOVA, $p=2.99e-25$), becoming saturated at an optical density (OD_{600}) 0.34 lower than that of parental strain Cg2001 $\Delta his3$ (Table 4.1).

Within the subset of *C. glabrata* deletion mutants showing significantly altered fitness in rich media, the majority scored distinct growth defects in one fitness measure only. For example, *C. glabrata* $\Delta CAGL0K10318g$ had a pronounced increase in lag phase yet showed no significant variation in doubling time or maximum culture density (Appendix 7 Table 1; Appendix 8 Figure 51). Significant deviation in fitness by at least two growth measurements were observed in 12 *C. glabrata* isolates corresponding to seven individual gene deletions (Table 4.1). Interestingly, this subset includes two computationally identified adhesins, encoded by *CAGL0E00275g* and *CAGL0G10175g*,

designated *EPA20* and *AWP6* (de Groot *et al.*, 2008). Of all isolates tested, *C. glabrata* Δ CAGL0A04565g showed the most notable reduction in fitness (Figure 4.3), scoring significant growth defects in all fitness measures. The lag phase for Δ CAGL0A04565g was extended by 110 minutes and the doubling time was increased approximately 2-fold that of the parental strain (Table 4.1). Furthermore, Δ CAGL0A04565g yielded a significantly lower final cell density compared with the parental strains.

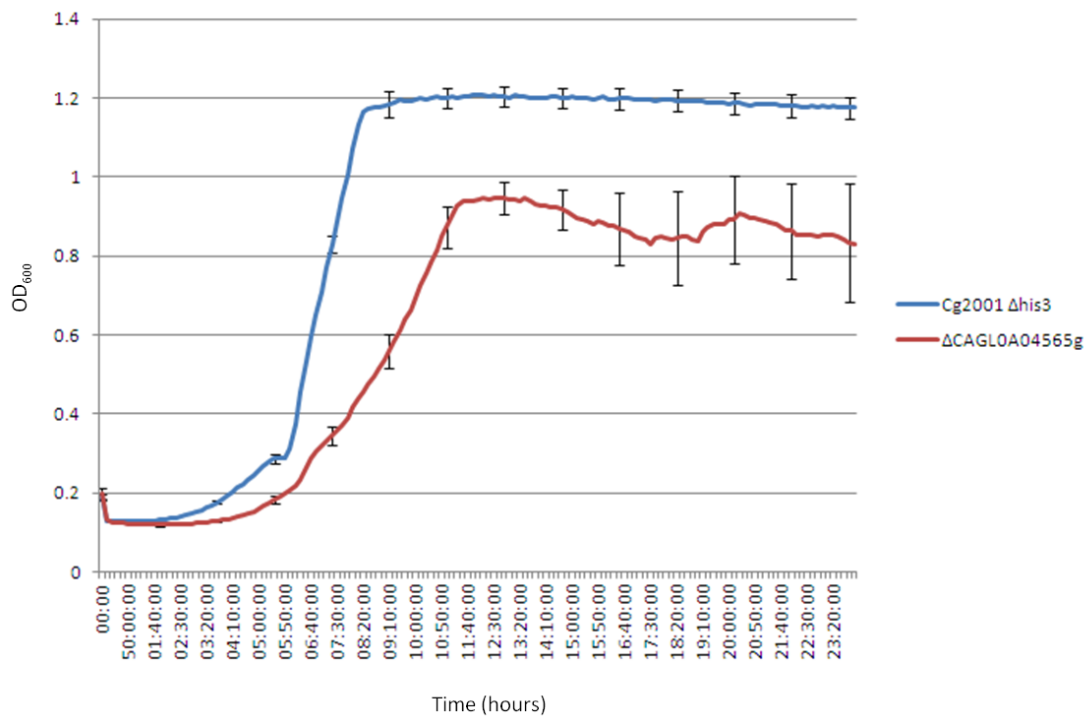


Figure 4.3 Growth profiles of *C. glabrata* Δ CAGL0A04565g and parental strain Cg2001 Δ his3. Cultures of *C. glabrata* Δ CAGL0A04565g and Cg2001 Δ his3 at OD₆₀₀ 0.1 in YPD were transferred to a 96-well microtitre plate and growth was measured every 10 minutes over a 24 hour period at 30 °C with continuous shaking between reads. Blue and red lines represent the average optical density of replicate Cg2001 Δ his3 and Δ CAGL0A04565g cultures, respectively. Error bars denote the standard deviation across replicates.

Table 4.1: *C. glabrata* mutants with altered fitness. Table summarises seven *C. glabrata* mutants for which fitness significantly deviated from the parental strain in a minimum of two fitness measures (ANOVA $p < 2.99e-25$, Dunnett's critical value 3.37). *S. cerevisiae* orthologues and predicted functional domains for *C. glabrata* ORFs are stated (yjob.ucd.ie; ebi.ac.uk/interpro/). All values indicate a significant change in each measurement compared to parental strain Cg2001 $\Delta his3$. Lag time (minutes) the time taken for deletion strains to reach exponential growth at a threshold OD_{600} 0.2. Doubling time (minutes) was measured as the maximum growth rate during exponential phase. Maximum density (OD_{600}) indicates the final yield of cultures in saturation, 24 hours post inoculation. Fitness measures which did not significantly deviate from the parental strain are marked with an asterisk (*).

<i>C. glabrata</i> isolate	<i>S. cerevisiae</i> orthologue	Functional domain	Change in lag time (minutes)	Change in doubling time (minutes)	Change in maximum density (OD_{600})
$\Delta CAGL0A04565g A$	<i>SWI4</i>	APSES-type DNA-binding domain	+110.00	+109.03	-0.3452
$\Delta CAGL0E00275g A$	-	PA14; GLEYA adhesin domain	+63.33	+11.80	*
$\Delta CAGL0F05159g A$	<i>VPS72</i>	YL1 Nuclear	+28.00	+21.94	*
$\Delta CAGL0F05159g B$			+21.67	+18.87	*
$\Delta CAGL0F08767g A$	-	-	-20.00	+23.50	*
$\Delta CAGL0F08767g B$			-22.50	+15.34	*
$\Delta CAGL0G04279g A$	-	Alpha mannosyl-transferase	-20.00	+14.71	*
$\Delta CAGL0G04279g B$			-16.67	+17.28	*
$\Delta CAGL0G05522g A$	-	-	40.00	+121.52	*
$\Delta CAGL0G05522g B$			44.00	+109.38	*
$\Delta CAGL0G10175g A$	-	-	-48.00	+20.90	*
$\Delta CAGL0G10175g B$			-107.50	+22.24	*

4.3.2 High-throughput Phenotypic Screening of *C. glabrata* Deletion Mutants

An automated, high-throughput phenotypic screening platform was optimised for the functional characterisation of *C. glabrata* strains. *C. glabrata* mutants were tested for growth on 61 conditions targeting a range of cellular structures and processes, singly or in combination (Table 4.2). Colony growth of strains in response to screening conditions was used as a phenotypic read-out for fitness. In addition to the library of 65 *C. glabrata* deletion mutants generated in this study (see 3.3.8), 67 *C. glabrata* deletion mutants and parental strain Cg2001 Δ HTL from a previous study (Schwartzmüller *et al.*, 2013; Appendix 13) were also screened due to their lack of an obvious *S. cerevisiae* orthologue in reciprocal best hit (RBH) searches (Appendix 9 Table 1; see 3.3.1). Previous phenotypic screening of these mutants included 5 screening conditions only. Together, a total of 132 individual *C. glabrata* gene deletion mutants were phenotypically screened on 61 conditions in a minimum of three biological replicates. Where available, two independent isolates of each deletion mutant were phenotypically screened to ensure phenotypes were not due to second site mutations. Initial screens identified a growth defect for *C. glabrata* Δ CAGL0A04565g on rich broth (Figure 4.3). Furthermore, Δ CAGL0A04565g growth was inhibited on all phenotypic screening conditions.

Table 4.2: Phenotypic screening conditions and the associated functional implications of phenotypes (Hampsey, 1997; Ram & Klis, 2006; Kaloriti *et al.*, 2012). The total number of *C. glabrata* deletion mutants with phenotypes corresponding to each functional category are stated. All screens were performed on YPD agar in biological triplicate and incubated at 30 °C unless otherwise stated.

Functional implication	Screening condition	No. of mutants displaying phenotype
Reduced fitness on rich media	YPD, SC	2
General protein defect	Reduced temperature (4 °C and 16 °C), Increased temperature (42 °C), Heat shock (55 °C), Ethanol	5
pH sensitivity, defective vacuole function	pH 3	1
Respiratory deficiency; inability to produce respiratory-competent mitochondria	Glycerol	0
Sensitivity to divalent cations and heavy metals; altered expression of membrane ATPases.	LiCl, ZnCl ₂ , CdCl ₂ , CoCl ₂ , BaCl ₂ , FeCl ₂ , CsCl, KCl, NaCl, MnCl ₂ , CaCl ₂ , CuSO ₄ , MgCl ₂ , CuCl ₂ , Arsenic (III) oxide, Sodium metaarsenite	15
Defect in components of MAP kinase signalling pathways	Caffeine	4
Osmotic sensitivity	Sorbitol, NaCl	0
Deficiency in the utilisation of non-glucose carbon sources.	Carbon source: Lactose, Starch, Galactose, Raffinose, Xylose, Sodium acetate, Ethanol, Sorbitol, Glycerol, Sucrose, Maltose, Trehalose	1
Defective DNA damage repair	UV light, MMS	4
Defective DNA replication	Hydroxyurea	1
Sensitivity to oxidative stress	tBOOH, H ₂ O ₂ , Menadione	0
Sensitivity to combinatorial stress	H ₂ O ₂ + NaCl, H ₂ O ₂ + 42 °C	3
Defective microtubule formation	Benomyl	0
Defective sterol biosynthesis	Nystatin	1
Defective protein glycosylation; secretory defects	Sodium orthovanadate	1
Defective in cell wall biosynthesis	Calcofluor white, Congo red, SDS	9
Defects in protein synthesis and cell cycle	Cycloheximide	1
Deficient iron uptake	BPS	0
Susceptibility to antifungal drugs	Casposfungin, Fluconazole	3

Screens identified 22 *C. glabrata* deletion mutants (Table 4.2; Table 4.3) with growth altered from that of the parental strain on at least one screening condition. Phenotypes of *C. glabrata* mutants occurred on 29 of 61 screening conditions. In total, 110 *C. glabrata* deletion mutants displayed no observable growth phenotype on any tested condition. In particular, no phenotypes were observed for bioinformatically identified horizontal gene transfer ORFs *CAGL0D01210g*, *CAGL0K11066g* and *CAGL0M14091g* (see 3.3.4). For analysis, screening conditions were grouped according to the functional implications of associated phenotypes (Table 4.2). The largest number of phenotypes was found in the group encompassing metal and metalloid compounds on which 15 *C. glabrata* mutants showed phenotypes (Table 4.2; Table 4.3). Second to this, nine *C. glabrata* mutants (Table 4.2; Table 4.3) showed phenotypes on cell-wall perturbing agents calcofluor white, congo red or SDS, suggestive of a role for deleted *C. glabrata* ORFs in cell wall biogenesis. Four *C. glabrata* mutants were also found to be defective in DNA damage repair due to their sensitivity to DNA damage agent MMS (Table 4.2; Table 4.3). Antifungal susceptibility testing was performed by observing the growth of *C. glabrata* mutants on YPD supplemented with caspofungin or fluconazole. Importantly, deletion of *C. glabrata* *CAGL0D03850g*, *CAGL0L07480g* and *CAGL0K05841g* rendered *C. glabrata* sensitive to fluconazole, a member of the azole class of antifungal drugs (Figure 4.4). *CAGL0D03850g*, *CAGL0L07480g* and *CAGL0K05841g* encode putative zinc finger transcription factors with similarity to *S. cerevisiae* *RSC30*, *NRG2* and *HAP1* respectively.

ORF	Condition																												
	YPD 30 °C	EtOH 6 %	YPD 16 °C	YPD 42 °C	YPD pH3	Meta arsenite 0.5 mM	Arsenic (III) oxide 1 mM	LiCl 80 mM	CaCl ₂ 0.5 M	CoCl ₂ 1 mM	CsCl 250 mM	ZnCl ₂ 8 mM	CaCl ₂ 2 mM	MgCl ₂ 600 mM	MnCl ₂ 30 mM	NaCl 1 M	Sorbitol 1 M	Caffeine 20 mM	Xylse 2 % C-source	MMS 0.05 %	Hydroxyurea 100 mM	Combi H ₂ O ₂ 2 mM	Combi NaCl 0.5 M + H ₂ O ₂ 2 mM	Nystatin 5 µg/ml	Sodium orthovanadate 2.5 mM	SDS 0.1 %	Calcofluor white 1 mg/ml	Cyclohexamide 1 µg/ml	Fluconazole 32 µg/ml
CAGL0D03850g	N	S	SS	S	N	N	N	S	S	N	NG	N	S	N	SS	S	N	SS	N	NG	N	SS	S	SS	N	NG	N	N	S
CAGL0D05170g	N	N	N	N	N	N	N	N	N	N	N	N	N	S	N	S	N	N	N	N	N	N	N	N	N	N	N	N	N
CAGL0F05159g	N	N	S	NG	N	N	N	N	N	S	S	N	N	N	N	N	N	SS	N	N	N	SS	N	N	N	N	N	N	N
CAGL0F03905g	N	N	N	N	N	N	N	N	N	N	FG	N	N	N	N	N	N	FG	N	N	N	N	N	N	N	N	N	N	N
CAGL0K06479g	N	N	N	N	N	N	N	N	N	S	N	N	N	N	N	N	N	N	N	N	N	N	N	N	N	N	NG	N	N
CAGL0M02299g	N	N	N	N	N	N	FG	N	N	N	N	N	N	N	N	N	N	N	N	N	N	N	N	N	N	N	N	N	N
CAGL0K10318g	N	N	N	N	N	N	N	N	N	N	N	N	N	N	S	N	N	N	N	N	N	N	N	N	N	N	N	N	N
CAGL0D05434g	N*	N*	N*	N*	N*	SS	NG	N*	N*	S	NG	N*	N*	N*	NG	N*	N*	N*	N*	NG	NG	N*	N*	N*	N*	N*	N*	N*	N*
CAGL0G03201g	N	N	N	N	N	N	FG	N	N	N	N	N	N	N	N	N	N	N	N	N	N	N	N	N	N	N	N	N	N
CAGL0K03245g	N	N	N	N	N	N	N	N	N	S	N	N	N	N	N	N	N	N	N	N	N	N	N	N	N	N	NG	N	N
CAGL0M02321g	N	N	S	N	N	N	N	N	N	N	N	N	N	N	N	N	N	N	N	N	N	N	N	N	N	N	N	N	N
CAGL0M01914g	N	N	N	N	N	N	N	N	N	N	N	N	N	N	N	N	N	N	N	N	N	N	N	N	N	N	S	N	N
CAGL0E00275g	N	N	N	N	N	N	N	N	N	N	N	N	N	N	N	SS	N	N	N	N	N	N	N	N	N	N	S	N	N
CAGL0D02750g	N	S	N	NG	N	N	N	SS	S	N	NG	N	N	N	NG	N	N	NG	N	N	N	SS	N	N	N	NG	N	S	N
CAGL0M06831g	N	N	N	N	N	N	N	N	S	N	N	N	N	N	NG	N	N	N	N	N	N	N	N	N	N	NG	S	N	N
CAGL0M04169g	N	N	NG	N	S	N	N	N	N	N	N	N	NG	N	N	N	N	N	S	N	N	N	N	N	NG	NG	N	N	N
CAGL0A01892g	N	N	N	N	N	N	N	N	S	S	N	S	N	N	N	N	N	N	N	S	N	N	N	N	N	N	NG	N	N
CAGL0L00627g	N	N	N	N	N	N	N	N	N	N	SS	N	N	N	N	N	N	N	N	N	N	N	N	N	S	N	N	N	N
CAGL0D05654g	N	N	N	N	N	N	N	N	S	N	N	N	N	N	N	N	N	N	N	N	N	N	N	N	N	N	N	N	N
CAGL0C03311g	N	N	N	N	N	N	N	N	N	N	N	N	N	N	N	N	N	N	N	S	N	N	N	N	N	N	N	N	N
CAGL0L07480g	N	N	N	N	N	N	N	N	N	N	N	N	N	N	N	N	N	N	N	N	N	N	N	N	N	N	N	N	S
CAGL0K05851g	N	N	N	N	N	N	N	N	N	N	N	N	N	N	N	N	N	N	N	N	N	N	N	N	N	N	N	N	S

S Sick
 SS Severely sick
 NG No growth
 FG Fast growth
 N Normal fitness
 * decreased colony size

Table 4.3: Chemogenomic screening of the *C. glabrata* deletion library. *C. glabrata* deletion mutants were pinned on YPD agar supplemented with stated chemicals and incubated at 30 °C (unless otherwise stated). After 48 hours, colony phenotypes were inspected visually for growth. For each ORF, phenotypes corresponding to growth under the stated screening condition is listed, relative to the parental strain. Table includes *C. glabrata* ORFs for which deletion conferred altered growth under a minimum of one screening condition. Deletion mutants displaying no observable phenotypes are excluded from the table. Conditions under which no *C. glabrata* mutants showed growth phenotypes were also excluded.

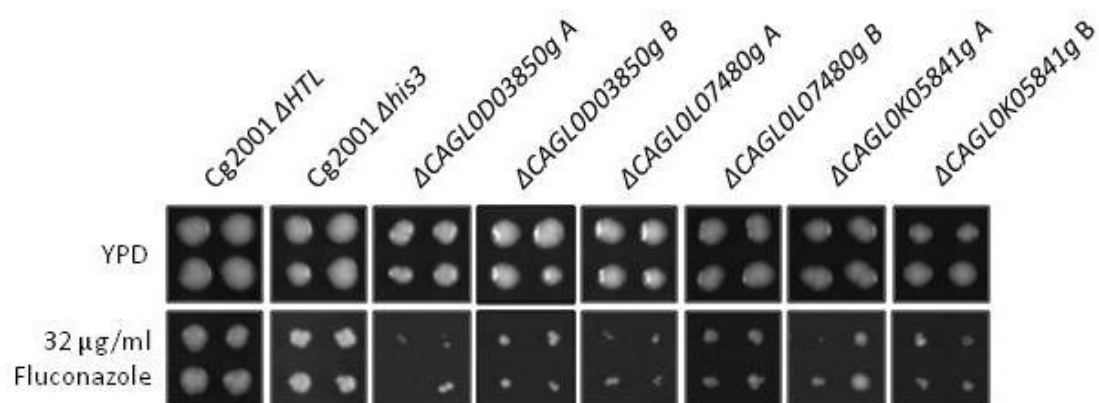


Figure 4.4 Fluconazole-sensitive *C. glabrata* mutants. *C. glabrata* deletion mutants and parental strains Cg2001 $\Delta his3$ and Cg2001 ΔHTL were pinned in quadruplicate onto YPD agar supplemented with 32 $\mu\text{g/ml}$ fluconazole and incubated at 30 °C for 48 hours. *C. glabrata* strains with reduced fitness on fluconazole ($\Delta CAGL0D03850g$, $\Delta CAGL0L07480g$ and $\Delta CAGL0K05841g$) were visually identified.

Deletion of *C. glabrata* *CAGL0D03850g* conferred the most observed phenotypes in screens. Of the 61 conditions tested, $\Delta CAGL0D03850g$ isolates yielded altered growth phenotypes on 17 stress conditions (Figure 4.5) covering a broad range of functional categories. *C. glabrata* $\Delta CAGL0D03850g$ yielded sensitive or no growth phenotypes on compounds targeting cellular MAP kinase signalling (caffeine), compounds inducing cell membrane stress (SDS), DNA damage (MMS) and metal ion toxicity (MnCl_2 , CaCl_2 , LiCl and CdCl_2). The mutant also exhibited phenotypes suggestive of a general protein defect (increased and decreased temperature, ethanol), sensitivity to combinatorial stress and susceptibility to antifungal drugs (Figure 4.5).

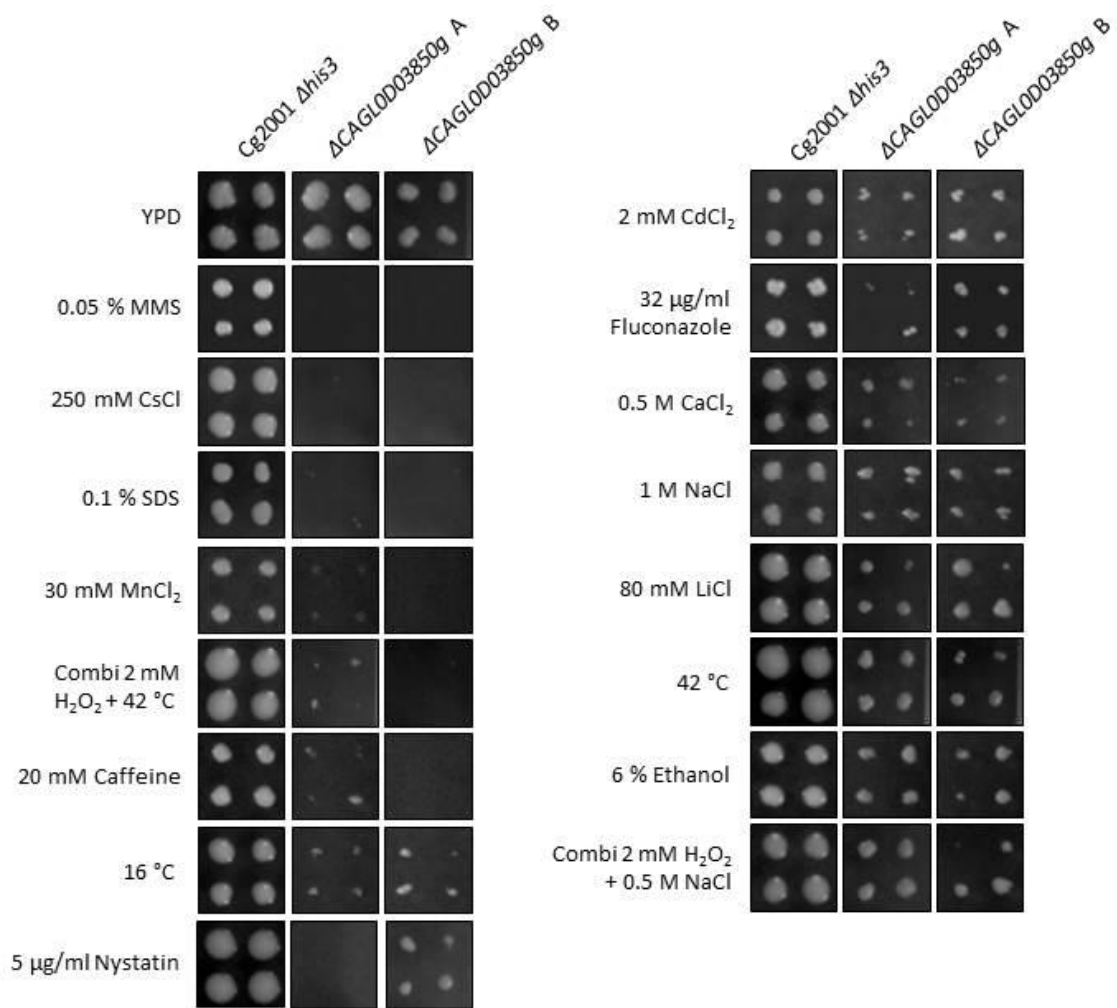


Figure 4.5 Phenotypic screening of *C. glabrata* Δ CAGL0D03850g isolates and parental strain Cg2001 Δ his3. *C. glabrata* parental strain Cg2001 Δ his3 and Δ CAGL0D03850g isolates A and B were pinned in quadruplicate using a Singer HDA ROTOR© robot onto YPD agar plates supplemented with stated chemical agents. Plates were incubated for 48 hours at 30 °C unless otherwise stated and inspected manually for phenotypes.

Bioinformatic searches predicted *C. glabrata* CAGL0D03850g to encode a putative Zn(2)-C6 fungal-type DNA-binding domain with sequence-specific DNA binding RNA polymerase II transcription factor activity (GO:0000981) (Appendix 4 Table 1). Despite being identified as a *C. glabrata* ORF with no *S. cerevisiae* orthologue by RBH searches (Appendix 3 Table 1), YGOB assigned CAGL0D03850g as an orthologue of *S. cerevisiae* RSC30 (ygob.ucd.ie), a zinc cluster protein component of the RSC chromatin remodelling complex (Angus-Hill *et al.*, 2001). Therefore, complementation studies were used to identify

whether *S. cerevisiae* *RSC30* is a functional orthologue of *C. glabrata* *CAGL0D03850g*. The complemented strain was tested for restoration of normal growth under two conditions (16 °C and 20 mM caffeine) for which *C. glabrata* Δ *CAGL0D03850g* conferred sensitive phenotypes. As expected, *C. glabrata* Δ *CAGL0D03850g* and a Δ *CAGL0D03850g* strain transformed with empty vector conferred sensitivity to growth on caffeine and to growth at 16 °C compared with parental strain Cg2001 Δ *his3* (Figure 4.6). Complementation was achieved by expression of *S. cerevisiae* *RSC30*, restoring growth of *C. glabrata* Δ *CAGL0D03850g* to that of the parental strain at 16 °C. Complementation of growth was also observed on YPD supplemented with caffeine (Figure 4.6). Thus in these instances, *S. cerevisiae* *RSC30* was able to functionally complement *C. glabrata* *CAGL0D03850g* and hence may be a functional orthologue.

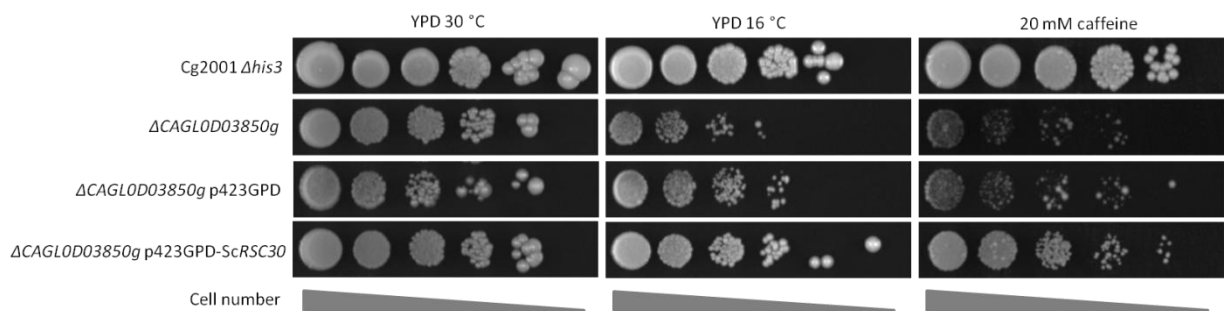


Figure 4.6: Complementation of *C. glabrata* Δ *CAGL0D03850g* with putative orthologue *S. cerevisiae* *RSC30*. Serial dilutions of *C. glabrata* parental strain Cg2001 Δ *his3*, deletion mutant Δ *CAGL0D03850g*, deletion mutant carrying empty vector Δ *CAGL0D03850g* p423GPD and deletion mutant expressing *S. cerevisiae* *RSC30* Δ *CAGL0D03850g* p423GPD-Sc*RSC30* (See Table 2.1). Ten fold serial dilutions commencing at OD₆₀₀ 0.1 were spotted onto YPD agar plates and incubated at 30 °C for 48 hours unless otherwise specified.

C. glabrata deletion mutants Δ *CAGL0D05434g* and Δ *CAGL0D02750g* also conferred multiple phenotypes in screens. Deletion of *CAGL0D05434g*, a predicted chromatin remodeler, yielded a general slow growth phenotype as well as sensitivities to seven conditions tested (see 5.3.1). Deletion of *CAGL0D02750g* rendered *C. glabrata* sensitive to 10 tested conditions. Phenotypes included sensitivity to metal ions, increased temperature, caffeine and SDS (Figure 4.7). *CAGL0D02750g* was identified to have no *S. cerevisiae*

orthologue by RBH searches (Appendix 3 Table 1) and bears no orthologue in any species included on the YGOB database (Figure 4.8; ygob.ucd.ie/). Bioinformatic searches of the protein encoded by *CAGL0D02750g* indicated the presence of a myosin and kinesin motor domain (cl00206; NCBI Conserved Domains).

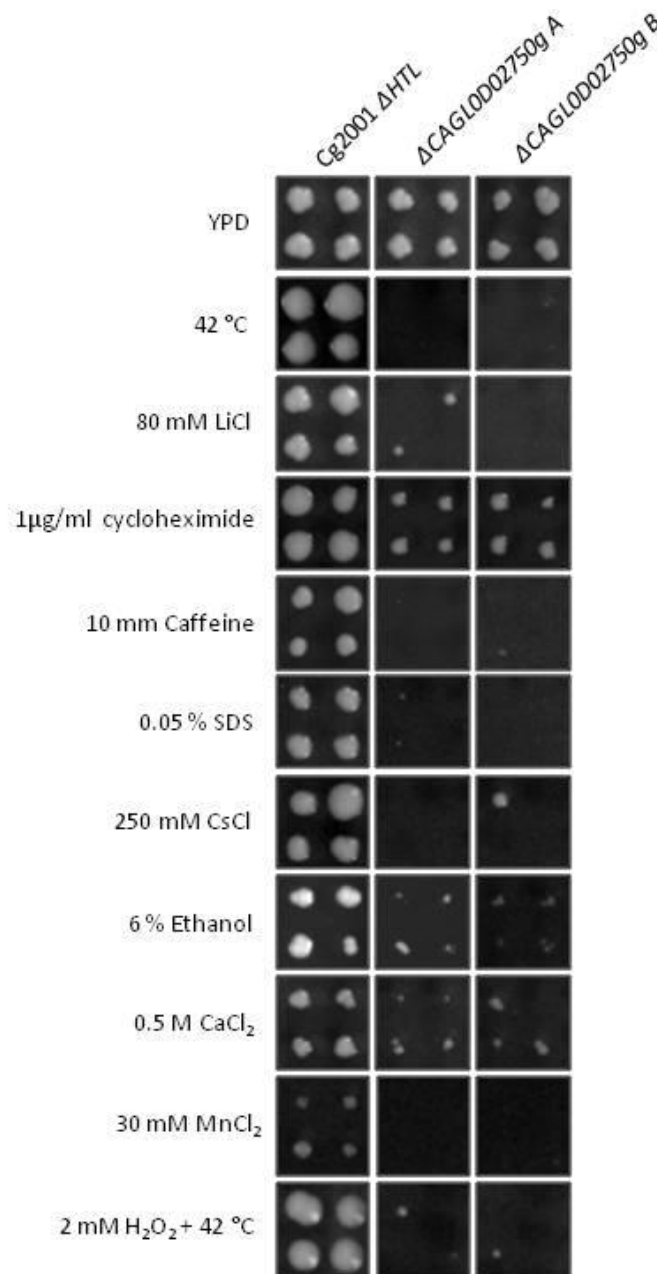


Figure 4.7: Phenotypic screening of $\Delta CAGL0D02750g$. *C. glabrata* parental strain Cg2001 ΔHTL and $\Delta CAGL0D02750g$ isolates A and B were spotted in quadruplicate onto YPD supplemented with chemical agents described and incubated at 30 °C for 48 hours.



Figure 4.8 YGOB alignment of *C. glabrata* *CAGL0D02750g* (ygob.ucd.ie). The *CAGL0D02750g* pillar aligns with no ORFs from any species in the YGOB database.

4.3.3 Screening *C. glabrata* Mutants for Biofilm Formation

C. glabrata mutants were tested for their ability to form biofilms, a growth form of significant clinical relevance (see 1.5.2). Biofilm structures formed *in vitro* by *C. glabrata* mutants on a polystyrene surface were quantified using an XTT reduction assay which proportionately indicates the metabolic activity of the biofilm thus providing an estimate for biofilm size (Iraqi *et al.*, 2005). Accordingly, the *C. glabrata* deletion library of 65 mutants (see 3.4.3) was screened for altered biofilm formation compared to that of the parental strain

Cg2001 $\Delta his3$. *C. glabrata* $\Delta CAGL0A04565g$ was excluded from the biofilm screen due to its growth defect in rich broth medium (Figure 4.3). Screening identified eight *C. glabrata* mutants which showed increased XTT reduction and thus increased biofilm formation (Anova $p < 1.45E-05$; Figure 4.9). Increased biofilm forming mutants included deletion of *CAGL0M01870g*, encoding a putative zinc finger transcription factor, as well as deletion of *C. glabrata* *CAGL0G03201g* and *CAGL0K05687g*, both of which contain putative oxidoreductase domains in the encoding protein (Figure 4.9; Appendix 4 Table 1). Deletion of *CAGL0M10153g*, a paralogue of *S. cerevisiae* MAP kinase signalling component *STE20*, conferred the greatest increase in biofilm formation amongst *C. glabrata* deletion mutants, yielding a 30.2 % average increase in XTT reduction (Appendix 11 Table 1). Less pronounced increases in biofilm formation were also observed for deletion mutants of *CAGL0A02343g*, *CAGL0A02299g* and *CAGL0C04763g* for which bioinformatic searches were unable to detect any known functional domains. Screens also identified six *C. glabrata* mutants with reduced biofilm forming capacity, indicated by decreased XTT reduction (Figure 4.9 B). Biofilm formation was most significantly decreased by 54.2 % for *C. glabrata* $\Delta CAGL0E00275g$ (Figure 4.9 B), encoding a putative PA14 domain adhesin belonging to the *EPA* family. Decreased biofilm formation was observed for *C. glabrata* deletion mutants of *CAGL0D03850g*, *CAGL0F05159g* and *CAGL0L07480g* – orthologues of *S. cerevisiae* *RSC30*, *VPS72* and *NRG2*, respectively (ygob.ucd.ie). Screening revealed reduced biofilm formation in deletion mutants of *C. glabrata* ORFs *CAGL0M02299g* and *CAGL0G04279g* which have no orthologue in *S. cerevisiae*. *CAGL0M02299g* encodes a putative serine/threonine kinase and *CAGL0G04279g* encodes a putative alpha mannosyltransferase (Appendix 4 Table 1). Biofilm formation for the remaining 51 *C. glabrata* deletion strains did not significantly deviate from that of the parental strain.

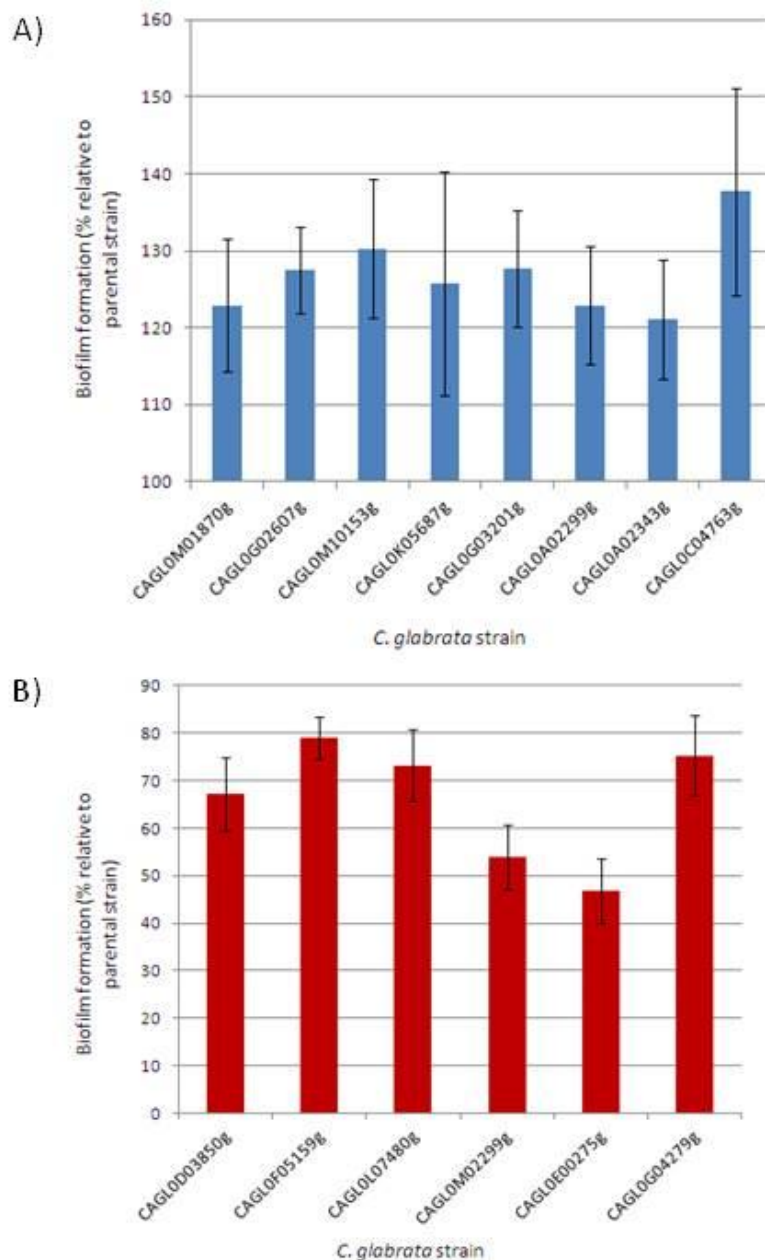


Figure 4.9: Biofilm formation by *C. glabrata* mutants. Cultures of *C. glabrata* were distributed in a polystyrene 96-well microtitre plate and incubated at 37 °C in SC broth for 24 hours to allow biofilm formation. Biofilm formation was subsequently quantified by measuring XTT reduction in a spectrophotometer. All OD₄₉₂ measurements (n=18) were normalised to parental strain Cg2001 $\Delta his3$ (Anova p<1.97E-05, Dunnett's critical value 3.37). A) Percentage biofilm formation of *C. glabrata* mutants with significantly increased biofilm-forming capacity relative to parental strain Cg2001 $\Delta his3$. B) Percentage biofilm formation of *C. glabrata* mutants with significantly decreased biofilm-forming capacity relative to parental strain Cg2001 $\Delta his3$.

4.3.4 Virulence Screening of *C. glabrata* Mutants

A *Drosophila melanogaster* model of *Candida* gastrointestinal (GI) infection was used to characterise the role *C. glabrata* ORFs with no *S. cerevisiae* orthologues which may play a role in virulence. Firstly, survival of immunocompromised Dif/Key *D. melanogaster* larvae, in which major signalling components of the IMD and Toll pathway are deactivated (Figure 4.1 and 4.2), was examined following *C. glabrata* infection (Figure 4.10 A). Secondly, Toll pathway activation in response to *C. glabrata* infection was examined in Drs-GFP larvae in which Drosomycin, a major antimicrobial peptide produced upon Toll pathway activation following pathogen recognition, was GFP-tagged thus serving as an indicator of innate immune activation (Figure 4.10 B).

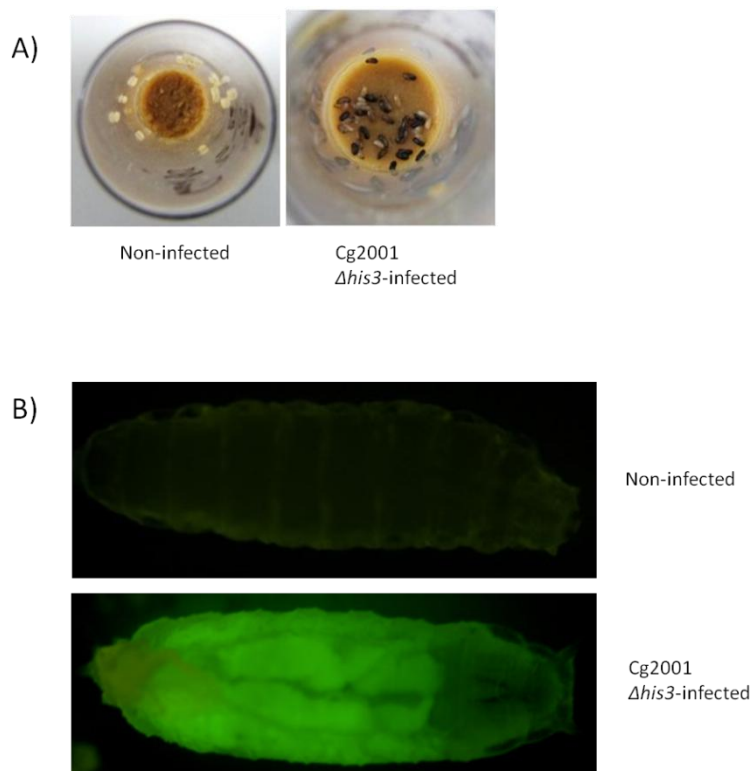


Figure 4.10: A *D. melanogaster* model of *C. glabrata* GI infection. A) Infection of *D. melanogaster* Dif/Key larvae with *C. glabrata* parental strain Cg2001 $\Delta his3$ resulted in 90-100 % death of larvae 48 hours post infection compared with non-infected controls in which 90 – 100 % Dif/Key larvae survived. **B)** Infection of *D. melanogaster* Drs-GFP larvae with *C. glabrata* parental strain Cg2001 $\Delta his3$ caused activation of the Toll pathway and subsequent expression of Drs-GFP 48 hours post infection. No Drs-GFP expression was observed in non-infected controls.

Challenge of immunocompromised Dif/Key larvae with *C. glabrata* parental strain Cg2001 $\Delta his3$ in positive controls resulted in 0-10 % Dif/Key larvae survival 48 hours post infection (Figure 4.11 A). Conversely, uninfected Dif/Key larvae controls yielded 90-100 % larvae survival (Figure 4.11 A). Infection of immunocompromised larvae with 59 of 65 *C. glabrata* mutants resulted in low levels of larvae survival, showing similar levels of virulence to parental strain Cg2001 $\Delta his3$ (Appendix 10 Table 2). However, six *C. glabrata* mutants were attenuated for virulence in Dif/Key larvae which resulted in increased larvae survival (Figure 4.11 A). Despite being initially identified to have no *S. cerevisiae* orthologue in RBH searches (see 3.3.1), YGOB (ygob.ucd.ie) indicated the presence of *S. cerevisiae* orthologues for four of the six *C. glabrata* ORFs which upon deletion rendered *C. glabrata* attenuated for virulence in the immunocompromised *D. melanogaster* infection model. These included *C. glabrata* CAGL0D03850g, a putative orthologue of *S. cerevisiae* RSC chromatin remodelling complex component *RSC30*; CAGL0B00726g, an orthologue of glucokinase *GLK1*; CAGL0L03674g, an orthologue of putative zinc-finger transcription factor *GSM1*; and CAGL0L07480g, an orthologue of transcriptional repressor *NRG2* (ygob.ucd.ie). Also attenuated for virulence in the immunocompromised infection model were two *C. glabrata* ORFs, CAGL0K05687g and CAGL0H01749g, which were found to have no orthologue in both RBH and YGOB searches (Appendix 3 Table 1 and 2). Bioinformatic searches identified an oxidoreductase domain in the CAGL0K05687g encoding protein (Appendix 4 Table 1). However, searches were unable to bioinformatically identify any recognisable functional domains within the CAGL0H01749g protein coding sequence.

All *C. glabrata* deletion mutants, including those which were attenuated for virulence in immunocompromised larvae, induced GFP expression following infection of *D. melanogaster* Dros-GFP larvae (Figure 4.11 B; Appendix 10 Table 1). Thus all *C. glabrata* mutants tested were able to activate innate immune signalling via the Toll pathway and subsequent production of antimicrobial peptide Drosomycin.

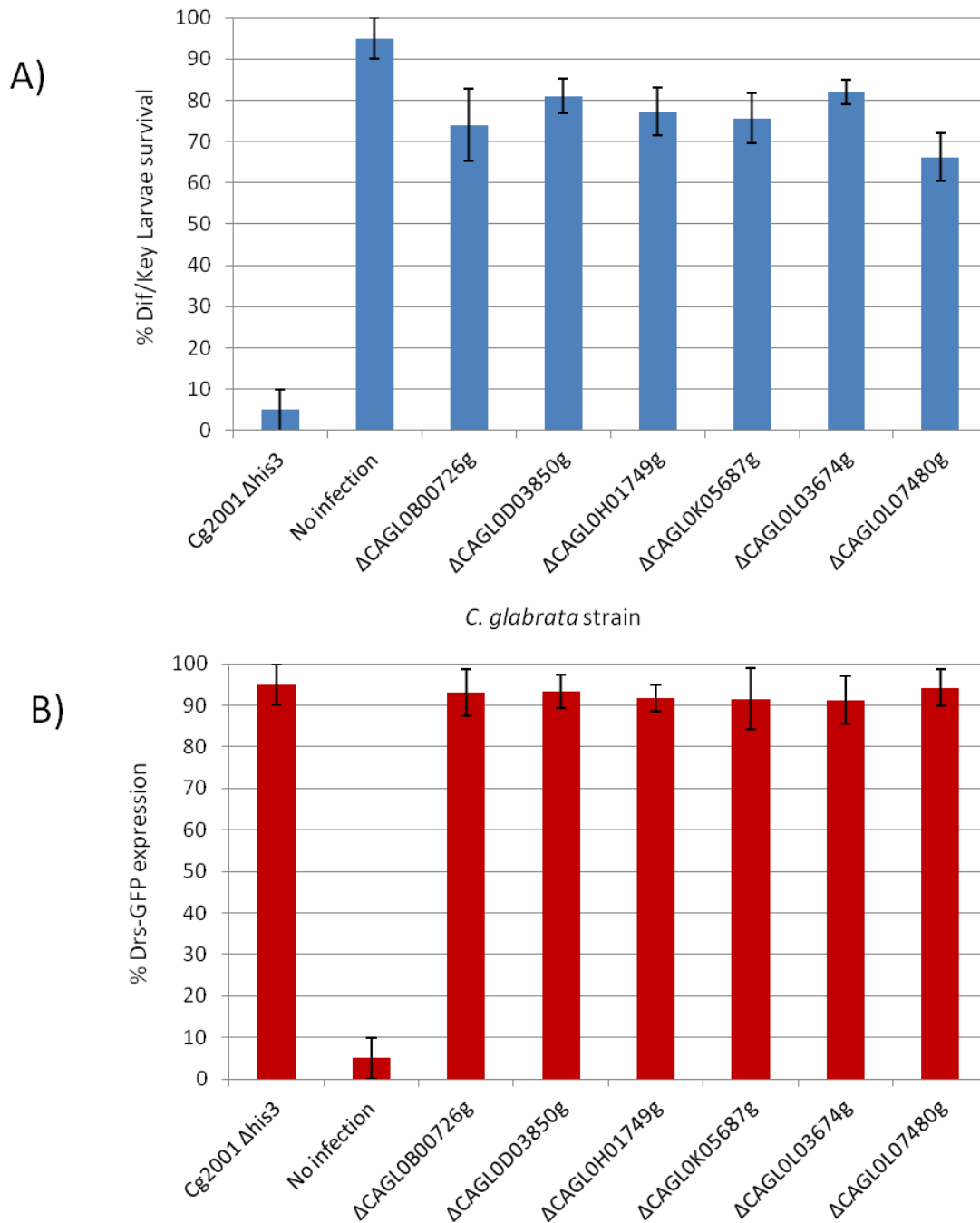


Figure 4.11 *C. glabrata* mutants attenuated for virulence in a *D. melanogaster* model of *C. glabrata* infection. A) Average percentage of surviving Dif/Key larvae 48 hours post infection with *C. glabrata* mutants, parental strain Cg2001 $\Delta his3$ and uninfected controls. B) Average number of Dros-GFP larvae expressing GFP 48 hours following challenge by *C. glabrata* mutants, parental strain Cg2001 $\Delta his3$ and parental controls.

Screening the *C. glabrata* Deletion Library: Summary

Taken together, four different screening approaches identified 23 *C. glabrata* ORFs with no orthologue in *S. cerevisiae* (using both RBH and YGOB criteria) which showed phenotypes in at least one screen (Table 4.4). The majority of deletion mutants showed observable phenotypes in one screening method only. No *C. glabrata* mutants showed phenotypes in all screens, however two mutants (Δ CAGL0F05159g and Δ CAGL0E00275g) showed phenotypes in three out of four screens (Table 4.4).

Table 4.4: Summary of all phenotypes conferred by deletion of *C. glabrata* ORFs with no orthologue in *S. cerevisiae*. Table includes deletions of *C. glabrata* ORFs which were defined to have no *S. cerevisiae* orthologue by both RBH and YGOB searches (Appendix 3 Table 1 and 2) and predicted function domains (interpro.ebi.ac.uk). “+” represents increased fitness for the given strain in fitness profiling or chemogenomic screens or increased biofilm formation. “-“ denotes decreased fitness in fitness and chemogenomic screens, reduced biofilm formation or reduced virulence in the *D. melanogaster* immunocompromised infection model. “None” indicates no significant increase or decrease in fitness was conferred by deletion of the *C. glabrata* ORF under the given screen.

<i>C. glabrata</i> strain	Predicted functional domain	Fitness profiling	Chemogenomic screens	Biofilm formation	Virulence in <i>D. melanogaster</i>
<i>ΔCAGL0A01892g</i>	None	None	-	None	None
<i>ΔCAGL0A02299g</i>	None	None	None	+	None
<i>ΔCAGL0A02343g</i>	None	None	None	+	None
<i>ΔCAGL0A04565g</i>	APSES-type DNA-binding domain; Ankyrin repeat-containing domain	-	None	None	None
<i>ΔCAGL0C03311g</i>	None	None	-	None	None
<i>ΔCAGL0C04763g</i>	None	None	None	+	None
<i>ΔCAGL0D02750g</i>	None	None	-	None	None
<i>ΔCAGL0D05434g</i>	Repressor Rox1, High mobility group box domain	None	-	None	None
<i>ΔCAGL0D05654g</i>	None	None	-	None	None
<i>ΔCAGL0E00275g</i>	PA14; GLEYA adhesin domain	-	-	-	None
<i>ΔCAGL0F05159g</i>	YL1 Nuclear	-	-	-	None

<i>ΔCAGL0F08767g</i>	None	-	None	None	None
<i>ΔCAGL0G03201g</i>	FMN-binding split barrel; Flavin-reductase-like, FMN-binding	None	+	+	None
<i>ΔCAGL0G04279g</i>	Alpha mannosyltransferase	-	None	-	None
<i>ΔCAGL0G05522g</i>	None	-	None	None	None
<i>ΔCAGL0G10175g</i>	None	-	None	None	None
<i>ΔCAGL0H01749g</i>	None	None	None	None	-
<i>ΔCAGL0K03245g</i>	None	None	-	None	None
<i>ΔCAGL0K05687g</i>	Aldolase-type TIM barrel; NADH:flavin oxidoreductase/NADH oxidase, N-terminal	None	None	+	-
<i>ΔCAGL0K05851g</i>	None	None	-	None	None
<i>ΔCAGL0M01870g</i>	Zinc finger, C2H2	None	None	+	None
<i>ΔCAGL0M01914g</i>	Tetratricopeptide-like helical	None	-	None	None
<i>ΔCAGL0M02321g</i>	None	None	-	None	None

4.4 Discussion

The *C. glabrata* deletion library provided a molecular tool for the study of *C. glabrata* ORFs with no orthologue in *S. cerevisiae*. In this work, the development of high-throughput phenotypic screening platforms, biofilm screening and the establishment of *D. melanogaster* as a host for infection studies facilitated the functional characterisation of *C. glabrata* deletion mutants. Most notably, this study has contributed function information regarding previously unstudied *C. glabrata* genes, facilitating our understanding of *C. glabrata* genes required for growth and for virulence in this medically important pathogen.

4.4.1 Fitness Analysis of the *C. glabrata* Deletion Library

Upon encountering the varied environment of the host niche, fitness can be a vital prerequisite for survival and the establishment of infection. Fitness profiling revealed seven *C. glabrata* ORFs which when genetically perturbed conferred a significant variation in *C. glabrata* fitness in rich media. More specifically, deletion of these ORFs resulted in altered lag phase and increased doubling time. Alterations in lag phase could be indicative of the ability of cells to adapt to the environment whilst altered doubling times reflects the capacity of cells to proliferate. Fitness profiling highlighted a significant impairment of *C. glabrata* growth upon deletion of *CAGL0A04565g*. Despite bioinformatically being classified as a *C. glabrata*-specific ORF (Appendix 3 Table 1), CGD and YGOB databases identified *CAGL0A04565g* to encode an orthologue of *S. cerevisiae* *SWI4*, the DNA-binding component of the SBF complex which regulates the transcription of G1-specific genes (ygob.ucd.ie; candidagenome.org). It is likely that orthology between the two encoding proteins was not recognised in RBH searches due to the conserved APSES-type DNA-binding domain encompassing approximately 10 % of the total protein sequence. Hence orthology was not detected by RBH searches due to filters requiring sequence conservation throughout a minimum of 50 % of orthologous protein sequences. In *S. cerevisiae*, *SWI4* and the SBF complex is known to regulate the expression of genes involved in cell budding, cell wall morphogenesis and membrane biosynthesis during the G1/S transition of the cell cycle (Iyer *et al.*, 2001; Levin, 2005). *S. cerevisiae* $\Delta swi4$ mutants were viable yet no reduction of fitness has been observed (Gaiever *et al.*, 2002; Córcoles-Sáez *et al.*, 2012) as

opposed to the distinct fitness defect incurred upon deletion of putative *C. glabrata* orthologue *CAGL0A04565g* (Figure 4.3). However, *S. cerevisiae* $\Delta swi4$ cells showed delayed cell cycle progression and showed increased susceptibility to cell wall perturbing agents (Levin, 2005; White *et al.*, 2009). Thus further experimentation could explore the hypothesis that inhibition of growth in *C. glabrata* $\Delta CAGL0A04565g$ is due to cell cycle delay or defective cell wall biogenesis.

A limitation of the fitness profiling approach lies in the analysis of growth in rich media under laboratory conditions. Although this methodology identified *C. glabrata* ORFs that were required for normal growth under defined laboratory conditions in rich media, it is unclear whether fitness data could be extrapolated to the human host niche in which invading microorganisms encounter multiple stresses simultaneously and in competition with the existing host microflora. Thus for fitness screening more relevant to the host niche, more extensive fitness profiling could explore growth of *C. glabrata* mutants in minimal media at elevated temperatures. Furthermore, to reflect competition for nutrients in the host niche, barcode tags in the *C. glabrata* deletion mutant collection could be exploited in pooled growth experiments whereby mixed cultures of *C. glabrata* mutants are analysed for competitive fitness. Such approaches have been extensively used for *S. cerevisiae* deletion collections and other organisms with available barcoded deletion libraries (Mazurkiewicz *et al.*, 2006; see 1.3.1.1).

4.4.2 Phenotypic Screening of the *C. glabrata* Deletion Library

Development of an automated, high-throughput screening platform facilitated the functional characterisation of *C. glabrata* deletion mutants, identifying conditions under which certain gene products were required for growth. Most notably, together with deletion mutants generated from a previous gene deletion study (Schwartzmüller *et al.*, 2013; Appendix 13), phenotypic screens revealed novel phenotypes associated with the deletion of 22 previously unstudied *C. glabrata* ORFs, accounting for 17 % of the deletion mutants tested (Table 4.3). Growth phenotypes were found for uncharacterised *C. glabrata* putative transcription factors encoded by *CAGL0D05434g*, *CAGL0D03850g* and *CAGL0D05170g* as well as for putative kinases encoded by *CAGL0F03905g*, *CAGL0K06479g* and *CAGL0M02299g* (Table 4.3). A total of 110 *C. glabrata*

mutants did not yield any observable alteration of growth in phenotypic screens. This could be due to the presence of genes with similar function in *C. glabrata* masking phenotypes. Alternatively, two *C. glabrata* ORFs targeted for gene deletion may have been dubious ORFs due to misannotation. For example, *C. glabrata* ORF *CAGLOB02946g* was removed from CGD during the course of the study and thus is unlikely to encode a transcribed ORF (candidagenome.org).

C. glabrata Δ *CAGL0D03850g*, a putative orthologue of *S. cerevisiae* *RSC30* was found to be defective for growth on a number of conditions such as increased temperature, NaCl, caffeine, SDS and fluconazole (Figure 4.5). These phenotypes are contrary to a study by Rai *et al.*, 2012, of a Tn7 insertion mutant of *CAGL0D03850g* (in which *CAGL0D03850g* was designated an orthologue of *S. cerevisiae* *RSC3*) which found this strain to show no altered phenotype in response to growth on these compounds (Rai *et al.*, 2012). Rather, the *CAGL0D03850g* Tn7 insertional mutant from the Rai *et al.*, (2012) study was found to have increased susceptibility to H₂O₂ and hydroxyurea. The discrepancy between the two studies could be a consequence of the different methods by which *C. glabrata* ORF *CAGL0D03850g* was genetically altered since insertional mutagenesis introduces an interruption into the still-present target ORF whereas in the current study, the target ORF was completely replaced by a Nourseothricin resistance cassette (see 3.2.2). Alternatively, differences could be attributed to different phenotypic screening techniques, conditions or concentrations used. However, both studies demonstrate the requirement of *CAGL0D03850g* for growth on a number of stress conditions with functional implications including general protein defects and decreased tolerance to metal compounds and antifungal drugs in *C. glabrata*. In *S. cerevisiae*, *RSC30* comprises a DNA-binding component of the RSC chromatin remodelling complex (Shim *et al.*, 2005). Through the mobilisation of nucleosomes, the RSC complex regulates genes implicated in stress response, cell wall integrity, cell cycle progression and the repair of double stranded DNA breaks (Angus-Hill *et al.*, 2001; Shim *et al.*, 2005). In particular, *RSC30*, *MRE11* and Ku encoded proteins are required for recruitment of *RSC30* to double strand breaks in DNA (Shim *et al.*, 2005). Consistent with its *S. cerevisiae* orthologue *RSC30*, deletion of *CAGL0D03850g* rendered *C. glabrata* unable to grow on DNA-damaging agent MMS and sensitive to osmotic and cationic

stressor NaCl (Figure 4.5; Angus-Hill *et al.*, 2001; Shim *et al.*, 2005). Furthermore, *S. cerevisiae* RSC30 was able to complement deletion of CAGL0D03850g on two tested conditions (Figure 4.6). Thus, contrary to the study by Rai *et al.*, 2012, this work provides evidence for *C. glabrata* CAGL0D03850g being a functional orthologue of *S. cerevisiae* RSC30 (Rai *et al.*, 2012).

All *C. glabrata* deletion mutants were screened for increased or decreased susceptibility to antifungal drugs caspofungin and fluconazole, since the antifungal resistance of *C. glabrata* poses a significant challenge for treatment of infections in the clinical setting (see 1.9). Screening deletion collections for growth on antifungal compounds can facilitate our understanding of genes which contribute to drug resistance in pathogenic microorganisms (Homann *et al.*, 2009; Schwartzmüller *et al.*, 2013; Appendix 13). Three *C. glabrata* mutants showed decreased resistance to fluconazole in this study: Δ CAGL0D03850g, Δ CAGL0L07480g and Δ CAGL0K05841g (Figure 4.4). *C. glabrata* CAGL0L07480g is designated as an orthologue of *S. cerevisiae* NRG1 (candidagenome.org) or NRG2 (ygob.ucd.ie), encoding paralogous zinc finger transcriptional repressors of carbon-source responsive genes, stress response, filamentous growth and response to alkaline pH (Vyas *et al.*, 2005; Santangelo, 2006). In *C. albicans*, NRG1 and NRG2 are known to negatively regulate filamentous growth and chlamyospore formation (Uhl *et al.*, 2003; Staib *et al.*, 2005; Kadosh & Johnson, 2005). Similarly to *C. glabrata* Δ CAGL0L07480g, NRG1 deletion mutants yield increased susceptibility of *C. albicans* to fluconazole (Homann *et al.*, 2009). *C. albicans* NRG1 deletion also increased sensitivity to caspofungin (Wheeler *et al.*, 2008) however no consistent phenotype for *C. glabrata* Δ CAGL0L07480g was observed in response to growth on caspofungin in this study. Contrary to *S. cerevisiae* Δ nrg1 and Δ nrg2 mutants (Vyas *et al.*, 2005), increased tolerance to osmotic or oxidative stress was not observed for deletion of their putative *C. glabrata* orthologue CAGL0L07480g. Phenotypic screening identified a second *C. glabrata* deletion mutant of putative transcription factor CAGL0K05841g which when deleted rendered *C. glabrata* sensitive to fluconazole. CAGL0K05891g is orthologous to *S. cerevisiae* HAP1 and *C. albicans* ZCF20 (candidagenome.org). *C. albicans* ZCF20 was found to be upregulated more than 7-fold in a fluconazole-resistant

lab strain, which was hypothesised to regulate *ERG2* due to decreased ergosterol in the fluconazole-resistant strain (Yan *et al.*, 2008 B). However, targets of *CAGL0K05841g* (*HAP1*) and their role in fluconazole tolerance have not been investigated in *C. glabrata*.

4.4.3 Screening of *C. glabrata* Deletion Mutants for Biofilm Formation

This study sought to investigate the role *C. glabrata* ORFs with no orthologue in *S. cerevisiae* may play in biofilm formation due to the medical relevance of this growth form both as a source of *Candida* infections associated with medical devices and for its enhanced virulence properties. Studies into the mechanisms underlying *C. glabrata* biofilm formation have uncovered a crucial role for Epa6 and Epa7 in biofilm formation whose expression is primarily regulated by the subtelomeric silencing machinery (Iraqi *et al.*, 2005; see 1.5.2). A number of Epa and Awp family proteins were found to be expressed in biofilm forming cells however the influence they have on biofilm formation is unknown (Kraneveld *et al.*, 2011). Further to this, bioinformatic studies identified 67 putative adhesins in *C. glabrata*, many of which have no orthologue in *S. cerevisiae* or other *Candida* species and three of which were included in the deletion library (de Groot *et al.*, 2008). Screening the *C. glabrata* deletion library identified *C. glabrata* mutants with increased or decreased biofilm forming capacity – further expanding the repertoire of *C. glabrata* ORFs known to affect biofilm formation. Biofilm quantification of the *C. glabrata* deletion library identified 14 mutants with significantly altered biofilm forming capacity (Figure 4.9 A and B). The greatest reduction in biofilm-forming capacity was observed in a deletion mutant of *C. glabrata* *CAGL0E00275g* (Figure 4.9 B), which was previously identified bioinformatically as a member of the Epa family (de Groot *et al.*, 2008). Similarly to many adhesins in *C. glabrata*, *CAGL0E00275g* (or *EPA20*) is located at the telomere of the left arm of chromosome E and encodes a PA14 GLEYA adhesin domain (Appendix 4 Table 1). This study presents the first experimental evidence of the involvement of uncharacterised adhesin *EPA20* in *C. glabrata* biofilm formation. Further experimentation could more extensively validate the role of *EPA20* as an adhesin implicated in biofilm formation and whether *EPA20* is subject to subtelomeric silencing similarly to *EPA6* and *EPA7* (see 1.5.2; Iraqi *et al.*, 2005). Screening also implicated 3 putative transcription factors (encoded by *CAGL0M01870g*, *CAGL0D03850g* and *CAGL0L07480g*) and 4

ORFs encoding predicted kinase domains (*CAGLOG02607g*, *CAGLOM10153g*, *CAGLOG03201g* and *CAGLOM02299g*) in *C. glabrata* biofilm formation (Figure 4.9 A and B). Deletion of *CAGL0L07480g*, orthologue of *S. cerevisiae* transcriptional repressors *NRG1* or *NRG2*, reduced biofilm formation in *C. glabrata* (Figure 4.9 B). This is contrary to reports of improved adherence and biofilm formation in an *S. cerevisiae* $\Delta nrg1\Delta nrg2$ double mutant (Kuchin *et al.*, 2002) whereas deletion of *C. albicans* *NRG1* resulted in no detectable alteration in biofilm formation (Nobile *et al.*, 2012). Hence the effect on biofilm formation following deletion of *CAGL0L07480g* could be specific to *C. glabrata*. Interestingly, eight deletion mutants of *C. glabrata* ORFs with no orthologue in *S. cerevisiae* showed altered biofilm formation including putative zinc-finger transcription factor *CAGLOM01870g*, putative kinase *CAGLOG03201g*, oxidoreductase *CAGL0K05687g* and mannosyltransferase *CAGLOG04279g* (Appendix 4 Table 1). No functional domains were detected bioinformatically for the remaining *C. glabrata* ORFs. Further investigation of biofilm altered mutants could explore whether the identified transcription factors regulate *EPA6* or *EPA7* adhesin expression during biofilm formation in *C. glabrata*.

4.4.4 Virulence Screening of *C. glabrata* deletion mutants

Due to the size of the *C. glabrata* deletion library and the unsuitability of a murine infection model in this instance, a *D. melanogaster* larvae model of *C. glabrata* gastrointestinal infection was used to study the virulence of *C. glabrata* mutants. All *C. glabrata* mutants caused Toll pathway (Figure 4.1) activation to similar levels as the parental strain in *D. melanogaster* Dros-GFP larvae 48 hours post infection (Figure 4.11 B; Appendix 10 Table 1). However, six *C. glabrata* mutants were attenuated for virulence in immunocompromised Dif/Key larvae (Figure 4.11 A). Attenuated mutants included deletions of *CAGL0L07480g* and *CAGL0D03850g* which are orthologues of *S. cerevisiae* *NRG1/2* and *RSC30*, respectively.

During the course of the study, a role for *C. glabrata* *CAGL0D03850g* in virulence was reported (Rai *et al.*, 2012). Firstly, $\Delta CAGL0D03850g$ survival and replication was found to be decreased in THP-1 macrophages. Secondly, *C. glabrata* $\Delta CAGL0D03850g$ was attenuated for virulence in a murine model of disseminated Candidiasis. This report provided validation for the use of *D.*

melanogaster larvae as an alternative to mammalian infection models since *C. glabrata* Δ CAGL0D03850g was found to be attenuated for virulence in this host also (Figure 4.11 A). Transcriptional profiling highlighted the regulation of genes involved in metabolic adaptation by *RSC30* upon macrophage internalisation. It was also proposed that the remodelling of chromatin architecture by *RSC30* is a prerequisite for adaptation to the macrophage environment (Rai *et al.*, 2012). Although it has not previously been reported for *C. glabrata*, avirulence in *NRG1* deletion mutants has been described in a number of fungal pathogens. For example, *NRG1* mutants were attenuated for virulence in murine models of both *C. albicans* and *C. neoformans* infection (Braun *et al.*, 2001; Cramer *et al.*, 2006). Subsequently, the avirulence of *C. albicans* *NRG1* deletion strains has made them candidates for vaccine development in which a *C. albicans* tet-*NRG1* strain was administered in a murine model as a vaccine protecting against disseminated Candidiasis (Saville *et al.*, 2009). Thus, the attenuation of virulence of *C. glabrata* Δ CAGL0L07480g is also consistent with previous reports for *NRG* mutants in other fungal pathogens.

Two *C. glabrata* ORFs with orthologues in related species but no previous association with pathogenicity were also found to be required for virulence in *C. glabrata*. Virulence of deletion strains Δ CAGL0B00726g and Δ CAGL0L03674g was attenuated in the *D. melanogaster* immunocompromised Dif/Key larvae infection model (see 4.3.4), allowing increased larvae survival (Figure 4.11 A). Firstly, *C. glabrata* CAGL0B00726g encodes an orthologue of *S. cerevisiae* *GLK1*, a glucokinase involved in glucose metabolism (yeastgenome.org). In the pathogenic yeast *C. albicans*, *GLK1* is a member of a subset of metabolic genes regulated by Efg1 during filamentation and is also upregulated following fluconazole exposure (Doedt *et al.*, 2004; Copping *et al.*, 2005). Despite morphogenesis and drug resistance being contributing factors to the pathogenicity of *C. albicans*, no direct role for *GLK1* in *C. albicans* virulence has been described. The sole report exploring the role of *GLK1* in virulence exists in the plant pathogen *Botrytis cinerea* which found *GLK1* not to be required for pathogenicity (Rui & Hahn, 2007). Thus, this work provides the first evidence for the implication of *GLK1* (CAGL0B00726g) in virulence in *C. glabrata*. The role *C. glabrata* *GLK1* may play in virulence however remains unclear. Since *C. glabrata* does not undergo a morphological switch it could be proposed that

attenuated virulence in the Δ CAGL0B00726g strain could be due to altered glucose metabolism. Alternatively, attenuated virulence of Δ CAGL0B00726g could be conferred by an altered core stress response, although no stress-related phenotypes were observed in phenotypic screens. Concordantly in *C. albicans*, *GLK1* transcripts are regulated by osmotic, oxidative and heavy metal stress as a constituent of the core stress response (Enjalbert et al., 2005). Secondly, *C. glabrata* CAGL0L03674g was identified as an orthologue of *S. cerevisiae* *GSM1* (ygob.ucd.ie), a zinc cluster transcription factor also implicated in energy metabolism (yeastgenome.org). Together, the alteration in virulence for *C. glabrata* CAGL0B00726g and CAGL0L03674g suggests glucose metabolism is an important contributor to *C. glabrata* virulence in a *D. melanogaster* larvae infection. This study also provides the first evidence of a role for *C. glabrata* CAGL0B00726g (*GLK1*) and CAGL0L03674g (*GSM1*) in pathogenicity.

Screening identified the requirement for *C. glabrata* CAGL0K05687g and CAGL0H01749g for full virulence in immunocompromised *D. melanogaster* larvae. Both ORFs are *C. glabrata*-specific and have no orthologue in *S. cerevisiae*. Bioinformatic searches revealed a NADH:flavin oxidoreductase domain in the CAGL0K05687g encoding protein with predicted zinc ion binding (GO:0008270) and ubiquitin-protein ligase activity (GO:0004842). Thus, functional characterisation of a *C. glabrata* deletion library identified *C. glabrata* ORFs with no orthologue in *S. cerevisiae* which could be implicated in virulence. Indeed, *D. melanogaster* has proven a useful model for the evaluation of virulence in large strain collections. The requirement of candidate *C. glabrata* ORFs for virulence could be further verified in a mammalian infection model.

This study took a four-pronged approach for the functional analysis of a *C. glabrata* deletion library. Each of the screening methods employed highlighted the requirement of *C. glabrata* ORFs for growth, taking into consideration different aspects of *C. glabrata* fitness under a variety of environmental stresses and by analysing growth forms relevant to infection. Individually, phenotypic analyses identified *C. glabrata* ORFs implicated in particular cellular processes. In total, novel phenotypes in at least one screen associated with the deletion of 23 *C. glabrata* ORFs with no strict *S. cerevisiae* orthologue were found in this

study (Table 4.4). However, together the different analyses complemented each other and highlighted the importance of ORFs such as *CAGL0D03850g* for growth and virulence in *C. glabrata*. As such, the utilisation of such tools aids the dissection of the roles of *C. glabrata*-specific ORFs for which the inference of gene function through study of orthologues in model organisms such as *S. cerevisiae* is not possible. This platform has also proved useful for the study of *C. glabrata* ORFs with orthologues in *S. cerevisiae* and has allowed the comparison of datasets between related species, highlighting the evolutionary differences between the two species. For example, the orthologue of *S. cerevisiae* *RSC30* has been implicated in virulence in *C. glabrata*, suggesting genetic rewiring between the two species and highlighting the importance for the direct study of medically-relevant pathogens. The study has also highlighted similarities between pathogenic species through the identification of common ORFs which are required for virulence such as *C. albicans* *NRG1* and its putative *C. glabrata* orthologue *CAGL0L07480g*.

Chapter 5: Functional Characterisation of *CAGL0D05434g* and *CAGL0K05687g*

5.1 Overview

High-throughput phenotypic screening of the *C. glabrata* deletion library (see Chapter 4) identified novel phenotypes associated with the deletion of previously uncharacterised *C. glabrata* ORF *CAGL0D05434g*. *CAGL0D05434g* has no orthologue in *S. cerevisiae* and was a prime candidate for functional characterisation as a possible novel regulator of the stress response in *C. glabrata* due to predicted DNA-binding functional domains (Appendix 4 Table 1). The work presented herein aims to gain insight into the function of *CAGL0D05434g* through examining phenotypes associated with deletion and/or overexpression mutants in *C. glabrata* and the identification of conditions under which *CAGL0D05434g* is required for *C. glabrata* growth.

Due to the limited molecular tools available for the functional characterisation of genes in *C. glabrata* (see 1.4), this chapter aims to exploit the Synthetic Genetic Array (SGA) system established in the model yeast *S. cerevisiae* to further dissect the pathways *CAGL0D05434g* may function within through the generation of genome-wide genetic interaction maps. The development of SGA has proven a powerful tool for the functional annotation of *S. cerevisiae* both essential and non-essential genes (see 1.3.3). For example, examination of the essential genetic interaction network enabled the annotation of uncharacterised *S. cerevisiae* gene *PGA1* in protein sorting or modification in the endoplasmic reticulum (Davierwala *et al.*, 2005). Interrogation of genetic interaction clusters also assigned uncharacterised genes *PAR32*, *ECM30* and *UBP15* to be members of the Gap1-sorting module based on genetic network connectivity (Costanzo *et al.*, 2010).

SGA profiling in species such as *C. glabrata* is hindered by the lack of an apparent sexual cycle and genome-wide deletion arrays. However, *S.*

cerevisiae SGA mediated genetic interaction profiling has been extended to the characterisation of non-*S. cerevisiae* ORFs. Using SGA methods, Brown & Madhani, 2012, were able to successfully predict the function of genes required for virulence in a murine model of *C. neoformans* infection. Comparison of genetic interaction profiles of *C. neoformans* *LIV7* with those of the *S. cerevisiae* genetic landscape found a strong correlation with the genetic interaction profile of *S. cerevisiae* *TRS33*, a vesicle tethering complex involved in ER-to-Golgi transport. Further experimentation validated the function of *LIV7* in Golgi transport in *C. neoformans*. Additionally, *LIV7* was found to genetically interact with *TRS33* in *C. neoformans*, as inferred from genetic interaction profiling in *S. cerevisiae* (Brown & Madhani, 2012). Thus following from genetic interaction studies for *C. neoformans* ORFs and *C. glabrata* ORFs with *S. cerevisiae* orthologues (personal communication, Dr. Jane Usher, University of Exeter), the *S. cerevisiae* SGA platform will be used to dissect the function of *C. glabrata* ORFs with no orthologue in *S. cerevisiae*.

Aims of the chapter:

- 1) Study the impact on deletion and/or overexpression of *CAGL0D05434g* on *C. glabrata* fitness.
- 2) Identify conditions under which *CAGL0D05434g* is required for *C. glabrata* growth using high-throughput phenotypic screening.
- 3) Perform genome-wide genetic interaction profiling to reveal functional information for *CAGL0D05434g* and *CAGL0K05687g* through the use of *S. cerevisiae* SGA methods.

5.2 Materials and Methods

5.2.1 Quantification of *C. glabrata* Colony Size

Images of plates from phenotypic screens (see 4.2.1.1) were acquired using a Syngene G:BOX and uploaded into Gene Tools for automated quantification of colony volume.

5.2.2 Synthetic Genetic Interaction Profiling of *C. glabrata* ORFs

S. cerevisiae query strains overexpressing *C. glabrata* *CAGL0D05434g* were generated for genome-wide genetic interaction profiling. An SGA methodology

previously described by Tong *et al.*, (2005) was used to study genetic interactions of *C. glabrata* CAGL0D05434g with the *S. cerevisiae* non-essential deletion array. All automated pinning steps were performed using a Singer ROTOR HDA robot, Singer PlusPlates© and Singer Repads©.

5.2.2.1 Construction of the SGA Query Strain

C. glabrata ORF CAGL0D05434g was amplified using primers GW-D05434-F and GW-D05434-R (Appendix 1 Table 5), cloned into pENTRY vector pDONR™221 (Life Technologies™; see 2.5) and shuttled into pDEST vectors pAG426GPD-ccdB and pAG416GPD-ccdB (Addgene; Table 2.5). Correct clones were verified by colony PCR using ORF specific primers GW-D05434-F and GW-D05434-R (Appendix 1 Table 5) or plasmid specific primers M13-For and M13-Rev (Appendix 1 Table 4). Destination vectors carrying *C. glabrata* ORF CAGL0D05434g were transformed into *S. cerevisiae* SGA starter strains Y7092 and KH01 (see 2.4.7). Correct transformants were selected for on SC-ura agar. Three correct transformants of each SGA query strain were stored.

5.2.2.2 Condensing the *S. cerevisiae* Deletion Array

The *S. cerevisiae* haploid *MAT α* deletion collection was pinned from 96-well microtiter plate glycerol stocks onto YPD G418 agar PlusPlates© in 96-format and incubated for 24 hours at 30 °C. The deletion array was condensed into 1536-format on fresh YPD G418 PlusPlates©, pinning two technical replicates of each strain. Condensed deletion arrays were incubated at 30 °C for 24 hours.

5.2.2.3 Automated Pinning Steps for the Generation of Double Mutants

SC –ura broth was inoculated with a single colony of *S. cerevisiae* SGA query strains Y7093-D05434, Y7094-D05434, KH02-D05434, KH03-D05434 (see Table 2.2) and grown overnight. 1 ml of overnight culture was transferred and spread onto PlusPlates© containing Sc –ura agar and grown overnight at 30 °C to produce lawns of the SGA query strain. To allow mating to take place between the SGA query strain and the *S. cerevisiae* deletion mutants, cells from the SGA query lawn and the deletion array were pinned onto mating PlusPlates© and incubated for 48 hours at 30 °C. For selection of diploids, cells from mating PlusPlates© were pinned onto diploid selection agar and incubated for 48 hours at 30 °C. Diploids were transferred onto sporulation agar and

incubated for 5 to 21 days at room temperature, checking daily for tetrads. Following observation of approximately 70 % tetrad formation, cells were pinned onto two rounds of *MAT a* haploid selection plates and incubated at 30 °C for 48 hours. Further rounds pinning onto KanR plates and Double Mutant Selection plates allowed for the selection of meiotic progeny and double mutants, respectively. All SGA screens were performed in triplicate biological replicates. The resultant double mutant PlusPlates® were imaged in a Syngene G:BOX imager. Analysis of genetic interactions was performed by visual inspection using colony growth as a read-out for strain fitness. Genetic interactions were categorised as SS (synthetic sick), SL (synthetic lethal), S (suppressor) or NI (no interaction) in instances where a minimum of two out of three biological replicates were in agreement. Functional classification and enrichment analysis of genetic interaction datasets was performed in FunSpec (funspec.med.utoronto.ca; Robinson *et al.*, 2002).

5.2.2.4 Visualisation of Genetic Interactions

Text files containing interaction data were uploaded into Osprey version 1.2.0 for the visualisation of genetic interaction networks.

5.3 Results

5.3.1 Phenotypic Screening of *C. glabrata* Δ CAGL0D05434g

Initial selection of *C. glabrata* CAGL0D05434g for deletion was based on the lack of an orthologue in *S. cerevisiae* according to both Reciprocal Best Hit (RBH) and Yeast Gene Order Browser (YGOB) based searches (Appendix 3 Table 1 and 2). Additionally, InterproScan searches of the CAGL0D05434g encoding sequence identified the presence of a putative DNA-binding domain, predicting this ORF to regulate transcription in response to stress (GO:0043618) and to have nuclear chromatin localisation (GO:0000790) (ebi.ac.uk/interpro/; Appendix 4, Table 1).

The deletion of CAGL0D05434g altered the growth of *C. glabrata* both on rich media and on phenotypic screening conditions. On YPD rich medium, visual inspection found Δ CAGL0D05434g formed smaller colonies than their Cg2001 Δ his3 counterparts (Figure 5.1 A). Volume quantification of 336 individual colonies formed by the parental strain (Cg2001 Δ his3) and Δ CAGL0D05434g

revealed a significant difference (T-test, $p=4.19e-56$) in average colony size. Cg2001 $\Delta his3$ colonies yielded an average colony size of 8187.56 units (Syngene Gene Tools) compared to an average volume of 7642.56 units (Syngene Gene Tools) for $\Delta CAGL0D05434g$ colonies (Figure 5.1 B). Subsequently, FACS analysis was used to decipher whether reduced colony size in the $\Delta CAGL0D05434g$ mutant was accountable to a reduced cell volume in this strain. However, comparison of FACS forward scatter profiles (FSC) revealed Cg2001 $\Delta his3$ and $\Delta CAGL0D05434g$ to have similar cell volume (Figure 5.1 C). Thus, it is proposed that deletion of *C. glabrata* $CAGL0D05434g$ has a negative impact on *C. glabrata* fitness that is independent of cell volume.

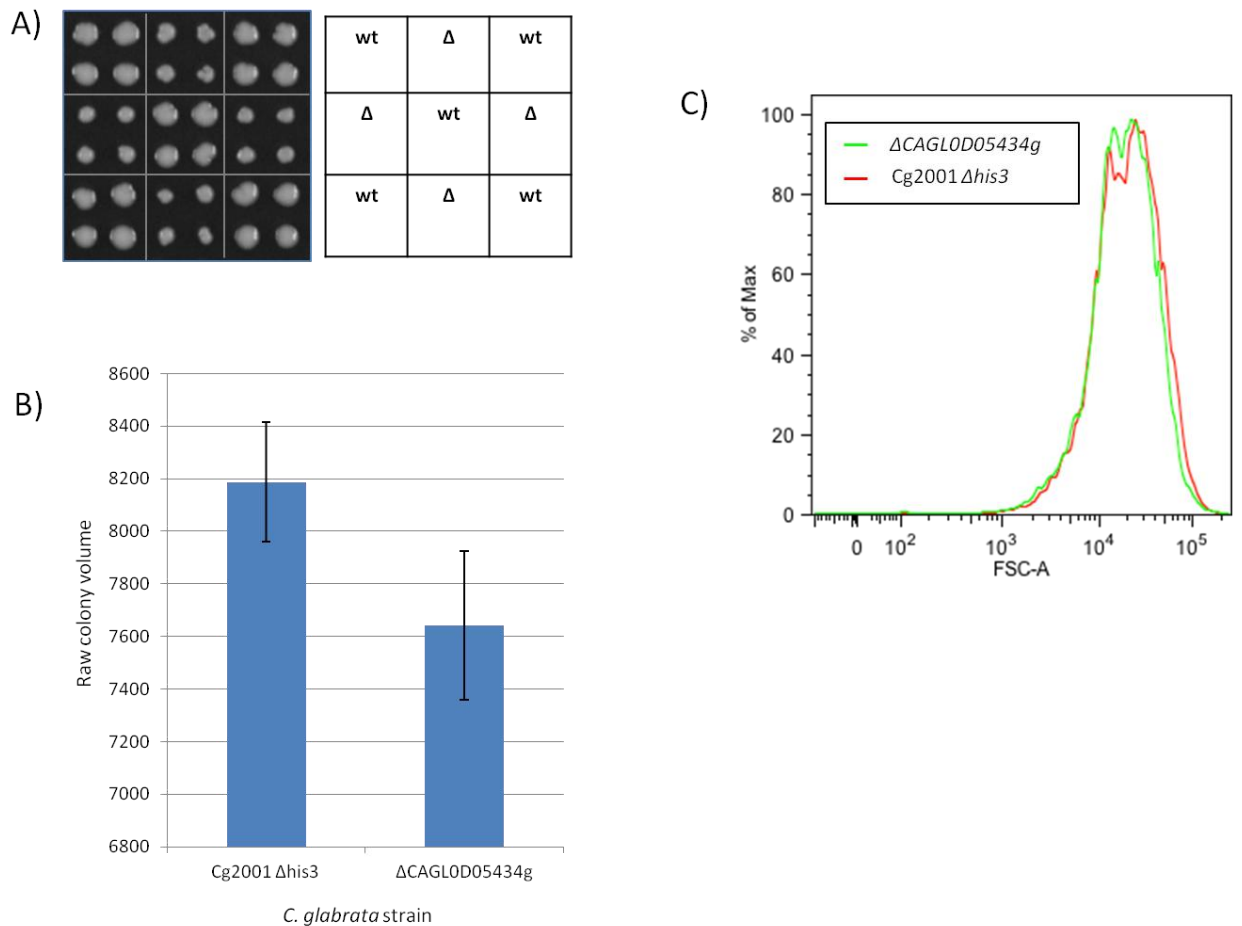


Figure 5.1: Deletion of *CAGL0D05434g* confers reduced *C. glabrata* colony size. A) Comparison of colony size between parental strain *Cg2001 Δ his3* (“wt”) and mutant *Δ CAGL0D05434g* (“ Δ ”) following 48 hours growth on YPD, 30 °C. Strains were spotted from a cell suspension of OD₆₀₀ 0.1 in quadruplicate onto agar plates using a Singer ROTOR HDA robot. B) Volume quantification (Syngene Gene Tools) of 336 *C. glabrata* colonies after 48 hours growth on YPD plates at 30 °C. Bars represent average volume for each strain. Error bars denote standard deviation. C) FACS forward scatter (FSC) profiles for populations of 20,000 *Cg Δ his3* and *Δ CAGL0D05434g* cells.

High-throughput phenotypic screening highlighted the requirement for *C. glabrata CAGL0D05434g* under specific growth conditions. As was observed on YPD controls, *Δ CAGL0D05434g* isolates A and B showed a reduced colony size on all screening conditions tested (Figure 5.2). However, *Δ CAGL0D05434g* mutants showed increased sensitivity to cobalt chloride (1 mM CoCl₂) (Figure 5.2). Moreover, growth of *Δ CAGL0D05434g* isolates was completely inhibited on YPD agar containing arsenic compounds sodium metaarsenite (0.5 mM) and

arsenic (III) oxide (1 mM) as well as manganese chloride (30 mM MnCl₂) and caesium chloride (250 mM CsCl) (Figure 5.2). Therefore, *C. glabrata* CAGL0D05434g is required for growth on arsenic-containing compounds and some metal chlorides, implicating CAGL0D05434g in metal and metalloid tolerance.

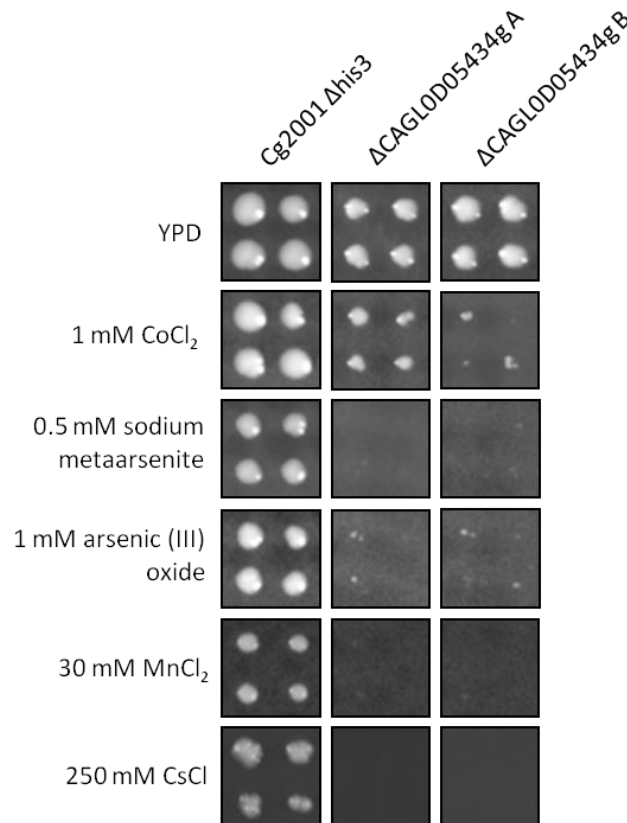


Figure 5.2: Phenotypic screening of ΔCAGL0D05434g. Images show growth of parental strain Cg2001 Δhis3 and two ΔCAGL0D05434g isolates, A and B, in phenotypic screens. Strains were pinned in quadruplicate using a Singer ROTOR HDA robot onto YPD agar plates supplemented with stated chemical agents and incubated at 30 °C for 48 hours. Images not shown for conditions which induced no observable growth defect in deletion mutants.

To further investigate the requirement of *C. glabrata* CAGL0D05434g for growth, liquid growth time courses were performed in YPD broth. In contrast to phenotypic screens, growth profiling of ΔCAGL0D05434g mutants in YPD broth found little significant difference in growth compared with the parental strain Cg2001 Δhis3 (Figure 5.3). *C. glabrata* ΔCAGL0D05434g isolates yielded a significantly extended lag phase, 50-55 minutes longer than that of the parental

strain (ANOVA $p < 0.05$; Appendix 7 Table 1). However, no significant difference in doubling times and saturation density were observed between strains thus highlighting differences between using broth- and agar-based assays for measuring strain fitness. As such, the impact on growth incurred by deletion of *C. glabrata* *CAGL0D05434g* observed in phenotypic screens performed on agar was not fully supported by liquid growth profiles of *C. glabrata* Δ *CAGL0D05434g* mutants. It could be hypothesised that growth phenotypes are exacerbated in phenotypic screening assays where strains are densely pinned and consequently may need to compete for nutrients. In contrast, the monocultures used for liquid growth time courses do not experience competition for nutrients.

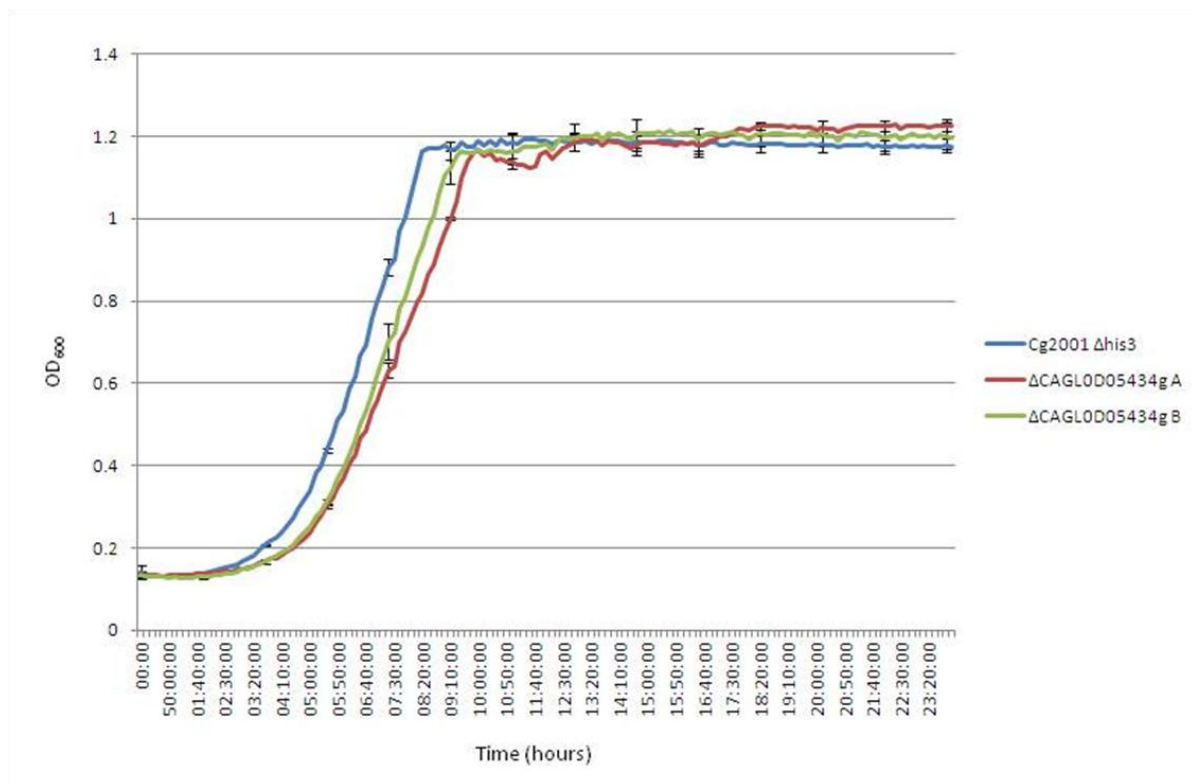


Figure 5.3: Growth profile of two *C. glabrata* Δ CAGL0D05434g isolates A and B (red and green lines) compared with the parental strain Cg2001 Δ his3 in YPD. Starting cultures of OD₆₀₀ 0.1 were incubated at 30 °C for 48 hours in a VersaMax™ Absorbance Microplate Reader (Molecular Devices). OD readings were taken at 10 minute intervals with 550 seconds shaking between reads.

5.3.2 *C. glabrata* CAGL0D05434g Encodes a Putative HMG box Chromatin Remodeler

To further elucidate the functional role *CAGL0D05434g* may have in *C. glabrata*, functional domains encoded by the ORF were predicted bioinformatically. Conserved domain searches of the *C. glabrata* *CAGL0D05434g* protein sequence predicted a High Mobility Group-box (HMG-box) domain at the C-terminus of the protein. The HMG superfamily of chromatin remodelers are well conserved in eukaryotes and are the most prevalent non-histone chromatin-binding proteins in eukaryotic cells (Štros *et al.*, 2007). HMG-box proteins influence transcription, replication, recombination, DNA repair and stability in the cell by binding chromatin via the HMG-box DNA-binding motif and inducing structural changes (Štros, 2010). Multiple sequence alignments of *C. glabrata* *CAGL0D05434g* with well characterised HMG-box proteins *HMGB1* and *HMGB2* from *Homo sapiens* and *HMO1* and *NHP6A* from *S. cerevisiae* shows conservation of the HMG-box DNA binding domain in these sequences, further confirming bioinformatically the presence of an HMG-box DNA binding domain in *C. glabrata* *CAGL0D05434g* (Figure 5.4). The N-terminus of the *C. glabrata* *CAGL0D05434g* protein sequence however shows no alignment, nor does it produce any significant BLASTP hits (e-value < 1e-5) with any other sequences.

HMG-box protein sequences

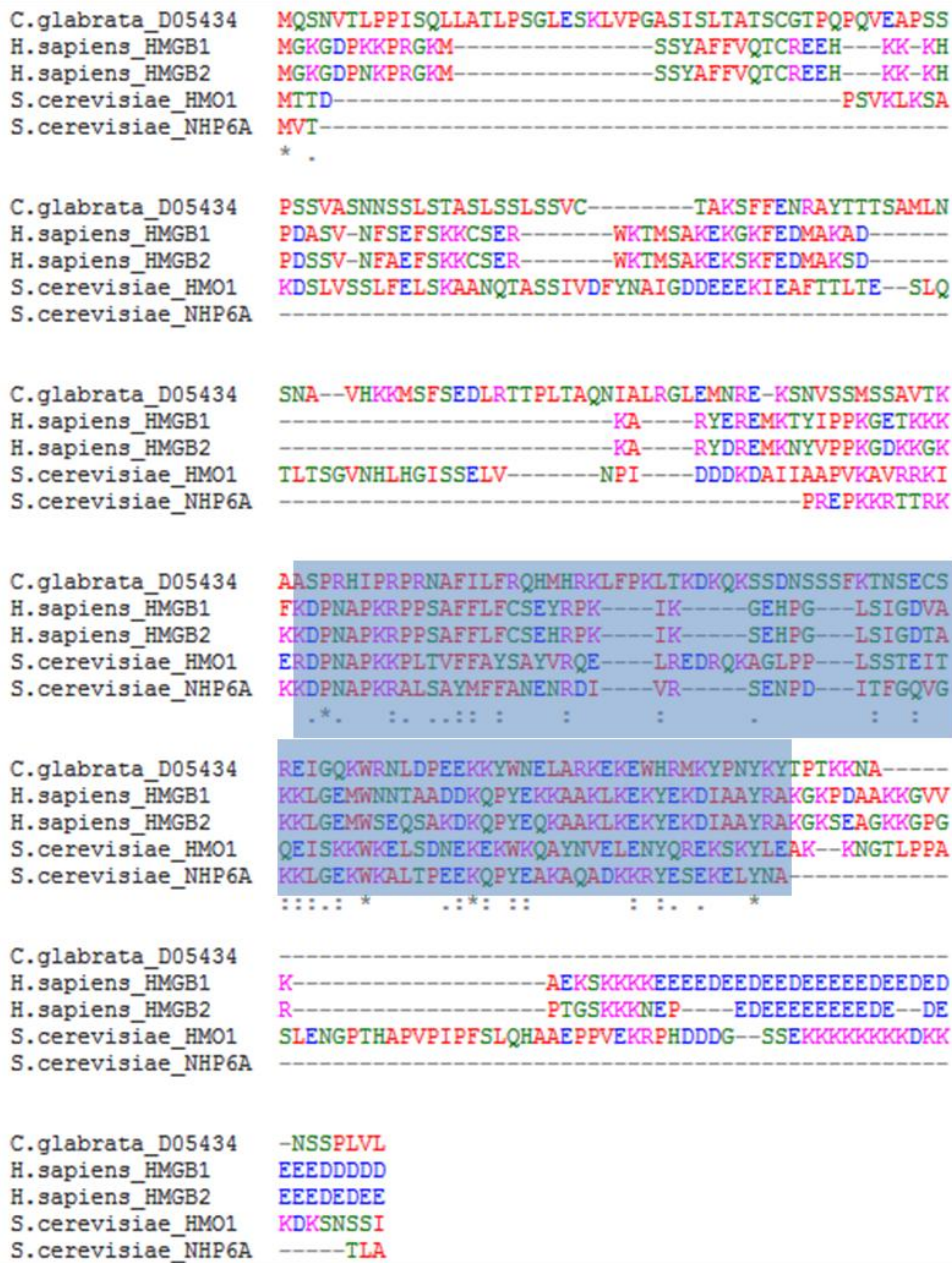


Figure 5.4: Multiple sequence alignment of *C. glabrata* CAGL0D05434g with characterised HMGB proteins HMGB1 & HMGB2 (*Homo sapiens*) and HMO1 & NHP6A (*S. cerevisiae*) showing conservation of a DNA-binding HMG-box domain highlighted in blue. The N-terminus of the protein shows no significant sequence similarity.

More specifically, NCBI Conserved domain searches (ncbi.nlm.nih.gov/Structure/cdd/wrpsb.cgi) further identified the DNA-binding domain of *C. glabrata* CAGL0D05434g to belong to the MATA HMG-box (NCBI cd01389) group, a class I member of the HMG superfamily. Known MATA HMG

proteins includes fungal *MAT* locus genes including *Candida albicans* *MTLa*, *Yarrowia lipolytica* *MATA2*, *Kluyveromyces lactis* *MATa2* (Butler *et al.*, 2004) and *Aspergillus fumigatus* *MAT1-2* (Paoletti *et al.*, 2005) and this group are characterised by the presence of a single HMG-box domain which binds DNA in a strict sequence specific manner (NCBI cl00082). Hence, *CAGL0D05434g* may regulate transcription in *C. glabrata* through binding DNA in a sequence-specific manner via an HMG MATA DNA-binding domain. The prevalence of class I HMG-box proteins associated with the *MAT* locus in both sexual and asexual fungi could implicate a role for *CAGL0D05434g* in a yet unelucidated sexual cycle in *C. glabrata*.

Although *C. glabrata* *CAGL0D05434g* has no orthologue in *S. cerevisiae*, YGOB assigned orthologues for *CAGL0D05434g* in twelve sequenced species (ygob.ucd.ie/). *CAGL0D05434g* orthologues are present in the non-pathogenic species *Vanderwaltozyma polyspora*, *Naumovozya dairenensis*, *Lachancea* species and the cotton pathogen *Eromothecium gossypii* (Table 5.1). However, all orthologues remain uncharacterised in these species. In contrast to *C. glabrata*, all species with orthologues of *CAGL0D05434g* have a known sexual cycle. *S. cerevisiae*, *Naumovozya castellii* and *Kazachstania africana* do not encode orthologues of *C. glabrata* *CAGL0D05434g* and thus it is hypothesised that *CAGL0D05434g* orthologues may have been lost in these species.

Table 5.1: Orthologues of *C. glabrata* CAGL0D05434g in related yeast species (ygob.ucd.ie/)

Species	Orthologue	Sexual reproduction	Pathogen
<i>Vanderwaltozyma polyspora</i>	401.4	Yes	No
<i>Tetrapisispora phaffii</i>	TPHA0C04350	Yes	No
<i>Tetrapisispora blattae</i>	TBLA0J01680	Yes	No
<i>Naumovozyma dairenensis</i>	NDAI0E03570	Yes	No
<i>Naumovozyma castellii</i>	-	Yes	No
<i>Kazachstania naganishii</i>	-	Yes	No
<i>Kazachstania africana</i>	KAFR0G02830	Yes	No
<i>Saccharomyces cerevisiae</i>	-	Yes	No
<i>Zygosaccharomyces rouxii</i>	ZYR0D15312g	Yes	No
<i>Torulaspora delbrueckii</i>	TDEL0H02760	Yes	No
<i>Kluyveromyces lactis</i>	KLLA0B11495g	Yes	No
<i>Eromothecium gossypii</i>	AAR026W	Yes	Yes
<i>Lachancea kluyveri</i>	SAKL0F03872g	Yes	No
<i>Lachancea thermotolerans</i>	KLTH0F13926g	Yes	No
<i>Lachancea waltii</i>	55.21061	Yes	No

5.3.3 SGA Analysis of *C. glabrata* CAGL0D05434g

To dissect the functional role of *C. glabrata* CAGL0D05434g and due to the lack of molecular tools available in *C. glabrata*, further functional analysis was performed in *S. cerevisiae*. In particular the SGA platform was exploited for genetic interaction analysis with the hypothesis that genetic interaction profiling of *C. glabrata* ORF CAGL0D05434g in *S. cerevisiae* may elucidate the pathways and processes it may regulate.

5.3.3.1 Expression of *C. glabrata* CAGL0D05434g Inhibits Growth in *S. cerevisiae*

Firstly, *C. glabrata* CAGL0D05434g was cloned using the Gateway® system. Destination vectors containing CAGL0D05434g were transformed into *S. cerevisiae* SGA strains Y7092 and KH01 for SGA analysis. SGA strains Y7093-

D05434 and KH02-D05434 expressed *CAGL0D05434g* from low copy number destination vector pAG416GPD-ccdB (Addgene; Table 2.2). SGA strains Y7094-D05434 and KH03-D05434 expressed *CAGL0D05434g* from high copy number destination vector pAG426GPD-ccdB (Addgene; Table 2.2).

Growth inhibition was observed for all *S. cerevisiae* SGA strains expressing *C. glabrata CAGL0D05434g*. Liquid growth profiling of SGA query strains KH02-D05434 and KH03-D05434 and their respective control strains, KH02 and KH03, containing empty vector revealed significantly increased doubling times and a reduced final optical density in strains expressing *CAGL0D05434g* (Figure 5.5; Appendix 5 Table 1). The most pronounced difference in doubling times were observed in *S. cerevisiae* strain KH03-D05434 and control strain KH03 which during exponential phase growth, yielded maximum doubling times of 451 and 283 minutes, respectively (two sample T-test, $p=1.35e-11$). Similarly, *S. cerevisiae* KH03-D05434 reached a significantly lower (87.7 %) final saturation OD_{600} of 0.674, compared with a final OD_{600} of 0.768 for control strain KH03 (two sample T-test, $p=1.98e-14$). A less pronounced trend was observed for *S. cerevisiae* KH02-D05434 compared with respective empty vector control KH02 (Appendix 5 Table 1). The lag time for *S. cerevisiae* KH03-D05434 was also significantly increased compared with empty vector controls (two sample T-test, $p=4.94e-5$; Appendix 5 Table 1). For all three measures of growth fitness, a greater impact on *S. cerevisiae* growth was observed upon expression of *C. glabrata CAGL0D05434g* from a high-copy number plasmid. Thus, growth profiling of strains suggested the expression of *C. glabrata CAGL0D05434g* in *S. cerevisiae* inhibits growth in a dose dependent manner (Figure 5.5).

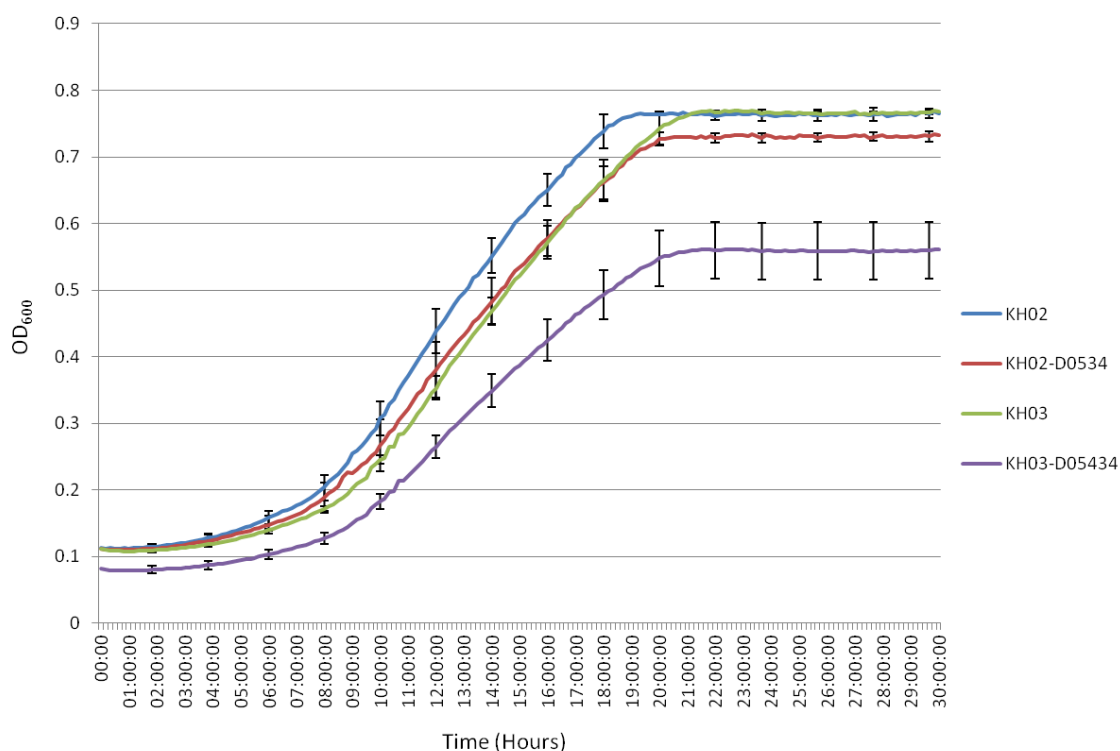


Figure 5.5 Growth profile of *S. cerevisiae* SGA strains expressing *C. glabrata* ORF *CAGL0D05434g*. KH02-D05434 expresses *CAGL0D05434g* from a low copy number plasmid pAG416GPD-ccdB (empty vector control KH02). KH03-D05434 expresses *CAGL0D05434g* from a high copy number plasmid pAG426GPD (empty vector control KH03). The optical density of cultures of strains at a starting OD₆₀₀ of 0.1 were measured every ten minutes for 30 hours at 30 °C with continuous shaking.

5.3.3.2 Expression of *C. glabrata* *CAGL0D05434g* Inhibits the Formation of Double Mutants by SGA

Four SGA screens were performed using two *S. cerevisiae* query strains expressing *C. glabrata* *CAGL0D05434g*: KH02-D05434, KH03-D05434, Y7093-D05434 and Y7094-D05434 (see Table 2.2). Following selection of diploid cells, no tetrad formation was observed up to 30 days post transfer in all screens. To confirm that sporulation had not taken place, cells from sporulation plates were taken forward for continuation of the Mata haploid and double mutant selection stages of the SGA screen. However, no *S. cerevisiae* mutants overexpressing *C. glabrata* *CAGL0D05434g* were obtained following double mutant selection. Thus, SGA screens using an *S. cerevisiae* starter strain overexpressing *C. glabrata* ORF *CAGL0D05434g* were unable to yield double mutants for genetic interaction analysis (Figure 5.6).

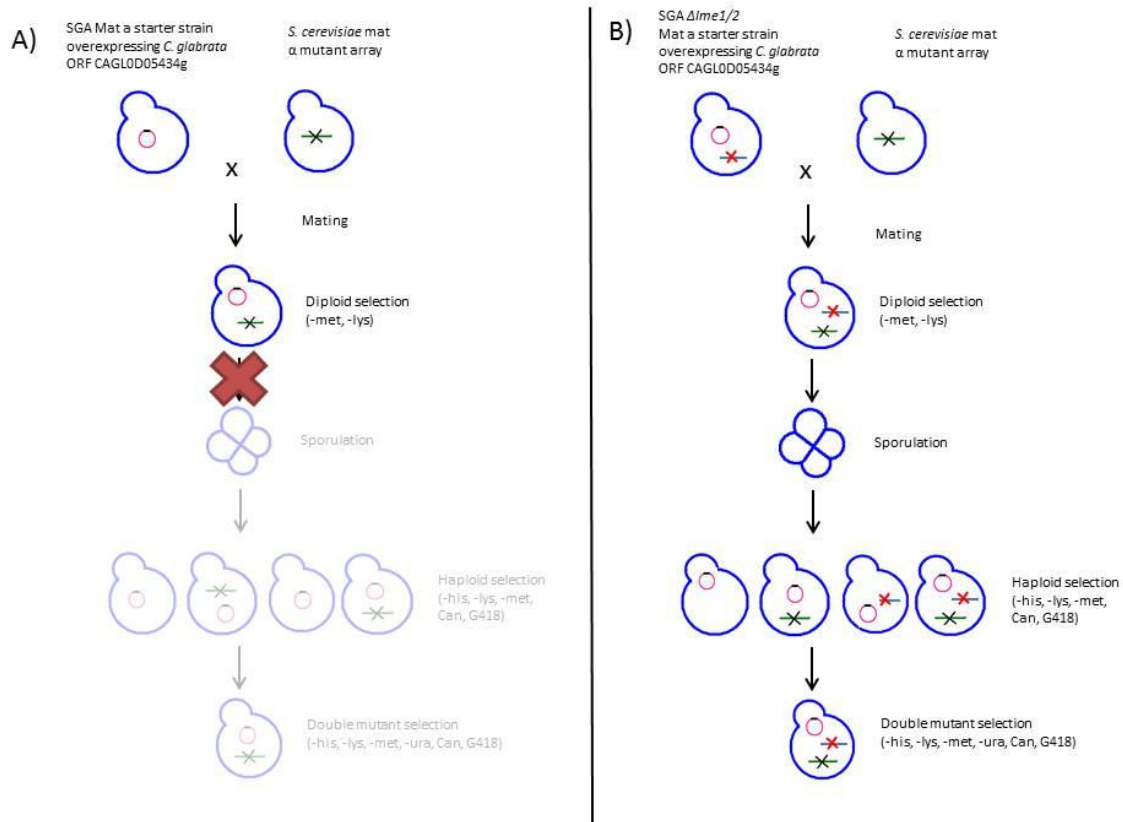


Figure 5.6: Schematic describing the formation of double mutants by SGA. *S. cerevisiae* SGA query strains expressing *C. glabrata* *CAGL0D05434g* were mated with the *S. cerevisiae* non-essential deletion array. From mating plates, diploid cells were selected (-met, -lys) and allowed to sporulate. Following sporulation, 3 rounds of pinning enabled the selection of haploid meiotic progeny (-his, -met -lys, 100 mg/ml canavanine, 200 μ g/ml G418). Lastly, *S. cerevisiae* deletion mutants expressing *CAGL0D05434g* were selected on double mutant selection agar (-ura, -his, -met -lys, 100 mg/ml canavanine, 200 μ g/ml G418). A) SGA query strains expressing *CAGL0D05434g* were unable to proceed past the diploid selection stages of SGA and no tetrads were formed. B) Expression of *CAGL0D05434g* in *S. cerevisiae* $\Delta IME1$ or $\Delta IME2$ starter strains enabled progression through all selection stages of SGA forming *S. cerevisiae* mutants expressing *C. glabrata* *CAGL0D05434g*.

Due to the inability of *S. cerevisiae* query strains expressing *C. glabrata* *CAGL0D05434g* to generate double mutants, the impact of expressing *C.*

glabrata CAGL0D05434g in *S. cerevisiae* backgrounds lacking major regulators of meiosis was investigated. In *S. cerevisiae* *IME1* encodes the major transcriptional regulator of meiosis and *IME2* encodes a meiosis-specific kinase (Kassir *et al.*, 2003). As such *C. glabrata* CAGL0D05434g was transformed into *S. cerevisiae* Δ *IME1* or Δ *IME2* background strains on a high copy number plasmid yielding two SGA strains: Δ *IME1*-D05434 or Δ *IME2*-D05434 (see Table 2.2). Following mating and selection for diploids, Δ *IME1*-D05434 and Δ *IME2*-D05434 were able to form viable tetrads. Therefore, Δ *IME1*-D05434 and Δ *IME2*-D05434 query strains were used to investigate the genetic interactions of *C. glabrata* CAGL0D05434g (personal communication Dr. Jane Usher, University of Exeter; Figure 5.6).

5.3.3.3 Genetic Interactions for *C. glabrata* CAGL0D05434g

SGA screens were performed on *S. cerevisiae* query strains Δ *IME1*-D05434 and Δ *IME2*-D05434. In order to examine genetic interactions specifically associated with the expression of *C. glabrata* ORF CAGL0D05434g, genetic interaction data from Δ *IME1*-D05434 or Δ *IME2*-D05434 SGA screens were compared with that of *S. cerevisiae* Δ *IME1* and *S. cerevisiae* Δ *IME2* (Figure 5.7; personal communication Dr Jane Usher, University of Exeter). Surprisingly, few genetic interactions were common between two or more query strains. Whilst the majority of genetic interactors were unique to each query strain, Sc Δ *Ime1*-D05434 and Sc Δ *Ime1* shared four genetic interactions including *S. cerevisiae* *DDC1*, encoding a DNA damage checkpoint protein; threonine synthase, *THR4*; DNA-dependent ATPase, *RDH54*; and inner mitochondrial membrane protein, *MDM31* (Figure 5.8). Similarly, just 4 genetic interactions were common to both query strains Sc Δ *Ime2*-D05434 and Sc Δ *Ime2*. The majority of interacting genes were unique to each query strain (Figure 5.9). Common interactors included *S. cerevisiae* polyubiquitin gene *UBI4*; alanine transaminase, *ALT1*; mitochondrial fatty acid synthase, *OAR4*; and *KES1*, a negative regulator of Golgi secretory function.

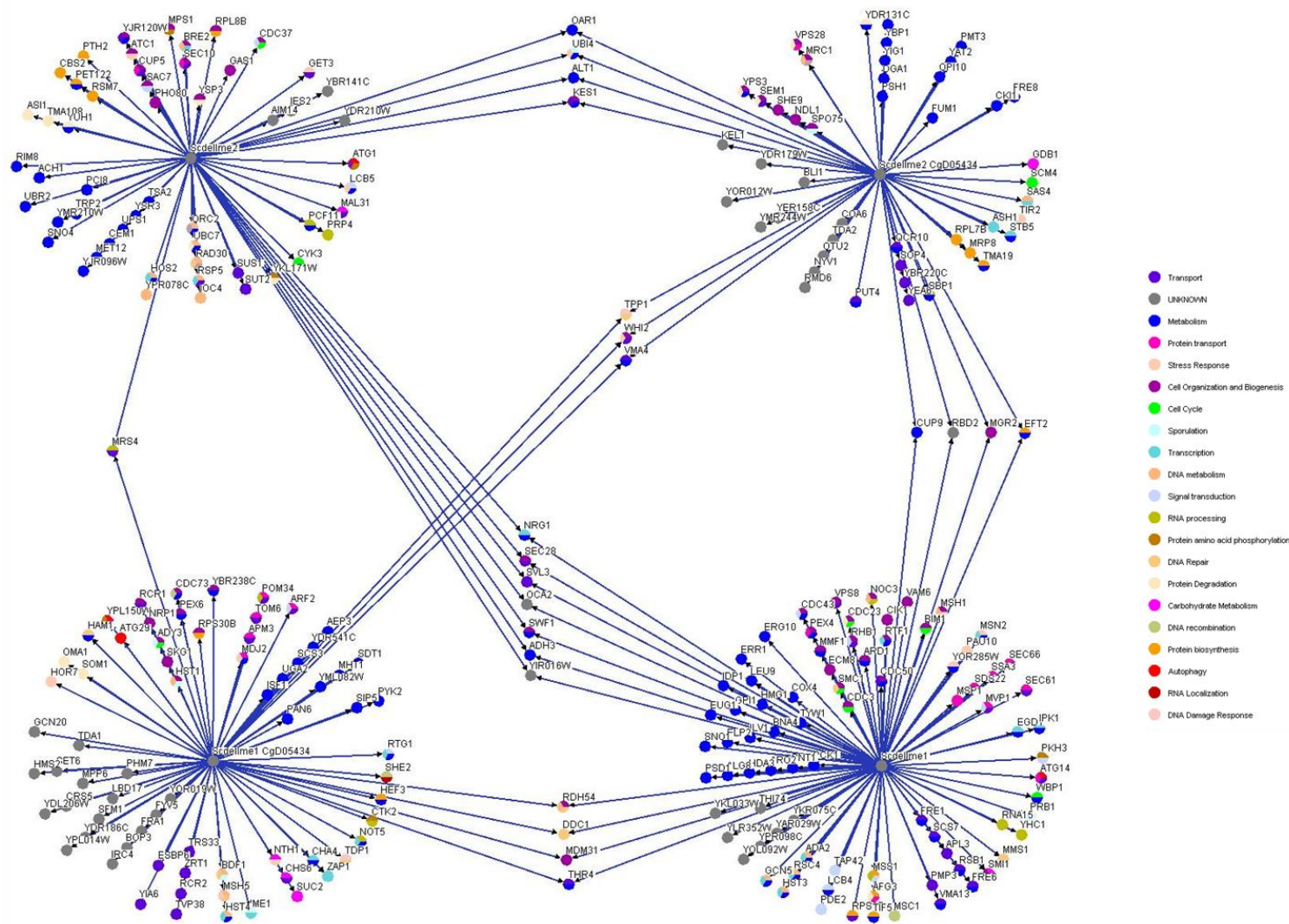


Figure 5.7: Genetic interaction maps for SGA query strains *S. cerevisiae* Δ *IME1* “ScdellIME2” and Δ *IME2* “ScdellIME2” and *S. cerevisiae* Δ *IME1* and Δ *IME2* overexpressing *C. glabrata* *CAGL0D05434g* “ScdellIME1 CgD05434” and “ScdellIME2 CgD05434” respectively. Query strains are represented by central grey nodes. Edges connecting nodes represent genetic interactions between genes. Nodes are coloured according to associated GO terms.

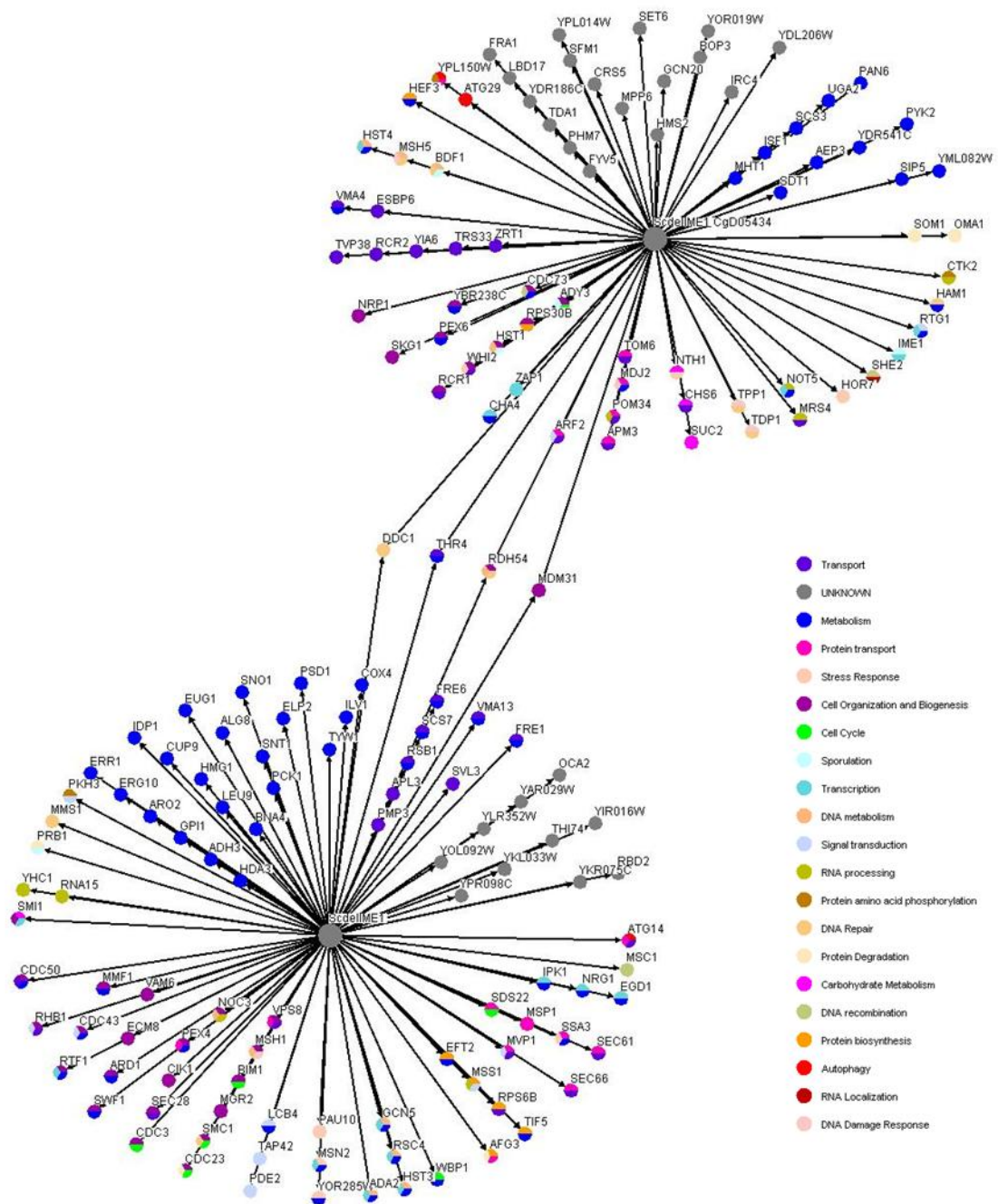


Figure 5.8: Genetic interaction maps for SGA query strains *S. cerevisiae* Δ IME1 "ScdellIME1" and *S. cerevisiae* Δ IME1-D05434 overexpressing *C. glabrata* CAGL0D05434g "ScdellIME1 CgD05434" represented by enlarged grey nodes. Edges represent genetic interactions between connected genes represented by their respective node. Nodes are coloured according to associated GO terms.

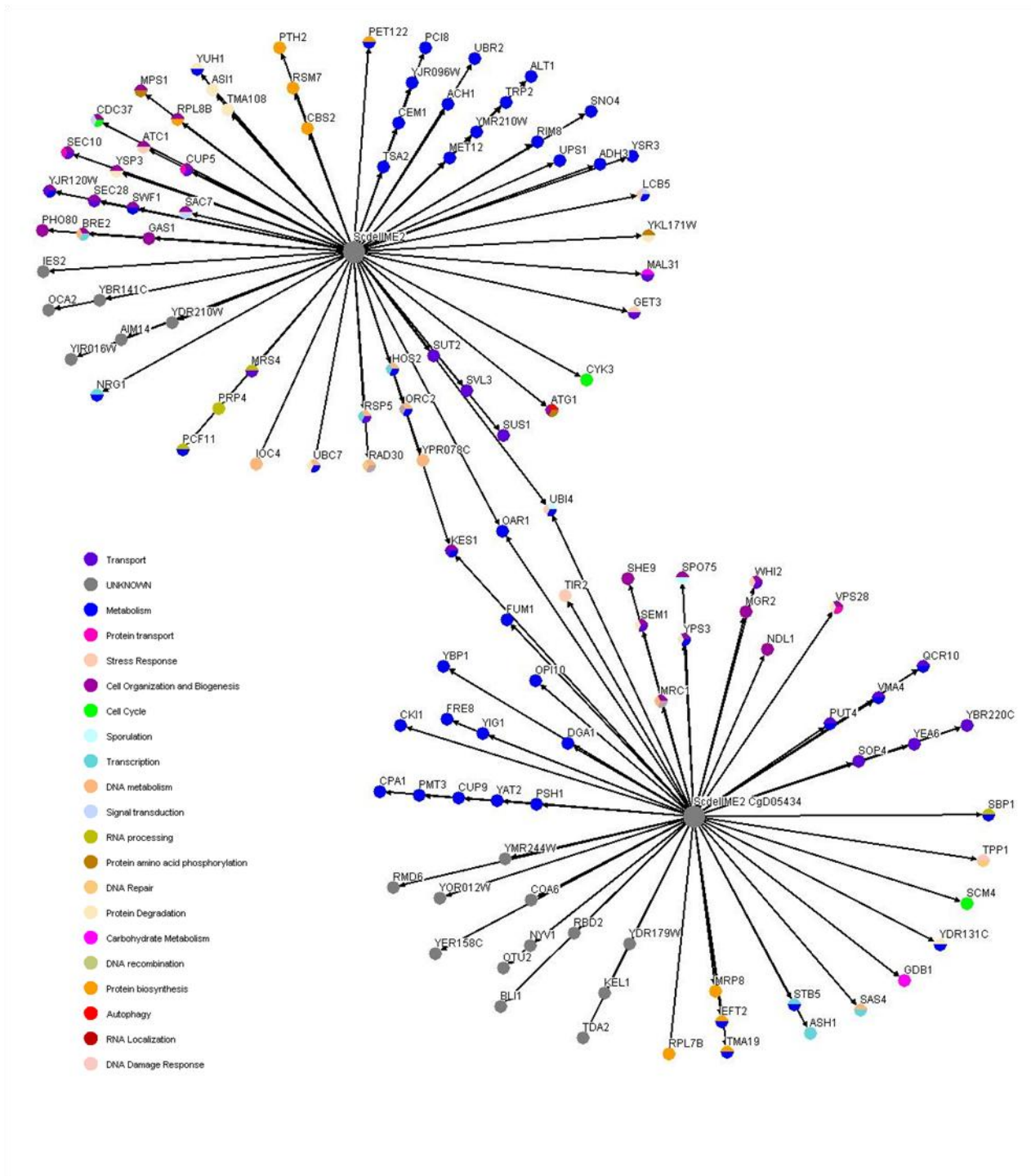


Figure 5.9: Genetic interaction maps for SGA query strains *S. cerevisiae* Δ IME2 “Scd1IME2” and *S. cerevisiae* Δ IME2 over-expressing *C. glabrata* CAGL0D05434g “Scd1IME2 CgD05434” represented by enlarged grey nodes. Edges connecting nodes represent genetic interactions between genes. Nodes are coloured according to associated GO terms.

S. cerevisiae Sc Δ *Ime1*-D05434 and Sc Δ *Ime2*-D05434 showed genetic interactions with 79 and 57 *S. cerevisiae* genes, respectively (Figure 5.7; Appendix 6 Table 1 & 2). Common to both *CAGL0D05434g*-expressing query strains were genetic interactions with *TPP1*, encoding a DNA 3'-phosphatase required for the repair of endogenous DNA damage; *WHI2*, an activator of the general stress response; and *VMA4*, which encodes a V1 subunit of V-ATPase and whose abundance is increased in response to DNA replication stress (yeastgenome.org). To elucidate the pathways *C. glabrata* *CAGL0D05434g* may function within, functional classification analysis of interacting *S. cerevisiae* genes from Sc Δ *Ime1*-D05434 and Δ *Ime2*-D05434 SGA screens was performed using FunSpec (funspec.med.utoronto.ca/). For *S. cerevisiae* genes which yielded genetic interactions with the Sc Δ *Ime1*-D05434 query strain, analysis found six significantly enriched GO Biological Process terms (Table 5.2). Protein deacetylation was significantly represented ($p=0.0020552$) in the genetic interaction list due to interactions with sirtuins *HST1* and *HST4*, NAD(+)-dependent histone deacetylase components of the transcriptional silencing machinery associated with maintenance and silencing at telomeres. The presence of core stress response activator *WHI2*, autophagy-specific gene *ATG29* and an uncharacterised ORF *YOR019W* in the genetic interaction list significantly represent mitochondrion degradation ($p=0.004815$). Functional classification also highlighted significant enrichment of genes implicated in vesicle-mediated transport ($p=0.00638$; Table 5.2) including endosomal vacuolar trafficking pathway genes, *RCR1* and *RCR2*, and regulator of coated vesicle formation, *ARF2*. Enrichment of DNA damage ($p=0.002314$), sporulation ($p=0.007581$) and ion homeostasis ($p=0.008631$) genes were also significantly represented in the Δ *Ime1*-D05434 genetic interaction list (Table 5.2).

Table 5.2: Significantly enriched GO Biological Process terms amongst *S. cerevisiae* genes which showed genetic interactions with *C. glabrata* CAGL0D05434g in SGA screens of query strain Δ Ime1-D05434

(funspec.med.utoronto.ca/). “k” represents the number of genes from the input cluster in a given category. “f” represents the number of genes total in a given category.

Category	p-value	In Category from Cluster	k	F
protein deacetylation [GO:0006476]	0.002055	<i>HST4 HST1</i>	2	6
response to DNA damage stimulus [GO:0006974]	0.002314	<i>RDH54 TDP1 MSH5 CTK2 HAM1 BDF1 TPP1 DDC1</i>	8	197
mitochondrion degradation [GO:0000422]	0.004815	<i>YOR019W WHI2 ATG29</i>	3	29
vesicle-mediated transport [GO:0016192]	0.00638	<i>RCR1 APM3 ARF2 RCR2 TVP38 TRS33</i>	6	140
sporulation resulting in formation of a cellular spore [GO:0030435]	0.007581	<i>OAF1 ADY3 IME1 BDF1 HST1</i>	5	103
cellular ion homeostasis [GO:0006873]	0.008631	<i>FYV5 MDM31</i>	2	12

Automated functional specification analysis of Δ IME2-D05434 interactors yielded functional annotation of low significance. However, manual inspection and annotation of both Δ IME1-D05434 and Δ IME2-D05434 genetic interaction datasets identified three major groups of *S. cerevisiae* genes implicated in DNA replication/damage stress, metal ion homeostasis and mating, meiosis and sporulation. Firstly, a total of 16 *S. cerevisiae* genes with known functional roles in mating, meiosis and sporulation were identified within Δ IME1-D05434 and Δ IME2-D05434 genetic interaction datasets (Appendix 6 Tables 1 & 2). Genetic interactors included meiosis genes *MSH5*, a facilitator of homologue crossover during meiosis; *RMD6*, required for meiotic nuclear division; and spore wall formation genes *SPO75* and *ADY3*. Secondly, manual inspection of the genetic interaction datasets also identified 27 *S. cerevisiae* genes associated with DNA replication stress and DNA damage repair (Appendix 6 Tables 1 & 2), for example *DDC1*, a known major DNA-damage checkpoint protein; *TPP1*, a DNA 3'-phosphatase required for the repair of endogenous damage to double-

stranded DNA; and *MRC1*, an S-phase checkpoint protein required for DNA replication. Within the genetic interaction datasets were also genes whose protein abundance increase in response to DNA damage including *ATG29*, *CDC73*, *HAM1*, *COA6*, *CUP9* and *MRP8* (Appendix 6 Tables 1 & 2). Lastly, a group of metal ion homeostasis and transport genes were represented in the genetic interaction dataset. Of particular interest were iron transporter, *MRS4*; an iron/copper reductase involved in iron homeostasis, *FRE8*; and *FRA1*, a negative regulator of cellular iron concentration. Also present in the list are zinc-regulated transcription factor, *ZAP1*, and zinc transporter, *ZRT1* (Appendix 6 Tables 1 & 2). Taken together, *S. cerevisiae* genetic interaction data can be used to drive hypotheses relating to a putative functional role for *C. glabrata* *CAGL0D05434g* DNA replication/damage stress, metal ion homeostasis or in meiosis and sporulation, perhaps in an undiscovered sexual cycle.

5.3.4 *C. glabrata* *CAGL0D05434g* is required for growth in response to DNA damage

Genetic interaction profiling of *C. glabrata* *CAGL0D05434g* revealed significant enrichment of genetic interactions with *S. cerevisiae* genes implicated in DNA damage response (Table 5.2). To investigate whether genetic interaction data for *C. glabrata* ORFs gained in *S. cerevisiae* could be extrapolated to reveal relevant insights into *C. glabrata* biology, the role of *C. glabrata* *CAGL0D05434g* was explored by phenotypic screening of deletion and overexpression mutants in response to DNA damage agents (Figure 5.10). In support of this hypothesis, deletion mutant Δ *CAGL0D05434g* showed greatly reduced growth on YPD supplemented with 50 mM HU (hydroxyurea) and 0.05 % MMS (methyl methanesulfonate) (Figure 5.10). HU inhibits ribonucleotide reductase hence preventing dNTP production and DNA synthesis (Hampsey, 1997) thus sensitivity of Δ *CAGL0D05434g* to growth on HU implies a defect in DNA replication. Sensitivity to growth on MMS, an alkylating agent inducing DNA damage (Hampsey, 1997), also signifies defective DNA damage repair in Δ *CAGL0D05434g*. Consistent with these observations, *C. glabrata* *CAGL0D05434g* overexpression strain (Cg2001 Δ *his3* p423GPD-D05434) showed increased resistance to growth on 0.1 % MMS and 100 mM HU compared with an empty vector control strain (Cg2001 Δ *his3* p423GPD) (Figure 5.10). Surprisingly, Δ *CAGL0D05434g* showed no reduction in growth compared

with parental strain Cg2001 $\Delta his3$ in response to exposure to UV light which induces DNA damage (Figure 5.10). Thus $\Delta CAGL0D05434g$ growth was inhibited by chemically-induced DNA damage only.

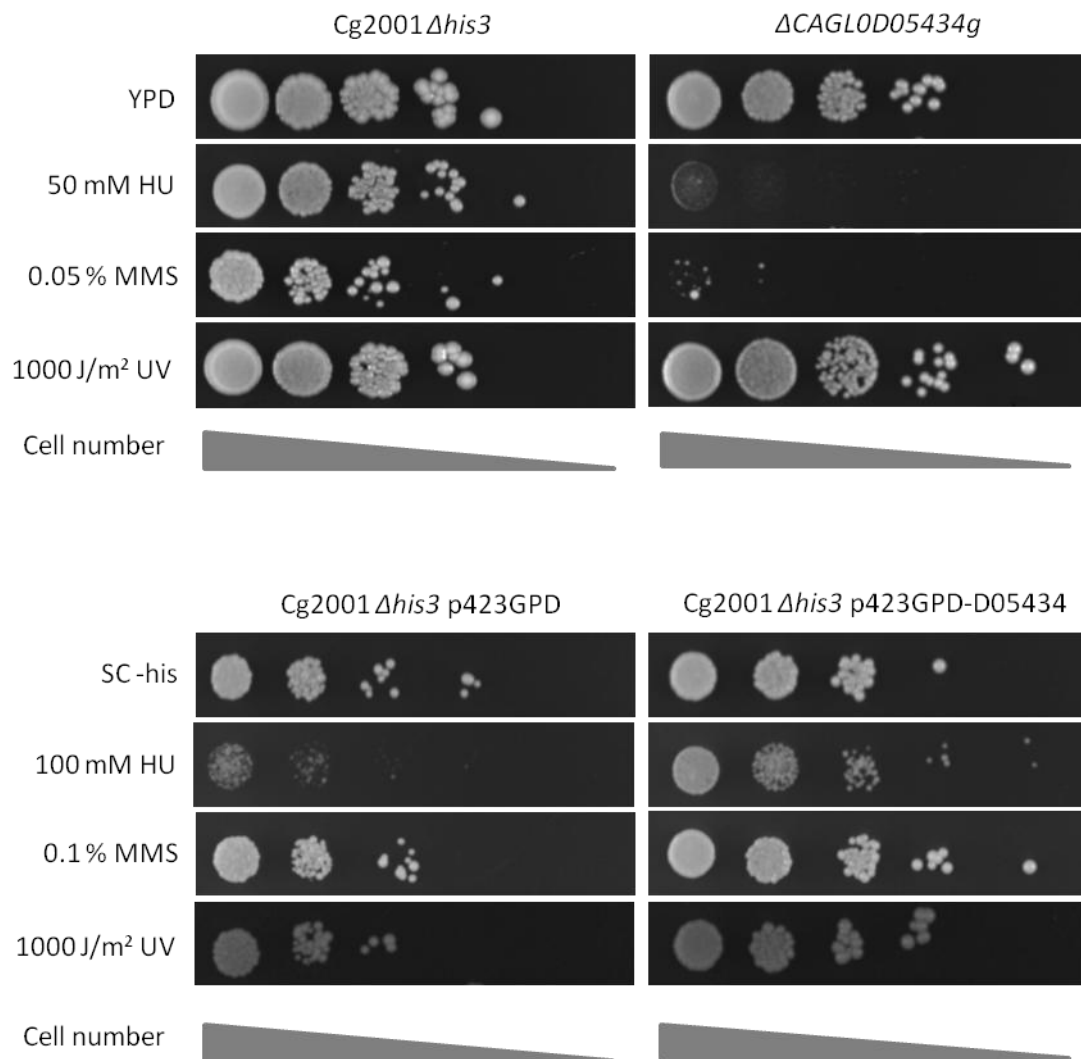


Figure 5.10: Phenotypic screening of *C. glabrata* *CAGL0D05434g* deletion and overexpression mutants on DNA damage agents hydroxyurea (HU), methyl methanesulfonate (MMS) and UV light. Deletion mutant Cg $\Delta CAGL0D05434g$ and parental strain Cg2001 $\Delta his3$ were grown on YPD and incubated at 30 °C for 2 days. Overexpression mutant Cg2001 $\Delta his3$ p423GPD-D05434 and empty vector control strain Cg2001 $\Delta his3$ p423GPD were incubated at 30 °C for 3 days.

5.3.5 Genetic Interactions of *C. glabrata* CAGL0K05687g

Deletion of *CAGL0K05687g* rendered *C. glabrata* attenuated for virulence in an immunocompromised *Drosophila melanogaster* larvae model of infection (Figure 4.11 A). In addition, Δ *CAGL0K05687g* strains were observed to have increased biofilm forming capacity compared with parental strain Cg2001 Δ *his3* (Figure 4.9 A). Bioinformatic searches identified an NADH:flavin oxidoreductase domain throughout the *CAGL0K05687g* encoding protein (Appendix 4 Table 1). However, phenotypic screens yielded no observable phenotypes for Δ *CAGL0K05687g* isolates (Table 4.3). Following the successful use of genetic interaction profiling to identify a role for *C. glabrata* CAGL0D05434g in the DNA-damage response (Table 5.2; see 5.3.4), systematic genetic interaction analysis was employed to identify pathways or processes *C. glabrata* CAGL0K05687g may act within and thus uncover how *CAGL0K05687g* may contribute to *C. glabrata* virulence. SGA screens were performed for *S. cerevisiae* query strain KH03-K05687, expressing *C. glabrata* CAGL0K05687g. Double mutant analysis found *C. glabrata* CAGL0K05687g to genetically interact with 115 *S. cerevisiae* ORFs (Figure 5.11; Appendix 12 Table 1).

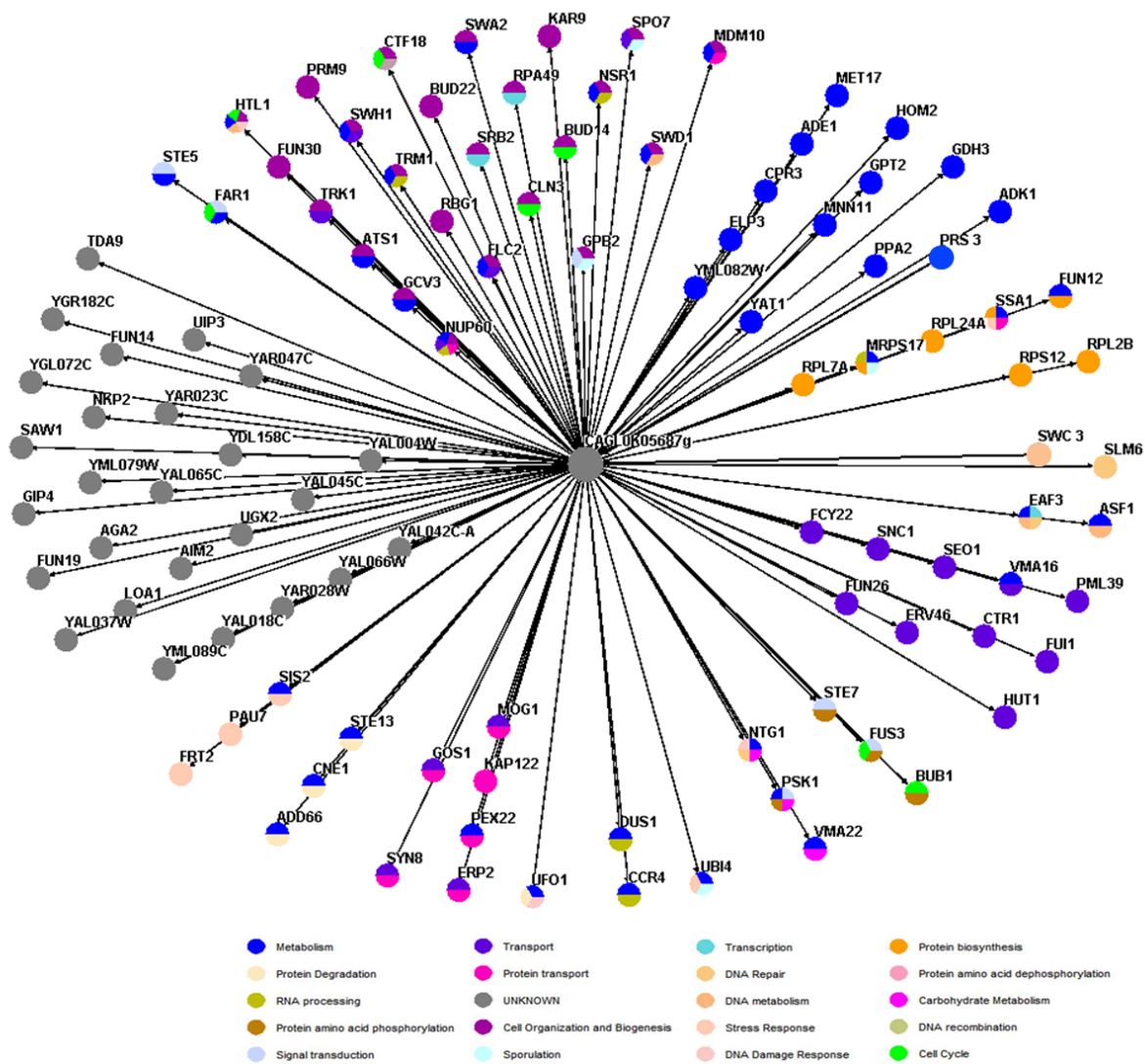


Figure 5.11: Genetic interaction maps for SGA query strains KH03-K05687 expressing *C. glabrata* CAGL0K05687g. Query strains are represented by central grey nodes. Edges connecting nodes represent positive and negative genetic interactions between genes. Nodes are coloured according to associated GO terms.

Table 5.3: Significantly enriched GO terms relating to the molecular function, biological process and cellular component of *S. cerevisiae* genes which showed genetic interactions with *C. glabrata* CAGL0K05687g in SGA screens of query strain KH03-K05687 (funspec.med.utoronto.ca/). “k” represents the number of genes from the input cluster in a given category. “f” represents the number of genes total in a given category.

Category	p-value	In Category from Cluster	K	f
Molecular Function				
SNAP receptor activity [GO:0005484]	0.003204	<i>SYN8 SNC1 GOS1</i>	3	24
nucleobase transmembrane transporter activity [GO:0015205]	0.00658	<i>FUI1 FCY22</i>	2	10
Biological process				
regulation of cell size [GO:0008361]	0.000496	<i>CLN3 KAP122 PRS3 RPA49</i>	4	30
nucleobase transport [GO:0015851]	0.00658	<i>FUI1 FCY22</i>	2	10
histone exchange [GO:0043486]	0.007977	<i>SWC3 ASF1</i>	2	11
Cellular Component				
integral to membrane [GO:0016021]	0.007835	<i>MDM10 SYN8 YAL018C FRT2 SNC1 ERV46 FLC2 PEX22 CNE1 YAL065C SEO1 NUP60 YAR023C UIP3 YAR028W PRM9 FUI1 FCY22 KAP122 GOS1 TRK1 MNN1 GPT2 HUT1 CTR1 VPS66</i>	26	1303

Statistical analysis of the *S. cerevisiae* genetic interaction dataset found a significant enrichment of genes implicated in SNAP receptor activity (GO:0005484; p=0.003204) (Table 5.3). This category included *S. cerevisiae* *SYN8*, an endosomal SNARE (SNAP receptor protein), as well as vesicle associated SNARES (v-SNARES) *SNC1* and *GOS1* (yeastgenome.org) implicated in vesicle-mediated transport of cargo between cellular organelles (Bonifacino & Glick, 2004). Manual inspection of the genetic interaction dataset further identified two *S. cerevisiae* genes *VSP8* and *ERV46* which are also implicated in vesicle tethering and membrane fusion (Appendix 12 Table 1; yeastgenome.org). Additionally, *C. glabrata* CAGL0K05687g showed genetic interactions with 26 membrane proteins (GO:0016021, p=0.007835), including

nucleobase transporters *FUI1* and *FCY22* (GO:0015851; p=0.658) and high affinity potassium and copper transporters *TRK1* and *CRT1* (Appendix 12 Table 1). Genetic interactions of *C. glabrata* *CAGL0K05687g* was also observed amongst *S. cerevisiae* histone exchange genes (GO:0043486, p=0.007977) including *SWC3*, a component of the SWR chromatin remodelling complex, and *ASF1*, a nucleosome assembly factor with anti-silencing properties (Table 5.3; yeastgenome.org). Genetic interactions were also identified with transcriptional silencing factors *SWD1* and *FUN30* (Appendix 12 Table 1).

5.4 Discussion

Bioinformatic searches identified uncharacterised *C. glabrata* ORF *CAGL0D05434g* to encode a putative transcription factor with no orthologue in *S. cerevisiae* (Appendix 3 Table 1 and 2). In this chapter, screening of a *CAGL0D05434g* mutant for growth phenotypes was used to uncover novel phenotypes associated with the deletion of this uncharacterised ORF and elucidate the functional role this ORF may play in *C. glabrata*. The use of the *S. cerevisiae* SGA system for mapping genome-wide genetic interactions of *C. glabrata* ORFs was explored as tool to identify pathways *CAGL0D05434g* may regulate.

5.4.1 *C. glabrata* *CAGL0D05434g* is required for fitness and growth on metal and metalloid compounds

Phenotypic screens revealed reduced fitness of *CAGL0D05434g* deletion strains on rich media, resulting in reduced colony size (Figure 5.1 A and B) and raising speculation that *CAGL0D05434g* may be important for fitness in *C. glabrata*. Further, *C. glabrata* *CAGL0D05434g* was found to be required for growth on metal compounds (cobalt-, manganese- and caesium chloride) and metalloid compounds (arsenic (III) oxide and sodium metaarsenite) (Figure 5.2). Whilst low levels of metals are required for normal cell physiology (Hood & Skaar, 2012), for example as cofactors of enzymes or for protein structure (Ragsdale, 2006), increased levels of metals/metalloids are highly toxic to cells (Avery, 2001; Lin *et al.*, 2010). In yeast, the accumulation of reactive oxygen species (ROS) and depletion of cellular glutathione (GSH) is a major cause of metal/metalloid-induced cytotoxicity and thus could contribute to the sensitive growth phenotype of *C. glabrata* *CAGL0D05434g* mutants (Avery, 2000;

Wysocki & Tamás *et al.*, 2010; Thorsen *et al.*, 2012). Yeast cells exposed to metals and metalloids, in particular arsenic, elicit an oxidative stress transcriptional response mediated by Yap1p, accompanied by chronic activation of Msn2p and Msn4p, regulators of the general stress response (Hosiner *et al.*, 2009). However, it is unlikely that oxidative stress encountered as a consequence of metal/metalloid toxicity inhibited growth of *C. glabrata* *CAGL0D05434g* deletion mutants since no phenotypes were observed for these strains in response to oxidative stress-inducing agents hydrogen peroxide (H₂O₂), t-butyl hydroperoxide (tBOOH) or menadoine. It is more likely that the metal/metalloid-induced growth defect in *C. glabrata* *CAGL0D05434g* was caused by other mechanisms of metal/metalloid-induced toxicity such as impaired DNA repair, inhibition of enzyme function or disturbance of cell cycle progression (Wysocki & Tamás, 2010). Therefore, it was hypothesised that *C. glabrata* *CAGL0D05434g* may function in the tolerance to cytotoxicity induced by metal and metalloid compounds.

5.4.2 *C. glabrata* *CAGL0D05434g* Encodes a Putative MATA HMG-box Domain

Bioinformatic analysis revealed the presence of a conserved HMG-box domain at the C- terminus of the *CAGL0D05434g* encoding protein, which is highly similar to that of other chromatin remodelling HMG-box proteins in yeast and humans (Štros, 2010; Figure 5.4). In particular, the HMG-box domain of *C. glabrata* *CAGL0D05434g* was assigned to the class I MATA HMG-box family. MATA HMG-box proteins are present at the MAT loci of many fungi where they play regulatory roles in the mating systems of these species (Butler *et al.*, 2004). In filamentous fungi such as the *Aspergillus* species, MATA HMG proteins drive the expression of sex-specific genes, sexual development and the coordination of ascospore formation (Shiu & Glass, 2000; Paoletti *et al.*, 2005; O'Garman *et al.*, 2009; Czaja *et al.*, 2011). In several hemiascomycete species (excluding *S. cerevisiae*) HMG-box protein *MATa2* are found in the *MATa* idiomorph (Butler *et al.*, 2004), expression of which has been shown to regulate mating in *Y. lipolytica* and *C. albicans* (Kurischko *et al.*, 1999; Tsong *et al.*, 2003). Despite *C. glabrata* *CAGL0D05434g* belonging to the MATA HMG domain family, *CAGL0D05434g* is not an orthologue of the *MATA2* gene. However, *C. glabrata* *CAGL0D05434g* has uncharacterised orthologues in a number of related

species - many of which have a sexual cycle, although it is unknown whether these ORFs encode proteins implicated in mating, meiosis or sporulation (Table 5.1). Due to a high number of genetic interactions with mating, meiosis and sporulation genes and the association of MATA HMG-box proteins with the MAT loci, *C. glabrata* *CAGL0D05434g* is hypothesised to play a role in an undiscovered sexual cycle, or may have evolved new functions following the loss of a sexual cycle in *C. glabrata*.

5.4.3 *C. glabrata* *CAGL0D05434g* Genetic Interactions

Previous work has shown the utility of the *S. cerevisiae* SGA platform for genetic interaction profiling of *C. glabrata* ORFs with orthologues in *S. cerevisiae* (personal communication, Dr. Jane Usher, University of Exeter). This present study aimed to use the *S. cerevisiae* SGA platform to uncover genetic interaction networks for *C. glabrata* ORF *CAGL0D05434g*, for which there is no orthologue in *S. cerevisiae*, to reveal the pathways this ORF may function in. It was hypothesised that due to the conservation of genetic interactions between yeasts (Dixon *et al.*, 2008; Ryan *et al.*, 2012), genetic interaction data for *C. glabrata* ORFs in the closely related yeast *S. cerevisiae* would hold true biological relevance to ORF function in *C. glabrata*. Indeed, such hypotheses are supported by recent work in which genetic interaction mapping in *S. cerevisiae* was used for functional characterisation of more distantly related *C. neoformans* virulence factors, which also have no orthologue (Brown & Madhani, 2012). In this study, genome-wide genetic interaction analysis of *C. glabrata* *CAGL0D05434g* found enrichment of interacting genes implicated in meiosis and sporulation, ion homeostasis and DNA damage repair and replication (Figure 5.7).

5.4.4 *C. glabrata* *CAGL0D05434g* – a Role in Meiosis?

Consistent with the prevalence of HMG MATA proteins in fungal mating systems, functional characterisation of *C. glabrata* *CAGL0D05434g* in *S. cerevisiae* implied a role for *CAGL0D05434g* in the mating process. Firstly, *S. cerevisiae* SGA query strains expressing *C. glabrata* *CAGL0D05434g* did not form tetrads following mating thus preventing the formation of double mutants for genetic interaction analysis (Figure 5.6). Although growth on auxotrophic selection implied *CAGL0D05434g*-expressing *S. cerevisiae* strains were

successful in the formation of diploids, further experimentation and verification is required to dissect at which step in mating, meiosis or sporulation inhibition occurred and whether this is directly linked to the expression of *C. glabrata* *CAGL0D05434g*. However, it seems likely to be associated with expression of *C. glabrata* *CAGL0D05434g* since the SGA platform has previously been successfully used for the genetic interaction profiling of numerous *C. glabrata* ORFs (personal communication, Dr. Jane Usher, University of Exeter). Secondly, examination of *CAGL0D05434g* genetic interactions in *S. cerevisiae* Δ *IME1* and Δ *IME2* strains uncovered significant enrichment of interacting genes with known functions in mating, meiosis and sporulation (Table 5.2; Appendix 6 Tables 1 and 2). Since genetic interactions often occur between genes within the same or related biological pathways (Dixon *et al.*, 2009; see 1.3.3), genetic interactions provide a strong indicator for gene function thus proposing a putative function for *CAGL0D05434g* in the mating machinery. Although the presence of a mating-associated gene does not comply with the asexual lifestyle of *C. glabrata*, numerous orthologues of the mating machinery have been described in this species (Wong *et al.*, 2003) – some of which, for example *STE12*, are able to complement mating in their respective *S. cerevisiae* deletion mutants but uniquely to *C. glabrata* has emerged as an important virulence attribute (Calcagno *et al.*, 2003). Thus, in agreement with the universal function of MATA HMG-box proteins in fungal mating systems taken together with genetic interaction data, it is proposed that *C. glabrata* *CAGL0D05434g* may have a functional role in mating, meiosis or sporulation. Alternatively, through evolutionary driven genetic rewiring, *CAGL0D05434g* may also have evolved a novel role specific to *C. glabrata* as has been shown for other mating-associated *C. glabrata* genes (Calcagno *et al.*, 2003).

5.4.5 *CAGL0D05434g* and the DNA-damage Response

Genetic interaction mapping of *C. glabrata* *CAGL0D05434g* revealed an enrichment of genetic interactions with *S. cerevisiae* genes implicated in DNA replication stress and DNA damage repair (Table 5.2; Appendix 6 Table 1 and 2), driving the hypothesis that *CAGL0D05434g* may be involved in the DNA damage response of *C. glabrata*. Further investigation confirmed this hypothesis, demonstrating experimentally by phenotypic screening the requirement of *CAGL0D05434g* for *C. glabrata* growth on MMS and

hydroxyurea as well as increased tolerance to these compounds upon overexpression of *CAGL0D05434g* (Figure 5.10). MMS is a DNA-damaging agent which physically impedes and reduces the rate of DNA replication fork progression by alkylation of genomic DNA. Previously, MMS-induced cytotoxicity has been found to occur when cells are allowed to enter S-phase with DNA alkylation damage, often as a result of mutation of vital checkpoint control genes (Tercero & Diffley, 2001). In DNA repair-competent cells, MMS-induced DNA damage is remediated by a group of base excision repair proteins including *RAD6*, a checkpoint control protein involved in replication repair and double stranded DNA break repair; *RAD52*, which functions in the repair of double strand DNA breaks during meiosis; *MEC1*, a genome integrity checkpoint protein and component of the signal transduction pathway in response to DNA damage; and *RAD53*, a protein kinase required for DNA damage-induced cell cycle arrest (Hanway *et al.*, 2002). Treatment of yeast with hydroxyurea reversibly inhibits ribonucleotide reductase, preventing the reduction of ribonucleotides to deoxyribonucleotides (dNTPs), thereby diminishing cellular dNTP pools, hampering DNA synthesis and progression through S-phase (Hampsey, 1997; Alvino *et al.*, 2007). Similarly to MMS-induced DNA damage, checkpoint genes *MEC1* and *RAD53* are engaged in response to hydroxyurea treatment, prohibiting a lethal passage through the cell cycle into mitosis (Alvino *et al.*, 2007). Due to the sensitivity of *C. glabrata* *CAGL0D05434g* to DNA damage agents MMS and hydroxyurea (Figure 5.10), it is proposed that *CAGL0D05434g* is a novel regulator of the DNA damage response in *C. glabrata*. Further experimentation to investigate whether *CAGL0D05434g* confers tolerance to MMS and hydroxyurea could explore the regulation of DNA damage checkpoint controls such as *RAD53*, *MEC1*, *RAD6* or *RAD52* by *CAGL0D05434g*. In agreement with such hypotheses, *C. glabrata* *CAGL0D05434g* showed genetic interactions with S-phase DNA damage checkpoint proteins encoded by *MRC1* and *DDC1*; and *MSH1*, *COA6*, *TDP3*, *TOM6* and *UBI4* which are required for growth on MMS (Appendix 6 Tables 1 and 2; Hanway *et al.*, 2002). Such involvement of *CAGL0D05434g* in DNA damage regulation could also explain the sensitivity of *CAGL0D05345g* deletion mutants to metals and arsenic compounds since treatment of yeast cells with metal and arsenic compounds has been associated with increased DNA mutation and damage frequency (Yu *et al.*, 2009; Litwin *et al.*, 2013). The

involvement of *C. glabrata* *CAGL0D05434g* in DNA replication and damage repair could also be linked to the proposed role of *CAGL0D05434g* in mating, meiosis and sporulation since double strand breaks and their repair is a vital stage in meiosis (Haber, 2000; Murakami & Keeney, 2008). However, further experimentation of *CAGL0D05434g* function is required to validate such speculation.

5.4.6 Genetic Interaction Mapping of *C. glabrata* *CAGL0K05687g* – a Role in Transport?

This work exploited the SGA platform to investigate the genome-wide genetic interactions of putative *C. glabrata* oxidoreductase *CAGL0K05687g*. *CAGL0K05687g* was previously identified to be required for full *C. glabrata* virulence in an immunocompromised *D. melanogaster* infection model (Figure 4.11 A) and deletion modulated the biofilm-forming capacity of *C. glabrata* (Figure 4.9 A). However, chemogenomic screening of a *CAGL0K05687g* deletion mutant revealed no phenotypes (Table 4.3). As such, the pathways *CAGL0K05687g* may act within and how this relates to *C. glabrata* virulence remains unclear.

Systematic genetic interaction profiling of *C. glabrata* *CAGL0K05687g* identified genetic interactions with 115 *S. cerevisiae* genes (Figure 5.11). In particular, genetic interactions were enriched amongst integral membrane proteins, SNARE proteins and membrane transporters (Table 5.3). In *S. cerevisiae*, SNAREs comprise a diverse group of C-terminal anchored transmembrane proteins which together constitute the machinery governing vesicle targeting and fusion and as such play an important role in endo- or exo-cytosis and the transport of cargo between organelles (Bonifacino & Glick, 2004). Thus, given that *C. glabrata* *CAGL0K05687g* genetically interacts with a number of SNAREs, it could be proposed that *CAGL0K05687g* functions in vesicle-mediated transport. Additionally, *CAGL0K05687g* was found to genetically interact with 26 membrane proteins, some of which (such as *CTR1* and *TRK1*) have transporter activity which could implicate *CAGL0K05687g* in nutrient transport. Further experimentation could be used to validate genetic interaction-driven hypotheses and explore the implications this may have on *C. glabrata* virulence. Genetic interactions with histone modification and chromatin

remodelling proteins encoded by *S. cerevisiae* *SWC3*, *ASF1*, *SWD1* and *FUN30* were also uncovered (Appendix 12 Table 1), many of which are involved in telomeric silencing (Daganzo *et al.*, 2003; Mueller *et al.*, 2006). It could be further studied whether interactions between *CAGL0K05687g* and chromatin remodelers in *C. glabrata* have an impact on subtelomeric silencing. Such an interaction could alter expression of the *EPA* adhesins and provide a link with the increased biofilm-forming capacity of the *CAGL0K05687g* deletion mutant.

Chemogenomic screening of deletion mutants has been used as an effective tool in the functional characterisation of previously unstudied genes in yeasts (Winzeler *et al.*, 1999; Homann *et al.*, 2009; Schwartzmüller *et al.*, 2013; see 1.3.1.2). However, dissection of ORF function is hampered when gene deletion confers no observable phenotypes in chemogenomic screens. For many ORFs, genetic redundancy or the presence of parallel pathways which are able to functionally compensate for the other may mask growth phenotypes (Dixon, 2009). Alternatively, gene deletion may confer a phenotype other than alteration of colony growth or fitness. Thus, alternative approaches for functional characterisation must be employed for ORFs with no observable screening phenotypes. In this instance, the SGA platform was used due to its application in uncovering redundant gene function (Tong *et al.*, 2001).

Taken together, approaches to functionally characterise *CAGL0D05434g* have lead to the hypothesis that this ORF may play a role in meiosis, sporulation or the regulation of the DNA damage and replication response in *C. glabrata*. Further, high-throughput genetic interaction profiling of a *C. glabrata*-specific ORF in *S. cerevisiae* was used to drive hypotheses regarding *C. glabrata* function which were experimentally validated in *C. glabrata*.

Chapter 6: Discussion

6.1 Overview

The development of molecular tools (such as barcoded deletion libraries and ORF collections) have enabled genome-wide studies in the model yeast *S. cerevisiae* leading to rapid and systematic characterisation of unstudied genes, uncovering novel regulatory networks, protein-protein interactions and genetic interaction networks (Giaever *et al.*, 2002; Tong *et al.*, 2004; Krogan *et al.*, 2006; Costanzo *et al.*, 2010). Such tools have been instrumental in the understanding of orthologous gene function in related yeasts such as *C. glabrata*. However the non-pathogenic nature of *S. cerevisiae* limits the use of these tools in the dissection of traits specific to pathogenic yeast species. As a result, this study addresses problems posed by the lack of molecular tools available for the large-scale study of ORF function in non-model organisms, focusing on the pathogenic yeast *C. glabrata*.

A focus on *C. glabrata* ORFs with no orthologue in *S. cerevisiae* was driven by comparative genomic studies which found *C. glabrata* to be more closely related to the non-pathogenic yeast *S. cerevisiae* (Dujon *et al.*, 2004; see 1.2). In particular, phylogenetic analysis found *C. glabrata* to lie in the WGD (whole genome duplication) clade, distinct from other pathogenic yeast species constituting the *Candida* clade (Figure 1.3). It was thus hypothesised that *C. glabrata* and *S. cerevisiae* shared a common ancestor and following divergence from this ancestor *C. glabrata* emerged as a pathogen of humans (Byrne & Wolfe, 2005). Therefore, this study aimed to address *C. glabrata* attributes which may contribute to virulence in this species through the direct comparison of orthologous genes between *C. glabrata* and *S. cerevisiae*. It was subsequently hypothesised that genes specific to *C. glabrata* may elucidate virulence factors.

A bespoke reciprocal best hit (RBH) pipeline (see 3.3.1) was used to bioinformatically identify 727 *C. glabrata* ORFs which may have no orthologue in *S. cerevisiae*. Further refinement criteria were used to supplement RBH

searches and select candidate *C. glabrata* ORFs to be taken forward for functional characterisation. This was mainly achieved through the detection of predicted functional domains in the encoding protein sequences and identification of orthologous genes in other related species using the Yeast Gene Order Browser (YGOB; ygob.ucd.ie) and the Candida Genome Database (CGD; candidagenome.org). A resultant list of 100 *C. glabrata* ORFs of interest was taken forward for targeted gene deletion. Subsequently, a total of 65 *C. glabrata* ORFs were individually deleted (see 3.4.3) to produce a barcoded *C. glabrata* deletion library to be used as a molecular tool for their study. This work further contributed to a collaborative gene deletion project of approximately 700 *C. glabrata* mutants constructed in the Haynes, Kuchler and Cormack labs, providing a lasting resource for the study of *C. glabrata* biology (Schwartzmüller *et al.*, 2013; Appendix 13).

A series of assays were used to characterise the *C. glabrata* deletion library, facilitating the dissection of ORF function with respect to growth conditions and growth forms relevant to virulence. Data presented in this study highlights seven *C. glabrata* ORFs found to be required for *C. glabrata* fitness *in vitro* (see 4.3.1) and 22 *C. glabrata* ORFs required for growth under stress conditions tested in phenotypic screens (Table 4.3). As a result, screening provided a link between unstudied ORFs and functional processes such as tolerance to heavy metals, the DNA damage response and resistance to antifungal drugs (Table 4.2). Additionally, 14 *C. glabrata* ORFs were implicated in biofilm formation (see 4.3.3) and 6 ORFs were required for virulence in a *Drosophila melanogaster* infection model (see 4.3.4), providing the first evidence for the involvement of these ORFs in virulence and pathogenesis-related growth forms. Hence, the multi-faceted approach to the functional characterisation of the *C. glabrata* deletion library has led to the identification of *C. glabrata* ORFs which play a role in a variety of aspects related to *C. glabrata* biology. The use of a *D. melanogaster* infection model has also broadened the availability of animal models applicable to large strain collections. Together, the screening platforms developed in this work are applicable to other fungal pathogens to facilitate the functional characterisation of ORFs in these species.

This work also introduced the *S. cerevisiae* synthetic genetic array (SGA) method for the functional characterisation of *C. glabrata* ORFs with no orthologue in *S. cerevisiae* (see 5.3.3). Genetic interaction networks were presented representing genetically interacting partners of *C. glabrata* *CAGL0D05434g*, a putative HMG-box chromatin remodeler (Figure 5.7). Analysis of genetic interactions led to the finding that *C. glabrata* *CAGL0D05434g* was required for growth on DNA-damaging agents (see 5.3.4). Preliminary genetic interaction profiling was also used to uncover the pathways the virulence-associated ORF *CAGL0K05687g* may act within and how this may relate to virulence.

6.2 Defining *C. glabrata* ORFs with no Orthologue in *S. cerevisiae*

This study focused on *C. glabrata* ORFs with no *S. cerevisiae* orthologue as an approach for the identification of *C. glabrata* virulence attributes as it was hypothesised that the emergence of *C. glabrata*-specific genes may have accompanied the adaptation of *C. glabrata* to the human host niche and evolution of pathogenicity. During the course of this study Desai *et al.*, 2011, also focused on *C. glabrata*-specific ORFs leading to the identification of novel endothelial adhesin factors Pwp7 and Aed1. Also supporting the hypothesis that *C. glabrata*-specific ORFs play important roles in infection related processes, expression profiling of macrophage-internalised *C. glabrata* cells found 15-30 % of all differentially regulated genes were either specific to *C. glabrata* or had uncharacterised *S. cerevisiae* orthologues (Rai *et al.*, 2012). The study of species-specific ORFs could be applied to other fungal pathogens for the identification of pathogenicity factors.

The current study also explored the possibility that the acquisition of prokaryotic genes by *C. glabrata* may have accompanied the emergence of this species as a human pathogen. More specifically, three ORFs encoding a putative aspartate racemase (*CAGL0D01210g*), an NADPH dehydrogenase (*CAGL0M14091g*) and transferase enzyme (*CAGL0K11066g*) were proposed to be of prokaryotic origin, most likely from horizontal gene transfer events from species in the Firmicute, Proteobacteria or Actinobacteria phyla (see 3.3.4). It was previously reported that HGT events from prokaryotes to fungi may accompany the adaptation of pathogens to a new host niche. In particular the acquisition of

racemase enzymes could facilitate the detoxification of D-amino acid forms found in mammalian tissues or the peptidoglycan layer of the bacterial cell wall (Yoshimura & Esaki, 2003; Marcet-Houben & Gabaldón, 2010). It is hypothesised that horizontal gene transfer between bacterial and yeast species could take place in the competitive environment of the host microflora and that such transfer could confer a fitness advantage in the host niche.

The identification of *C. glabrata* ORFs with no orthologue in *S. cerevisiae* in the current study highlighted discrepancies in orthologue assignment by different search methods and databases. RBH searches in this study initially identified 727 *C. glabrata* ORFs to have no orthologue in *S. cerevisiae* (see 3.4.1). Contrarily, comparison of orthologues in *S. cerevisiae* and *C. glabrata* by Desai *et al.*, 2011, identified 337 ORFs unique to *C. glabrata* whilst YGOB identified 294 ORFs (Desai *et al.*, 2011; ygob.ucd.ie). It is likely that filters assigned to RBH searches (requiring 30 % sequence identity throughout 50 % of the coding sequence) greatly increased the number of *C. glabrata* genes which were identified in these searches and consequently many of the 727 *C. glabrata* ORFs may have orthologues. This was exemplified through the study of *C. glabrata* *CAGL0D03850g* which was identified to be *C. glabrata*-specific by RBH searches but was assigned as an orthologue of *S. cerevisiae* *RSC30* by YGOB (ygob.ucd.ie). Complementation experiments provided evidence that *S. cerevisiae* *RSC30* can functionally compensate for deletion of *C. glabrata* *CAGL0D03850g* (Figure 4.6), despite sequence identity lying in only 200 bp of the ORF sequence encompassing the Zn(2)-C6 fungal-type DNA-binding domain (yeastgenome.org). Thus it is proposed that some of the 727 *C. glabrata* ORFs identified by RBH searches may have *S. cerevisiae* orthologues, however, these were not identified due to the functional orthology lying within less than 50 % of the encoding sequence.

Sequence comparison-based bioinformatic searches were the main criterion used for the selection of *C. glabrata* ORFs for gene deletion in this study (see 3.4.3). Based on this selection, 65 *C. glabrata* deletion mutants were generated to create a library with defined features making the library compatible with the Schwartzmüller *et al.*, 2013 study (Appendix 13). Each deletion mutant was tagged with two unique DNA barcodes and universal flanking sequences

enabling their amplification by PCR and flippase recognition target (FRT) sites to allow further downstream genetic manipulations such as recycling the resistance cassette to delete a second ORF. Subsequent screening of the deletion library facilitated the functional characterisation of previously unstudied *C. glabrata* ORFs (see Chapter 4). Of particular note was the identification of three ORFs required for tolerance of antifungal drug fluconazole (Figure 4.4) and the implication of putative chromatin modeller *CAGL0D05434g* in tolerance to DNA damage-inducing agents, metal and metalloid compounds. Furthermore, screening implicated 16 *C. glabrata* ORFs in biofilm formation (Figure 4.9) and identified six gene products required for virulence in an immunocompromised *D. melanogaster* larvae infection model (Figure 4.11).

However, a large proportion of *C. glabrata* mutants showed no phenotype in any screen. For example, in chemogenomic screens 110 of 132 deletion mutants did not yield altered growth under any tested condition, likely due to the presence of compensatory pathways masking the effects of genetic perturbation (see 4.3.2). Alternatively, the ORFs targeted by gene deletion could be dubious ORFs or pseudogenes. Selection of ORFs for functional characterisation could be improved by the incorporation of experimental data in combination with bioinformatic selection criterion. For example, *C. glabrata* expression data could be used to identify *C. glabrata*-specific ORFs which are differentially regulated in response to stress, since stress resistance is a vital prerequisite to surviving the host environment. As such a more targeted strategy for ORF selection may increase the number of deletion mutants showing observable phenotypes.

Taking both RBH- and YGOB-based searches into account, this study proposes that 197 *C. glabrata* ORFs have no strict orthologue in *S. cerevisiae* (Figure 3.4). Of the 65 *C. glabrata* ORFs deleted in this study, 37 have no *S. cerevisiae* orthologue according to YGOB (ygob.ucd.ie). Within this list, 23 *C. glabrata* ORFs were associated with novel phenotypes during the course of this study (Table 4.4), expanding the functional annotation of uncharacterised ORFs in this species and the role they may play in *C. glabrata* stress adaptation and survival of the host environment.

6.3 The Use of a Non-Mammalian Host for Virulence Studies of *C. glabrata* Strains

The current study introduced the use of a *D. melanogaster* larvae infection model for virulence analysis of large collections of *C. glabrata* mutants. In this instance, *in vitro* studies of *C. glabrata* –immune cell interactions were not selected as a model for virulence since macrophage studies of *C. glabrata* virulence were previously found to not correlate well with *in vivo* murine models of *C. glabrata* infection (personal communication, Dr. Hsueh-lui Ho, University of Exeter). Although murine models remain the mammalian host model of choice for *Candida* infection studies, their use is limited by high labour intensity (in particular to achieve statistically significant sample sizes), high costs and ethical issues. As such, mammalian host models are not amenable to high-throughput virulence screens. This work addressed the requirement for alternative non-mammalian model host for virulence studies of *Candida* species. Such a model host is required for *C. glabrata* in particular due to the unsuitability of *Galleria mellonella* as a host for this species (Cotter *et al.*, 2000). Alternative models such as zebrafish have been used to study *C. albicans* infection (Chao *et al.*, 2010) however such a host model requires the availability of specialist aquarium equipment. A *D. melanogaster* infection model offers a number of advantages including the ready availability of large sample numbers of larvae thus providing statistically sound experimental pool sizes. In addition, the maintenance of *Drosophila* stocks requires only a fraction of the cost and labour required of a mammalian host. As a model organism, a variety of *Drosophila* tools (such as flybase.org), strain collections (RNAi collections) and stock centres (Bloomington Stock Centre) exist, enabling the analysis of *C. glabrata* virulence in a variety of chosen strain backgrounds. The ability to screen collections of *C. glabrata* deletion mutants in different *D. melanogaster* backgrounds offers the opportunity to study host-pathogen interactions – for example, dissecting interactions with components of host immunity. The use of a non-mammalian infection model also alleviates any ethical issues surrounding the use of animals for experimentation. The biological relevance of *D. melanogaster* as a model host for virulence studies has previously been validated in *C. albicans* in which both *D. melanogaster* and murine hosts showed strong correlation (Glittenberg *et al.*, 2011 B). Thus, with the increasing availability and size of strain collections of pathogenic fungi, the use of non-

mammalian infection models for high-throughput pathogenesis studies is likely to increase. During the course of this study, another group published work in which *D. melanogaster* was used as a model host for the study of *C. glabrata* infection, showing similarities to results obtained from mammalian host models. Namely, as has been observed in murine host models (Calcagno *et al.*, 2003; Calcagno *et al.*, 2004; Kaur *et al.*, 2007), components of MAPK signalling pathways and yapsins were required for virulence in wild-type *D. melanogaster* (Quintin *et al.*, 2013). They also found that wild-type *D. melanogaster* was unable to kill *C. glabrata* cells (administered by injection) but rather *C. glabrata* infection was contained via a Toll-pathway mediated mechanism (Quintin *et al.*, 2013). Together, these studies have extended the utility of *D. melanogaster* as a suitable host for *C. glabrata* virulence studies. The use of such models will subsequently reduce the number of strains tested in mammalian hosts.

The implementation of *D. melanogaster* as a model for *C. glabrata* virulence studies uncovered six deletion mutants which were attenuated for virulence (see 4.3.4; Figure 4.11 A). Of the deleted *C. glabrata* ORFs identified, five had no previous implication in *C. glabrata* pathogenicity. Infection of immunocompromised *D. melanogaster* larvae with all six *C. glabrata* mutants resulted in increased larvae survival compared with infection with parental strains (Figure 4.11 A). However, all mutants were able to activate the Toll Pathway, signifying that all *C. glabrata* mutants were recognised by *D. melanogaster* PRRs (pathogen recognitions receptors), instigating innate immune signalling (Figure 4.11 B). Activation of the Toll pathway, allows *D. melanogaster* larvae to control (but not clear) *C. glabrata* infection resulting in survival of larvae following infection (Quintin *et al.*, 2013).

Most strikingly, three of the six *C. glabrata* ORFs (*CAGL0D03850g*, *CAGL0B00726g* and *CAGL0L03674g*) required for virulence in the *D. melanogaster* immunocompromised infection model have *S. cerevisiae* orthologues with known function in metabolic adaptation, most notably with regard to glucose metabolism. *C. glabrata* *CAGL0L03674g* shares orthology with *S. cerevisiae* *GSM1*, encoding a zinc finger transcription factor implicated in the regulation of energy metabolism; and *CAGL0B00726g* has orthology with *S. cerevisiae* *GLK1* which encodes a glucokinase which functions in glucose

metabolism pathways (yeastgenome.org). *C. glabrata* *CAGL0D03850g*, which is orthologous to *S. cerevisiae* *RSC30*, has been shown to regulate metabolic adaptation genes in *C. glabrata* including carbohydrate metabolism (Rai *et al.*, 2012). Therefore, in agreement with Rai *et al.*, 2012, this study proposes that remodelling of carbon metabolism may be a vital prerequisite for *C. glabrata* pathogenicity. The ability to readily alter carbohydrate metabolism could be an important factor in adaptation to the host niche, in which invading microorganisms such as *C. glabrata* experience competition for limited nutrients and must survive host-driven nutrient starvation strategies. As such, effective remodelling of carbon metabolism via ORFs such as *CAGL0D03850g*, *CAGL0B00726g* and *CAGL0L03674g* may confer a competitive advantage in the host environment and promote survival under nutrient-depleted conditions such as the phagosome. Such a theory is corroborated by the Rai *et al.*, 2012, study in which *CAGL0D03850g* was found to be required for macrophage survival and for full virulence in a murine model of *C. glabrata* infection (Rai *et al.*, 2012). Given its requirement for *C. glabrata* survival in macrophages and virulence, carbon metabolism pathways could be pursued as a potential drug target in the treatment of *C. glabrata* infections.

A limitation of the *D. melanogaster* infection model used in this study lies in its restriction for detecting mutants with virulence levels either similar or reduced compared to that of the parental strains. Due to the 90 – 100 % killing levels of *D. melanogaster* larvae following infection with *C. glabrata* parental strains, this host model does not provide scope for identifying *C. glabrata* mutants with enhanced virulence. As such, adaptation of the model or use of another virulence model may be required for identifying mutants with enhanced virulence.

6.4 Genetic Interaction Analysis Facilitates the Functional Characterisation of *C. glabrata* ORFs

Virulence screening also identified two *C. glabrata* ORFs with no detectable orthologue in *S. cerevisiae* which were required for virulence in *D. melanogaster*: *CAGL0K05687g* and *CAGL0H01749g*. However, the lack of other observable phenotypes associated with the deletion of either ORF in *C. glabrata* prevented the identification of functional mechanisms by which these

ORFs may contribute to virulence. As such, alternative strategies were required for functional characterisation of *C. glabrata* ORFs. This study exploited the synthetic genetic array (SGA) platform as a tool to identify genetic interactors of *C. glabrata* ORFs in *S. cerevisiae*. The large scale study of genetic interactions in *S. cerevisiae* has greatly facilitated functional annotation of previously unknown genes based on genetic interactions most frequently occurring between genes which lie in the same or parallel functional pathways, form part of the same protein complex and which share a similar cellular location (Tong *et al.*, 2004). Comparison of networks of evolutionary distanced yeasts *S. cerevisiae* and *Schizosaccharomyces pombe* showed that genetic interaction networks retained conserved features with highly similar connectivity between different biological processes (Ryan *et al.*, 2012). As such, it was hypothesised that systematic analysis of genetic interactions of *C. glabrata* ORFs in *S. cerevisiae* would reveal relevant functional information about ORFs that could be extrapolated back to *C. glabrata* biology. In this instance, genetic interaction analysis of *C. glabrata* *CAGL0K05687g* led to the implication of *CAGL0K05687g* in transport due to the high number of genetic interactions with *S. cerevisiae* membrane proteins, transporters (for example *TRK1*, *CTR1* and *FUI1*) and SNAREs (SNAP receptor proteins) (see 5.4.6). Thus it could be speculated that the attenuation of *C. glabrata* Δ *CAGL0K05687g* in *D. melanogaster* could be due to defects in transport processes.

SGA was also used to further dissect the function of putative *C. glabrata* chromatin remodeler *CAGL0D05434g*, following the observation that *CAGL0D05434g* was required for *C. glabrata* growth on metal and metalloid compounds in phenotypic screens (Figure 5.2). In agreement with screening observations, *CAGL0D05434g* was found to interact with a number of metal ion transporters (Appendix 6 Table 1 and 2). Genetic interactions and phenotypic screens also implied a role for *CAGL0D05434g* in DNA damage and replication stress which could impact fitness of *C. glabrata* cells upon macrophage uptake where DNA-damage repair mechanisms are crucial for survival (Rai *et al.*, 2012). Subsequent analysis of the *C. glabrata* Δ *CAGL0D05434g* mutants confirmed that *CAGL0D05434g* was required for growth under DNA damage and replication stresses, thus validating the biological relevance of studying *C. glabrata* genes in *S. cerevisiae*. During the course of this study, Brown &

Madhani, 2012, reported the use of SGA in *S. cerevisiae* in the characterisation of *Cryptococcus neoformans* virulence factors. Together, the current study and work by Brown & Madhani *et al.*, 2012, extend the scope of systematic genetic interaction profiling using SGA to non-*S. cerevisiae* species. Such approaches could be applied to dissect the function of ORFs in other fungal species, inclusive of ORFs with or without an *S. cerevisiae* orthologue.

6.5 Future work

6.5.1 Studying the Evolutionary Differences of *C. glabrata* CAGL0D03850g and *S. cerevisiae* RSC30

Preliminary complementation studies confirmed that *S. cerevisiae* RSC30 was able to functionally complement phenotypes associated with the deletion of CAGL0D03850g despite sequence identity lying in the N-terminal zinc-finger DNA binding domain only. Thus it is predicted that the functional domains only of these proteins are required for maintaining orthologous gene function. Further experimentation using truncated *C. glabrata* CAGL0D03850g and *S. cerevisiae* RSC30 mutants could investigate whether the DNA-binding domain is sufficient to complement orthologue function. Additionally, the evolutionary differences between orthologues could be explored since *C. glabrata* CAGL0D03850g was found to be required for virulence in the *D. melanogaster* infection model yet its orthologue RSC30 has been retained in the non-pathogenic yeast *S. cerevisiae*. Thus it could be of interest to consider whether complementation of *C. glabrata* CAGL0D03850g with *S. cerevisiae* RSC30 extends to the virulence phenotype. Exploiting technologies such as ChIP-seq could be used to compare different target genes of the two transcription factors and identify instances of genetic rewiring that may have accompanied the emergence of *C. glabrata* as a pathogen. Comparison of *S. cerevisiae* RSC30 orthologues in pathogenic *S. cerevisiae* isolates and recently identified emerging pathogens of the *C. glabrata* clade (Gabaldón *et al.*, 2013) could also identify whether RSC30 orthologues are more similar to *C. glabrata* RSC30 and whether this RSC30 is also related to pathogenicity in these species.

6.5.2 Understanding the Role of Horizontal Gene Transfer in *C. glabrata*

To complement bioinformatic analysis which linked three *C. glabrata* ORFs to horizontal gene transfer (HGT) events from bacteria, experimental analysis

could verify the functionality of *C. glabrata* ORFs in bacterial species. For example, expression of *CAGL0D01210g* in bacterial species (such as model organism *E. coli* or alternatively in *Lactobacillus* species from which it was predicted to originate from) could investigate whether *CAGL0D01210g* confers increased tolerance to D-aspartate enantiomers. It has been predicted that the ability to metabolise and detoxify D-aspartate by *C. glabrata* may confer a competitive advantage in the host niche or enhances virulence. This could be investigated using competitive growth experiments in a mammalian host, exploiting the unique barcodes built into the *C. glabrata* deletion library, to verify whether the presence of aspartate racemase encoded by *CAGL0D01210g* does confer a competitive advantage. It could also be tested whether Δ *CAGL0D01210g* mutants are altered for virulence or stress resistance following treatment with D-aspartate. Such work would greatly enhance understanding regarding the physiological role of fungal genes acquired from bacteria and the impact such genes have with regards to adaptation to the host environment. Although some such studies exist (Garcia-Vallvé et al., 2000; Uo et al., 2001), the wider implication HGT may have in the evolution of pathogenicity remains relatively unstudied.

6.5.3 Exploiting Barcoded *C. glabrata* Mutants for Competitive Growth Analysis

Both *C. glabrata* deletion libraries constructed in this study and by Schwartzmüller et al., 2013, incorporated two unique 20 bp DNA barcodes into each individual deletion mutant, making the prevalence of each strain detectable within mixed populations of mutants (see 1.3.1.1). In the current study, the functional characterisation assays were performed using monocultures of each individual mutant. Whilst this yielded biological insight into the function of previously uncharacterised ORFs under controlled conditions *in vitro*, it does not reflect the environmental conditions and the competition *C. glabrata* cells would experience in the mammalian host. Therefore, competitive growth assays or STM-like screens in a murine host could be of use for the identification of mutant phenotypes which could otherwise have been masked in non-competitive growth assays performed using rich media and could increase the biological relevance of phenotypic screening observations.

6.5.4 Further Characterising *C. glabrata* Fluconazole-Susceptible Mutants

Importantly, phenotypic screens in this study highlighted three *C. glabrata* ORFs which were found to be required for fluconazole tolerance (Figure 4.4), all of which encode putative transcriptional regulators. To further validate the role of identified *C. glabrata* ORFs in fluconazole resistance, increased tolerance to fluconazole following overexpression of *CAGL0D03850g*, *CAGL0L07480g* and *CAGL0K05841g* could be tested. Furthermore, future work could uncover the mechanisms by which deletion of *CAGL0D03850g*, *CAGL0L07480g* and *CAGL0K05841g* confer fluconazole susceptibility in deletion strains. In particular, it is predicted that susceptibility to fluconazole in these strains could be dependent on the major regulator of drug resistance encoded by *PDR1* (*CAGL0A00451g*) or (see 1.9.1). This could be investigated using techniques such as RT-PCR or northern blotting to identify whether transcripts of *PDR1* or its targets (such as *CDR1*, *CDR2*, *SNQ2*, *QDR1*) are altered in deletion mutants compared with parental strains. As a result, this work could expand our understanding of the mechanisms underlying drug resistance in *C. glabrata*.

6.5.5 Dissecting the Role of Novel Biofilm-Associated ORFs in *C. glabrata*

Following the identification of *C. glabrata* mutants with altered biofilm forming capacity in high-throughput screens (see 4.3.3), the role selected *C. glabrata* ORFs may play in biofilm formation could be further investigated using more direct methods to measure biofilm mass. In this study, enzymatic screens in which the colourimetric change accompanying XTT reduction in response to cellular metabolism was used as a readout for biofilm size. To increase the confidence of hits identified in biofilm screens, direct measurement of dried *C. glabrata* biofilm mass could be employed. Additionally, scanning EM could be used to observe altered structure of biofilms in biofilm-altered mutants. Lastly, candidate *C. glabrata* mutants from biofilm screens could be explored for altered expression (by Northern blotting or RT-PCR) or for interactions (protein pull-downs) with *EPA6* (*CAGL0C00110g*) and *EPA7* (*CAGL0C05643g*), which encode the major adhesins mediating biofilm formation in *C. glabrata* (see 1.5.2). The adhesion-properties of the Δ *CAGL0E00275g* should be explored

further since biofilm formation was most significantly stunted in this strain. *CAGL0E00275g* encodes a protein encompassing a PA14 adhesin domain which was previously denoted *EPA20* (de Groot *et al.*, 2008). As such, future work should explore the possibility that *EPA20* could be required for biofilm formation in *C. glabrata*. It is predicted that overexpression of *EPA20* in *C. glabrata* may increase adherence and biofilm forming capability of cells both *in vitro* and *in vivo*. Studying the interaction of *EPA20* with immune cells could validate such hypotheses.

6.5.6 Validating *C. glabrata* ORFs Required for Virulence

Previous studies have shown a strong correlation between *D. melanogaster* and murine models of *C. albicans* infection, making *D. melanogaster* a suitable model for *C. albicans* virulence studies (Glittenberg *et al.*, 2011 B). Recent work by Quintin *et al.*, 2013, also presented similarities in both host and pathogen factors required for the establishment of *C. glabrata* infection in both mammalian and *D. melanogaster* infection models. However, *C. glabrata* mutants identified to be attenuated for virulence in the immunocompromised *D. melanogaster* infection model (see 4.3.4) should be further validated in a murine model of *C. glabrata* infection.

6.5.7 Functional Characterisation of *C. glabrata* *CAGL0D05434g*

C. glabrata *CAGL0D05434g* was bioinformatically predicted to encode a chromatin remodeler acting in response to stress (GO:0043618; Appendix 4 Table 1). To experimentally verify the role of *CAGL0D05434g* as a chromatin remodeler, MNase (micrococcal nuclease) assays could be used to investigate chromatin dynamics in Δ *CAGL0D05434g* and parental strains in response to stress. In this work, *C. glabrata* *CAGL0D05434g* was found to be required for growth following stress induced by metals, metalloids and DNA-damaging agents (Figure 5.2 and 5.10). Therefore it is predicted that *CAGL0D05434g* may play a role in regulating adaptation to stress in *C. glabrata*. Further experimentation could verify genetic interactions of *C. glabrata* *CAGL0D05434g*

with DNA damage checkpoint control proteins encoded by *RAD53*, *MEC1*, *RAD6* or *RAD52* in *C. glabrata* (Appendix 6 Table 1 and 2) and whether *CAGL0D05434g* influences the DNA damage response through these proteins. Additionally, Δ *CAGL0D05434g* cells could be tested for altered survival following uptake by macrophages. It is predicted that survival of Δ *CAGL0D05434g* would be reduced following macrophage uptake due to the finding that *C. glabrata* mutants defective in DNA repair mechanisms are more susceptible to macrophage killing (Rai *et al.*, 2012). Such a finding would provide a link between phenotypes observed *in vitro* with *in vivo* phenotypes.

Further to this, the HMG-box domain encoded by *CAGL0D05434g* belongs to the MATA group of HMG-box proteins, many of which are found at the mating type loci of other fungal species (Butler *et al.*, 2004; Paoletti *et al.*, 2005). In addition, expression of *C. glabrata CAGL0D05434g* in *S. cerevisiae* inhibited the formation of double mutants by classical mating methods in the SGA platform (see 5.3.3.2). As such it was hypothesised that *CAGL0D05434g* may function in mating, despite *C. glabrata* yielding no natural sexual cycle. Following the engineering of mating *C. glabrata* strains (Dr. Jane Usher, University of Exeter, personal communication), the involvement of *CAGL0D05434g* could be further investigated in these strains. It could be observed whether the presence or absence of *CAGL0D05434g* in these strains positively or negatively affects the efficiency of mating. The stage at which *CAGL0D05434g* may inhibit the sexual cycle of *S. cerevisiae* could also be further dissected since tetrads were never observed for *S. cerevisiae* strains expressing *CAGL0D05434g*.

6.6 Conclusion

In order to explore *C. glabrata* attributes associated with virulence, orthologous genes between *C. glabrata*, a significant pathogen of humans, and the non-pathogenic yeast *S. cerevisiae* were compared. *C. glabrata*-specific ORFs were selected to generate a *C. glabrata* deletion library. A multifaceted approach was taken for the functional characterisation of the *C. glabrata* deletion library leading to the identification of *C. glabrata* ORFs required for fitness and for survival under a plethora of stress conditions. The study highlighted *C. glabrata*

ORFs implicated in biofilm formation, most notably that deletion of putative adhesin *EPA20* results in decreased *C. glabrata* biofilm formation. Use of a *D. melanogaster* infection model highlighted novel *C. glabrata* ORFs required for virulence including a putative oxidoreductase encoded by *CAGL0K05687g* and unannotated ORF *CAGL0H01749g*. Synthetic genetic interaction profiling of *C. glabrata* ORFs in *S. cerevisiae* was used to uncover functional pathways proteins encoded by *C. glabrata* *CAGL0K05687g* and *CAGL0D05434g* may act within. Study of genetic interactions lead to the hypothesis that reduced virulence of a Δ *CAGL0K05687g* strain may be due to altered nutrient transport. Further, genetic interaction profiling may lead to the finding that putative chromatin modeller *CAGL0D05434g* may function in the DNA damage response of *C. glabrata*.

Together, this work has expanded the molecular toolkit available to the *Candida* community for the study of *C. glabrata* ORFs. Phenotypic analysis of the *C. glabrata* deletion library has enabled the functional characterisation of previously unstudied *C. glabrata* ORFs and highlighted novel functions for *C. glabrata* ORFs in stress resistance, biofilm formation and virulence.

Appendix 1: List of oligonucleotides used in this study

Table 1: General oligonucleotides used in this study for the generation of the *C. glabrata* deletion library.

Primer	Sequence
U2-BC-NAT	CGTACGCTGCAGGTCGACGCCTTCCGCTGCTAGGCGC
D2-BC-NAT	CTACGAGACCGACACCGTCGGGCCGCTGACGAAGTTC
NAT-5'-R	CATCCAAAGTAGTAGAC
NAT-3'-F	ATGTCTATGCCATGTCC

Table 2: ORF-specific oligonucleotides used for the construction of *C. glabrata* fusion cassettes for targeted gene deletion. Underlined sequences represent Up- and Down- barcode sequences.

Primer name	Sequence	ORF deleted
A01870-500-F	ACTCAGTGGAGTGATGC	CAGL0A01870g
A01870+500-R	CTTGCAGAAGTAGAAGG	
A01870-1-NAT-R	<u>GCGTCGACCTGCAGCGTACGTTGAGGAGACCACTTAC</u> <u>GCCACGGCGCGCCTAGCAGCGG</u> GACATTGAAGGAGATAC	
A01870+1-NAT-F	<u>CGACGGTGTCCGGTCTCGTAGGGAGACTCTTTGTGCGT</u> <u>ATAGTCAGCGGCCGCATCCCTGCGTGTATGTTCCGGT</u> AGG	
A02255-500-F	CTGAAGCAAATG GATGC	CAGL0A02255g
A02255+500-R	GGTTAACCACGCTCTCC	
A02255-1-NAT-R	<u>GCGTCGACCTGCAGCGTACGGACTTCACGAGCCTTAT</u> <u>CAGCACGGCGCGCCTAGCAGCGGGCGAATGTAGTGAA</u> TGG	
A02255+1-NAT-F	<u>CGACGGTGTCCGGTCTCGTAGGTATTATTACATCTCCC</u> <u>GGGTCAGCGGCCGCATCCCTGCCAATGTGATGCTCA</u> CT	
A02299-500-F	GAAAGTGGGATGTAGAC	CAGL0A02299g
A02299+500-R	CACTACCAACTGATCAC	
A02299-1-NAT-R	<u>GCGTCGACCTGCAGCGTACGGATGAGCTTCAGTGTAC</u> <u>TTCCACGGCGCGCCTAGCAGCGGGGA</u> ACTACTATGAG TGAG	
A02299+1-NAT-F	<u>CGACGGTGTCCGGTCTCGTAGTTAGAGACGAGACCACG</u> <u>CTCGTCAGCGGCCGCATCCCTGCGACATCTCTCGCAA</u> ACA	
A02343-500-F	CAGAGACCTGCGTAGTAC	CAGL0A02343g
A02343+500-R	GATCTATCGAGAGACAC	
A02343-1-NAT-R	<u>GCGTCGACCTGCAGCGTACGCACCGATCTGACTCAAT</u> <u>GATCACGGCGCGCCTAGCAGCGGCTCCTGTACAGCCG</u> TGT	
A02343+1-NAT-F	<u>CGACGGTGTCCGGTCTCGTAGCATGGCATTGAAGCTCA</u> <u>CTCGTCAGCGGCCGCATCCCTGCAGAGATCGGTGCTA</u>	

	GAT	
A03608-500-F	CCAGTGACTTCTGTTGC	CAGL0A03608g
A03608+500-R	GACAAGAGTAAGACTTC	
A03608-1-NAT-R	GCGTCGACCTGCAGCGTACGGCCTATTTCAAACGAGG GAACACGGCGCGCCTAGCAGCGG ACAATACGGAGCGACCG	
A03608+1-NAT-F	CGACGGTGTCCGGTCTCGTAGAGGTATAATAAGGTGCC CGCGTCAGCGGCCGCATCCCTGCTCTGCATGCTTTGT CGA	
A04257-500-F	CGTACAAACACCTGACCC	CAGL0A04257g
A04257+500-R	AACTGAAGAAAGCGACCC	
A04257-1-NAT-R	GCGTCGACCTGCAGCGTACGCGATGGGTGATAGTCAT ACCCACGGCGCGCCTAGCAGCGGCCAAGCAAAACAGC AATC	
A04257+1-NAT-F	CGACGGTGTCCGGTCTCGTAGGAAATCCACTGTCACATT CGGTCAGCGGCCGCATCCCTGCTAACAAAGTCTGGCT GGC	
A04565-500-F	GCCTGTCTAGGGCTTTC	CAGL0A04565g
A04565+500-R	CCTCTTGAACCTCTTCCT	
A04565-1-NAT-R	GCGTCGACCTGCAGCGTACGCGCGGAACGTCCATAC TGTCACGGCGCGCCTAGCAGCGGCTTCTGATTAACCA CCTC	
A04565+1-NAT-F	CGACGGTGTCCGGTCTCGTAGAAAGGCCAGTGGATTAC ATGGTCAGCGGCCGCATCCCTGCCTCATATCCTTTAAG GG	
B00726-500-F	ACCGTGAAGGTGATTCAA	CAGL0B00726
B00726+500-R	ACTTAGCTTCCACCGCTC	
B00726-1-NAT-R	GCGTCGACCTGCAGCGTACGCATGCTGGTCCCTACTA GAGCACGGCGCGCCTAGCAGCGGAGATCGAGTTAATA GGTGTC	
B00726+1-NAT-F	CGACGGTGTCCGGTCTCGTAGATGATGTAACCTAGAGCG CAGGTCAGCGGCCGCATCCCTGCGCATTCTCACCTA CAA	
B01287-500-F	CGATGTGATCCTGTTTCG	CAGL0B01287g
B01287+500-R	GGTCTTGCTGTAGGGAT	
B01287-1-NAT-R	GCGTCGACCTGCAGCGTACGGACCCGTTCAACTATCT GTTACAGGCGCGCCTAGAGCGGCTGAAAGTAAAGGTA CC	
B01287+1-NAT-F	CGACGGTGTCCGGTCTCGTAGAGCCAGCGTACATTATCT TCGTCAGCGGCCGCATCCCTGCCGAATATGAATCCAG GG	
B02882-500-F	GCGTTTACTGTAAGGTG	CAGL0B02882g
B02882+500-R	CCAGTAATCTGCTCTTC	
B02882-1-NAT-R	GCGTCGACCTGCAGCGTACGGTGAGCTAATACTCGAT CAGCACGGCGCGCCTAGCAGCGGGTTGTCTTTGTCTT TAGC	
B02882+1-NAT-F	CGACGGTGTCCGGTCTCGTAGCTCCAATGTCGAGTGAT ATGGTCAGCGGCCGCATCCCTGCAGGAGTTTGGCGTT TCT	
B02926-500-F	TGTTGCGGTAGGTGGAC	CAGL0B02926g
B02926+500-R	CATCTACCATCTCAAGC	
B02926-1-NAT-R	GCGTCGACCTGCAGCGTACGATACAGTAGACAGATGT GGCCACGGCGCGCCTAGCAGCGGGGAGAAAGAGCAA TTGG	
B02926+1-NAT-F	CGACGGTGTCCGGTCTCGTAGGCAACCTTCAATGCGCT TAGGTCAGCGGCCGCATCCCTGCGTCCATGAATCATC CTC	
B02948-500-F	TGGCGACGACTGGCTCA	CAGL0B02948g
B02948+500-R	GGTGACTTCGTGTGTCT	
B02948-1-NAT-R	GCGTCGACCTGCAGCGTACGATATCTTTGCGCCCGGT GGTCACGGCGCGCCTAGCAGCGG	

	AGGAGGACGAGTTGGTC	
B02948+1-NAT-F	<u>CGACGGTGTCCGGTCTCGTAGTTATCTCCTTTCCACGAG</u> <u>GGGTCAGCGGCCGCATCCCTGC</u> <u>CGCAGGCAACTCACGAG</u>	
B02970-500-F	ACCACTTTGCTTCTGTG	CAGL0B02870g
B02970+500-R	GACTTCGTGTGTCTTC	
B02970-1-NAT-R	<u>GCGTCGACCTGCAGCGTACGTTGAGGACTCGCCACAA</u> <u>TGCCACGGCGCGCCTAGCAGCGGGCATCTGAGTTATG</u> <u>CAAG</u>	
B02970+1-NAT-F	<u>CGACGGTGTCCGGTCTCGTAGGCAAACCTTCCGCGCTGT</u> <u>GTTGTCAGCGGCCGCATCCCTGCGGCTTACGCAGGCA</u> <u>ACT</u>	
B03223-500-F	CTTAGGAGAAGCCAGTG	CAGL0B03223g
B03223+500-R	TCTCCATTCTCACCAGC	
B03223-1-NAT-R	<u>GCGTCGACCTGCAGCGTACGGCGACCACTCGAATAAG</u> <u>GACCACGGCGCGCCTAGCAGCGGTGCTAAGTC</u> <u>TGTGCGCT</u>	
B03223+1-NAT-F	<u>CGACGGTGTCCGGTCTCGTAGGGTTTGTAATACTTAGC</u> <u>GCGTCAGCGGCCGCATCCCTGC</u> <u>CCAGTGATGTTTCGTATG</u>	
B03883-500-F	GACTGAGCACAAATACC	CAGL0B03883g
B03883+500-R	CTTGCCATGAGATGGTC	
B03883-1-NAT-R	<u>GCGTCGACCTGCAGCGTACGGTTTACACCACTGTTCCG</u> <u>GTACACGGCGCGCCTAGCAGCGGTGCTGTTGGTCTGC</u> <u>TGG</u>	
B03883+1-NAT-F	<u>CGACGGTGTCCGGTCTCGTAGGCGCTAACACTTACTCAA</u> <u>GACGTCAGCGGCCGCATCCCTGCCATCGATATTTCCG</u> <u>CCG</u>	
C00110-500-F	GAACAGGTA CTCTATTCC	CAGL0C00110g
C00110+500-R	CAACTCTTTCTCTACGA	
C00110-1-NAT-R	<u>GCGTCGACCTGCAGCGTACGAGGCAGATACGATTAGT</u> <u>ACGCACGGCGCGCCTAGCAGCGGAGACCTCACCTCAT</u> <u>GTT</u>	
C00110+1-NAT-F	<u>CGACGGTGTCCGGTCTCGTAGCCGAAGTGTCATCGAAT</u> <u>CTTGTCAGCGGCCGCATCCCTGCTGTGATACCACATTT</u> <u>CC</u>	
C00253-500-F	CCATAGCGAAGTCCTTG	CAGL0C00253g
C00253+500-R	CTCGGTAGGTGTTATGC	
C00253-1-NAT-R	<u>GCGTCGACCTGCAGCGTACGGCCTTGACAAATGCTC</u> <u>AAACACGGCGCGCCTAGCAGCGG GAATGTGCA</u> <u>AGTTCACC</u>	
C00253+1-NAT-F	<u>CGACGGTGTCCGGTCTCGTAGGCGTCAAATATCGGATT</u> <u>CCAGTCAGCGGCCGCATCCCTGCCCTGAACTCTTCCA</u> <u>ACA</u>	
C00847-500-F	CCTAAAGGCAAGCTCTAG	CAGL0C00847g
C00847+500-R	TGTAATGGCGGTCAAGG	
C00847-1-NAT-R	<u>GCGTCGACCTGCAGCGTACGCATACACCTCTCGGATA</u> <u>GTACACGGCGCGCCTAGCAGCGGGATGTAAACCTTGA</u> <u>TCG</u>	
C00847+1-NAT-F	<u>CGACGGTGTCCGGTCTCGTAGTTTGTGCGACGCTCACC</u> <u>GATGTCAGCGGCCGCATCCCTGCCATCACTGTGTATT</u> <u>GTG</u>	
C01837-500-F	TCAAGCACACTGTGTGG	CAGL0C01837g
C01837+500-R	CGCCATCCTTACGCTGG	
C01837-1-NAT-R	<u>GCGTCGACCTGCAGCGTACGGAGTCGTCTCTCACTGC</u> <u>GTTACAGGGCGCGCCTAGCAGCGGCACCTGAAACACTA</u> <u>CTG</u>	
C01837+1-NAT-F	<u>CGACGGTGTCCGGTCTCGTAGGTTCTCGCTGTCTG</u> <u>TCCAAAGTCAGCGGCCGCATCCCTGC</u> <u>CATTCGAACGAGATCAG</u>	

C02277-500-F	CTTCACTGTCACTGCTG	CAGL0C02277g
C02277+500-R	GAAACAACAGCCAATGC	
C02277-1-NAT-R	GCGTCGACCTGCAGCGTACGAGACGGACGCGATCCTA TATCACGGCGCGCCTAGCAGCGGGTATGTGTGTTGCT TTC	
C02277+1-NAT-F	CGACGGTGTCCGGTCTCGTAGAGAAGTGACGGGGCTCTC CATGTCAGCGGCCGCATCCCTGCCTGCCATTACAGATA CC	CAGL0C04763g
C04763-500-F	TGCACTCAGCATCATTG	
C04763+500-R	CGAGACACTACTACGAA	
C04763-1-NAT-R	GCGTCGACCTGCAGCGTACGTTCCGACGCGAGACTCTA GTGCACGGCGCGCCTAGCAGCGGGCGTCTAATAC TCAGAG	CAGL0D03850g
C04763+1-NAT-F	CGACGGTGTCCGGTCTCGTAGCACGGATATGAGTGGAA ATCGTCAGCGGCCGCATCCCTGCTCCCACTTCTTTAGG CC	
D03850-500-F	CCACAGACACACTCGAT	
D03850+500-R	CTGAGTTAGCCAACCCTG	CAGL0D00682g
D03850-1-NAT-R	GCGTCGACCTGCAGCGTACGCCTCTCCGTGGCAAGTG TATCACGGCGCGCCTAGCAGCGGAGCAATAGACGGGA CTC	
D03850+1-NAT-F	CGACGGTGTCCGGTCTCGTAGACCGTTACGAGATGTAT GTG <u>GTCAGCGGCCGCATCCCTGC</u> <u>CAATTCTGGTGTATGGAC</u>	
D00682-500-F	CAGACAGCAGCGCAGAG	CAGL0D01210g
D00682+500-R	CTACAAGGTGTGACACA	
D00682-1-NAT-R	GCGTCGACCTGCAGCGTACGGTGCTCCACAGTAATAC AACCACGGCGCGCCTAGCAGCGGGGTTATTGAG AGCCACT	
D00682+1-NAT-F	CGACGGTGTCCGGTCTCGTAGGTCTAAATTCCGTTACTG CGGTCAGCGGCCGCATCCCTGCGCTTCGTA ACTACAT AAC	CAGL0D03872g
D01210-500-F	CGTGTTGCTTGTCTTAC	
D01210+500-R	TCCTCCTCACTACCTC	
D01210-1-NAT-R	GCGTCGACCTGCAGCGTACGGCAAGGTATGTGAGCTA ATCCACGGCGCGCCTAGCAGCGG GAGTCTTCAACCAAACC	CAGL0D05170g
D01210+1-NAT-F	CGACGGTGTCCGGTCTCGTAGAGAGCAGAGACATTATT CCCGTCAGCGGCCGCATCCCTGCGCAGCAAGAGCACT AAC	
D03872-500-F	TCAACGCTCCTCTTG TG	
D03872+500-R	GTGCGAGCTGTT CAGTG	CAGL0D05434g
D03872-1-NAT-R	GCGTCGACCTGCAGCGTACGGAGGCAACTGTCTAGGT ATCCACGGCGCGCCTAGCAGCGG GATCCTGACTCAATTGA	
D03872+1-NAT-F	CGACGGTGTCCGGTCTCGTAGAACCATTCTGAAGACG GTCGTCAGCGGCCGCATCCCTGCCGTGCTCTACAAGA AAG	
D05170-500-F	GCAGGATGTT CGCAACA	CAGL0D05434g
D05170+500-R	TGTTGATTGCAGCTGGG	
D05170-1-NAT-R	GCGTCGACCTGCAGCGTACGTGTAGCTGTTTCATCCG CGCCACGGCGCGCCTAGCAGCGGGGTGTCTAGCTGG TCAG	
D05170+1-NAT-F	CGACGGTGTCCGGTCTCGTAGATATGGATGCCGCACTC CTGGTCAGCGGCCGCATCCCTGCCTACAGATACTCCA AGAC	CAGL0D05434g
D05434-500-F	GTCCTCTTGCTACCAGAC	
D05434+500-R	GAGTTAGATCGTGGATG	
D05434-1-NAT-R	GCGTCGACCTGCAGCGTACGTTATTGGCAGACGCCCA TCGCACGGCGCGCCTAGCAGCGGGTCCGGGACTGCCA GGGC	

D05434+1-NAT-F	CGACGGTGTCCGGTCTCGTAGCCAATGGTAAATAGTGC GTCGTCAGCGGCCGCATCCCTGCGCATCGTTCCCACC GAAC	
D06226-500-F	TGTTGGATCGGCTTTGA	CAGL0D06226g
D06226+500-R	CAGAGAAGAGCAAGGAG	
D06226-1-NAT-R	GCGTCGACCTGCAGCGTACGATAGAGCCGTGCCACTC GATCACGGCGCGCCTAGCAGCGG GATG CTAGAAGAGT GTC	
D06226+1-NAT-F	CGACGGTGTCCGGTCTCGTAGCATGCGCTGCCGTCAGA TAAGTCAGCGGCCGCATCCCTGCGACTCCGCACACTC TAC	
D06380-500-F	CCGGAGTTCTTCCACTG	CAGL0D06380g
D06380+500-R	GAGTTGGTGAACGTGAC	
D06380-1-NAT-R	GCGTCGACCTGCAGCGTACGCGGTGCTATACGGTGTT ACTCACGGCGCGCCTAGCAGCGGGACTCTTAGTAGCT TTCC	
D06380+1-NAT-F	CGACGGTGTCCGGTCTCGTAGTACCTACACGGGAGTAA GCGGTCAGCGGCCGCATCCCTGCTGCAACCAGCGTCT ACA	
E00275-500-F	GTC AACGTAATAGTGGG	CAGL0E00275g
E00275+500-R	GATCAAGGAGTACGTTG	
E00275-1-NAT-R	GCGTCGACCTGCAGCGTACGCGGTTAAGGCGCGTTAC CAACACGGCGCGCCTAGCAGCGG GACCAAATGTTTGCCTG	
E00275+1-NAT-F	CGACGGTGTCCGGTCTCGTAGCGTACGAGTATCATATTTCC CGGTCAGCGGCCGCATCCCTGCGAGAACTCTTTG GCTACC	
E06600-500-F	GGTATGATCTGAAGGCA	CAGL0E06600g
E06600+500-R	GATCGCATCTGGCAGGC	
E06600-1-NAT-R	GCGTCGACCTGCAGCGTACGGAGGTCTTCCGCTCGCT TAACACGGCGCGCCTAGCAGCGG TCAGATCAGAGGCATTAC	
E06600+1-NAT-F	CGACGGTGTCCGGTCTCGTAGGTTTACCACTAATCGTCG TCGTCAGCGGCCGCATCCCTGCGATTATCCTTTGCACT G	
E06644-500-F	GCTGTGCGATATCGCTG	CAGL0E06644g
E06644+500-R	GGTCTAACTTCATGGAC	
E06644-1-NAT-R	GCGTCGACCTGCAGCGTACGAATGGAATGCCACTCT CGGCACGGCGCGCCTAGCAGCGGCCAACATGGGTAC GAAC	
E06644+1-NAT-F	CGACGGTGTCCGGTCTCGTAGTAGAAACACACACCCCGT GGGTCAGCGGCCGCATCCCTGCGAGCAGGGACCAT TGTT	
F00627-500-F	GTCACAGATCAGCTCAC	CAGL0F00627g
F00627+500-R	TCTCCAAATAGTTCTGG	
F00627-1-NAT-R	GCGTCGACCTGCAGCGTACGACACTTCTCTCAGTTGC GGTCACGGCGCGCCTAGCAGCGGCTATCGCTTGCAGG TGG	
F00627+1-NAT-F	CGACGGTGTCCGGTCTCGTAGAAACCAGGTCATCACTC AGTGTGTCAGCGGCCGCATCCCTGCCTGATCAAGTGTC AGCG	
F01265-500-F	CTGTATCCCCTCCACTG	CAGL0F01265g
F01265+500-R	CCAAGAATGGTGCAGCTGC	
F01265-1-NAT-R	GCGTCGACCTGCAGCGTACGGAGGATTATTAACCTG GGCCACGGCGCGCCTAGCAGCGGCGAGATGCCGATG GCCTC	
F01265+1-NAT-F	CGACGGTGTCCGGTCTCGTAGATCAGAGGCACATTCCG GTCGTCAGCGGCCGCATCCCTGCGATTTGTTAGGCGT TTG	
F01815-500-F	ACTGAGAGCACTAGGAG	CAGL0F01815g
F01815+500-R	GGC TGC ACTGGGCAATT	

F01815-1-NAT-R	<u>GCGTCGACCTGCAGCGTACGTAGGACGAGTCACTGCA</u> <u>TCGCACGGCGCGCCTAGCAGCGGAGT GTTGTGTCTC</u> <u>TTGG</u>	
F01815+1-NAT-F	<u>CGACGGTGTCCGGTCTCGTAGCGAATGACTGTCCCAGC</u> <u>TAGGTCAGCGGCCGCATCCCTGCGCAGTGTGAGTGTA</u> <u>TGC</u>	
F02057-500-F	<u>TTGTTAAGACAGCACTG</u>	<i>CAGL0F02057g</i>
F02057+500-R	<u>ACTCTCGGATGGTGTG</u>	
F02057-1-NAT-R	<u>GCGTCGACCTGCAGCGTACGTCACTGTGTTAGAATGCT</u> <u>GGCCACGGCGCGCCTAGCAGCGG AAG TAGCGTTCTT</u> <u>ATGC</u>	
F02057+1-NAT-F	<u>CGACGGTGTCCGGTCTCGTAGAACAACTCTATCAGCCG</u> <u>ATGGTCAGCGGCCGCATCCCTGCGTTCAGACTACATC</u> <u>ACA</u>	
F03069-500-F	<u>AGAAAGAGATGGACTCC</u>	<i>CAGL0F03069g</i>
F03069+500-R	<u>CAAAGAATGCATCGTTCC</u>	
F03069-1-NAT-R	<u>GCGTCGACCTGCAGCGTACGTCACTTGGACCAGTTTG</u> <u>GCGCACGGCGCGCCTAGCAGCGGCCACTGACACGCT</u> <u>TATC</u>	
F03069+1-NAT-F	<u>CGACGGTGTCCGGTCTCGTAGAGGTAATCTGGCGACCG</u> <u>TCAGTCAGCGGCCGCATCCCTGCCAATAATGCATAGC</u> <u>GGC</u>	
F03905-500-F	<u>CCCGTTAAGACTAGGGC</u>	<i>CAGL0F03905g</i>
F03905+500-R	<u>CGCTGCTGCTGTCCCGC</u>	
F03905-1-NAT-R	<u>GCGTCGACCTGCAGCGTACGCCGTGTACTGAATTACG</u> <u>ATCCACGGCGCGCCTAGCAGCGG GCCCTTATCA</u> <u>GAATCCA</u>	
F03905+1-NAT-F	<u>CGACGGTGTCCGGTCTCGTAGCCTCACATTACCAAAGAT</u> <u>GGGTCAGCGGCCGCATCCCTGCCCCAGTCATCAGAG</u> <u>AC</u>	
F05159-500-F	<u>GTTCTGTCGCAGTAAATTC</u>	<i>CAGL0F05159g</i>
F05159+500-R	<u>AATACTGGAGTAGCTGA</u>	
F05159-1-NAT-R	<u>GCGTCGACCTGCAGCGTACGTGGCCGCATTTCCGAGA</u> <u>TGTCACGGCGCGCCTAGCAGCGGCCAGTTCACTCACC</u> <u>GAC</u>	
F05150+1-NAT-F	<u>CGACGGTGTCCGGTCTCGTAGTCATGCTGTACCATATTG</u> <u>GGGTCAGCGGCCGCATCCCTGCGATCATCAATGGACG</u> <u>GG</u>	
F04081-500-F	<u>ACTTCATCGTAACTGAG</u>	<i>CAGL0F04081g</i>
F04081+500-R	<u>GGAACCTCAAGTAGGCA</u>	
F04081-1-NAT-R	<u>GCGTCGACCTGCAGCGTACGTGGCCGCATTTCCGAGA</u> <u>TGTCACGGCGCGCCTAGCAGCGGGTCAGTTTTTGTCT</u> <u>CTAAG</u>	
F04081+1-NAT-F	<u>CGACGGTGTCCGGTCTCGTAGTCATGCTGTACCATATTG</u> <u>GGGTCAGCGGCCGCATCCCTGCGTATGATTCTAGTCG</u> <u>TCC</u>	
F05973-500-F	<u>GGTCTTGCTGTAGGGAT</u>	<i>CAGL0F05973g</i>
F05973+500-R	<u>CGATGTGATCCTGTTTCG</u>	
F05973-1-NAT-R	<u>GCGTCGACCTGCAGCGTACGAATTACAGCGACTCGAT</u> <u>GCGCACGGCGCGCCTAGCAGCGGCAATATGAATCCAG</u> <u>GG</u>	
F05973+1-NAT-F	<u>CGACGGTGTCCGGTCTCGTAGGCATCAAGTGGTGTGTCAG</u> <u>TCTGTCAGCGGCCGCATCCCTGCCTGAAAGTAAAGGT</u> <u>ACC</u>	
F06237-500-F	<u>CGCGATGATCTGCTCG</u>	<i>CAGL0F06237g</i>
F06237+500-R	<u>TCAACTGCCTAGCTTCC</u>	
F06237-1-NAT-R	<u>GCGTCGACCTGCAGCGTACGACACCAGGGAAAGGGCT</u> <u>TCACACGGCGCGCCTAGCAGCGGGCGTACAGAGTGTA</u> <u>TAG</u>	
F06237+1-NAT-F	<u>CGACGGTGTCCGGTCTCGTAGGAGGTTACTCGGTCTTA</u> <u>GCTGTCAGCGGCCGCATCCCTGCGAGGTCTCTACTGG</u>	

	TTA	
F08195-500-F	CCAGAGATAGCATCTAC	CAGL0F08195g
F08195+500-R	CACTACCAATGGACAACC	
F08195-1-NAT-R	GCGTCGACCTGCAGCGTACGTCGCCACCTTTACGAAT GTTACAGGCGCGCCTAGCAGCGGCTGCATTGCAAGTG AAAGGC	
F08195+1-NAT-F	CGACGGTGTCCGGTGTCTAGAAAGATAGAGTAACCCGC CTCGTCAGCGGCCGCATCCCTGCGTGTGCCAGTTAGA CCA	
F08767-500-F	GTAGACAACCTGGGTGTG	CAGL0F08767g
F08767+500-R	GGTTCTCCACGAACGAG	
F08767-1-NAT-R	GCGTCGACCTGCAGCGTACGCGGTGTGAGATGATATA CTCCACGGCGCGCCTAGCAGCGGCTACTAGGGCTGTC TCTC	
F08767+1-NAT-F	CGACGGTGTCCGGTCTCGTAGTTATCCATGCGGTGCAA GCGGTCAGCGGCCGCATCCCTGCTGGCTACACCACGG CTC	
F09229-500-F	CTTCCTATCAGAGCATA	CAGL0F09229g
F09229+500-R	GAACTTGTGACGGCTCC	
F09229-1-NAT-R	GCGTCGACCTGCAGCGTACGAGCGTACTAGGCATCTA TTGCACGGCGCGCCTAGCAGCGGCAGCGTGGGTATAA CCGG	
F09229+1-NAT-F	CGACGGTGTCCGGTCTCGTAGCGAGCGAATGATCTACT ATCGTCAGCGGCCGCATCCCTGCGTAAGTCGTAGAGG CT	
G02607-500-F	GTAAGCCTACTTCCCCG	CAGL0G02607g
G02607+500-R	CTGATGGTGCCGCTGCTC	
G02607-1-NAT-R	GCGTCGACCTGCAGCGTACGATAGCATGAACATCACG GCCACGGCGCGCCTAGCAGCGGCGGTTGATTCATA ACTC	
G02607+1-NAT-F	CGACGGTGTCCGGTCTCGTAGAATGCCGAAAGCTCCAG CAGGTCAGCGGCCGCATCCCTGC CCTAGCGCTGTGTAATA	
G03201-500-F	GAACGGAGCTGCTCCTG	CAGL0G03201g
G03201+500-R	ATCTAGTTGCAGCCGCT	
G03201-1-NAT-R	GCGTCGACCTGCAGCGTACGTCGTAGTACAGATCAGG TAGCACGGCGCGCCTAGCAGCGG CTGCCAGTTCTTTCATGC	
G03201+1-NAT-F	CGACGGTGTCCGGTCTCGTAGCGTGGAAATGCTGGTAA TACGTCAGCGGCCGCATCCCTGCGATCACATCACGGT TGG	
G03421-500-F	TGCAGTGCCATCTAAACC	CAGL0G03421g
G03421+500-R	TTTCGGCATAATACTGGG	
G03421-1-NAT-R	GCGTCGACCTGCAGCGTACGCGCCTGTTACAAAGTCT GTTACAGGCGCGCCTAGCAGCGGCCTATTTGGTTG GTG	
G03421+1-NAT-F	CGACGGTGTCCGGTCTCGTAGATGATTGACCCGCAGAC TCGGTCAGCGGCCGCATCCCTGCCACTACACTCATTCA TTTCG	
G04279-500-F	GAATCCAAATGAGTGCG	CAGL0G04279g
G04279+500-R	GGCGGCATCCGTTTATG	
G04279-1-NAT-R	GCGTCGACCTGCAGCGTACGCCGGTTGCCAAAGCGAG AAACACGGCGCGCCTAGCAGCGGCCGGATTACTTTAG C TG	
G04279+1-NAT-F	CGACGGTGTCCGGTCTCGTAGGTGGGAACTTCTTCTCCT CGGTCAGCGGCCGCATCCCTGCGTTAACGGTGCTTGA AC	
G04389-500-F	GCACTTTATCGGCACCTG	CAGL0G04389g
G04389+500-R	AACGCTGGTTTTGACGC	
G04389-1-NAT-R	GCGTCGACCTGCAGCGTACGCGATGGCTGCGTATCCC TAACACGGCGCGCCTAGCAGCGGCTAGATGCTTCTCA	

	CTC	
G04389+1-NAT-F	CGACGGTGTCCGGTCTCGTAGTTAAGATACCTGCCATT CGGTCAGCGGCCGCATCCCTGCTTCGCGTAGTTAGAC GC	
G05522-500-F	CTCCTTGAGCAAATGCG	CAGL0G05522g
G05522+500-R	CGTTATCCATGGCTCAC	
G05522-1-NAT-R	GCGTCGACCTGCAGCGTACGCCGCCTTAACACTATGG GATCACGGCGCGCCTAGCAGCGGGGCGTTTGAGTTGT CGG	
G05522+1-NAT-F	CGACGGTGTCCGGTCTCGTAGTATTCTTGACGCAGCTC GGGGTCAGCGGCCGCATCCCTGCCCGTTTAGGTATT TCC	
G10175-500-F	CGTGGACATTGAACGGC	CAGL0G10175g
G10175+500-R	CAGTATCTTATCAGGCC	
G10175-1-NAT-R	GCGTCGACCTGCAGCGTACGGCAGCAATGTGGTCCGC TATCACGGCGCGCCTAGCAGCGGGATAGACAAGCAGT CTC	
G10175+1-NAT-F	CGACGGTGTCCGGTCTCGTAGCCGTCGTATGAATCTACA TCGTCAGCGGCCGCATCCCTGCCGGCGCATATTTTGA CA	
H01749-500-F	CACTTCTCAGGGTATCC	CAGL0H01749g
H01749+500-R	GGTATACTGTGCAAACG	
H01749-1-NAT-R	GCGTCGACCTGCAGCGTACGGAGGTGCATCTCACTCC ATGCACGGCGCGCCTAGCAGCGGCTCTAGCGGTGCT TTCT	
H01749+1-NAT-F	CGACGGTGTCCGGTCTCGTAGGCATGTCATTCACTACTAC GGGTCAGCGGCCGCATCCCTGCCAACTCTGTGAACTT CC	
H04037-500-F	GTGTCAAGACGAGAAGG	CAGL0H04037g
H04037+500-R	CACTCTGAAGTGTGGTA	
H04037-1-NAT-R	GCGTCGACCTGCAGCGTACGCATTATGCACGATGGAT GCGCACGGCGCGCCTAGCAGCGGCAGGTCAAGAAG TGTAC	
H04037+1-NAT-F	CGACGGTGTCCGGTCTCGTAGCTGCAACATGGCCGCTG ATAGTCAGCGGCCGCATCCCTGCCGTGCGAAATAGGT TGC	
H06765-500-F	TCGTCCGGATGTTGCTC	CAGL0H06765g
H06765+500-R	GTAGGTCTGGCCAGACA	
H06765-1-NAT-R	GCGTCGACCTGCAGCGTACGAATCATCAGTAAGGAGG GTCCACGGCGCGCCTAGCAGCGGGCATCCAGCATCAG TCG	
H06765+1-NAT-F	CGACGGTGTCCGGTCTCGTAGGAAGATATTATGACCGA GCGGTCAGCGGCCGCATCCCTGCAGCGTCTAACATAC GCC	
H08712-500-F	ATAGAAGCAGACGTGTC	CAGL0H08712g
H08712+500-R	AGACACGAAG GCCTGCA	
H08712-1-NAT-R	GCGTCGACCTGCAGCGTACGCATTATTGTGAGCATG GTGCACGGCGCGCCTAGCAGCGG CCTGGTGT TTGTTCTG	
H08712+1-NAT-F	CGACGGTGTCCGGTCTCGTAGGCATGGGTGTGAATACT ATCGTCAGCGGCCGCATCCCTGC CACAAATGTGTTGCTAC	
H09592-500-F	GCTTGTG GACACAGAAG	CAGL0H09592g
H09592+500-R	CAACGGATTGGTCTGCG	
H09592-1-NAT-R	GCGTCGACCTGCAGCGTACGACAAACTCGGGCGCTAG GATCACGGCGCGCCTAGCAGCGG GAAATTATGAGCGAGTG	
H09592+1-NAT-F	CGACGGTGTCCGGTCTCGTAGCTGGCTGGGAAACCGAA ACA GTCAGCGGCCGCATCCCTGC CTATTGCA GGGCTTATAG	

H09988-500-F	CTTTAACGACCTGCATC	CAGL0H09988g
H09988+500-R	CGACCCTGATGAGCTTG	
H09988-1-NAT-R	GCGTCGACCTGCAGCGTACGAAGGATGTCTAACACTC TCCCACGGCGCGCCTAGCAGCGGTAGTCGTTTGGGCG CCA	
H09988+1-NAT-F	CGACGGTGTCCGGTCTCGTAGGAGGGAGCTTCCACCCA TATGTCAGCGGCCGCATCCCTGCGCATTTCATGGACATT GC	
H10208-500-F	ATCTATTCCTCGGTGCTC	CAGL0H10208g
H10208+500-R	CTCCCTCCTTTCTT	
H10208-1-NAT-R	GCGTCGACCTGCAGCGTACGTTACGGAGGCTTGGCAT ATTACGGCGCGCCTAGCAGCGG TATTTGGCCT TTCCATTGTG TA	
H10208+1-NAT-F	CGACGGTGTCCGGTCTCGTAGGGAGCCGTTCCGACCAT ATTGTCAGCGGCCGCATCCCTGC GTGAGAAACAAGCTACC	
I02244-500-F	CTTCGTACCTAGCACTG	CAGL0I02244g
I02244+500-R	TTGATCTGATCGCCGCT	
I02244-1-NAT-R	GCGTCGACCTGCAGCGTACGAGGCATTTGTCACACTG GTGCACGGCGCGCCTAGCAGCGG GAGAACGATTAAGTAGC	
I02244+1-NAT-F	CGACGGTGTCCGGTCTCGTAGGCATGGCTTCCAATGTC TGTGTCAGCGGCCGCATCCCTGC CAATGTGCTGAAGTGTC	
I08151-500-F	GAAGCAGACCACCACGA	CAGL0I08185g
I08151+500-R	GTTAGAGTAGCTGTTGG	
I08151-1-NAT-R	GCGTCGACCTGCAGCGTACGCGATGTATCCCGCTGTC GAACACGGCGCGCCTAGCAGCGG GAGGAAACTAAGACGAC	
I08151+1-NAT-F	CGACGGTGTCCGGTCTCGTAGTACAAACCAAGAGTGTC TCGGTCAGCGGCCGCATCCCTGCCATGACATGTAACA GCC	
I08437-500-F	GATCAGTCGGTCATTTCG	CAGL0I08437g
I08437+500-R	CGACTTGTTGCGACATC	
I08437-1-NAT-R	GCGTCGACCTGCAGCGTACGTATGCCTCTTGCTCCTA GAACACGGCGCGCCTAGCAGCGG CCGACATCAACTTACCG	
I08437+1-NAT-F	CGACGGTGTCCGGTCTCGTAGGCGGATATAACAGTAGT CACGTCAGCGGCCGCATCCCTGC GCA CACGAAGCAG GTCT	
I08613-500-F	AGACAATACCGCACAGG	CAGL0I08613g
I08613+500-R	CCTCTCCATTTCGTCCTTG	
I08613-1-NAT-R	GCGTCGACCTGCAGCGTACGGCGCATTAAAGTCCATTG AAGCACGGCGCGCCTAGCAGCGG GCTTGTCTGTTCTGCT	
I08613+1-NAT-F	CGACGGTGTCCGGTCTCGTAGCTGTAATGGACTGGTAG CTTGTGTCAGCGGCCGCATCCCTGCGCCTCCACCTACAA TTT	
I10362-500-F	GTGCCTATTT TCTGTCT	CAGL0I10362g
I10362+500-R	AGACGCTGCAGATGTGC	
I10362-1-NAT-R	GCGTCGACCTGCAGCGTACGTCTCTCTGTTGATCGCC GGACACGGCGCGCCTAGCAGCGG GTGGACACAAACTAGAC	
I10362+1-NAT-F	CGACGGTGTCCGGTCTCGTAGGCGCGACACTAATTTATC ACGTCAGCGGCCGCATCCCTGCCGAAATGTTCCGTC	
J01177-500-F	AACACGCTAAGCACAGG	CAGL0J01177g
J01177+500-R	ACAGCTATCTAGACAGG	
J01177-1-NAT-R	GCGTCGACCTGCAGCGTACGCGGTGTAATCGGATCTC GATCACGGCGCGCCTAGCAGCGGTTGTGTTCTCGTTG GCG	

J01177+1-NAT-F	CGACGGTGTCCGGTCTCGTAGACTACCATCGCAGTTGA GGGGTTCAGCGGCCGCATCCCTGCCTTAAATGGTAGCT CCA	
J02530-500-F	CTTCCGAACCAGGAACG	CAGL0J02530g
J02530+500-R	TACCCACGGAGCGAAGA	
J02530-1-NAT-R	GCGTCGACCTGCAGCGTACGGATGATAGACCATACCT CGCCACGGCGCGCCTAGCAGCGG GGCAAAACGA GAGTTTC	
J02530+1-NAT-F	CGACGGTGTCCGGTCTCGTAGTCTGATTCTTGCTCGGG AGAGTCAGCGGCCGCATCCCTGC GCAGGATCAGGTCAAGC	
J04972-500-F	GAGTCTTGGAGTTGCTAG	CAGL0J04972g
J04972+500-R	GCGAGATAGCGAGAGAG	
J04972-1-NAT-R	GCGTCGACCTGCAGCGTACGAATACTGGCAGAAGAGT TGCCACGGCGCGCCTAGCAGCGG TGCAATACGTGGCATCC	
J04972+1-NAT-F	CGACGGTGTCCGGTCTCGTAGTCCGTCATAACAGGCAA CTA GTCAGCGGCCGCATCCCTGC GAAGATC GACAACAAGG	
J05786-500-F	CCACTTCGTA CTACTACC	CAGL0J05786g
J05786+500-R	CTCGTGCTTGAAGAAAC	
J05786-1-NAT-R	GCGTCGACCTGCAGCGTACGAGTCTACCCACATGCTTT AGCACGGCGCGCCTAGCAGCGGCAAGAACTTCGCTTG AC	
J05786+1-NAT-F	CGACGGTGTCCGGTCTCGTAGCCGGCAAGTGTCCGATG AATGTCAGCGGCCGCATCCCTGCCAGATGGCAAAGAC AG	
J05852-500-F	CCAGATCGAAGTTGCCG	CAGL0J05852g
J05852+500-R	CTCTGTGTCCATGTCTG	
J05852-1-NAT-R	GCGTCGACCTGCAGCGTACGTCTACGTGCGTCAGGTA TGTCACGGCGCGCCTAGCAGCGG AGCAGTTCT CAGGTGCT	
J05852+1-NAT-F	CGACGGTGTCCGGTCTCGTAGTACCACACTTGGAAGAG TCTGTCAGCGGCCGCATCCCTGC TGTTCTCAACGGTGCCG	
K02013-500-F	CCTATTCTTGCCACTATG	CAGL0K02013g
K02013+500-R	TCGGTGAATATCCGTGG	
K02013-1-NAT-R	GCGTCGACCTGCAGCGTACGCGTGTGAATGAATGGCC TCTCACGGCGCGCCTAGCAGCGGCATACGAGCTTCCA TCAG	
K02013+1-NAT-F	CGACGGTGTCCGGTCTCGTAGTAGACATCTGTTCAAGTC GCGTCAGCGGCCGCATCCCTGCCTGGCATATGTGAGA GG	
K02145-500-F	CGCTTTGGATTATAGCCG	CAGL0K02145g
K02145+500-R	CAAAAGATCGGACCTCA	
K02145-1-NAT-R	GCGTCGACCTGCAGCGTACGAGCGGGCATCGTAGCAT ACTCACGGCGCGCCTAGCAGCGG CGTATACTGCGGCAGAA	
K02145+1-NAT-F	CGACGGTGTCCGGTCTCGTAGGCACGTATCACAATGAC GCAGTCAGCGGCCGCATCCCTGCGGTATTTGCTT GAATGC	
K02585-500-F	TTCATCAGCCAGTTTCG	CAGL0K02585g
K02585+500-R	GAGTTACTCTGCTGCTC	
K02585-1-NAT-R	GCGTCGACCTGCAGCGTACGTATGTCGCAGCCACTTC AGGCACGGCGCGCCTAGCAGCGGCCACGTATTAACCT TGAC	
K02585+1-NAT-F	CGACGGTGTCCGGTCTCGTAGGCAATCATGTTAGAACCT CGGTCAGCGGCCGCATCCCTGCGGCTATTTGAGTCGT CTG	
K05687-500-F	GCCAGAGCTTTAGGGTTGG	CAGL0K05687g
K05687+500-R	GGCAGTTCGTCTAGCAA	

K05687-1-NAT-R	<u>GCGTCGACCTGCAGCGTACGCAGTGATAGGGATGATA</u> <u>CACCACGGCGCGCCTAGCAGCGG</u> <u>AGAGAGATACGTTCGACAG</u>	
K05687+1-NAT-F	<u>CGACGGTGTCCGGTCTCGTAGCCATCCATGAGATATGT</u> <u>GAGGTCAGCGGCCGCATCCCTGCGTCACTTAAGTTGA</u> <u>CTG GC</u>	
K07634-500-F	<u>TCCTTGCTCCCATGTTC</u>	CAGL0K07634g
K07634+500-R	<u>GCCTTGTTGGGTCATTCT</u>	
K07634-1-NAT-R	<u>GCGTCGACCTGCAGCGTACGCGTCTACGAGTATTTGC</u> <u>AGTCACGGCGCGCCTAGCAGCGGGCTAGGAGAGTGG</u> <u>ACTA</u>	
K07634+1-NAT-F	<u>CGACGGTGTCCGGTCTCGTAGAAAGATCCTACATACGCT</u> <u>CGGTCAGCGGCCGCATCCCTGCCTGGGTAATGGTAAT</u> <u>CGC</u>	
K08294-500-F	<u>GTGGCAGACCTGGGTCCG</u>	CAGL0K08294g
K08294+500-R	<u>GGAGAACAGAACCGGAACC</u>	
K08294-1-NAT-R	<u>GCGTCGACCTGCAGCGTACGTATGTTGTCCCATCCGA</u> <u>CGGCACGGCGCGCCTAGCAGCGGTCCAGCTGTAAG</u> <u>GCGG</u>	
K08294+1-NAT-F	<u>CGACGGTGTCCGGTCTCGTAGAGCCTAAGTGCCGAGAC</u> <u>CTAGTCAGCGGCCGCATCCCTGCGCCTATCAAGACAT</u> <u>AAGC</u>	
K10318-500-F	<u>CACGCTCTCGCAACGCC</u>	CAGL0K10318g
K10318+500-R	<u>CTCAGCACACAGAACTCC</u>	
K10318-1-NAT-R	<u>GCGTCGACCTGCAGCGTACGCATGAGCTGAGTGCGAT</u> <u>CCACACGGCGCGCCTAGCAGCGGAACGGCCCTGGTA</u> <u>ACTA</u>	
K10318+1-NAT-F	<u>CGACGGTGTCCGGTCTCGTAGCGAGAAGTGTGCGATAAT</u> <u>CAGGTCAGCGGCCGCATCCCTGCCAAGCAAAGACTAA</u> <u>CTGG</u>	
K11066-500-F	<u>GTCCCAGT TCTTGTGCGAC</u>	CAGL0K11066g
K11066+500-R	<u>GACTCCTGTAGAATCGC</u>	
K11066-1-NAT-R	<u>GCGTCGACCTGCAGCGTACGGGCTGTCTGTGGCTTA</u> <u>CATCACGGCGCGCCTAGCAGCGGGGGCAATGAGACTC</u> <u>TG</u>	
K11066+1-NAT-F	<u>CGACGGTGTCCGGTCTCGTAGGTACACTTTGTCAACGAT</u> <u>CCGTCAGCGGCCGCATCCCTGCTGCTATCTCCATGTC</u> <u>GG</u>	
L03916-500-F	<u>GGCTCACCAAGGTCATC</u>	CAGL0L03916g
L03916+500-R	<u>GGTTGACGAGTTCTCTGG</u>	
L03916-1-NAT-R	<u>GCGTCGACCTGCAGCGTACGATCAGCTACCTCATTGC</u> <u>GATCACGGCGCGCCTAGCAGCGGAGAGAACTGGAA</u> <u>ATG</u>	
L03916+1-NAT-F	<u>CGACGGTGTCCGGTCTCGTAGCATGCGGATGCGTCCAC</u> <u>ATTGTCAGCGGCCGCATCCCTGCTCGGTGAACACCTA</u> <u>ACA</u>	
L06072-500-F	<u>CAAGTTTTCTCTCTTG</u>	CAGL0L06072g
L06072+500-R	<u>GCTGCATTGAGAAGGAC</u>	
L06072-1-NAT-R	<u>GCGTCGACCTGCAGCGTACGGCCGTAGTAACAAGCTC</u> <u>ACACACGGCGCGCCTAGCAGCGGCACTTCGGAACCTT</u> <u>AGA</u>	
L06072+1-NAT-F	<u>CGACGGTGTCCGGTCTCGTAGATACACATGACTACGAGT</u> <u>GCGTCAGCGGCCGCATCCCTGCGTTCTTTGTGTTTGA</u> <u>TC</u>	
L06776-500-F	<u>AGTATCTGTGGGCTGAT</u>	CAGL0L06776g
L06776+500-R	<u>CATCAATAGAGAGTGCG</u>	
L06776-1-NAT-R	<u>GCGTCGACCTGCAGCGTACGTATGACTTGTAGCAG</u> <u>TGGCACGGCGCGCCTAGCAGCGG</u> <u>GGCGTGTTCTAAGAAAC</u>	
L06776+1-NAT-F	<u>CGACGGTGTCCGGTCTCGTAGCGATGCACTAAATGACC</u> <u>TCAGTCAGCGGCCGCATCCCTGC A GATAGCGTGT</u>	

	CGGAAC	
L07480-500-F	CACTATACTCAGGACAC	CAGL0L07480g
L07480+500-R	CTGAATCTAAAGGCTAG	
L07480-1-NAT-R	GCGTCGACCTGCAGCGTACGGGGTCATCACGGCTCAT CATCACGGCGCGCCTAGCAGCGG TGCAAAT GAGGCTTGTG	
L07480+1-NAT-F	CGACGGTGTCCGGTCTCGTAGGCCATAGCTTCGACACG ATTGTCAGCGGCCGCATCCCTGC GAAAGTCACCTTCACGC	
M00770-500-F	CCGTGGCCACGGCCTTG	CAGL0M00770g
M00770+500-R	CTTACTTACCCGATCAGG	
M00770-1-NAT-R	GCGTCGACCTGCAGCGTACGTCGCGCTTGGTGCAAAT TCTCACGGCGCGCCTAGCAGCGG	
M00770+1-NAT-F	CGACGGTGTCCGGTCTCGTAGCGCCGCAAGTATGGTAA ATAGTCAGCGGCCGCATCCCTGCGACAAGTCTCATCTC CTC	
M01716-500-F	CTATTCGTTGTCGTTCTC	CAGL0M01716g
M01716+500-R	AGTCGTTGCTGGTAGTG	
M01716-1-NAT-R	GCGTCGACCTGCAGCGTACGTTGTACCCACTAGACGT GCGCACGGCGCGCCTAGCAGCGG GAGG GCGTTATTTG TGG	
M01716+1-NAT-F	CGACGGTGTCCGGTCTCGTAGAGGGTATGCCGGACACT CAAGTCAGCGGCCGCATCCCTGC GAGAGATGTAGGAATGC	
M01870-500-F	AGTAGATGGGATTACCA	CAGL0M01870g
M01870+500-R	CCATAGCCTTCCAAGAT	
M01870-1-NAT-R	GCGTCGACCTGCAGCGTACGCTTCATTGAGGATCAGA GGGCACGGCGCGCCTAGCAGCGG CTA TCAGCGAGATATTG	
M01870+1-NAT-F	CGACGGTGTCCGGTCTCGTAGCCATAGCTTAAAGGCCG TTCGTCAGCGGCCGCATCCCTGC CACTATCCCTCCATTAG	
M01914-500-F	CAAGGATTGACCCATCT	CAGL0M01914g
M01914+500-R	CACTGGCATTCTGGTCC	
M01914-1-NAT-R	GCGTCGACCTGCAGCGTACGCTACAAGCTCTGCGGTG CATCACGGCGCGCCTAGCAGCGGCCTTGTACTTTCTT GC	
M01914+1-NAT-F	CGACGGTGTCCGGTCTCGTAGCAGCATTGGCAACGAGT TTAGTCAGCGGCCGCATCCCTGCCAATGGCTCATAT TTCAC	
M02299-500-F	GGCA CCGCACTGTGCTA	CAGL0M02299g
M02299+500-R	TCGCTGACATGAACGAG	
M02299-1-NAT-R	GCGTCGACCTGCAGCGTACGACCGTACTGAGACATCC TGACACGGCGCGCCTAGCAGCGG CTATGCGTCTATGTGACC	
M02299+1-NAT-F	CGACGGTGTCCGGTCTCGTAGAGAGCCTTCCAATATCC GTAGTCAGCGGCCGCATCCCTGC GAACCACCATGCAAT CA	
M02321-500-F	CCTTCAGGAACGCCATC	CAGL0M02321g
M02321+500-R	CAGACAACGACGAAACTG	
M02321-1-NAT-R	GCGTCGACCTGCAGCGTACGCAGCCTAGTACATTAGC TTCCACGGCGCGCCTAGCAGCGG CCAATCGCT AAGTGAGT	
M02321+1-NAT-F	CGACGGTGTCCGGTCTCGTAGTAAAGACATTGCC TCACTGGTCAGCGGCCGCATCCCTGC GATTGCATGGTGGTTCT	
M04543-500-F	TCGCGGCACACATTGTT	CAGL0M04543g
M04543+500-R	GCATTGGTCAACAGATCG	
M04543-1-NAT-R	GCGTCGACCTGCAGCGTACGCAACCAGTGGACGGTAA TCTCACGGCGCGCCTAGCAGCGG	

	CTTTACAATTGGCCAGT	
M04543+1-NAT-F	CGACGGTGTCCGGTCTCGTAGAAGTACGCTTCATCCTTC GTGTCAGCGGCCGCATCCCTGC GCA AGACATGTCAAATG	
M05137-500-F	ACGGAGAGGGAGAGAA	CAGL0M05157g
M05137+500-R	CCGAAGATCGAAGAAGC	
M05137-1-NAT-R	GCGTCGACCTGCAGCGTACGTGACATCTTGTATTGCG GGCCACGGCGCGCCTAGCAGCGG TACGGTCAGTACCTAGC	
M05137+1-NAT-F	CGACGGTGTCCGGTCTCGTAGCAACCGTGAGGAGATCA TGTGTCAGCGGCCGCATCCCTGCCGTACGTGAAAGAG ATGC	
M10065-500-F	TCTTCGCATGTGGC TAG	CAGL0M10065g
M10065+500-R	AGTAGAGAGACAGCCAC	
M10065-1-NAT-R	GCGTCGACCTGCAGCGTACGTGACATCCTTTAGTAGCT GGCACGGCGCGCCTAGCAGCGG CTTCCAACCTTCCTTCAGG	
M10065+1-NAT-F	CGACGGTGTCCGGTCTCGTAGAAGCCTTCAGTGCGTCA TGT_GTCAGCGGCCGCATCCCTGC GAAGTCC TGCCACATTC	
M10153-500-F	ATACTATCAGAGTCCAC	CAGL0M10153g
M10153+500-R	GCATTTGCCAGTGGGAT	
M10153-1-NAT-R	GCGTCGACCTGCAGCGTACGATGTCAGAGACGGTACT ACGCACGGCGCGCCTAGCAGCGGGAAGGGAAAGGTA GTGC	
M10153+1-NAT-F	CGACGGTGTCCGGTCTCGTAGCCGACATATCCCTAGAG TATGTCAGCGGCCGCATCCCTGCGTATACTACCATA CG	
M10978-500-F	ACTGGCTTACAGCATCC	CAGL0M10978g
M10978+500-R	CGACAACGAACAATAGTG	
M10978-1-NAT-R	GCGTCGACCTGCAGCGTACGTACTGAGCGGCATGTCA CTGCACGGCGCGCCTAGCAGCGG GTAGGGCAGTTTACGTT	
M10978+1-NAT-F	CGACGGTGTCCGGTCTCGTAGCTCAATGTGCAGTGGTA TGCGTCAGCGGCCGCATCCCTGC TCGAGCTATCAGTAGCG	
M12881-500-F	CCTTGCCATGGACTAC	CAGL0M12881g
M12881+500-R	CTAGAAGCTGTCCAGCTG	
M12881-1-NAT-R	GCGTCGACCTGCAGCGTACGATGACCGGGCTGTACT ACTCACGGCGCGCCTAGCAGCGGGCTTCAGGCTTTAT CCAG	
M12881+1-NAT-F	CGACGGTGTCCGGTCTCGTAGAATTACGAGGCGTCAG GCTGTCAGCGGCCGCATCCCTGCCATTTCCGCCGTCT AGA	

Table 3: ORF-specific oligonucleotides for the verification of *C. glabrata* deletion mutants

Primer name	Sequence	Deletion verified
A01870 int-F	GGTATCATGGTCGCGCA	CAGL0A01870g
A01870 int-R	CGGAATCCTCTTCTGCT	
A01870-600-F	GGCTGATTGGCTTGAGA	
A01870+600-R	GGAAAGATCCGACATGG	
A02255 int-F	GGTGACTTGGATGTCGT	CAGL0A02255g
A02255 int-R	CATCTGGTCCAGCATTC	
A02255-600-F	CCAGAGGACTTCTAATGC	
A02255+600-R	AGTGCTCACACCGTGTG	
A02299 int-F	GGAGAGCATACGTCCCA	CAGL0A02299g
A02299 int-R	GTGCATTCTGTGTCTG	
A02299-600-F	CATTGGCAGCCATTCGG	
A02299+600-R	CCGAAAGAGATGACAGC	
A02343 int-F	CGGGTGTCTACTCTGG	CAGL0A02343g
A02343 int-R	GATGGAAATCCCTGCAC	
A02343-600-F	GTTGGGCAGCTCATCGG	
A02343+600-R	GCGTTTCTGCGATGAGAG	
A03608 int-F	GTTTGCTCGCCTTGAAC	CAGL0A03608g
A03608 int-R	GCTGACAGCGCTGATCT	
A03608-600-F	GGACTCTGCTCCTATGTC	
A03608+600-R	GCATCAGCAGCCATGGA	
A04257 int-F	CCCGAGTATGCGAATATG	CAGL0A04257g
A04257 int-R	GCCATGTGCATTTTCTTC	
A04257-600-F	GAGAGGTACATCCTGGGG	
A04257+600-R	GCACGTAAGCTCCCTCT	
A04565 int-F	TCACACAGCAAGACGAA	CAGL0A04565g
A04565 int-R	CACTGAGTTCGACAAGG	
A04565-600-F	GCACAATACGGTACTCAG	
A04565+600-R	CACAACATGGTTAATACCG	
B00726 int-F	GTGACTTCCGAATCCCTT	CAGL0B00726g
B00726 int-R	ACATGCACCACCAATTTT	
B00726-600-F	CAACAGACATAAAGGCGG	
B00726+600-R	ACTGAAGCAGAAGCAGTCA	
B01287 int-F	AATTAGGGATACCATGG	CAGL0B01287g
B01287 int-R	AGGAGCGAAAGCGGCAG	
B01287-600-F	GGCTTTGAATCCCGGTT	
B01287+600-R	CAACCAACAACGCGTTG	
B02882 int-F	GCAATGCTAGCAGAGG	CAGL0B02882g
B02882 int-R	GAGACTGTCTATCTCGT	
B02882-600-F	AAGGTGCAGTGGAACGC	
B02882+600-R	CCCAGCTCCAGTATAAT	
B02926 int-F	CTGGAGACTTGCGTTTC	CAGL0B02926g
B02926 int-R	GTACCCGAACAAAGGAT	
B02926-600-F	TCTAGAACTCAGCGTGC	
B02926+600-R	GCACGGATTGCGATTGGA	
B02948 int-F	GATGGGACGCTAGAGCC	CAGL0B02948g
B02948 int-R	GTCTGCCTCGCTGAAGG	
B02948-600-F	CCTACGCACACCGTATG	
B02948+600-R	GCGTCTGATGGGAAGAG	
B02970 int-F	CAGCCTATAGATACCAC	CAGL0B02970g
B02970 int-R	TATCCAAGACCGTTGGA	
B02970-600-F	ATCGTACTCGGAAACGC	
B02970+600-R	GCGTCTGATGGGAAGAG	
B03223 int-F	GAGTGCATGTGAACTC	CAGL0B03223g
B03223 int-R	TGTTGTGGCGACGCTTC	

B03223-600-F	GGCGAAATTCACCAACG	
B03223+600-R	CGAGAATCCTGAATTCC	
B03883 int-F	GGCAGTGGTGTGTTAT	CAGL0B03883g
B03883 int-R	CCTTCTGTACCACATCG	
B03883-600-F	GCTGCCTTCTTGTACAG	
B03883+600-R	CTCGAAGTCCATCACAC	
C00110 int-F	CTATCTCATCGATCACC	CAGL0C00110g
C00110 int-R	GCCTCTGTTCTGTTACG	
C00110-600-F	GTGCAGAGGATAACTGA	
C00110+600-R	CAGTCCTTTCCGTACAAG	
C00253 int-F	CAGACAGCACACTGTTT	CAGL0C00253g
C00253 int-R	CGAGGTGGAATACACTG	
C00253-600-F	CATGTTGAGCTCGACCC	
C00253+600-R	CTGAGATGATCACAGGAG	
C00847 int-F	CCAGGAACAG ACATTCC	CAGL0C00847g
C00847 int-R	TTGGACTTGGCGATGGA	
C00847-600-F	CAAGAAGGAGTGGCTCC	
C00847+600-R	GTGTGCGCTGCCTTCAA	
C01837 int-F	GAAGCTGGACGTCCGGCG	CAGL0C01837g
C01837 int-R	CATGACGCGTACATCTC	
C01837-600-F	CCATGGAATTCCGTCC	
C01837+600-R	GTGGTATCCGAAGTGCC	
C02277 int-F	GTCTCATCTTCTGAACGA	CAGL0C02277g
C02277 int-R	GAATACTCTGGTCATCG	
C02277-600-F	CAATGGACTTATCACGC	
C02277+600-R	GTCTTCCTTCGATCCTT	
C04763 int-F	AAGAGCACCAGGTGTTG	CAGL0C04763g
C04763 int-R	AAGAGCACCAGGTGTTG	
C04763-600-F	CAGATTGACCGACGAGG	
C04763+600-R	GAGCACGCAAAGTAGAG	
D00682 int-F	CACAGACAGGCAAATGC	CAGL0D00682g
D00682 int-R	GATCTGGAGC AGCATGA	
D00682-600-F	ATCACGGCAGAGACTGG	
D00682+600-R	GTTGTCAGAAGGGCAAG	
D01210 int-F	CGAGATGGTGGTTGAGAG	CAGL0D01210g
D01210 int-R	CATCAAGTCCATGCTCC	
D01210-600-F	GTGACCGGTGGTAGTAG	
D01210+600-R	CCTGCAGGAAGTGGCTG	
D03850 int-F	GGGCAAGTAGGGCAGTTG	CAGL0D03850g
D03850 int-R	CCTAGCAGCCAACAGTTG	
D03850-600-F	GGAGCTAACACTATGGC	
D03850+600-R	ACATTGGATCTAGGCAC	
D03872 int-F	CAATCTACACGGTGAGC	CAGL0D03872g
D03872 int-R	AGGCACAACCTGGCATG	
D03872-600-F	CGAAGCATACCGTAAGC	
D03872+600-R	CATCCGTCTGCAGAGA	
D05170 int-F	CAGCGGATTACAGCACG	CAGL0D05170g
D05170 int-R	CCGATGCTGCCACCAGT	
D05170-600-F	GACCGGTATGCATTACC	
D05170+600-R	CCTATTGGGCGAAGATC	
D05434 int-F	GCTACCTCTTGTGGGACC	CAGL0D05434g
D05434 int-R	CTAGCGAGCTCATTCCAG	
D05434-600-F	CCACAACCTCAGTGCAACCC	
D05434+600-R	GGCGAGGACTAGTTAGAG	
D06226 int-F	CGTCTGTTACTCACACC	CAGL0D06226g
D06226 int-R	GCAAGACCGTCAAGGTT	
D06226-600-F	GCACTCAGCTTGAGTAG	
D06226+600-R	GCTCAGCATGTGAGTTG	
D06380 int-F	CGAAGCTCGCCAATGAG	CAGL0D06380g

D06380 int-R	ACGGTGCCTTCGACCAG	
D06380-600-F	GCACTGGGAACAATGCAG	
D06380+600-R	CACAGTCTCGTCTCGGT	
E00275 int-F	CACAGAAAGGCCAACTG	CAGL0E00275g
E00275 int-R	GGATGGCTTGACACAAC	
E00275-600-F	TACATCAGATAGCAGTC	
E00275+600-R	CCGGGACAATCAAAACCT	
E06600 int-F	CAGCTACTCGACTAGCG	CAGL0E06600g
E06600 int-R	GAATGTGCAGCAGGTGT	
E06600-600-F	GATCGTGGGAATCCTGT	
E06600+600-R	GTGGTGAATATGCGCAC	
E06644 int-F	CAGTTCGCAGAAGACTC	CAGL0E06644g
E06644 int-R	CTTAGGACAGATGAGCTC	
E06644-600-F	ATCGCAA GCATGCGATC	
E06644+600-R	GTTAGTTCTTGTGTCCAG	
F00627 int-F	AACTTGTCGCCACCA	CAGL0F00627g
F00627 int-R	CCGCCACGGCTGTAAGA	
F00627-600-F	GCACCTTACCTACTGATGC	
F00627+600-R	CTGATAAACGGGTTAGTTGGC	
F01265 int-F	GGTGCTAGTCCCAACGG	CAGL0F01265g
F01265 int-R	TCAGCTGGAGTCCCGGC	
F01265-600-F	GGCTCTCCGCCTCCTAC	
F01265+600-R	CATCTTCTCCTCCACAC	
F01815 int-F	GGCAAGAGACCATCACC	CAGL0F01815g
F01815 int-R	GGTCTGTTG GTCGAGGA	
F01815-600-F	ACACGAAGCAGAACATG	
F01815+600-R	GGCTGTAGGTTATCTGA	
F02057 int-F	GCTAGCATTACCTTAGAG	CAGL0F02057g
F02057 int-R	CTGTCTGAGTTGTCCTC	
F02057-600-F	TATCTCTTCGGACCTTG	
F02057+600-R	TGCAAACACGCGATTCA	
F03069 int-F	CCGATAAGCAAGCGGAT	CAGL0F03069g
F03069 int-R	GACAGCTGTTAGCTTTG	
F03069-600-F	CTGATATGGGCGATGAG	
F03069+600-R	ATCGACGACGTCAGCGA	
F03905 int-F	CTGGGCCAAATGGCAGAC	CAGL0F03905g
F03905 int-R	ATAAGACGGGAAGTCCCC	
F03905-600-F	GAGAGTACTGAGAACCG	
F03905+600-R	GGCTTCTAAGAGCACATCG	
F04081 int-F	GGACACGACAAGTGGCC	CAGL0F04081g
F04081 int-R	TGCTGGGTAGCTGTAGC	
F04081-600-F	TCCCGCACTTGACGTCA	
F04081+600-R	CTACATATTCGCCTTC	
F05159 int-F	CGTCAGAAGATGAGCCGG	CAGL0F05159g
F05159 int-R	CCCTTCAGCCTGAGCC	
F05159-600-F	CGCCGACAATGTTAAACC	
F05159+600-R	ACCATCTGCAATTGACG	
F05973 int-F	AGGAGCGAAAGCGGCAG	CAGL0F05973g
F05973 int-R	GGAGGTCTCGGCAATCC	
F05973-600-F	CAACCAACAACGCGTTG	
F05973+600-R	GGCTTTGAATCCCGGTT	
F06237 int-F	CAGGGACACAAGTACTG	CAGL0F06237g
F06237 int-R	GGACCCTTGCCCTGTTG	
F06237-600-F	GCAACTGTGAGAATACCC	
F06237+600-R	GCCTTCAGCAACTTCTT	
F08195 int-F	CTGGAATGACGACGAGA	CAGL0F08195g
F08195 int-R	CCTGATTTCGATTTCCCGG	
F08195-600-F	CGCCAATAACTTCACCA	
F08195+600-R	CCGGCTGCACCAATAGA	
F08767 int-F	GTGCTTCCTTCCAGCCA	CAGL0F08767g

F08767 int-R	CGACTTACACGTGTTTTCG	
F08767-600-F	CCAAGACCAAGACCAAG	
F08767+600-R	GCTTTGTATCCTAGGGC	
F09229 int-F	ATGATGGGGAGGGATCG	CAGL0F09229g
F09229 int-R	CGTGTCTATGTGGTCTTG	
F09229-600-F	CAGCTAGTTTCTATGTTG	
F09229+600-R	CCACAACCTCAAGCGGCAG	
G02607 int-F	TGGATCAGTCAGTGGTG	CAGL0G02607g
G02607 int-R	GTCCCTGTGGAAG AAAGCTC	
G02607-600-F	TGAAACTTGCCGTGGTCC	
G02607+600-R	CAAATACGGCAAGATCC	
G03201 int-F	CATGTCGTGACACAGCA	CAGL0G03201g
G03201 int-R	GCAGATGATAGCCAGTT	
G03201-600-F	CTTGATGCGAAACCAAAC	
G03201+600-R	GCCTCCAGCCTCACCAT	
G03421 int-F		CAGL0G03421g
G03421 int-R		
G03421-600-F	GAGAGCACAGGAGCACAG	
G03421+600-R	ACCTTGGTAATAGTTTGGG	
G04279 int-F	GGGCTTTGCTGCATGCG	CAGL0G04279g
G04279 int-R	GTACCGGTTGAACAGTG	
G04279-600-F	TGAGCAGCCAGCACCCA	
G04279+600-R	GCGCTTATCTGATCTTG	
G04389 int-F	CCGCGCCAGTCTGTAAG	CAGL0G04389g
G04389 int-R	CTGCCTCTTCTAATTGGC	
G04389-600-F	CGTGTTGTGAAGCTGGC	
G04389+600-R	GTTGCAGGTGGTGGTGC	
G05522 int-F	GGCAAGCGAAGTCCACG	CAGL0G05522g
G05522 int-R	GCATTTGCCATAACCGG	
G05522-600-F	CCTCGACGCTAACTTTG	
G05522+600-R	TCAAGCTGGCCACAACC	
G10175 int-F	GCAAGATTGGCTGACGC	CAGL0G10175g
G10175 int-R	GCCGATGATGGCTCTGT	
G10175-600-F	CTCATCTCGTATCTGAG	
G10175+600-R	GTAATGGTCATGCAGTG	
H01749 int-F	ACGACAGGATGCAGCAT	CAGL0H01749g
H01749 int-R	CCGTATCGCTGCTTCTG	
H01749-600-F	TGGATTCTCCTCGCATC	
H01749+600-R	TGACCTGCGTTTTGGGT	
H04037 int-F		CAGL0H04037g
H04037 int-R	TCTCAGATCCTTAGCAG	
H04037-600-F	CAGTGCAAGAGGAATCAG	
H04037+600-R	GCTCAACTCTCTCCAAC	
H06765 int-F	GTGTCTGTTGTGCAGTC	CAGL0H06765g
H06765 int-R	GAGATCTTGACAGACCAA	
H06765-600-F	AACGTGTCGATGAACCTC	
H06765+600-R	GCAGCATTGCTGCGTT	
H08712 int-F	GAGGATTCAAGACTCCG	CAGL0H08712g
H08712 int-R	CTGAGCAAGGCGTGCAA	
H08712-600-F	GGCTTCTCGAAGCCATT	
H08712+600-R	CGAGTTCGAAACTGCTG	
H09592 int-F	GCTAACTTGCCAGCTGG	CAGL0H09592g
H09592 int-R	AGAAGATGGAGCAGCAG	
H09592-600-F	CGCTTCATTGTTCTCGC	
H09592+600-R	GTACTACGTCTCATAGG	
H09988 int-F	TACCGAACAGCCCCAAG	CAGL0H09988g
H09988 int-R	GTAGCTACCTCGGTTGG	
H09988-600-F	GTCATGACATCTGGCTATG	
H09988+600-R	GCCGGACGACTCAAAC	
H10208 int-F	TGTACACACAACCTCCGC	CAGL0H10208g

H10208 int-R	GGCTTCGAGG CAGTGT	
H10208-600-F	GAGGTACCGTAACCTCTC	
H10208+600-R	AGATAGT ATGGCATGTGG	
I02244 int-F	GATTGATGACGCAGGCG	CAGL0I02244g
I02244 int-R	GTCTGCTCATCCACAGC	
I02244-600-F	TGAACCAAACACTACAGTG	
I02244+600-R	GAGTAAGATCGACTGTCC	
I08151 int-F	GCTGGTGAGCAAGAGGA	CAGL0I08185g
I08151 int-R	TGCAGACCACGACAAGG	
I08151-600-F	GGTTGCTCTAGCGTAAC	
I08151+600-F	CCATCAAGGAGACGATTC	
I08437 int-F	GTCGTTGAGTGTGGAAG	CAGL0I08437g
I08437 int-R	GCATACAGGAGTCATCC	
I08437-600-F	GACTGCTCAATCCACAG	
I08437+600-R	GACAGGTCTTACCACAG	
I08613 int-F	CATCATGCTTGTGCGTG	CAGL0I08613g
I08613 int-R	CTCAGCGAGATGTCCGA	
I08613-600-F	TGTTGTCTCTCTGCGTG	
I08613+600-R	TCCTGCCAGTCTCCGCT	
I10362 int-F	GACGACTGTTGTGACTG	CAGL0I10362g
I10362 int-R	CAACTGGGAACTACCAG	
I10362-600-F	CTGGAGGCTAGTTGAAGC	
I10362+600-R	CAAGTCAAGAGAGCTGC	
J01177 int-F	AGCGTCAGACCTAACTC	CAGL0J01177g
J01177 int-R	CTTTCTTCTGGTTCTGC	
J01177-600-F	TGTGGCAGTGGTATGCC	
J01177+600-R	GGTCAGATCACTGAGAG	
J02530 int-F	GTTGAGCCATCCTCATC	CAGL0J02530g
J02530 int-R	CTGGAGGTACTIONCAGGA	
J02530-600-F	CCACACATAGCCGGTGT	
J02530+600-R	AGGCAGTGACCTACTAG	
J04972 int-F	GACATGCATCTTCGAGAC	CAGL0J04972g
J04972 int-R	CAACACTGGAAAGCGCT	
J04972-600-F	GACCCTATCACTGACAC	
J04972+600-R	GTGTTTACCCTGGCGTC	
J05786 int-F	GAACGTATGCGTGACAC	CAGL0J05786g
J05786 int-R	GAGACTGTTGTACGTAG	
J05786-600-F	GTCTACTGTATGCAC	
J05786+600-R	GAGAGAGGCCATTGTAG	
J05852 int-F	CGTTGTCAGTGGCTGCG	CAGL0J05852g
J05852 int-R	GGTGCCAGTCTCTCTGC	
J05852-600-F	CATCCTATAGCTGCTAC	
J05852+600-R	CAACAGCAGGCCGAGTACC	
K02013 int-F	ACCTGTGTTTGCCTGCC	CAGL0K02013g
K02013 int-R	CAGGCTGTTTCCCTCGCA	
K02013-600-F	GTCGAGAAGATGAAGGAG	
K02013+600-R	CAAGGTCCTAGCTTGC	
K02145 int-F	CGAGATGCTCAAACGAC	CAGL0K02145g
K02145 int-R	TCAGGCACTAAAGAAGG	
K02145-600-F	GCACACACATACAAACG	
K02145+600-R	GCTCCATTCTTTAGGC	
K02585 int-F	ATAGTGCGAACTTGACC	CAGL0K02585g
K02585 int-R	TGCTTAGCACCTTCTGC	
K02585-600-F	TTAACACGCAGAACGTC	
K02585+600-R	CACTTTGCGCTGTTCTTC	
K05687 int-F	CCCTTGAAGATTAGGGC	CAGL0K05687g
K05687 int-R	TTTCGGACTTGGGACCG	
K05687-600-F	CCTCGAACA GCTAAGACGG	
K05687+600-R	GCCTACAGTCAACATGA	

K07634 int-F	TGATGACAAAGGCACCT	CAGL0K07634g
K07634 int-R	CTCAGTGCTACTGACAC	
K07634-600-F	AGTATTCTCAACTGCTGAAATAA	
K07634+600-R	GTGGCCGATGATTGGTA	
K08294 int-F	GGCCTGTTGTGCTCACC	CAGL0K08294g
K08294 int-R	GCAAGCACGACTCGATG	
K08294-600-F	CCCGCAGACTTAGTTGA	
K08294+600-R	GGTGATAAAGCATTCTTC	
K10318 int-F	GTGCTGTATCAGAGAAGC	CAGL0K10318g
K10318 int-R	CCTCTAGCCTCACTAATC	
K10318-600-F	CCTCTTGTCAACAACGTC	
K10318+600-R	GGGATCCGATTCTGATT	
K11066 int-F	CTGGAGAACCAGTCTTC	CAGL0K11066g
K11066 int-R	CCTGCTGCAACAACGTC	
K11066-600-F	CAGGCGCTAAGCCC AAG	
K11066+600-R	CCGTACGATGTGGAACG	
L03916 int-F	CAACAATACTCCCTACGG	CAGL0L03916g
L03916 int-R	GATCGTTTGTGGGTGGTAC	
L03916-600-F	GCATTCCCCTTGACAACG	
L03916+600-R	GACGGCCTATATTACCA	
L06072 int-F	CTGGATATGTCGTCGCT	CAGL0L06072g
L06072 int-R	CACTTCTGCTGAAAGAC	
L06072-600-F	TGTAAGAAACACCAGTG	
L06072+600-R	CTATCGCGCACCTTAAT	
L06776 int-F	GTATCCAGATTGGAGAG	CAGL0L06776g
L06776 int-R	CTCTAGAGCTTCTATC	
L06776-600-F	TAAGTCCAGGTTGGGAA	
L06776+600-R	CTGAACCCACTTGTCTT	
L07480 int-F	GGTACTCATCTCAAGTC	CAGL0L07480g
L07480 int-R	CGTGTCTGCTGAAGCTT	
L07480-600-F	CTAGCAATCGTTGCTAC	
L07480+600-R	TGCTGGTTCCAAGACAT	
M00770 int-F	GGAGTTCAAGCCCGAGT	CAGL0M00770g
M00770 int-R	ACAATCTTGCTCCTCGG	
M00770-600-F	CACGCACTAGCAAGTGA	
M00770+600-R	CACTGTTAACCATGCGGC	
M01716 int-F	CCACAACAGACTGATGA	CAGL0M01716g
M01716 int-R	CGTGTATGAGTTCTGGA	
M01716-600-F	CTCGCCAAAAGGATGGA	
M01716+600-R	GAACGCTTGATACAGAA	
M01870 int-F	CTCCAGAAGAGATACTC	CAGL0M01870g
M01870 int-R	TCTGATGGGTAGCCATC	
M01870-600-F	CTGTATCAACCGTAGAT	
M01870+600-R	CTCTTGATGCCCTGTTG	
M01914 int-F	GCTGTTGACTACGCTCTG	CAGL0M01914g
M01914 int-R	ATAGCGTAGCAGCATGG	
M01914-600-F	GATGAGAAGGACAGGAAG	
M01914+600-R	TCTTGTCGATAGCGAGG	
M02299 int-F	GGTGCTG TACTACGC	CAGL0M02299g
M02299 int-R	CCACCCGAACGGAAAGC	
M02299-600-F	CGCC AATACTCATCCC GC	
M02299+600-R	GAGACTCACTGATCCTG	
M02321 int-F	CACTGATACTGCTGGCG	CAGL0M02321g
M02321 int-R	AGTCTGTGCGCCATATAG	
M02321-600-F	GTGGTGTGTAGATGGCT	
M02321+600-R	CTAGATTTGGAGCACATC	
M04543 int-F	GCTAGAGTTGCATGGAG	CAGL0M04543g
M04543 int-R	TCACTGATACGTAAGGC	
M04543-600-F	AGACACTAGTGCCGAGT	
M04543+600-R	TCACTGGACACTCGTGG	

M05137 int-F	GACGGGTGTCAGACATG	CAGL0M05137g
M05137 int-R	ACGTCAGCCGATATCGT	
M05137-600-F	CATAAGAGAGGAACCAAC	
M05137+600-R	ACTTCCAAGACGTCCGC	
M10065 int-F	CACGATCACG GGCACAG	CAGL0M10065g
M10065 int-R	CCTCAGTAACAGACGC	
M10065-600-F	TGGATGCCTTCTAGTCC	
M10065+600-R	CGGCTACAAGATCTATG	
M10153 int-F	CCAGGAACACCTGAGGA	CAGL0M10153g
M10153 int-R	CTTCTCTACACACAGCA	
M10153-600-F	GGCTGAGCTATTGGTGA	
M10153+600-R	GCGAAGCCAAAACCTGAG	
M10978 int-F	CATTGTACGCTATGAGC	CAGL0M10978g
M10978 int-R	AACGGAGACCTCTCAGC	
M10978-600-F	CCTTGTGTATCAATCGTG	
M10978+600-R	GTTCCATGATGCTGAAGG	
M12881 int-F	CGGTAGTGCCGGTACT	CAGL0M12881g
M12881 int-R	CCAAGGTTACACAGCAAGC	
M12881-600-F	GAGCAACTCCTCAGTTC	
M12881+600-R	ACTACTGAAGCCCAATC	

Table 4: General oligonucleotides for cloning of *C. glabrata* ORFs into the Invitrogen Gateway® System.

Primer	Sequence
AttB-For	GGGACAAGTTTGTACAAAAAAGCAGGCTTC
AttB-Rev	GGGGACCACTTTGTACAAGAAAGCTGGGTC
M13-For	GTAAAACGACGGCCAG
M13-Rev	CAGGAAACAGCTATGAC

Table 5: ORF-specific primers for amplification of *C. glabrata* and *S. cerevisiae* ORFs for cloning into the Gateway® System.

Primer	Sequence
GW-D05434-F	ACAAAAAGCAGGCTTCATGCAATCTAACGTTACTCTTCCACCTATC
GW-D05434-R	TACAAGAAAGCTGGGTCTAACACTAGTGGTGAAGAGTTTGCCTTCTT
GW-RSC30-F	ACAAAAAGCAGGCTTCATGATGGACATGCAAGTGAGAAAAGTGAC
GW-RSC30-R	TACAAGAAAGCTGGGTCTAATTATAAAATGCATCATAGAAATCGTT

Appendix 2: Phenotypic Screening Media

Table 1: Summary of conditions used for phenotypic screens. For chemicals added to the media, stock concentrations, solutes and final concentrations are listed. All screening was performed on YPD agar plates and incubated at 30 °C (unless otherwise stated). For chemicals listed as “carbon source”, glucose was omitted from the media. All filter sterilised stocks were added to YPD agar following autoclaving.

Chemical/condition	Stock concentration	Final concentration	Notes
YPD	-	-	-
Reduced temperature	-	-	Incubation at 16 °C
Increased temperature	-	-	Incubation at 42 °C
Heat shock	-	-	Heat shock for 1 hour at 55 °C, return to incubation at 30 °C
Glycerol	100 %	3 %	-
LiCl	4 M	80 mM	Filter sterilise stock
SDS (Sodium dodecyl sulphate)	20 %	0.1 % and 0.05 %	-
ZnCl ₂	1 M	8 mM	Filter sterilise stock
CdCl ₂	100 mM	2 mM	Filter sterilise stock
CoCl ₂	100 mM	1 mM and 2 mM	Filter sterilise stock
BaCl ₂	2 M	50 mM	Filter sterilise stock
FeCl ₂	100 mM	200 µM	Filter sterilise stock
CsCl	5 M	250 mM	Filter sterilise stock
KCl	2.5 M	200 mM and 400 mM	Filter sterilise stock
NaCl	-	0.5 M, 1 M and 1.5 M	-
Ethanol	100 %	6 %	-
Caffeine	150 mM	10 mM and 20 mM	Filter sterilise stock
Sorbitol	-	1 M	-
MnCl ₂	1 M	30 mM	Filter sterilise stock
CaCl ₂	5 M	0.5 M	Filter sterilise stock
CuSO ₄	1 M	7.5 mM	Filter sterilise stock

MgCl ₂	5 M	600 mM	Filter sterilise stock
CuCl ₂	100 mM	5 mM	Filter sterilise stock
Lactose (carbon source)	-	2 %	No glucose
Starch (carbon source)	-	2 %	No glucose
Galactose (carbon source)	-	2 %	No glucose
Raffinose (carbon source)	-	2 %	No glucose
Xylose (carbon source)	-	2 %	No glucose
Sodium acetate (carbon source)	-	2 %	No glucose
Ethanol (carbon source)	-	2 %	No glucose
Sorbitol (carbon source)	-	2 %	No glucose
Glycerol (carbon source)	-	2 %	No glucose
Sucrose (carbon source)	-	2 %	No glucose
Maltose (carbon source)	-	2 %	No glucose
Maltose (carbon source) + bromocresol purple		2.5 % bromocresol purple	No glucose. Bromocresol stock dissolved in ethanol. Filter sterilise stock.
Trehalose (carbon source)	-	2 %	No glucose
Nitrogen starvation	-	-	YNB no ammonium sulphate
Arsenic (III) oxide	50 mM	1 mM	Filter sterilise stock
UV light	-	800 J/M ²	-
MMS (methyl methanesulphonate)	99 %	0.05 %	-
Sodium metaarsenite	5 mM	0.5 mM	Filter sterilise stock
Hydroxyurea	2 M	100 mM	Filter sterilise stock
tBOOH (t-butyl hydroperoxide)	7.2 M	5 mM	-
H ₂ O ₂	8.8 M	5 mM	-
H ₂ O ₂ + NaCl	-	2 mM H ₂ O ₂ + 0.5 M NaCl	-
H ₂ O ₂ + 42 °C	-	2 mM H ₂ O ₂	Incubate at 42 °C
Benomyl	10 mg/ml	1 µg/ml	Stock solute DMSO. Filter sterilise stock.
Nystatin	8 mg/ml	5 µg/ml	Stock solute DMSO. Filter sterilise stock.

Sodium orthovanadate	200 mM	2.5 mM	Filter sterilise stock
Calcofluor white	50 mg/ml	1 mg/ml	Stock solute DMSO. Filter sterilise stock. Store in dark.
Congo red	10 mg/ml	250 µg/ml	Filter sterilise stock
Menadione	50 mM	50 µM	Stock solute ethanol
Caspofungin			Filter sterilise stock
Cycloheximide	50 mg/ml	1 µg/ml	Stock solute DMSO. Filter sterilise stock.
BPS (bathophenanthroline disulfonic acid)	10 mM	0.1 mM	Filter sterilise stock.
Fluconazole	2 mM	32 µg/ml	Filter sterilise stock.

Appendix 3: *C. glabrata* ORFs with no orthologue in *S. cerevisiae*

Table 1: List of 727 *C. glabrata* ORFs identified by RBH searches to have no orthologue in *S. cerevisiae*. ORFs with no coordinates have been disregarded by CGD during the course of this study (candidagenome.org).

ORF name	<i>C. glabrata</i> Gene name	Chromosome	Start coordinate	Stop coordinate	Strand
<i>CAGLOA00143g</i>					
<i>CAGLOA00165g</i>		ChrA_C_glabrata_CBS138	18876	18037	C
<i>CAGLOA00583g</i>		ChrA_C_glabrata_CBS138	65286	67226	W
<i>CAGLOA00649g</i>		ChrA_C_glabrata_CBS138	70937	71320	W
<i>CAGLOA00715g</i>		ChrA_C_glabrata_CBS138	73333	73623	W
<i>CAGLOA00913g</i>		ChrA_C_glabrata_CBS138	92985	97265	W
<i>CAGLOA01364g</i>					
<i>CAGLOA01366g</i>	<i>EPA9</i>	ChrA_C_glabrata_CBS138	140305	144693	W
<i>CAGLOA01408g</i>		ChrA_C_glabrata_CBS138	145388	146833	W
<i>CAGLOA01474g</i>		ChrA_C_glabrata_CBS138	153155	154933	W
<i>CAGLOA01650g</i>		ChrA_C_glabrata_CBS138	163770	164126	W
<i>CAGLOA01694g</i>		ChrA_C_glabrata_CBS138	169167	167242	C
<i>CAGLOA01870g</i>		ChrA_C_glabrata_CBS138	193719	191335	C
<i>CAGLOA01892g</i>		ChrA_C_glabrata_CBS138	194560	194826	W
<i>CAGLOA02024g</i>		ChrA_C_glabrata_CBS138	213901	211829	C
<i>CAGLOA02255g</i>		ChrA_C_glabrata_CBS138	244683	245501	W
<i>CAGLOA02277g</i>		ChrA_C_glabrata_CBS138	248522	249340	W
<i>CAGLOA02299g</i>		ChrA_C_glabrata_CBS138	250851	251690	W
<i>CAGLOA02343g</i>		ChrA_C_glabrata_CBS138	254861	255127	W
<i>CAGLOA02596g</i>		ChrA_C_glabrata_CBS138	278467	281085	W
<i>CAGLOA02838g</i>		ChrA_C_glabrata_CBS138	300358	297872	C
<i>CAGLOA02882g</i>		ChrA_C_glabrata_CBS138	302262	302576	W
<i>CAGLOA03344g</i>		ChrA_C_glabrata_CBS138	340501	342378	W
<i>CAGLOA03410g</i>		ChrA_C_glabrata_CBS138	348708	349451	W
<i>CAGLOA03608g</i>		ChrA_C_glabrata_CBS138	366934	366290	C
<i>CAGLOA03872g</i>		ChrA_C_glabrata_CBS138	394454	392922	C
<i>CAGLOA03883g</i>		ChrA_C_glabrata_CBS138	394613	395029	W
<i>CAGLOA04081g</i>		ChrA_C_glabrata_CBS138	408064	409188	W
<i>CAGLOA04257g</i>		ChrA_C_glabrata_CBS138	424289	422355	C
<i>CAGLOA04565g</i>		ChrA_C_glabrata_CBS138	450575	453700	W
<i>CAGLOA04609g</i>					
<i>CAGLOA04631g</i>		ChrA_C_glabrata_CBS138	456156	457241	W

CAGL0A04763g					
CAGL0A04851g					
CAGL0B00242g		ChrB_C_glabrata_CBS138	11136	10582	C
CAGL0B00440g		ChrB_C_glabrata_CBS138	31504	32313	W
CAGL0B00572g		ChrB_C_glabrata_CBS138	49506	48898	C
CAGL0B00726g		ChrB_C_glabrata_CBS138	63903	65153	W
CAGL0B00946g		ChrB_C_glabrata_CBS138	83143	84327	W
CAGL0B00968g		ChrB_C_glabrata_CBS138	84713	85951	W
CAGL0B01287g	<i>BUD5</i>	ChrB_C_glabrata_CBS138	114832	118575	W
CAGL0B01353g	<i>SPT20</i>	ChrB_C_glabrata_CBS138	122519	120462	C
CAGL0B01595g		ChrB_C_glabrata_CBS138	146542	148740	W
CAGL0B01743g		ChrB_C_glabrata_CBS138	161784	162653	W
CAGL0B01793g		ChrB_C_glabrata_CBS138	165053	165349	W
CAGL0B01859g		ChrB_C_glabrata_CBS138	168976	170844	W
CAGL0B02277g		ChrB_C_glabrata_CBS138	216745	216053	C
CAGL0B02299g		ChrB_C_glabrata_CBS138	217341	219272	W
CAGL0B02409g		ChrB_C_glabrata_CBS138	231172	230087	C
CAGL0B02860g		ChrB_C_glabrata_CBS138	278657	278007	C
CAGL0B02882g	<i>BMT2</i>	ChrB_C_glabrata_CBS138	281184	279334	C
CAGL0B02904g	<i>BMT6</i>	ChrB_C_glabrata_CBS138	283910	282093	C
CAGL0B02926g	<i>BMT3</i>	ChrB_C_glabrata_CBS138	286753	284897	C
CAGL0B02948g	<i>BMT4</i>	ChrB_C_glabrata_CBS138	289799	288006	C
CAGL0B02970g	<i>BMT5</i>	ChrB_C_glabrata_CBS138	293137	291248	C
CAGL0B02992g	<i>MNT3</i>	ChrB_C_glabrata_CBS138	294942	297019	W
CAGL0B03025g					
CAGL0B03179g		ChrB_C_glabrata_CBS138	312599	309816	C
CAGL0B03201g		ChrB_C_glabrata_CBS138	314195	313239	C
CAGL0B03223g		ChrB_C_glabrata_CBS138	314992	314690	C
CAGL0B03861g		ChrB_C_glabrata_CBS138	383336	382452	C
CAGL0B04235g	<i>SCP120</i>	ChrB_C_glabrata_CBS138	416601	415660	C
CAGL0B04763g		ChrB_C_glabrata_CBS138	458314	457409	C
CAGL0B04895g		ChrB_C_glabrata_CBS138	475072	476955	W
CAGL0C00110g	<i>EPA6</i>	ChrC_C_glabrata_CBS138	4284	2137	C
CAGL0C00209g	<i>AWP7</i>	ChrC_C_glabrata_CBS138	12939	11626	C
CAGL0C00253g		ChrC_C_glabrata_CBS138	23710	18884	C
CAGL0C00583g		ChrC_C_glabrata_CBS138	62224	63396	W
CAGL0C00781g		ChrC_C_glabrata_CBS138	81411	82193	W
CAGL0C00803g					
CAGL0C00825g					
CAGL0C00847g	<i>EPA8</i>	ChrC_C_glabrata_CBS138	86130	88502	W
CAGL0C00869g					
CAGL0C00968g		ChrC_C_glabrata_CBS138	96914	100018	W
CAGL0C01111g					
CAGL0C01133g		ChrC_C_glabrata_CBS138	114805	117915	W
CAGL0C01155g		ChrC_C_glabrata_CBS138	119007	119954	W
CAGL0C01265g	<i>GLM4</i>	ChrC_C_glabrata_CBS138	134389	129884	C

CAGL0C01463g		ChrC_C_glabrata_CBS138	162501	160384	C
CAGL0C01485g		ChrC_C_glabrata_CBS138	164613	162991	C
CAGL0C01617g		ChrC_C_glabrata_CBS138	174618	175334	W
CAGL0C01837g		ChrC_C_glabrata_CBS138	193387	191463	C
CAGL0C01859g		ChrC_C_glabrata_CBS138	196167	193730	C
CAGL0C01969g		ChrC_C_glabrata_CBS138	208511	206652	C
CAGL0C01991g		ChrC_C_glabrata_CBS138	208793	209806	W
CAGL0C02057g		ChrC_C_glabrata_CBS138	213539	213180	C
CAGL0C02167g		ChrC_C_glabrata_CBS138	220619	222061	W
CAGL0C02277g	GLN3	ChrC_C_glabrata_CBS138	232967	230496	C
CAGL0C02299g	KRE29	ChrC_C_glabrata_CBS138	233339	234424	W
CAGL0C02365g		ChrC_C_glabrata_CBS138	239122	238940	C
CAGL0C02431g		ChrC_C_glabrata_CBS138	246581	243792	C
CAGL0C02519g		ChrC_C_glabrata_CBS138	253051	254007	W
CAGL0C02739g		ChrC_C_glabrata_CBS138	276663	277250	W
CAGL0C02915g					
CAGL0C03311g		ChrC_C_glabrata_CBS138	334443	333898	C
CAGL0C03575g		ChrC_C_glabrata_CBS138	358209	356203	C
CAGL0C03740g		ChrC_C_glabrata_CBS138	372123	370762	C
CAGL0C03872g		ChrC_C_glabrata_CBS138	380268	379501	C
CAGL0C04026g		ChrC_C_glabrata_CBS138	399213	397303	C
CAGL0C04213g		ChrC_C_glabrata_CBS138	412104	411409	C
CAGL0C04763g		ChrC_C_glabrata_CBS138	445881	444934	C
CAGL0C04785g		ChrC_C_glabrata_CBS138	447874	447029	C
CAGL0C04829g		ChrC_C_glabrata_CBS138	451489	451151	C
CAGL0C05577g		ChrC_C_glabrata_CBS138	536419	538278	W
CAGL0C05621g					
CAGL0D00286g	BMT1	ChrD_C_glabrata_CBS138	37583	39784	W
CAGL0D00374g		ChrD_C_glabrata_CBS138	45775	46086	W
CAGL0D00462g		ChrD_C_glabrata_CBS138	55305	57443	W
CAGL0D00682g		ChrD_C_glabrata_CBS138	90825	89194	C
CAGL0D00726g		ChrD_C_glabrata_CBS138	93895	93272	C
CAGL0D01210g		ChrD_C_glabrata_CBS138	137954	138646	W
CAGL0D01254g		ChrD_C_glabrata_CBS138	140355	141038	W
CAGL0D01276g		ChrD_C_glabrata_CBS138	142618	143949	W
CAGL0D01364g		ChrD_C_glabrata_CBS138	152033	155479	W
CAGL0D01474g		ChrD_C_glabrata_CBS138	163480	161495	C
CAGL0D02200g		ChrD_C_glabrata_CBS138	224941	228159	W
CAGL0D02222g		ChrD_C_glabrata_CBS138	229223	228285	C
CAGL0D02310g		ChrD_C_glabrata_CBS138	239213	237084	C
CAGL0D02486g		ChrD_C_glabrata_CBS138	253763	256399	W
CAGL0D02750g		ChrD_C_glabrata_CBS138	288647	289021	W
CAGL0D02794g		ChrD_C_glabrata_CBS138	292034	293425	W
CAGL0D03234g		ChrD_C_glabrata_CBS138	334913	336145	W
CAGL0D03608g		ChrD_C_glabrata_CBS138	364790	363465	C
CAGL0D03630g		ChrD_C_glabrata_CBS138	366246	367025	W

CAGL0D03850g		ChrD_C_glabrata_CBS138	384689	387193	W
CAGL0D03872g		ChrD_C_glabrata_CBS138	387624	388433	W
CAGL0D03938g		ChrD_C_glabrata_CBS138	392433	394304	W
CAGL0D04400g		ChrD_C_glabrata_CBS138	432398	432126	C
CAGL0D04444g		ChrD_C_glabrata_CBS138	437288	435564	C
CAGL0D04488g		ChrD_C_glabrata_CBS138	438456	439238	W
CAGL0D04840g		ChrD_C_glabrata_CBS138	471574	472164	W
CAGL0D05104g					
CAGL0D05148g		ChrD_C_glabrata_CBS138	493013	492687	C
CAGL0D05170g	<i>PHO4</i>	ChrD_C_glabrata_CBS138	493897	495498	W
CAGL0D05236g		ChrD_C_glabrata_CBS138	499006	500337	W
CAGL0D05324g		ChrD_C_glabrata_CBS138	512450	510087	C
CAGL0D05434g		ChrD_C_glabrata_CBS138	518767	518042	C
CAGL0D05456g		ChrD_C_glabrata_CBS138	521445	522071	W
CAGL0D05544g		ChrD_C_glabrata_CBS138	530217	527482	C
CAGL0D05610g		ChrD_C_glabrata_CBS138	536192	534849	C
CAGL0D05654g		ChrD_C_glabrata_CBS138	538337	537378	C
CAGL0D05764g		ChrD_C_glabrata_CBS138	547259	549880	W
CAGL0D06226g		ChrD_C_glabrata_CBS138	588725	586395	C
CAGL0D06380g		ChrD_C_glabrata_CBS138	601040	602083	W
CAGL0D06622g		ChrD_C_glabrata_CBS138	632859	629323	C
CAGL0D06644g		ChrD_C_glabrata_CBS138	634224	636926	W
CAGL0D06666g		ChrD_C_glabrata_CBS138	638537	638737	W
CAGL0D06710g		ChrD_C_glabrata_CBS138	643127	641982	C
CAGL0E00165g					
CAGL0E00187g		ChrE_C_glabrata_CBS138	13227	12511	C
CAGL0E00275g	<i>EPA20</i>	ChrE_C_glabrata_CBS138	25881	28523	W
CAGL0E01265g		ChrE_C_glabrata_CBS138	119454	113167	C
CAGL0E01375g					
CAGL0E01397g		ChrE_C_glabrata_CBS138	131689	129962	C
CAGL0E01661g		ChrE_C_glabrata_CBS138	160703	164950	W
CAGL0E02057g		ChrE_C_glabrata_CBS138	203578	205509	W
CAGL0E02145g		ChrE_C_glabrata_CBS138	212223	213179	W
CAGL0E02893g		ChrE_C_glabrata_CBS138	273462	276254	W
CAGL0E03025g		ChrE_C_glabrata_CBS138	285579	285911	W
CAGL0E03069g		ChrE_C_glabrata_CBS138	288878	286341	C
CAGL0E03135g					
CAGL0E03421g		ChrE_C_glabrata_CBS138	315140	315493	W
CAGL0E03498g		ChrE_C_glabrata_CBS138	324961	324476	C
CAGL0E03542g		ChrE_C_glabrata_CBS138	328583	326046	C
CAGL0E03652g		ChrE_C_glabrata_CBS138	342099	341431	C
CAGL0E03696g					
CAGL0E03718g	<i>SNF6</i>	ChrE_C_glabrata_CBS138	348294	347116	C
CAGL0E04026g		ChrE_C_glabrata_CBS138	386039	387946	W
CAGL0E04202g					
CAGL0E04224g		ChrE_C_glabrata_CBS138	404636	405310	W

CAGL0E04268g		ChrE_C_glabrata_CBS138	406619	407983	W
CAGL0E04466g		ChrE_C_glabrata_CBS138	427512	428360	W
CAGL0E04554g		ChrE_C_glabrata_CBS138	439395	440117	W
CAGL0E04862g		ChrE_C_glabrata_CBS138	466023	469223	W
CAGL0E05852g					
CAGL0E05984g		ChrE_C_glabrata_CBS138	595299	595727	W
CAGL0E06116g		ChrE_C_glabrata_CBS138	606786	604945	C
CAGL0E06402g		ChrE_C_glabrata_CBS138	643478	643768	W
CAGL0E06578g					
CAGL0E06600g		ChrE_C_glabrata_CBS138	658435	661332	W
CAGL0E06622g					
CAGL0E06644g	EPA1	ChrE_C_glabrata_CBS138	665110	668214	W
CAGL0E06666g	EPA2	ChrE_C_glabrata_CBS138	674692	670430	C
CAGL0E06688g	EPA3	ChrE_C_glabrata_CBS138	683331	680404	C
CAGL0F00209g		ChrF_C_glabrata_CBS138	23731	22109	C
CAGL0F00627g		ChrF_C_glabrata_CBS138	67393	65516	C
CAGL0F00781g					
CAGL0F00803g	GAL11B	ChrF_C_glabrata_CBS138	88454	90970	W
CAGL0F00935g	PEX15	ChrF_C_glabrata_CBS138	101230	102354	W
CAGL0F01067g					
CAGL0F01177g		ChrF_C_glabrata_CBS138	123471	121015	C
CAGL0F01265g	YAP7	ChrF_C_glabrata_CBS138	131725	133596	W
CAGL0F01441g					
CAGL0F01463g	TIR1	ChrF_C_glabrata_CBS138	149905	150570	W
CAGL0F01485g	TIR2	ChrF_C_glabrata_CBS138	152334	151321	C
CAGL0F01507g		ChrF_C_glabrata_CBS138	153593	154864	W
CAGL0F01683g		ChrF_C_glabrata_CBS138	168297	167401	C
CAGL0F01815g		ChrF_C_glabrata_CBS138	180414	179470	C
CAGL0F01881g		ChrF_C_glabrata_CBS138	186169	186711	W
CAGL0F02057g		ChrF_C_glabrata_CBS138	199689	197149	C
CAGL0F02475g		ChrF_C_glabrata_CBS138	240391	239243	C
CAGL0F02783g		ChrF_C_glabrata_CBS138	271798	274317	W
CAGL0F03003g		ChrF_C_glabrata_CBS138	289923	293480	W
CAGL0F03069g	CAD1	ChrF_C_glabrata_CBS138	303110	301650	C
CAGL0F03377g					
CAGL0F03619g		ChrF_C_glabrata_CBS138	354565	352409	C
CAGL0F03905g		ChrF_C_glabrata_CBS138	380088	377962	C
CAGL0F03971g		ChrF_C_glabrata_CBS138	386224	390591	W
CAGL0F04037g					
CAGL0F04059g					
CAGL0F04081g		ChrF_C_glabrata_CBS138	406151	407998	W
CAGL0F04125g		ChrF_C_glabrata_CBS138	412378	411161	C
CAGL0F04147g					
CAGL0F04169g					
CAGL0F04521g		ChrF_C_glabrata_CBS138	453943	453083	C

CAGL0F04543g		ChrF_C_glabrata_CBS138	456591	456866	W
CAGL0F04785g		ChrF_C_glabrata_CBS138	482637	484547	W
CAGL0F05159g		ChrF_C_glabrata_CBS138	525230	527617	W
CAGL0F05357g		ChrF_C_glabrata_CBS138	541830	543635	W
CAGL0F05533g		ChrF_C_glabrata_CBS138	558329	557208	C
CAGL0F05687g		ChrF_C_glabrata_CBS138	570280	572649	W
CAGL0F05709g		ChrF_C_glabrata_CBS138	573128	574174	W
CAGL0F05819g		ChrF_C_glabrata_CBS138	586189	584882	C
CAGL0F05973g		ChrF_C_glabrata_CBS138	597353	595752	C
CAGL0F06237g		ChrF_C_glabrata_CBS138	619632	618976	C
CAGL0F06259g		ChrF_C_glabrata_CBS138	621027	620431	C
CAGL0F06567g		ChrF_C_glabrata_CBS138	646495	648012	W
CAGL0F06699g		ChrF_C_glabrata_CBS138	659539	658958	C
CAGL0F06787g		ChrF_C_glabrata_CBS138	665038	666156	W
CAGL0F06985g		ChrF_C_glabrata_CBS138	684832	686724	W
CAGL0F07271g		ChrF_C_glabrata_CBS138	709510	707309	C
CAGL0F07359g		ChrF_C_glabrata_CBS138	718650	717856	C
CAGL0F07513g		ChrF_C_glabrata_CBS138	730505	729306	C
CAGL0F07667g	MSS11	ChrF_C_glabrata_CBS138	746653	744275	C
CAGL0F07909g		ChrF_C_glabrata_CBS138	776659	779808	W
CAGL0F07997g		ChrF_C_glabrata_CBS138	788613	785803	C
CAGL0F08019g	PEX21	ChrF_C_glabrata_CBS138	791508	790810	C
CAGL0F08195g		ChrF_C_glabrata_CBS138	813050	814027	W
CAGL0F08591g		ChrF_C_glabrata_CBS138	855132	855620	W
CAGL0F08767g		ChrF_C_glabrata_CBS138	867394	867789	W
CAGL0F08811g		ChrF_C_glabrata_CBS138	869467	871308	W
CAGL0F08833g		ChrF_C_glabrata_CBS138	873849	876659	W
CAGL0F09141g		ChrF_C_glabrata_CBS138	904448	904239	C
CAGL0F09229g		ChrF_C_glabrata_CBS138	910693	908186	C
CAGL0F09251g					
CAGL0G00198g					
CAGL0G00396g		ChrG_C_glabrata_CBS138	40467	39655	C
CAGL0G00836g		ChrG_C_glabrata_CBS138	74216	74605	W
CAGL0G00968g		ChrG_C_glabrata_CBS138	88130	85791	C
CAGL0G01012g		ChrG_C_glabrata_CBS138	90335	91672	W
CAGL0G01122g		ChrG_C_glabrata_CBS138	106218	105880	C
CAGL0G01408g		ChrG_C_glabrata_CBS138	134524	134928	W
CAGL0G01562g		ChrG_C_glabrata_CBS138	146521	145796	C
CAGL0G01848g		ChrG_C_glabrata_CBS138	168670	168200	C
CAGL0G02123g		ChrG_C_glabrata_CBS138	186276	187691	W
CAGL0G02387g		ChrG_C_glabrata_CBS138	212288	214417	W
CAGL0G02409g		ChrG_C_glabrata_CBS138	215952	214837	C
CAGL0G02431g					
CAGL0G02519g		ChrG_C_glabrata_CBS138	229958	228822	C
CAGL0G02607g		ChrG_C_glabrata_CBS138	242310	240244	C
CAGL0G03201g		ChrG_C_glabrata_CBS138	299668	299021	C

CAGLOG03421g	FLO8	ChrG_C_glabrata_CBS138	330883	327833	C
CAGLOG03531g		ChrG_C_glabrata_CBS138	343866	343363	C
CAGLOG03553g		ChrG_C_glabrata_CBS138	345689	345057	C
CAGLOG03685g		ChrG_C_glabrata_CBS138	354696	354923	W
CAGLOG03751g		ChrG_C_glabrata_CBS138	360146	361096	W
CAGLOG03949g		ChrG_C_glabrata_CBS138	375421	375924	W
CAGLOG03993g		ChrG_C_glabrata_CBS138	379229	378876	C
CAGLOG04125g		ChrG_C_glabrata_CBS138	393879	396170	W
CAGLOG04279g		ChrG_C_glabrata_CBS138	406126	404144	C
CAGLOG04389g		ChrG_C_glabrata_CBS138	414764	413376	C
CAGLOG04477g					
CAGLOG04565g		ChrG_C_glabrata_CBS138	435706	434012	C
CAGLOG04609g	PKH2	ChrG_C_glabrata_CBS138	440059	437162	C
CAGLOG04785g		ChrG_C_glabrata_CBS138	456307	456011	C
CAGLOG04829g		ChrG_C_glabrata_CBS138	459677	462151	W
CAGLOG04939g		ChrG_C_glabrata_CBS138	474854	473085	C
CAGLOG05467g		ChrG_C_glabrata_CBS138	518000	516813	C
CAGLOG05511g		ChrG_C_glabrata_CBS138	524050	522026	C
CAGLOG05522g		ChrG_C_glabrata_CBS138	524170	524448	W
CAGLOG05544g		ChrG_C_glabrata_CBS138	527250	524827	C
CAGLOG05588g		ChrG_C_glabrata_CBS138	533711	531450	C
CAGLOG05808g		ChrG_C_glabrata_CBS138	560227	558635	C
CAGLOG05830g		ChrG_C_glabrata_CBS138	564474	561943	C
CAGLOG05896g		ChrG_C_glabrata_CBS138	568221	567337	C
CAGLOG06050g		ChrG_C_glabrata_CBS138	581306	581530	W
CAGLOG06160g		ChrG_C_glabrata_CBS138	587971	588246	W
CAGLOG06182g		ChrG_C_glabrata_CBS138	589050	591095	W
CAGLOG06446g		ChrG_C_glabrata_CBS138	622068	622394	W
CAGLOG06600g		ChrG_C_glabrata_CBS138	631430	630714	C
CAGLOG06644g		ChrG_C_glabrata_CBS138	634825	634475	C
CAGLOG06710g		ChrG_C_glabrata_CBS138	643070	642819	C
CAGLOG06820g		ChrG_C_glabrata_CBS138	650668	649676	C
CAGLOG06842g		ChrG_C_glabrata_CBS138	654152	651033	C
CAGLOG06996g		ChrG_C_glabrata_CBS138	667930	667115	C
CAGLOG07183g		ChrG_C_glabrata_CBS138	683243	678730	C
CAGLOG07293g		ChrG_C_glabrata_CBS138	693448	690620	C
CAGLOG07645g		ChrG_C_glabrata_CBS138	725540	725259	C
CAGLOG07887g		ChrG_C_glabrata_CBS138	748964	748236	C
CAGLOG08107g		ChrG_C_glabrata_CBS138	768772	770649	W
CAGLOG08382g		ChrG_C_glabrata_CBS138	792588	793943	W
CAGLOG08492g		ChrG_C_glabrata_CBS138	802604	804190	W
CAGLOG08580g					
CAGLOG08602g		ChrG_C_glabrata_CBS138	808355	811147	W
CAGLOG08866g		ChrG_C_glabrata_CBS138	850923	852752	W
CAGLOG08954g		ChrG_C_glabrata_CBS138	858788	857016	C
CAGLOG09064g		ChrG_C_glabrata_CBS138	865891	864422	C

CAGLOG09086g		ChrG_C_glabrata_CBS138	867382	867894	W
CAGLOG09108g		ChrG_C_glabrata_CBS138	869367	868327	C
CAGLOG09229g		ChrG_C_glabrata_CBS138	881783	881448	C
CAGLOG09603g		ChrG_C_glabrata_CBS138	918130	917738	C
CAGLOG09625g		ChrG_C_glabrata_CBS138	918731	919138	W
CAGLOG09647g		ChrG_C_glabrata_CBS138	919676	919350	C
CAGLOG09779g		ChrG_C_glabrata_CBS138	935346	935969	W
CAGLOG10175g	AWP6	ChrG_C_glabrata_CBS138	977483	979216	W
CAGLOG10197g					
CAGLOG10219g		ChrG_C_glabrata_CBS138	988766	991744	W
CAGLOH00110g		ChrH_C_glabrata_CBS138	3711	2611	C
CAGLOH00352g		ChrH_C_glabrata_CBS138	33180	34292	W
CAGLOH00638g	VIK1	ChrH_C_glabrata_CBS138	62769	61015	C
CAGLOH00704g		ChrH_C_glabrata_CBS138	69547	69155	C
CAGLOH00715g					
CAGLOH00913g		ChrH_C_glabrata_CBS138	91592	90756	C
CAGLOH01749g		ChrH_C_glabrata_CBS138	168634	168305	C
CAGLOH01815g	CBF1	ChrH_C_glabrata_CBS138	175972	174644	C
CAGLOH02145g		ChrH_C_glabrata_CBS138	192690	190804	C
CAGLOH02167g		ChrH_C_glabrata_CBS138	197907	196897	C
CAGLOH02277g		ChrH_C_glabrata_CBS138	206023	206397	W
CAGLOH02475g		ChrH_C_glabrata_CBS138	224077	226485	W
CAGLOH02497g		ChrH_C_glabrata_CBS138	228775	228026	C
CAGLOH02783g		ChrH_C_glabrata_CBS138	251169	256526	W
CAGLOH02959g	TOS8	ChrH_C_glabrata_CBS138	277540	278319	W
CAGLOH03047g		ChrH_C_glabrata_CBS138	285868	288093	W
CAGLOH03311g		ChrH_C_glabrata_CBS138	310699	311430	W
CAGLOH03421g		ChrH_C_glabrata_CBS138	320386	319316	C
CAGLOH03465g		ChrH_C_glabrata_CBS138	323129	323524	W
CAGLOH03751g		ChrH_C_glabrata_CBS138	347169	344104	C
CAGLOH03927g		ChrH_C_glabrata_CBS138	367018	365612	C
CAGLOH04015g		ChrH_C_glabrata_CBS138	378264	377281	C
CAGLOH04037g		ChrH_C_glabrata_CBS138	381916	379169	C
CAGLOH04059g		ChrH_C_glabrata_CBS138	383690	383247	C
CAGLOH04147g		ChrH_C_glabrata_CBS138	392825	393643	W
CAGLOH04191g		ChrH_C_glabrata_CBS138	397001	396831	C
CAGLOH04257g	MT-II	ChrH_C_glabrata_CBS138	405073	405231	W
CAGLOH04279g	MT-IIB	ChrH_C_glabrata_CBS138	406327	406485	W
CAGLOH04455g		ChrH_C_glabrata_CBS138	419033	421033	W
CAGLOH04609g		ChrH_C_glabrata_CBS138	441790	433499	C
CAGLOH04763g		ChrH_C_glabrata_CBS138	454589	455740	W
CAGLOH05027g		ChrH_C_glabrata_CBS138	481654	483762	W
CAGLOH05247g		ChrH_C_glabrata_CBS138	506947	507891	W
CAGLOH05577g		ChrH_C_glabrata_CBS138	552456	545740	C
CAGLOH05621g	RLM1	ChrH_C_glabrata_CBS138	556498	558378	W
CAGLOH05929g		ChrH_C_glabrata_CBS138	582132	584999	W

CAGL0H06215g	GAL11A	ChrH_C_glabrata_CBS138	609128	612415	W
CAGL0H06413g	SSR1	ChrH_C_glabrata_CBS138	632432	631794	C
CAGL0H06765g	BNR1	ChrH_C_glabrata_CBS138	676503	672619	C
CAGL0H07337g		ChrH_C_glabrata_CBS138	718141	718590	W
CAGL0H07557g		ChrH_C_glabrata_CBS138	738086	739516	W
CAGL0H07645g		ChrH_C_glabrata_CBS138	747508	749538	W
CAGL0H07843g	HAP2	ChrH_C_glabrata_CBS138	766126	765236	C
CAGL0H08107g		ChrH_C_glabrata_CBS138	792971	793987	W
CAGL0H08151g					
CAGL0H08712g		ChrH_C_glabrata_CBS138	849446	848229	C
CAGL0H08756g		ChrH_C_glabrata_CBS138	853968	853720	C
CAGL0H08866g		ChrH_C_glabrata_CBS138	866293	864317	C
CAGL0H08910g		ChrH_C_glabrata_CBS138	871136	870096	C
CAGL0H08998g		ChrH_C_glabrata_CBS138	877952	879595	W
CAGL0H09394g		ChrH_C_glabrata_CBS138	921373	920468	C
CAGL0H09482g		ChrH_C_glabrata_CBS138	928788	928384	C
CAGL0H09592g		ChrH_C_glabrata_CBS138	937859	938569	W
CAGL0H09614g		ChrH_C_glabrata_CBS138	939996	939286	C
CAGL0H09702g		ChrH_C_glabrata_CBS138	949553	948066	C
CAGL0H09922g		ChrH_C_glabrata_CBS138	970713	967366	C
CAGL0H09988g		ChrH_C_glabrata_CBS138	975811	973850	C
CAGL0H10010g		ChrH_C_glabrata_CBS138	977299	976466	C
CAGL0H10164g		ChrH_C_glabrata_CBS138	992579	991125	C
CAGL0H10208g		ChrH_C_glabrata_CBS138	999936	996853	C
CAGL0H10626g		ChrH_C_glabrata_CBS138	1043943	1047923	W
CAGL0I00220g	EPA23	ChrI_C_glabrata_CBS138	14903	12309	C
CAGL0I00374g		ChrI_C_glabrata_CBS138	28154	27597	C
CAGL0I00396g		ChrI_C_glabrata_CBS138	29592	29245	C
CAGL0I00550g		ChrI_C_glabrata_CBS138	41775	41539	C
CAGL0I00726g		ChrI_C_glabrata_CBS138	52931	52542	C
CAGL0I00902g		ChrI_C_glabrata_CBS138	69090	67387	C
CAGL0I00968g		ChrI_C_glabrata_CBS138	78375	81368	W
CAGL0I01210g		ChrI_C_glabrata_CBS138	99925	101580	W
CAGL0I01606g		ChrI_C_glabrata_CBS138	128683	132156	W
CAGL0I01650g		ChrI_C_glabrata_CBS138	138286	134918	C
CAGL0I01782g		ChrI_C_glabrata_CBS138	146481	149636	W
CAGL0I01914g		ChrI_C_glabrata_CBS138	159798	160229	W
CAGL0I01936g		ChrI_C_glabrata_CBS138	161109	160546	C
CAGL0I01958g		ChrI_C_glabrata_CBS138	162266	165565	W
CAGL0I02068g		ChrI_C_glabrata_CBS138	176743	177165	W
CAGL0I02134g	PEX21B	ChrI_C_glabrata_CBS138	183860	183081	C
CAGL0I02244g		ChrI_C_glabrata_CBS138	195726	195217	C
CAGL0I02596g		ChrI_C_glabrata_CBS138	235250	234648	C
CAGL0I02816g		ChrI_C_glabrata_CBS138	248692	247817	C
CAGL0I02838g		ChrI_C_glabrata_CBS138	250671	248704	C
CAGL0I03014g		ChrI_C_glabrata_CBS138	262731	262249	C

CAGL0I03212g		ChrI_C_glabrata_CBS138	275826	278717	W
CAGL0I03982g					
CAGL0I04466g		ChrI_C_glabrata_CBS138	397172	399460	W
CAGL0I05082g		ChrI_C_glabrata_CBS138	475276	473462	C
CAGL0I05170g	CST6	ChrI_C_glabrata_CBS138	490959	493064	W
CAGL0I05610g		ChrI_C_glabrata_CBS138	530369	529962	C
CAGL0I06226g		ChrI_C_glabrata_CBS138	597520	598887	W
CAGL0I06314g		ChrI_C_glabrata_CBS138	605636	607507	W
CAGL0I06446g		ChrI_C_glabrata_CBS138	624290	622713	C
CAGL0I06644g		ChrI_C_glabrata_CBS138	644830	644156	C
CAGL0I06919g		ChrI_C_glabrata_CBS138	669200	667962	C
CAGL0I06941g		ChrI_C_glabrata_CBS138	670718	669657	C
CAGL0I07183g		ChrI_C_glabrata_CBS138	692395	690080	C
CAGL0I07293g		ChrI_C_glabrata_CBS138	708640	703325	C
CAGL0I07425g		ChrI_C_glabrata_CBS138	715390	714551	C
CAGL0I07491g		ChrI_C_glabrata_CBS138	720444	719539	C
CAGL0I07711g		ChrI_C_glabrata_CBS138	740473	742197	W
CAGL0I07887g		ChrI_C_glabrata_CBS138	762373	763521	W
CAGL0I08151g		ChrI_C_glabrata_CBS138	793917	795065	W
CAGL0I08415g		ChrI_C_glabrata_CBS138	820773	824699	W
CAGL0I08437g		ChrI_C_glabrata_CBS138	825046	829038	W
CAGL0I08591g		ChrI_C_glabrata_CBS138	839319	837766	C
CAGL0I08613g	DUR3	ChrI_C_glabrata_CBS138	841861	840182	C
CAGL0I08811g		ChrI_C_glabrata_CBS138	858471	859535	W
CAGL0I09196g		ChrI_C_glabrata_CBS138	889696	891537	W
CAGL0I09636g		ChrI_C_glabrata_CBS138	923436	921232	C
CAGL0I09768g		ChrI_C_glabrata_CBS138	934608	933082	C
CAGL0I09834g		ChrI_C_glabrata_CBS138	939751	938648	C
CAGL0I09856g		ChrI_C_glabrata_CBS138	942327	943151	W
CAGL0I10098g	PWP7	ChrI_C_glabrata_CBS138	964074	959218	C
CAGL0I10246g	PWP2	ChrI_C_glabrata_CBS138	1002627	1006349	W
CAGL0I10252g					
CAGL0I10340g	PWP5	ChrI_C_glabrata_CBS138	1013299	1016337	W
CAGL0I10362g	PWP4	ChrI_C_glabrata_CBS138	1020373	1025691	W
CAGL0I10692g					
CAGL0I10725g		ChrI_C_glabrata_CBS138	1060071	1058860	C
CAGL0I10769g		ChrI_C_glabrata_CBS138	1065957	1065199	C
CAGL0I11011g		ChrI_C_glabrata_CBS138	1096813	1100349	W
CAGL0J00253g		ChrJ_C_glabrata_CBS138	17376	15883	C
CAGL0J00913g		ChrJ_C_glabrata_CBS138	94620	95756	W
CAGL0J01177g		ChrJ_C_glabrata_CBS138	111185	112624	W
CAGL0J01419g		ChrJ_C_glabrata_CBS138	133832	130812	C
CAGL0J01573g					
CAGL0J01595g	GLM6	ChrJ_C_glabrata_CBS138	151584	152618	W
CAGL0J01683g					
CAGL0J01727g		ChrJ_C_glabrata_CBS138	160781	157842	C

CAGL0J01774g		ChrJ_C_glabrata_CBS138	172073	164808	C
CAGL0J01958g		ChrJ_C_glabrata_CBS138	196501	194396	C
CAGL0J02024g		ChrJ_C_glabrata_CBS138	204836	203412	C
CAGL0J02046g		ChrJ_C_glabrata_CBS138	205632	205871	W
CAGL0J02464g		ChrJ_C_glabrata_CBS138	238695	241445	W
CAGL0J02508g	AWP1	ChrJ_C_glabrata_CBS138	248822	246210	C
CAGL0J02530g		ChrJ_C_glabrata_CBS138	252893	250629	C
CAGL0J02552g		ChrJ_C_glabrata_CBS138	257549	254862	C
CAGL0J02618g		ChrJ_C_glabrata_CBS138	261400	261843	W
CAGL0J02706g		ChrJ_C_glabrata_CBS138	269104	267965	C
CAGL0J03014g		ChrJ_C_glabrata_CBS138	291832	290111	C
CAGL0J03388g		ChrJ_C_glabrata_CBS138	327822	329105	W
CAGL0J03432g		ChrJ_C_glabrata_CBS138	330031	331899	W
CAGL0J03564g		ChrJ_C_glabrata_CBS138	340647	343736	W
CAGL0J03982g		ChrJ_C_glabrata_CBS138	377534	377881	W
CAGL0J04708g		ChrJ_C_glabrata_CBS138	447836	449728	W
CAGL0J04862g		ChrJ_C_glabrata_CBS138	462163	464562	W
CAGL0J04884g		ChrJ_C_glabrata_CBS138	465532	466518	W
CAGL0J04972g		ChrJ_C_glabrata_CBS138	475587	476606	W
CAGL0J05192g					
CAGL0J05302g		ChrJ_C_glabrata_CBS138	510020	510943	W
CAGL0J05390g		ChrJ_C_glabrata_CBS138	517202	516870	C
CAGL0J05786g		ChrJ_C_glabrata_CBS138	553406	551562	C
CAGL0J05808g		ChrJ_C_glabrata_CBS138	553745	554044	W
CAGL0J05830g		ChrJ_C_glabrata_CBS138	556054	554231	C
CAGL0J05852g		ChrJ_C_glabrata_CBS138	557558	556527	C
CAGL0J05896g		ChrJ_C_glabrata_CBS138	559944	560519	W
CAGL0J06160g		ChrJ_C_glabrata_CBS138	584111	585373	W
CAGL0J06556g		ChrJ_C_glabrata_CBS138	630978	634214	W
CAGL0J06622g		ChrJ_C_glabrata_CBS138	637316	638311	W
CAGL0J06798g		ChrJ_C_glabrata_CBS138	654817	655521	W
CAGL0J07348g		ChrJ_C_glabrata_CBS138	711496	713091	W
CAGL0J07502g		ChrJ_C_glabrata_CBS138	727961	726663	C
CAGL0J08327g					
CAGL0J08701g					
CAGL0J09130g		ChrJ_C_glabrata_CBS138	902880	904658	W
CAGL0J09174g		ChrJ_C_glabrata_CBS138	906232	907293	W
CAGL0J09548g		ChrJ_C_glabrata_CBS138	940777	936524	C
CAGL0J10076g		ChrJ_C_glabrata_CBS138	989186	988050	C
CAGL0J10142g					
CAGL0J10318g		ChrJ_C_glabrata_CBS138	1009995	1008835	C
CAGL0J10582g		ChrJ_C_glabrata_CBS138	1035745	1037154	W
CAGL0J10714g		ChrJ_C_glabrata_CBS138	1046800	1047771	W
CAGL0J10956g		ChrJ_C_glabrata_CBS138	1068578	1070431	W
CAGL0J11044g		ChrJ_C_glabrata_CBS138	1078322	1076112	C
CAGL0J11088g		ChrJ_C_glabrata_CBS138	1081270	1081962	W

CAGL0J11176g		ChrJ_C_glabrata_CBS138	1088473	1090362	W
CAGL0J11374g		ChrJ_C_glabrata_CBS138	1106466	1106215	C
CAGL0J11418g		ChrJ_C_glabrata_CBS138	1108949	1107909	C
CAGL0J11594g		ChrJ_C_glabrata_CBS138	1129709	1126896	C
CAGL0J11616g		ChrJ_C_glabrata_CBS138	1130080	1130436	W
CAGL0J11968g	EPA15	ChrJ_C_glabrata_CBS138	1172919	1175795	W
CAGL0K00110g	AWP2	ChrK_C_glabrata_CBS138	5830	3332	C
CAGL0K00341g		ChrK_C_glabrata_CBS138	37953	37531	C
CAGL0K00385g		ChrK_C_glabrata_CBS138	42643	43347	W
CAGL0K00495g		ChrK_C_glabrata_CBS138	53462	55564	W
CAGL0K01221g	PEX8	ChrK_C_glabrata_CBS138	114592	116427	W
CAGL0K01507g		ChrK_C_glabrata_CBS138	134490	131704	C
CAGL0K01639g		ChrK_C_glabrata_CBS138	147354	146143	C
CAGL0K01727g	RPN4	ChrK_C_glabrata_CBS138	154897	153398	C
CAGL0K01903g		ChrK_C_glabrata_CBS138	169974	169669	C
CAGL0K01947g		ChrK_C_glabrata_CBS138	172658	172341	C
CAGL0K02013g		ChrK_C_glabrata_CBS138	176257	177375	W
CAGL0K02101g		ChrK_C_glabrata_CBS138	182946	187847	W
CAGL0K02145g		ChrK_C_glabrata_CBS138	190884	191837	W
CAGL0K02519g		ChrK_C_glabrata_CBS138	228185	227541	C
CAGL0K02585g	YAP3	ChrK_C_glabrata_CBS138	235078	233972	C
CAGL0K02695g		ChrK_C_glabrata_CBS138	245459	244992	C
CAGL0K03003g		ChrK_C_glabrata_CBS138	277585	279528	W
CAGL0K03245g		ChrK_C_glabrata_CBS138	299646	298216	C
CAGL0K03663g		ChrK_C_glabrata_CBS138	339486	339752	W
CAGL0K03905g		ChrK_C_glabrata_CBS138	363233	364318	W
CAGL0K04191g		ChrK_C_glabrata_CBS138	386857	388446	W
CAGL0K04257g		ChrK_C_glabrata_CBS138	393759	392116	C
CAGL0K04631g		ChrK_C_glabrata_CBS138	444591	441550	C
CAGL0K04653g		ChrK_C_glabrata_CBS138	448486	446732	C
CAGL0K04675g		ChrK_C_glabrata_CBS138	455284	455718	W
CAGL0K04697g		ChrK_C_glabrata_CBS138	459195	460742	W
CAGL0K04719g		ChrK_C_glabrata_CBS138	462817	462359	C
CAGL0K04763g					
CAGL0K04895g		ChrK_C_glabrata_CBS138	476625	475558	C
CAGL0K05247g		ChrK_C_glabrata_CBS138	509508	513182	W
CAGL0K05511g		ChrK_C_glabrata_CBS138	542127	539944	C
CAGL0K05643g		ChrK_C_glabrata_CBS138	551022	552314	W
CAGL0K05687g		ChrK_C_glabrata_CBS138	555370	556536	W
CAGL0K06039g		ChrK_C_glabrata_CBS138	589631	592027	W
CAGL0K06083g		ChrK_C_glabrata_CBS138	594349	593405	C
CAGL0K06127g		ChrK_C_glabrata_CBS138	597610	598566	W
CAGL0K06171g					
CAGL0K06325g		ChrK_C_glabrata_CBS138	623378	621549	C
CAGL0K06435g		ChrK_C_glabrata_CBS138	630381	635204	W

CAGL0K06479g		ChrK_C_glabrata_CBS138	637125	640100	W
CAGL0K06655g		ChrK_C_glabrata_CBS138	648911	651319	W
CAGL0K06721g		ChrK_C_glabrata_CBS138	655617	656933	W
CAGL0K07183g		ChrK_C_glabrata_CBS138	705897	706220	W
CAGL0K07205g		ChrK_C_glabrata_CBS138	708222	707503	C
CAGL0K07271g		ChrK_C_glabrata_CBS138	714624	712294	C
CAGL0K07502g		ChrK_C_glabrata_CBS138	742349	742990	W
CAGL0K07634g		ChrK_C_glabrata_CBS138	756054	754675	C
CAGL0K07678g		ChrK_C_glabrata_CBS138	764843	764196	C
CAGL0K07920g		ChrK_C_glabrata_CBS138	788342	786915	C
CAGL0K08294g		ChrK_C_glabrata_CBS138	837573	825448	C
CAGL0K08470g		ChrK_C_glabrata_CBS138	852119	851940	C
CAGL0K08624g		ChrK_C_glabrata_CBS138	870380	869340	C
CAGL0K08690g		ChrK_C_glabrata_CBS138	879137	877494	C
CAGL0K09130g		ChrK_C_glabrata_CBS138	907965	907150	C
CAGL0K09504g		ChrK_C_glabrata_CBS138	939088	938579	C
CAGL0K09746g		ChrK_C_glabrata_CBS138	955125	952549	C
CAGL0K09812g		ChrK_C_glabrata_CBS138	959122	960138	W
CAGL0K09834g		ChrK_C_glabrata_CBS138	964855	960893	C
CAGL0K10032g		ChrK_C_glabrata_CBS138	981372	980068	C
CAGL0K10164g		ChrK_C_glabrata_CBS138	990940	990287	C
CAGL0K10318g		ChrK_C_glabrata_CBS138	1004753	1007506	W
CAGL0K10428g		ChrK_C_glabrata_CBS138	1019646	1020206	W
CAGL0K10648g		ChrK_C_glabrata_CBS138	1039063	1036025	C
CAGL0K11319g		ChrK_C_glabrata_CBS138	1098955	1097846	C
CAGL0K11396g	SIR4	ChrK_C_glabrata_CBS138	1108107	1103764	C
CAGL0K11484g		ChrK_C_glabrata_CBS138	1114883	1115206	W
CAGL0K11638g		ChrK_C_glabrata_CBS138	1125950	1124172	C
CAGL0K11946g		ChrK_C_glabrata_CBS138	1153568	1153891	W
CAGL0K11990g		ChrK_C_glabrata_CBS138	1159199	1156224	C
CAGL0K12078g		ChrK_C_glabrata_CBS138	1171209	1169818	C
CAGL0K12298g		ChrK_C_glabrata_CBS138	1201583	1200966	C
CAGL0K12320g		ChrK_C_glabrata_CBS138	1201918	1204275	W
CAGL0K12364g		ChrK_C_glabrata_CBS138	1206621	1207109	W
CAGL0K12540g	HAC1	ChrK_C_glabrata_CBS138	1225334	1224345	C
CAGL0K12980g	BMT7	ChrK_C_glabrata_CBS138	1286134	1283966	C
CAGL0K13002g	AED2	ChrK_C_glabrata_CBS138	1291683	1294496	W
CAGL0K13024g	AED1	ChrK_C_glabrata_CBS138	1297775	1301002	W
CAGL0L00176g					
CAGL0L00473g		ChrL_C_glabrata_CBS138	53395	54774	W
CAGL0L00583g		ChrL_C_glabrata_CBS138	71544	72710	W
CAGL0L01023g		ChrL_C_glabrata_CBS138	119978	119691	C
CAGL0L01045g		ChrL_C_glabrata_CBS138	120342	120109	C
CAGL0L01507g		ChrL_C_glabrata_CBS138	167209	171099	W
CAGL0L01573g		ChrL_C_glabrata_CBS138	176421	176894	W
CAGL0L01771g		ChrL_C_glabrata_CBS138	198971	200278	W

CAGL0L02013g		ChrL_C_glabrata_CBS138	237127	235616	C
CAGL0L02453g		ChrL_C_glabrata_CBS138	280524	278611	C
CAGL0L02541g		ChrL_C_glabrata_CBS138	300308	300988	W
CAGL0L02981g		ChrL_C_glabrata_CBS138	349506	348799	C
CAGL0L03157g		ChrL_C_glabrata_CBS138	367003	367563	W
CAGL0L03388g		ChrL_C_glabrata_CBS138	388777	389391	W
CAGL0L03674g		ChrL_C_glabrata_CBS138	422571	424460	W
CAGL0L03784g		ChrL_C_glabrata_CBS138	439813	437192	C
CAGL0L03894g		ChrL_C_glabrata_CBS138	448634	448143	C
CAGL0L03916g		ChrL_C_glabrata_CBS138	452880	450952	C
CAGL0L04114g		ChrL_C_glabrata_CBS138	484447	482705	C
CAGL0L04818g		ChrL_C_glabrata_CBS138	553653	552334	C
CAGL0L05038g		ChrL_C_glabrata_CBS138	571776	573317	W
CAGL0L05192g		ChrL_C_glabrata_CBS138	585066	585383	W
CAGL0L05214g					
CAGL0L05324g		ChrL_C_glabrata_CBS138	592217	591903	C
CAGL0L05786g		ChrL_C_glabrata_CBS138	639219	638173	C
CAGL0L05830g		ChrL_C_glabrata_CBS138	651511	652161	W
CAGL0L05940g		ChrL_C_glabrata_CBS138	662250	663698	W
CAGL0L05984g		ChrL_C_glabrata_CBS138	669527	669150	C
CAGL0L06072g		ChrL_C_glabrata_CBS138	682823	681921	C
CAGL0L06226g		ChrL_C_glabrata_CBS138	707044	705599	C
CAGL0L06424g		ChrL_C_glabrata_CBS138	728331	728999	W
CAGL0L06512g		ChrL_C_glabrata_CBS138	736479	736255	C
CAGL0L06644g		ChrL_C_glabrata_CBS138	750307	752793	W
CAGL0L06688g		ChrL_C_glabrata_CBS138	758073	756016	C
CAGL0L06776g		ChrL_C_glabrata_CBS138	763580	766066	W
CAGL0L07194g		ChrL_C_glabrata_CBS138	800960	801430	W
CAGL0L07480g		ChrL_C_glabrata_CBS138	825181	824237	C
CAGL0L07502g		ChrL_C_glabrata_CBS138	829066	828380	C
CAGL0L07524g					
CAGL0L07568g		ChrL_C_glabrata_CBS138	837713	837393	C
CAGL0L07590g		ChrL_C_glabrata_CBS138	838499	838293	C
CAGL0L08008g		ChrL_C_glabrata_CBS138	875742	875861	W
CAGL0L08470g		ChrL_C_glabrata_CBS138	930917	930435	C
CAGL0L08536g		ChrL_C_glabrata_CBS138	934441	934662	W
CAGL0L08954g		ChrL_C_glabrata_CBS138	979515	980879	W
CAGL0L09251g		ChrL_C_glabrata_CBS138	1004824	1003976	C
CAGL0L09339g		ChrL_C_glabrata_CBS138	1014256	1016889	W
CAGL0L09361g		ChrL_C_glabrata_CBS138	1018071	1018406	W
CAGL0L09383g		ChrL_C_glabrata_CBS138	1020856	1021956	W
CAGL0L09845g		ChrL_C_glabrata_CBS138	1056009	1054843	C
CAGL0L09889g		ChrL_C_glabrata_CBS138	1057762	1059915	W
CAGL0L09911g		ChrL_C_glabrata_CBS138	1064342	1068697	W
CAGL0L10186g		ChrL_C_glabrata_CBS138	1097625	1097104	C
CAGL0L10626g		ChrL_C_glabrata_CBS138	1136212	1137753	W

CAGL0L11484g		ChrL_C_glabrata_CBS138	1222937	1224250	W
CAGL0L11880g		ChrL_C_glabrata_CBS138	1274920	1277862	W
CAGL0L12122g		ChrL_C_glabrata_CBS138	1303778	1302987	C
CAGL0L12298g		ChrL_C_glabrata_CBS138	1331972	1331112	C
CAGL0L12320g		ChrL_C_glabrata_CBS138	1332269	1333105	W
CAGL0L12496g		ChrL_C_glabrata_CBS138	1349053	1348769	C
CAGL0L12518g		ChrL_C_glabrata_CBS138	1349621	1349271	C
CAGL0L12782g		ChrL_C_glabrata_CBS138	1370285	1371082	W
CAGL0L13090g		ChrL_C_glabrata_CBS138	1397800	1400046	W
CAGL0L13332g	EPA13	ChrL_C_glabrata_CBS138	1436026	1439133	W
CAGL0M00132g	EPA12	ChrM_C_glabrata_CBS138	14404	11636	C
CAGL0M00308g		ChrM_C_glabrata_CBS138	39072	38758	C
CAGL0M00440g		ChrM_C_glabrata_CBS138	56009	56707	W
CAGL0M00638g		ChrM_C_glabrata_CBS138	78077	76881	C
CAGL0M00704g		ChrM_C_glabrata_CBS138	81930	82796	W
CAGL0M00726g		ChrM_C_glabrata_CBS138	83656	82968	C
CAGL0M00770g	SIR3	ChrM_C_glabrata_CBS138	86290	89556	W
CAGL0M00792g		ChrM_C_glabrata_CBS138	91057	90755	C
CAGL0M00968g		ChrM_C_glabrata_CBS138	107989	109311	W
CAGL0M01254g	STE12	ChrM_C_glabrata_CBS138	143315	141519	C
CAGL0M01716g		ChrM_C_glabrata_CBS138	193696	192389	C
CAGL0M01870g		ChrM_C_glabrata_CBS138	220760	219813	C
CAGL0M01914g		ChrM_C_glabrata_CBS138	232780	234810	W
CAGL0M02013g		ChrM_C_glabrata_CBS138	245581	244928	C
CAGL0M02079g		ChrM_C_glabrata_CBS138	253472	251658	C
CAGL0M02299g		ChrM_C_glabrata_CBS138	273725	276406	W
CAGL0M02321g		ChrM_C_glabrata_CBS138	277990	276554	C
CAGL0M02453g		ChrM_C_glabrata_CBS138	287732	288094	W
CAGL0M02541g		ChrM_C_glabrata_CBS138	294479	294348	C
CAGL0M02717g		ChrM_C_glabrata_CBS138	309656	310444	W
CAGL0M02915g		ChrM_C_glabrata_CBS138	329923	329147	C
CAGL0M03069g		ChrM_C_glabrata_CBS138	349230	347584	C
CAGL0M03157g		ChrM_C_glabrata_CBS138	358599	361211	W
CAGL0M03421g		ChrM_C_glabrata_CBS138	391586	390927	C
CAGL0M03773g		ChrM_C_glabrata_CBS138	427099	426518	C
CAGL0M04015g		ChrM_C_glabrata_CBS138	447889	447059	C
CAGL0M04169g		ChrM_C_glabrata_CBS138	459618	460739	W
CAGL0M04345g		ChrM_C_glabrata_CBS138	478693	477731	C
CAGL0M04389g		ChrM_C_glabrata_CBS138	481522	483702	W
CAGL0M04455g		ChrM_C_glabrata_CBS138	491183	489048	C
CAGL0M04543g		ChrM_C_glabrata_CBS138	498691	499533	W
CAGL0M04851g		ChrM_C_glabrata_CBS138	532127	532318	W
CAGL0M04917g		ChrM_C_glabrata_CBS138	537760	539520	W
CAGL0M05115g		ChrM_C_glabrata_CBS138	549946	551247	W
CAGL0M05137g		ChrM_C_glabrata_CBS138	552160	556215	W
CAGL0M05313g		ChrM_C_glabrata_CBS138	568646	567906	C

CAGL0M05401g		ChrM_C_glabrata_CBS138	575952	575740	C
CAGL0M05819g		ChrM_C_glabrata_CBS138	615435	615635	W
CAGL0M06149g		ChrM_C_glabrata_CBS138	642556	640964	C
CAGL0M06325g		ChrM_C_glabrata_CBS138	659269	657290	C
CAGL0M06479g		ChrM_C_glabrata_CBS138	671810	671472	C
CAGL0M06831g	CRZ1	ChrM_C_glabrata_CBS138	695162	697099	W
CAGL0M07007g		ChrM_C_glabrata_CBS138	713125	712268	C
CAGL0M07205g		ChrM_C_glabrata_CBS138	726724	727449	W
CAGL0M07337g		ChrM_C_glabrata_CBS138	743961	743020	C
CAGL0M07491g		ChrM_C_glabrata_CBS138	754350	753496	C
CAGL0M07590g		ChrM_C_glabrata_CBS138	758940	760310	W
CAGL0M07634g		ChrM_C_glabrata_CBS138	763929	764702	W
CAGL0M07744g		ChrM_C_glabrata_CBS138	779985	779281	C
CAGL0M07766g		ChrM_C_glabrata_CBS138	781830	782546	W
CAGL0M07832g		ChrM_C_glabrata_CBS138	784724	783505	C
CAGL0M08096g		ChrM_C_glabrata_CBS138	809185	809559	W
CAGL0M08316g		ChrM_C_glabrata_CBS138	829069	831963	W
CAGL0M08536g		ChrM_C_glabrata_CBS138	853376	852150	C
CAGL0M08558g		ChrM_C_glabrata_CBS138	855342	855046	C
CAGL0M08580g		ChrM_C_glabrata_CBS138	856036	855443	C
CAGL0M08778g		ChrM_C_glabrata_CBS138	873232	873642	W
CAGL0M08800g	YAP6	ChrM_C_glabrata_CBS138	878328	879119	W
CAGL0M09042g		ChrM_C_glabrata_CBS138	901459	902817	W
CAGL0M09691g		ChrM_C_glabrata_CBS138	963159	961939	C
CAGL0M09955g		ChrM_C_glabrata_CBS138	984334	982943	C
CAGL0M10065g		ChrM_C_glabrata_CBS138	1002184	1002933	W
CAGL0M10153g		ChrM_C_glabrata_CBS138	1013291	1010688	C
CAGL0M10395g		ChrM_C_glabrata_CBS138	1038860	1043857	W
CAGL0M10978g		ChrM_C_glabrata_CBS138	1090119	1088278	C
CAGL0M11088g		ChrM_C_glabrata_CBS138	1095910	1095254	C
CAGL0M11858g		ChrM_C_glabrata_CBS138	1178837	1179550	W
CAGL0M12056g		ChrM_C_glabrata_CBS138	1207001	1206666	C
CAGL0M12078g					
CAGL0M12100g		ChrM_C_glabrata_CBS138	1209814	1210788	W
CAGL0M12254g		ChrM_C_glabrata_CBS138	1222321	1224765	W
CAGL0M12342g		ChrM_C_glabrata_CBS138	1235565	1234192	C
CAGL0M12364g		ChrM_C_glabrata_CBS138	1236300	1236064	C
CAGL0M12452g		ChrM_C_glabrata_CBS138	1241018	1241242	W
CAGL0M12474g		ChrM_C_glabrata_CBS138	1242276	1243610	W
CAGL0M12507g					
CAGL0M12793g		ChrM_C_glabrata_CBS138	1262305	1263201	W
CAGL0M12815g		ChrM_C_glabrata_CBS138	1263880	1266834	W
CAGL0M12881g		ChrM_C_glabrata_CBS138	1273254	1274573	W
CAGL0M13035g		ChrM_C_glabrata_CBS138	1286086	1284308	C
CAGL0M13123g		ChrM_C_glabrata_CBS138	1291605	1289611	C
CAGL0M13211g		ChrM_C_glabrata_CBS138	1299931	1300689	W

<i>CAGL0M13233g</i>		ChrM_C_glabrata_CBS138	1304297	1300974	C
<i>CAGL0M13365g</i>		ChrM_C_glabrata_CBS138	1314673	1316544	W
<i>CAGL0M13387g</i>		ChrM_C_glabrata_CBS138	1317526	1316747	C
<i>CAGL0M13607g</i>		ChrM_C_glabrata_CBS138	1338688	1339728	W
<i>CAGL0M13695g</i>		ChrM_C_glabrata_CBS138	1345104	1344157	C
<i>CAGL0M14069g</i>	<i>PWP6</i>	ChrM_C_glabrata_CBS138	1391579	1394179	W
<i>CAGL0M14091g</i>		ChrM_C_glabrata_CBS138	1395548	1396189	W

Table 2: 294 *C. glabrata* ORFs with no *S. cerevisiae* orthologues based on the Yeast Gene

Order Browser (<http://ygob.ucd.ie/>).

ORF name	<i>C. glabrata</i> gene name	Chromosome	Start coordinate	Stop coordinate	Strand
CAGL0A00165g		ChrA_C_glabrata_CBS138	18876	18037	C
CAGL0A00583g		ChrA_C_glabrata_CBS138	65286	67226	W
CAGL0A00649g		ChrA_C_glabrata_CBS138	70937	71320	W
CAGL0A00715g		ChrA_C_glabrata_CBS138	73333	73623	W
CAGL0A00737g		ChrA_C_glabrata_CBS138	74767	76416	W
CAGL0A01221g		ChrA_C_glabrata_CBS138	125780	126661	W
CAGL0A01243g	<i>GIT1</i>	ChrA_C_glabrata_CBS138	129101	127506	C
CAGL0A01284g	<i>EPA10</i>	ChrA_C_glabrata_CBS138	131362	135567	W
CAGL0A01325g	<i>PGD1</i>	ChrA_C_glabrata_CBS138	136262	137695	W
CAGL0A01366g	<i>EPA9</i>	ChrA_C_glabrata_CBS138	140305	144693	W
CAGL0A01870g		ChrA_C_glabrata_CBS138	193719	191335	C
CAGL0A01892g		ChrA_C_glabrata_CBS138	194560	194826	W
CAGL0A02255g		ChrA_C_glabrata_CBS138	244683	245501	W
CAGL0A02299g		ChrA_C_glabrata_CBS138	250851	251690	W
CAGL0A02343g		ChrA_C_glabrata_CBS138	254861	255127	W
CAGL0A02882g		ChrA_C_glabrata_CBS138	302262	302576	W
CAGL0A03410g		ChrA_C_glabrata_CBS138	348708	349451	W
CAGL0A03608g		ChrA_C_glabrata_CBS138	366934	366290	C
CAGL0B00220g		ChrB_C_glabrata_CBS138	10385	10615	W
CAGL0B00440g		ChrB_C_glabrata_CBS138	31504	32313	W
CAGL0B00572g		ChrB_C_glabrata_CBS138	49506	48898	C
CAGL0B01595g		ChrB_C_glabrata_CBS138	146542	148740	W
CAGL0B02882g	<i>BMT2</i>	ChrB_C_glabrata_CBS138	281184	279334	C
CAGL0B02904g	<i>BMT6</i>	ChrB_C_glabrata_CBS138	283910	282093	C
CAGL0B02926g	<i>BMT3</i>	ChrB_C_glabrata_CBS138	286753	284897	C
CAGL0B02948g	<i>BMT4</i>	ChrB_C_glabrata_CBS138	289799	288006	C
CAGL0B02970g	<i>BMT5</i>	ChrB_C_glabrata_CBS138	293137	291248	C
CAGL0B03223g		ChrB_C_glabrata_CBS138	314992	314690	C
CAGL0B03611g		ChrB_C_glabrata_CBS138	360952	360764	C
CAGL0B03883g		ChrB_C_glabrata_CBS138	383602	384522	W
CAGL0B03949g		ChrB_C_glabrata_CBS138	389759	387861	C
CAGL0B04235g	<i>SCP120</i>	ChrB_C_glabrata_CBS138	416601	415660	C
CAGL0C00110g	<i>EPA6</i>	ChrC_C_glabrata_CBS138	4284	2137	C
CAGL0C00209g	<i>AWP7</i>	ChrC_C_glabrata_CBS138	12939	11626	C
CAGL0C00231g		ChrC_C_glabrata_CBS138	15916	17538	W
CAGL0C00253g		ChrC_C_glabrata_CBS138	23710	18884	C
CAGL0C00781g		ChrC_C_glabrata_CBS138	81411	82193	W
CAGL0C00847g	<i>EPA8</i>	ChrC_C_glabrata_CBS138	86130	88502	W
CAGL0C00968g		ChrC_C_glabrata_CBS138	96914	100018	W
CAGL0C01133g		ChrC_C_glabrata_CBS138	114805	117915	W
CAGL0C01617g		ChrC_C_glabrata_CBS138	174618	175334	W

<i>CAGL0C01837g</i>		ChrC_C_glabrata_CBS138	193387	191463	C
<i>CAGL0C01859g</i>		ChrC_C_glabrata_CBS138	196167	193730	C
<i>CAGL0C01919g</i>	<i>MFA2</i>	ChrC_C_glabrata_CBS138	202488	202384	C
<i>CAGL0C02057g</i>		ChrC_C_glabrata_CBS138	213539	213180	C
<i>CAGL0C02365g</i>		ChrC_C_glabrata_CBS138	239122	238940	C
<i>CAGL0C03311g</i>		ChrC_C_glabrata_CBS138	334443	333898	C
<i>CAGL0C03916g</i>		ChrC_C_glabrata_CBS138	385875	383989	C
<i>CAGL0C03938g</i>		ChrC_C_glabrata_CBS138	388586	386673	C
<i>CAGL0C03960g</i>		ChrC_C_glabrata_CBS138	391121	389250	C
<i>CAGL0C03982g</i>		ChrC_C_glabrata_CBS138	393798	391909	C
<i>CAGL0C04004g</i>		ChrC_C_glabrata_CBS138	396512	394614	C
<i>CAGL0C04026g</i>		ChrC_C_glabrata_CBS138	399213	397303	C
<i>CAGL0C04048g</i>		ChrC_C_glabrata_CBS138	401596	399734	C
<i>CAGL0C04763g</i>		ChrC_C_glabrata_CBS138	445881	444934	C
<i>CAGL0C05401g</i>		ChrC_C_glabrata_CBS138	515623	515886	W
<i>CAGL0D00154g</i>	<i>AQY1</i>	ChrD_C_glabrata_CBS138	17914	17042	C
<i>CAGL0D00286g</i>	<i>BMT1</i>	ChrD_C_glabrata_CBS138	37583	39784	W
<i>CAGL0D00374g</i>		ChrD_C_glabrata_CBS138	45775	46086	W
<i>CAGL0D00396g</i>		ChrD_C_glabrata_CBS138	46558	46316	C
<i>CAGL0D01210g</i>		ChrD_C_glabrata_CBS138	137954	138646	W
<i>CAGL0D01254g</i>		ChrD_C_glabrata_CBS138	140355	141038	W
<i>CAGL0D01265g</i>	<i>MT-I</i>	ChrD_C_glabrata_CBS138	142000	142191	W
<i>CAGL0D02486g</i>		ChrD_C_glabrata_CBS138	253763	256399	W
<i>CAGL0D02640g</i>		ChrD_C_glabrata_CBS138	274285	275979	W
<i>CAGL0D02662g</i>		ChrD_C_glabrata_CBS138	279793	278099	C
<i>CAGL0D02750g</i>		ChrD_C_glabrata_CBS138	288647	289021	W
<i>CAGL0D03608g</i>		ChrD_C_glabrata_CBS138	364790	363465	C
<i>CAGL0D03872g</i>		ChrD_C_glabrata_CBS138	387624	388433	W
<i>CAGL0D04840g</i>		ChrD_C_glabrata_CBS138	471574	472164	W
<i>CAGL0D05434g</i>		ChrD_C_glabrata_CBS138	518767	518042	C
<i>CAGL0D05456g</i>		ChrD_C_glabrata_CBS138	521445	522071	W
<i>CAGL0D05654g</i>		ChrD_C_glabrata_CBS138	538337	537378	C
<i>CAGL0D06226g</i>		ChrD_C_glabrata_CBS138	588725	586395	C
<i>CAGL0D06380g</i>		ChrD_C_glabrata_CBS138	601040	602083	W
<i>CAGL0D06534g</i>		ChrD_C_glabrata_CBS138	622492	622178	C
<i>CAGL0D06666g</i>		ChrD_C_glabrata_CBS138	638537	638737	W
<i>CAGL0D06710g</i>		ChrD_C_glabrata_CBS138	643127	641982	C
<i>CAGL0E00187g</i>		ChrE_C_glabrata_CBS138	13227	12511	C
<i>CAGL0E00275g</i>	<i>EPA20</i>	ChrE_C_glabrata_CBS138	25881	28523	W
<i>CAGL0E00363g</i>		ChrE_C_glabrata_CBS138	30527	30336	C
<i>CAGL0E01661g</i>		ChrE_C_glabrata_CBS138	160703	164950	W
<i>CAGL0E01727g</i>	<i>YPS3</i>	ChrE_C_glabrata_CBS138	171119	172738	W
<i>CAGL0E01749g</i>	<i>YPS4</i>	ChrE_C_glabrata_CBS138	174323	172875	C
<i>CAGL0E01771g</i>	<i>YPS5</i>	ChrE_C_glabrata_CBS138	177211	175652	C
<i>CAGL0E01793g</i>	<i>YPS6</i>	ChrE_C_glabrata_CBS138	179961	178411	C
<i>CAGL0E01815g</i>	<i>YPS8</i>	ChrE_C_glabrata_CBS138	182713	181154	C

<i>CAGL0E01837g</i>	<i>YPS9</i>	ChrE_C_glabrata_CBS138	184802	183237	C
<i>CAGL0E01859g</i>	<i>YPS10</i>	ChrE_C_glabrata_CBS138	187387	185870	C
<i>CAGL0E01881g</i>	<i>YPS11</i>	ChrE_C_glabrata_CBS138	188277	189803	W
<i>CAGL0E02211g</i>		ChrE_C_glabrata_CBS138	215568	215768	W
<i>CAGL0E03498g</i>		ChrE_C_glabrata_CBS138	324961	324476	C
<i>CAGL0E04554g</i>		ChrE_C_glabrata_CBS138	439395	440117	W
<i>CAGL0E05192g</i>		ChrE_C_glabrata_CBS138	507868	506831	C
<i>CAGL0E05214g</i>		ChrE_C_glabrata_CBS138	509315	508275	C
<i>CAGL0E05236g</i>		ChrE_C_glabrata_CBS138	510749	509715	C
<i>CAGL0E05280g</i>	<i>GRE2(B)</i>	ChrE_C_glabrata_CBS138	513263	512208	C
<i>CAGL0E06094g</i>		ChrE_C_glabrata_CBS138	603704	603877	W
<i>CAGL0E06402g</i>		ChrE_C_glabrata_CBS138	643478	643768	W
<i>CAGL0E06600g</i>		ChrE_C_glabrata_CBS138	658435	661332	W
<i>CAGL0E06644g</i>	<i>EPA1</i>	ChrE_C_glabrata_CBS138	665110	668214	W
<i>CAGL0E06666g</i>	<i>EPA2</i>	ChrE_C_glabrata_CBS138	674692	670430	C
<i>CAGL0E06688g</i>	<i>EPA3</i>	ChrE_C_glabrata_CBS138	683331	680404	C
<i>CAGL0F00209g</i>		ChrF_C_glabrata_CBS138	23731	22109	C
<i>CAGL0F01815g</i>		ChrF_C_glabrata_CBS138	180414	179470	C
<i>CAGL0F02057g</i>		ChrF_C_glabrata_CBS138	199689	197149	C
<i>CAGL0F03641g</i>		ChrF_C_glabrata_CBS138	356059	354791	C
<i>CAGL0F04543g</i>		ChrF_C_glabrata_CBS138	456591	456866	W
<i>CAGL0F06699g</i>		ChrF_C_glabrata_CBS138	659539	658958	C
<i>CAGL0F07381g</i>		ChrF_C_glabrata_CBS138	720934	719330	C
<i>CAGL0F08767g</i>		ChrF_C_glabrata_CBS138	867394	867789	W
<i>CAGL0F09141g</i>		ChrF_C_glabrata_CBS138	904448	904239	C
<i>CAGL0F09273g</i>		ChrF_C_glabrata_CBS138	925942	926406	W
<i>CAGL0G00836g</i>		ChrG_C_glabrata_CBS138	74216	74605	W
<i>CAGL0G01408g</i>		ChrG_C_glabrata_CBS138	134524	134928	W
<i>CAGL0G02519g</i>		ChrG_C_glabrata_CBS138	229958	228822	C
<i>CAGL0G02563g</i>		ChrG_C_glabrata_CBS138	237393	235498	C
<i>CAGL0G02871g</i>		ChrG_C_glabrata_CBS138	264266	263943	C
<i>CAGL0G03201g</i>		ChrG_C_glabrata_CBS138	299668	299021	C
<i>CAGL0G03685g</i>		ChrG_C_glabrata_CBS138	354696	354923	W
<i>CAGL0G03949g</i>		ChrG_C_glabrata_CBS138	375421	375924	W
<i>CAGL0G03993g</i>		ChrG_C_glabrata_CBS138	379229	378876	C
<i>CAGL0G04279g</i>		ChrG_C_glabrata_CBS138	406126	404144	C
<i>CAGL0G04785g</i>		ChrG_C_glabrata_CBS138	456307	456011	C
<i>CAGL0G04829g</i>		ChrG_C_glabrata_CBS138	459677	462151	W
<i>CAGL0G05522g</i>		ChrG_C_glabrata_CBS138	524170	524448	W
<i>CAGL0G06050g</i>		ChrG_C_glabrata_CBS138	581306	581530	W
<i>CAGL0G06160g</i>		ChrG_C_glabrata_CBS138	587971	588246	W
<i>CAGL0G06446g</i>		ChrG_C_glabrata_CBS138	622068	622394	W
<i>CAGL0G06644g</i>		ChrG_C_glabrata_CBS138	634825	634475	C
<i>CAGL0G06710g</i>		ChrG_C_glabrata_CBS138	643070	642819	C
<i>CAGL0G06996g</i>		ChrG_C_glabrata_CBS138	667930	667115	C
<i>CAGL0G07183g</i>		ChrG_C_glabrata_CBS138	683243	678730	C

CAGL0G07645g		ChrG_C_glabrata_CBS138	725540	725259	C
CAGL0G09086g		ChrG_C_glabrata_CBS138	867382	867894	W
CAGL0G09625g		ChrG_C_glabrata_CBS138	918731	919138	W
CAGL0G09647g		ChrG_C_glabrata_CBS138	919676	919350	C
CAGL0G10175g	<i>AWP6</i>	ChrG_C_glabrata_CBS138	977483	979216	W
CAGL0G10219g		ChrG_C_glabrata_CBS138	988766	991744	W
CAGL0H00110g		ChrH_C_glabrata_CBS138	3711	2611	C
CAGL0H00418g		ChrH_C_glabrata_CBS138	42181	41327	C
CAGL0H01749g		ChrH_C_glabrata_CBS138	168634	168305	C
CAGL0H02277g		ChrH_C_glabrata_CBS138	206023	206397	W
CAGL0H03465g		ChrH_C_glabrata_CBS138	323129	323524	W
CAGL0H04015g		ChrH_C_glabrata_CBS138	378264	377281	C
CAGL0H04059g		ChrH_C_glabrata_CBS138	383690	383247	C
CAGL0H04147g		ChrH_C_glabrata_CBS138	392825	393643	W
CAGL0H04257g	<i>MT-II</i>	ChrH_C_glabrata_CBS138	405073	405231	W
CAGL0H04279g	<i>MT-IIB</i>	ChrH_C_glabrata_CBS138	406327	406485	W
CAGL0H06017g	<i>FLR1</i>	ChrH_C_glabrata_CBS138	590229	588556	C
CAGL0H06039g		ChrH_C_glabrata_CBS138	594295	592526	C
CAGL0H06853g	<i>ADH6</i>	ChrH_C_glabrata_CBS138	681266	680184	C
CAGL0H07337g		ChrH_C_glabrata_CBS138	718141	718590	W
CAGL0H08712g		ChrH_C_glabrata_CBS138	849446	848229	C
CAGL0H08756g		ChrH_C_glabrata_CBS138	853968	853720	C
CAGL0H09240g		ChrH_C_glabrata_CBS138	907598	905670	C
CAGL0H09262g		ChrH_C_glabrata_CBS138	910135	908258	C
CAGL0H09394g		ChrH_C_glabrata_CBS138	921373	920468	C
CAGL0H09482g		ChrH_C_glabrata_CBS138	928788	928384	C
CAGL0H09592g		ChrH_C_glabrata_CBS138	937859	938569	W
CAGL0H10010g		ChrH_C_glabrata_CBS138	977299	976466	C
CAGL0H10626g		ChrH_C_glabrata_CBS138	1043943	1047923	W
CAGL0I00220g	<i>EPA23</i>	ChrI_C_glabrata_CBS138	14903	12309	C
CAGL0I00242g		ChrI_C_glabrata_CBS138	18146	17649	C
CAGL0I00286g		ChrI_C_glabrata_CBS138	22188	20521	C
CAGL0I00396g		ChrI_C_glabrata_CBS138	29592	29245	C
CAGL0I02024g	<i>OYE2</i>	ChrI_C_glabrata_CBS138	173433	172231	C
CAGL0I02046g		ChrI_C_glabrata_CBS138	176085	175036	C
CAGL0I02244g		ChrI_C_glabrata_CBS138	195726	195217	C
CAGL0I02596g		ChrI_C_glabrata_CBS138	235250	234648	C
CAGL0I05874g		ChrI_C_glabrata_CBS138	558845	558102	C
CAGL0I07293g		ChrI_C_glabrata_CBS138	708640	703325	C
CAGL0I08151g		ChrI_C_glabrata_CBS138	793917	795065	W
CAGL0I08437g		ChrI_C_glabrata_CBS138	825046	829038	W
CAGL0I08613g	<i>DUR3</i>	ChrI_C_glabrata_CBS138	841861	840182	C
CAGL0I09108g		ChrI_C_glabrata_CBS138	884075	882180	C
CAGL0I09724g		ChrI_C_glabrata_CBS138	929606	928113	C
CAGL0I10147g	<i>PWP1</i>	ChrI_C_glabrata_CBS138	983741	970731	C
CAGL0I10200g	<i>PWP3</i>	ChrI_C_glabrata_CBS138	992434	996555	W

CAGL0I10246g	PWP2	ChrI_C_glabrata_CBS138	1002627	1006349	W
CAGL0I10340g	PWP5	ChrI_C_glabrata_CBS138	1013299	1016337	W
CAGL0I10362g	PWP4	ChrI_C_glabrata_CBS138	1020373	1025691	W
CAGL0J00451g		ChrJ_C_glabrata_CBS138	37169	36171	C
CAGL0J01727g		ChrJ_C_glabrata_CBS138	160781	157842	C
CAGL0J01774g		ChrJ_C_glabrata_CBS138	172073	164808	C
CAGL0J01800g		ChrJ_C_glabrata_CBS138	177152	173901	C
CAGL0J02024g		ChrJ_C_glabrata_CBS138	204836	203412	C
CAGL0J02046g		ChrJ_C_glabrata_CBS138	205632	205871	W
CAGL0J02508g	AWP1	ChrJ_C_glabrata_CBS138	248822	246210	C
CAGL0J02530g		ChrJ_C_glabrata_CBS138	252893	250629	C
CAGL0J02552g		ChrJ_C_glabrata_CBS138	257549	254862	C
CAGL0J03982g		ChrJ_C_glabrata_CBS138	377534	377881	W
CAGL0J04554g		ChrJ_C_glabrata_CBS138	434978	433719	C
CAGL0J04972g		ChrJ_C_glabrata_CBS138	475587	476606	W
CAGL0J05159g		ChrJ_C_glabrata_CBS138	494336	489747	C
CAGL0J05390g		ChrJ_C_glabrata_CBS138	517202	516870	C
CAGL0J05786g		ChrJ_C_glabrata_CBS138	553406	551562	C
CAGL0J05852g		ChrJ_C_glabrata_CBS138	557558	556527	C
CAGL0J10714g		ChrJ_C_glabrata_CBS138	1046800	1047771	W
CAGL0J11000g		ChrJ_C_glabrata_CBS138	1073752	1074513	W
CAGL0J11088g		ChrJ_C_glabrata_CBS138	1081270	1081962	W
CAGL0J11374g		ChrJ_C_glabrata_CBS138	1106466	1106215	C
CAGL0J11616g		ChrJ_C_glabrata_CBS138	1130080	1130436	W
CAGL0J11891g	AWP3	ChrJ_C_glabrata_CBS138	1165100	1161474	C
CAGL0K00110g	AWP2	ChrK_C_glabrata_CBS138	5830	3332	C
CAGL0K00170g	EPA22	ChrK_C_glabrata_CBS138	14140	18411	W
CAGL0K00341g		ChrK_C_glabrata_CBS138	37953	37531	C
CAGL0K02013g		ChrK_C_glabrata_CBS138	176257	177375	W
CAGL0K02519g		ChrK_C_glabrata_CBS138	228185	227541	C
CAGL0K03245g		ChrK_C_glabrata_CBS138	299646	298216	C
CAGL0K04609g		ChrK_C_glabrata_CBS138	440457	438628	C
CAGL0K04675g		ChrK_C_glabrata_CBS138	455284	455718	W
CAGL0K05665g		ChrK_C_glabrata_CBS138	553943	552804	C
CAGL0K05687g		ChrK_C_glabrata_CBS138	555370	556536	W
CAGL0K07183g		ChrK_C_glabrata_CBS138	705897	706220	W
CAGL0K07337g		ChrK_C_glabrata_CBS138	724973	725914	W
CAGL0K07502g		ChrK_C_glabrata_CBS138	742349	742990	W
CAGL0K07546g	PMU2	ChrK_C_glabrata_CBS138	745201	746172	W
CAGL0K07568g	PMU3	ChrK_C_glabrata_CBS138	747658	748629	W
CAGL0K07678g		ChrK_C_glabrata_CBS138	764843	764196	C
CAGL0K08338g		ChrK_C_glabrata_CBS138	841389	840409	C
CAGL0K08470g		ChrK_C_glabrata_CBS138	852119	851940	C
CAGL0K10890g		ChrK_C_glabrata_CBS138	1063220	1064422	W
CAGL0K11484g		ChrK_C_glabrata_CBS138	1114883	1115206	W
CAGL0K11946g		ChrK_C_glabrata_CBS138	1153568	1153891	W

<i>CAGL0K12364g</i>		ChrK_C_glabrata_CBS138	1206621	1207109	W
<i>CAGL0K12980g</i>	<i>BMT7</i>	ChrK_C_glabrata_CBS138	1286134	1283966	C
<i>CAGL0K13002g</i>	<i>AED2</i>	ChrK_C_glabrata_CBS138	1291683	1294496	W
<i>CAGL0L00157g</i>		ChrL_C_glabrata_CBS138	5931	736	C
<i>CAGL0L00227g</i>		ChrL_C_glabrata_CBS138	27536	17811	C
<i>CAGL0L01023g</i>		ChrL_C_glabrata_CBS138	119978	119691	C
<i>CAGL0L01045g</i>		ChrL_C_glabrata_CBS138	120342	120109	C
<i>CAGL0L01831g</i>		ChrL_C_glabrata_CBS138	212208	212366	W
<i>CAGL0L03388g</i>		ChrL_C_glabrata_CBS138	388777	389391	W
<i>CAGL0L03894g</i>		ChrL_C_glabrata_CBS138	448634	448143	C
<i>CAGL0L04832g</i>		ChrL_C_glabrata_CBS138	554478	554284	C
<i>CAGL0L04836g</i>		ChrL_C_glabrata_CBS138	554702	554508	C
<i>CAGL0L05192g</i>		ChrL_C_glabrata_CBS138	585066	585383	W
<i>CAGL0L05324g</i>		ChrL_C_glabrata_CBS138	592217	591903	C
<i>CAGL0L05984g</i>		ChrL_C_glabrata_CBS138	669527	669150	C
<i>CAGL0L06688g</i>		ChrL_C_glabrata_CBS138	758073	756016	C
<i>CAGL0L07194g</i>		ChrL_C_glabrata_CBS138	800960	801430	W
<i>CAGL0L07568g</i>		ChrL_C_glabrata_CBS138	837713	837393	C
<i>CAGL0L07590g</i>		ChrL_C_glabrata_CBS138	838499	838293	C
<i>CAGL0L08470g</i>		ChrL_C_glabrata_CBS138	930917	930435	C
<i>CAGL0L08536g</i>		ChrL_C_glabrata_CBS138	934441	934662	W
<i>CAGL0L09361g</i>		ChrL_C_glabrata_CBS138	1018071	1018406	W
<i>CAGL0L09537g</i>		ChrL_C_glabrata_CBS138	1029031	1030233	W
<i>CAGL0L10092g</i>		ChrL_C_glabrata_CBS138	1084445	1088695	W
<i>CAGL0L12496g</i>		ChrL_C_glabrata_CBS138	1349053	1348769	C
<i>CAGL0L12518g</i>		ChrL_C_glabrata_CBS138	1349621	1349271	C
<i>CAGL0L13266g</i>		ChrL_C_glabrata_CBS138	1418408	1420147	W
<i>CAGL0L13299g</i>	<i>EPA11</i>	ChrL_C_glabrata_CBS138	1426694	1431586	W
<i>CAGL0L13332g</i>	<i>EPA13</i>	ChrL_C_glabrata_CBS138	1436026	1439133	W
<i>CAGL0L13354g</i>	<i>TNR1</i>	ChrL_C_glabrata_CBS138	1441319	1439574	C
<i>CAGL0L13365r</i>	<i>RDN25-1</i>	ChrL_C_glabrata_CBS138	1448197	1444790	C
<i>CAGL0L13387r</i>	<i>RDN58-1</i>	ChrL_C_glabrata_CBS138	1448584	1448427	C
<i>CAGL0L13398r</i>	<i>RDN18-1</i>	ChrL_C_glabrata_CBS138	1450786	1448987	C
<i>CAGL0L13409r</i>	<i>RDN5-1</i>	ChrL_C_glabrata_CBS138	1452956	1453076	W
<i>CAGL0M00154g</i>	<i>CYN1</i>	ChrM_C_glabrata_CBS138	22039	23691	W
<i>CAGL0M00308g</i>		ChrM_C_glabrata_CBS138	39072	38758	C
<i>CAGL0M00704g</i>		ChrM_C_glabrata_CBS138	81930	82796	W
<i>CAGL0M00792g</i>		ChrM_C_glabrata_CBS138	91057	90755	C
<i>CAGL0M01760g</i>	<i>CDR1</i>	ChrM_C_glabrata_CBS138	203616	208115	W
<i>CAGL0M01870g</i>		ChrM_C_glabrata_CBS138	220760	219813	C
<i>CAGL0M01914g</i>		ChrM_C_glabrata_CBS138	232780	234810	W
<i>CAGL0M02321g</i>		ChrM_C_glabrata_CBS138	277990	276554	C
<i>CAGL0M02541g</i>		ChrM_C_glabrata_CBS138	294479	294348	C
<i>CAGL0M03421g</i>		ChrM_C_glabrata_CBS138	391586	390927	C
<i>CAGL0M04543g</i>		ChrM_C_glabrata_CBS138	498691	499533	W
<i>CAGL0M04851g</i>		ChrM_C_glabrata_CBS138	532127	532318	W

<i>CAGL0M05115g</i>		ChrM_C_glabrata_CBS138	549946	551247	W
<i>CAGL0M05137g</i>		ChrM_C_glabrata_CBS138	552160	556215	W
<i>CAGL0M05819g</i>		ChrM_C_glabrata_CBS138	615435	615635	W
<i>CAGL0M07744g</i>		ChrM_C_glabrata_CBS138	779985	779281	C
<i>CAGL0M07766g</i>		ChrM_C_glabrata_CBS138	781830	782546	W
<i>CAGL0M08096g</i>		ChrM_C_glabrata_CBS138	809185	809559	W
<i>CAGL0M08558g</i>		ChrM_C_glabrata_CBS138	855342	855046	C
<i>CAGL0M10065g</i>		ChrM_C_glabrata_CBS138	1002184	1002933	W
<i>CAGL0M10263g</i>		ChrM_C_glabrata_CBS138	1027902	1027450	C
<i>CAGL0M10395g</i>		ChrM_C_glabrata_CBS138	1038860	1043857	W
<i>CAGL0M10978g</i>		ChrM_C_glabrata_CBS138	1090119	1088278	C
<i>CAGL0M11088g</i>		ChrM_C_glabrata_CBS138	1095910	1095254	C
<i>CAGL0M11660g</i>		ChrM_C_glabrata_CBS138	1160862	1160116	C
<i>CAGL0M12056g</i>		ChrM_C_glabrata_CBS138	1207001	1206666	C
<i>CAGL0M12364g</i>		ChrM_C_glabrata_CBS138	1236300	1236064	C
<i>CAGL0M12452g</i>		ChrM_C_glabrata_CBS138	1241018	1241242	W
<i>CAGL0M12881g</i>		ChrM_C_glabrata_CBS138	1273254	1274573	W
<i>CAGL0M12947g</i>	<i>PUP1</i>	ChrM_C_glabrata_CBS138	1277761	1278396	W
<i>CAGL0M13123g</i>		ChrM_C_glabrata_CBS138	1291605	1289611	C
<i>CAGL0M14069g</i>	<i>PWP6</i>	ChrM_C_glabrata_CBS138	1391579	1394179	W
<i>CAGL0M14091g</i>		ChrM_C_glabrata_CBS138	1395548	1396189	W
<i>CAGL0M14113g</i>	<i>TNR2</i>	ChrM_C_glabrata_CBS138	1399152	1397407	C

Appendix 4: Functional information for targeted *C. glabrata* gene deletions

Table 1: Deleted and verified *C. glabrata* ORFs. Coordinates of the deletion cassette are given as chromosomal location followed by position relative to the start of the coding sequence. Predicted domains encoded by each ORF (ebi.ac.uk/interpro/) and their associated GO terms are also listed.

<i>C. glabrata</i> ORF	<i>S. cerevisiae</i> orthologue (YGOB)	Coordinates of deletion construct	Interpro domains	Interpro: GO Biological Process	Interpro: GO Molecular Function	Interpro: GO Cellular Compartment
CAGLOA02299g	None	250844 to 251762 (-7 to +912)	None	None	None	None
CAGLOA02343g	None	254831 to 255132 (-30 to +272)	None	None	None	None
CAGLOA04565g	SWI4	445874 to 449018 (-9 to +3136)	APSES-type DNA-binding domain; Ankyrin repeat-containing domain	GO:0006355 regulation of transcription, DNA-dependent	GO:0003677 DNA binding GO:0003700 sequence-specific DNA binding transcription factor activity	None
CAGLOB00726g	GLK1	63877 to 65154 (-26 to +1252)	Hexokinase	GO:0005975 carbohydrate metabolic process	GO:0005524 ATP binding GO:0016773 phosphotransferase activity, alcohol group as acceptor	None
CAGLOB02926g	None	284892 to 286823	None	None	None	None

		(-6 to +1927)				
<i>CAGLOB02946g</i>	None	252227 to 254950 (-33 to 2692)	None	None	None	None
<i>CAGLOB02948g</i>	None	287995 to 289873 (-11 to +1868)	None	None	None	None
<i>CAGLOB02970g</i>	None	291235 to 293148 (-14 to +1902)	None	None	None	None
<i>CAGLOB03223g</i>	None	314580 to 315021 (-110 to +332)	None	None	None	None
<i>CAGLOB03883g</i>	None	383602 to 384523 (+1 to +922)	Mitochondrial carrier domain	None	None	None
<i>CAGLOC00253g</i>	None	18868 to 23731 (-16 to +4848)	None	None	None	None
<i>CAGLOC01837g</i>	None	191460 to 193408 (-3 to +1945)	None	None	None	GO:0016021 integral to membrane
<i>CAGLOC04763g</i>	None	444889 to 445883 (-35 to +950)	None	None	None	GO:0016021 integral to membrane
<i>CAGL0D00682g</i>	<i>SFP1</i>	89099 to 90871 (-95 to +1677)	Zinc finger C2H2- type/integrase DNA binding domain; zinc finger, C2H2	None	GO:0003676 nucleic acid binding; GO:0046872 metal ion binding	None
<i>CAGL0D01210g</i>	None	137908 to 138661 (-46 to +708)	Aspartate racemase	GO:0006520 cellular amino acid metabolic process GO:0006807 nitrogen compound metabolic process GO:0008152 metabolic process	GO:0016855 racemas e and epimerase activity, acting on amino acids and derivatives GO:0036361 racemase activity, acting on amino acids and derivatives	None
<i>CAGL0D03850g</i>	<i>RSC30</i>	384666 to 387223 (-23 to +2535)	Zn(2)-C6 fungal- type DNA-binding domain	GO:0006355 regulatio n of transcription, DNA-dependent	GO:0000981 sequenc e-specific DNA binding RNA polymerase II transcription factor activity GO:0008270 zinc ion	GO:0005634 nucleus

					binding	
<i>CAGL0D03872g</i>	None	387620 to 388433 (-3 to +810)	None	None	None	None
<i>CAGL0D05170g</i>	<i>PHO4</i>	493835 to 495498 (-44 to +1602)	Myc-type, basic helix-loop-helix domain	None	GO:0046983 protein dimerization activity	None
<i>CAGL0D05434g</i>	None	518011 to 518813 (-31 to +772)	Repressor Rox1, High mobility group box domain	GO:0043618 regulatio n of transcription from RNA polymerase II promoter in response to stress	GO:0043565 sequenc e-specific DNA binding	GO:0000790 nuclear chromatin
<i>CAGL0D06226g</i>	None	586360 to 588754 (-35 to +2342)	None	None	None	None
<i>CAGL0E00275g</i>	None	25857 to 28568 (-5 to +2688)	PA14; GLEYA adhesin domain	None	None	None
<i>CAGL0E06600g</i>	None	658325 to 661393 (-110 to 2959)	Hyphally-regulated cell wall protein; Flocculin	GO:0000128 flocculati on	None	None
<i>CAGL0E06644g</i>	None	665109 to 668298 (-1 to +3171)	PA14; GLEYA adhesin domain	None	None	None
<i>CAGL0F01815g</i>	None	179369 to 180475 (-101 to +988)	RmlC-like cupin domain; Pirin	None	None	None
<i>CAGL0F03905g</i>	<i>SKY1</i>	377984 to 380088 (+22 to +2109)	Protein kinase domain	GO:0006468 protein phosphorylation	GO:0004672 protein kinase activity GO:0004674 protein serine/threonine kinase activity GO:0005524 ATP binding; GO:0016772 transferase activity, transferring phosphorus-containing groups	None
<i>CAGL0F04081g</i>	<i>TEC1</i>	406040 to 408033 (-110 to +1883)	TEA/ATTS	GO:0006355 regulatio n of transcription, DNA-dependent	GO:0003700 sequenc e-specific DNA binding transcription factor	GO:0005634 nucleus

					activity	
<i>CAGL0F05159g</i>	<i>VPS72</i>	525178 to 527640 (-51 to +2411)	YL1 Nuclear	GO:0006355 regulation of transcription, DNA-dependent	None	None
<i>CAGL0F05973g</i>	<i>MIH1</i>	595747 to 597393 (-5 to +1642)	M-phase inducer phosphatase; Rhodanese-like domain	GO:0000087 M phase of mitotic cell cycle GO:0006470 protein dephosphorylation	GO:0004725 protein tyrosine phosphatase activity	GO:0005622 intracellular
<i>CAGL0F06237g</i>	<i>MCM1</i>	618975 to 619693 (-1 to +718)	Transcription factor; MADS-box	None	GO:0003677 DNA binding GO:0046983 protein dimerization activity	KO
<i>CAGL0F08767g</i>	None	867393 to 867813 (-1 to +420)	None	None	None	None
<i>CAGL0F09229g</i>	<i>YER184c</i>	908185 to 910715 (-1 to 2530)	Zn(2)-C6 fungal-type DNA binding domain; Transcription factor domain, fungi	GO:0006351 transcription, DNA-dependent GO:0006355 regulation of transcription, DNA-dependent	GO:0000981 sequence-specific DNA binding RNA polymerase II transcription factor activity GO:0003677 DNA binding GO:0008270 zinc ion binding	GO:0005634 nucleus
<i>CAGL0G02607g</i>	<i>ARK1</i>	240259 to 242297 (+16 to 2054)	Protein kinase-like domain; Serine/threonine-protein kinase, active site	GO:0006468 protein phosphorylation	GO:0004672 protein kinase activity GO:0004674 protein serine/threonine kinase activity GO:0005524 ATP binding GO:0016772 transferase activity, transferring phosphorus-containing groups	None

<i>CAGL0G03201g</i>	None	299019 to 299680 (-2 to +660)	FMN-binding split barrel; Flavin-reductase-like, FMN-binding	GO:0055114 oxidation-reduction process	GO:0010181 FMN binding GO:0016491 oxidoreductase activity GO:0042602 riboflavin reductase (NADPH) activity	KO
<i>CAGL0G04279g</i>	None	404052 to 406165 (-74 to +2022)	Alpha mannosyltransferase	GO:0006486 protein glycosylation	None	None
<i>CAGL0G05522g</i>	None	524159 to 524473 (-11 to 304)	None	None	None	None
<i>CAGL0G08866g</i>	<i>FKH1</i>	850934 to 852770 (+12 to 1848)	SMAO/FHA domain; Winged helix-turn-helix DNA-binding domain	GO:0006355 regulation of transcription, DNA-dependent	GO:0003700 sequence-specific DNA binding transcription factor activity GO:0005515 protein binding GO:0043565 sequence-specific DNA binding	None
<i>CAGL0G10175g</i>	None	977401 to 979260 (-82 to +1778)	None	None	None	None
<i>CAGL0H01749g</i>	None	168264 to 168654 (-43 to +333)	None	None	None	None
<i>CAGL0H06765g</i>	<i>BNR1</i>	672619 to 676510 (-1 to +3892)	Formin, GTP-ase-binding and FH3 domain; Formin, FH2 domain; Formin, diaphanous autoregulatory (DAD) domain	GO:0007015 actin filament organization ; actin cytoskeleton organization GO:0045010 actin nucleation	GO:0003779 actin binding GO:0005488 binding GO:0017048 Rho GTPase binding	GO:0005884 actin filament
<i>CAGL0H08712g</i>	None	848226 to 849480 (-3 to +1253)	Src homology-3 domain; Phox homology domain	GO:0007154 cell communication	GO:0005515 protein binding GO:0035091 phosphatidylinositol	None

					binding	
<i>CAGL0H09988g</i>	<i>REB1</i>	973838 to 975840 (-12 to 1990)	Homeodomain-like; SANT/Myb domain	None	GO:0003677 DNA binding GO:0003682 chromatin binding	None
<i>CAGL0H10208g</i>	<i>AKL1</i>	996857 to 999925 (+5 to +3073)	Protein kinase domain; Serine/threonine- protein kinase, active site	GO:0006468 protein phosphorylation	GO:0004672 protein kinase activity GO:0004674 protein serine/threonine kinase activity GO:0005524 ATP binding GO:0016772 transferase activity, transferring phosphorus-containing groups	None
<i>CAGL0I02244g</i>	None	195216 to 195798 (-1 to +582)	no hit	None	None	None
<i>CAGL0I08437g</i>	None	825005 to 829037 (-41 to +3992)	no hit	None	None	None
<i>CAGL0I08613g</i>	None	839182 to 842886 (+1 to +1705)	Sodium/solute symporter	GO:0006810 transport GO:0055085 transmembrane transport	GO:0005215 transport er activity	GO:0016020 membra ne
<i>CAGL0J05786g</i>	None	550495 to 554463 (-67 to +1902)	Zinc finger, B-box	None	GO:0008270 zinc ion binding	GO:0005622 intracell ular
<i>CAGL0J05852g</i>	None	556482 to 557601 (-45 to +1075)	NAD(P)-binding domain	GO:0008152 metaboli c process	GO:0016491 oxidored uctase activity	None
<i>CAGL0K02145g</i>	<i>YER130C</i>	189978 to 191009 (-28 to +955)	Zinc finger C2H2- type/integrase DNA-binding domain	None	GO:0003676 nucleic acid binding GO:0046872 metal ion binding	None
<i>CAGL0K05687g</i>	None	554478 to 555693 (-63 to +1153)	Aldolase-type TIM barrel; NADH:flavin oxidoreductase/NA	None	GO:0004842 ubiquitin- protein ligase activity GO:0008270 zinc ion	None

			DH oxidase, N-terminal		binding	
<i>CAGL0K07634g</i>	<i>GAT1</i>	753820 to 755228 (-25 to +1384)	Zinc finger, GATA-type	GO:0006355 regulation of transcription, DNA-dependent	GO:0003700 sequence-specific DNA binding transcription factor activity GO:0008270 zinc ion binding GO:0043565 sequence-specific DNA binding	None
<i>CAGL0K10318g</i>	<i>RGA1</i>	1003916 to 1006756 (-8 to +2833)	Zinc finger, LIM-type; Rho GTPase activation protein domain	GO:0007165 signal transduction	GO:0008270 zinc ion binding	GO:0005622 intracellular
<i>CAGL0K11066g</i>	None	1078268 to 1078921 (-32 to +605)	Trimeric LpxA-like; Hexapeptide transferase, conserved site	None	GO:0016740 transferase activity	None
<i>CAGL0L03674g</i>	<i>GSM1</i>	420554 to 422473 (-20 to +1901)	Zn(2)-C6 fungal-type DNA-binding domain; PAS domain	GO:0006355 regulation of transcription, DNA-dependent GO:0007165 signal transduction	GO:0000981 sequence-specific DNA binding RNA polymerase II transcription factor activity GO:0004871 signal transducer activity GO:0004871 signal transducer activity	GO:0005634 nucleus
<i>CAGL0L06776g</i>	<i>GAT2</i>	761565 to 764069 (-18 to +2487)	Zinc finger, GATA-type	GO:0006355 regulation of transcription, DNA-dependent	GO:0003700 sequence-specific DNA binding transcription factor activity GO:0008270 zinc ion binding GO:0043565 sequence-specific	None

					DNA binding	
<i>CAGL0L07480g</i>	<i>NRG2</i>	822201 to 823243 (-39 to +1004)	Zinc finger, C2H2	None	GO:0003676 nucleic acid binding GO:0046872 metal ion binding	None
<i>CAGL0L09383g</i>	<i>SUT2</i>	1018870 - 1019987 (+12 to +1129)	Zn(2)-C6 fungal- type DNA-binding domain	None	None	None
<i>CAGL0M01716g</i>	<i>TEC1</i>	192371 to 193706 (+1 to +1318)	TEA/ATTS	GO:0006355 regulatio n of transcription, DNA-dependent	GO:0003700 sequenc e-specific DNA binding transcription factor activity	None
<i>CAGL0M01870g</i>	None	219810 to 220787 (-3 to +975)	Zinc finger, C2H2	None	GO:0003676 nucleic acid binding GO:0046872 metal ion binding	None
<i>CAGL0M01914g</i>	None	232780 to 234877 (+1 to +2098)	Tetratricopeptide- like helical	None	GO:0005515 protein binding	None
<i>CAGL0M02299g</i>	<i>YPL150W</i>	273683 to 276535 (-42 to +2811)	Protein kinase domain; Serine/threonine- /dual specificity protein kinase, catalytic domain	GO:0006468 protein phosphorylation	GO:0004672 protein kinase activity GO:0004674 protein serine/threonine kinase activity GO:0005524 ATP binding GO:0016772 transferase activity, transferring phosphorus-containing groups	None
<i>CAGL0M02321g</i>	None	276552 to 277991 (-2 to +1438)	None	None	None	None
<i>CAGL0M05137g</i>	None	552098 to 556242 (-62 to +4083)	Regulator of chromosome condensation1/beta-lactamase-inhibitor	None	GO:0005515 protein binding	GO:0005634 nucleus

			protein II; BTB/POZ fold			
<i>CAGL0M10153g</i>	<i>STE20</i>	1010630 to 1013383 (-58 to +2696)	PAK-box/P21-Rho-binding; Serine/threonine-/dual specificity protein kinase, catalytic domain	GO:0006468 protein phosphorylation	GO:0004672 protein kinase activity GO:0004674 protein serine/threonine kinase activity GO:0005515 protein binding GO:0005524 ATP binding GO:0016772 transferase activity, transferring phosphorus-containing groups	None
<i>CAGL0M10978g</i>	None	1098987 to 10990393 (-13 to +1842)	no hit	None	None	None

Table 2: *C. glabrata* ORFs for which fusion constructs were generated but were not successfully transformed or verified into *C. glabrata*. Coordinates of the deletion cassette are given as chromosomal location followed by position relative to the start of the coding sequence. Predicted domains encoded by each ORF (ebi.ac.uk/interpro/) and their associated GO terms are also listed.

<i>C. glabrata</i> ORF	<i>S. cerevisiae</i> orthologue (YGOB)	Coordinates of deletion construct	Interpro domains	Interpro: GO biological process	Interpro: GO Molecular Function	Interpro: GO Cellular Compartment
<i>CAGL0A01870g</i>	None	191328 to 193764 (-7 to +2630)	Sialidases; Collagen triple helix repeat	None	None	GO:0016021 integral to membrane
<i>CAGL0A01892g</i>	None	194514 to 194873 (-46 to +314)	no hits	None	None	None
<i>CAGL0A02255g</i>	None	244674 to 245446 (-9 to +781)	no hits	None	None	None
<i>CAGL0A03608g</i>	None	366262 to 366991 (-28 to +702)	no hits	None	None	None
<i>CAGL0A04257g</i>	<i>TOD6</i>	417613 to 419632 (-31 to +1970)	Myb domain; homeodomain-like	None	GO:0003677 DNA binding GO:0003682 chromatin binding	None
<i>CAGL0B01287g</i>	<i>BUD5</i>	114798 to 118596 (-33 to +3765)	Ras guanine nucleotide exchange factor; Src homology-3 domain	GO:0007264 small GTPase mediated signal transduction GO:0051056 regulation of small GTPase mediated signal transduction	GO:0005085 guanyl-nucleotide exchange factor activity GO:0005515 protein binding	GO:0005622 intracellular
<i>CAGL0B02882g</i>	None	279334 to 281185 (+1 to +1852)	no hits	None	None	None
<i>CAGL0C00110g</i>	None	2132 to 4352 (-6 to +2198)	PA14; GLEYA adhesin domain	None	None	None
<i>CAGL0C00847g</i>	None	86017 to 88562 (-113 to +2433)	PA14; GLEYA adhesin domain	None	None	None
<i>CAGL0C02277g</i>	<i>GLN3</i>	230471 to 232986 (-26 to +2491)	Zinc finger; GATA-type	GO:0006355 regulation of transcription, DNA-dependent	GO:0003700 sequence-specific DNA binding transcription factor activity GO:0008270 zinc ion	None

					binding GO:0043565 sequence-specific DNA binding	
<i>CAGL0D02750g</i>	None	288623 to 289032 (-24 to +386)	no hits	None	None	None
<i>CAGL0D06380g</i>	None	601021 to 602088 (+1 to +1149)	no hits	None	None	None
<i>CAGL0F02057g</i>	None	197109 to 199697 (-41 to +2549)	Homeodomain-like	None	GO:0003677 DNA binding	None
<i>CAGL0F03069g</i>	<i>CAD1</i>	301624 to 303133 (-28 to +1484)	Basic-leucine zipper domain	GO:0006355 regulation of transcription, DNA-dependent;	GO:0003700 sequence-specific DNA binding transcription factor activity GO:0043565 sequence-specific DNA binding	None
<i>CAGL0F08195g</i>	<i>MGA1</i>	813027 to 814110 (-2 to +1061)	Heat shock factor (HSF)-type, DNA binding	GO:0006355 regulation of transcription, DNA-dependent	GO:0003700 sequence-specific DNA binding transcription factor activity GO:0043565 sequence-specific DNA binding	GO:0005634 nucleus
<i>CAGL0G03421g</i>	<i>FLO8</i>	327810 to 330923 (-23 to +3091)	Sequence-specific single-strand DNA-binding; LisH dimerisation motif	None	GO:0003697 single-stranded DNA binding GO:0005515 protein binding	None
<i>CAGL0G04389g</i>	<i>GZF3</i>	413333 to 414803 (-43 to +1431)	Zinc finger, GATA-type	GO:0006355 regulation of transcription, DNA-dependent	GO:0003700 sequence-specific DNA binding transcription factor activity GO:0008270 zinc ion binding GO:0043565 sequence-specific DNA binding	None
<i>CAGL0H04037g</i>	<i>GAC1</i>	379158 to 381918 (-12 to +2750)	Putative phosphatase regulatory subunit	None	GO:0005515 protein binding	None
<i>CAGL0H09592g</i>	None	937855 to 938662 (-4 to +804)	Yeast PIR protein repeat	GO:0006950 response to stress	GO:0005199 structural constituent of cell wall	GO:0005618 cell wall
<i>CAGL0I08151g</i>	None	793860 to 795117 (-57 to +1201)	RmlC-like cupin domain; Pirin	None	None	None

<i>CAGL0I10362g</i>	None	1020342 to 1025748 (-13 to +5376)	PA14	None	None	None
<i>CAGL0J01177g</i>	<i>ABF1</i>	111179 to 112625 (-6 to +1441)	no hits	GO:0006338 chromatin remodeling	GO:0003677 DNA binding	GO:0005634 nucleus
<i>CAGL0J02530g</i>	None	250910 to 252989 (-18 to +2362)	no hits	None	None	None
<i>CAGL0J04972g</i>	None	475550 to 476623 (-37 to +1037)	Protein kinase domain; serine/threonine-protein kinase, active site	GO:0006468 protein phosphorylation;	GO:0004672 protein kinase activity GO:0004674 protein serine/threonine kinase activity GO:0005524 ATP binding GO:0016772 transferase activity, transferring phosphorus-containing groups	None
<i>CAGL0K02013g</i>	None	175201 to 178434 (-56 to +1178)	Zinc finger, N-recognin	None	GO:0004842 ubiquitin-protein ligase activity GO:0008270 zinc ion binding	None
<i>CAGL0K02585g</i>	<i>YAP3</i>	233130 to 234278 (-12 to +1136)	Basic-leucine zipper domain	GO:0006355 regulation of transcription, DNA-dependent	GO:0003700 sequence-specific DNA binding transcription factor activity GO:0043565 sequence-specific DNA binding	None
<i>CAGL0K08294g</i>	<i>DYN1</i>	824611 to 836743 (-13 to +12125)	Dynein heavy chain, domain-1; Dynein heavy chain-domain-2; AAA+ ATPase domain; Dynein heavy chain, P-loop containing D4 domain; Dynein heavy chain, coiled coil stalk	GO:0007018 microtubule-based movement ;	GO:0000166 nucleotide binding GO:0003777 microtubule motor activity GO:0005524 ATP binding; GO:0016887 ATPase activity GO:0016887 ATPase activity	None
<i>CAGL0L03916g</i>	<i>AZF1</i>	448927 to 450883 (-28 to +1929)	Zing finger C2H2-type/integrase DNA-	None	GO:0003676 nucleic acid binding	None

			binding domain		GO:0046872 metal ion binding	
<i>CAGL0L05686g</i>	None			no hits	None	None
<i>CAGL0L06072g</i>	<i>YER130C</i>	679893 to 680866 (-31 to +943)	Zing finger, C2H2	None	GO:0003676 nucleic acid binding GO:0046872 metal ion binding	None
<i>CAGL0M00770g</i>	<i>SIR3</i>	86279 to 89665 (-11 to +3376)	Bromo adjacent homology (BAH) domain	None	GO:0003677 DNA binding	None
<i>CAGL0M04543g</i>	None	498649 to 499607 (-42 to +917)	no hits	None	None	None
<i>CAGL0M10065g</i>	None	1002100 to 1002963 (-83 to +780)	Galactose-binding domain-like; PITH domain	None	None	None
<i>CAGL0M12881g</i>	None	1273191 to 1274626 (-63 to +1373)	dihydroorotate dehydrogenase, class 1/2; aldolase-type TIM barrel	GO:0006207 'de novo' pyrimidine nucleobase biosynthetic process GO:0006222 UMP biosynthetic process GO:0055114 oxidation-reduction process	GO:0003824 catalytic activity GO:0004152 dihydroorotate dehydrogenase activity GO:0004158 dihydroorotate oxidase activity	GO:0016020 membrane
<i>CAGL0F00627g</i>	<i>SLF1</i>	65464 to 67407 (-52 to +1892)	Winged helix-turn-helix DNA-binding domain; RNA-binding protein Lupus La	None	None	None
<i>CAGL0F01265g</i>	<i>YAP7</i>	131674 to 133622 (-32 to +1898)	Basic-leucine zipper domain	GO:0006355 regulation of transcription, DNA-dependent	GO:0003700 sequence-specific DNA binding transcription factor activity GO:0043565 sequence-specific DNA binding	None

Appendix 5: Statistical Analysis of Fitness Profiles

Table1: Average lag time, doubling time and final OD₆₀₀ readings for *S. cerevisiae* SGA strains expressing *C. glabrata* CAGL0D05434g compared with empty vector controls. P-values correspond to two-sample T-test comparing data sets from the previous cells.

Strain	Lag time (minutes)	T-test p value	Doubling Time (minutes)	T-test p-value	Final OD	T-test p value
KH02	480	0.089	248	9.17e-13	0.766	1.6e-8
KH02-D05434	499		301		0.733	
KH03	546	4.94e-5	283	1.35e-11	0.768	1.98e-14
KH03-D05434	603		451		0.674	

Appendix 6: Genetic interactions with *C. glabrata* *CAGL0D05434g*

Table 1: *S. cerevisiae* ORFs and SGD description (yeastgenome.org) which showed genetic interactions with *C. glabrata* *CAGL0D05434g* expressed from *S. cerevisiae* strain Δ *Ime1-D05434*. Genes highlighted in blue are implicated in mating, meiosis or sporulation. Orange denotes genes which function in DNA replication, DNA damage stress or whose expression increases in abundance or re-localises in response to DNA damage stress. Red represents genes involved in metal ion homeostasis, transport or resistance.

Gene Name	ORF name	SGD Description
<i>ADH5</i>	<i>YBR145W</i>	Alcohol dehydrogenase isoenzyme V; involved in ethanol production; ADH5 has a paralog, ADH1, that arose from the whole genome duplication
<i>ADY3</i>	<i>YDL239C</i>	Protein required for spore wall formation; thought to mediate assembly of a Don1p-containing structure at the leading edge of the prospore membrane via interaction with spindle pole body components; potentially phosphorylated by Cdc28p; ADY3 has a paralog, CNM67, that arose from the whole genome duplication
<i>AEP3</i>	<i>YPL005W</i>	Protein that may facilitate use of unformylated tRNA-Met in mitochondrial translation initiation; localized to the matrix face of the mitochondrial inner membrane; stabilizes the bicistronic AAP1-ATP6 mRNA
<i>APM3</i>	<i>YBR288C</i>	Mu3-like subunit of the clathrin associated protein complex (AP-3); functions in transport of alkaline phosphatase to the vacuole via the alternate pathway
<i>ARF2</i>	<i>YDL137W</i>	ADP-ribosylation factor; GTPase of the Ras superfamily involved in regulation of coated formation vesicles in intracellular trafficking within the Golgi; ARF2 has a paralog, ARF1, that arose from the whole genome duplication
<i>ATG29</i>	<i>YPL166W</i>	Autophagy-specific protein; required for recruiting other ATG proteins to the pre-autophagosomal structure (PAS); interacts with Atg17p and localizes to the PAS in a manner interdependent with Atg17p and Cis1p; not conserved; relocates from nucleus to cytoplasmic foci upon DNA replication stress
<i>BDF1</i>	<i>YLR399C</i>	Protein involved in transcription initiation at TATA-containing promoters; associates with the basal transcription factor TFIID; contains two bromodomains; corresponds to the C-terminal region of mammalian TAF1; redundant with Bdf2p
<i>BOP3</i>	<i>YNL042W</i>	Protein of unknown function, potential Cdc28p substrate; overproduction confers resistance to methylmercury
<i>CDC73</i>	<i>YLR418C</i>	Component of the Paf1p complex; binds to and modulates the activity of RNA polymerases I and II; required for expression of certain genes, modification of some histones, and telomere maintenance; involved in transcription elongation as demonstrated by

		the G-less-based run-on (GLRO) assay; protein abundance increases in response to DNA replication stress
<i>CHA4</i>	<i>YLR098C</i>	DNA binding transcriptional activator, mediates serine/threonine activation of the catabolic L-serine (L-threonine) deaminase (CHA1); Zinc-finger protein with Zn[2]-Cys[6] fungal-type binuclear cluster domain
<i>CHS6</i>	<i>YJL099W</i>	Member of the ChAPs (Chs5p-Arf1p-binding proteins) family; part of the exomer complex that mediates export of specific cargo proteins, including Chs3p, from the Golgi to the plasma membrane; CHS6 has a paralog, BCH2, that arose from the whole genome duplication
<i>CRS5</i>	<i>YOR031W</i>	Copper-binding metallothionein, required for wild-type copper resistance
<i>CTK2</i>	<i>YJL006C</i>	Beta subunit of C-terminal domain kinase I (CTDK-I), which phosphorylates both RNA pol II subunit Rpo21p to affect transcription and pre-mRNA 3' end processing, and ribosomal protein Rps2p to increase translational fidelity
<i>DDC1</i>	<i>YPL194W</i>	DNA damage checkpoint protein; part of a PCNA-like complex required for DNA damage response, required for pachytene checkpoint to inhibit cell cycle in response to unrepaired recombination intermediates; potential Cdc28p substrate; forms nuclear foci upon DNA replication stress
<i>ESBP6</i>	<i>YNL125C</i>	Protein with similarity to monocarboxylate permeases, appears not to be involved in transport of monocarboxylates such as lactate, pyruvate or acetate across the plasma membrane
<i>FRA1</i>	<i>YLL029W</i>	Protein involved in negative regulation of transcription of iron regulon; forms an iron independent complex with Fra2p, Grx3p, and Grx4p; cytosolic; mutant fails to repress transcription of iron regulon and is defective in spore formation
<i>FYV5</i>	<i>YCL058C</i>	Protein involved in regulation of the mating pathway; binds with Matalpha2p to promoters of haploid-specific genes; required for survival upon exposure to K1 killer toxin; involved in ion homeostasis
<i>GCN20</i>	<i>YFR009W</i>	Positive regulator of the Gcn2p kinase activity, forms a complex with Gcn1p; proposed to stimulate Gcn2p activation by an uncharged tRNA
<i>HAM1</i>	<i>YJR069C</i>	Nucleoside triphosphate pyrophosphohydrolase; active against a wide range of substrates including ITP, dITP and XTP; mediates exclusion of noncanonical purines and pyrimidines from deoxyribonucleoside triphosphate pools; mutant is sensitive to the base analog 6-N-hydroxylaminopurine; protein abundance increases in response to DNA replication stress
<i>HEF3</i>	<i>YNL014W</i>	Translational elongation factor EF-3; member of the ABC superfamily; stimulates EF-1 alpha-dependent binding of aminoacyl-tRNA by the ribosome; normally expressed in zinc deficient cells; HEF3 has a paralog, YEF3, that arose from the whole genome duplication
<i>HMS2</i>	<i>YJR147W</i>	Protein with similarity to heat shock transcription factors; overexpression suppresses the pseudohyphal filamentation defect of a diploid <i>mep1 mep2</i> homozygous null mutant; HMS2 has a paralog, SKN7, that arose from the whole genome duplication
<i>HOR7</i>	<i>YMR251W-A</i>	Protein of unknown function; overexpression suppresses Ca ²⁺ sensitivity of mutants lacking inositol phosphorylceramide mannosyltransferases Csg1p and Csh1p; transcription is induced under hyperosmotic stress and repressed by alpha factor; HOR7 has a paralog, DDR2, that arose from the whole genome duplication
<i>HST1</i>	<i>YOL068C</i>	NAD(+)-dependent histone deacetylase; essential subunit of the Sum1p/Rfm1p/Hst1p complex required for ORC-dependent silencing and mitotic repression; non-essential subunit of the Set3C deacetylase complex; involved in telomere maintenance
<i>HST4</i>	<i>YDR191W</i>	Member of the Sir2 family of NAD(+)-dependent protein deacetylases; involved along with Hst3p in silencing at telomeres, cell cycle progression, radiation resistance, genomic stability and short-chain fatty acid metabolism

<i>IME1</i>	<i>YJR094C</i>	Master regulator of meiosis that is active only during meiotic events, activates transcription of early meiotic genes through interaction with Ume6p, degraded by the 26S proteasome following phosphorylation by Ime2p
<i>IRC4</i>	<i>YDR540C</i>	Putative protein of unknown function; null mutant displays increased levels of spontaneous Rad52p foci; green fluorescent protein (GFP)-fusion protein localizes to the cytoplasm and nucleus
<i>ISF1</i>	<i>YMR081C</i>	Serine-rich, hydrophilic protein with similarity to Mbr1p; overexpression suppresses growth defects of hap2, hap3, and hap4 mutants; expression is under glucose control; cotranscribed with NAM7 in a <i>cyp1</i> mutant
<i>MDJ2</i>	<i>YNL328C</i>	Constituent of the mitochondrial import motor associated with the presequence translocase; function overlaps with that of Pam 18p; stimulates the ATPase activity of Ssc1p to drive mitochondrial import; contains a J domain
<i>MDM31</i>	<i>YHR194W</i>	Mitochondrial protein that may have a role in phospholipid metabolism; inner membrane protein with similarity to Mdm32p; required for normal mitochondrial morphology and inheritance; interacts genetically with MMM1, MMM2, MDM10, MDM12, and MDM34
<i>MHT1</i>	<i>YLL062C</i>	S-methylmethionine-homocysteine methyltransferase, functions along with Sam4p in the conversion of S-adenosylmethionine (AdoMet) to methionine to control the methionine/AdoMet ratio
<i>MPP6</i>	<i>YNR024W</i>	Nuclear exosome-associated RNA binding protein; involved in surveillance of pre-rRNAs and pre-mRNAs, and the degradation of cryptic non-coding RNAs (ncRNA); copurifies with ribosomes
<i>MRF1</i>	<i>YGL143C</i>	Mitochondrial translation release factor, involved in stop codon recognition and hydrolysis of the peptidyl-tRNA bond during mitochondrial translation; lack of MRF1 causes mitochondrial genome instability
<i>MRS4</i>	<i>YKR052C</i>	Iron transporter of the mitochondrial carrier family; mediates Fe ²⁺ transport across the inner mitochondrial membrane; active under low-iron conditions; may transport other cations; protein abundance increases in response to DNA replication stress; MRS4 has a paralog, MRS3, that arose from the whole genome duplication
<i>MSH5</i>	<i>YDL154W</i>	Protein of the MutS family, forms a dimer with Msh4p that facilitates crossovers between homologs during meiosis; <i>msh5</i> -Y823H mutation confers tolerance to DNA alkylating agents; homologs present in <i>C. elegans</i> and humans
<i>NOT5</i>	<i>YPR072W</i>	Subunit of the CCR4-NOT complex, which is a global transcriptional regulator with roles in transcription initiation and elongation and in mRNA degradation
<i>NRP1</i>	<i>YDL167C</i>	Putative RNA binding protein of unknown function; localizes to stress granules induced by glucose deprivation; predicted to be involved in ribosome biogenesis
<i>NTH1</i>	<i>YDR001C</i>	Neutral trehalase, degrades trehalose; required for thermotolerance and may mediate resistance to other cellular stresses; may be phosphorylated by Cdc28p; NTH1 has a paralog, NTH2, that arose from the whole genome duplication.
<i>OAF1</i>	<i>YAL051W</i>	Oleate-activated transcription factor; acts alone and as a heterodimer with Pip2p; activates genes involved in beta-oxidation of fatty acids and peroxisome organization and biogenesis; OAF1 has a paralog, PIP2, that arose from the whole genome duplication
<i>OMA1</i>	<i>YKR087C</i>	Metalloendopeptidase of the mitochondrial inner membrane; involved in turnover of membrane-embedded proteins; mediates degradation of Cox1p in <i>coa2</i> mutant cells; member of a family of predicted membrane-bound metallopeptidases in prokaryotes and higher eukaryotes
<i>PAN6</i>	<i>YIL145C</i>	Pantothenate synthase, also known as pantoate-beta-alanine ligase, required for pantothenic acid biosynthesis, deletion causes pantothenic acid auxotrophy, homologous to <i>E. coli</i> panC

<i>PEX6</i>	<i>YNL329C</i>	AAA-peroxin that heterodimerizes with AAA-peroxin Pex1p and participates in the recycling of peroxisomal signal receptor Pex5p from the peroxisomal membrane to the cytosol
<i>PHM7</i>	<i>YOL084W</i>	Protein of unknown function; expression is regulated by phosphate levels; green fluorescent protein (GFP)-fusion protein localizes to the cell periphery and vacuole; protein abundance increases in response to DNA replication stress
<i>POM34</i>	<i>YLR018C</i>	Subunit of the transmembrane ring of the nuclear pore complex (NPC); contributes to nucleocytoplasmic transport, NPC biogenesis and spindle pole body duplication
<i>PYK2</i>	<i>YOR347C</i>	Pyruvate kinase; appears to be modulated by phosphorylation; transcription repressed by glucose, and Pyk2p may be active under low glycolytic flux; PYK2 has a paralog, CDC19, that arose from the whole genome duplication
<i>RCR1</i>	<i>YBR005W</i>	Protein of the ER membrane involved in cell wall chitin deposition; may function in the endosomal-vacuolar trafficking pathway, helping determine whether plasma membrane proteins are degraded or routed to the plasma membrane; RCR1 has a paralog, RCR2, that arose from the whole genome duplication
<i>RCR2</i>	<i>YDR003W</i>	Vacuolar protein; presumably functions within the endosomal-vacuolar trafficking pathway, affecting events that determine whether plasma membrane proteins are degraded or routed to the plasma membrane; RCR2 has a paralog, RCR1, that arose from the whole genome duplication
<i>RDH54</i>	<i>YBR073W</i>	DNA-dependent ATPase; stimulates strand exchange by modifying the topology of double-stranded DNA; involved in recombinational repair of DNA double-strand breaks during mitosis and meiosis; proposed to be involved in crossover interference; interacts with Dmc1p; stimulates Dmc1p and Rad51p
<i>RPS30B</i>	<i>YOR182C</i>	Protein component of the small (40S) ribosomal subunit; homologous to mammalian ribosomal protein S30, no bacterial homolog; RPS30B has a paralog, RPS30A, that arose from the whole genome duplication; protein abundance increases in response to DNA replication stress
<i>RTG1</i>	<i>YOL067C</i>	Transcription factor (bHLH) involved in interorganelle communication between mitochondria, peroxisomes, and nucleus
<i>SCS3</i>	<i>YGL126W</i>	Protein required for inositol prototrophy; required for normal ER membrane biosynthesis; ortholog of the FIT family of proteins involved in triglyceride droplet biosynthesis and homologous to human FIT2; disputed role in the synthesis of inositol phospholipids from inositol
<i>SDT1</i>	<i>YGL224C</i>	Pyrimidine nucleotidase; overexpression suppresses the 6-AU sensitivity of transcription elongation factor S-II, as well as resistance to other pyrimidine derivatives
<i>SET6</i>	<i>YPL165C</i>	SET domain protein of unknown function; deletion heterozygote is sensitive to compounds that target ergosterol biosynthesis, may be involved in compound availability
<i>SFM1</i>	<i>YOR021C</i>	SPOUT methyltransferase; catalyzes omega-monomethylation of Rps3p on Arg-146; not an essential gene; predicted to be involved in rRNA processing and ribosome biogenesis and in biopolymer catabolism
<i>SHE2</i>	<i>YKL130C</i>	RNA-binding protein that binds specific mRNAs and interacts with She3p; part of the mRNA localization machinery that restricts accumulation of certain proteins to the bud
<i>SIP5</i>	<i>YMR140W</i>	Protein of unknown function; interacts with both the Reg1p/Glc7p phosphatase and the Snf1p kinase; forms cytoplasmic foci upon DNA replication stress
<i>SKG1</i>	<i>YKR100C</i>	Transmembrane protein with a role in cell wall polymer composition; localizes on the inner surface of the plasma membrane at the

		bud and in the daughter cell
<i>SOM1</i>	<i>YEL059C-A</i>	Subunit of the mitochondrial inner membrane peptidase, which is required for maturation of mitochondrial proteins of the intermembrane space; Som1p facilitates cleavage of a subset of substrates; contains twin cysteine-x9-cysteine motifs
<i>SUC2</i>	<i>YIL162W</i>	Invertase, sucrose hydrolyzing enzyme; a secreted, glycosylated form is regulated by glucose repression, and an intracellular, nonglycosylated enzyme is produced constitutively
<i>TDA1</i>	<i>YMR291W</i>	Protein kinase of unknown cellular role; green fluorescent protein (GFP)-fusion protein localizes to the cytoplasm and nucleus; null mutant is sensitive to expression of the top1-T722A allele; not an essential gene; relocates from nucleus to cytoplasm upon DNA replication stress
<i>TDP1</i>	<i>YBR223C</i>	Tyrosyl-DNA phosphodiesterase I; hydrolyzes 3' and 5'-phosphotyrosyl bonds; involved in the repair of DNA lesions created by topoisomerase I and topoisomerase II; mutations in human homolog result in the neurodegenerative disease SCAN1
<i>THR4</i>	<i>YCR053W</i>	Threonine synthase, conserved protein that catalyzes formation of threonine from O-phosphohomoserine; expression is regulated by the GCN4-mediated general amino acid control pathway
<i>TOM6</i>	<i>YOR045W</i>	Component of the TOM (translocase of outer membrane) complex responsible for recognition and initial import steps for all mitochondrially directed proteins; promotes assembly and stability of the TOM complex
<i>TPP1</i>	<i>TPP1</i>	DNA 3'-phosphatase; functions in repair of endogenous damage of double-stranded DNA, activity is specific for removal of 3' phosphates at strand breaks; similar to the I-2-haloacid dehalogenase superfamily; homolog of human polynucleotide kinase/3'-phosphatase
<i>TRS33</i>	<i>YOR115C</i>	One of 10 subunits of the transport protein particle (TRAPP) complex of the cis-Golgi which mediates vesicle docking and fusion; involved in endoplasmic reticulum (ER) to Golgi membrane traffic
<i>TVP38</i>	<i>YKR088C</i>	Integral membrane protein localized to late Golgi vesicles along with the v-SNARE Tlg2p; required for asymmetric localization of Kar9p during mitosis; GFP-fusion protein localizes to the cytoplasm in a punctate pattern
<i>UGA2</i>	<i>YBR006W</i>	Succinate semialdehyde dehydrogenase involved in the utilization of gamma-aminobutyrate (GABA) as a nitrogen source; part of the 4-aminobutyrate and glutamate degradation pathways; localized to the cytoplasm
<i>VMA4</i>	<i>YOR332W</i>	Subunit E of the V1 domain of the vacuolar H ⁺ -ATPase (V-ATPase); V-ATPase is an electrogenic proton pump found throughout the endomembrane system; V1 domain has eight subunits; required for the V1 domain to assemble onto the vacuolar membrane; protein abundance increases in response to DNA replication stress
<i>WHI2</i>	<i>YOR043W</i>	Protein required, with binding partner Psr1p, for full activation of the general stress response, possibly through Msn2p dephosphorylation; regulates growth during the diauxic shift; negative regulator of G1 cyclin expression
<i>YBR238C</i>	<i>YBR238C</i>	Mitochondrial membrane protein with similarity to Rmd9p; not required for respiratory growth but causes a synthetic respiratory defect in combination with rmd9 mutations; transcriptionally up-regulated by TOR; deletion increases life span
<i>YDL206W</i>	<i>YDL206W</i>	Putative protein of unknown function; YDL206W is not an essential protein
<i>YDR186C</i>	<i>YDR186C</i>	Putative protein of unknown function; may interact with ribosomes, based on co-purification experiments; green fluorescent protein (GFP)-fusion protein localizes to the cytoplasm
<i>YDR541C</i>	<i>YDR541C</i>	Putative dihydrokaempferol 4-reductase

YIA6	YIL006W	Mitochondrial NAD ⁺ transporter, involved in the transport of NAD ⁺ into the mitochondria (see also YEA6); member of the mitochondrial carrier subfamily; disputed role as a pyruvate transporter; has putative mouse and human orthologs
YML082W	YML082W	Putative protein predicted to have carbon-sulfur lyase activity; transcriptionally regulated by Upc2p via an upstream sterol response element; green fluorescent protein (GFP)-fusion protein localizes to the nucleus and the cytoplasm; YML082W is not an essential gene
YOR019W	YOR019W	Protein of unknown function that may interact with ribosomes, based on co-purification experiments
YPL014W	YPL014W	Putative protein of unknown function; green fluorescent protein (GFP)-fusion protein localizes to the cytoplasm and to the nucleus
YPL150W	YPL150W	Protein kinase of unknown cellular role; binds phosphatidylinositols and cardiolipin in a large-scale study
ZAP1	YJL056C	Zinc-regulated transcription factor; binds to zinc-responsive promoters to induce transcription of certain genes in presence of zinc, represses other genes in low zinc; regulates its own transcription; contains seven zinc-finger domains
ZRT1	YGL255W	High-affinity zinc transporter of the plasma membrane, responsible for the majority of zinc uptake; transcription is induced under low-zinc conditions by the Zap1p transcription factor

Table 2: *S. cerevisiae* ORFs and SGD description (yeastgenome.org) which showed genetic interactions with *C. glabrata* CAGL0D05434g expressed from *S. cerevisiae* strain Δ Ime2-D05434. Genes highlighted in blue are implicated in mating, meiosis or sporulation. Orange denotes genes which function in DNA replication, DNA damage stress or whose expression increases in abundance or re-localises in response to DNA damage stress. Red represents genes involved in metal ion homeostasis, transport or resistance.

Gene Name	ORF name	SGD Description
ALT1	YLR089C	Alanine transaminase (glutamic pyruvic transaminase); involved in alanine biosynthetic and catabolic processes; expression is induced in the presence of alanine; repression is mediated by Nrg1p; the authentic, non-tagged protein is detected in highly purified mitochondria in high-throughput studies; paralogous gene ALT2 is catalytically inactive
ASH1	YKL185W	Zinc-finger inhibitor of HO transcription; mRNA is localized and translated in the distal tip of anaphase cells, resulting in accumulation of Ash1p in daughter cell nuclei and inhibition of HO expression; potential Cdc28p substrate
BLI1	YKL061W	Putative protein of unknown function; likely member of BLOC complex involved in endosomal cargo sorting; green fluorescent protein (GFP)-fusion protein localizes to the endosome
CKI1	YLR133W	Choline kinase; catalyzes the first step in phosphatidylcholine synthesis via the CDP-choline (Kennedy pathway); exhibits some ethanolamine kinase activity contributing to phosphatidylethanolamine synthesis via the CDP-ethanolamine pathway; CKI1 has a paralog, EKI1, that arose from the whole genome duplication

<i>COA6</i>	<i>YMR244C</i>	Protein involved in cytochrome c oxidase assembly; also required for efficient formation of respiratory supercomplexes comprised of Complexes III and IV; localizes to the mitochondrial intermembrane space; has a human homolog; transcription is induced in response to the DNA-damaging agent MMS; protein abundance increases in response to DNA replication stress
<i>CPA1</i>	<i>YOR303W</i>	Small subunit of carbamoyl phosphate synthetase, which catalyzes a step in the synthesis of citrulline, an arginine precursor; translationally regulated by an attenuator peptide encoded by <i>YOR302W</i> within the <i>CPA1</i> mRNA 5'-leader
<i>CUP9</i>	<i>YPL177C</i>	Homeodomain-containing transcriptional repressor; regulates expression of <i>PTR2</i> , which encodes a major peptide transporter; imported peptides activate ubiquitin-dependent proteolysis, resulting in degradation of Cup9p and de-repression of <i>PTR2</i> transcription; <i>CUP9</i> has a paralog, <i>TOS8</i> , that arose from the whole genome duplication; protein abundance increases in response to DNA replication stress
<i>DGA1</i>	<i>YOR245C</i>	Diacylglycerol acyltransferase, catalyzes the terminal step of triacylglycerol (TAG) formation, acylates diacylglycerol using acyl-CoA as an acyl donor, localized to lipid particles
<i>EFT2</i>	<i>YDR385W</i>	Elongation factor 2 (EF-2), also encoded by <i>EFT1</i> ; catalyzes ribosomal translocation during protein synthesis; contains diphthamide, the unique posttranslationally modified histidine residue specifically ADP-ribosylated by diphtheria toxin; <i>EFT2</i> has a paralog, <i>EFT1</i> , that arose from the whole genome duplication
<i>FRE8</i>	<i>YLR047C</i>	Protein with sequence similarity to iron/copper reductases, involved in iron homeostasis; deletion mutant has iron deficiency/accumulation growth defects; expression increased in the absence of copper-responsive transcription factor Mac1p
<i>FUM1</i>	<i>YPL262W</i>	Fumarase, converts fumaric acid to L-malic acid in the TCA cycle; cytosolic and mitochondrial distribution determined by the N-terminal targeting sequence, protein conformation, and status of glyoxylate shunt; phosphorylated in mitochondria
<i>GDB1</i>	<i>YPR184W</i>	Glycogen debranching enzyme; contains glucanotransferase and alpha-1,6-amyloglucosidase activities; required for glycogen degradation; phosphorylated in mitochondria; activity is inhibited by Igd1p; protein abundance increases in response to DNA replication stress
<i>KEL1</i>	<i>YHR158C</i>	Protein required for proper cell fusion and cell morphology; functions in a complex with Kel2p to negatively regulate mitotic exit, interacts with Tem1p and Lte1p; localizes to regions of polarized growth; potential Cdc28p substrate
<i>KES1</i>	<i>YPL145C</i>	One of seven members of the yeast oxysterol binding protein family; involved in negative regulation of Sec14p-dependent Golgi complex secretory functions, peripheral membrane protein that localizes to the Golgi complex; <i>KES1</i> has a paralog, <i>HES1</i> , that arose from the whole genome duplication
<i>MGR2</i>	<i>YPL098C</i>	Subunit of the TIM23 translocase complex; acts to couple Tim21p with the core Tim23 translocase; absolutely required for mitochondrial import of presequence-containing proteins at elevated temperature; required for viability of cells lacking the mitochondrial genome (petite-negative phenotype)
<i>MRC1</i>	<i>YCL061C</i>	S-phase checkpoint protein required for DNA replication; interacts with and stabilizes Pol2p at stalled replication forks during stress, where it forms a pausing complex with Tof1p and is phosphorylated by Mec1p; protects uncapped telomeres
<i>MRP8</i>	<i>YKL142W</i>	Protein of unknown function; undergoes sumoylation; transcription induced under cell wall stress; protein levels are reduced under anaerobic conditions; protein abundance increases in response to DNA replication stress; originally thought to be a mitochondrial ribosomal protein based on sequence analysis
<i>NDL1</i>	<i>YLR254C</i>	Homolog of nuclear distribution factor NudE, NUDEL; interacts with Pac1p and regulates dynein targeting to microtubule plus ends

<i>NYV1</i>	<i>YLR093C</i>	v-SNARE component of the vacuolar SNARE complex involved in vesicle fusion; inhibits ATP-dependent Ca(2+) transport activity of Pmc1p in the vacuolar membrane
<i>OAR1</i>	<i>YKL055C</i>	Mitochondrial 3-oxoacyl-[acyl-carrier-protein] reductase, may comprise a type II mitochondrial fatty acid synthase along with Mct1p
<i>OPI10</i>	<i>YOL032W</i>	Protein with a possible role in phospholipid biosynthesis; null mutant displays an inositol-excreting phenotype that is suppressed by exogenous choline; protein abundance increases in response to DNA replication stress
<i>OTU2</i>	<i>YHL013C</i>	Protein of unknown function; may interact with ribosomes, based on co-purification experiments; member of the ovarian tumor-like (OTU) superfamily of predicted cysteine proteases; shows cytoplasmic localization; protein abundance increases in response to DNA replication stress
<i>PMT3</i>	<i>YOR321W</i>	Protein O-mannosyltransferase; transfers mannose residues from dolichyl phosphate-D-mannose to protein serine/threonine residues; acts in a complex with Pmt5p, can instead interact with Pmt1p in some conditions; antifungal drug target; PMT3 has a paralog, PMT2, that arose from the whole genome duplication
<i>PSH1</i>	<i>YOL054W</i>	E3 ubiquitin ligase that mediates polyubiquitination and degradation of centromere-binding protein Cse4p and prevents Cse4p from mislocalizing to euchromatin; ubiquitylation of Cse4p may be antagonized by Scm3p
<i>PUT4</i>	<i>YOR348C</i>	Proline permease, required for high-affinity transport of proline; also transports the toxic proline analog azetidine-2-carboxylate (AzC); PUT4 transcription is repressed in ammonia-grown cells
<i>QCR10</i>	<i>YHR001W</i>	Subunit of the ubiquinol-cytochrome c oxidoreductase complex which includes Cobp, Rip1p, Cyt1p, Cor1p, Qcr2p, Qcr6p, Qcr7p, Qcr8p, Qcr9p, and Qcr10p and comprises part of the mitochondrial respiratory chain
<i>RBD2</i>	<i>YPL246C</i>	Possible rhomboid protease, has similarity to eukaryotic rhomboid proteases including Pcp1p
<i>RMD6</i>	<i>YEL072W</i>	Required for Meiotic nuclear Division
<i>RPL7B</i>	<i>YPL198W</i>	Ribosomal 60S subunit protein L7B; contains a conserved C-terminal Nucleic acid Binding Domain (NDB2); homologous to mammalian ribosomal protein L7 and bacterial L30; RPL7B has a paralog, RPL7A, that arose from the whole genome duplication
<i>SAS4</i>	<i>YDR181C</i>	Subunit of the SAS complex (Sas2p, Sas4p, Sas5p), which acetylates free histones and nucleosomes and regulates transcriptional silencing; required for the HAT activity of Sas2p
<i>SBP1</i>	<i>YHL034C</i>	Protein that binds eIF4G and has a role in repression of translation; has an RGG motif; found in cytoplasmic P bodies; found associated with small nucleolar RNAs snR10 and snR11
<i>SCM4</i>	<i>YGR049W</i>	Mitochondrial outer membrane protein of unknown function; predicted to have 4 transmembrane segments; import is mediated by Tom70p and Mim1p; interacts genetically with a cdc4 mutation
<i>SEM1</i>	<i>YDR363W</i>	Component of lid subcomplex of the 26S proteasome regulatory subunit; involved in mRNA export mediated by the TREX-2 complex (Sac3p-Thp1p); ortholog of human DSS1; protein abundance increases in response to DNA replication stress
<i>SHE9</i>	<i>YDR393W</i>	Mitochondrial inner membrane protein required for normal mitochondrial morphology, may be involved in fission of the inner membrane; forms a homo-oligomeric complex
<i>SOP4</i>	<i>YJL192C</i>	ER-membrane protein; suppressor of pma1-7, deletion of SOP4 slows down the export of wild-type Pma1p and Pma1-7 from the ER
<i>SPO75</i>	<i>YLL005C</i>	Meiosis-specific protein of unknown function, required for spore wall formation during sporulation; dispensable for both nuclear

		divisions during meiosis
<i>STB5</i>	<i>YHR178W</i>	Transcription factor, involved in regulating multidrug resistance and oxidative stress response; forms a heterodimer with Pdr1p; contains a Zn(II) ₂ Cys ₆ zinc finger domain that interacts with a pleiotropic drug resistance element in vitro
<i>TDA2</i>	<i>YER071C</i>	Protein of unknown function; green fluorescent protein (GFP)-fusion protein localizes to the cytoplasm in a punctate pattern; null mutant is sensitive to expression of the top1-T722A allele
<i>TIR2</i>	<i>YOR010C</i>	Putative cell wall mannoprotein of the Srp1p/Tip1p family of serine-alanine-rich proteins; transcription is induced by cold shock and anaerobiosis
<i>TMA19</i>	<i>YKL056C</i>	Protein that associates with ribosomes; homolog of translationally controlled tumor protein; green fluorescent protein (GFP)-fusion protein localizes to the cytoplasm and relocates to the mitochondrial outer surface upon oxidative stress
<i>TPP1</i>	<i>YMR156C</i>	DNA 3'-phosphatase; functions in repair of endogenous damage of double-stranded DNA, activity is specific for removal of 3' phosphates at strand breaks; similar to the I-2-haloacid dehalogenase superfamily; homolog of human polynucleotide kinase/3'-phosphatase
<i>UBI4</i>	<i>YLL039C</i>	Ubiquitin; becomes conjugated to proteins, marking them for selective degradation via the ubiquitin-26S proteasome system; essential for the cellular stress response; encoded as a polyubiquitin precursor comprised of 5 head-to-tail repeats; protein abundance increases in response to DNA replication stress
<i>VMA4</i>	<i>YOR332W</i>	Subunit E of the V1 domain of the vacuolar H ⁺ -ATPase (V-ATPase); V-ATPase is an electrogenic proton pump found throughout the endomembrane system; V1 domain has eight subunits; required for the V1 domain to assemble onto the vacuolar membrane; protein abundance increases in response to DNA replication stress
<i>VPS28</i>	<i>YPL065W</i>	Component of the ESCRT-I complex (Stp22p, Srn2p, Vps28p, and Mvb12p), which is involved in ubiquitin-dependent sorting of proteins into the endosome; conserved C-terminal domain interacts with ESCRT-III subunit Vps20p
<i>WHI2</i>	<i>YOR043W</i>	Protein required, with binding partner Psr1p, for full activation of the general stress response, possibly through Msn2p dephosphorylation; regulates growth during the diauxic shift; negative regulator of G1 cyclin expression
<i>YAT2</i>	<i>YER024W</i>	Carnitine acetyltransferase; has similarity to Yat1p, which is a carnitine acetyltransferase associated with the mitochondrial outer membrane
<i>YBP1</i>	<i>YBR216C</i>	Protein required for oxidation of specific cysteine residues of the transcription factor Yap1p, resulting in the nuclear localization of Yap1p in response to stress
<i>YBR220C</i>	<i>YBR220C</i>	Putative protein of unknown function; YBR220C is not an essential gene
<i>YDR131C</i>	<i>YDR131C</i>	F-box protein, substrate-specific adaptor subunit that recruits substrates to a core ubiquitination complex
<i>YDR179W</i>	<i>YDR179W</i>	Putative protein of unknown function
<i>YEA6</i>	<i>YEL006W</i>	Putative mitochondrial NAD ⁺ transporter, member of the mitochondrial carrier subfamily (see also YIA6); has putative human ortholog
<i>YER158C</i>	<i>YER158C</i>	Protein of unknown function; potentially phosphorylated by Cdc28p; YER158C has a paralog, AFR1, that arose from the whole genome duplication
<i>YIG1</i>	<i>YPL201C</i>	Protein that interacts with glycerol 3-phosphatase and plays a role in anaerobic glycerol production; localizes to the nucleus and

		cytosol
<i>YMR244W</i>	<i>YMR244W</i>	Putative protein of unknown function
<i>YOR012W</i>	<i>YOR012W</i>	Putative protein of unknown function
<i>YPS3</i>	<i>YLR121C</i>	Aspartic protease, member of the yapsin family of proteases involved in cell wall growth and maintenance; attached to the plasma membrane via a glycosylphosphatidylinositol (GPI) anchor
<i>YSP3</i>	<i>YOR003W</i>	Putative precursor to the subtilisin-like protease III

Appendix 7: Fitness Measures for *C. glabrata* Deletion Mutants

Table 1: Summary of fitness measures for *C. glabrata* deletion mutants relative to the parental strain. Numbers represent either a positive or negative increase in the specified fitness measure compared with parental strain Cg2001 $\Delta his3$. Lag time was measured as time taken for cultures to reach OD₆₀₀ 0.2. Doubling time was calculated as described (see 2.6.3) taking measurements from cultures in exponential phase (approximately OD₆₀₀ 0.4 to 0.8). Maximum density was taken as the final OD₆₀₀ of cultures at 24 hours of growth profiling. Strains with fitness significantly different from the parental strain are highlighted in yellow (Anova $p < 0.05$; Dunnett's critical value 3.37).

<i>C. glabrata</i> strain	Change in lag time (minutes)	Change in doubling time (minutes)	Change in maximum density (OD ₆₀₀)
$\Delta CAGL0A02299g$ A	-20.00	9.75	0.0027
$\Delta CAGL0A02299g$ B	-18.33	2.42	-0.0052
$\Delta CAGL0A02343g$ A	0.00	5.91	-0.0071
$\Delta CAGL0A02343g$ B	10.00	-6.58	-0.0369
$\Delta CAGL0A04565g$ A	110.00	109.03	-0.3452
$\Delta CAGL0B00726g$ A	-13.33	12.29	0.0343
$\Delta CAGL0B00726g$ B	2.00	-2.86	0.0105
$\Delta CAGL0B02926g$ A	0.00	0.29	0.0160
$\Delta CAGL0B02946g$ A	-12.50	-8.18	1.1513
$\Delta CAGL0B02946g$ B	-6.67	0.56	1.1475
$\Delta CAGL0B02948g$ A	22.50	115.19	0.0004
$\Delta CAGL0B02948g$ B	10.00	114.76	0.0299
$\Delta CAGL0B02970g$ A	31.67	5.03	0.0110
$\Delta CAGL0B03223g$ A	13.33	-11.16	0.0270
$\Delta CAGL0B03223g$ B	6.67	-3.39	0.0141
$\Delta CAGL0B03883g$ A	30.00	1.45	-0.0478
$\Delta CAGL0B03883g$ B	40.00	6.75	-0.0429
$\Delta CAGL0C00253g$ A	20.00	19.49	-0.0185
$\Delta CAGL0C00253g$ B	38.00	-7.20	0.0016
$\Delta CAGL0C01837g$ A	12.50	3.06	-0.0039
$\Delta CAGL0C01837g$ B	6.67	0.73	0.0159
$\Delta CAGL0C04763g$ A	2.50	4.01	-0.0073
$\Delta CAGL0C04763g$ B	8.00	4.83	-0.0086
$\Delta CAGL0D00682g$ A	-16.67	7.91	0.0191
$\Delta CAGL0D00682g$ B	4.00	6.95	-0.0041
$\Delta CAGL0D01210g$ A	-3.33	-5.69	0.0312
$\Delta CAGL0D01210g$ B	-15.00	4.97	0.0187
$\Delta CAGL0D03850g$ A	75.00	38.40	0.0136

Δ CAGL0D03850g B	42.50	24.89	0.0202
Δ CAGL0D03872g A	-21.67	8.14	-0.0021
Δ CAGL0D03872g B	-22.50	9.52	-0.0168
Δ CAGL0D05170g A	8.33	1.63	0.0096
Δ CAGL0D05170g B	-16.67	4.97	0.0148
Δ CAGL0D05434g A	55.00	15.58	0.0509
Δ CAGL0D05434g B	50.00	2.23	0.0231
Δ CAGL0D06226g A	-2.00	0.45	0.0228
Δ CAGL0D06226g B	-20.00	1.68	0.0243
Δ CAGL0E00275g A	63.33	11.80	-0.0670
Δ CAGL0E06600g A	0.00	5.56	-0.0118
Δ CAGL0E06600g B	-1.67	-0.03	-0.0176
Δ CAGL0E06644g A	1.67	-1.54	0.0091
Δ CAGL0E06644g B	-10.00	6.76	-0.0031
Δ CAGL0F01815g A	11.67	2.51	-0.0363
Δ CAGL0F01815g B	3.33	5.83	-0.0423
Δ CAGL0F03905g A	0.00	11.55	0.0172
Δ CAGL0F03905g B	1.67	12.31	0.0320
Δ CAGL0F04081g A	8.00	2.15	0.0103
Δ CAGL0F05159g A	28.00	21.94	-0.0648
Δ CAGL0F05159g B	21.67	18.87	-0.1109
Δ CAGL0F05973g A	11.67	-7.12	0.0385
Δ CAGL0F06237g A	1.67	28.98	0.0008
Δ CAGL0F06237g B	12.50	22.83	-0.0113
Δ CAGL0F08767g A	-20.00	23.50	0.0419
Δ CAGL0F08767g B	-22.50	15.34	0.0244
Δ CAGL0F09229g A	-1.67	-4.54	-0.1747
Δ CAGL0F09229g B	-20.00	4.07	-0.0069
Δ CAGL0G02607g A	0.00	8.01	0.0200
Δ CAGL0G03201g A	-20.00	12.06	0.0115
Δ CAGL0G04279g A	-20.00	14.71	-0.0128
Δ CAGL0G04279g B	-16.67	17.28	-0.0003
Δ CAGL0G05522g A	40.00	121.52	-0.0237
Δ CAGL0G05522g B	44.00	109.38	-0.0026
Δ CAGL0G08866g A	-6.00	18.62	-0.0148
Δ CAGL0G08866g B	-4.00	16.21	-0.0079
Δ CAGL0G10175g A	-48.00	20.90	0.0253
Δ CAGL0G10175g B	-107.50	22.24	-0.0036
Δ CAGL0H01749g A	8.00	-7.86	0.0212
Δ CAGL0H01749g B	-13.33	4.86	0.0157
Δ CAGL0H06765g A	30.00	-0.91	-0.0044
Δ CAGL0H06765g B	13.33	-5.19	-0.0126
Δ CAGL0H08712g A	2.50	17.09	0.0151
Δ CAGL0H08712g B	0.00	15.84	0.0495
Δ CAGL0H09988g A	23.33	1.44	-0.0009
Δ CAGL0H09988g B	4.00	5.02	-0.0376

Δ CAGL0H10208g A	18.00	3.56	-0.1050
Δ CAGL0H10208g B	-3.33	3.70	-0.1326
Δ CAGL0H10208g C	-8.33	-5.04	0.0242
Δ CAGL0I02244g A	6.67	0.50	0.0113
Δ CAGL0I08437g A	28.33	12.25	0.0011
Δ CAGL0I08613g A	41.67	-3.72	-0.0515
Δ CAGL0I08613g B	10.00	2.42	-0.0193
Δ CAGL0J05786g A	23.33	7.74	-0.0301
Δ CAGL0J05786g B	36.00	-4.96	-0.0467
Δ CAGL0J05852g A	12.00	-6.42	0.0254
Δ CAGL0J05852g B	6.67	5.55	0.0267
Δ CAGL0K02145g A	-12.50	-5.13	0.0359
Δ CAGL0K02145g B	-32.50	1.90	0.0176
Δ CAGL0K05687g A	26.67	-1.19	-0.0178
Δ CAGL0K05687g A	5.00	3.37	-0.0221
Δ CAGL0K05687g B	34.00	-1.56	-0.0201
Δ CAGL0K05687g B	-1.67	3.40	-0.0281
Δ CAGL0K07634g A	30.00	-12.59	-0.0064
Δ CAGL0K07634g B	-12.50	8.22	0.0594
Δ CAGL0K10318g A	42.50	14.74	-0.0454
Δ CAGL0K10318g B	60.00	9.81	-0.0639
Δ CAGL0K11066g A	36.67	8.26	-0.0206
Δ CAGL0L03674g A	14.00	-2.52	0.0290
Δ CAGL0L03674g B	6.67	-0.37	0.0243
Δ CAGL0L06776g A	6.67	2.60	0.0264
Δ CAGL0L06776g B	5.00	-0.66	0.0416
Δ CAGL0L07480g A	20.00	-3.31	0.0102
Δ CAGL0L07480g B	-23.33	7.90	0.0362
Δ CAGL0L09383g A	16.67	4.92	0.0252
Δ CAGL0L09383g B	30.00	-4.96	0.0152
Δ CAGL0M01716g A	-2.00	-1.76	-0.0090
Δ CAGL0M01716g B	-6.00	4.17	0.0234
Δ CAGL0M01870g A	-23.33	3.86	0.0436
Δ CAGL0M01914g A	14.00	0.61	0.0612
Δ CAGL0M02299g A	36.67	4.22	-0.0805
Δ CAGL0M02321g A	0.00	16.37	-0.0068
Δ CAGL0M02321g B	0.00	3.38	0.0291
Δ CAGL0M04543g A	6.67	4.31	-0.0051
Δ CAGL0M04543g B	12.50	4.31	0.0037
Δ CAGL0M05137g A	-2.50	29.04	-0.0032
Δ CAGL0M05137g B	15.00	8.98	0.0166
Δ CAGL0M10153g A	-2.50	10.11	0.0110
Δ CAGL0M10978g A	-2.50	7.26	-0.0090
Δ CAGL0M10978g B	30.00	-4.21	-0.0687

Appendix 8: Growth profiling of *C. glabrata* mutants

Fitness of *C. glabrata* deletion mutants and parental strain Cg2001 $\Delta his3$ was assessed by measuring growth in YPD broth at 30 °C (see 2.6.3). Growth profiles represent average optical density readings of *C. glabrata* cultures taken every ten minutes over a 24 hour period with continuous shaking between reads. Error bars represent standard deviation across replicates.

Figure 1: Growth profile of *C. glabrata* parental strain Cg2001 $\Delta his3$ and $\Delta CAGL0A02299g$ isolates A and B.

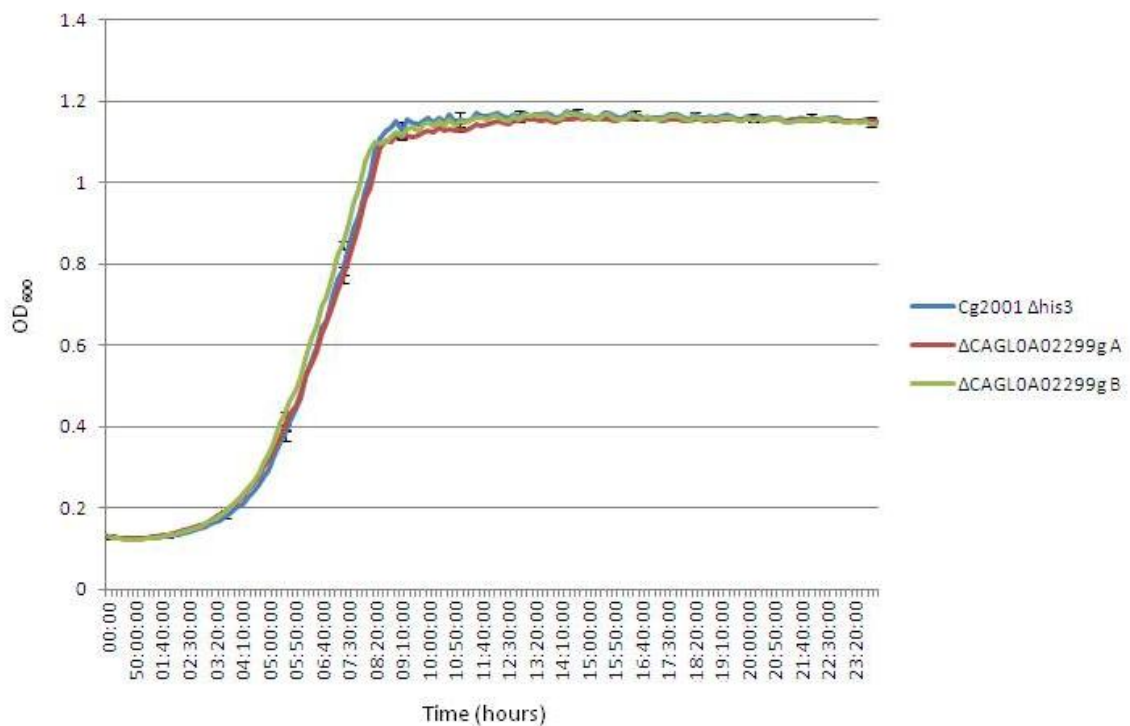


Figure 2: Growth profile of *C. glabrata* parental strain Cg2001 $\Delta his3$ and $\Delta CAGL0A02343g$ isolates A and B.

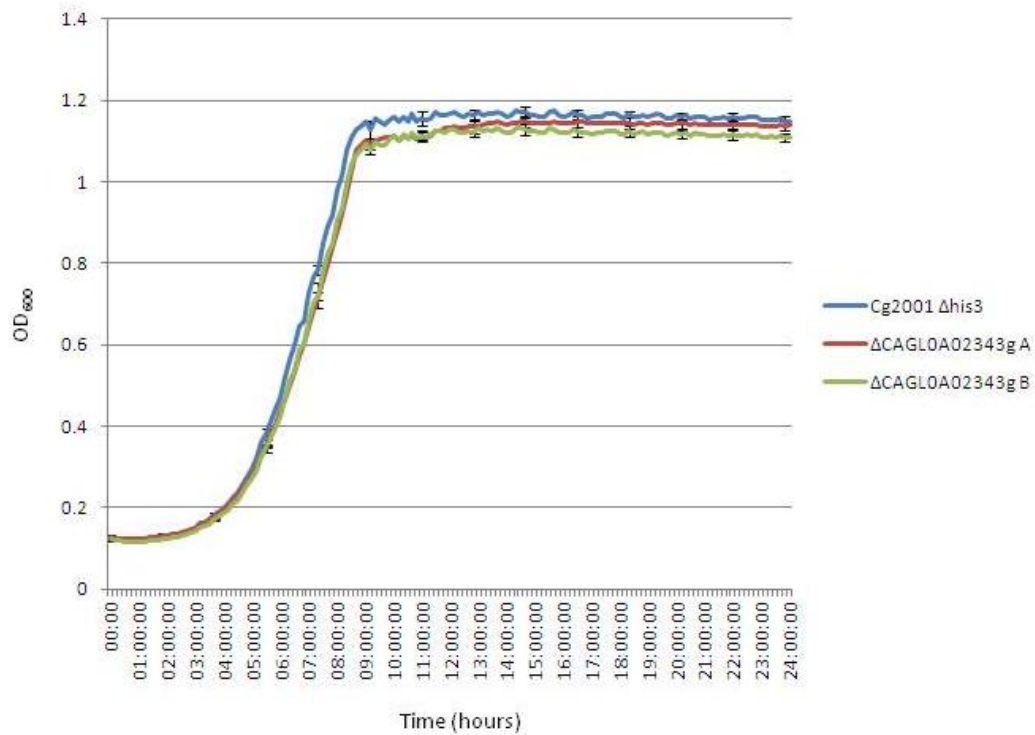


Figure 3: Growth profile of *C. glabrata* parental strain Cg2001 $\Delta his3$ and $\Delta CAGL0A04565g$.

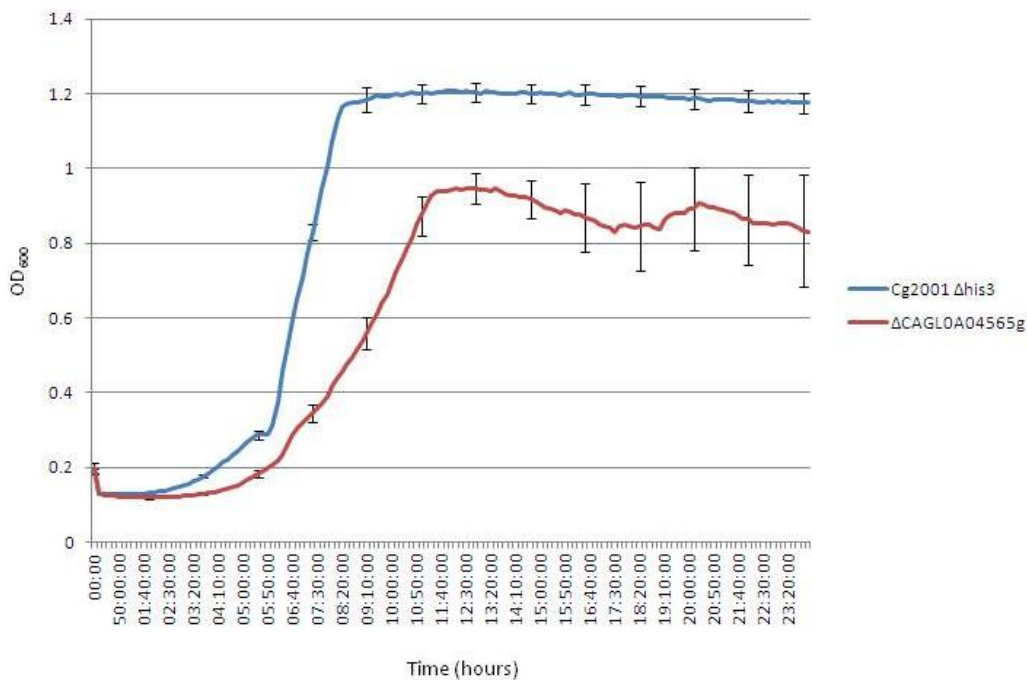


Figure 4: Growth profile of *C. glabrata* parental strain Cg2001 $\Delta his3$ and $\Delta CAGL0B00726g$ isolates A and B.

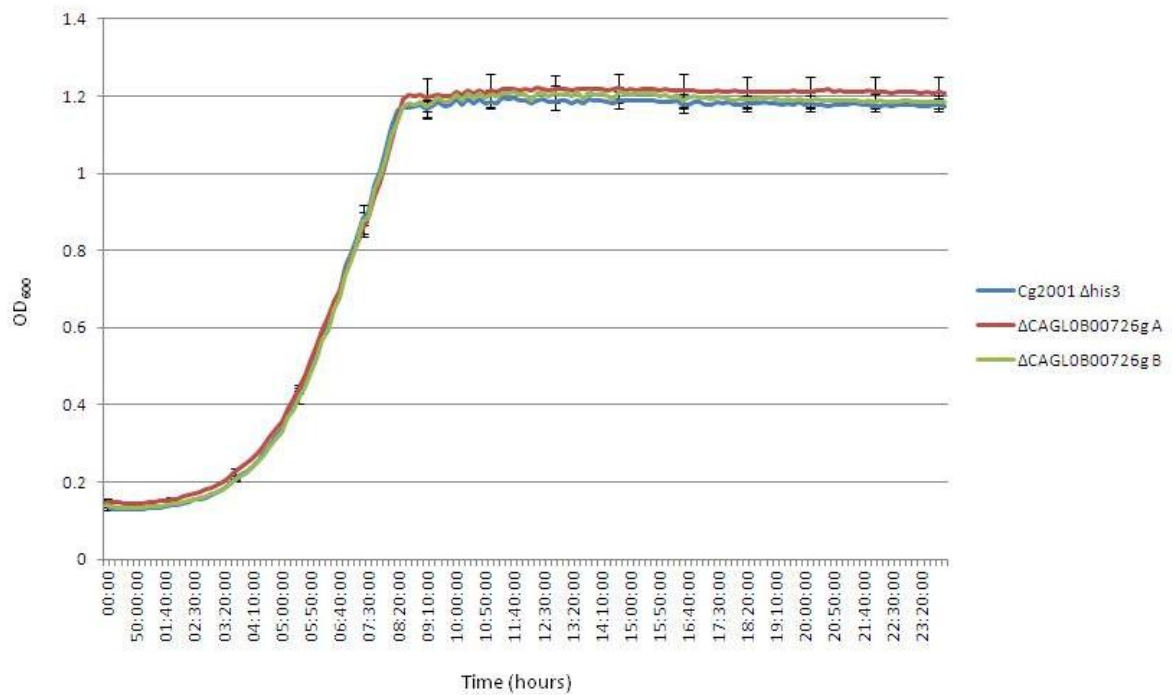


Figure 5: Growth profile of *C. glabrata* parental strain Cg2001 $\Delta his3$ and $\Delta CAGL0B02926g$.

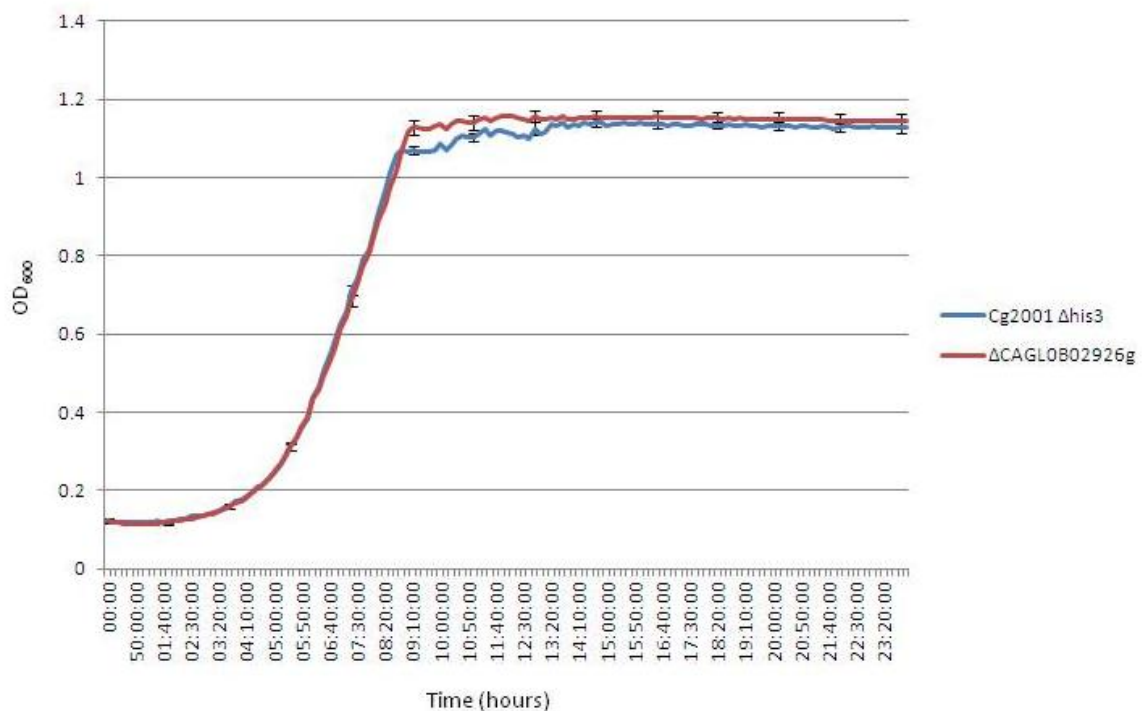


Figure 6: Growth profile of *C. glabrata* parental strain Cg2001 $\Delta his3$ and $\Delta CAGL0B02946g$ isolates A and B.

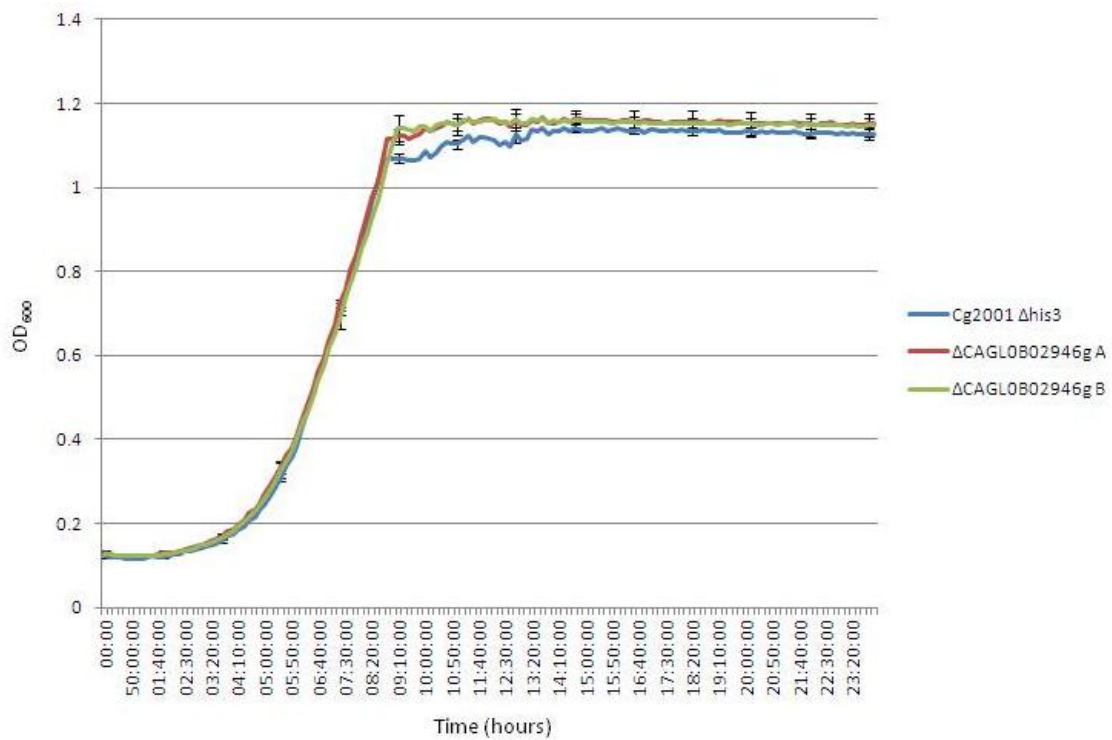


Figure 7: Growth profile of *C. glabrata* parental strain Cg2001 $\Delta his3$ and $\Delta CAGL0B02948g$ isolates A and B.

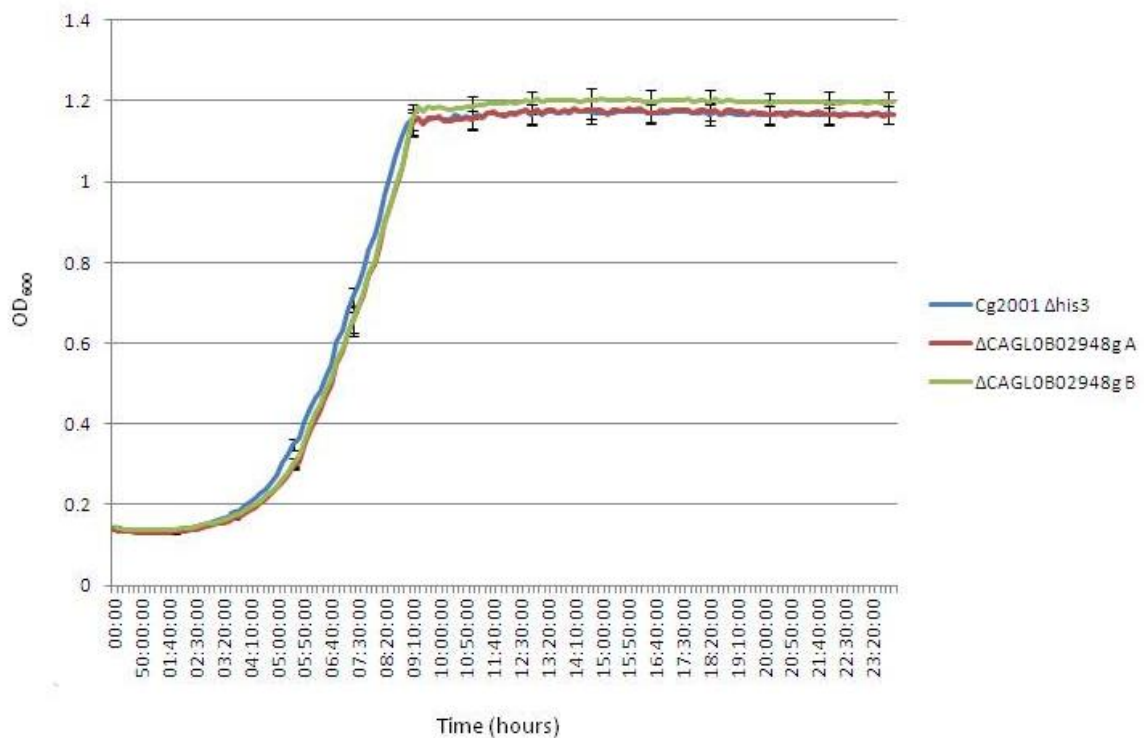


Figure 8: Growth profile of *C. glabrata* parental strain Cg2001 $\Delta his3$ and $\Delta CAGL0B02970g$.

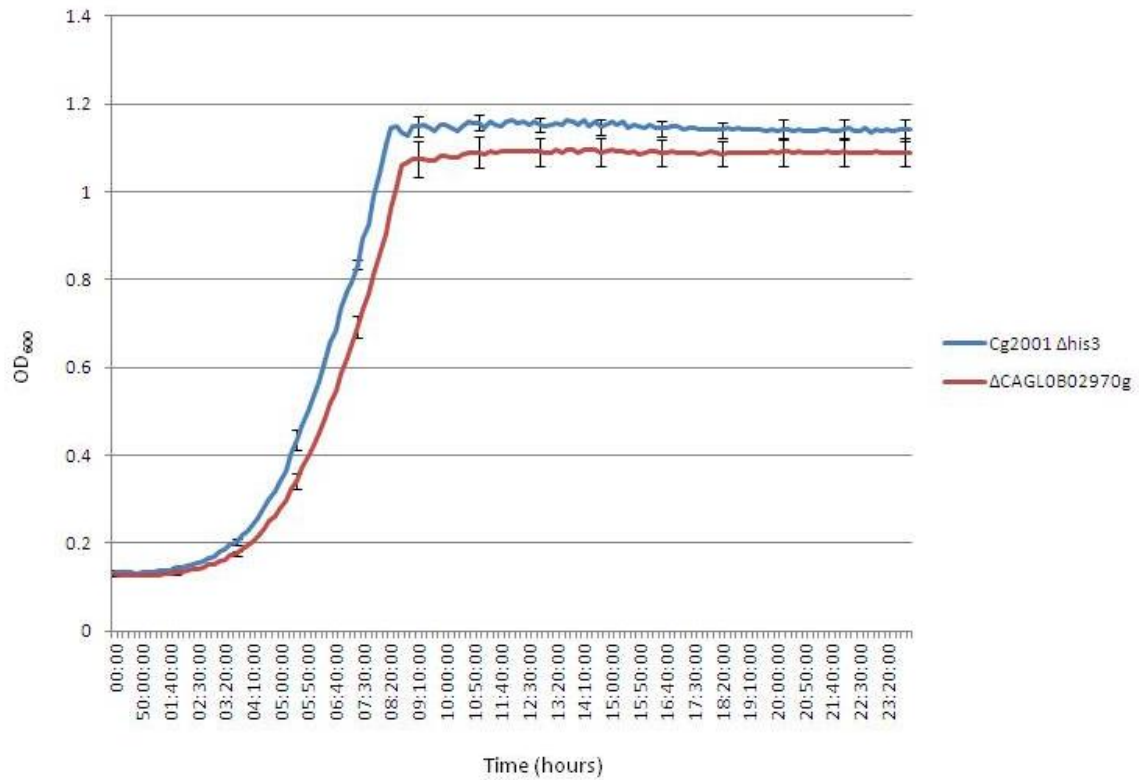


Figure 9: Growth profile of *C. glabrata* parental strain Cg2001 $\Delta his3$ and $\Delta CAGL0B03223g$ isolates A and B.

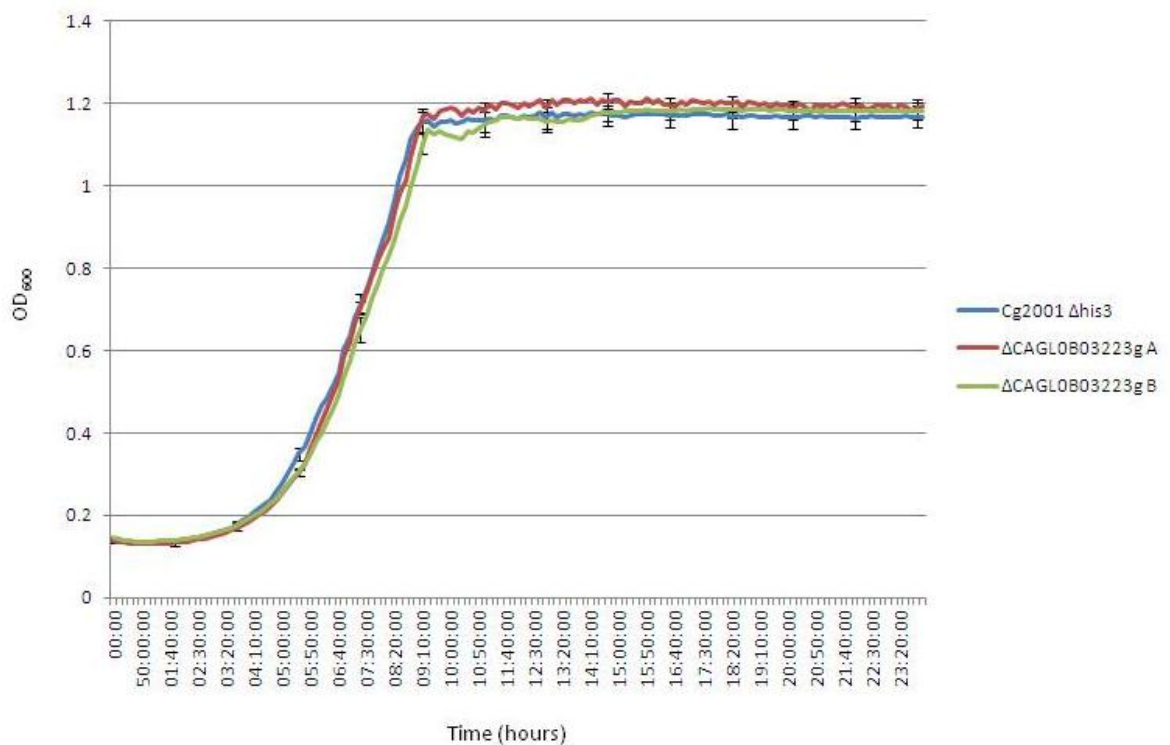


Figure 10: Growth profile of *C. glabrata* parental strain Cg2001 $\Delta his3$ and $\Delta CAGL0B03883g$ isolates A and B.

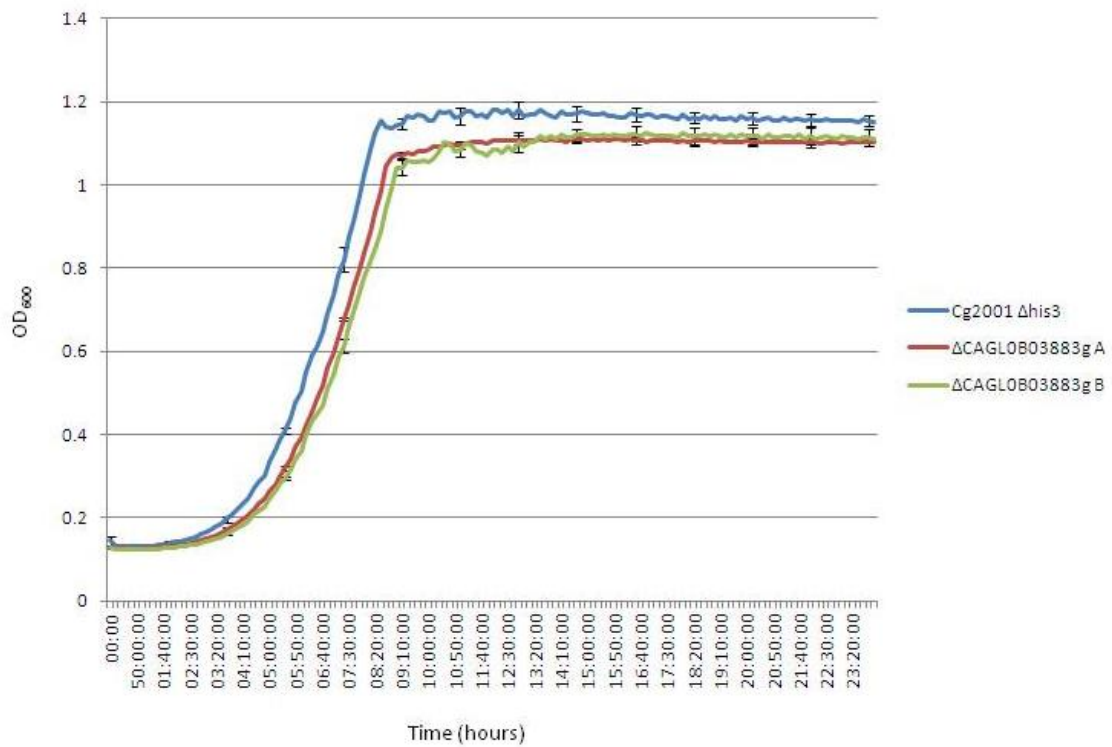


Figure 11: Growth profile of *C. glabrata* parental strain Cg2001 $\Delta his3$ and $\Delta CAGL0C00253g$ isolates A and B.

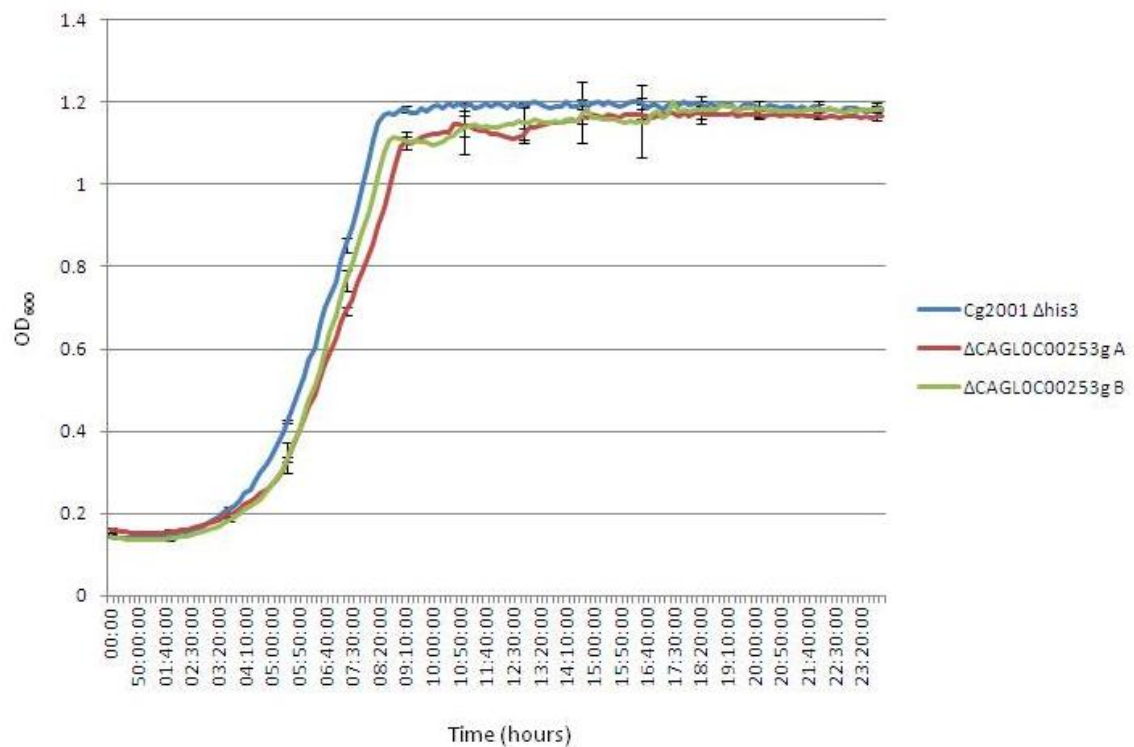


Figure 12: Growth profile of *C. glabrata* parental strain Cg2001 $\Delta his3$ and $\Delta CAGLOC01837g$ isolates A and B.

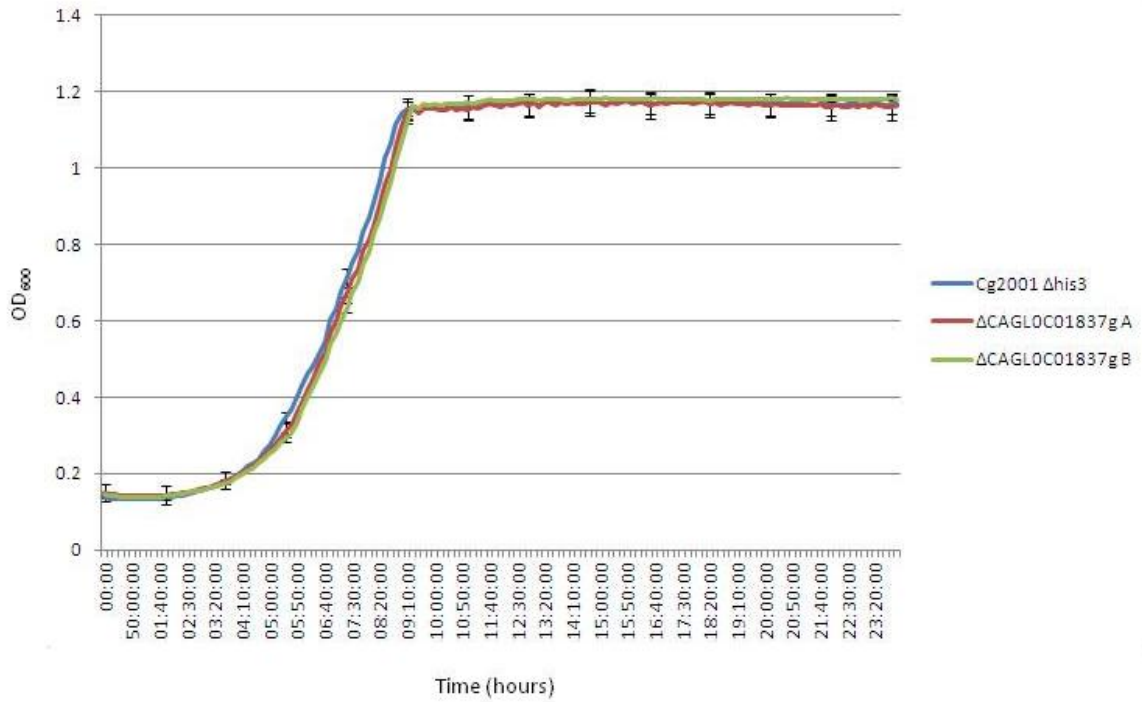


Figure 13: Growth profile of *C. glabrata* parental strain Cg2001 $\Delta his3$ and $\Delta CAGLOC04763g$ isolates A and B.

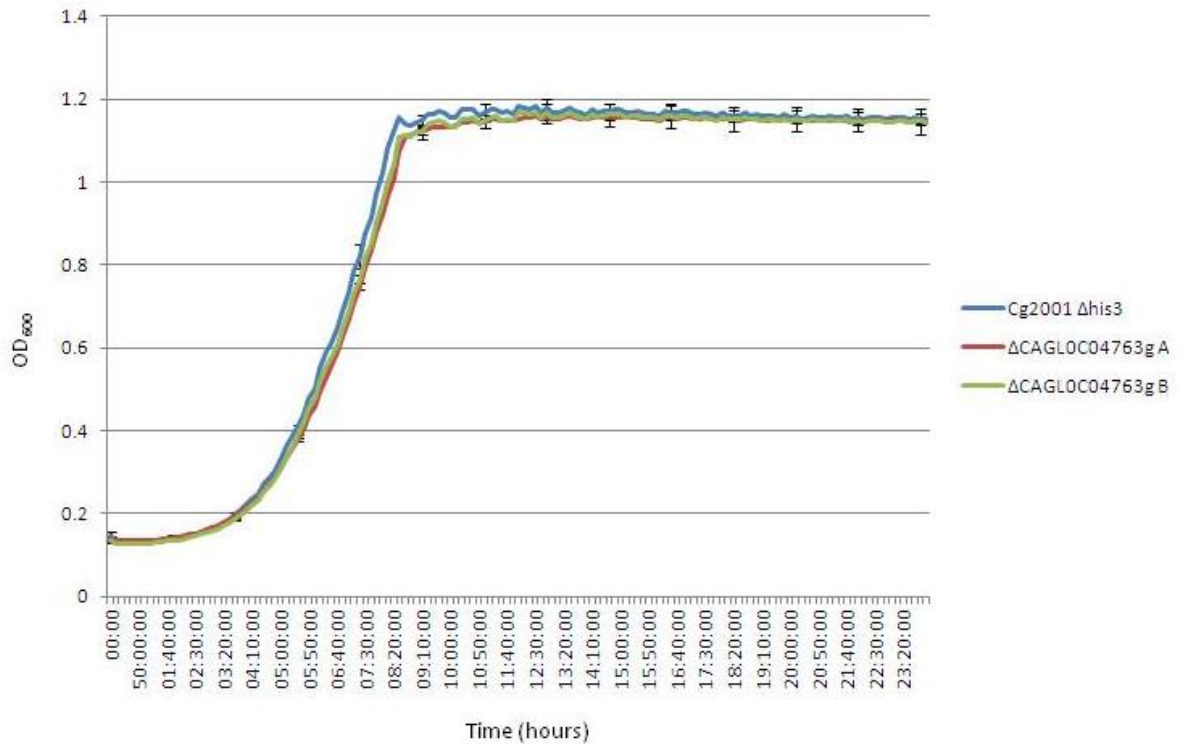


Figure 14: Growth profile of *C. glabrata* parental strain Cg2001 $\Delta his3$ and $\Delta CAGL0D00682g$ isolates A and B.

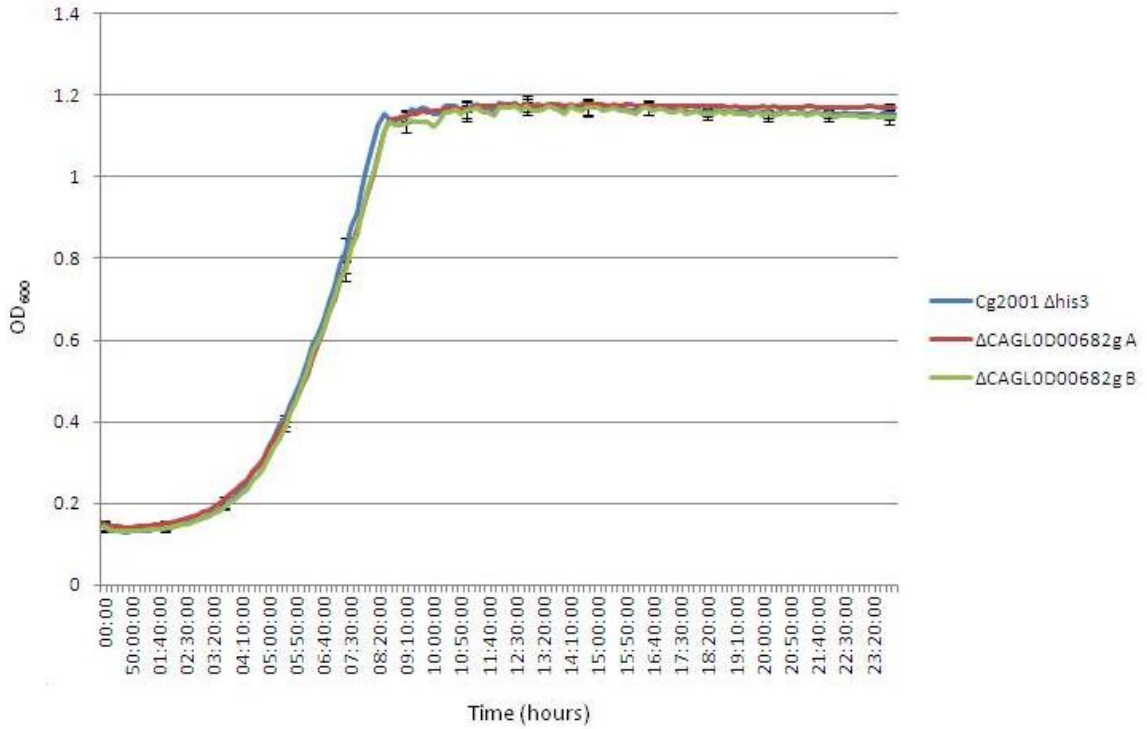


Figure 15: Growth profile of *C. glabrata* parental strain Cg2001 $\Delta his3$ and $\Delta CAGL0D01210g$ isolates A and B.

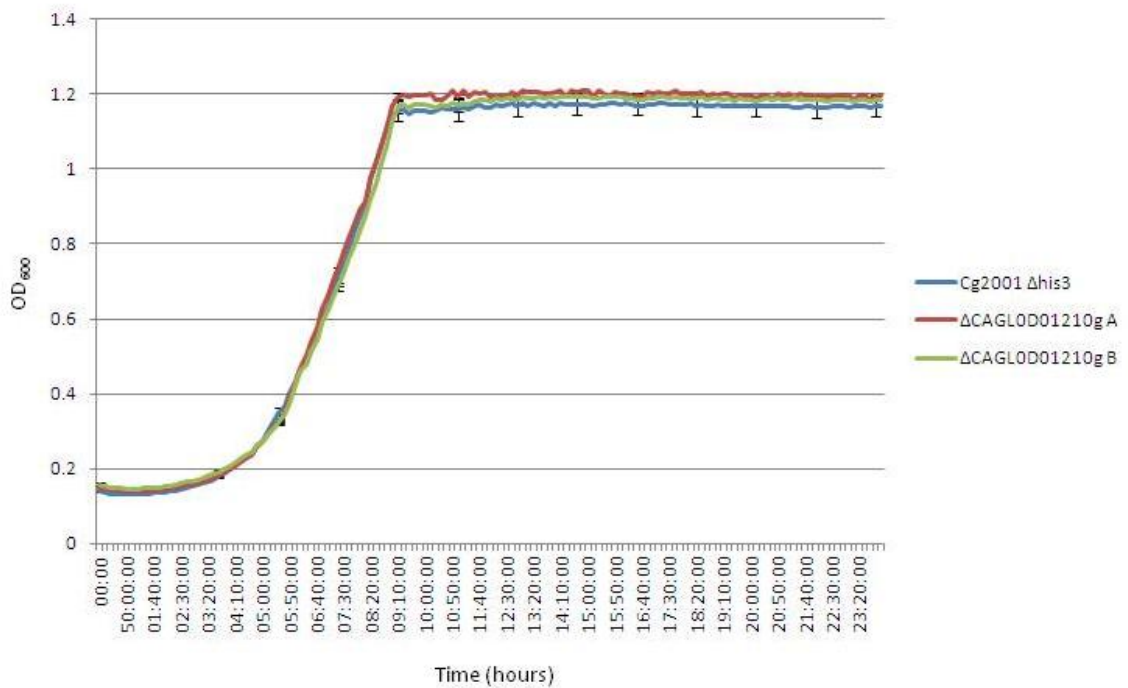


Figure 16: Growth profile of *C. glabrata* parental strain Cg2001 $\Delta his3$ and $\Delta CAGL0D03850g$ isolates A and B.

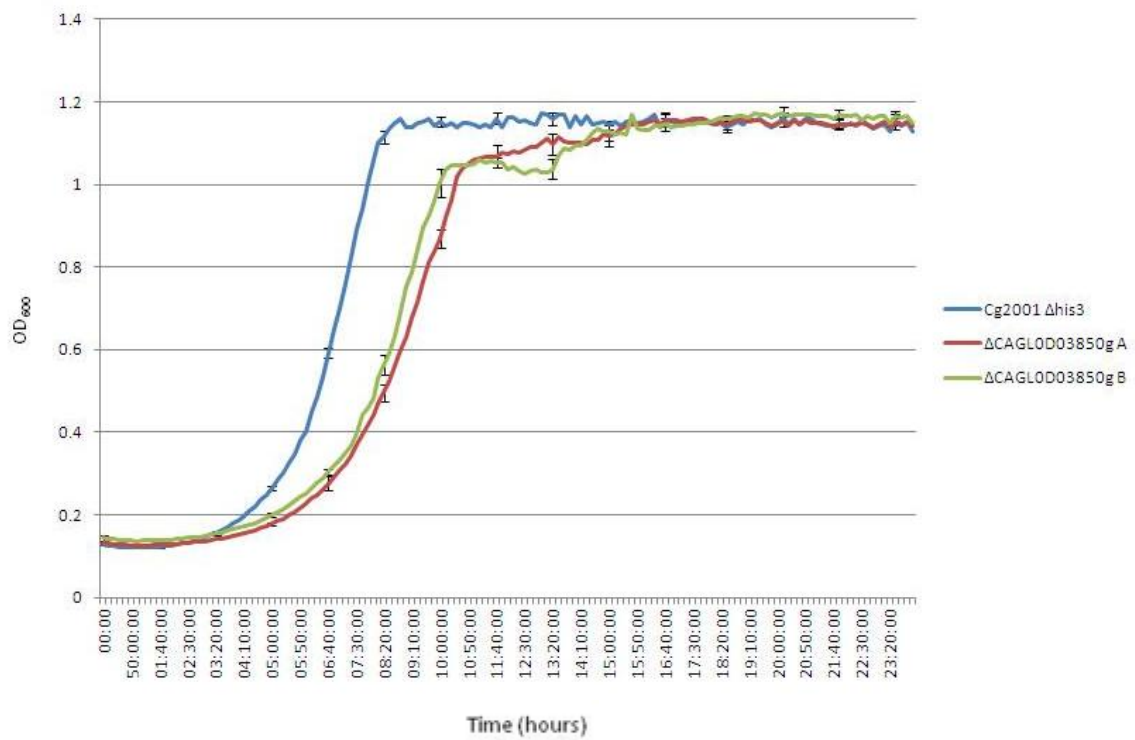


Figure 17: Growth profile of *C. glabrata* parental strain Cg2001 $\Delta his3$ and $\Delta CAGL0D03872g$ isolates A and B.

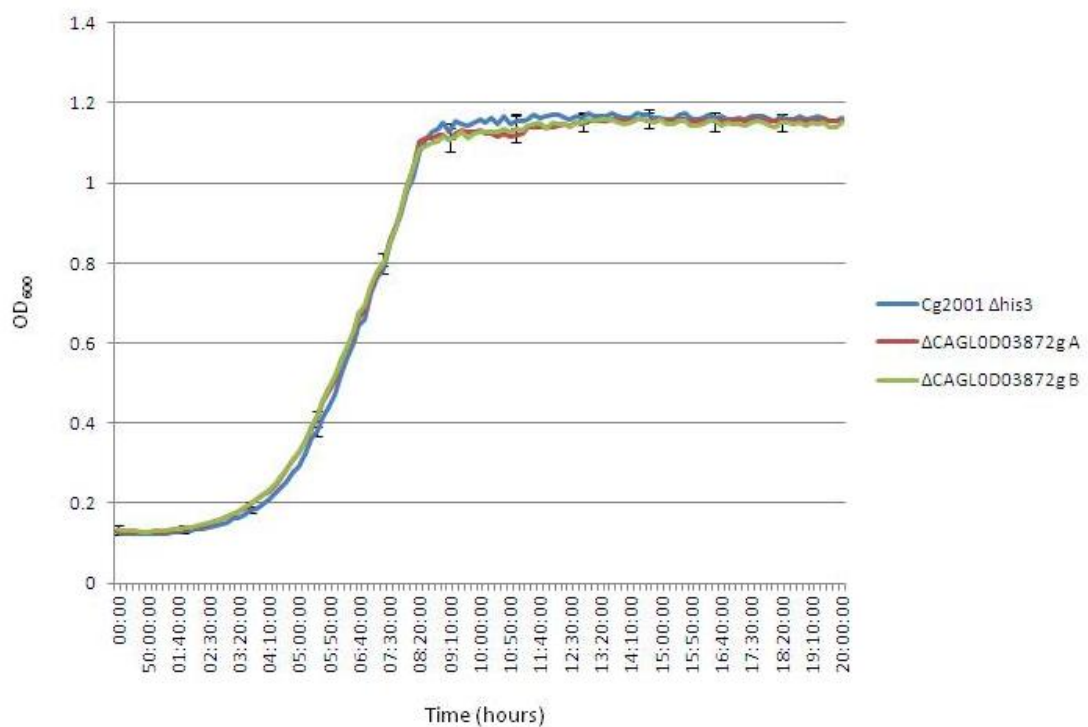


Figure 18: Growth profile of *C. glabrata* parental strain Cg2001 $\Delta his3$ and $\Delta CAGL0D05170g$ isolates A and B.

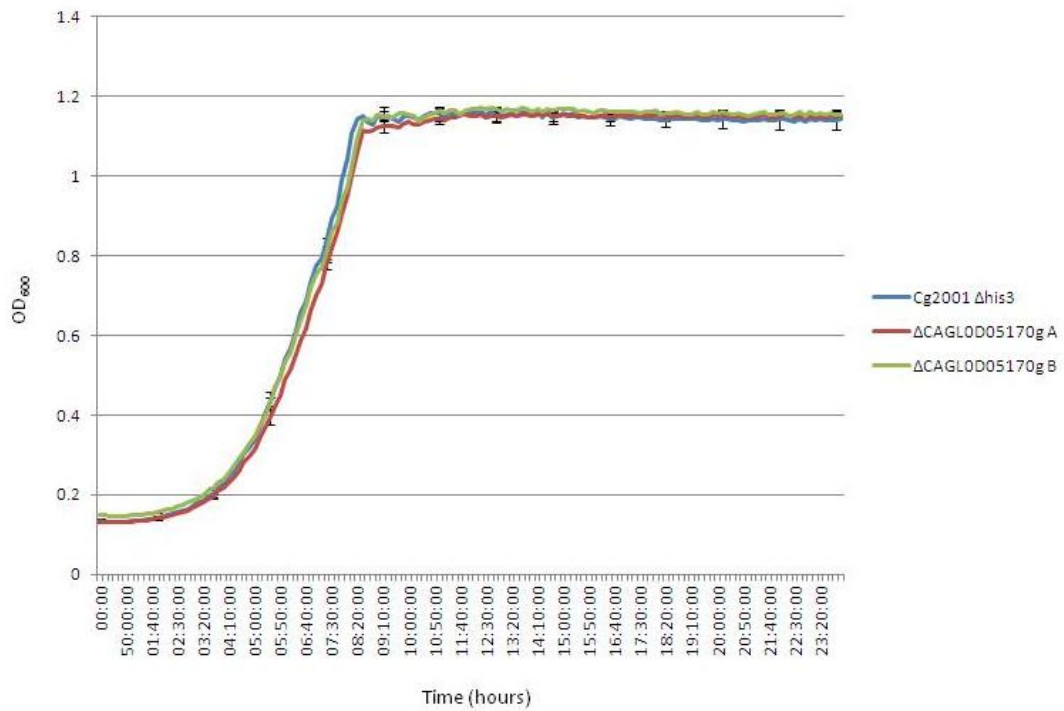


Figure 19: Growth profile of *C. glabrata* parental strain Cg2001 $\Delta his3$ and $\Delta CAGL0D05434g$ isolates A and B.

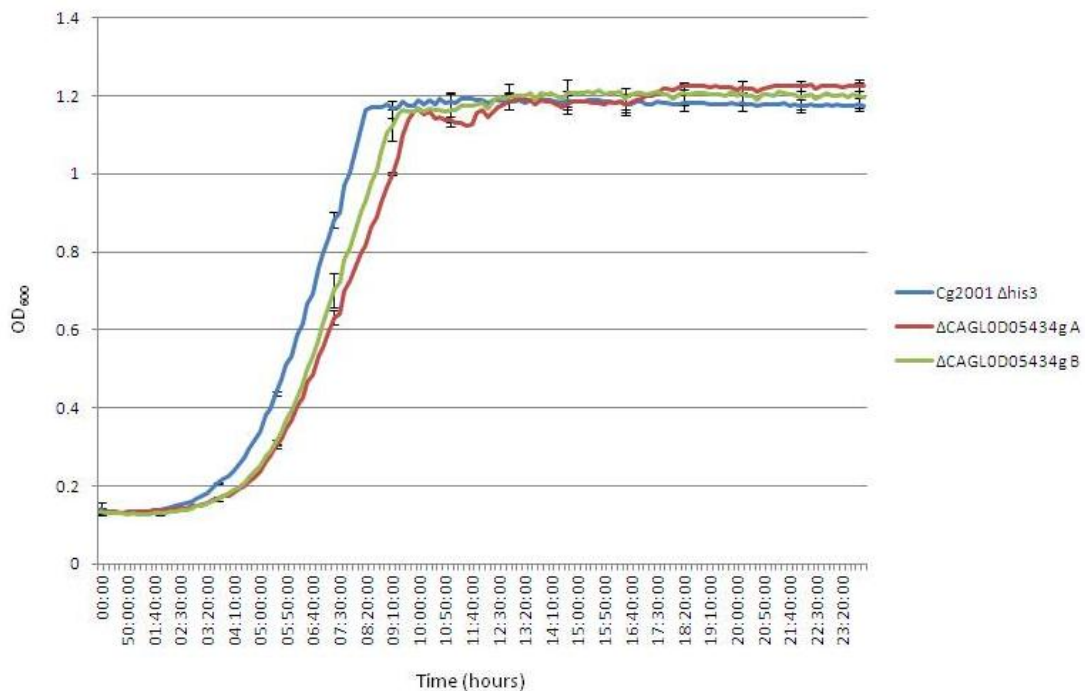


Figure 20: Growth profile of *C. glabrata* parental strain Cg2001 $\Delta his3$ and $\Delta CAGL0D06226g$ isolates A and B.

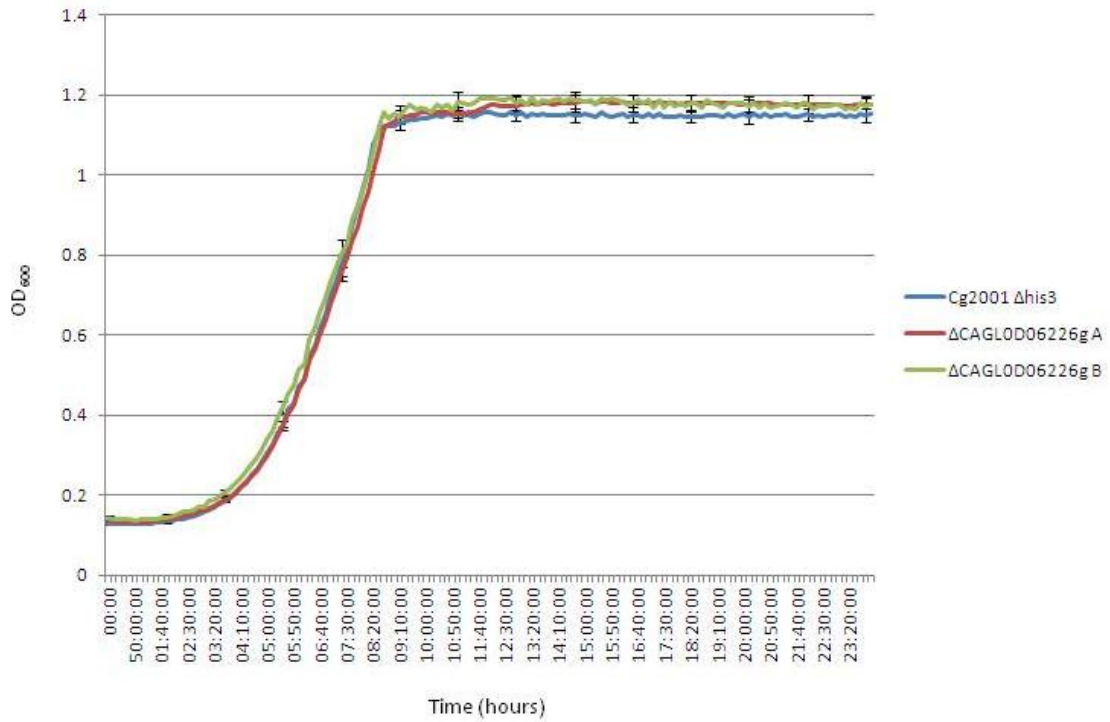


Figure 21: Growth profile of *C. glabrata* parental strain Cg2001 $\Delta his3$ and $\Delta CAGL0E00275g$.

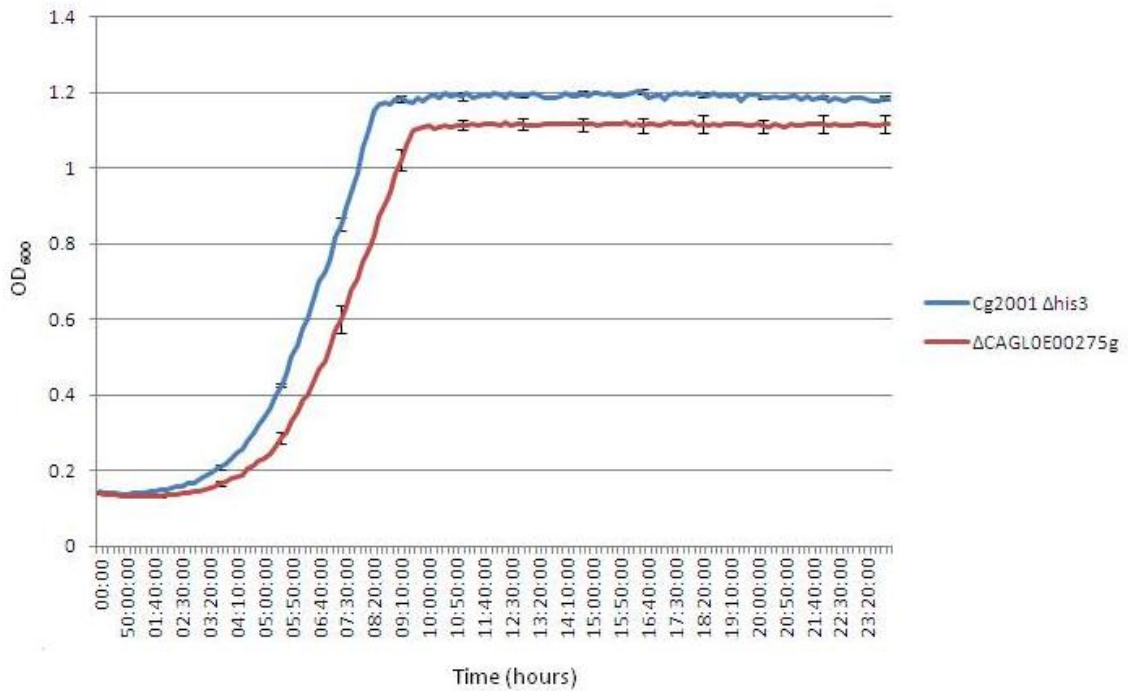


Figure 22: Growth profile of *C. glabrata* parental strain Cg2001 $\Delta his3$ and $\Delta CAGL0E06600g$ isolates A and B.

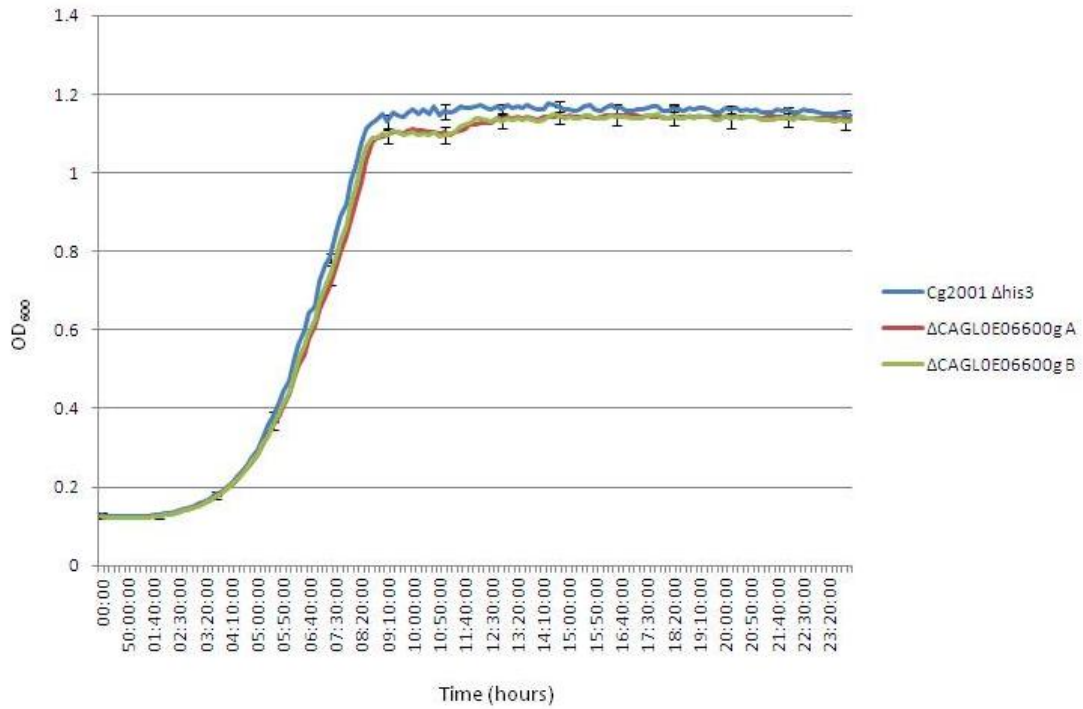


Figure 23: Growth profile of *C. glabrata* parental strain Cg2001 $\Delta his3$ and $\Delta CAGL0E06644g$ isolates A and B.

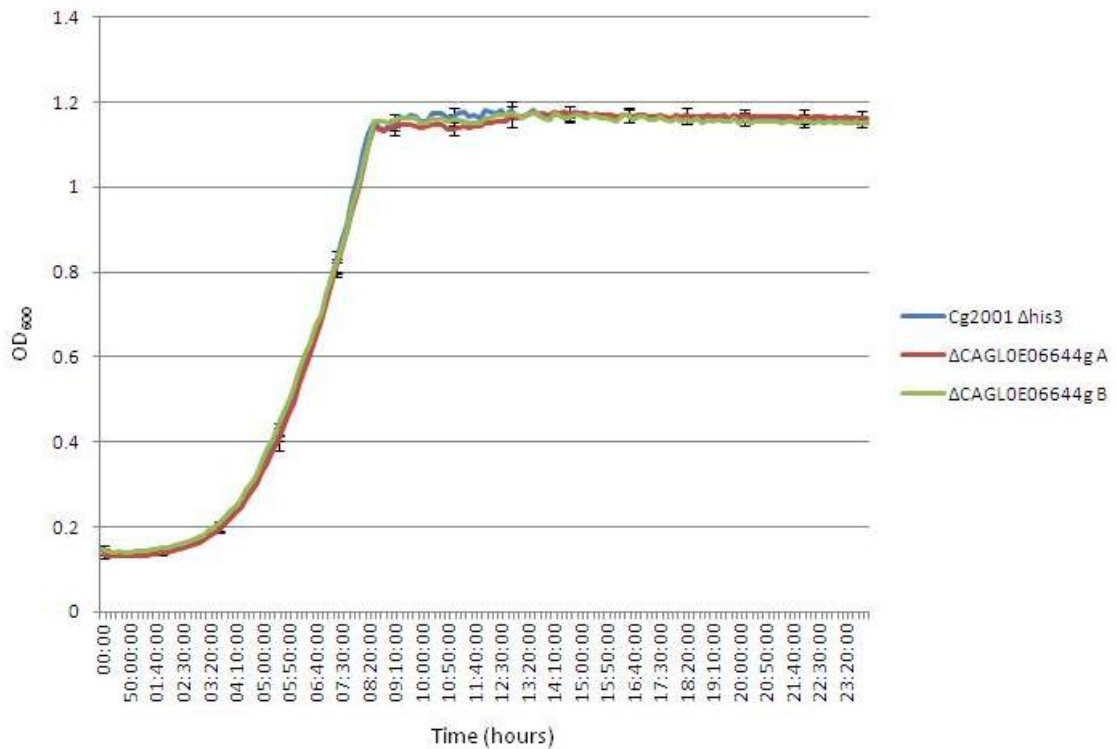


Figure 24: Growth profile of *C. glabrata* parental strain Cg2001 $\Delta his3$ and $\Delta CAGL0F01815g$ isolates A and B.

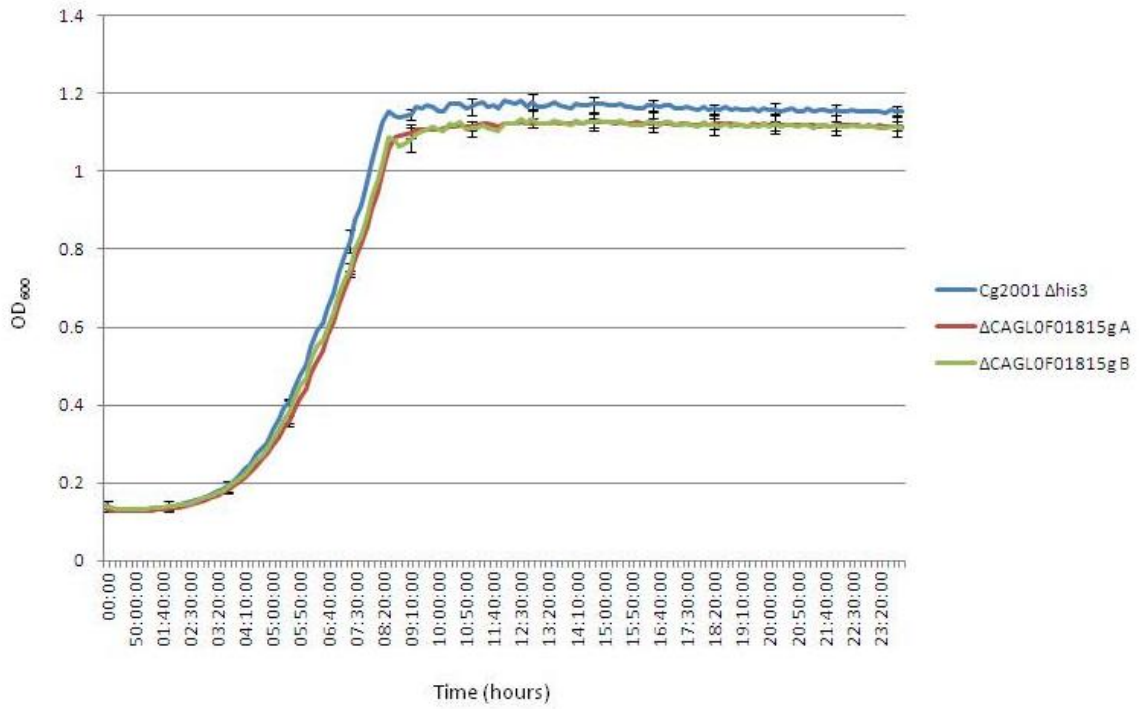


Figure 25: Growth profile of *C. glabrata* parental strain Cg2001 $\Delta his3$ and $\Delta CAGL0F03905g$ isolates A and B.

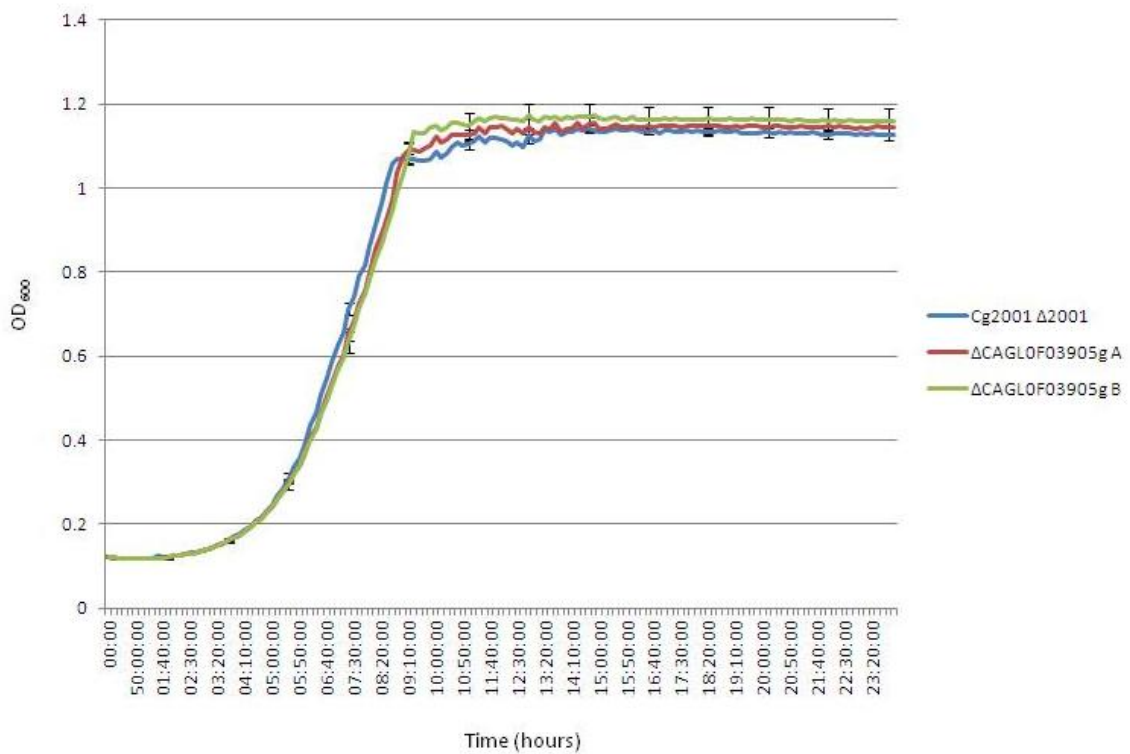


Figure 26: Growth profile of *C. glabrata* parental strain Cg2001 $\Delta his3$ and $\Delta CAGL0F04081g$.

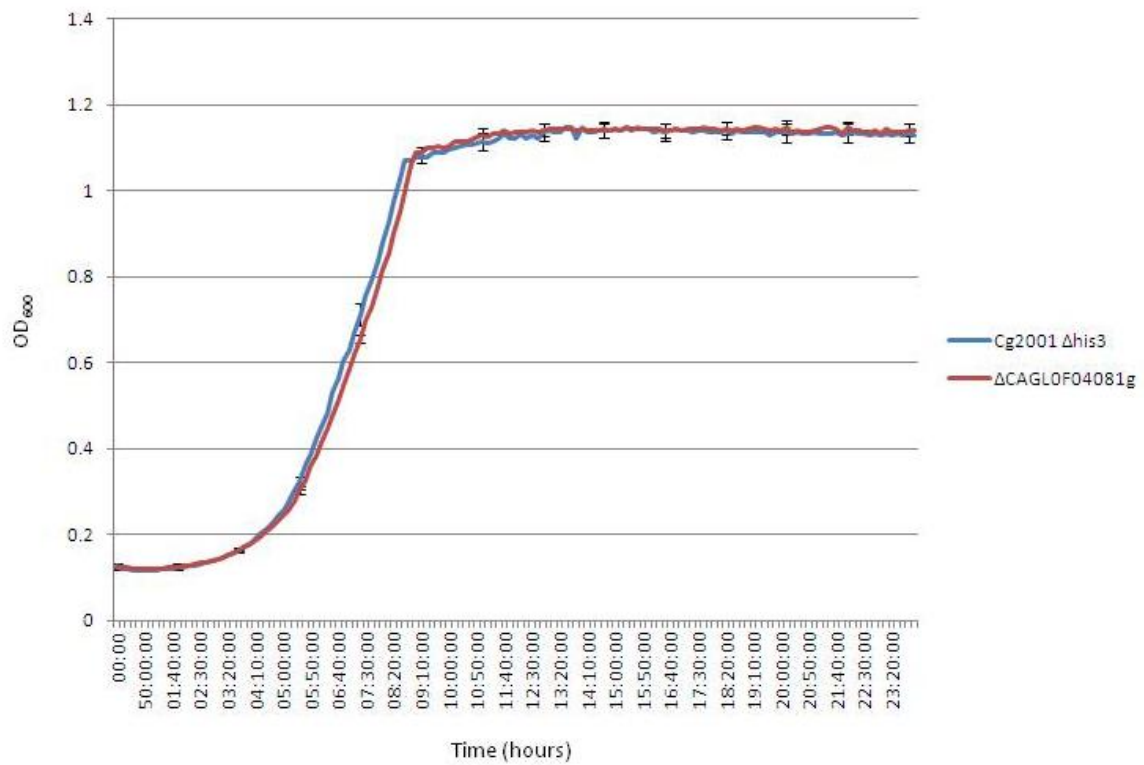


Figure 27: Growth profile of *C. glabrata* parental strain Cg2001 $\Delta his3$ and $\Delta CAGL0F05159g$ isolates A and B.

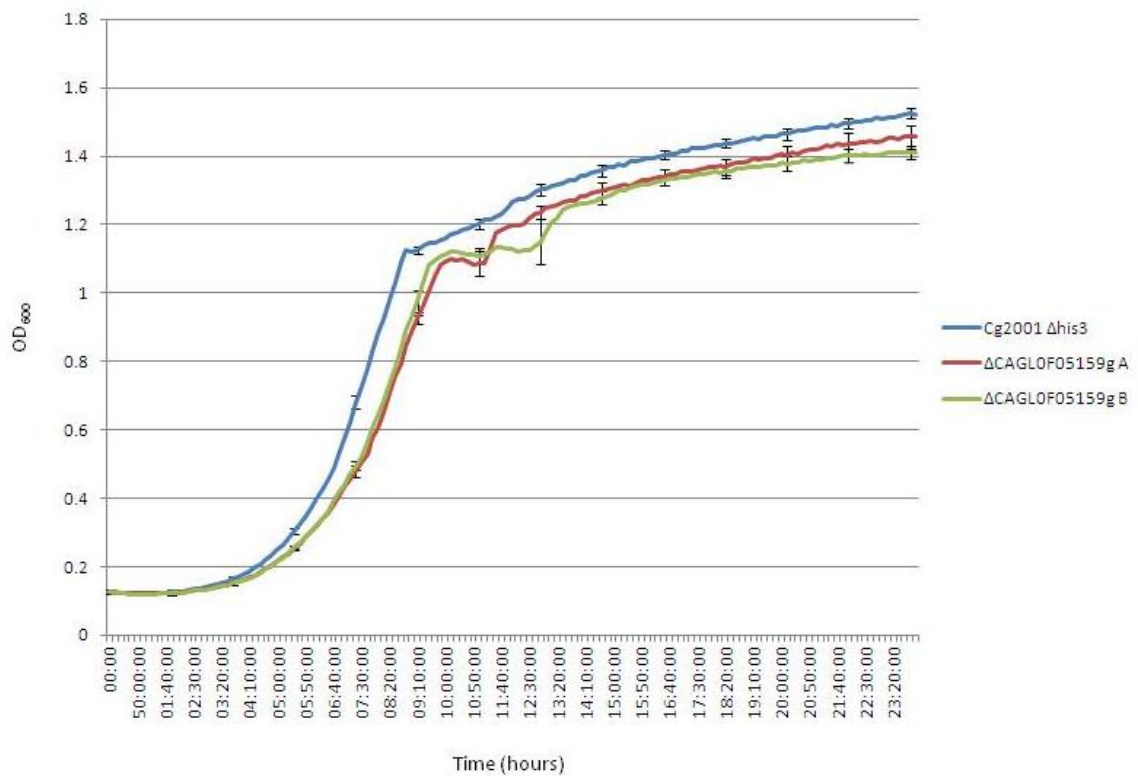


Figure 28: Growth profile of *C. glabrata* parental strain Cg2001 $\Delta his3$ and $\Delta CAGL0F05973g$.

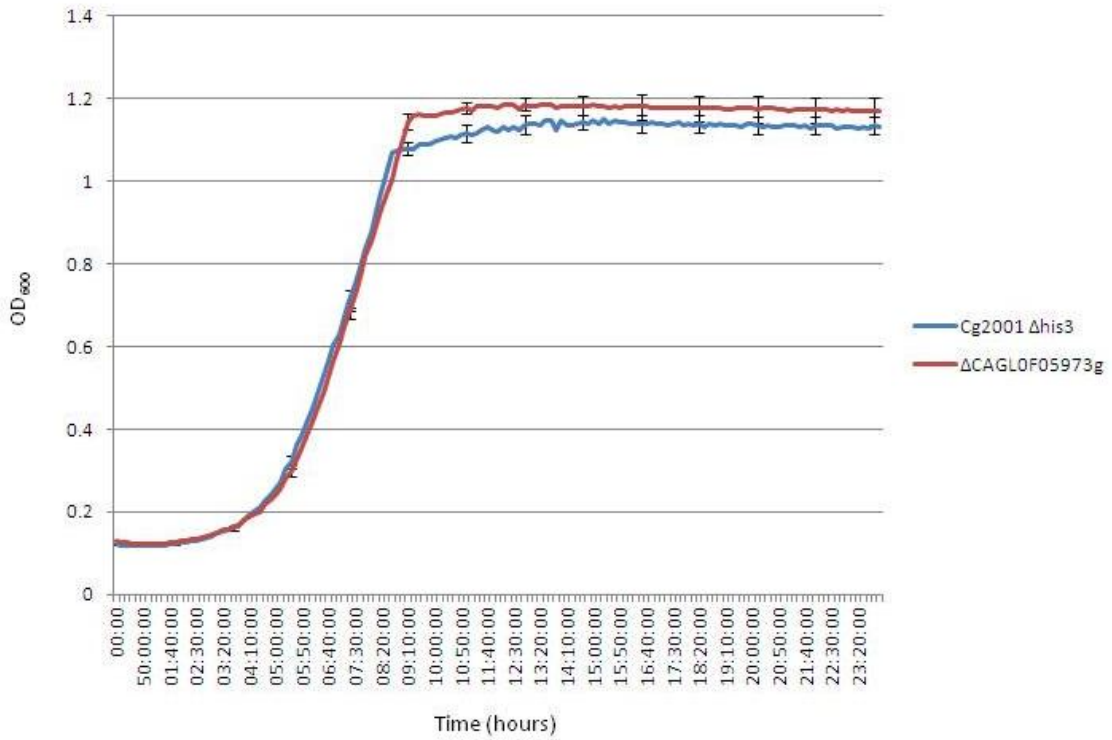


Figure 29: Growth profile of *C. glabrata* parental strain Cg2001 $\Delta his3$ and $\Delta CAGL0F06237g$ isolates A and B.

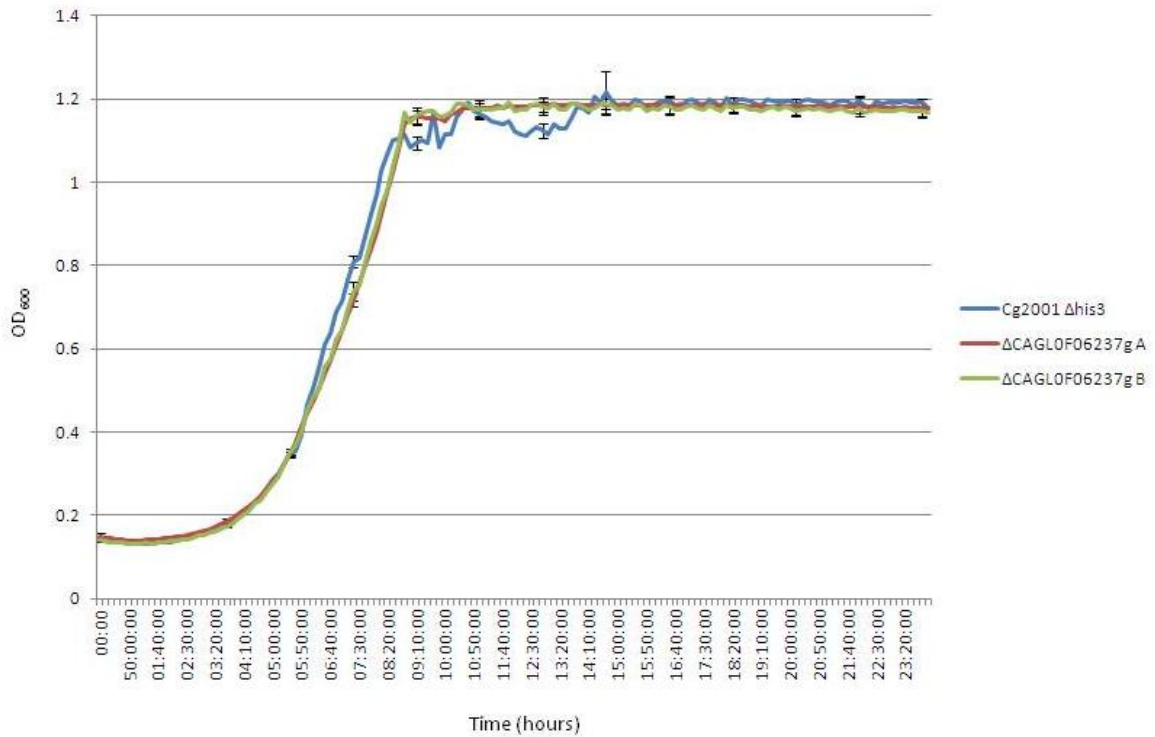


Figure 30: Growth profile of *C. glabrata* parental strain Cg2001 $\Delta his3$ and $\Delta CAGL0F08767g$ isolates A and B.

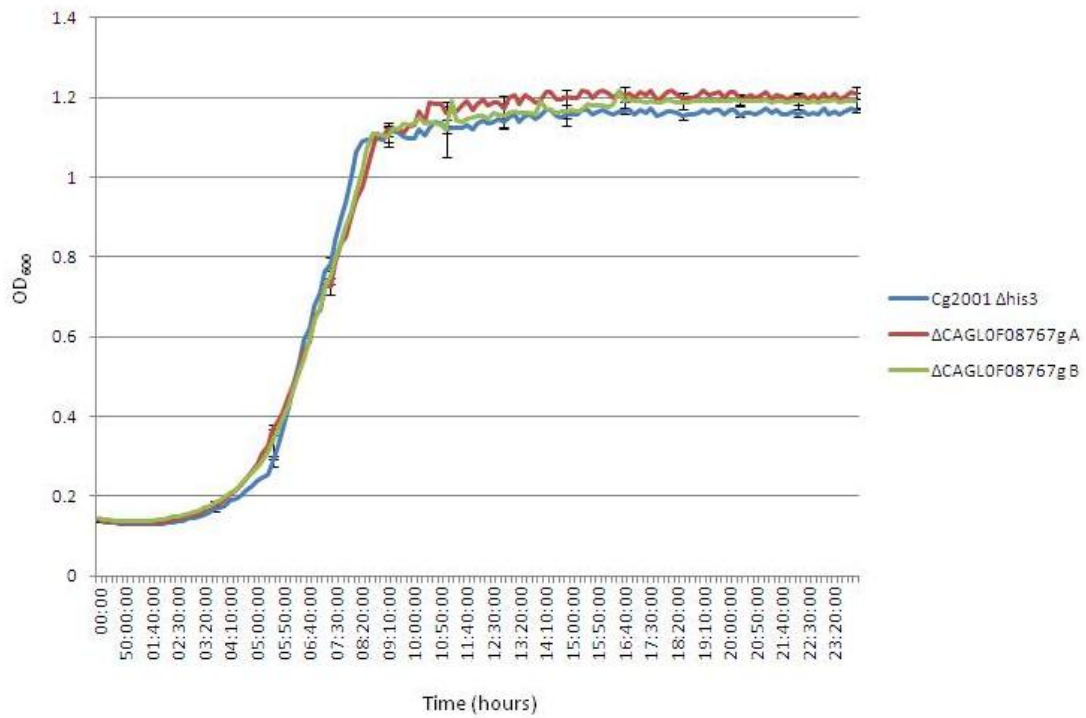


Figure 31: Growth profile of *C. glabrata* parental strain Cg2001 $\Delta his3$ and $\Delta CAGL0F09229g$ isolates A and B.

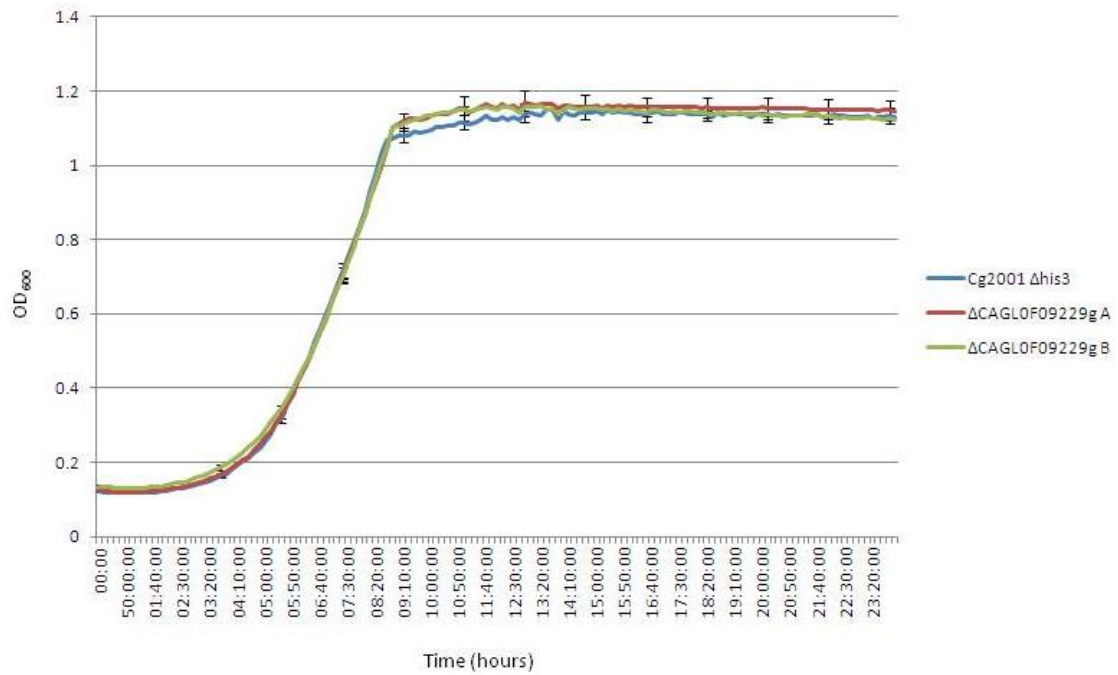


Figure 32: Growth profile of *C. glabrata* parental strain Cg2001 $\Delta his3$ and $\Delta CAGL0G02607g$.

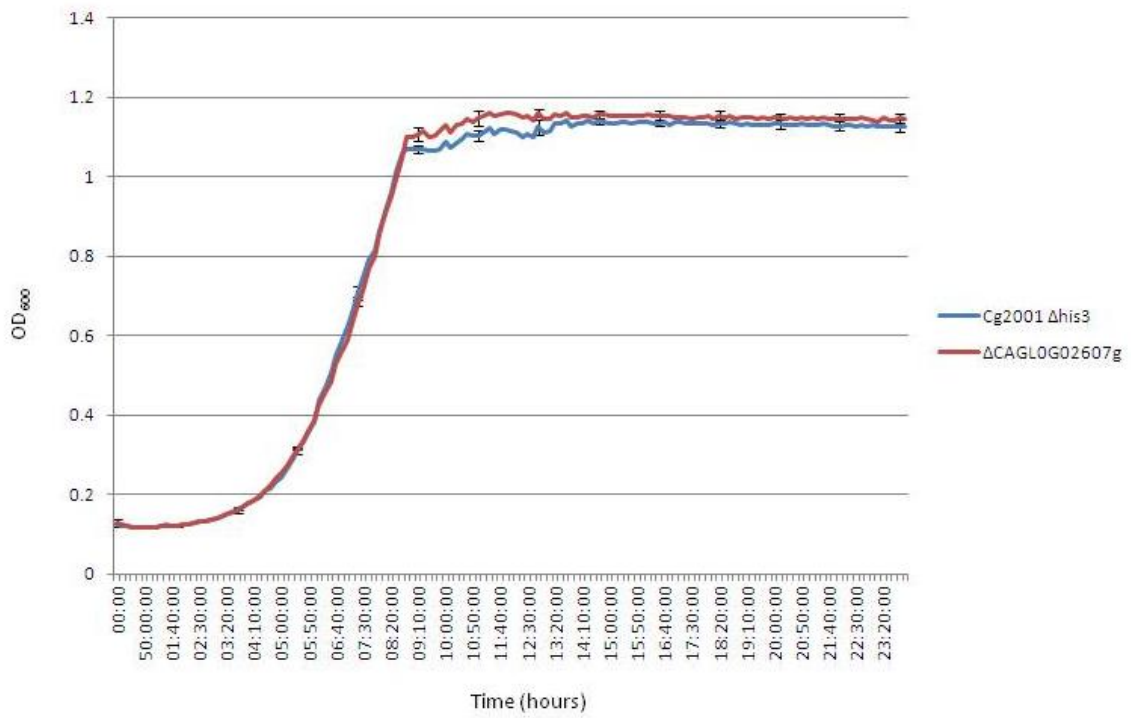


Figure 33: Growth profile of *C. glabrata* parental strain Cg2001 $\Delta his3$ and $\Delta CAGL0G03201g$.

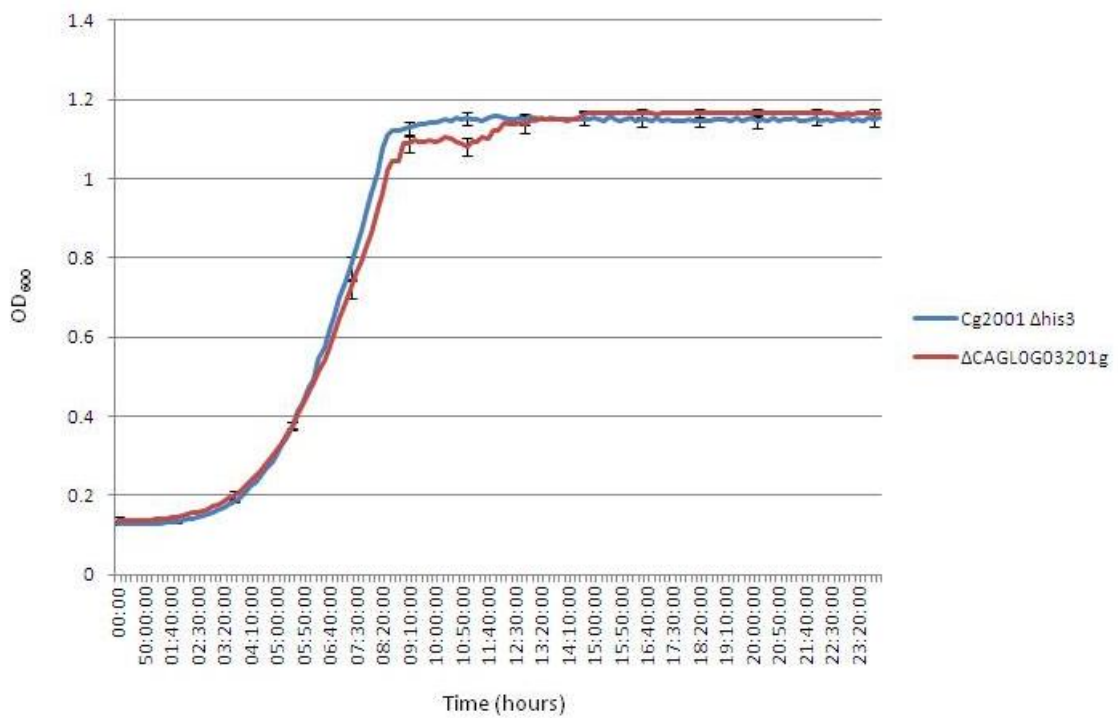


Figure 34: Growth profile of *C. glabrata* parental strain Cg2001 $\Delta his3$ and $\Delta CAGL0G04279g$ isolates A and B.

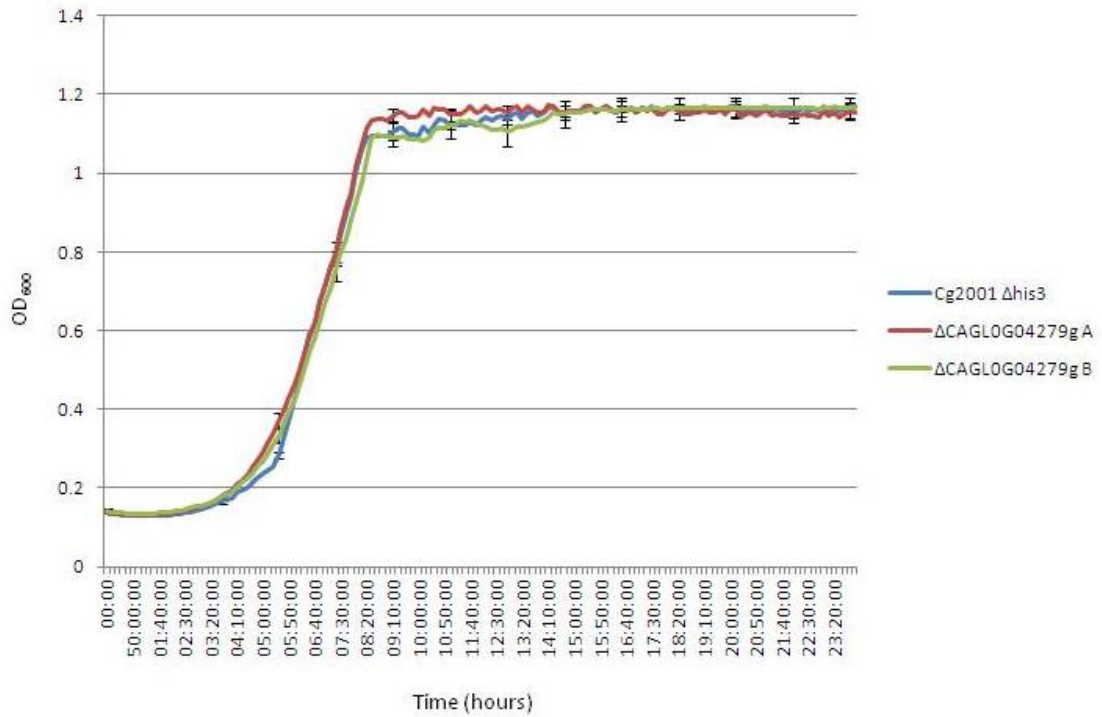


Figure 35: Growth profile of *C. glabrata* parental strain Cg2001 $\Delta his3$ and $\Delta CAGL0G05522g$ isolates A and B.

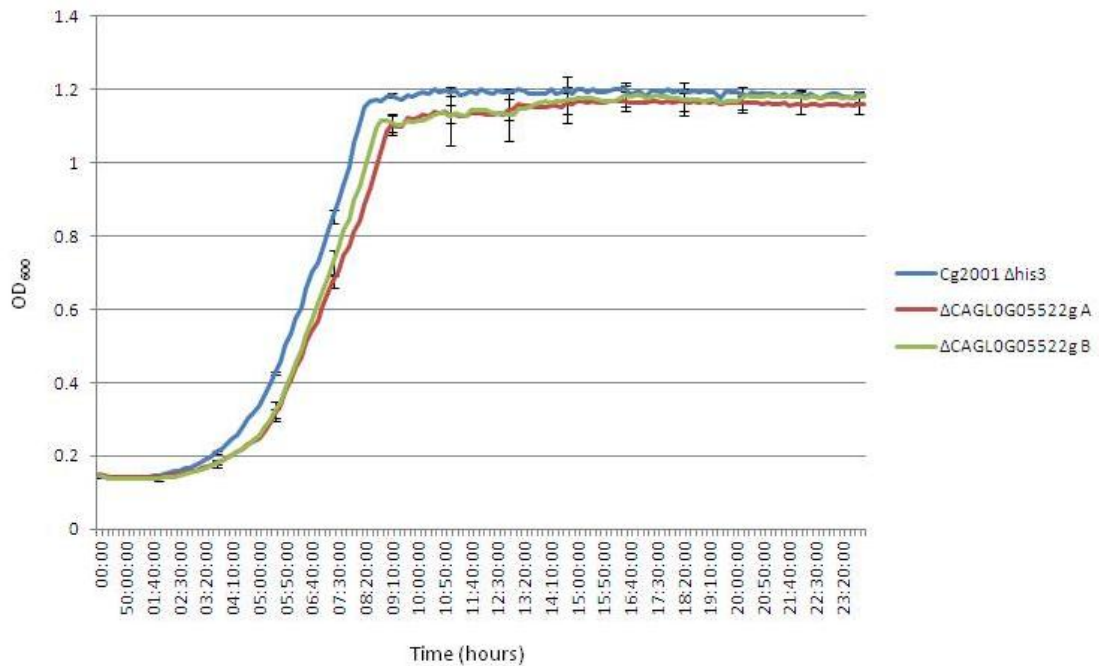


Figure 36: Growth profile of *C. glabrata* parental strain Cg2001 $\Delta his3$ and $\Delta CAGL0G08866g$ isolates A and B.

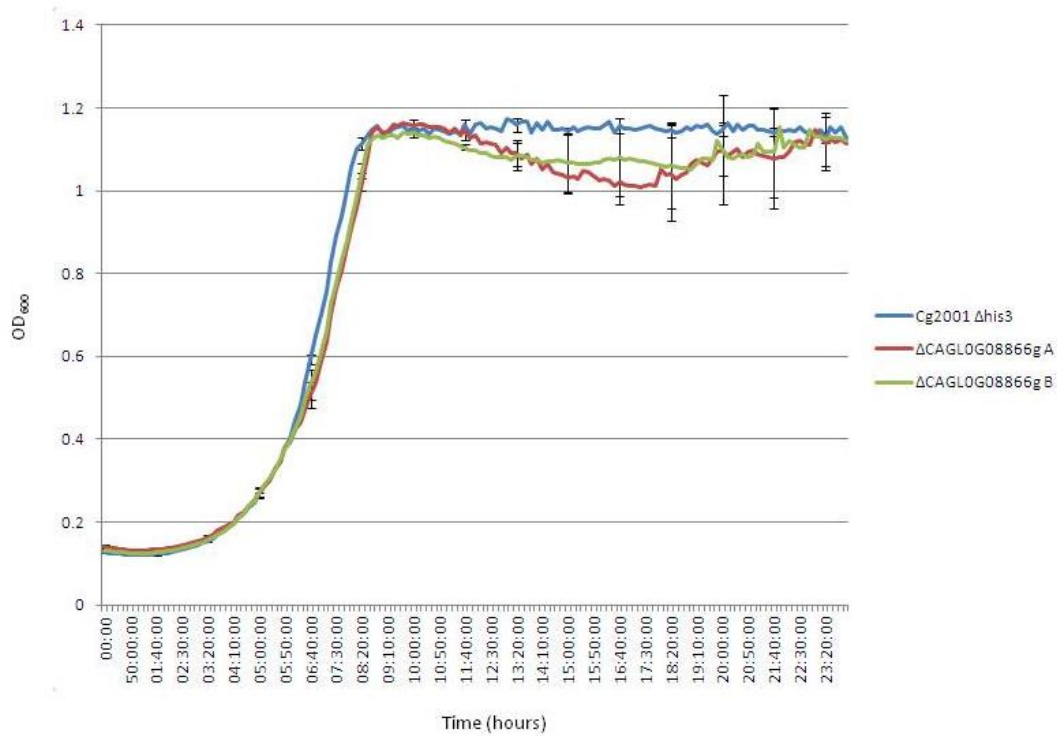


Figure 37: Growth profile of *C. glabrata* parental strain Cg2001 $\Delta his3$ and $\Delta CAGL0G10175g$ isolates A and B.

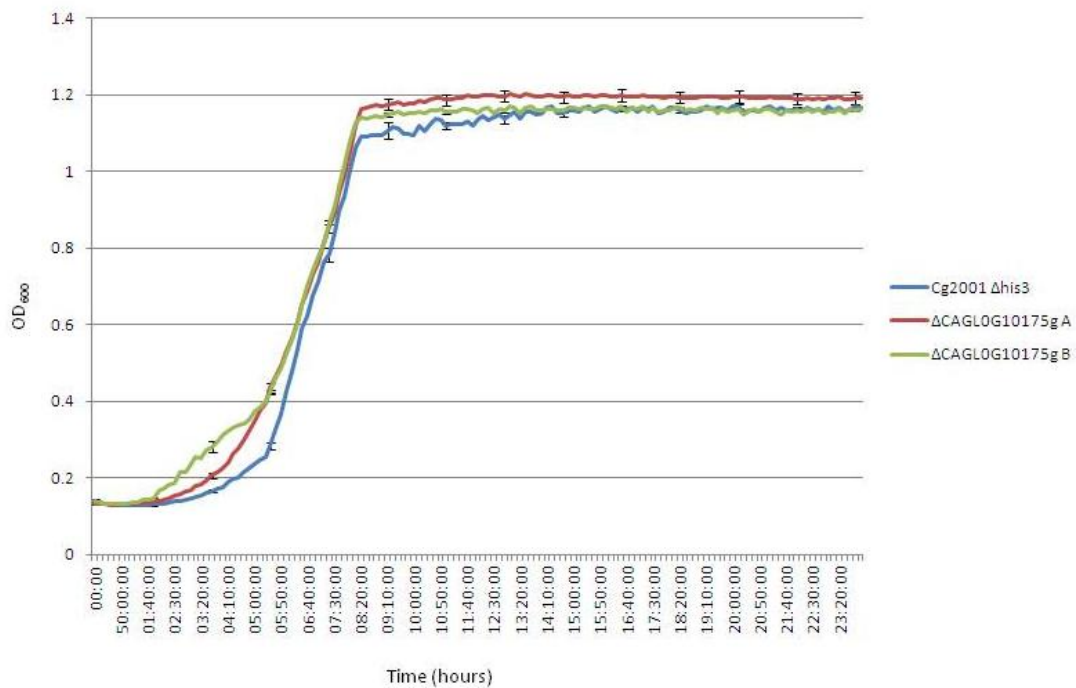


Figure 38: Growth profile of *C. glabrata* parental strain Cg2001 $\Delta his3$ and $\Delta CAGL0H01749g$ isolates A and B.

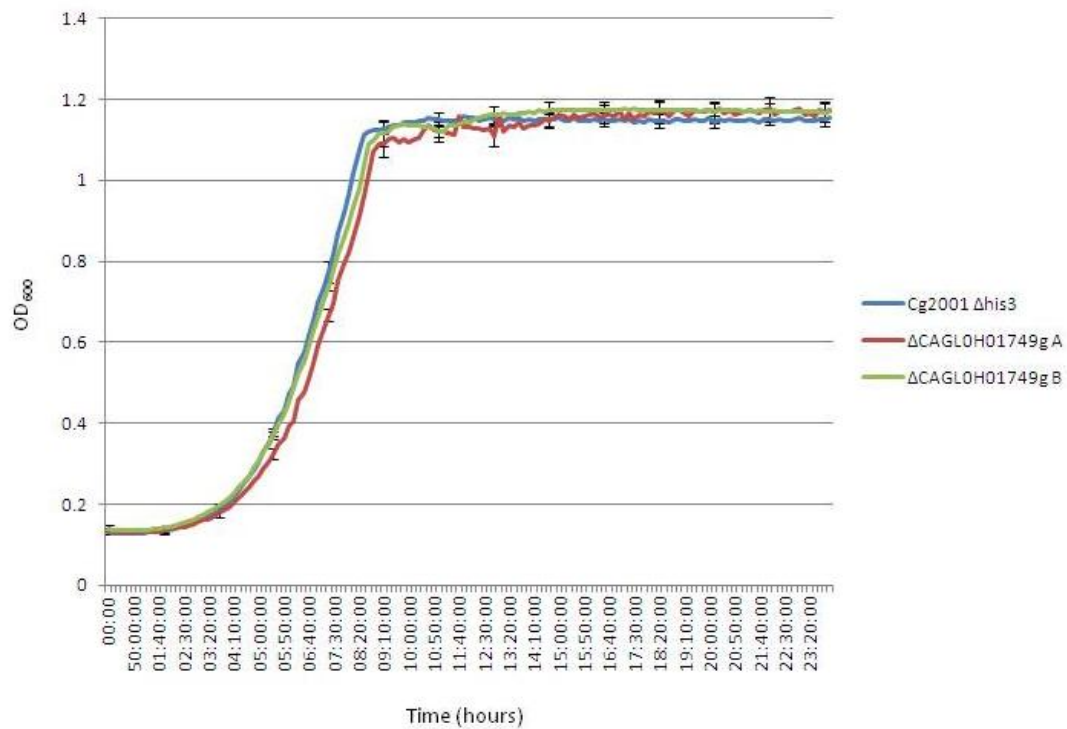


Figure 39: Growth profile of *C. glabrata* parental strain Cg2001 $\Delta his3$ and $\Delta CAGL0H06765g$ isolates A and B.

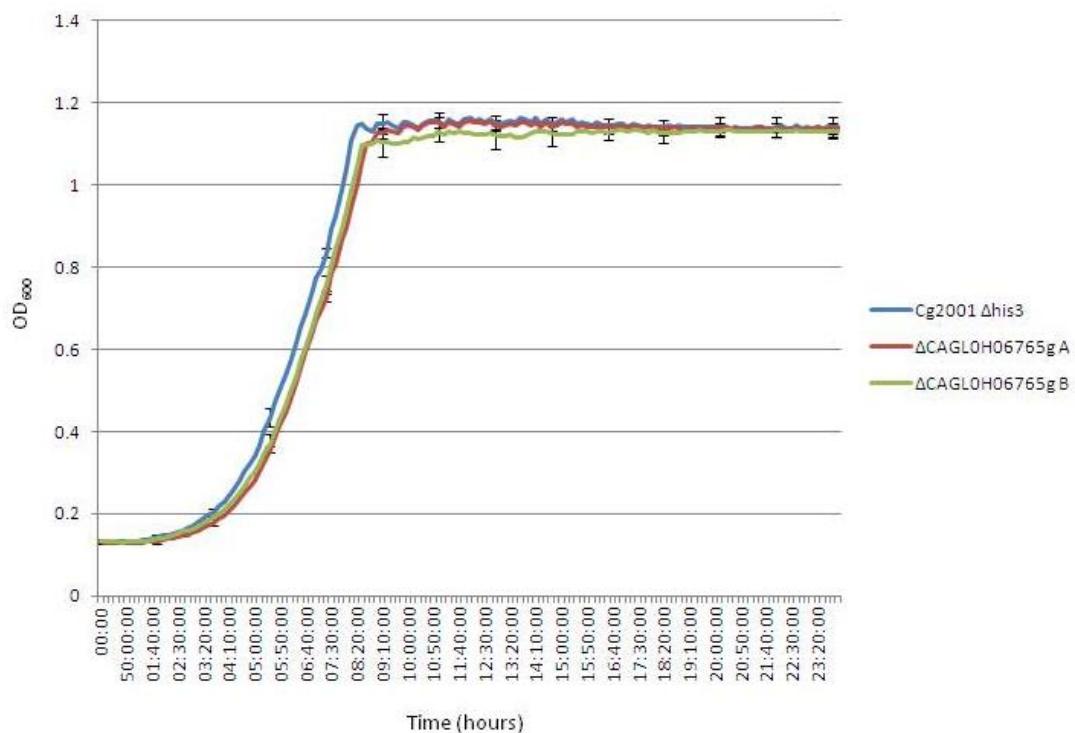


Figure 40: Growth profile of *C. glabrata* parental strain Cg2001 $\Delta his3$ and $\Delta CAGL0H08712g$ isolates A and B.

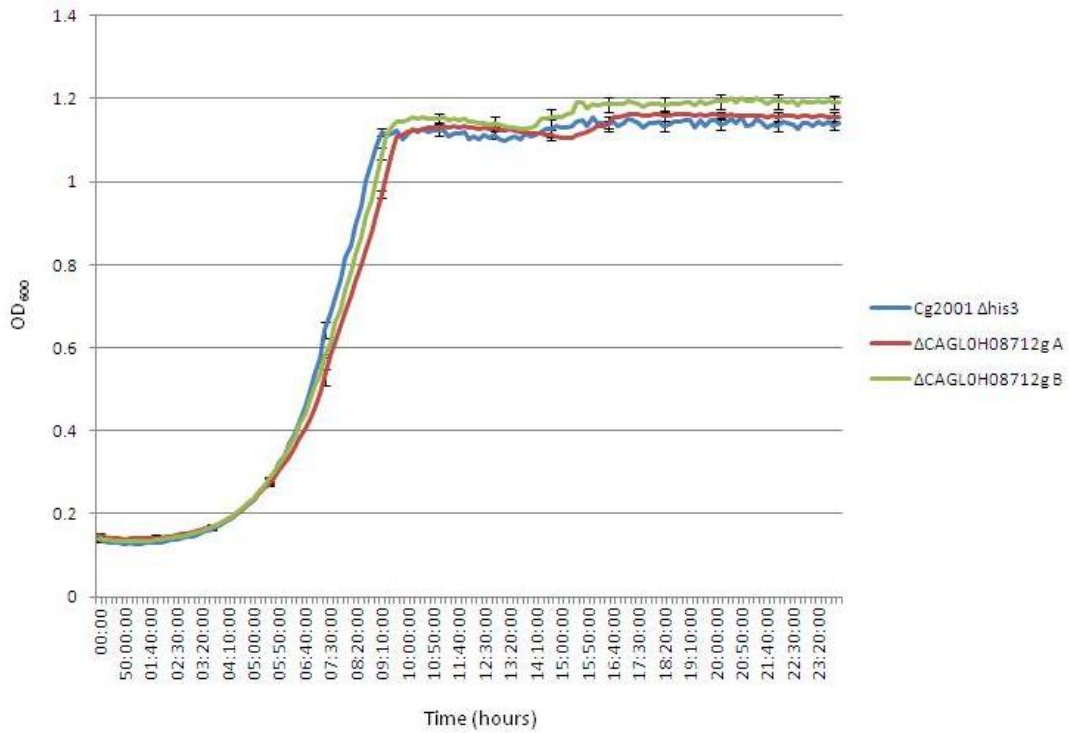


Figure 41: Growth profile of *C. glabrata* parental strain Cg2001 $\Delta his3$ and $\Delta CAGL0H09988g$ isolates A and B.

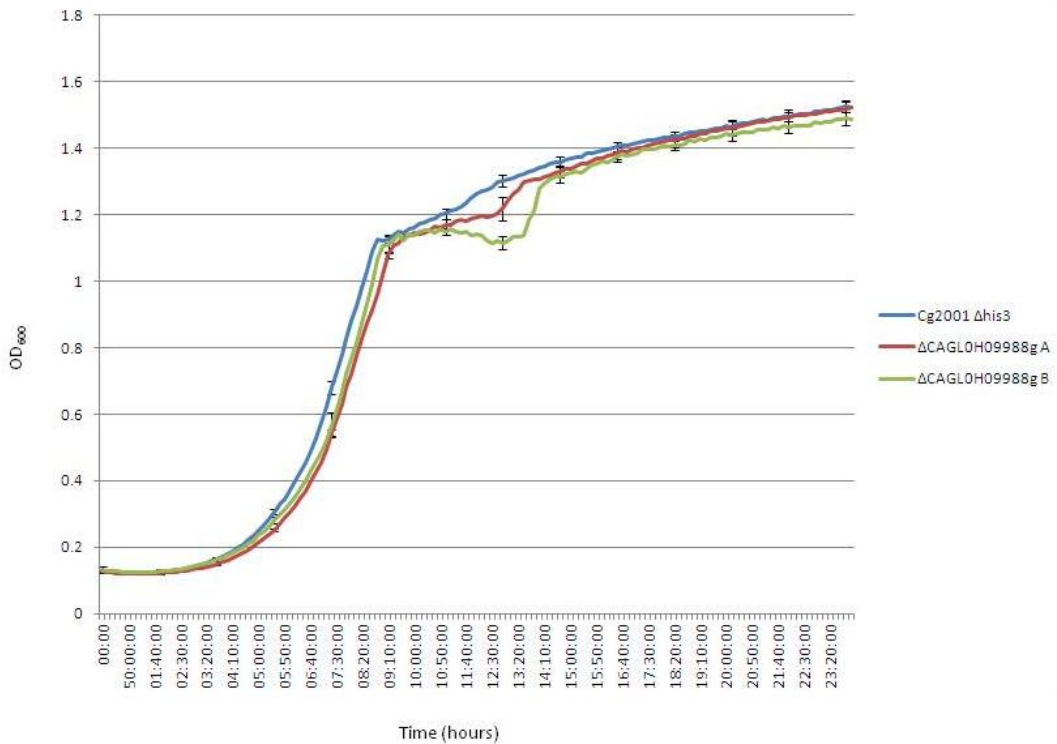


Figure 42: Growth profile of *C. glabrata* parental strain Cg2001 $\Delta his3$ and $\Delta CAGL0H10208g$ isolates A and B.

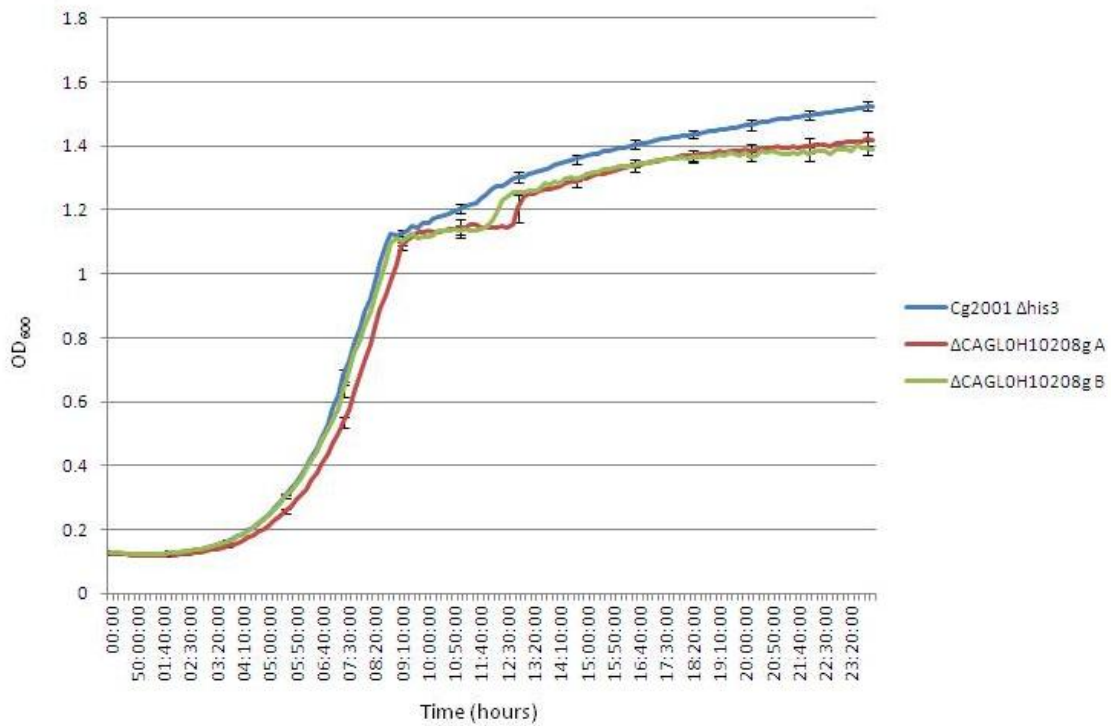


Figure 43: Growth profile of *C. glabrata* parental strain Cg2001 $\Delta his3$ and $\Delta CAGL0I02244g$.

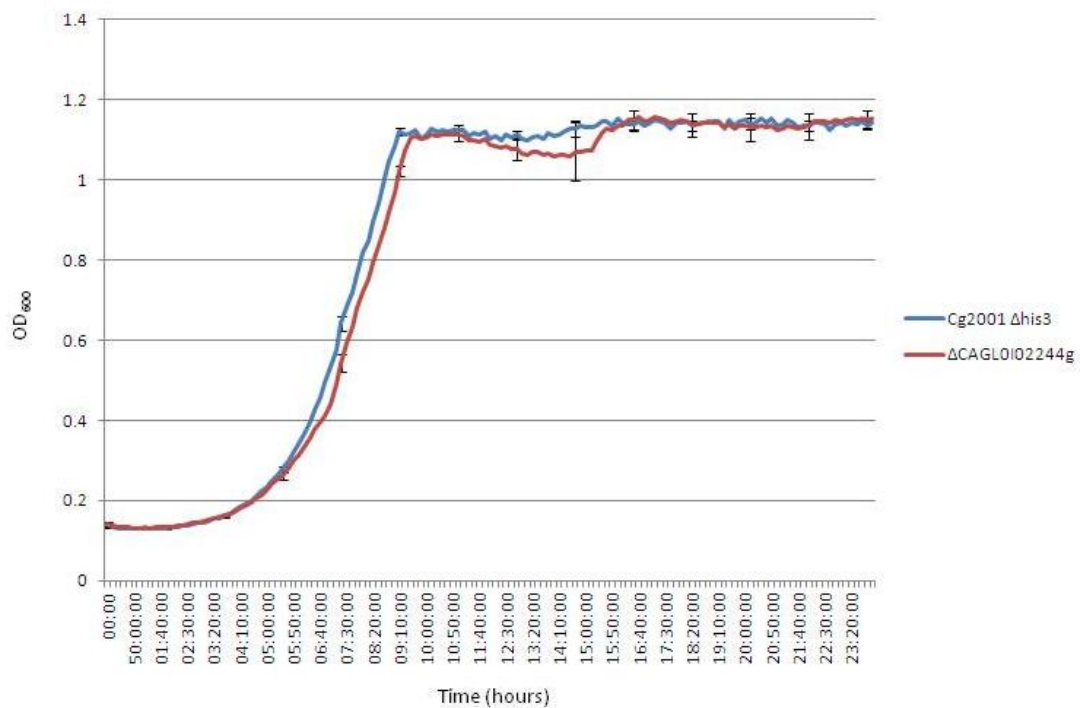


Figure 44: Growth profile of *C. glabrata* parental strain Cg2001 $\Delta his3$ and $\Delta CAGL0108437g$.

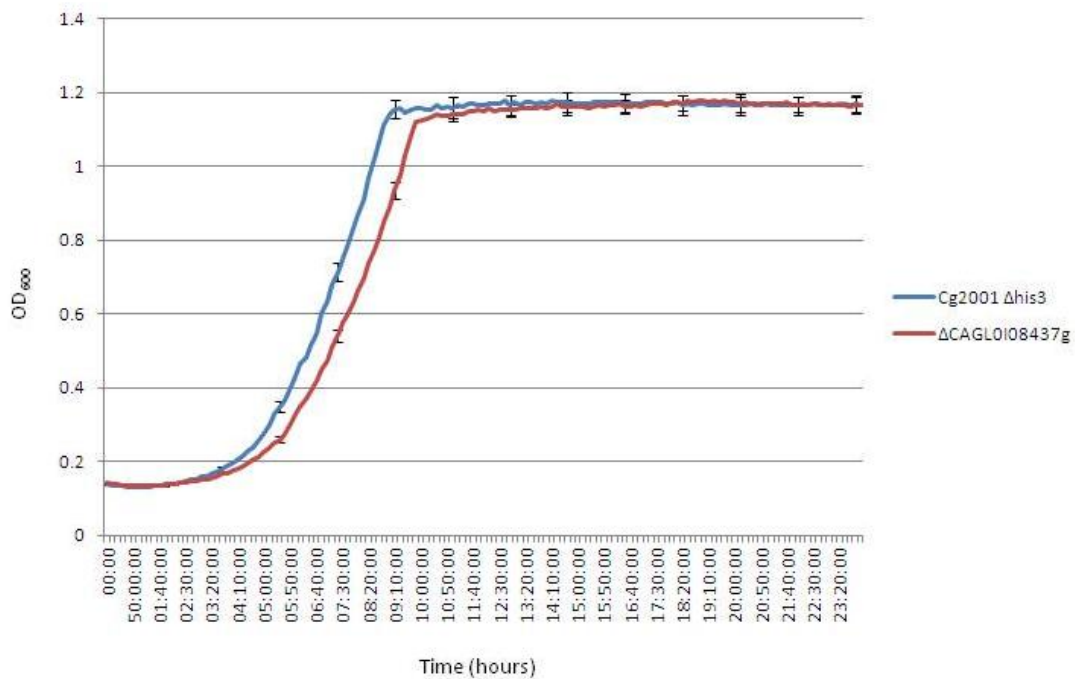


Figure 45: Growth profile of *C. glabrata* parental strain Cg2001 $\Delta his3$ and $\Delta CAGL0108613g$ isolates A and B.

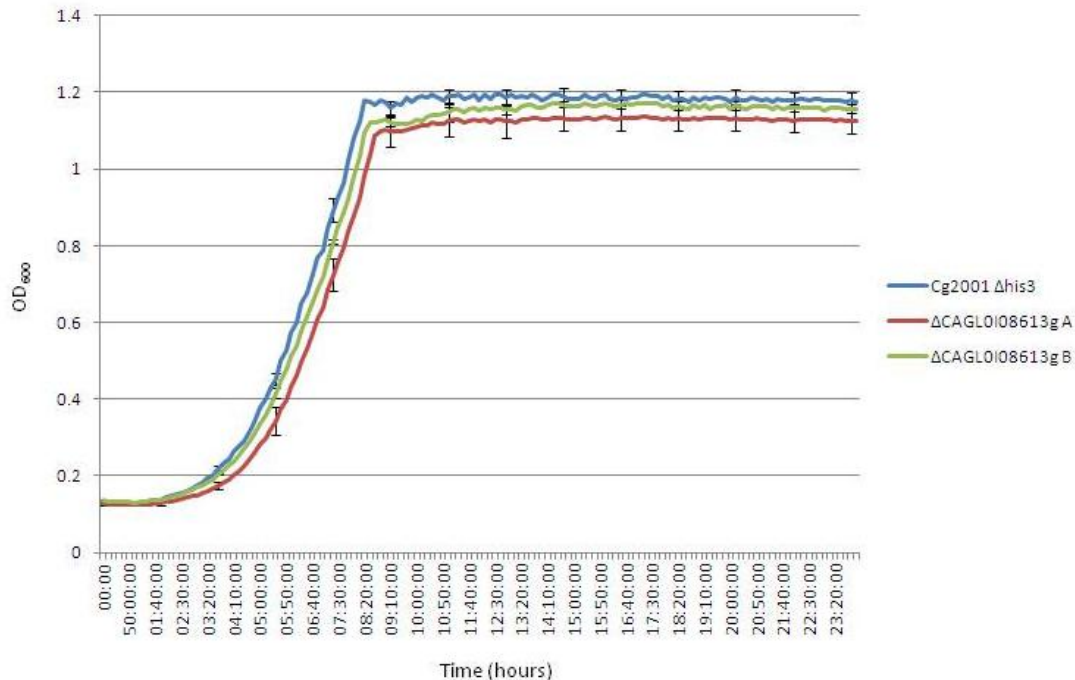


Figure 46: Growth profile of *C. glabrata* parental strain Cg2001 $\Delta his3$ and $\Delta CAGL0J05786g$ isolates A and B.

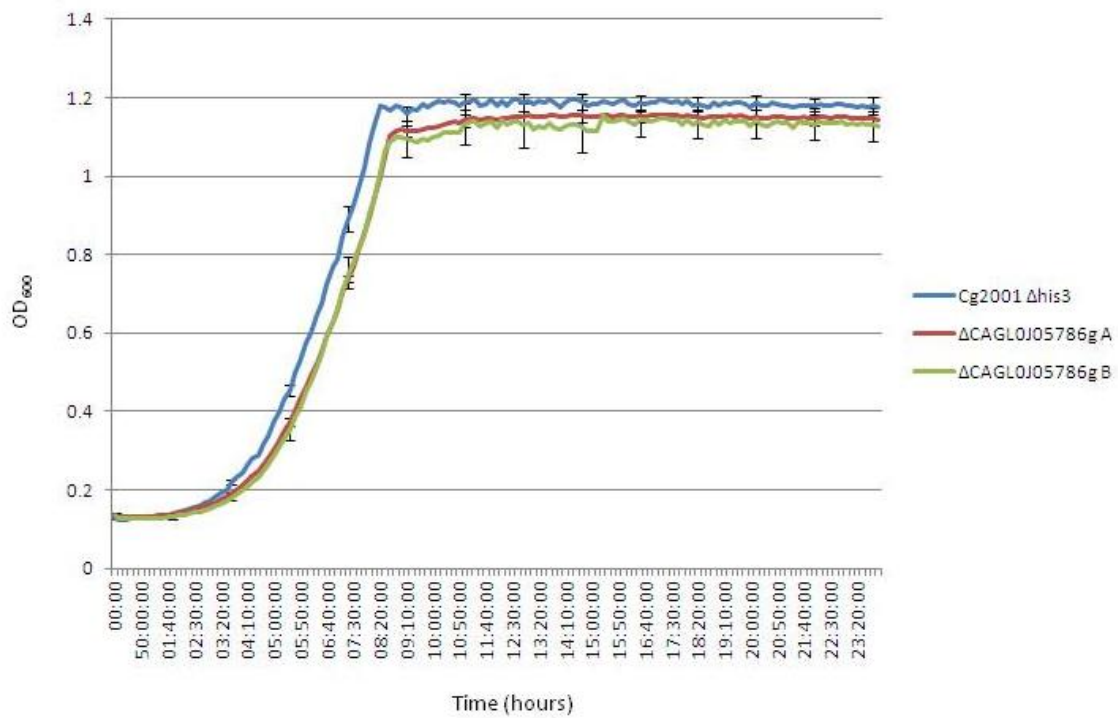


Figure 47: Growth profile of *C. glabrata* parental strain Cg2001 $\Delta his3$ and $\Delta CAGL0J05852g$ isolates A and B.

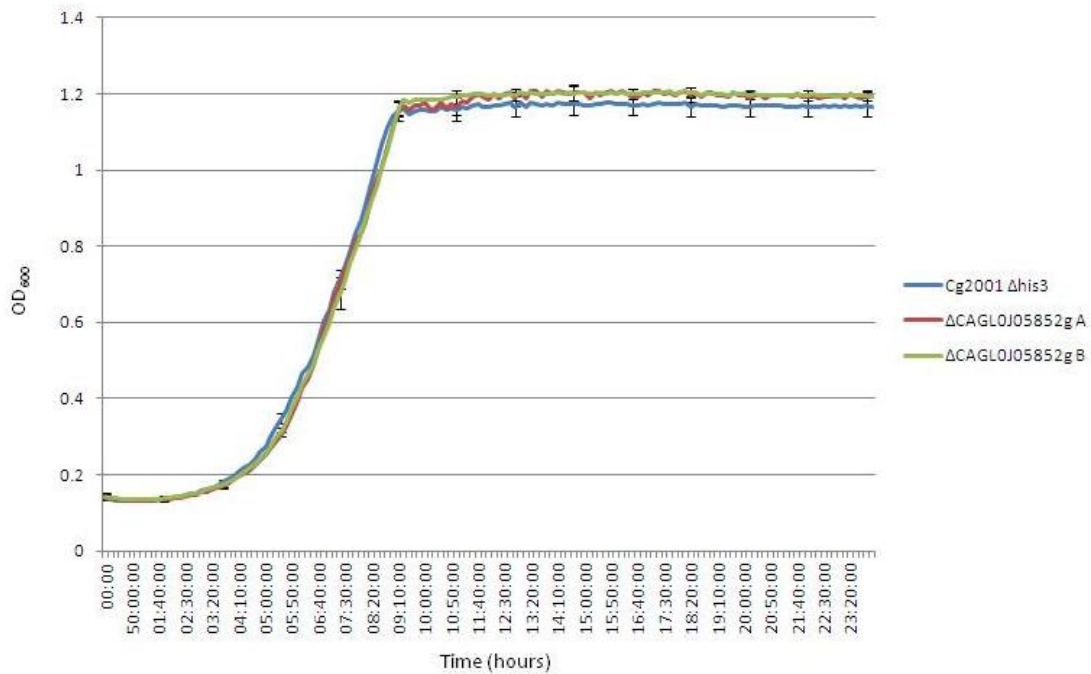


Figure 48: Growth profile of *C. glabrata* parental strain Cg2001 $\Delta his3$ and $\Delta CAGL0K02145g$ isolates A and B.

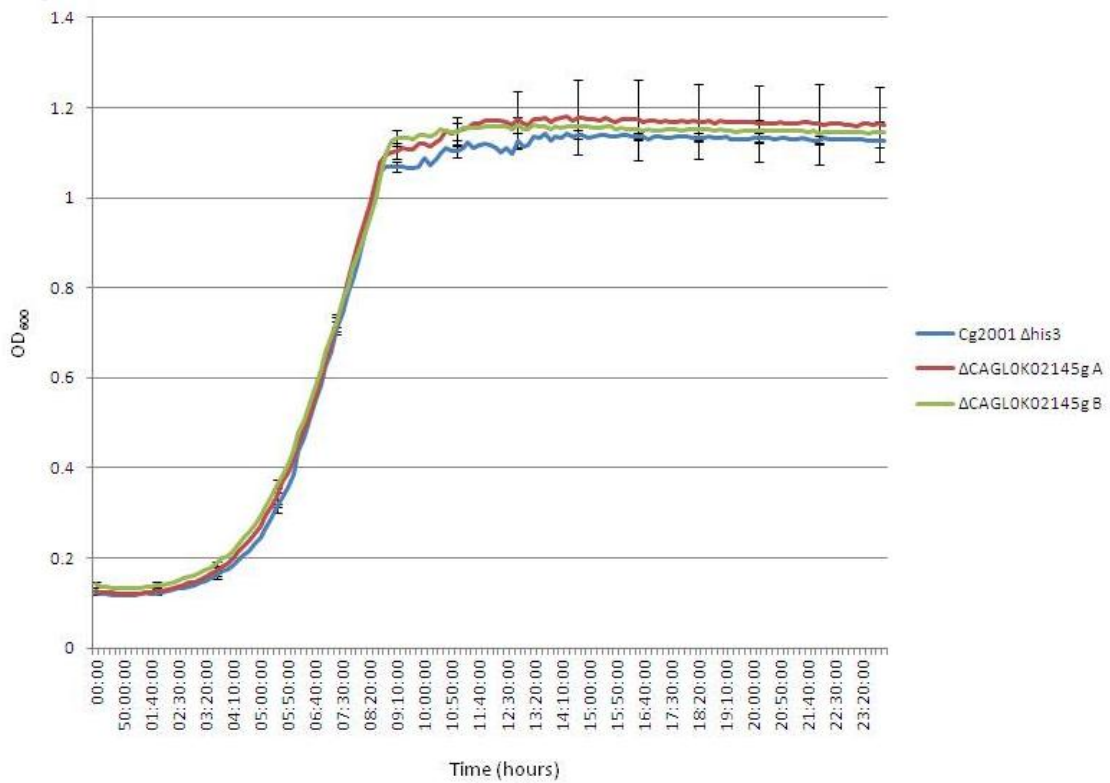


Figure 49: Growth profile of *C. glabrata* parental strain Cg2001 $\Delta his3$ and $\Delta CAGL0K05687g$ isolates A and B.

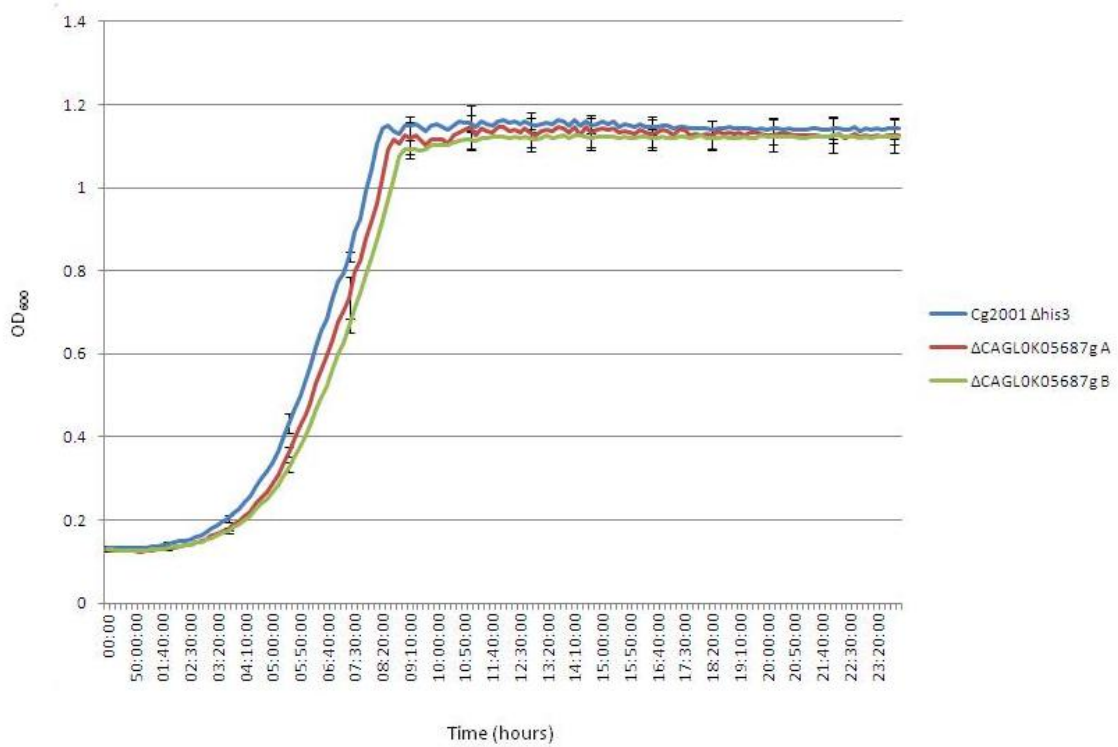


Figure 50: Growth profile of *C. glabrata* parental strain Cg2001 $\Delta his3$ and $\Delta CAGL0K07634g$.

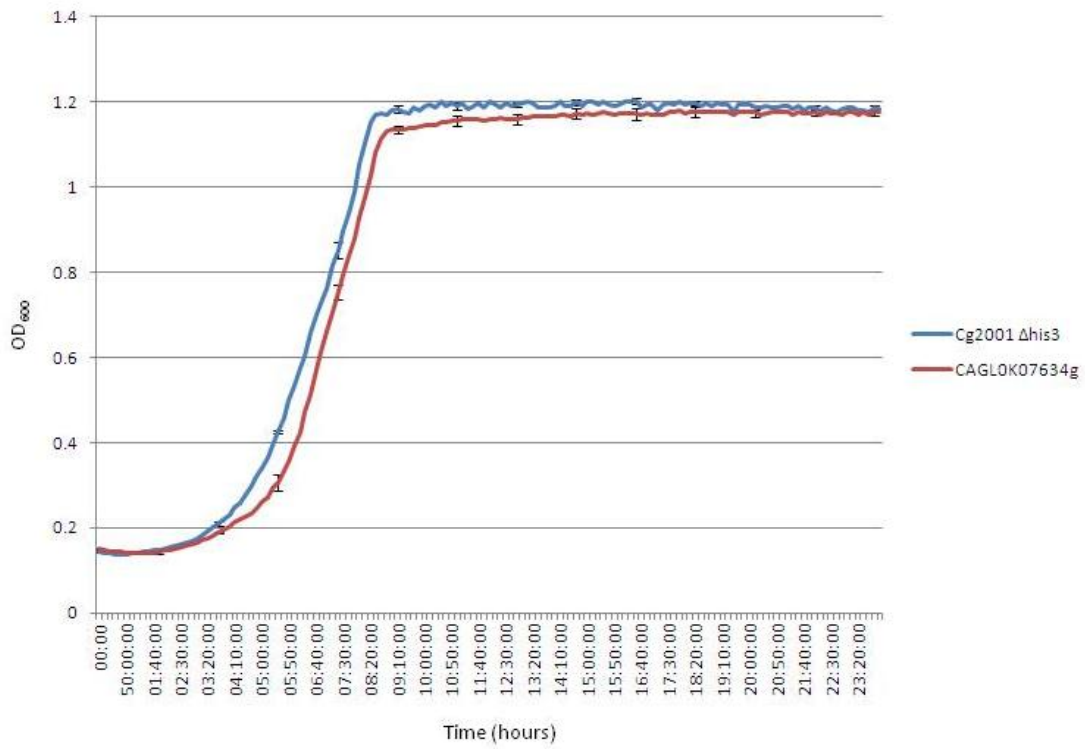


Figure 51: Growth profile of *C. glabrata* parental strain Cg2001 $\Delta his3$ and $\Delta CAGL0K10318g$ isolates A and B.

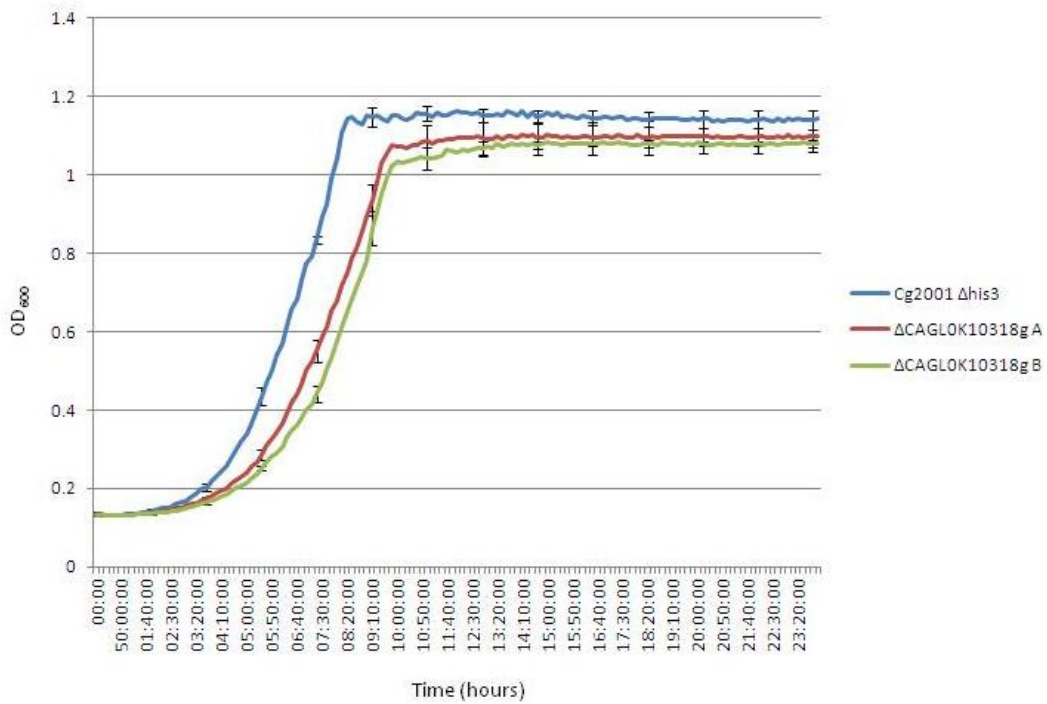


Figure 52: Growth profile of *C. glabrata* parental strain Cg2001 $\Delta his3$ and $\Delta CAGL0K11066g$.

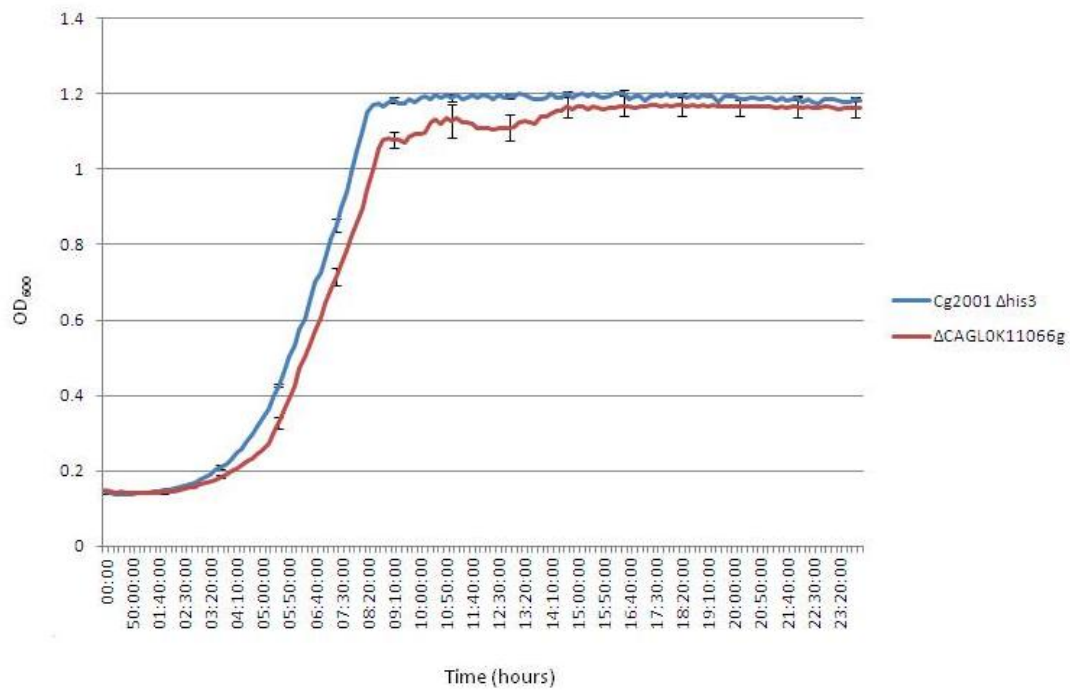


Figure 53: Growth profile of *C. glabrata* parental strain Cg2001 $\Delta his3$ and $\Delta CAGL0L03674g$ isolates A and B.

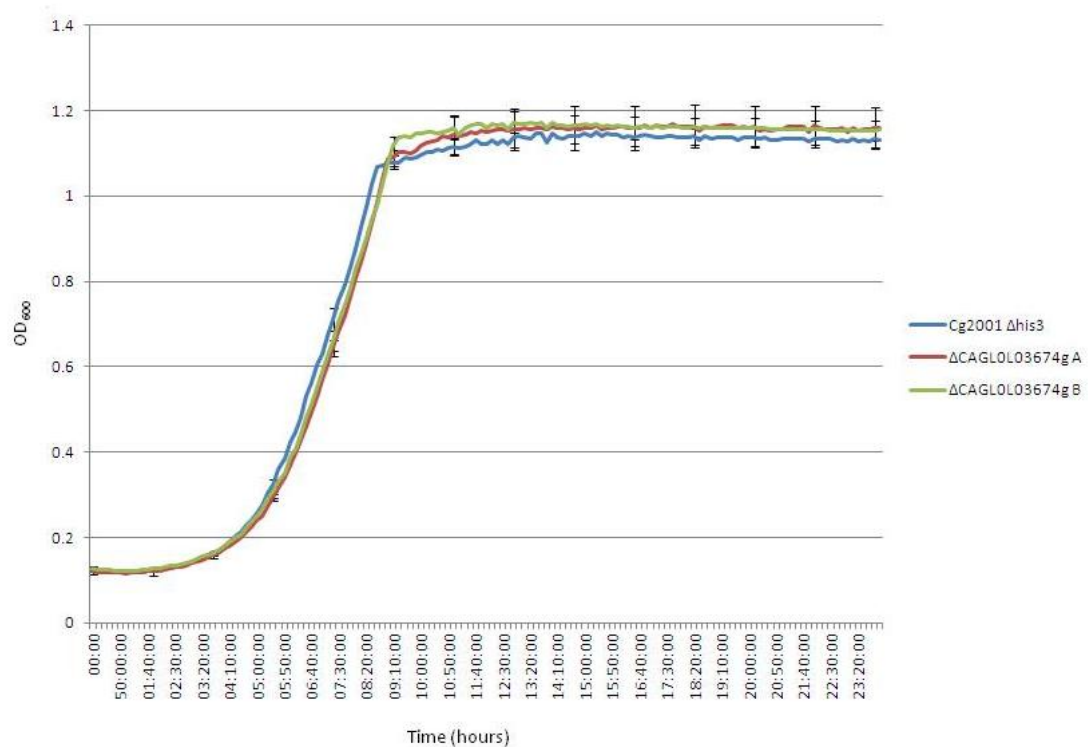


Figure 54: Growth profile of *C. glabrata* parental strain Cg2001 $\Delta his3$ and $\Delta CAGL0L06776g$ isolates A and B.

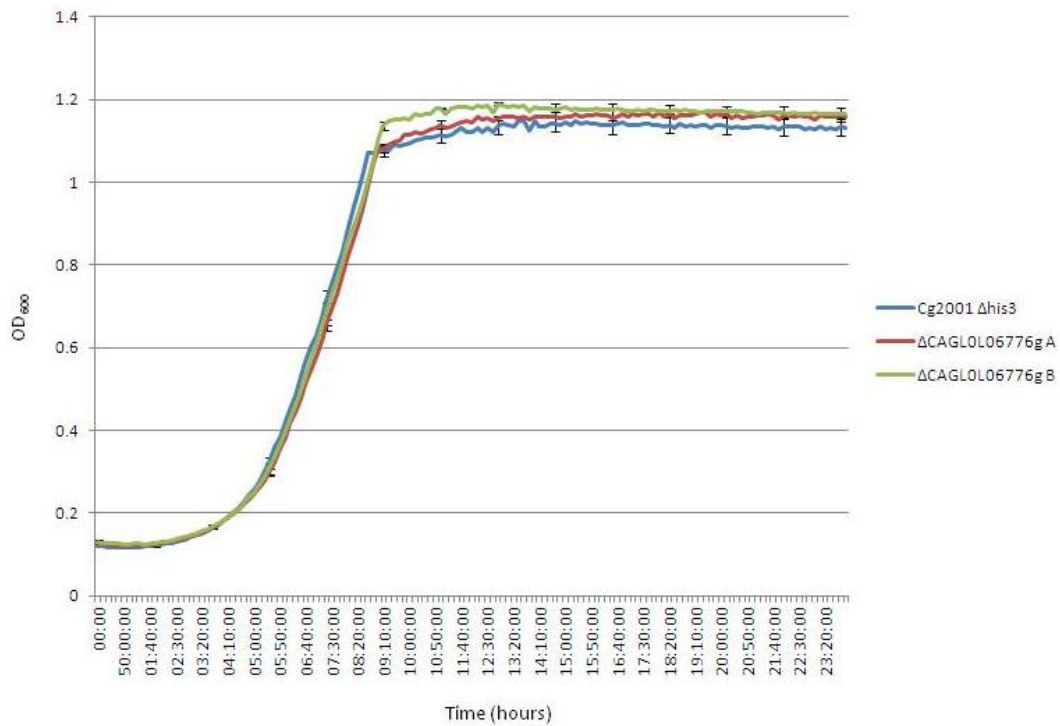


Figure 55: Growth profile of *C. glabrata* parental strain Cg2001 $\Delta his3$ and $\Delta CAGL0L07480g$ isolates A and B.

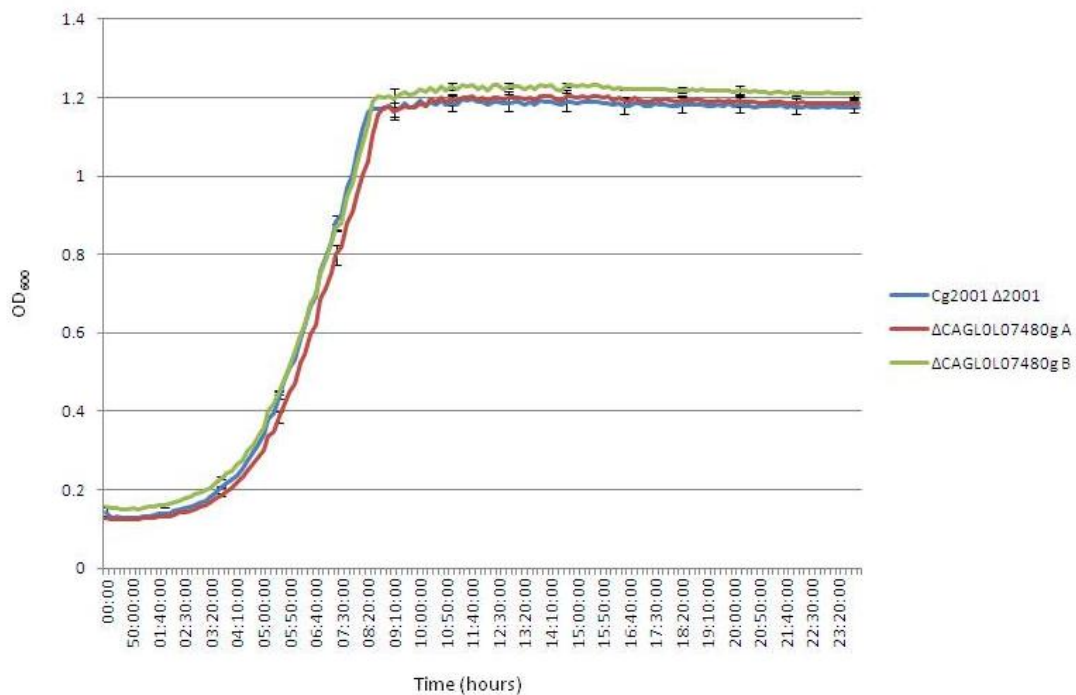


Figure 56: Growth profile of *C. glabrata* parental strain Cg2001 $\Delta his3$ and $\Delta CAGL0L09383g$ isolates A and B.

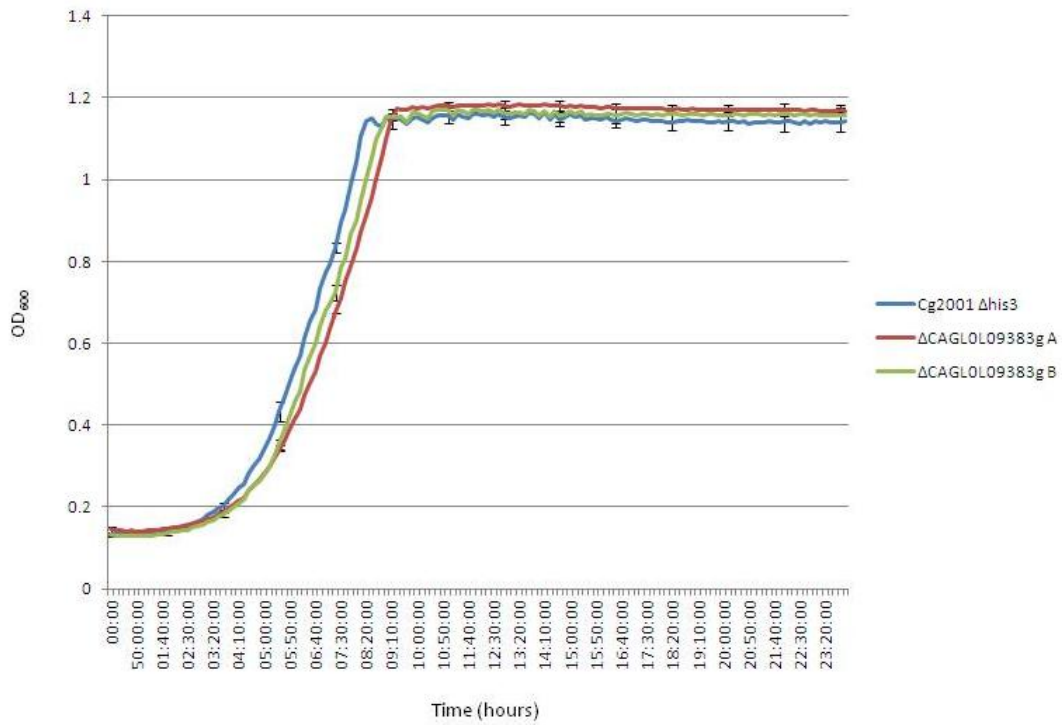


Figure 57: Growth profile of *C. glabrata* parental strain Cg2001 $\Delta his3$ and $\Delta CAGL0M01716g$ isolates A and B.

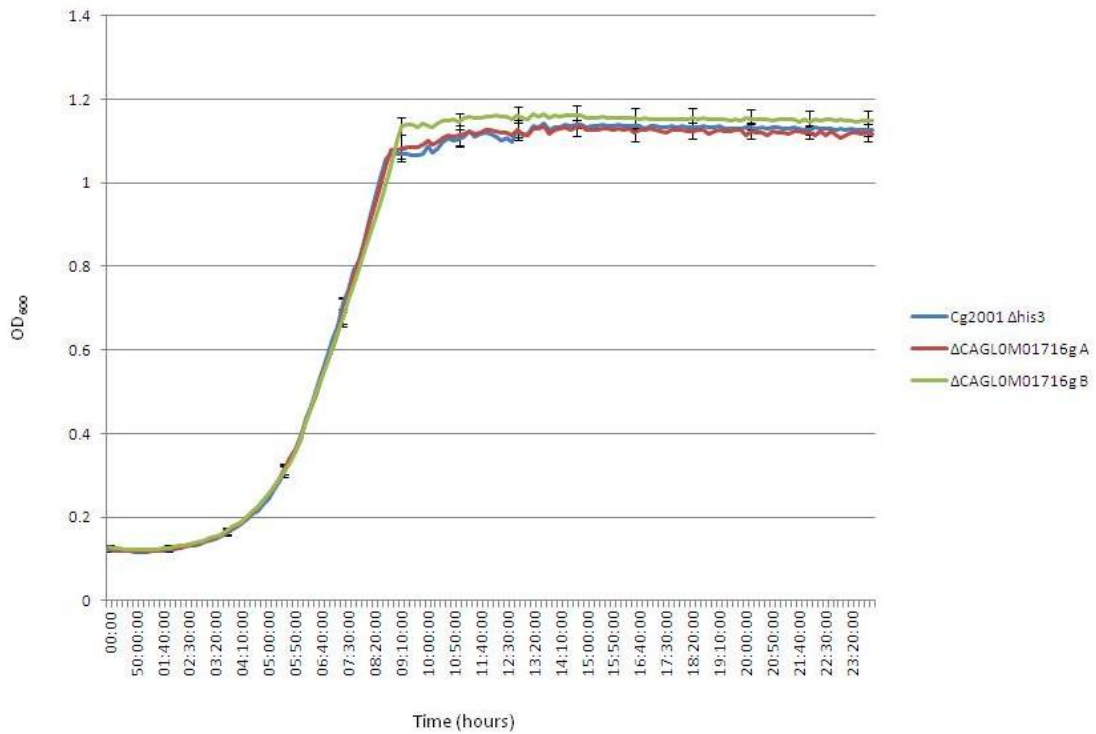


Figure 58: Growth profile of *C. glabrata* parental strain Cg2001 $\Delta his3$ and $\Delta CAGL0M01870g$.

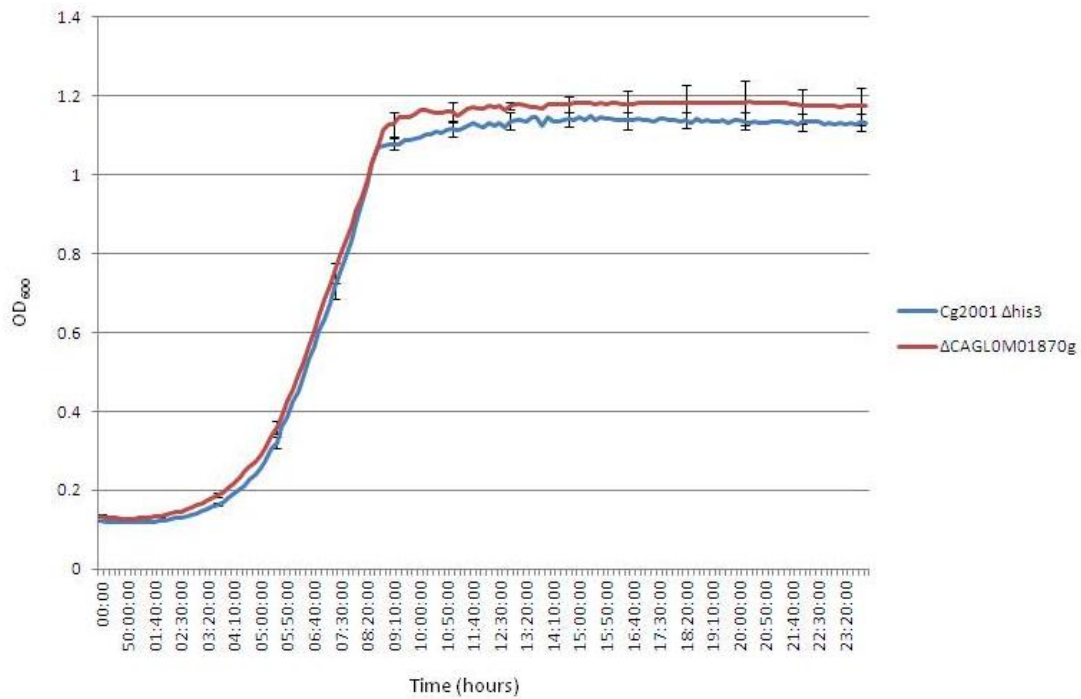


Figure 59: Growth profile of *C. glabrata* parental strain Cg2001 $\Delta his3$ and $\Delta CAGL0M01914g$.

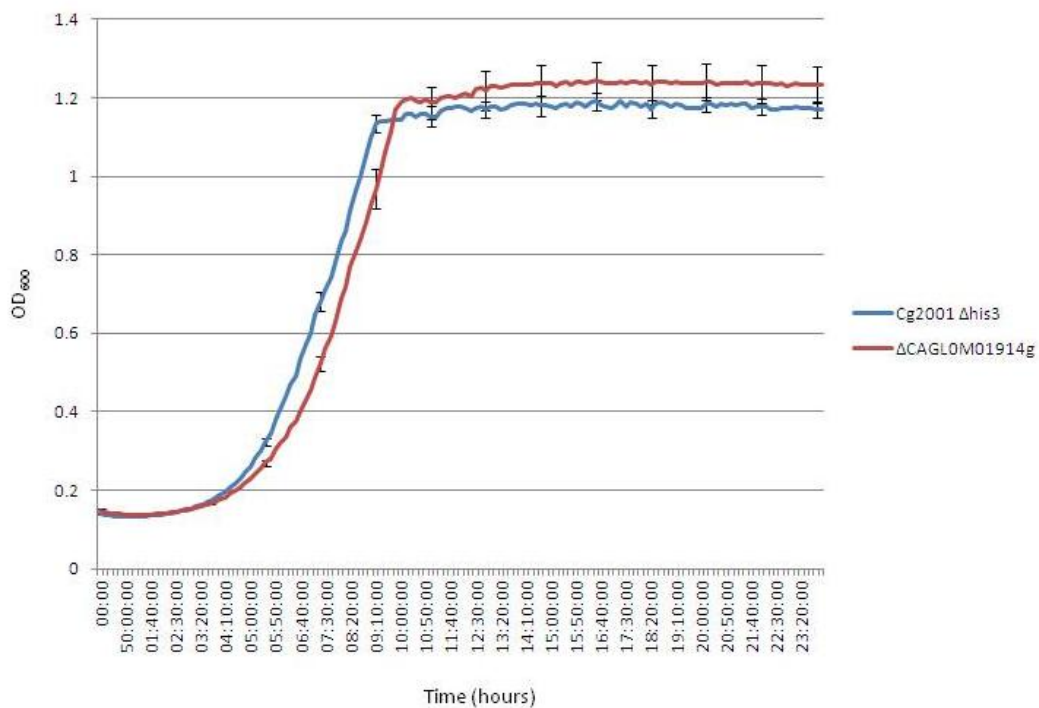


Figure 60: Growth profile of *C. glabrata* parental strain Cg2001 $\Delta his3$ and $\Delta CAGL0M02299g$.

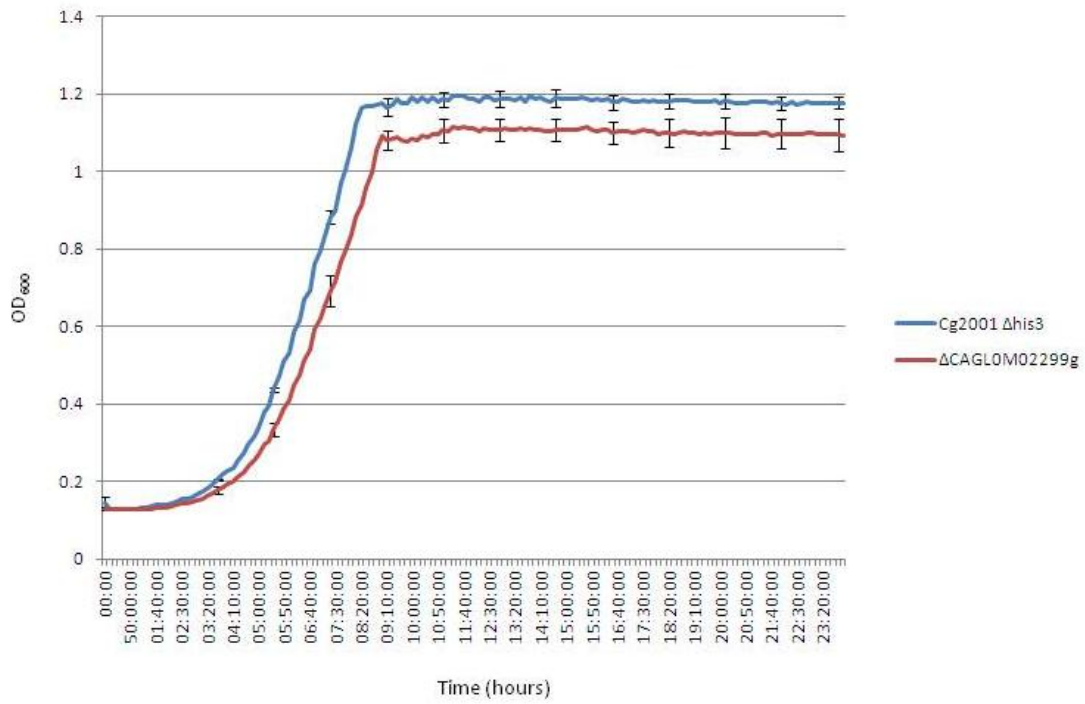


Figure 61: Growth profile of *C. glabrata* parental strain Cg2001 $\Delta his3$ and $\Delta CAGL0M02321g$ isolates A and B.

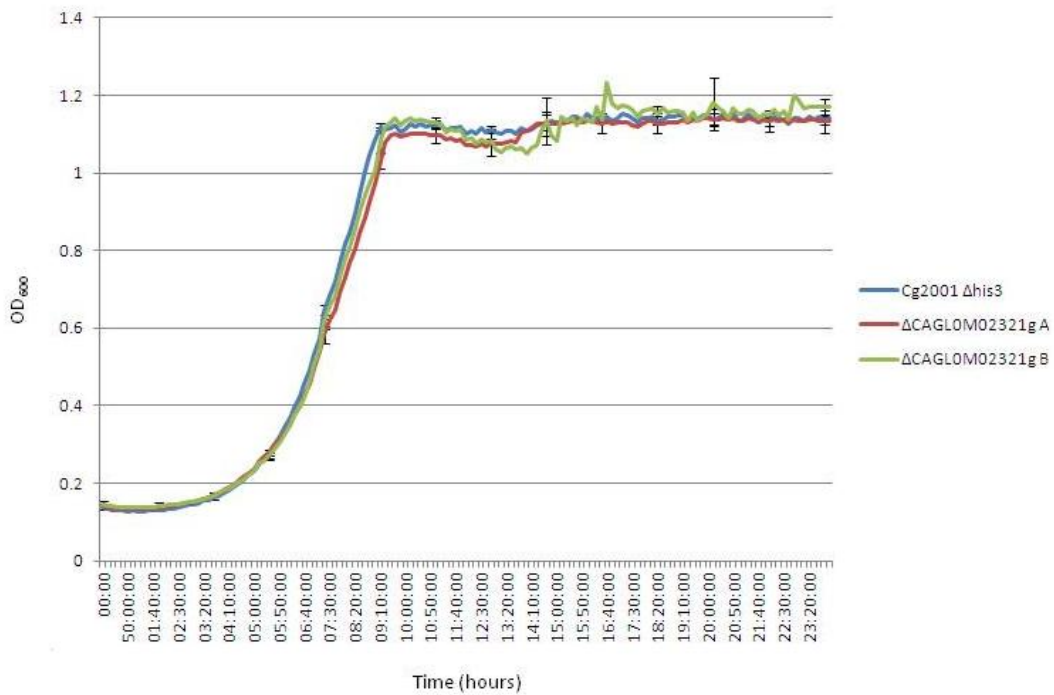


Figure 62: Growth profile of *C. glabrata* parental strain Cg2001 $\Delta his3$ and $\Delta CAGL0M05137g$ isolates A and B.

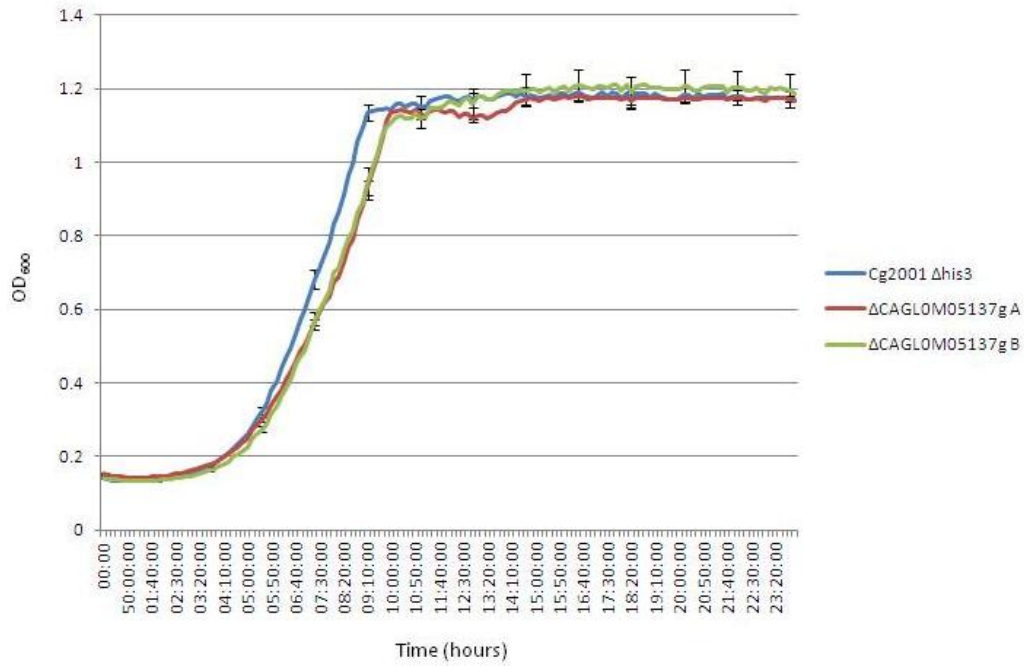


Figure 63: Growth profile of *C. glabrata* parental strain Cg2001 $\Delta his3$ and $\Delta CAGL0M10153g$.

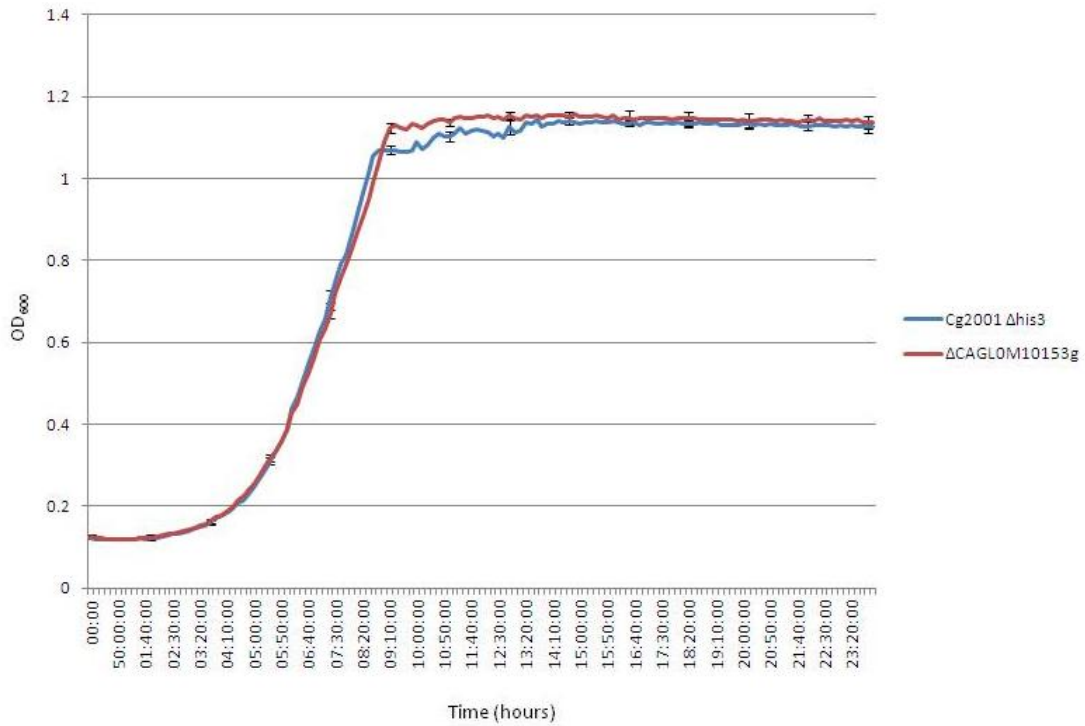
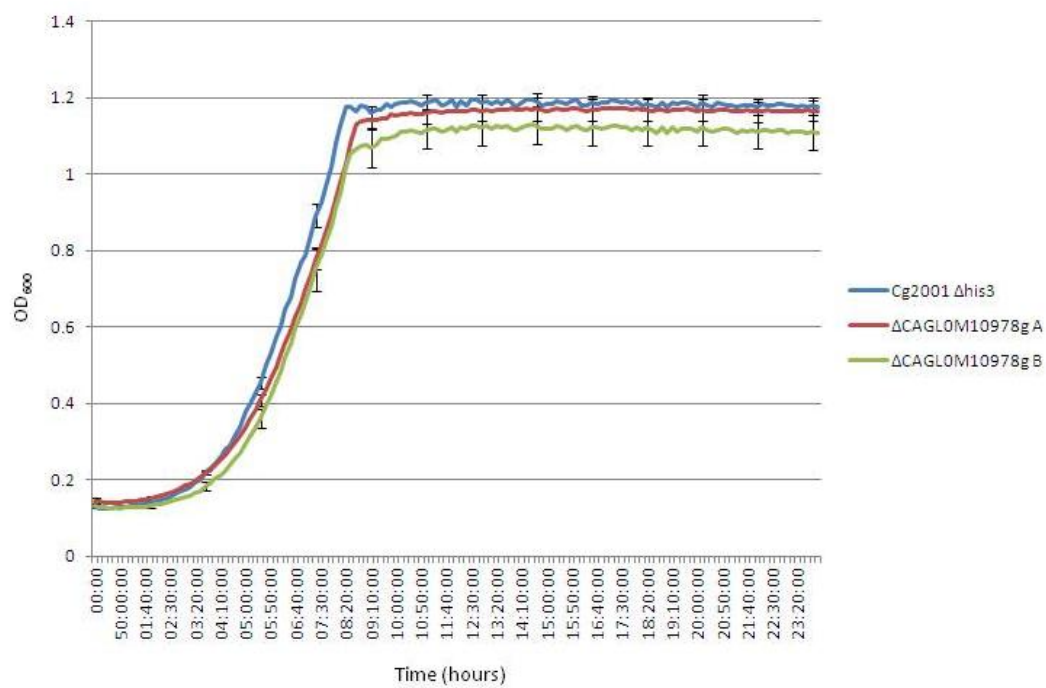


Figure 64: Growth profile of *C. glabrata* parental strain Cg2001 $\Delta his3$ and $\Delta CAGL0M10978g$ isolates A and B.



Appendix 9: *C. glabrata* deletion mutants from the Schwarzmüller *et al.*, 2013 study with no *S. cerevisiae* orthologue used in phenotypic screens

Table 1: List of 67 *C. glabrata* ORFs from the Scharzmüller *et al.*, 2013 study identified by RBH searches to have no orthologue in *S. cerevisiae*. ORFs with no coordinates have been disregarded by CGD during the course of this study (candidagenome.org).

<i>C. glabrata</i> ORF	Start coordinate	Stop coordinate	Strand	<i>S. cerevisiae</i> best hit
CAGLOA00143g				-
CAGLOA01892g	194560	194826	W	-
CAGLOA02299g	250851	251690	W	-
CAGLOA03410g	348708	349451	W	-
CAGLOA03586g	365696	365127	C	YLR040C
CAGLOA04609g				-
CAGLOA04763g				-
CAGLOB00440g	31504	32313	W	-
CAGLOB00572g	49506	48898	C	-
CAGLOB03223g	314992	314690	C	-
CAGLOC00803g				-
CAGLOC00869g				-
CAGLOC01111g				-
CAGLOC02365g	239122	238940	C	-
CAGLOC02915g				-
CAGLOC03311g	334443	333898	C	-
CAGLOC05401g	515623	515886	W	-
CAGL0D01210g	137954	138646	W	-
CAGL0D02750g	288647	289021	W	-
CAGL0D04840g	471574	472164	W	MSS18
CAGL0D05104g				-
CAGL0D05654g	538337	537378	C	-
CAGL0D06534g	622492	622178	C	-
CAGL0D06666g	638537	638737	W	-
CAGL0E00165g				-
CAGL0E01375g				-
CAGL0E01771g	177211	175652	C	-
CAGL0E02211g	215568	215768	W	-

<i>CAGL0E03135g</i>				-
<i>CAGL0E03498g</i>	324961	324476	C	-
<i>CAGL0E04202g</i>				-
<i>CAGL0E04620g</i>	446284	447573	W	<i>PST1</i>
<i>CAGL0E06094g</i>	603704	603877	W	-
<i>CAGL0E06578g</i>				-
<i>CAGL0E06622g</i>				-
<i>CAGL0F00341g</i>	37817	38098	W	-
<i>CAGL0F00781g</i>				-
<i>CAGL0F01441g</i>				-
<i>CAGL0F05995g</i>	600612	598819	C	-
<i>CAGL0F07601g</i>	739068	738412	C	<i>CWP2</i>
<i>CAGL0F07865g</i>	770804	768270	C	<i>ECM22</i>
<i>CAGL0G01386g</i>	133878	132280	C	<i>SLM2</i>
<i>CAGL0G09757g</i>	930351	934622	W	<i>YLR278C</i>
<i>CAGL0H02563g</i>	232068	231892	C	<i>DDR2</i>
<i>CAGL0H03861g</i>	362520	361189	C	<i>HRB1</i>
<i>CAGL0I04092g</i>	358219	359889	W	<i>SHE10</i>
<i>CAGL0J00253g</i>	17376	15883	C	<i>MID2</i>
<i>CAGL0K01507g</i>	134490	131704	C	<i>GPR1</i>
<i>CAGL0K03003g</i>	277585	279528	W	<i>MOT3</i>
<i>CAGL0K03245g</i>	299646	298216	C	-
<i>CAGL0K04037g</i>	373375	379068	W	-
<i>CAGL0K05841g</i>	573144	577262	W	<i>HAP1</i>
<i>CAGL0K06479g</i>	637125	640100	W	<i>PKH3</i>
<i>CAGL0K10164g</i>	990940	990287	C	<i>SPI1</i>
<i>CAGL0K12078g</i>	1171209	1169818	C	-
<i>CAGL0L00627g</i>	77798	80341	W	<i>GPB1</i>
<i>CAGL0L01771g</i>	198971	200278	W	-
<i>CAGL0L01903g</i>	220700	224563	W	<i>RGT1</i>
<i>CAGL0L03674g</i>	422571	424460	W	<i>GSM1</i>
<i>CAGL0L04400g</i>	516722	513759	C	<i>YRR1</i>
<i>CAGL0L12782g</i>	1370285	1371082	W	<i>DIG1</i>
<i>CAGL0M03773g</i>	427099	426518	C	<i>TOS6</i>
<i>CAGL0M04169g</i>	459618	460739	W	<i>KRE1</i>
<i>CAGL0M06831g</i>	695162	697099	W	<i>CRZ1</i>
<i>CAGL0M10791g</i>				-
<i>CAGL0M11726g</i>	1166748	1166308	C	-

Appendix 10: Screening *C. glabrata* deletion mutants for virulence using a *Drosophila melanogaster* gastrointestinal infection model

Table 1: *D. melanogaster* Toll pathway activation in response to infection by *C. glabrata* mutants. Pools of 50 5-day old Drs-GFP larvae were fed *C. glabrata* cell. Larval GFP expression was observed 48 hours post infection as a read-out of Toll-pathway activation. For each *C. glabrata* isolate four pools of 50 *D. melanogaster* Drs-GFP larvae were infected.

<i>C. glabrata</i> strain	No. of GFP-expressing larvae				Average
	Pool 1	Pool 2	Pool 3	Pool 4	
Δ CAGL0A02299g A	48	48	50	50	49
Δ CAGL0A02299g B	44	48	45	44	45.25
Δ CAGL0A02343g A	44	42	47	47	45
Δ CAGL0A02343g B	45	48	49	47	47.25
Δ CAGL0A04565g A	48	50	47	46	47.75
Δ CAGL0B00726g A	48	45	47	41	45.25
Δ CAGL0B00726g B	50	48	48	45	47.75
Δ CAGL0B02926g A	50	48	48	50	49
Δ CAGL0B02946g A	41	42	42	48	43.25
Δ CAGL0B02946g B	42	47	49	50	47
Δ CAGL0B02948g A	44	45	49	49	46.75
Δ CAGL0B02948g B	45	48	44	50	46.75
Δ CAGL0B02970g A	48	49	47	45	47.25
Δ CAGL0B03223g A	47	47	43	48	46.25
Δ CAGL0B03223g B	40	42	41	47	42.5
Δ CAGL0B03883g A	50	48	50	48	49
Δ CAGL0B03883g B	48	48	47	46	47.25
Δ CAGL0C00253g A	48	48	42	43	45.25
Δ CAGL0C00253g B	50	47	45	47	47.25
Δ CAGL0C01837g A	48	46	45	46	46.25
Δ CAGL0C01837g B	43	41	40	44	42
Δ CAGL0C04763g A	50	50	47	42	47.25
Δ CAGL0C04763g B	45	49	41	44	44.75
Δ CAGL0D00682g A	44	47	42	45	44.5
Δ CAGL0D00682g B	50	48	47	50	48.75
Δ CAGL0D01210g A	45	47	42	46	45

Δ CAGL0D01210g B	45	43	49	48	46.25
Δ CAGL0D03850g A	50	48	45	44	46.75
Δ CAGL0D03850g B	47	45	46	48	46.5
Δ CAGL0D03872g A	50	50	50	50	50
Δ CAGL0D03872g B	39	44	42	42	41.75
Δ CAGL0D05170g A	50	50	49	49	49.5
Δ CAGL0D05170g B	38	44	44	41	41.75
Δ CAGL0D05434g A	44	44	49	49	46.5
Δ CAGL0D05434g B	50	49	50	47	49
Δ CAGL0D06226g A	50	46	50	45	47.75
Δ CAGL0D06226g B	46	48	48	46	47
Δ CAGL0E00275g A	50	45	42	41	44.5
Δ CAGL0E06600g A	50	49	47	50	49
Δ CAGL0E06600g B	46	46	48	46	46.5
Δ CAGL0E06644g A	44	46	47	46	45.75
Δ CAGL0E06644g B	50	41	45	44	45
Δ CAGL0F01815g A	47	44	42	41	43.5
Δ CAGL0F01815g B	49	47	50	44	47.5
Δ CAGL0F03905g A	42	50	44	46	45.5
Δ CAGL0F03905g B	50	47	50	50	49.25
Δ CAGL0F04081g A	50	50	50	47	49.25
Δ CAGL0F05159g A	42	48	41	41	43
Δ CAGL0F05159g B	45	45	41	47	44.5
Δ CAGL0F05973g A	50	50	47	46	48.25
Δ CAGL0F06237g A	45	45	42	48	45
Δ CAGL0F06237g B	50	47	47	46	47.5
Δ CAGL0F08767g A	45	43	43	50	45.25
Δ CAGL0F08767g B	47	48	43	44	45.5
Δ CAGL0F09229g A	45	50	50	50	48.75
Δ CAGL0F09229g B	40	49	50	50	47.25
Δ CAGL0G02607g A	50	48	49	50	49.25
Δ CAGL0G03201g A	48	47	47	46	47
Δ CAGL0G04279g A	39	47	48	44	44.5
Δ CAGL0G04279g B	45	47	45	46	45.75
Δ CAGL0G05522g A	40	45	46	44	43.75
Δ CAGL0G05522g B	48	49	45	45	46.75
Δ CAGL0G08866g A	50	48	48	48	48.5
Δ CAGL0G08866g B	50	47	50	50	49.25
Δ CAGL0G10175g A	48	49	50	50	49.25
Δ CAGL0G10175g B	48	47	47	44	46.5
Δ CAGL0H01749g A	44	45	45	45	44.75
Δ CAGL0H01749g B	49	45	47	47	47
Δ CAGL0H06765g A	44	41	40	48	43.25
Δ CAGL0H06765g B	50	44	48	50	48
Δ CAGL0H08712g A	50	50	48	48	49
Δ CAGL0H08712g B	50	50	45	50	48.75

Δ CAGL0H09988g A	45	50	45	48	47
Δ CAGL0H09988g B	50	50	48	47	48.75
Δ CAGL0H10208g A	48	50	48	48	48.5
Δ CAGL0H10208g B	50	47	46	44	46.75
Δ CAGL0I02244g A	44	48	49	42	45.75
Δ CAGL0I02244g B	45	50	47	44	46.5
Δ CAGL0I08437g A	45	45	42	48	45
Δ CAGL0I08613g A	50	47	44	47	47
Δ CAGL0I08613g B	46	49	47	45	46.75
Δ CAGL0J05786g A	44	42	41	47	43.5
Δ CAGL0J05786g B	44	41	38	43	41.5
Δ CAGL0J05852g A	50	49	48	47	48.5
Δ CAGL0J05852g B	45	48	49	48	47.5
Δ CAGL0K02145g A	50	50	48	48	49
Δ CAGL0K02145g B	50	48	48	49	48.75
Δ CAGL0K05687g A	41	42	47	41	42.75
Δ CAGL0K05687g B	48	50	50	50	49.5
Δ CAGL0K05687g B	41	45	48	46	45
Δ CAGL0K07634g A	50	50	48	50	49.5
Δ CAGL0K10318g A	50	48	47	48	48.25
Δ CAGL0K10318g B	48	45	44	44	45.25
Δ CAGL0L03674g A	50	47	46	46	47.25
Δ CAGL0L03674g B	43	44	41	48	44
Δ CAGL0L06776g A	48	48	42	44	45.5
Δ CAGL0L06776g B	50	48	47	47	48
Δ CAGL0L07480g A	50	46	47	44	46.75
Δ CAGL0L07480g B	45	50	48	47	47.5
Δ CAGL0L09383g A	50	48	48	46	48
Δ CAGL0L09383g B	47	45	46	45	45.75
Δ CAGL0M01716g A	46	50	47	47	47.5
Δ CAGL0M01716g B	44	45	47	47	45.75
Δ CAGL0M01870g A	50	50	48	42	47.5
Δ CAGL0M01914g A	50	42	47	41	45
Δ CAGL0M02299g A	50	43	44	47	46
Δ CAGL0M02321g A	47	47	48	48	47.5
Δ CAGL0M02321g B	45	41	48	45	44.75
Δ CAGL0M04543g A	50	47	48	49	48.5
Δ CAGL0M04543g B	43	41	47	47	44.5
Δ CAGL0M05137g A	47	44	46	43	45
Δ CAGL0M05137g B	46	48	42	47	45.75
Δ CAGL0M10153g A	50	48	48	50	49
Δ CAGL0M10978g A	46	42	50	50	47
Δ CAGL0M10978g B	47	48	49	50	48.5

Table 2: Survival of immunocompromised dif/key *D. melanogaster* larvae in response to infection by *C. glabrata* mutants. Pools of 50 5-day old dif/key larvae were fed *C. glabrata* cells. Survival of larvae was observed 48 hours post infection. For each *C. glabrata* isolate four pools of 50 *D. melanogaster* dif/key larvae were infected.

<i>C. glabrata</i> strain	No. of surviving dif/key larvae				Average
	Pool 1	Pool 2	Pool 3	Pool 4	
Δ CAGL0A02299g A	2	8	4	4	4.5
Δ CAGL0A02299g B	4	5	0	4	3.25
Δ CAGL0A02343g A	2	7	7	3	4.75
Δ CAGL0A02343g B	1	4	4	2	2.75
Δ CAGL0A04565g A	1	3	1	4	2.25
Δ CAGL0B00726g A	44	40	41	38	40.75
Δ CAGL0B00726g B	32	35	33	33	33.25
Δ CAGL0B02926g A	0	7	4	2	3.25
Δ CAGL0B02946g A	6	8	7	6	6.75
Δ CAGL0B02946g B	4	1	1	7	3.25
Δ CAGL0B02948g A	3	3	5	1	3
Δ CAGL0B02948g B	2	0	3	0	1.25
Δ CAGL0B02970g A	9	11	5	8	8.25
Δ CAGL0B03223g A	5	6	6	2	4.75
Δ CAGL0B03223g B	3	9	4	0	4
Δ CAGL0B03883g A	4	2	0	0	1.5
Δ CAGL0B03883g B	10	14	18	26	17
Δ CAGL0C00253g A	10	12	9	3	8.5
Δ CAGL0C00253g B	11	4	8	8	7.75
Δ CAGL0C01837g A	9	4	6	1	5
Δ CAGL0C01837g B	7	3	5	4	4.75
Δ CAGL0C04763g A	5	6	6	1	4.5
Δ CAGL0C04763g B	3	2	2	3	2.5
Δ CAGL0D00682g A	3	2	3	2	2.5
Δ CAGL0D00682g B	0	4	2	1	1.75
Δ CAGL0D01210g A	4	8	8	2	5.5
Δ CAGL0D01210g B	2	5	2	0	2.25
Δ CAGL0D03850g A	38	41	42	44	41.25
Δ CAGL0D03850g B	39	38	41	41	39.75
Δ CAGL0D03872g A	0	8	0	4	3
Δ CAGL0D03872g B	0	3	0	4	1.75
Δ CAGL0D05170g A	0	8	5	5	4.5
Δ CAGL0D05170g B	7	4	1	1	3.25
Δ CAGL0D05434g A	4	4	0	0	2
Δ CAGL0D05434g B	5	5	6	4	5
Δ CAGL0D06226g A	6	7	2	2	4.25
Δ CAGL0D06226g B	4	8	2	8	5.5

Δ CAGL0E00275g A	4	4	1	1	2.5
Δ CAGL0E06600g A	5	5	4	4	4.5
Δ CAGL0E06600g B	1	0	5	0	1.5
Δ CAGL0E06644g A	4	4	1	5	3.5
Δ CAGL0E06644g B	2	6	0	4	3
Δ CAGL0F01815g A	0	3	2	0	1.25
Δ CAGL0F01815g B	3	4	7	8	5.5
Δ CAGL0F03905g A	3	8	4	4	4.75
Δ CAGL0F03905g B	12	7	6	6	7.75
Δ CAGL0F04081g A	8	8	4	2	5.5
Δ CAGL0F05159g A	0	0	2	0	0.5
Δ CAGL0F05159g B	0	0	1	1	0.5
Δ CAGL0F05973g A	3	5	4	1	3.25
Δ CAGL0F06237g A	4	3	2	2	2.75
Δ CAGL0F06237g B	2	1	1	2	1.5
Δ CAGL0F08767g A	1	4	0	0	1.25
Δ CAGL0F08767g B	0	2	1	1	1
Δ CAGL0F09229g A	5	5	4	4	4.5
Δ CAGL0F09229g B	6	5	5	6	5.5
Δ CAGL0G02607g A	9	6	3	4	5.5
Δ CAGL0G03201g A	0	4	4	1	2.25
Δ CAGL0G04279g A	6	6	3	3	4.5
Δ CAGL0G04279g B	5	1	2	4	3
Δ CAGL0G05522g A	1	2	3	1	1.75
Δ CAGL0G05522g B	1	1	1	0	0.75
Δ CAGL0G08866g A	2	2	3	4	2.75
Δ CAGL0G08866g B	3	2	5	5	3.75
Δ CAGL0G10175g A	0	0	0	0	0
Δ CAGL0G10175g B	1	1	0	1	0.75
Δ CAGL0H01749g A	36	33	40	41	37.5
Δ CAGL0H01749g B	39	41	41	38	39.75
Δ CAGL0H06765g A	5	8	7	7	6.75
Δ CAGL0H06765g B	5	2	2	0	2.25
Δ CAGL0H08712g A	4	4	8	7	5.75
Δ CAGL0H08712g B	3	1	4	3	2.75
Δ CAGL0H09988g A	10	8	7	7	8
Δ CAGL0H09988g B	4	4	4	1	3.25
Δ CAGL0H10208g A	9	2	0	1	3
Δ CAGL0H10208g B	2	4	5	6	4.25
Δ CAGL0I02244g A	8	8	4	7	6.75
Δ CAGL0I02244g B	4	7	2	4	4.25
Δ CAGL0I08437g A	0	0	0	1	0.25
Δ CAGL0I08613g A	2	2	0	4	2
Δ CAGL0I08613g B	1	0	0	2	0.75
Δ CAGL0J05786g A	4	0	7	6	4.25
Δ CAGL0J05786g B	1	4	1	4	2.5

Δ CAGL0J05852g A	2	8	4	3	4.25
Δ CAGL0J05852g B	4	3	4	8	4.75
Δ CAGL0K02145g A	2	2	0	1	1.25
Δ CAGL0K02145g B	8	4	4	2	4.5
Δ CAGL0K05687g A	39	42	42	38	40.25
Δ CAGL0K05687g B	38	38	35	33	36
Δ CAGL0K05687g B	40	40	36	33	37.25
Δ CAGL0K07634g A	0	0	0	1	0.25
Δ CAGL0K10318g A	2	4	6	0	3
Δ CAGL0K10318g B	5	0	2	4	2.75
Δ CAGL0L03674g A	41	38	42	42	40.75
Δ CAGL0L03674g B	42	40	41	42	41.25
Δ CAGL0L06776g A	8	7	7	2	6
Δ CAGL0L06776g B	8	7	5	7	6.75
Δ CAGL0L07480g A	35	34	32	39	35
Δ CAGL0L07480g B	33	32	30	30	31.25
Δ CAGL0L09383g A	2	2	0	1	1.25
Δ CAGL0L09383g B	6	4	4	5	4.75
Δ CAGL0M01716g A	0	5	5	8	4.5
Δ CAGL0M01716g B	0	4	4	0	2
Δ CAGL0M01870g A	6	5	6	4	5.25
Δ CAGL0M01914g A	0	1	0	4	1.25
Δ CAGL0M02299g A	4	4	2	1	2.75
Δ CAGL0M02321g A	11	8	6	4	7.25
Δ CAGL0M02321g B	1	3	2	1	1.75
Δ CAGL0M04543g A	2	7	1	1	2.75
Δ CAGL0M04543g B	2	5	4	6	4.25
Δ CAGL0M05137g A	3	3	7	4	4.25
Δ CAGL0M05137g B	6	4	5	10	6.25
Δ CAGL0M10153g A	4	7	2	5	4.5
Δ CAGL0M10978g A	4	2	2	1	2.25
Δ CAGL0M10978g B	0	1	4	1	1.5

Appendix 11: Screening *C. glabrata* deletion mutants for Biofilm Formation

Table 1: Quantification of biofilm formation for 117 *C. glabrata* isolates corresponding to 65 *C. glabrata* ORF deletions. Values indicate the average OD₄₉₂ of XTT solution incubated with *C. glabrata* biofilms for 1 hour at 37 °C as well as that of the parental strain control Cg2001 $\Delta his3$. Where available, two independent isolates of each *C. glabrata* deletion mutant were tested for biofilm formation. *C. glabrata* isolates for which biofilm formation was significantly increased or decreased compared with the parental strain are highlighted in yellow (Anova $p < 1.45E-05$, Dunnett's critical value 3.37).

<i>C. glabrata</i> isolate	Average XTT reduction (OD ₄₉₂)	Average Cg2001 $\Delta his3$ control XTT reduction (OD ₄₉₂)
$\Delta CAGL0A02299g A$	0.4793	0.3740
$\Delta CAGL0A02299g B$	0.4402	0.3740
$\Delta CAGL0A02343g A$	0.4623	0.3740
$\Delta CAGL0A02343g B$	0.4437	0.3740
$\Delta CAGL0A03608g A$	0.7953	0.8035
$\Delta CAGL0A03608g B$	0.8133	0.8035
$\Delta CAGL0B00726g A$	0.7512	0.8247
$\Delta CAGL0B00726g B$	0.7558	0.8247
$\Delta CAGL0B02926g A$	0.4247	0.4150
$\Delta CAGL0B02946g B$	0.4027	0.3038
$\Delta CAGL0B02948g A$	0.8056	0.8035
$\Delta CAGL0B02948g B$	0.8156	0.8035
$\Delta CAGL0B02970g A$	0.6341	0.6341
$\Delta CAGL0B03223g A$	0.6943	0.8035
$\Delta CAGL0B03223g B$	0.6746	0.8035
$\Delta CAGL0B03883g A$	0.3508	0.4150
$\Delta CAGL0B03883g B$	0.3655	0.4150
$\Delta CAGL0C00253g A$	0.8133	0.8035
$\Delta CAGL0C00253g B$	0.8086	0.8035
$\Delta CAGL0C01837g A$	0.7983	0.8035
$\Delta CAGL0C01837g B$	0.7806	0.8035
$\Delta CAGL0C04763g A$	0.4015	0.3038
$\Delta CAGL0C04763g B$	0.4352	0.3038
$\Delta CAGL0D00682g A$	0.2808	0.3038
$\Delta CAGL0D00682g B$	0.3757	0.3038

Δ CAGL0D01210g A	0.8156	0.8035
Δ CAGL0D01210g B	0.8056	0.8035
Δ CAGL0D03850g A	0.3987	0.5490
Δ CAGL0D03850g B	0.3372	0.5490
Δ CAGL0D03872g A	0.7550	0.8035
Δ CAGL0D05170g A	0.5133	0.5490
Δ CAGL0D05170g B	0.5238	0.5490
Δ CAGL0D05434g A	0.5452	0.5490
Δ CAGL0D05434g B	0.5383	0.5490
Δ CAGL0D06226g A	0.8533	0.8035
Δ CAGL0E00275g A	0.3786	0.8035
Δ CAGL0E06600g A	0.4518	0.3740
Δ CAGL0E06600g B	0.4028	0.3740
Δ CAGL0E06644g A	0.3305	0.3038
Δ CAGL0E06644g B	0.2907	0.3038
Δ CAGL0F01815g A	0.3965	0.4150
Δ CAGL0F01815g B	0.3757	0.4150
Δ CAGL0F03905g A	0.6948	0.8247
Δ CAGL0F03905g B	0.7097	0.8247
Δ CAGL0F04081g A	0.5572	0.5382
Δ CAGL0F05159g A	0.6300	0.8247
Δ CAGL0F05159g B	0.6718	0.8247
Δ CAGL0F05973g A	0.5718	0.5382
Δ CAGL0F06237g A	0.5165	0.5490
Δ CAGL0F06237g B	0.5147	0.5490
Δ CAGL0F08767g A	0.7423	0.8035
Δ CAGL0F08767g B	0.7265	0.8035
Δ CAGL0F09229g A	0.7348	0.8247
Δ CAGL0F09229g B	0.7738	0.8247
Δ CAGL0G02607g A	0.6863	0.5382
Δ CAGL0G02607g B	0.4992	0.5725
Δ CAGL0G03201g A	0.4775	0.3740
Δ CAGL0G04279g A	0.6233	0.8035
Δ CAGL0G04279g B	0.5921	0.8035
Δ CAGL0G05522g A	0.8150	0.8035
Δ CAGL0G05522g B	0.8518	0.8035
Δ CAGL0G08866g A	0.5525	0.5490
Δ CAGL0G08866g B	0.5552	0.5490
Δ CAGL0G10175g A	0.8353	0.8035
Δ CAGL0G10175g B	0.8213	0.8035
Δ CAGL0H01749g A	0.4668	0.4268
Δ CAGL0H01749g B	0.4158	0.4268
Δ CAGL0H06765g A	0.5893	0.5725
Δ CAGL0H06765g B	0.6737	0.5725
Δ CAGL0H08712g A	0.4495	0.4268
Δ CAGL0H08712g B	0.3323	0.4268

Δ CAGL0H09988g A	0.5015	0.5490
Δ CAGL0H09988g B	0.5087	0.5490
Δ CAGL0H10208g A	0.4992	0.5725
Δ CAGL0H10208g B	0.6195	0.5382
Δ CAGL0I02244g A	0.4378	0.4268
Δ CAGL0I02244g B	0.4302	0.4268
Δ CAGL0I08437g A	0.8183	0.8035
Δ CAGL0I08613g A	0.4422	0.3740
Δ CAGL0I08613g B	0.3905	0.3740
Δ CAGL0J05786g A	0.4563	0.4268
Δ CAGL0J05786g B	0.4730	0.4268
Δ CAGL0J05852g A	0.8260	0.8035
Δ CAGL0J05852g B	0.7993	0.8035
Δ CAGL0K02145g A	0.4172	0.4150
Δ CAGL0K02145g B	0.3547	0.4150
Δ CAGL0K05687g A	0.7322	0.5725
Δ CAGL0K05687g A	0.5028	0.4268
Δ CAGL0K05687g B	0.7068	0.5725
Δ CAGL0K07634g A	0.6883	0.5382
Δ CAGL0K10318g A	0.6403	0.5725
Δ CAGL0K10318g B	0.8353	0.8035
Δ CAGL0K11066g A	0.8740	0.8035
Δ CAGL0L03674g A	0.7520	0.8247
Δ CAGL0L03674g B	0.7583	0.8247
Δ CAGL0L06776g A	0.8480	0.8247
Δ CAGL0L06776g B	0.7787	0.8247
Δ CAGL0L07480g A	0.6498	0.8247
Δ CAGL0L07480g B	0.5578	0.8247
Δ CAGL0L09383g A	0.5018	0.5490
Δ CAGL0L09383g B	0.4840	0.5490
Δ CAGL0M01716g A	0.3927	0.4150
Δ CAGL0M01716g B	0.3588	0.4150
Δ CAGL0M01870g A	0.6615	0.5382
Δ CAGL0M01914g A	0.7176	0.8035
Δ CAGL0M02299g A	0.3093	0.5725
Δ CAGL0M02321g A	0.4727	0.4268
Δ CAGL0M02321g B	0.4308	0.4268
Δ CAGL0M04543g A	0.8583	0.8035
Δ CAGL0M04543g B	0.8643	0.8035
Δ CAGL0M05137g A	0.8583	0.8035
Δ CAGL0M05137g B	0.8643	0.8035
Δ CAGL0M10153g A	0.7008	0.5382
Δ CAGL0M10978g A	0.4728	0.3740
Δ CAGL0M10978g B	0.3765	0.3740

Appendix 12: *CAGL0K05687g* genetic interactions

Table 1: *S. cerevisiae* ORFs and SGD description (yeastgenome.org) which showed genetic interactions with *C. glabrata* *CAGL0K05687g* expressed from *S. cerevisiae* strain KH03-K05687. Genes highlighted in orange highlight *S. cerevisiae* membrane proteins and transporters. *S. cerevisiae* genes involved in transcriptional regulation are highlighted in blue. ORFs highlighted green are associated with the vesicle.

ORF name	Gene name	SGD Description
<i>YAL002W</i>	<i>VPS8</i>	Membrane-binding component of the CORVET complex; involved in endosomal vesicle tethering and fusion in the endosome to vacuole protein targeting pathway; interacts with Vps21p; contains RING finger motif
<i>YAL004W</i>	<i>YAL004W</i>	Dubious open reading frame; unlikely to encode a functional protein, based on available experimental and comparative sequence data; completely overlaps verified gene SSA1/YAL005C
<i>YAL005C</i>	<i>SSA1</i>	ATPase involved in protein folding and NLS-directed nuclear transport; member of HSP70 family; forms chaperone complex with Ydj1p; localized to nucleus, cytoplasm, and cell wall; 98% identical with paralogue Ssa2p, but subtle differences between the two proteins provide functional specificity with respect to propagation of yeast [URE3] prions and vacuolar-mediated degradations of gluconeogenesis enzymes; general targeting factor of Hsp104p to prion fibrils
<i>YAL010C</i>	<i>MDM10</i>	Subunit of both the ERMES complex and the SAM complex; the ERMES complex links the ER to mitochondria; the SAM complex is mitochondrial sorting and assembly machinery that functions in import and assembly of outer membrane beta-barrel proteins
<i>YAL011W</i>	<i>SWC3</i>	Protein of unknown function; component of the SWR1 complex, which exchanges histone variant H2AZ (Htz1p) for chromatin-bound histone H2A; required for formation of nuclear-associated array of smooth endoplasmic reticulum known as karmellae
<i>YAL014C</i>	<i>SYN8</i>	Endosomal SNARE related to mammalian syntaxin 8
<i>YAL015C</i>	<i>NTG1</i>	DNA N-glycosylase and apurinic/apyrimidinic (AP) lyase; involved in base excision repair; acts in both nucleus and mitochondrion; creates a double-strand break at mtDNA origins that stimulates replication in response to oxidative stress; required for maintaining mitochondrial genome integrity; NTG1 has a paralog, NTG2, that arose from the whole genome duplication
<i>YAL017W</i>	<i>PSK1</i>	PAS domain-containing serine/threonine protein kinase; coordinately regulates protein synthesis and carbohydrate metabolism and storage in response to a unknown metabolite that reflects nutritional status; PSK1 has a paralog, PSK2, that arose from the whole genome duplication
<i>YAL018C</i>	<i>YAL018C</i>	Protein involved in spore wall assembly; localizes to lipid droplets found on or outside of the prospore membrane; shares

		similarity with Lds2p and Rrt8p, and a strain mutant for all 3 genes exhibits reduced dityrosine fluorescence relative to the single mutants
YAL019W	FUN30	Snf2p family member with ATP-dependent chromatin remodeling activity; has a role in silencing at the mating type locus, telomeres and centromeres; enriched at centromeres and is required for correct chromatin structure around centromeres, as well as at the boundary element of the silent HMR; recruited to DNA double-strand breaks (DSBs) where it promotes 5' strand resection of DSBs; potential Cdc28p substrate
YAL020C	ATS1	Protein required for modification of wobble nucleosides in tRNA; acts with Elongator complex, Kti11p, and Kti12p; has a potential role in regulatory interactions between microtubules and the cell cycle
YAL027W	SAW1	5'- and 3'-flap DNA binding protein; recruits Rad1p-Rad10p to single-strand annealing intermediates with 3' non-homologous tails for removal during double-strand break repair; complexes with Rad1p-Rad10p and stimulates its endonuclease activity; green fluorescent protein (GFP)-fusion protein localizes to the nucleus
YAL028W	FRT2	Tail-anchored ER membrane protein of unknown function; interacts with homolog Frt1p; promotes growth in conditions of high Na ⁺ , alkaline pH, or cell wall stress, possibly via a role in posttranslational translocation; potential Cdc28p substrate; FRT2 has a paralog, FRT1, that arose from the whole genome duplication
YAL030W	SNC1	Vesicle membrane receptor protein (v-SNARE); involved in the fusion between Golgi-derived secretory vesicles with the plasma membrane; proposed to be involved in endocytosis; member of the synaptobrevin/VAMP family of R-type v-SNARE proteins; SNC1 has a paralog, SNC2, that arose from the whole genome duplication
YAL031C	GIP4	Cytoplasmic Glc7-interacting protein whose overexpression relocalizes Glc7p from the nucleus and prevents chromosome segregation; potential Cdc28p substrate
YAL034C	FUN19	Non-essential protein of unknown function; expression induced in response to heat stress; FUN19 has a paralog, YOR338W, that arose from the whole genome duplication
YAL036C	RBG1	Member of the DRG family of GTP-binding proteins; associates with translating ribosomes; interacts with Tma46p, Ygr250cp, Gir2p and Yap1p via two-hybrid
YAL037W	YAL037W	Putative protein of unknown function; YAL037W has a paralog, YOR342C, that arose from the whole genome duplication
YAL040C	CLN3	G1 cyclin involved in cell cycle progression; activates Cdc28p kinase to promote the G1 to S phase transition; plays a role in regulating transcription of the other G1 cyclins, CLN1 and CLN2; regulated by phosphorylation and proteolysis; acetyl-CoA induces CLN3 transcription in response to nutrient depletion to promote cell-cycle entry
YAL042W	ERV46	Protein localized to COPII-coated vesicles; forms a complex with Erv41p; involved in the membrane fusion stage of transport
YAL043C-a	YAL042C-A	Dubious open reading frame; unlikely to encode a functional protein, based on available experimental and comparative sequence data; partially overlaps verified ORF ERV46/YAL042W; YAL042C-A is a non-essential gene
YAL044C	GCV3	H subunit of the mitochondrial glycine decarboxylase complex; glycine decarboxylase is required for the catabolism of glycine to 5,10-methylene-THF; also required for all protein lipoylation; expression is regulated by levels of 5,10-methylene-THF
YAL045C	YAL045C	Dubious open reading frame; unlikely to encode a functional protein, based on available experimental and comparative sequence data; almost completely overlaps YAL044W-A

YAL049C	AIM2	Cytoplasmic protein involved in mitochondrial function or organization; null mutant displays reduced frequency of mitochondrial genome loss; potential Hsp82p interactor
YAL053W	FLC2	Putative FAD transporter; required for uptake of FAD into endoplasmic reticulum; involved in cell wall maintenance; FLC2 has a paralogue, YOR365C, that arose from the whole genome duplication
YAL055W	PEX22	Putative peroxisomal membrane protein required for import of peroxisomal proteins, functionally complements a <i>Pichia pastoris</i> pex22 mutation
YAL056W	GPB2	Multistep regulator of cAMP-PKA signaling; inhibits PKA downstream of Gpa2p and Cyr1p, thereby increasing cAMP dependency; inhibits Ras activity through direct interactions with Ira1p/2p; regulated by G-alpha protein Gpa2p; GPB2 has a paralogue, GPB1, that arose from the whole genome duplication
YAL058W	CNE1	Calnexin; integral membrane ER chaperone involved in folding and quality control of glycoproteins; chaperone activity is inhibited by Mpd1p, with which Cne1p interacts; 24% identical to mammalian calnexin; Ca ⁺ binding not yet shown in yeast
YAL062W	GDH3	NADP(+)-dependent glutamate dehydrogenase; synthesizes glutamate from ammonia and alpha-ketoglutarate; rate of alpha-ketoglutarate utilization differs from Gdh1p; expression regulated by nitrogen and carbon sources; GDH3 has a paralogue, GDH1, that arose from the whole genome duplication
YAL065C	YAL065C	Putative protein of unknown function; has homology to FLO1; possible pseudogene
YAL066W	YAL066W	Dubious open reading frame; unlikely to encode a functional protein, based on available experimental and comparative sequence data
YAL067C	SEO1	Putative permease; member of the allantoin transporter subfamily of the major facilitator superfamily; mutation confers resistance to ethionine sulfoxide
YAR002W	NUP60	FG-nucleoporin component of central core of the nuclear pore complex (NPC); contributes directly to nucleocytoplasmic transport and maintenance of the NPC permeability barrier and is involved in gene tethering at the nuclear periphery; relocalizes to the cytosol in response to hypoxia; both NUP1 and NUP60 are homologous to human NUP153
YAR003W	SWD1	Subunit of the COMPASS (Set1C) complex; COMPASS methylates histone H3 on lysine 4 and is required in transcriptional silencing near telomeres; WD40 beta propeller superfamily member with similarity to mammalian Rbbp7
YAR014C	BUD14	Protein involved in bud-site selection; Bud14p-Glc7p complex is a cortical regulator of dynein; inhibitor of the actin assembly factor Bnr1p (formin); diploid mutants display a random budding pattern instead of the wild-type bipolar pattern; relative distribution to the nucleus increases upon DNA replication stress
YAR015W	ADE1	N-succinyl-5-aminoimidazole-4-carboxamide ribotide synthetase; required for 'de novo' purine nucleotide biosynthesis; red pigment accumulates in mutant cells deprived of adenine; protein abundance increases in response to DNA replication stress
YAR018C	KIN3	Nonessential serine/threonine protein kinase; possible role in DNA damage response; influences tolerance to high levels of ethanol
YAR020C	PAU7	Member of the seripauperin multigene family; active during alcoholic fermentation, regulated by anaerobiosis, inhibited by oxygen, repressed by heme
YAR023C	YAR023C	Putative integral membrane protein; member of DUP240 gene family

YAR027W	UIP3	Putative integral membrane protein of unknown function; interacts with Ulp1p at the nuclear periphery; member of DUP240 gene family
YAR028W	YAR028W	Putative integral membrane protein; member of DUP240 gene family; GFP-fusion protein is induced in response to the DNA-damaging agent MMS
YAR031W	PRM9	Pheromone-regulated protein; contains 3 predicted transmembrane segments and an FF sequence, a motif involved in COPII binding; member of DUP240 gene family; PRM9 has a paralog, PRM8, that arose from a segmental duplication
YAR035W	YAT1	Outer mitochondrial carnitine acetyltransferase; minor ethanol-inducible enzyme involved in transport of activated acyl groups from the cytoplasm into the mitochondrial matrix; phosphorylated
YAR037W	None	None
YAR040C	None	None
YAR042W	SWH1	Protein similar to mammalian oxysterol-binding protein; contains ankyrin repeats; localizes to the Golgi and the nucleus-vacuole junction; SWH1 has a paralog, OSH2, that arose from the whole genome duplication
YAR043C-a	None	None
YAR044W	YAR044W	Protein similar to mammalian oxysterol-binding protein; contains ankyrin repeats; localizes to the Golgi and the nucleus-vacuole junction; SWH1 has a paralog, OSH2, that arose from the whole genome duplication
YAR047C	YAR047C	Dubious open reading frame; unlikely to encode a functional protein, based on available experimental and comparative sequence data
YBL042C	FUI1	High affinity uridine permease, localizes to the plasma membrane; also mediates low but significant transport of the cytotoxic nucleoside analog 5-fluorouridine; not involved in uracil transport; relative distribution to the vacuole increases upon DNA replication stress
YBR266C	SLM6	Protein with a potential role in actin cytoskeleton organization; gene exhibits synthetic genetic interaction with MSS4 encoding phosphatidylinositol 4-phosphate kinase
YDL158C	YDL158C	Dubious open reading frame; unlikely to encode a functional protein, based on available experimental and comparative sequence data
YDL169C	UGX2	Protein of unknown function; transcript accumulates in response to any combination of stress conditions
YDR120C	TRM1	tRNA methyltransferase; two forms of the protein are made by alternative translation starts; localizes to both the nucleus and mitochondrion to produce the modified base N2,N2-dimethylguanosine in tRNAs in both compartments
YDR158W	HOM2	Aspartic beta semi-aldehyde dehydrogenase; catalyzes the second step in the common pathway for methionine and threonine biosynthesis; expression regulated by Gcn4p and the general control of amino acid synthesis
YDR226W	ADK1	Adenylate kinase, required for purine metabolism; localized to the cytoplasm and the mitochondria; lacks cleavable signal sequence; protein abundance increases in response to DNA replication stress
YER060W-A	FCY22	Putative purine-cytosine permease; very similar to Fcy2p but cannot substitute for its function
YGL016W	KAP122	Karyopherin beta; responsible for import of the Toa1p-Toa2p complex into the nucleus; binds to nucleoporins Nup1p and Nup2p; may play a role in regulation of pleiotropic drug resistance

YGL031C	RPL24A	Ribosomal 60S subunit protein L24A; not essential for translation but may be required for normal translation rate; homologous to mammalian ribosomal protein L24, no bacterial homolog; RPL24A has a paralog, RPL24B, that arose from the whole genome duplication
YGL072C	YGL072C	Dubious open reading frame; unlikely to encode a functional protein, based on available experimental and comparative sequence data; partially overlaps the verified gene HSF1; null mutant displays increased resistance to antifungal agents gliotoxin, cycloheximide and H ₂ O ₂
YGR159C	NSR1	Nucleolar protein that binds nuclear localization sequences; required for pre-rRNA processing and ribosome biogenesis
YGR182C	YGR182C	Dubious open reading frame; unlikely to encode a functional protein, based on available experimental and comparative sequence data; partially overlaps the verified ORF TIM13/YGR181W
YGR188C	BUB1	Protein kinase involved in the cell cycle checkpoint into anaphase; forms complex with Mad1p and Bub3p crucial to preventing cell cycle progression into anaphase in presence of spindle damage; CDC28-mediated phosphorylation at Bub1p-T566 is important for degradation in anaphase and adaptation of checkpoint to prolonged mitotic arrest; associates with centromere DNA via Skp1p; BUB1 has a paralog, MAD3, that arose from the whole genome duplication
YHL011C	PRS3	5-phospho-ribosyl-1(alpha)-pyrophosphate synthetase; synthesizes PRPP, which is required for nucleotide, histidine, and tryptophan biosynthesis; one of five related enzymes, which are active as heteromultimeric complexes
YHL031C	GOS1	v-SNARE protein involved in Golgi transport; homolog of the mammalian protein GOS-28/GS28
YHR041C	SRB2	Subunit of the RNA polymerase II mediator complex; associates with core polymerase subunits to form the RNA polymerase II holoenzyme; general transcription factor involved in telomere maintenance
YHR060W	VMA22	Peripheral membrane protein that is required for vacuolar H ⁺ -ATPase (V-ATPase) function, although not an actual component of the V-ATPase complex; functions in the assembly of the V-ATPase; localized to the yeast endoplasmic reticulum (ER)
YJL115W	ASF1	Nucleosome assembly factor; involved in chromatin assembly and disassembly, anti-silencing protein that causes derepression of silent loci when overexpressed; plays a role in regulating Ty1 transposition; relocates to the cytosol in response to hypoxia
YJL129C	TRK1	Component of the Trk1p-Trk2p potassium transport system; 180 kDa high affinity potassium transporter; phosphorylated in vivo and interacts physically with the phosphatase Ppz1p, suggesting Trk1p activity is regulated by phosphorylation; TRK1 has a paralog, TRK2, that arose from the whole genome duplication
YJL183W	MNN11	Subunit of a Golgi mannosyltransferase complex; this complex also contains Anp1p, Mnn9p, Mnn10p, and Hoc1p, and mediates elongation of the polysaccharide mannan backbone; has homology to Mnn10p
YKL206C	ADD66	Protein involved in 20S proteasome assembly; forms a heterodimer with Pba1p that binds to proteasome precursors; interaction with Pba1p-Add66p may affect function of the mature proteasome and its role in maintaining respiratory metabolism; similar to human PAC2 constituent of the PAC1-PAC2 complex involved in proteasome assembly
YKR067W	GPT2	Glycerol-3-phosphate/dihydroxyacetone phosphate sn-1 acyltransferase; located in lipid particles and the ER; involved in the stepwise acylation of glycerol-3-phosphate and dihydroxyacetone in lipid biosynthesis; the most conserved motifs and functionally relevant residues are oriented towards the ER lumen

YKR072C	SIS2	Negative regulatory subunit of protein phosphatase 1 (Ppz1p); involved in coenzyme A biosynthesis; subunit of phosphopantothencysteine decarboxylase (PPCDC: Cab3p, Sis2p, Vhs3p) complex and the CoA-Synthesizing Protein Complex (CoA-SPC: Cab2p, Cab3p, Cab4p, Cab5p, Sis2p and Vhs3p); SIS2 has a paralog, VHS3, that arose from the whole genome duplication
YLR303W	MET17	Methionine and cysteine synthase (O-acetyl homoserine-O-acetyl serine sulfhydrylase), required for sulfur amino acid synthesis
YLR315W	NKP2	Central kinetochore protein and subunit of the Ctf19 complex; mutants have elevated rates of chromosome loss; orthologous to fission yeast kinetochore protein cnl2
YML088W	UFO1	F-box receptor protein; subunit of the Skp1-Cdc53-F-box receptor (SCF) E3 ubiquitin ligase complex; binds to phosphorylated Ho endonuclease, allowing its ubiquitylation by SCF and subsequent degradation
YML107C	PML39	Protein required for nuclear retention of unspliced pre-mRNAs along with Mlp1p and Pml1p; anchored to nuclear pore complex via Mlp1p and Mlp2p; found with the subset of nuclear pores farthest from the nucleolus; may interact with ribosomes
YMR014W	BUD22	Protein required for 18S rRNA maturation and small ribosomal subunit biogenesis; cosediments with pre-ribosomal particles; mutation decreases efficiency of +1 Ty1 frameshifting and transposition, and affects budding pattern
YMR188C	MRPS17	Mitochondrial ribosomal protein of the small subunit
YMR267W	PPA2	Mitochondrial inorganic pyrophosphatase; required for mitochondrial function and possibly involved in energy generation from inorganic pyrophosphate
YNL248C	RPA49	RNA polymerase I subunit A49
YOR369C	RPS12	Protein component of the small (40S) ribosomal subunit; homologous to mammalian ribosomal protein S12, no bacterial homolog
YPL086C	ELP3	Subunit of Elongator complex; Elongator is required for modification of wobble nucleosides in tRNA; exhibits histone acetyltransferase activity that is directed to histones H3 and H4; disruption confers resistance to K. lactis zymotoxin
YPL244C	HUT1	Protein with a role in UDP-galactose transport to the Golgi lumen; has similarity to human UDP-galactose transporter UGTrel1, exhibits a genetic interaction with S. cerevisiae ERO1
YPL269W	KAR9	Karyogamy protein required for correct positioning of the mitotic spindle and for orienting cytoplasmic microtubules, localizes at the shmoo tip in mating cells and at the tip of the growing bud in small-budded cells through anaphase
YPR023C	EAF3	Component of the Rpd3S histone deacetylase complex; Esa1p-associated factor, nonessential component of the NuA4 acetyltransferase complex, homologous to Drosophila dosage compensation protein MSL3; plays a role in regulating Ty1 transposition
YPR124W	CTR1	High-affinity copper transporter of the plasma membrane; mediates nearly all copper uptake under low copper conditions; transcriptionally induced at low copper levels and degraded at high copper levels; protein increases in abundance and relocalizes from nucleus to plasma membrane upon DNA replication stress
YPR139C	LOA1	Lysophosphatidic acid acyltransferase; involved in triacylglyceride homeostasis and lipid droplet formation; localized to lipid droplets and the ER; specificity for oleoyl-CoA

Appendix 13: Schwartzmüller *et al.*, 2013 paper submitted to PLoS Pathogens.

Systematic Phenotyping of a Genome-Scale *Candida glabrata* Deletion Collection Reveals Novel Antifungal Tolerance Genes

Tobias Schwarz Müller¹, Biao Ma^{2,3,*}, Ekkehard Hiller⁴, Fabian Istel¹, Michael Tschermer¹, Sascha Brunke^{5,6,7}, Lauren Ames^{2,8}, Arnaud Firon^{9,10,*}, Brian Green³, Vitor Cabral^{9,10,11}, Marina Marcet-Houben¹², Ilse D. Jacobsen^{5,6,7}, Jessica Quintin^{13,#}, Katja Seider⁵, Ingrid Frohner¹, Walter Glaser¹, Helmut Jungwirth¹⁴, Christophe d'Enfert^{9,10}, Dominique Ferrandon¹³, Toni Gabaldón^{12,15}, Bernhard Hube^{5,6,7}, Steffen Rupp⁴, Brendan Cormack^{3,§}, Ken Haynes^{2,8,§} & Karl Kuchler^{1,§}

From the

¹ Medical University Vienna, Max F. Perutz Laboratories, Department of Medical Biochemistry, A-1030 Vienna, Austria

² Department of Microbiology, Imperial College London, London, SW7 2AZ, UK

³ Department of Molecular Biology and Genetics, Johns Hopkins University School of Medicine, Baltimore, MD 21205, USA

⁴ Molekulare Biotechnologie MBT Fraunhofer Institut für Grenzflächen- und Bioverfahrenstechnik IGB Fraunhofer, 70569 Stuttgart, Germany

⁵ Department Microbial Pathogenicity Mechanisms, Hans-Knoell-Institute, 07745 Jena, Germany

⁶ Friedrich Schiller University, Jena, Germany

⁷ Center for Sepsis Control and Care, CSCC, Jena University Hospital, 07740 Jena, Germany

⁸ Biosciences, College of Life & Environmental Sciences, University of Exeter, EX4 4QD, UK

⁹ Institut Pasteur, Unité Biologie et Pathogénicité Fongiques, Département Génomes et Génétique, F-75015 Paris, France

¹⁰ INRA, USC2019, F-75015 Paris, France

¹¹ Univ. Paris Diderot, Sorbonne Paris Cité, Cellule Pasteur, rue du Docteur Roux, F-75015 Paris, France

¹² Bioinformatics and Genomics Programme. Centre for Genomic Regulation (CRG). Dr. Aiguader, 88. 08003 Barcelona

¹³ UPR 9022 du CNRS, Université de Strasbourg, Equipe Fondation Recherche Médicale, Institut de Biologie Moléculaire et Cellulaire, 67084 Strasbourg, France

¹⁴ Institut für Molekulare Biowissenschaften, Universität Graz, 8010 Graz

¹⁵ Universitat Pompeu Fabra (UPF), 08003 Barcelona, Spain

* Present address: Institut Pasteur, Unité de Biologie des Bactéries Pathogènes à Gram-positif, F-75015 Paris, France

+ Present address: The Babraham Institute, Babraham Research Campus, Cambridge, CB22 3AT, UK

Present address: Radboud University Nijmegen Medical Centre, Department of Experimental Internal Medicine, 6525 GA Nijmegen, The Netherlands

Keywords: *Candida glabrata*, gene deletion collection, chemogenetic profiling, biofilm formation, morphology, antifungal drug resistance, echinocandin, cell surface homeostasis

§ To whom correspondence should be addressed:

Karl Kuchler

Medical University Vienna; Max F. Perutz Laboratories

Department of Medical Biochemistry

Dr. Bohr-Gasse 9/2, A-1030 Vienna, Austria

Phone: +43-1-4277-61807; FAX: +43-1-4277-9618; E-mail:

karl.kuchler@meduniwien.ac.at

Ken Haynes

Biosciences - College of Life and Environmental Sciences, University of Exeter

Geoffrey Pope 325, Stocker Road, Exeter, EX4 4QD, UK

Phone: +44 1392 725152; FAX: +44 1392 263434; E-mail: k.haynes@exeter.ac.uk

Brendan Cormack

Department of Molecular Biology and Genetics; Johns Hopkins University School of Medicine

617 Hunterian, 725 N Wolfe Street, Baltimore, MD 21205, USA

Phone: +1410-614-4923; FAX: +1 410-502-6718; E-mail: bcormack@jhmi.edu

Abstract

The opportunistic fungal pathogen *Candida glabrata* is a frequent cause of candidiasis, causing infections ranging from superficial to life-threatening disseminated disease. The inherent tolerance of *C. glabrata* to azole drugs makes this pathogen a serious clinical threat. To identify genes implicated in drug resistance, we have constructed a genome-scale *C. glabrata* deletion library consisting of 619 unique individually bar-coded mutant strains, each lacking one specific gene. Functional analysis of this library in a series of phenotypic and fitness assays identified numerous genes required for growth of *C. glabrata* under normal or specific stress conditions, as well as a number of novel genes involved in tolerance to clinically important antifungal drugs such as azoles and echinocandins. We identified 39 deletions displaying increased susceptibility to caspofungin, 28 of which are novel, encoding functions that have not previously been linked to echinocandin tolerance. Our results demonstrate the potential of the *C. glabrata* mutant collection as a valuable resource in functional genomics studies of this important fungal pathogen of humans, and to facilitate the identification of putative novel antifungal drug target and virulence genes.

Author Summary

Clinical infections by the yeast-like pathogen *Candida glabrata* have been ever-increasing over the past years. Importantly, *C. glabrata* is one of the most prevalent causes of drug-refractory fungal infections in humans. We have generated a novel genome-scale collection of some 619 bar-coded *C. glabrata* mutants, each lacking a single gene. Extensive profiling of phenotypes reveals a number of novel genes implicated in tolerance to antifungal drugs that interfere with proper cell wall function, as well as genes affecting fitness of *C. glabrata* both during normal growth and under environmental stress. This fungal deletion collection will be an valuable resource for the community to study mechanisms of virulence and antifungal drug tolerance in *C. glabrata*, which is particularly relevant in view of the increasing prevalence of infections caused by this important human fungal pathogen.

Introduction

Candida glabrata, a small, asexual, haploid yeast, is the second most frequent cause of candidiasis after *Candida albicans*, accounting for approximately 15%-25% of clinical cases [1-4]. *C. glabrata* forms part of the normal microbial flora in humans, but can cause serious infections in immunocompromised and hospitalized patients; antibiotic exposure and presence of central venous catheter devices, being additional important risk factors for disease development [2]. In contrast to the pleomorphic diploid *C. albicans* [5], *C. glabrata* is found clinically, exclusively as monomorphic yeast cells. It also lacks several attributes considered key mediators of fungal pathogenicity in other *Candida* spp, such as secretion of proteases and lipases [6,7]. Despite the apparent absence of these well-known fungal virulence traits, *C. glabrata* remains highly pathogenic to humans. Hence, *C. glabrata* may rely upon distinct strategies and other virulence attributes to initiate infection, as well as to persist in infected patients.

Some traits that have been linked to the clinical importance and virulence of *C. glabrata* include an inherently elevated tolerance to azole antifungals [8-11]; the presence of a large repertoire of telomere-associated adhesins [12-18]; melanin-like pigment production [19]; adaptation to the acidic phagosomal environment and intra-phagosomal survival [20-22]; and Ace2-dependent components of the cell wall [23]. However, it is clear that the molecular basis of *C. glabrata* virulence is far from being completely understood.

C. glabrata clinical isolates generally exhibit a high inherent tolerance level to azole drugs [9]. While this trait has been extensively studied, the underlying mechanisms remain incompletely explained. Azole resistance can be acquired through increased expression of genes encoding ABC transporters (Cdr1, Pdh1, Snq2) or changes in their transcriptional regulatory system (Pdr1, Gal11) [24-28]. Mitochondrial dysfunction [29] and serum utilization via the putative sterol transporter Aus1 [30,31] also impact the ability of *C. glabrata* to tolerate high azole levels. It remains unclear if these are the only mechanisms driving azole resistance in *C. glabrata*. However, the

clinical implications of this resistance demand alternative antifungals for effective treatment *C. glabrata* infections in patients, especially since *C. glabrata* infections are globally rising, sometimes accounting for more than 30% of clinical cases [32].

Echinocandins such as caspofungin (CF), anidulafungin and micafungin are a relatively new class of effective yet high-cost antifungal drugs targeting fungal 1,3- β -D-glucan synthases and thereby impairing cell wall integrity [33]. Mutations in subunits of glucan synthases can render fungi resistant to echinocandin [33-36]. Surprisingly, even ectopic overexpression of the *C. albicans* Cdr2 efflux ABC transporter gene in both laboratory strains and clinical isolates markedly increases CF tolerance [37]. However, a better understanding of molecular mechanisms modulating echinocandin susceptibility is necessary, since it may facilitate targeted drug discovery, especially in the case of emerging resistant strains [38].

Reverse genetics coupled with global functional profiling has proven a powerful approach to identify genes required for specific phenotypes. Functional genomics studies in the non-pathogenic yeast *S. cerevisiae* have provided the starting point to decipher genotype-phenotype relations as it enabled answers about fundamentally important questions concerning complex genetic interactions and the genetic landscape of yeast. These approaches also unraveled stress response mechanisms and provided new insights into drug susceptibility and morphogenesis [39-46]. Heroic efforts by a few groups have recently resulted in highly useful genome-scale deletion collections of the major pathogen *C. albicans* [47-49] and *Cryptococcus neoformans* [50], enabling the identification of novel virulence genes and further demonstrating the power of a functional genomics approach.

Here, we have adapted a semi-automated approach [48] for constructing gene deletions to generate a collection of individually bar-coded strains in the sequenced *C. glabrata* strain ATCC 2001 [51], each lacking one defined open reading frame. We took advantage of this library to undertake the first systematic functional genomic analysis of *C. glabrata*, in particular examining the response to traits putatively implicated in

virulence and antifungal resistance. We performed a series of growth assays in distinct media to determine the impact of gene deletion on fitness. We then determined the susceptibility of the collection to major antifungal compounds (including azoles and caspofungin) and various other cell wall-damaging compounds. Finally, we investigated the effect on cellular morphology on fitness *in vitro*, and the ability to form biofilms. This enabled us to generate the first large-scale chemogenetic and phenotypic profile of *C. glabrata*. Our analysis revealed numerous novel genes implicated in stress response, cell wall homeostasis, growth morphology and fitness. Most importantly, we discover numerous novel genes implicated in susceptibility to echinocandins, demonstrating the usefulness of this deletion collection for the functional analysis of virulence-related, as well as clinically relevant traits, including the discovery of novel antifungal target genes.

Results

Gene selection. Using a large-scale phylogenetic approach across many fungal species [52], we identified 1047 putatively non-essential candidate genes in *C. glabrata* representing functional GO categories such as environmental stress sensing and signaling (MAPK pathways, TOR, RIM, PKA); transcriptional regulation; antifungal drug resistance (PDR network, membrane permeases); cell wall structure and homeostasis (glucan, mannan, chitin synthesis, glycosylation, adhesins, glycosylphosphatidylinositol (GPI)-anchor); chromatin and histone modification; iron metabolism and metal sensitivity; peroxisome biogenesis. We also selected genes lacking obvious orthologues in *S. cerevisiae* (Supplemental Table S1).

Parental recipient strains. To enable the rescue of deletion phenotypes and to facilitate double- or triple mutant construction, we engineered a triple-auxotrophic recipient strain in the sequenced type strain *C. glabrata* ATCC 2001 [51]. We used the dominant recyclable nourseothricin resistance marker *SAT1* [53] to replace the coding sequences of *HIS3*, *LEU2* and *TRP1* (Supplemental Figure S1-A). The repeated use of this marker cassette resulted in the new *C. glabrata* background recipient strain for deletions referred to as HTL (*his3Δ::FRT leu2Δ::FRT trp1Δ::FRT*), as well as all possible isogenic single deletions and all combinations of double deletion strains (Supplemental Table S2). We also constructed a bar-coded version of the HTL strain, *C. glabrata* HTL reference, by inserting 20bp barcodes flanking the *trp1* locus (Supplemental Table S2). The transcription factor (TF) mutants were made in a *his3* derivative of ATCC 2001, the majority using a codon-optimized version of the *NAT1* marker [54]. We avoided the use of the *URA3* marker in *C. glabrata*, since it is known to alter virulence properties of *C. albicans* [55,56]. The HTL strain displayed similar growth properties and rates as the parental strain, on both minimal and full media (Supplemental Figure S1C). Importantly, the auxotrophic markers did not significantly influence growth *in vitro*, or the survival in immunocompetent mice when compared to

the parental wild type strain [57]. While the growth behaviour of *C. glabrata* HTL was largely unchanged, these cells reached a slightly lower maximal cell density when growing in minimal media when compared to wild type cells (Supplemental Figure 1C).

Gene deletion strategy. Targeted gene disruption with short-homology flanking regions, as was done to construct the *S. cerevisiae* knock-out library, is inefficient in *C. glabrata*. Higher targeting efficiency requires the use of ≥ 500 base pair (bp) flanking regions [58]. Therefore, to maximise efficiency of gene replacement, we adapted and automated the fusion PCR technique [48] to generate gene deletion constructs containing ~ 500 bp homologous flanking regions for every gene, fused to the dominant marker *NAT1* and flanked by unique barcode identifiers (Figure 1A). We employed a limited set of barcode sequences selected from those successfully used in the *S. cerevisiae* genome deletion project [40,46]. These barcodes enable quantification and tracking of single mutants in pool experiments. A complete list of all barcode sequences corresponding to each deleted ORF in the collection is given in Supplemental Table S3.

C. glabrata recipient strains were transformed with these deletion cassettes using a modified 96-well format electroporation protocol. All resulting nourseothricin-resistant transformants were tested for correct genomic integration by colony PCR to verify both 5' and 3' junctions (Figure 1B). Single colonies of up to six verified transformants for each gene were isolated; the absence of the corresponding gene from the genome was confirmed using another PCR-based step and confirmed gene deletion strains were cryo-preserved (Figure 1C). A total of 24 PCR-verified gene deletion strains were randomly selected and subjected to Southern blot analysis to confirm correct genomic replacements (data not shown).

In all, we successfully deleted 619 of the 1047 genes initially selected for inactivation, yielding a total of 1601 independent unique deletion strains (Supplemental Table S3; <http://funpath.cdl.univie.ac.at>), representing 53% of the selected genes and

about 13% of the entire *C. glabrata* genome. Notably, for 77 genes only one deletion was obtained, while the majority of deletions result from two (246) or three (224) independent transformation and thus genomic removal events (Supplemental Table S2). We assume that a large fraction of the genes that we failed to inactivate is a consequence of inefficient homologous targeting, rather than a true representation of the frequency of essential genes.

Phenotypic screening and mutant characterization. We then carried out a preliminary pilot screen using a small set of selected deletion mutants displaying known phenotypes. Mutants lacking genes of the high osmolarity glycerol (HOG) pathway, the cell integrity protein kinase C (PKC) pathway and the pleiotropic drug resistance (PDR) network were tested for growth under conditions known to affect the corresponding mutants in *S. cerevisiae*. As expected, lack of *PBS2*, encoding the central MAPK (mitogen-activated protein kinase) of the HOG pathway [59], resulted in severe osmosensitivity (Supplemental Figure S2-A). Likewise, azole hypersensitivity was observed in *cdr1* and *pdr1* strains (Supplemental Figure S2-B) [24-26,28,60,61]. Finally, as previously shown, cells lacking the *SLT2* kinase of PKC pathway [62,63] displayed drastic hypersensitivities to CF (Supplemental Figure S2-C). Following these initial experiments, which served to establish and validate screening parameters, the collection of 1601 gene deletion mutants was subjected to extensive phenotypic profiling in four independent laboratories using the same conditions, including a variety of assays to monitor growth properties, fitness, stress and antifungal susceptibility, biofilm formation, as well as obvious colony or cellular morphology alterations.

Growth and fitness defects. Changes in the pathogenic potential of a fungus may be associated with a gain or loss of *in vitro* or *in vivo* growth, influencing the ability to efficiently replicate in the host or to withstand antifungal treatment [64]. Thus, we measured the growth rates of individual mutants in the deletion collection in YPD at

30°C. For each deletion strain, a relative fitness index [65] was calculated using the doubling times from at least two independent cultures of 1-6 independent mutants, and compared to the doubling time of all other strains. Notably, we identified 57 deletion mutants showing strong variations in relative fitness between independent cultures (Supplemental Table S4), all of which were omitted from further analysis along with deletions that were present in duplicate. Hence, reproducible fitness data could be obtained for 504 unique mutants (representing 1125 deletions). Out of these gene knock-outs, 399 had a relative fitness index within two standard deviations (SD) of the average relative fitness (Figure 2A, Supplemental Table S5). These data suggested that the corresponding genes are not necessary for efficient planktonic growth of *C. glabrata* in YPD at 30°C. However, some 71 strains showed a significant fitness defect (doubling time of ≥ 2 SD below the average fitness). Interestingly, another 34 deletions showed a gain in fitness (doubling time of ≥ 2 SD above the average fitness) under these growth conditions (Figure 2A, Supplemental Table S6).

Notably, many deletion strains exhibiting fitness defects *in vitro* also displayed obvious alterations to colony and cellular morphology (Figure 2B). Most morphology mutants grew as small or large wrinkled or smooth colonies. Microscopic inspection of deletion mutants then allowed for further classification of mutant morphologies into small round cells (*dse2*, *tos6*, *ace2*, *chs3*, *bni4*, *cwh41*), giant cells with obvious structural defects (*cdc21*, *cbk1*, *kre6*), cells with pseudohyphal-like elongated morphologies (*gin4*), and as pearl-string-like cells connected to each other as for *dse2* mutants (Figure 2B). Notably, except for pseudohyphal morphologies [66,67] or small round cells for *ace2* [23], many of these morphological alterations have not been described in *C. glabrata* to date.

Phenotypic profiling. Fungal pathogens need to adapt to diverse host environments and environmental stresses. Relevant stresses include perturbation of cell wall integrity, pH and osmostress during phagolysosome maturation, iron or nutrient

depletion, growth at elevated temperature and exposure to antifungal drugs. An efficient adaptation to particular stress conditions may also include formation of biofilms. We therefore phenotypically profiled the mutant collection to identify genes implicated in the response to host-mimicking adverse conditions such as osmostress. Interestingly, we identified remarkably strong osmosensitivity phenotypes caused by genes that have not been linked to osmostress in other fungi before, including *atm1*, *arb1*, *kre1*, *anp1*, *mps3* and *ptr3* (Supplemental Figure S3). Moreover, we scored for susceptibilities to the major antifungal drugs fluconazole, voriconazole, amphotericin B (AmB) and CF, as well as to the cell wall stressors Congo Red (CR) and Calcofluor White (CW). Finally, we also assessed the ability to form biofilms and to grow at elevated temperatures.

Biofilm and temperature sensitivity. Biofilm formation on medical devices represents a significant risk for invasive infections by *Candida* spp [68-70]. Hence, mutants in the deletion in the collection were scored for their ability to form biofilms. Strains were induced to form biofilms in 96-well polystyrene plates in minimal medium at 37°C; the biofilm biomass was quantified using a fluorescein diacetate (FDA) accumulation assay [71,72]. For each strain, a relative biofilm-forming index was calculated using FDA hydrolysis data from at least two independent cultures of the independent deletion mutants for each gene (see Materials and Methods; Supplemental Table S7, S8, S9). Independent deletions of the same gene including duplicates showing strong variations in relative biofilm formation between independent assays or independent cultures (Supplemental Table S7) were omitted from further analysis, leaving 420 deletions for which biofilm production was analyzed in detail (Figure 3; Supplemental Table S8). Out of these, 341 gene deletions resulted in a relative biofilm forming index within two standard deviations (SD) of the average relative biofilm-forming capacity (Figure 3; Supplemental Table S9), suggesting that the corresponding genes do not contribute to biofilm formation in minimal medium at 37°C. Isolates for the 46 gene deletions that

resulted in an alteration in biofilm formation (i.e. a biofilm fitness score 2 SD below or above the average relative biofilm-forming index) but not of planktonic growth at 30°C were retested in quadruplicate for their ability to form biofilms. Moreover, the planktonic growth rate of these strains in minimal medium at 37°C was monitored to assess possible effects of the higher incubation temperature on biofilm formation. Notably, a number of the corresponding deletions also displayed temperature-sensitive phenotypes and may therefore not be solely biofilm-specific. Yet, this analysis identified 14 gene deletions that resulted in significant defects in biofilm formation and no defect in planktonic growth (*AVO2*, *BCY1*, *CCW12*, *CCH1*, *CNB1*, *DCW1*, *GAS1*, *MHP1*, *PKH2*, *SLM1*, *SUB1*, *UTP14*, *YNL300W*, *YOR1*; Supplemental Table S8). Remarkably, we identified 11 gene knock-outs resulting in a gain in biofilm formation without an increase in planktonic growth (*BPH1*, *GAL11*, *GPB2*, *MIG1*, *PEX2*, *SSN2*, *SSN8*, *STE20*, *YAP6*, *YDR134C*, *YVC1*; Supplemental Table S8). Notably, the heat stress profiling on plates identified several genes implicated in cell wall biogenesis and organization, including *CWH41*, *ALG5*, *OST3*, *ALG6*, *KTR2*, *BIG1*, *CBK1*, *ALG3*. Interestingly, this gene set showed some overlap with the CF, CR or CW gene clusters (Figure 4), suggesting that heat stress triggers a distinct set of partially overlapping signaling response pathways, ranging from stress and cell integrity signaling to cell wall homeostasis and lipid membrane perturbation.

Susceptibility to azole and AmB antifungals. Azoles and AmB remain the most common drugs for treating fungal infections. The reduced azole susceptibility of the majority of *C. glabrata* clinical isolates is considered a major contributor to its clinical prevalence [73]. While this is mainly the consequence of transcriptional upregulation of the *CDR1* and *PDH1* (*CDR2*) encoding membrane efflux pumps or gain-of-function mutations in the *PDR1* regulator [28], additional mechanisms may play a role. The polyene AmB is thought to impair membrane function by binding to ergosterol, resulting in cellular leakage of cytoplasm [74]. While *C. glabrata* can develop AmB tolerance

[75,76], the underlying molecular mechanisms remain obscure. We have thus used the *C. glabrata* deletion collection to identify genes modulating azole as well as AmB susceptibility. A total of 14 deletions displayed marked hypersensitivities to azoles such as fluconazole and voriconazole albeit to a different extent (Supplemental Figure S5-A,C; Figure 4B). Moreover, 13 deletions were hypersusceptible AmB (Supplemental Figure S6-A, Figure 4B). The corresponding mutants were retested using microdilution assays to quantify their IC₅₀ values (Supplemental Figure S5-C,D; Supplemental Figure S6-B). The majority of the 14 azole-sensitive strains were sensitive to both fluconazole and voriconazole (Supplemental Figure S5-C,D), while 6 strains (*ktr2*, *cwh41*, *ssd1*, *ktr6*, *hap1* and *slt2*) appeared more sensitive to voriconazole. Notably, the strain lacking the *KTR2* gene encoding a mannosyltransferase [77] displayed the most significant voriconazole-specific hypersensitivity (Supplemental Figure S5-C,D). As expected, deletion of either the *PDR1* transcription factor or its target *CDR1* efflux pump resulted in marked azole hypersensitivity. Interestingly, calcineurin pathway mutants such as *cna1* and *cnb1* also displayed pronounced azole hypersensitivities. Several additional signaling mutants (*slt2*, *wsc1*, *ypk1*, *cka2*), as well as cell wall mutants (*ktr2*, *cwh41*, *ssd1*, *ktr6*) displayed slight to intermediate azole hypersensitivities (Supplemental Figure S5-A,B; Figure 4B). Among the 13 AmB-sensitive strains, the five genes displaying the most pronounced susceptibilities play diverse roles in phospho- and sphingolipid signaling, including *YPK1*, *CKA2*, *DEP1*, *SNF6* and *VPS15*.

Cell wall stress and CF sensitivity. The fungicidal echinocandins stand out as the most efficient clinically used drugs that block cell wall glucan biogenesis. Thus, we subjected the deletion collection to profiling for susceptibilities to caspofungin (CF), as well as other cell wall stressors such as CR and CW (Figure 4, Figure 5, Supplemental Figure 7). A total of 12 mutants were strongly hypersensitive to CR, and six to CW (Figure 4A; Supplemental Figure S7-BC). Unsurprisingly, deletion of genes encoding

functions implicated in cell wall integrity or polarity (*PSA1*, *KRE1*, *CWH41*, *OST3*, *KTR2*, *MNN10*, *ANP1*, *CBK1*) conferred hypersensitivity to CR and/or CW. Strikingly, we identified 48 mutants with altered CF susceptibilities (Figure 4A,B), 38 of which were strongly hypersensitive, while another 9 were mildly CF-sensitive, including *MET31*, *RTG3*, *OST3*, *KTR1*, *YFH1*, *TNA1*, *ATM1*, *SNF6*, *CRZ1* (Figure 4, Supplemental Figure 9).

To identify the functionally overlapping mutants, we used hierarchical clustering of stress-induced phenotypes, including heat, CF, CR and CW, identifying some 106 putative chemical-genetic interactions (Figure 5). The clustering approach identified three subsets of deletion mutants displaying distinct but partially overlapping hypersensitivities to high temperature, CR, CW and CF (Figure 5). Remarkably, the profiling analysis revealed some 28 novel CF tolerance genes, none of which had previously been associated with echinocandin hypersensitivities in *S. cerevisiae*, *C. albicans* or in other fungal pathogens (Figure 4, Figure 5). Notably, the group of genes affecting CF sensitivity was highly enriched in genes operating in the PKC cell integrity signaling pathway (*WSC1*, *SLT2*, *BCK1*, *MKK1*), in calcium / calcineurin signaling (*CNA1*, *CNB1*, *MID1*, *CCH1*), general cell wall homeostasis, including mannosylation and glycosylation (*MNN10*, *ANP1*, *MNS1*, *MNT3*, *PMT2*, *PSA1*, *KRE2*), as well as transcriptional regulators (*RLM1*, *DEP1*, *POP2*, *SPT3*, *MCM1*, *SIP3*, *SNF1*). Interestingly, deletion of several genes encoding components of the chromatin and histone modification machinery (*RPD3*, *HEK2*, *MPS3*, *SDS3*, *SIN3*, *ASF1*) also modulated CF susceptibility, suggesting an important regulatory role for chromatin in controlling surface homeostasis and CF susceptibility, as recently demonstrated for the *C. albicans* Hat1 acetyltransferase [78]. The removal of only three genes (*WSC1*, *CNB1* and *CNA1*) resulted in sensitivity to all three cell wall stressors (Figure 4A), confirming the pivotal roles PKC and calcineurin signaling pathways play in sensing and maintaining cell wall homeostasis in fungal pathogens [35,79,80].

Discussion

C. glabrata is an important human fungal pathogen, and after *C. albicans*, the second-most frequent cause of candidiasis, causing 15-30% of infections in humans [1-4]. Although *C. glabrata* appears similar to *S. cerevisiae* concerning gene synteny and conservation it is an obligate haploid, and the lack of a sexual cycle and elevated rates of non-homologous recombination have prevented a systematic genetic analysis. Importantly, the decreased sensitivity of *C. glabrata* clinical isolates to azoles antifungals is at least in part responsible for its clinical significance [32]. To address these issues, as well as to better understand virulence properties, we have generated a genome-scale deletion collection of *C. glabrata*. This deletion mutant collection comprising 619 unique strains each lacking a single gene has several advantages over known transposon-based mutant collections [81], since each ORF is completely removed. Thus, gene dosage effects or dominant phenotypes from truncated protein variants are excluded. Likewise, aberrantly expressed proteins due to insertion in promoters, which may result in partial loss or gain-of-function for the corresponding gene product, are precluded. The deletion collection was subjected to extensive phenotypic profiling, with a particular emphasis on susceptibility to major antifungal drugs, growth and morphology phenotypes, stress response pathways, cell wall biogenesis as well as biofilm formation, which has been associated with the initiation and development of candidiasis [82]. Importantly, we show here the feasibility to generate a genome-scale bar-coded gene deletion library in *C. glabrata*, revealing novel genes contributing to fitness, biofilm formation, antifungal drug resistance and several genes implicated in general cell wall homeostasis. We found a large number of mutants sensitive to at least one of the tested conditions. About 21% of the mutants display altered fitness and about 19% show alterations in biofilm formation, while only 2% exhibit abnormal cell and colony morphology. Approximately 15% of the mutants show severe stress-related phenotypes, including hypersensitivity to several antifungal drugs, heat and osmostress conditions.

General fitness defects and biofilm formation. *C. glabrata* and *S. cerevisiae* are phylogenetically related [51]. Hence, many orthologous gene functions may have been conserved between the two species. Remarkably however, several mutants with reduced or increased fitness in rich media corresponded to genes whose inactivation in *S. cerevisiae* resulted in entirely different or opposing phenotypes. These include homologous genes from the RAS-PKA pathway (*RAS2*, *GPA2* and *GPR1*) and genes involved in N-glycosylation and outer chain elongation (*ALG5*, *KTR2* and *MNN4*). Moreover, several genes known to be essential in *S. cerevisiae* were non-essential in *C. glabrata*, although their inactivation often confers reduced fitness or morphology defects. These include *MEC1*, encoding a master DNA damage checkpoint kinase [83], and *CBK1*, although the latter is only essential in the yeast background S288c [84]. *CBK1* encodes a RAM network kinase that is central to the establishment of cell polarity and involved in septum formation and cell separation and morphogenesis [85-88]. Notably, inactivation of the orthologous genes in *C. albicans* is not lethal [88-90]. Hence, Mec1- and Cbk1-dependent regulatory networks may operate differently between *S. cerevisiae* and *C. glabrata* and, possibly, other hemiascomycetous yeasts. Many biological processes and regulatory networks in fungi have evolved under distinct evolutionary pressures [91,92]. Because *Candida* spp have evolved as opportunistic pathogens of mammals, including humans, it is fair to propose that adaptation to the host environment and immunity surveillance may have been driving the evolution of functionally rewired genetic regulatory networks [93]. Finally, and as expected, mutants with altered abilities to form biofilms are enriched for cell wall-related genes. Notably, the biofilm mutant lacking the putative kinase gene *PKH2/CAGL0I07513g*, whose orthologue in *S. cerevisiae* encodes a component of the alternative cell wall integrity pathway, has two additional paralogues in *C. glabrata*, namely *CAGL0G04609g* and *CAGL0K06479g*. While *pkh2* mutants are defective in both biofilm formation and growth on solid media, lack of the other two paralogues leaves biofilm formation or

growth on solid media unaffected (data not shown). Thus, these data suggest that apparent *PKH* kinase homologues in *C. glabrata* have acquired some specialization concerning their roles in the sensing of cell integrity.

Antifungal drug sensitivity. We generated the first chemical-genetic profile of *C. glabrata* relevant to the understanding of drug susceptibilities *in vitro*. In addition to known genes implicated in azole resistance (*PDR1*, *CDR1*, *PDH1*), the profiling for azoles revealed only small number of novel genes (*YPK1*, *KTR2*) mediating azole tolerance, with *KTR2* even showing a significant a azole-specificity for voriconazole. These data imply that *C. glabrata* utilizes a limited set of mechanisms to mount azole resistance, with ABC transporter-mediated efflux by Cdr1 and Pdh1 being the most important one *in vitro* and *in vivo* [64].

The results from our screen showed some overlap with phenotypic screens in *S. cerevisiae* [94] and *C. albicans* [95] regarding sensitivity to CF, which belongs to the family of the fungicidal echinocandin drugs that inhibit the fungal 1,3- β -D-glucan synthase. Out of 38 mutants showing strong alterations in echinocandin sensitivities, 16 correspond to genes whose orthologues in baker's yeast and in *Candida spp* (at least for *FKS1*) have been linked to CF tolerance [35,94-96]. Hyperresistance to echinocandins can result from mutations in the glucan synthase genes *FKS1* or *FKS2* [34], as well as through the PKC pathway that mediates CF tolerance in *S. cerevisiae* [63] and *C. albicans* [97]. Accordingly, *wsc1*, *slt2*, *mkk1*, *bck1*, *rlm1* and *fks1* mutant cells, all lacking key genes of this central pathway, are also hypersensitive to CF in our assays. Despite the apparent differences between species, this overlap validates the phenotypic profiling to identify genes relevant for echinocandin susceptibility. Intriguingly, 23 genes whose deletion resulted in marked hypersensitivity to CF in *C. glabrata* have not previously been associated with CF susceptibility in yeast or any other fungal pathogens or heterozygous mutant collections from *C. albicans* [95]. While determining CF hypersensitivity phenotypes can be challenging, because many mutant

strains with aberrant cell morphologies (*cdc12*, *ace2*, *fkh2*, *cbk1*) or strong growth fitness defects (*kre6*) interfere with CF spot assays, our data clearly identify novel genes implicated in CF tolerance.

Interestingly, cells lacking chitin synthesis genes such as *CHS1* were also hypersensitive to the glucan synthase inhibitor, which is in line with reports from yeast [95], and recent data from *C. albicans* showing a role for chitin in regulating cell wall susceptibility to CF [98,99]. Likewise, the absence of calcineurin subunit genes *CNA1* or *CNB1* leads to CF hypersensitivity, indicating that calcineurin signaling is necessary for buffering or compensating cell wall stress, perhaps by affecting *FKS1* transcript levels through the transcription factor Crz1 [34]. In the mould *Aspergillus fumigatus*, a mutation or inhibition of calcineurin enhances the antifungal potency of CF [100]. Thus, calcineurin inhibitors may exert synergistic effects on cell wall mutants in other fungal species. The impact of CF on calcium signaling in *C. glabrata* is further confirmed by the hypersensitivity of mutants lacking *CCH1* and *MID1*, both of which encode stress-induced calcium channel proteins.

In *S. cerevisiae*, the Ypk1-mediated signaling pathway, which is activated by lipid-sensing [101], constitutes an alternative cell integrity signaling pathway connected to the classical PKC pathway [102,103]. Remarkably, *C. glabrata* cells lacking *YPK1* and *PKH2* are CF-hypersensitive, suggesting that the Ypk1-mediated signaling plays a major role in regulating CF tolerance or cell wall homeostasis in *C. glabrata* (Figure S4, Supplemental Figure S9). Taken together, these results indicate that *C. glabrata* employs several signaling pathways to respond to CF-induced cell wall damage and the required subsequent cell wall remodeling. It is therefore not unexpected that mutants displaying CF hypersensitivities include genes that affect trafficking of proteins or surface carbohydrate homeostasis, including chitin deposition and biogenesis.

Genes implicated in the susceptibility to both CF and azoles include those encoding the calcineurin subunits Cna1 and Cnb1 and the PKC pathway components Wsc1 and Slt2. These results confirm that both pathways are necessary for a response

to both drug classes and are consistent with data showing the synergistic action of calcineurin inhibitors and azoles or CF [35,80,104-106]. Comparison of azole-sensitive, AmB-sensitive and CF-sensitive mutants show that only a small number of gene deletion strains are susceptible to all three or to at least two compounds, which is consistent with their distinct mechanism of action. Notably, deletions that confer sensitivity to all three drugs occur in genes that may encode general stress sensing kinases such as Ypk1 and the mRNA-binding protein Ssd1, which is thought to control expression of surface genes in concert with Cbk1 [107-111]. Interestingly, the function of Ypk1, a mammalian SGK kinase homologue [112], remains unclear in *C. glabrata*. It is tempting to speculate though that Ypk1 is part of a distinctly wired kinase network implicated in regulating membrane perturbations, drug sensitivity and lipid-mediated stress signalling [92,113].

AmB is thought to interfere with normal membrane bilayer function by forming complexes with ergosterol [114]. Indeed, cells deficient in membrane biogenesis or organelle dynamics may show a synthetic fitness loss upon perturbation of the lipid composition, potentially explaining the AmB hypersensitivity of *snf7*, *vps15* and *sla1* mutants. A similar reason may explain the sensitivity of cells lacking *DEP1*, which, in *S. cerevisiae*, regulates transcription of structural phospholipid biosynthesis genes [115]. Notably, the profiling analysis reveals a strong genetic interaction between AmB action and genes implicated in cell wall function. AmB-sensitive strains include mutants lacking *KRE1* and *SAC7*, which encode proteins implicated in glucan homeostasis, as well as *KTR6*, *KTR2*, *CWH41*, whose products affect surface protein glycosylation. Remarkably, the latter three mutants show pronounced azole hypersensitivity, demonstrating a direct link between membrane lipid perturbation, cell wall function and antifungal sensitivity.

The hierarchical clustering of stress-induced phenotypes caused by heat, CF, CR and CW, identifies some 106 putative chemical-genetic interactions (Figure 5). We expected to discover distinct patterns for each compound, since CR and CW mainly

affect cell wall structure and composition, whereas CF targets Fks1. Remarkably though, all compounds strongly activate cell integrity signaling, which together drives cell wall remodeling and regulates surface homeostasis. Accordingly, the CF profile was enriched for genes involved in cell wall organization, signaling and transcriptional regulators, reflecting the activity of CF as an inhibitor of fungal cell wall biosynthesis (Figure 4). Only a few genes in the CF cluster overlap with genes associated with CR and CW sensitivity (Figure 4A), most of which are involved in stress and cell wall signaling (*CNA1*, *CNB1*, *WSC1*) or cell wall biogenesis (*KRE1*, *PSA1*, *ANP1*, *MNN10*), indicating that several distinct signaling pathways must cooperate to ensure maintenance of a functional cell wall under various adverse conditions.

Importantly, we identify numerous novel genes, whose function may have *C. glabrata*-specific roles in drug susceptibility and cell wall integrity signaling. Because the phenotypes are in general hypersensitivities, these data suggest that at least some of these genes may turn out as feasible targets for drug discovery. The discovery of a large number of deletion mutants affecting CF tolerance expands our knowledge about plausible mechanisms regulating CF sensitivity. For example, the fact that several CF-sensitive mutants are implicated in exocytic delivery of cell wall components such as chitin, glucan or mannan, implies a constant cross-talk of distinct signaling pathways to control proper cell wall remodeling upon CF-induced surface damage. As the number of chemical-genetic and genomic data in baker's yeast [42,43] is steadily increasing, our data add novel information concerning the function of related genes in an important human fungal pathogen. Hence, these data represent an important contribution towards a better understanding of drug resistance mechanisms, as well as species-specific differences.

These large-scale phenotypic profiling data also demonstrate the power of the *C. glabrata* knock-out collection, which is, in addition to the *C. albicans* and *C. neoformans* collections [47,50], to the best of our knowledge, among the three largest academic deletion collections for a human fungal pathogen. This library will facilitate

studies on novel virulence factors and other aspects of *C. glabrata* pathogenicity. The use of unique sequence tags, which were adopted from the *S. cerevisiae* gene deletion collection [40], allows for the functional analysis of single gene functions *in vitro* and *in vivo* [47,50]. The use of auxotrophic marker genes [57] do not affect *in vivo* dissemination of strains in standard mouse models of fungal virulence. The design of recipient strains will even enable to study genetic interactions and pathway epistasis through double and triple mutants. Moreover, *in vivo* organ-tropism and colonization, as well as virulence can be assessed in different infection models. Notably, screens of the collection in animal models and the understanding of virulence phenotypes (or lack thereof) can be challenging and laborious requiring a very large number of animals, due to the potential impact of fitness defects on growth *in vivo* or possible genetic redundancy. We suggest that interpretation of virulence phenotypes will be aided by the *in vitro* phenotypic analysis presented here, permitting correlation of *in vitro* phenotypes and *in vivo* fitness effects for *C. glabrata*.

Similar to existing *C. albicans* [47] or *C. neoformans* [50] collections, the *C. glabrata* mutant library constitutes a valuable tool for the fungal research community to study the function of virulence and drug resistance genes in *C. glabrata*. In view of rapid changes in the epidemiology of fungal infections, with *C. glabrata* infections showing ever-increasing clinical importance reaching up to 30% prevalence in some countries [32,116], this work is the first large-scale contribution to the systematic analysis of mechanisms implicated in antifungal drug resistance and *C. glabrata* pathogenicity. Notably, much of the previous work aimed at unraveling the molecular basis of drug resistance mechanisms in *C. glabrata* have been based on what is known from baker's yeast [94,117] or other *Candida* pathogens [95]. Although gene synteny has been largely conserved between pathogenic and non-pathogenic yeasts such as *C. glabrata* and *S. cerevisiae*, extensive rewiring of signaling pathways generated distinct and species-specific functions for seemingly orthologous genes. Indeed, our work clearly demonstrates that comparing and predicting drug resistance or virulence

phenotypes for *C. glabrata* based on data from even related yeasts requires extensive experimental verification and the use of loss-of-function approaches. This fungal pathogen deletion collection will pave the way for these future efforts.

Acknowledgments

We thank laboratory members for helpful discussions and critical comments on the manuscript. We are indebted to Julia Köhler for providing plasmid pJK863, and to Suzanne Noble and Alexander Johnson for their help in setting up the semi-automated deletion workflow. This work was supported by the Austrian Science Foundation FWF through the ERA-Net Pathogenomics project *FunPath* to KK (FWF-API-0125), SR (BMBF: 0313931A), TG, CD, DF and BH, and in part by the Christian Doppler Society to KK. BC and BM were supported in part by NIH RO1AI46223. BH and SB were supported by the German Federal Ministry of Education and Research (BMBF) through FKZ: 01EO1002. TG was funded in part by grants from the Spanish ministry of science and innovation (GEN2006-27784E, BFU2009-09168). KH was funded by the BBSRC (BB/F005210/1). DF was also partly supported by CNRS and the Fondation pour la recherche Médicale (Programme Equipe FRM). *There are no competing financial interests for authors. The funders had no role in study design, data collection and analysis, decision to publish, or preparation of the manuscript.*

Materials & Methods

Ethics Statement - The use of clinical *C. glabrata* isolates was approved through respective ethics committees according to national regulations.

Media and growth conditions. YPD (1% yeast extract, 2% peptone, 2% dextrose) media were prepared as described elsewhere [118]. Synthetic complete (SC) medium contained 0,67% YNB, 2% glucose supplemented with 1xCSM (ForMedium; complete synthetic mixture) containing histidine, tryptophane and leucine, which are required for growth of the deletion strains. Plates contained 2% agar.

Bioinformatic analysis and gene selection. Genes of different functional categories were manually selected based on potential function in virulence and drug resistance. The categories involved genes of signalling pathways, kinases, ABC transporters and permeases, GPI-anchored proteins, cell wall associated genes, genes involved in glycosylation, phospholipid biosynthesis, histone modification, iron metabolism, and several genes with no obvious homologue in *S. cerevisiae*. The genes were selected by their homology to *S. cerevisiae* based on these functional categories (SGD annotations; <http://www.yeastgenome.org/>). *C. glabrata* orthologues of the selected genes were first identified using a BLAST approach. The three best-aligned hits for each gene were saved and the *C. glabrata* homologue with the highest P-value was arbitrarily defined as the *C. glabrata* orthologue of a given gene in baker's yeast and named accordingly. In addition, a complete catalogue of orthology and paralogy relationships between *C. glabrata* genes and their homologues in 16 other fully-sequenced fungi was derived using a phylogenetic approach [119]. For this a complete collection of Maximum Likelihood phylogenetic trees for all *C. glabrata* genes, the so-called phylome, was generated using the automated pipeline described elsewhere [120]. Gene phylogenies, alignments and orthology and paralogy predictions are publicly available through PhylomeDB (www.phylomedb.org).

Primer design and generation. Oligonucleotide sequences for generation of the deletion cassettes and strain verification were automatically designed, using a custom-written Perl script called *PrimerList* (W. Glaser, unpublished data). PrimerList utilizes Bioperl to read and process nucleotide sequences and uses the EMBOSS [121] programs eprimer 3 and stssearch to find suitable primersets. Details on parameters used by PrimerList for primer design are found in Supplemental Table 1. For PCR-based generation of knock-out constructs, upstream and downstream fragments for genomic recombination were chosen to have a size between 450 and 550 nucleotides. 5'3' (forward) and 3'3' (reverse) primers were chosen to have a length of 20 to 30 bp, a GC content between 30 and 60% and a melting temperature of $50^{\circ}\text{C} \pm 4^{\circ}\text{C}$ with a GC clamp. 5'3', 3'5' primers were chosen to have a length of 20 to 30 bp plus the 20 bp constant overlap sequence (Fig. 1, Supplementary Table S2, 'barcode sequence sheet'), a GC content between 30 and 60% and a melting temperature of $50^{\circ}\text{C} \pm 4^{\circ}\text{C}$. 5'3' (reverse), 3'5' (forward) primers were chosen to bind exactly adjacent to the coding sequence, including the start codon ATG or the stop codon, respectively. 5c and 3c control primers have a length of 20 to 25 bp, a GC content between 40 and 60% and a melting temperature between 50°C to 60°C . The product size of the control PCR is between 750 and 900 bp. Internal control primers (5i and 3i) were designed to bind inside the coding sequence and to give a product of 400 to 500 bp in size. The primers have a length of 20 to 25 bp, a GC content between 40 and 60% and a melting temperature between 55°C to 60°C . Oligonucleotides were commercially purchased in 96-well plate format (Eurogentec, Belgium). Six plates were needed for each set. Each of the six plates (5'5', 5'3', 3'5', 3'3', 5c, 3c) contained the primers for a specific gene at the exact same well position.

Generation of gene deletion cassettes by fusion PCR. The dominant marker *NAT1* was amplified from plasmid pJK863 [54] using the primers fp_NAT1-U2 and rp_NAT1-

D2 to add the constant 20 bp sequences U2 and D2. The PCR product was ligated into a pGEM-T vector (Promega), generating plasmid pTS50. For the fusion PCR step, deletion cassettes were generated using a modified fusion PCR protocol [48]. Briefly, 500bp long flanking homology regions were amplified from ATCC2001 genomic DNA with primer pairs 5'5'/5'3' and 3'5'/3'3' adding the constant overlap sequence (U1/D1) of 20 bp and purified by ethanol precipitation. The conditions for a 50 µl reaction were as follows: 1x Taq buffer (50 mM KCl, 10 mM Tris-HCl (pH 9.0, 25°C), 0.1% TritonX-100, 1.5 mM MgCl₂), 0.2 µM dNTPs, 0.5 µM each primer, 1 µl Taq-Polymerase and genomic wild type DNA from strain ATCC2001; 93°C for 5 minutes, 35 cycles 93°C for 30s, 45°C for 30s, 72°C for 90s, finally 10 minutes at 72°C.

The dominant marker *NAT1* was amplified from plasmid pTS50 in a separate PCR reaction using primers 5M and 3M, adding unique barcode tags and constant complementary U1 and D1 sequences. Marker fragments were gel-purified in 0.7% agarose gels. The conditions for a 50 µl reaction were as follows: 1 x Taq buffer, 0.2 µM dNTPs, 0.5 µM each primer, 1 µl Taq-Polymerase and plasmid TS50; 93°C for 3 minutes, 32 cycles 93°C for 30s, 49°C for 30s, 72°C for 2.5 minutes, finally 10 minutes at 72°C. Fusion PCR was carried out in a 50 µl volume with the same conditions as above: 1x ExTaq buffer, 0.2 µM dNTPs, 0.5 µM each primer, 0.5 µl ExTaq-Polymerase (TaKaRa) and 3 µl marker fragment, 1.25 µl each flanking homology fragment; 93°C for 3 minutes, 35 cycles 93°C for 30s, 45°C for 30s, 72°C for 3 minutes, finally 10 minutes at 72°C. The final deletion construct was purified by ethanol precipitation.

Transformation of *C. glabrata* by electroporation. For transformation of the background strain HTL, we used a modified electroporation protocol [53]. Aliquots of 50 ml of a *C. glabrata* culture in YPD at an optical density of 600nm (OD₆₀₀) of 1.3 were harvested, washed with H₂O, resuspended in 1x TE buffer, 100mM LiAc and incubated at 30°C for 30 minutes with slow shaking (130xrpm). After addition of 250 µl 1M DTT and further incubation at 30°C for 60 minutes (130xrpm), 40 ml of H₂O were added and

the cells were harvested at 1000g for 5 minutes at 4°C. The cells were washed with 25 ml H₂O, subsequently with 5 ml 1 M cold sorbitol, finally resuspended in 550 µl 1 M sorbitol and kept on ice until use. Sterile electroporation cuvettes were precooled on ice and loaded with a mix of 40 - 45 µl electrocompetent cells and 5 - 10 µl linear DNA deletion construct (app. 2 - 3 µg DNA). Cells were left on ice for 10 minutes and electroporation was carried out with a BioRad GenePulser (200Ω, 1.5kV, 25µF). For recovery, 950 µl YPD was added and cells incubated for 4 h shaking at 30°C, before plating on YPD supplemented with 200 µg/ml Nourseothricin (Werner Bioagents, Jena). The plates were incubated for 48 hours at 30°C. For auxotrophic marker constructs the cells were recovered for 1 h at 30°C before plating on selective SC medium. Transformants were patched on YPD/Nourseothricin plates for colony PCR. For 96-well parallel electroporation, 300 ml of culture were grown to OD₆₀₀ of 1.3, split into 50 ml aliquots and treated as described above. For electroporation, we used a BTX Harvard Apparatus ECM630 electroporation device with a HT-100 plate handler.

Verification by yeast colony PCR. Strains were verified by colony PCR and “loss-of-gene” PCR according to the following protocol (Figure 1B). Transformants were patched on selective plates and incubated at 30°C for 24h. Cells were resuspended in 40 µl PCR mix 1 (0.2µM dNTPs, 0.5 µM of each gene specific primer 5c/3c up-/downstream of the homology region and marker specific primer 5M/3M) and heated for 10 minutes at 93°C. After cooling on ice, 10 µl polymerase mix (5 µl 10 x PCR buffer and 1 µl Taq-Pol.) were added per reaction and a regular PCR was performed (93°C for 5 min, 25 cycles 93°C for 30s, 45°C for 30s, 72°C for 90s, final 10 min 72°C). To verify the loss of the coding sequence (CDS), colony PCR was essentially performed the same way. Oligonucleotides used to screen for CDS loss bind inside the CDS to generate a product of 500 bp. All internal primers were also checked for functionality in a separate PCR reaction, amplifying the fragment from genomic wild type DNA.

Phenotypic profiling. For phenotypic analysis of the deletion collection, mutant cells were re-streaked from frozen stocks and grown for 48 h at 30°C on fresh YPD plates. Each of the three plates containing independent transformants of the same set of genes was arrayed into a 384-spot format serving as source plates. Phenotypic profiling of the deletion collection was performed using a robot on YPD plates (RoToR HDA, Singer Ltd., Roadwater, UK) or by manually spotting (two 1:10 dilutions from 24h culture in SC) on SC plates supplemented with the compounds to be tested. Plates were routinely incubated at 30°C for up to 3 days and scanned photographed with S&P Imaging system (S&P Imaging, Canada), after 24, 48 and 72h for documentation. Primary hits were manually rescreened for confirmation in 1:10 serial dilutions. Exponentially growing cells were adjusted to an OD₆₀₀ of 0.1. Equal volumes of serial dilutions (1:10, 1:100 and 1:1000) were spotted on YPD plates containing drugs and incubated as described above. Hypersensitive mutants identified as primary hits by robotic screening were independently re-screened manually in 96-well format, to verify growth phenotypes on agar plates containing various concentrations of xenobiotics. All manual re-screening assays were carried out independently at least in biological triplicates in four different laboratories, including the confirmation of hits by serial-dilution spot assays on agar plates or as appropriate by microdilution assays in liquid cultures.

Azole and drug susceptibility screenings. Azole susceptibility screenings were carried out by a modified endpoint method [122] in liquid culture in microtiter plates, using the following drug concentrations: 4 µg/ml Fluconazole, 0.1 µg/ml Voriconazole, 0.1 µg/ml Ketoconazole, 0.1 µg/ml Itraconazole (all azoles from Discovery Fine Chemicals), 3 µg/ml AmB (Discovery Fine Chemicals), 5 µg/ml 5-Flucytosine (Sigma-Aldrich). Cells were grown overnight in deep well plates to stationary phase, diluted 100-fold in sterile water and 100 µl suspension mixed with 100 µl of 2 x YPD containing a 2 x drug concentration (app. 10⁵ cells/well). After incubation at 30°C for 24 h and 48

h, cells were resuspended and the OD₆₀₀ was measured with a Victor plate reader (Perkin Elmer, USA). Finally, we added 120 ng/ml CF, 50 µg/ml CW (Sigma-Aldrich) or 250 µg/ml CR (Sigma-Aldrich) as supplements to media from sterile stock solutions after autoclaving. Plates were routinely incubated at 30°C for up to 3 days and documented every 24h.

Microbroth dilution assay for IC50 determination. To determine the IC50 of antifungal drugs a modified protocol of the microbroth dilution assay was used [123]. Briefly, an overnight culture was diluted 1:100 in YPD, regrown to an OD₆₀₀ of 1 and an inoculum of 2.5×10^4 cells/ml was prepared. Antifungal stock solutions were prepared in DMSO. Two fold serial dilutions of the drugs were then prepared in water in a deep well plate and stored at -20°C until use. 100 µl of two fold serial drug dilutions were distributed in triplicates into a flat bottom microtiter plate. The last wells free of antifungal drugs served as a growth control. After adding 100 µl of the inoculum (200 µl total volume), plates were incubated at 30°C for 24h and 48h in a humid environment to avoid evaporation. OD₆₀₀ was determined with a plate reader. Endpoint readings were set as the antifungal concentrations, causing at least 90% growth inhibition after 24 h of growth when compared to the control. The IC50 was determined by linear regression using Graph Pad Prism software.

Fitness analysis. Growth curves were performed in 96-well plates in a Tecan Infinite M200 microplate reader or a Tecan Sunrise microplate reader. *C. glabrata* strains were grown in YPD at 30°C. For each 96-well plate, the doubling times of each of the 96 tested strains were calculated based on the time necessary for a given strain to go from OD 0.15 to OD 0.6. The relative fitness of a strain was then calculated as the ratio of the average doubling time of all strains within the third to eighth deciles to the doubling time of the strain of interest [65]. Means and standard deviations are presented for fitness values determined for one or two independent knock-out mutants

in two biological replicates. Strains with standard deviation above 0.1 or an absolute difference between the relative fitness of two independent knock-out mutants above 0.1 were not considered further. In order to identify among the remaining strains those that showed significantly increased or decreased fitness, the average and standard deviation of the fitness for strains within the second to ninth deciles were calculated. Strains were classified based on the number of standard deviation between their fitness and the average fitness. Strains with decreased fitness had a fitness at least two standard deviations below the average fitness. Strains with increased fitness had a fitness at least two standard deviations above the average fitness.

Biofilm formation assays. Biofilms were produced in 96-well plates as previously described [72]. Briefly, saturated cultures in YPD were pin-inoculated diluted in 100 μ l SD 0.4% glucose medium in 96-well polystyrene plates and incubated at 37°C for 24 h. The 96-well plates were then washed with PBS using a HydroFlex platform (Tecan) and 100 μ l of a 1X FDA solution (50X stock: fluorescein diacetate, 2 g l⁻¹ in acetone; diluted to 1X in PBS) was added per well [71]. Plates were wrapped in aluminium foil and incubated for 1 h at 37°C before measuring fluorescence in a Tecan Infinite M200 microplate reader using an excitation filter of 486 \pm 9 nm and an emission filter of 535 \pm 20 nm. The relative biofilm fitness of a strain was then calculated as the ratio of the OD_{535nm} recording for the strain of interest to the average of the OD_{535nm} recordings obtained for strains within the third to eighth deciles of all OD_{535nm} recordings obtained within the 96-well plate to which the strain of interest belonged. Means and standard deviations are presented for fitness values determined for one or two independent knock-out mutants in two biological replicates. Strains with standard deviation above 0.3 or an absolute difference between the 2-4 relative biofilm fitness values above 0.5 were not considered further. In order to identify among the remaining strains those that showed significantly increased or decreased ability to form biofilm, the average and standard deviation of the relative biofilm fitness for strains within the second to ninth

deciles were calculated. Strains were classified based on the number of standard deviation between their biofilm fitness and the average biofilm fitness. Strains with decreased biofilm fitness had a relative biofilm fitness at least two standard deviations below the average relative biofilm fitness. Strains with increased biofilm fitness had a relative biofilm fitness at least two standard deviations above the average fitness. Strains with decreased or increased biofilm fitness were further evaluated by performing a biofilm assay in quadruplicate for each of two independent isolates. Data obtained for the 58 candidate strains were compared to those obtained for wild type isolates (96 independent values) using the Wilcoxon test. A p value below 0.01 was considered as indicative of a significant difference with the wild type strain. In this assay, a *yak1*Δ mutant was found significantly impaired in biofilm formation while a *sir3*Δ mutant showed significantly elevated biofilm production as previously shown [72].

References

1. Mean M, Marchetti O, Calandra T (2008) Bench-to-bedside review: *Candida* infections in the intensive care unit. *Crit Care* 12: 204.
2. Perlroth J, Choi B, Spellberg B (2007) Nosocomial fungal infections: epidemiology, diagnosis, and treatment. *Med Mycol* 45: 321-346.
3. Pfaller MA, Diekema DJ, Gibbs DL, Newell VA, Barton R, et al. (2010) Geographic variation in the frequency of isolation and fluconazole and voriconazole susceptibilities of *Candida glabrata*: an assessment from the ARTEMIS DISK Global Antifungal Surveillance Program. *Diagn Microbiol Infect Dis*.
4. Richardson M, Lass-Flörl C (2008) Changing epidemiology of systemic fungal infections. *Clin Microbiol Infect* 14 Suppl 4: 5-24.
5. Gow NA, van de Veerdonk FL, Brown AJ, Netea MG *Candida albicans* morphogenesis and host defence: discriminating invasion from colonization. *Nat Rev Microbiol* 10: 112-122.
6. Albrecht A, Felk A, Pichova I, Naglik JR, Schaller M, et al. (2006) Glycosylphosphatidylinositol-anchored proteases of *Candida albicans* target proteins necessary for both cellular processes and host-pathogen interactions. *J Biol Chem* 281: 688-694.
7. Ghannoum MA (2000) Potential role of phospholipases in virulence and fungal pathogenesis. *Clin Microbiol Rev* 13: 122-143, table of contents.
8. Panackal AA, Gribskov JL, Staab JF, Kirby KA, Rinaldi M, et al. (2006) Clinical significance of azole antifungal drug cross-resistance in *Candida glabrata*. *J Clin Microbiol* 44: 1740-1743.
9. Pfaller MA, Diekema DJ, Gibbs DL, Newell VA, Ellis D, et al. (2010) Results from the ARTEMIS DISK Global Antifungal Surveillance Study, 1997 to 2007: a 10.5-year analysis of susceptibilities of *Candida* Species to fluconazole and voriconazole as determined by CLSI standardized disk diffusion. *J Clin Microbiol* 48: 1366-1377.
10. Pfaller MA, Messer SA, Hollis RJ, Boyken L, Tendolkar S, et al. (2009) Variation in susceptibility of bloodstream isolates of *Candida glabrata* to fluconazole according to patient age and geographic location in the United States in 2001 to 2007. *J Clin Microbiol* 47: 3185-3190.
11. Ruan SY, Chu CC, Hsueh PR (2008) In vitro susceptibilities of invasive isolates of *Candida* species: rapid increase in rates of fluconazole susceptible-dose dependent *Candida glabrata* isolates. *Antimicrob Agents Chemother* 52: 2919-2922.
12. Castano I, Pan SJ, Zupancic M, Hennequin C, Dujon B, et al. (2005) Telomere length control and transcriptional regulation of subtelomeric adhesins in *Candida glabrata*. *Mol Microbiol* 55: 1246-1258.
13. Cormack BP, Ghori N, Falkow S (1999) An adhesin of the yeast pathogen *Candida glabrata* mediating adherence to human epithelial cells. *Science* 285: 578-582.
14. de Groot PW, Kraneveld EA, Yin QY, Dekker HL, Gross U, et al. (2008) The cell wall of the human pathogen *Candida glabrata*: differential incorporation of novel adhesin-like wall proteins. *Eukaryot Cell* 7: 1951-1964.
15. De Las Penas A, Pan SJ, Castano I, Alder J, Cregg R, et al. (2003) Virulence-related surface glycoproteins in the yeast pathogen *Candida glabrata* are encoded in subtelomeric clusters and subject to *RAP1*- and *SIR*-dependent transcriptional silencing. *Genes Dev* 17: 2245-2258.
16. Domergue R, Castano I, De Las Penas A, Zupancic M, Lockatell V, et al. (2005) Nicotinic acid limitation regulates silencing of *Candida* adhesins during UTI. *Science* 308: 866-870.
17. Kaur R, Domergue R, Zupancic ML, Cormack BP (2005) A yeast by any other name: *Candida glabrata* and its interaction with the host. *Curr Opin Microbiol* 8: 378-384.

18. Kaur R, Ma B, Cormack BP (2007) A family of glycosylphosphatidylinositol-linked aspartyl proteases is required for virulence of *Candida glabrata*. Proc Natl Acad Sci U S A 104: 7628-7633.
19. Brunke S, Seider K, Almeida RS, Heyken A, Fleck CB, et al. (2010) *Candida glabrata* tryptophan-based pigment production via the Ehrlich pathway. Mol Microbiol.
20. Roetzer A, Gratz N, Kovarik P, Schüller C (2010) Autophagy supports *Candida glabrata* survival during phagocytosis. Cell Microbiol 12: 199-216.
21. Seider K, Brunke S, Schild L, Jablonowski N, Wilson D, et al. (2011) The facultative intracellular pathogen *Candida glabrata* subverts macrophage cytokine production and phagolysosome maturation. J Immunol 187: 3072-3086.
22. Rai MN, Balusu S, Gorityala N, Dandu L, Kaur R (2012) Functional genomic analysis of *Candida glabrata*-macrophage interaction: role of chromatin remodeling in virulence. PLoS Pathog 8: e1002863.
23. Kamran M, Calcagno AM, Findon H, Bignell E, Jones MD, et al. (2004) Inactivation of transcription factor gene *ACE2* in the fungal pathogen *Candida glabrata* results in hypervirulence. Eukaryot Cell 3: 546-552.
24. Izumikawa K, Kakeya H, Tsai HF, Grimberg B, Bennett JE (2003) Function of *Candida glabrata* ABC transporter gene, *PDH1*. Yeast 20: 249-261.
25. Miyazaki H, Miyazaki Y, Geber A, Parkinson T, Hitchcock C, et al. (1998) Fluconazole resistance associated with drug efflux and increased transcription of a drug transporter gene, *PDH1*, in *Candida glabrata*. Antimicrob Agents Chemother 42: 1695-1701.
26. Sanglard D, Ischer F, Calabrese D, Majcherczyk PA, Bille J (1999) The ATP binding cassette transporter gene *CgCDR1* from *Candida glabrata* is involved in the resistance of clinical isolates to azole antifungal agents. Antimicrob Agents Chemother 43: 2753-2765.
27. Thakur JK, Arthanari H, Yang F, Pan SJ, Fan X, et al. (2008) A nuclear receptor-like pathway regulating multidrug resistance in fungi. Nature 452: 604-609.
28. Vermitsky JP, Earhart KD, Smith WL, Homayouni R, Edlind TD, et al. (2006) Pdr1 regulates multidrug resistance in *Candida glabrata*: gene disruption and genome-wide expression studies. Mol Microbiol 61: 704-722.
29. Brun S, Berges T, Poupard P, Vauzelle-Moreau C, Renier G, et al. (2004) Mechanisms of azole resistance in petite mutants of *Candida glabrata*. Antimicrob Agents Chemother 48: 1788-1796.
30. Nakayama H, Tanabe K, Bard M, Hodgson W, Wu S, et al. (2007) The *Candida glabrata* putative sterol transporter gene *CgAUS1* protects cells against azoles in the presence of serum. J Antimicrob Chemother 60: 1264-1272.
31. Nagi M, Tanabe K, Ueno K, Nakayama H, Aoyama T, et al. (2013) The *Candida glabrata* sterol scavenging mechanism, mediated by the ATP-binding cassette transporter Aus1p, is regulated by iron limitation. Mol Microbiol 88: 371-381.
32. Diekema D, Arbefeville S, Boyken L, Kroeger J, Pfaller M (2012) The changing epidemiology of healthcare-associated candidemia over three decades. Diagn Microbiol Infect Dis 73: 45-48.
33. Perlin DS (2011) Current perspectives on echinocandin class drugs. Future Microbiol 6: 441-457.
34. Perlin DS (2007) Resistance to echinocandin-class antifungal drugs. Drug Resist Updat 10: 121-130.
35. Singh-Babak SD, Babak T, Diezmann S, Hill JA, Xie JL, et al. (2012) Global analysis of the evolution and mechanism of echinocandin resistance in *Candida glabrata*. PLoS Pathog 8: e1002718.
36. Katiyar SK, Alastruey-Izquierdo A, Healey KR, Johnson ME, Perlin DS, et al. (2012) Fks1 and Fks2 are functionally redundant but differentially regulated in *Candida glabrata*: implications for echinocandin resistance. Antimicrob Agents Chemother 56: 6304-6309.

37. Schuetzner-Muehlbauer M, Willinger B, Krapf G, Enzinger S, Presterl E, et al. (2003) The *Candida albicans* Cdr2p ATP-binding cassette (ABC) transporter confers resistance to caspofungin. *Mol Microbiol* 48: 225-235.
38. Alexander BD, Johnson MD, Pfeiffer CD, Jimenez-Ortigosa C, Catania J, et al. (2013) Increasing Echinocandin Resistance in *Candida glabrata*: Clinical Failure Correlates With Presence of FKS Mutations and Elevated Minimum Inhibitory Concentrations. *Clin Infect Dis*.
39. Costanzo M, Baryshnikova A, Bellay J, Kim Y, Spear ED, et al. (2010) The genetic landscape of a cell. *Science* 327: 425-431.
40. Giaever G, Chu AM, Ni L, Connelly C, Riles L, et al. (2002) Functional profiling of the *Saccharomyces cerevisiae* genome. *Nature* 418: 387-391.
41. Hillenmeyer ME, Ericson E, Davis RW, Nislow C, Koller D, et al. (2010) Systematic analysis of genome-wide fitness data in yeast reveals novel gene function and drug action. *Genome Biol* 11: R30.
42. Hillenmeyer ME, Fung E, Wildenhain J, Pierce SE, Hoon S, et al. (2008) The chemical genomic portrait of yeast: uncovering a phenotype for all genes. *Science* 320: 362-365.
43. Parsons AB, Brost RL, Ding H, Li Z, Zhang C, et al. (2004) Integration of chemical-genetic and genetic interaction data links bioactive compounds to cellular target pathways. *Nat Biotechnol* 22: 62-69.
44. Ryan O, Shapiro RS, Kurat CF, Mayhew D, Baryshnikova A, et al. (2012) Global gene deletion analysis exploring yeast filamentous growth. *Science* 337: 1353-1356.
45. Tong AH, Lesage G, Bader GD, Ding H, Xu H, et al. (2004) Global mapping of the yeast genetic interaction network. *Science* 303: 808-813.
46. Winzeler EA, Shoemaker DD, Astromoff A, Liang H, Anderson K, et al. (1999) Functional characterization of the *S. cerevisiae* genome by gene deletion and parallel analysis. *Science* 285: 901-906.
47. Noble SM, French S, Kohn LA, Chen V, Johnson AD (2010) Systematic screens of a *Candida albicans* homozygous deletion library decouple morphogenetic switching and pathogenicity. *Nat Genet*.
48. Noble SM, Johnson AD (2005) Strains and strategies for large-scale gene deletion studies of the diploid human fungal pathogen *Candida albicans*. *Eukaryot Cell* 4: 298-309.
49. Roemer T, Jiang B, Davison J, Ketela T, Veillette K, et al. (2003) Large-scale essential gene identification in *Candida albicans* and applications to antifungal drug discovery. *Mol Microbiol* 50: 167-181.
50. Liu OW, Chun CD, Chow ED, Chen C, Madhani HD, et al. (2008) Systematic genetic analysis of virulence in the human fungal pathogen *Cryptococcus neoformans*. *Cell* 135: 174-188.
51. Dujon B, Sherman D, Fischer G, Durrens P, Casaregola S, et al. (2004) Genome evolution in yeasts. *Nature* 430: 35-44.
52. Marcet-Houben M, Gabaldon T (2009) The tree versus the forest: the fungal tree of life and the topological diversity within the yeast phylome. *PLoS ONE* 4: e4357.
53. Reuss O, Vik A, Kolter R, Morschhäuser J (2004) The SAT1 flipper, an optimized tool for gene disruption in *Candida albicans*. *Gene* 341: 119-127.
54. Shen J, Guo W, Köhler JR (2005) CaNAT1, a heterologous dominant selectable marker for transformation of *Candida albicans* and other pathogenic *Candida* species. *Infect Immun* 73: 1239-1242.
55. Brand A, MacCallum DM, Brown AJ, Gow NA, Odds FC (2004) Ectopic expression of URA3 can influence the virulence phenotypes and proteome of *Candida albicans* but can be overcome by targeted reintegration of URA3 at the RPS10 locus. *Eukaryot Cell* 3: 900-909.
56. Lay J, Henry LK, Clifford J, Koltin Y, Bulawa CE, et al. (1998) Altered expression of selectable marker URA3 in gene-disrupted *Candida albicans* strains complicates interpretation of virulence studies. *Infect Immun* 66: 5301-5306.

57. Jacobsen ID, Brunke S, Seider K, Schwarzmuller T, Firon A, et al. (2010) *Candida glabrata* persistence in mice does not depend on host immunosuppression and is unaffected by fungal amino acid auxotrophy. *Infect Immun* 78: 1066-1077.
58. Ueno K, Uno J, Nakayama H, Sasamoto K, Mikami Y, et al. (2007) Development of a highly efficient gene targeting system induced by transient repression of *YKU80* expression in *Candida glabrata*. *Eukaryot Cell* 6: 1239-1247.
59. Boguslawski G (1992) *PBS2*, a yeast gene encoding a putative protein kinase, interacts with the *RAS2* pathway and affects osmotic sensitivity of *Saccharomyces cerevisiae*. *J Gen Microbiol* 138: 2425-2432.
60. Sanglard D, Ischer F, Bille J (2001) Role of ATP-binding-cassette transporter genes in high-frequency acquisition of resistance to azole antifungals in *Candida glabrata*. *Antimicrob Agents Chemother* 45: 1174-1183.
61. Vermitsky JP, Edlind TD (2004) Azole resistance in *Candida glabrata*: coordinate upregulation of multidrug transporters and evidence for a Pdr1-like transcription factor. *Antimicrob Agents Chemother* 48: 3773-3781.
62. Cota JM, Grabinski JL, Talbert RL, Burgess DS, Rogers PD, et al. (2008) Increases in *SLT2* expression and chitin content are associated with incomplete killing of *Candida glabrata* by caspofungin. *Antimicrob Agents Chemother* 52: 1144-1146.
63. Reinoso-Martin C, Schüller C, Schuetzer-Muehlbauer M, Kuchler K (2003) The yeast protein kinase C cell integrity pathway mediates tolerance to the antifungal drug caspofungin through activation of Slt2p mitogen-activated protein kinase signaling. *Eukaryot Cell* 2: 1200-1210.
64. Ferrari S, Ischer F, Calabrese D, Posteraro B, Sanguinetti M, et al. (2009) Gain of function mutations in *CgPDR1* of *Candida glabrata* not only mediate antifungal resistance but also enhance virulence. *PLoS Pathog* 5: e1000268.
65. St Onge RP, Mani R, Oh J, Proctor M, Fung E, et al. (2007) Systematic pathway analysis using high-resolution fitness profiling of combinatorial gene deletions. *Nat Genet* 39: 199-206.
66. Csank C, Haynes K (2000) *Candida glabrata* displays pseudohyphal growth. *FEMS Microbiol Lett* 189: 115-120.
67. Vandeputte P, Tronchin G, Berges T, Hennequin C, Chabasse D, et al. (2007) Reduced susceptibility to polyenes associated with a missense mutation in the *ERG6* gene in a clinical isolate of *Candida glabrata* with pseudohyphal growth. *Antimicrob Agents Chemother* 51: 982-990.
68. Finkel JS, Mitchell AP (2011) Genetic control of *Candida albicans* biofilm development. *Nat Rev Microbiol* 9: 109-118.
69. Nobile CJ, Nett JE, Hernday AD, Homann OR, Deneault JS, et al. (2009) Biofilm matrix regulation by *Candida albicans* Zap1. *PLoS Biol* 7: e1000133.
70. Riera M, Mogensen E, d'Enfert C, Janbon G (2012) New regulators of biofilm development in *Candida glabrata*. *Res Microbiol* 163: 297-307.
71. Honraet K, Goetghebeur E, Nelis HJ (2005) Comparison of three assays for the quantification of *Candida* biomass in suspension and CDC reactor grown biofilms. *J Microbiol Methods* 63: 287-295.
72. Iraqui I, Garcia-Sanchez S, Aubert S, Dromer F, Ghigo JM, et al. (2005) The Yak1p kinase controls expression of adhesins and biofilm formation in *Candida glabrata* in a Sir4p-dependent pathway. *Mol Microbiol* 55: 1259-1271.
73. Pfaller MA, Castanheira M, Lockhart SR, Ahlquist AM, Messer SA, et al. (2012) Frequency of decreased susceptibility and resistance to echinocandins among fluconazole-resistant bloodstream isolates of *Candida glabrata*. *J Clin Microbiol* 50: 1199-1203.
74. Cowen LE (2008) The evolution of fungal drug resistance: modulating the trajectory from genotype to phenotype. *Nat Rev Microbiol* 6: 187-198.
75. Khan ZU, Ahmad S, Al-Obaid I, Al-Sweih NA, Joseph L, et al. (2008) Emergence of resistance to amphotericin B and triazoles in *Candida glabrata* vaginal isolates in a case of recurrent vaginitis. *J Chemother* 20: 488-491.

76. Krogh-Madsen M, Arendrup MC, Heslet L, Knudsen JD (2006) Amphotericin B and caspofungin resistance in *Candida glabrata* isolates recovered from a critically ill patient. *Clin Infect Dis* 42: 938-944.
77. Lussier M, Sdicu AM, Camirand A, Bussey H (1996) Functional characterization of the *YUR1*, *KTR1*, and *KTR2* genes as members of the yeast *KRE2/MNT1* mannosyltransferase gene family. *J Biol Chem* 271: 11001-11008.
78. Tscherner M, Stappler E, Hnisz D, Kuchler K The histone acetyltransferase Hat1 facilitates DNA damage repair and morphogenesis in *Candida albicans*. *Mol Microbiol*.
79. Miyazaki T, Inamine T, Yamauchi S, Nagayoshi Y, Saijo T, et al. (2010) Role of the Slt2 mitogen-activated protein kinase pathway in cell wall integrity and virulence in *Candida glabrata*. *FEMS Yeast Res* 10: 343-352.
80. Chen YL, Konieczka JH, Springer DJ, Bowen SE, Zhang J, et al. (2012) Convergent Evolution of Calcineurin Pathway Roles in Thermotolerance and Virulence in *Candida glabrata*. *G3 (Bethesda)* 2: 675-691.
81. Castano I, Kaur R, Pan S, Cregg R, Penas Ade L, et al. (2003) Tn7-based genome-wide random insertional mutagenesis of *Candida glabrata*. *Genome Res* 13: 905-915.
82. Kojic EM, Darouiche RO (2004) *Candida* infections of medical devices. *Clin Microbiol Rev* 17: 255-267.
83. Friedel AM, Pike BL, Gasser SM (2009) ATR/Mec1: coordinating fork stability and repair. *Curr Opin Cell Biol* 21: 237-244.
84. Jorgensen P, Nelson B, Robinson MD, Chen Y, Andrews B, et al. (2002) High-resolution genetic mapping with ordered arrays of *Saccharomyces cerevisiae* deletion mutants. *Genetics* 162: 1091-1099.
85. Bidlingmaier S, Weiss EL, Seidel C, Drubin DG, Snyder M (2001) The Cbk1p pathway is important for polarized cell growth and cell separation in *Saccharomyces cerevisiae*. *Mol Cell Biol* 21: 2449-2462.
86. Racki WJ, Becam AM, Nasr F, Herbert CJ (2000) Cbk1p, a protein similar to the human myotonic dystrophy kinase, is essential for normal morphogenesis in *Saccharomyces cerevisiae*. *EMBO J* 19: 4524-4532.
87. Bharucha N, Chabrier-Rosello Y, Xu T, Johnson C, Sobczynski S, et al. (2011) A large-scale complex haploinsufficiency-based genetic interaction screen in *Candida albicans*: analysis of the RAM network during morphogenesis. *PLoS Genet* 7: e1002058.
88. McNemar MD, Fonzi WA (2002) Conserved serine/threonine kinase encoded by *CBK1* regulates expression of several hypha-associated transcripts and genes encoding cell wall proteins in *Candida albicans*. *J Bacteriol* 184: 2058-2061.
89. Legrand M, Lephart P, Forche A, Mueller FM, Walsh T, et al. (2004) Homozygosity at the *MTL* locus in clinical strains of *Candida albicans*: karyotypic rearrangements and tetraploid formation. *Mol Microbiol* 52: 1451-1462.
90. Gutierrez-Escribano P, Zeidler U, Suarez MB, Bachellier-Bassi S, Clemente-Blanco A, et al. (2012) The NDR/LATS kinase Cbk1 controls the activity of the transcriptional regulator Bcr1 during biofilm formation in *Candida albicans*. *PLoS Pathog* 8: e1002683.
91. Lavoie H, Hogues H, Whiteway M (2009) Rearrangements of the transcriptional regulatory networks of metabolic pathways in fungi. *Curr Opin Microbiol* 12: 655-663.
92. Li H, Johnson AD (2010) Evolution of transcription networks - lessons from yeasts. *Curr Biol* 20: R746-753.
93. Casadevall A (2012) Fungi and the rise of mammals. *PLoS Pathog* 8: e1002808.
94. Lesage G, Sdicu AM, Menard P, Shapiro J, Hussein S, et al. (2004) Analysis of beta-1,3-glucan assembly in *Saccharomyces cerevisiae* using a synthetic interaction network and altered sensitivity to caspofungin. *Genetics* 167: 35-49.

95. Xu D, Jiang B, Ketela T, Lemieux S, Veillette K, et al. (2007) Genome-wide fitness test and mechanism-of-action studies of inhibitory compounds in *Candida albicans*. PLoS Pathog 3: e92.
96. Ben-Ami R, Kontoyiannis DP (2012) Resistance to echinocandins comes at a cost: the impact of FKS1 hotspot mutations on *Candida albicans* fitness and virulence. Virulence 3: 95-97.
97. Sussman A, Huss K, Chio LC, Heidler S, Shaw M, et al. (2004) Discovery of cercosporamide, a known antifungal natural product, as a selective Pkc1 kinase inhibitor through high-throughput screening. Eukaryot Cell 3: 932-943.
98. Lee KK, Maccallum DM, Jacobsen MD, Walker LA, Odds FC, et al. (2012) Elevated cell wall chitin in *Candida albicans* confers echinocandin resistance in vivo. Antimicrob Agents Chemother 56: 208-217.
99. Walker LA, Gow NA, Munro CA (2013) Elevated chitin content reduces the susceptibility of *Candida* species to caspofungin. Antimicrob Agents Chemother 57: 146-154.
100. Steinbach WJ, Cramer RA, Jr., Perfect BZ, Henn C, Nielsen K, et al. (2007) Calcineurin inhibition or mutation enhances cell wall inhibitors against *Aspergillus fumigatus*. Antimicrob Agents Chemother 51: 2979-2981.
101. Roelants FM, Breslow DK, Muir A, Weissman JS, Thorner J (2011) Protein kinase Ypk1 phosphorylates regulatory proteins Orm1 and Orm2 to control sphingolipid homeostasis in *Saccharomyces cerevisiae*. Proc Natl Acad Sci U S A 108: 19222-19227.
102. Inagaki M, Schmelzle T, Yamaguchi K, Irie K, Hall MN, et al. (1999) *PDK1* homologs activate the Pkc1-mitogen-activated protein kinase pathway in yeast. Mol Cell Biol 19: 8344-8352.
103. Roelants FM, Torrance PD, Bezman N, Thorner J (2002) Pkh1 and Pkh2 differentially phosphorylate and activate Ypk1 and Ykr2 and define protein kinase modules required for maintenance of cell wall integrity. Mol Biol Cell 13: 3005-3028.
104. Kaur R, Castano I, Cormack BP (2004) Functional genomic analysis of fluconazole susceptibility in the pathogenic yeast *Candida glabrata*: roles of calcium signaling and mitochondria. Antimicrob Agents Chemother 48: 1600-1613.
105. Onyewu C, Blankenship JR, Del Poeta M, Heitman J (2003) Ergosterol biosynthesis inhibitors become fungicidal when combined with calcineurin inhibitors against *Candida albicans*, *Candida glabrata*, and *Candida krusei*. Antimicrob Agents Chemother 47: 956-964.
106. Wiederhold NP, Kontoyiannis DP, Prince RA, Lewis RE (2005) Attenuation of the activity of caspofungin at high concentrations against *Candida albicans*: possible role of cell wall integrity and calcineurin pathways. Antimicrob Agents Chemother 49: 5146-5148.
107. Jansen JM, Wanless AG, Seidel CW, Weiss EL (2009) Cbk1 regulation of the RNA-binding protein Ssd1 integrates cell fate with translational control. Curr Biol 19: 2114-2120.
108. Gank KD, Yeaman MR, Kojima S, Yount NY, Park H, et al. (2008) *SSD1* is integral to host defense peptide resistance in *Candida albicans*. Eukaryot Cell 7: 1318-1327.
109. Colman-Lerner A, Chin TE, Brent R (2001) Yeast Cbk1 and Mob2 activate daughter-specific genetic programs to induce asymmetric cell fates. Cell 107: 739-750.
110. Kaeberlein M, Guarente L (2002) *Saccharomyces cerevisiae* *MPT5* and *SSD1* function in parallel pathways to promote cell wall integrity. Genetics 160: 83-95.
111. Kurischko C, Kuravi VK, Herbert CJ, Luca FC (2011) Nucleocytoplasmic shuttling of Ssd1 defines the destiny of its bound mRNAs. Mol Microbiol 81: 831-849.

112. Sun Y, Taniguchi R, Tanoue D, Yamaji T, Takematsu H, et al. (2000) Sli2 (Ypk1), a homologue of mammalian protein kinase SGK, is a downstream kinase in the sphingolipid-mediated signaling pathway of yeast. *Mol Cell Biol* 20: 4411-4419.
113. Roelants FM, Baltz AG, Trott AE, Fereres S, Thorner J (2010) A protein kinase network regulates the function of aminophospholipid flippases. *Proc Natl Acad Sci U S A* 107: 34-39.
114. Parks LW, Smith SJ, Crowley JH (1995) Biochemical and physiological effects of sterol alterations in yeast--a review. *Lipids* 30: 227-230.
115. Lamping E, Luckl J, Paltauf F, Henry SA, Kohlwein SD (1994) Isolation and characterization of a mutant of *Saccharomyces cerevisiae* with pleiotropic deficiencies in transcriptional activation and repression. *Genetics* 137: 55-65.
116. Pfaller M, Neofytos D, Diekema D, Azie N, Meier-Kriesche HU, et al. (2012) Epidemiology and outcomes of candidemia in 3648 patients: data from the Prospective Antifungal Therapy (PATH Alliance(R)) registry, 2004-2008. *Diagn Microbiol Infect Dis* 74: 323-331.
117. Morschhäuser J (2010) Regulation of multidrug resistance in pathogenic fungi. *Fungal Genet Biol* 47: 94-106.
118. Kaiser C, Michaelis S, Mitchell AP (1994) *Methods in yeast genetics. A laboratory course manual.* Cold Spring Harbor Laboratory Press, Cold Spring Harbor, NY.
119. Gabaldon T (2008) Large-scale assignment of orthology: back to phylogenetics? *Genome Biol* 9: 235.
120. Huerta-Cepas J, Capella-Gutierrez S, Pryszcz LP, Denisov I, Kormes D, et al. (2011) PhylomeDB v3.0: an expanding repository of genome-wide collections of trees, alignments and phylogeny-based orthology and paralogy predictions. *Nucleic Acids Res* 39: D556-560.
121. Rice P, Longden I, Bleasby A (2000) EMBOSS: the European Molecular Biology Open Software Suite. *Trends Genet* 16: 276-277.
122. Rex JH, Pfaller MA, Galgiani JN, Bartlett MS, Espinel-Ingroff A, et al. (1997) Development of interpretive breakpoints for antifungal susceptibility testing: conceptual framework and analysis of in vitro-in vivo correlation data for fluconazole, itraconazole, and candida infections. Subcommittee on Antifungal Susceptibility Testing of the National Committee for Clinical Laboratory Standards. *Clin Infect Dis* 24: 235-247.
123. Sanglard D, Kuchler K, Ischer F, Pagani JL, Monod M, et al. (1995) Mechanisms of resistance to azole antifungal agents in *Candida albicans* isolates from AIDS patients involve specific multidrug transporters. *Antimicrob Agents Chemother* 39: 2378-2386.

Figure Legends

Figure 1. Generation of *C. glabrata* mutants and systematic phenotypic analysis.

(a) Generation of gene deletion constructs by fusion PCR using the dominant selectable marker *NAT1*. A set of two times 96 unique barcode sequences was integrated in oligonucleotides to amplify the marker fragment and to add overlap sequences. (b) Transformants were verified by colony PCR for correct integration on the 5' and 3' junction and checked for absence of the target ORF. (c) Overview of the construction of the gene deletion strain library. **Primer design and deletion fragment construction.** For PCR-based generation of knock-out constructs, upstream and downstream fragments for genomic recombination were chosen to have a size between 450 and 550 nucleotides. 5'5' (forward) and 3'3' (reverse) primers were chosen to have a length of 20 to 30 bp, a GC content between 30 and 60% and a melting temperature of $50^{\circ}\text{C} \pm 4^{\circ}\text{C}$ with a GC clamp. 5'3', 3'5' primers were chosen to have a length of 20 to 30 bp plus the 20 bp constant overlap sequence (Figure 1, Supplemental Table S2, 'barcode sequence sheet'), a GC content between 30 and 60% and a melting temperature of $50^{\circ}\text{C} \pm 4^{\circ}\text{C}$. 5'3' (reverse), 3'5' (forward) primers were chosen to bind exactly adjacent to the coding sequence, including the start codon ATG or the stop codon, respectively. 5c and 3c control primers have a length of 20 to 25 bp, a GC content between 40 and 60% and a melting temperature between 50°C to 60°C . The product size of the control PCR is between 750 and 900 bp. Internal control primers (5i and 3i) were designed to bind inside the coding sequence and to give a product of 400 to 500 bp in size. The primers have a length of 20 to 25 bp, a GC content between 40 and 60% and a melting temperature between 55°C to 60°C . Oligonucleotides were commercially purchased in 96-well plate format (Eurogentec, Belgium). Six plates were needed per set. Each of the six plates (5'5', 5'3', 3'5', 3'3', 5c, 3c) contained the primers for a specific gene at the exact same well position.

Figure 2. Relative fitness distribution and morphology of *C. glabrata* gene deletion strains. (a) Wild type and mutant strains were grown in rich medium at 30°C and doubling times were recorded. The median doubling time of the wild type *C. glabrata* ATCC2001 strain under these conditions was 63.9 min while the median for mutant strains was 68.1 min. For each strain, the relative fitness was calculated using doubling times from at least two independent cultures of 1-6 independent mutants. Strains that showed strong variations in relative fitness between independent mutants or independent cultures were omitted from further analysis (Supplemental Table 6). Data were obtained for 551 knock-out mutants (Supplemental Table 5). (b) Colony and cell morphologies of *C. glabrata* deletion strains. Different types of distinct cell and colony morphologies were found. Cell morphology classes: ellipsoid (a), chains (b, f, g, i, k, l), elongated (c, d), large clumps (d, j, m, n), round (e), large and round (h); colony morphologies: smooth (a, b, c, e, f, g, i), small (h), slightly wrinkled (k, l), wrinkled (d, j, m, n). WT = HTL background strain; white bars correspond to 10 µm.

Figure 3. Relative biofilm fitness distribution. Wild type and mutant strains were induced to form biofilms in 96-well polystyrene plates in minimal medium at 37°C and the biofilm biomass was quantified using fluorescein diacetate (FDA). For each strain, a relative biofilm fitness was calculated based on FDA hydrolysis data from at least two independent cultures. Data were obtained for 420 knock-out mutants (Supplemental Table S8). Strains that showed strong variations in relative fitness between independent mutants or independent cultures were omitted from further analysis (Supplemental Table 8).

Figure 4. Classification of *C. glabrata* chemogenetic profiles. (A) Overlap between the chemical-genetic profile of CF (38 genes), CR (12 genes) and CW (6 genes). 28 genes (labeled in bold letters) were novel CF tolerance genes, since they have not been previously associated with echinocandin hypersensitivity in *S. cerevisiae* or *C.*

albicans. (B) Overlap between the chemical-genetic profile of CF, azoles and AmB. 61 genes displayed an increased sensitivity to CF (39 genes plus 9 genes with weak sensitivity), azoles (14 genes; fluconazole and voriconazole) and AmB (13 genes). The mutant strain collection was screened in a 96 well microplate format using an endpoint assay and medium was supplemented with 5 µg/ml fluconazole, 100 ng/ml voriconazole and 1,5 µg/ml AmB. The OD₆₀₀ was determined after 24 and 48 hours of incubation at 30°C. Grey-colored genes only display a weak sensitivity phenotype or were excluded from further analysis due to strong variations in the screening. Nodes represent compounds or genes and edges indicate chemical-genetic interactions. Gene nodes are color-coded according to GO annotation. Venn diagrams summarize distribution of genes affecting resistance to one of the three compounds.

Figure 5. Clustering of susceptibility data of the *C. glabrata* gene deletion collection. The set of mutants was screened on plates for hypersensitivity to four distinct stress conditions (CF, CR, CW and 42°C heat stress) using serial dilution assays on agar plates. (A) Two-dimensional hierarchical cluster plot of chemical-genetic profiles. On the horizontal axis genes are listed and stress conditions on the vertical axis. Interactions are shown in yellow depending on the degree of growth sensitivity (yellow = no growth, black = WT growth). Stress conditions and genes are clustered by the similarity of their interactions. (B) The clusters of genes are enlarged to highlight the chemical-genetic interaction profile of Caspofungin (blue bar in 'a' labeled 'b'). (C) A section of the cluster (orange bar labeled 'C') involved in heat stress (42°C) is enlarged. (D) Genes implicated in sensitivity to the cell wall-perturbing agents CR and CW (red and green bar labeled 'D').

Supplemental Figures

Figure S1. Generation of the new triple auxotrophic strain HTL. (A) Cloning strategy using the *SAT1* flipper for recyclable deletion cassettes of *C. glabrata* *TRP1*, *LEU2* and *HIS3* genes. 500bp homology flanking regions were ligated into *Apal/XhoI* and *SacII/SacI* restriction sites in pSFS2a, the deletion cassette excised with *Apal/SacI* and the resulting fragment used to transform *C. glabrata* ATCC2001. (B) Growth of ATCC2001 wild type strain, HTL and HTL reference strain on YPD, supplemented with 200 µg/ml Nourseothricin and SC plates lacking histidine, leucine or tryptophan. (C) Growth of ATCC 2001 wild type, HTL and HTL reference strains at 30°C and 37°C on solid YPD and minimal medium (YNB, ammonium sulfate, glucose, histidine, leucine or tryptophan), as well as in liquid YPD at 30°C and 37°C.

Figure S2. Verification of *C. glabrata* sensitivities to antifungals and hyperosmolarity. Deletions were tested for (A) osmostress (NaCl), (B) fluconazole (Flc) and (C) CF susceptibility. Serial dilutions of *C. glabrata* ATCC 2001, HTL and selected deletion strains were spotted onto YPD plates supplemented with the indicated compounds. Plates were incubated for two days at 30°C.

Figure S3. Sensitivity of *C. glabrata* strains to NaCl treatment. Confirmation of NaCl sensitivities of osmosensitivity mutants on agar plates. Deletions strains were spotted in serial dilutions on synthetic medium supplemented with 1M NaCl and growth was monitored over 3 days at 30°C.

Figure S4. Deletions with altered fitness under planktonic or biofilm growth conditions. VENN diagrams showing the overlap between planktonic and biofilm growth. (A) 36 strains showed a decrease in fitness in biofilm conditions, while 55 strains show a fitness decrease in planktonic conditions. 13 strains showed a decrease

in fitness under both conditions. (B) 36 mutants displayed a fitness gain under biofilm conditions, while 35 mutants showed increased fitness under planktonic conditions. 8 strains showed an increase in both growth conditions. SD (standard deviation), Fb (fitness biofilm growth), F (fitness planktonic growth).

Figure S5. Susceptibilities of *C. glabrata* mutants to azoles Susceptible strains identified in the primary screenings were subjected to IC₅₀ determination. Overnight cultures were grown to an OD₆₀₀ of 1.0 and a microdilution assay was carried out in YPD to determine IC₅₀ values as described in Materials and Methods. The OD₆₀₀ was determined in a microplate reader after 24 h and 48 h of incubation at 30°C. Each strain was tested in triplicates and mean values normalized to the untreated control were plotted against the antifungal concentration of fluconazole (A). The IC₅₀ was calculated by nonlinear regression (curve fit), using GraphPadPrism (B). Shown are data of 24 h measurements. Bars denote standard deviations.

Figure S6. Susceptibilities of *C. glabrata* mutants to AmB. AmB-susceptible strains identified in the primary robotic screening were subjected to IC₅₀ determination. Overnight cultures were grown to an OD₆₀₀ of 1.0 and a microdilution assay carried out in YPD to determine IC₅₀ for AmB (A) as described in Materials and Methods. The OD₆₀₀ was determined in a microplate reader after 24 h and 48 h of incubation at 30°C. Each strain was tested in triplicates and mean values normalized to the untreated control were plotted against the antifungal concentration. The IC₅₀ were calculated for each mutant by nonlinear regression (curve fit), using GraphPadPrism (B). Shown are data of 24 h measurement. Bars indicate standard deviations.

Figure S7. Sensitivity of *C. glabrata* deletion strains to cell integrity stressors. Deletion strain sensitivities were tested against CF, CW, CR, and 42°C in liquid culture and on plates. (A) Growth susceptibilities of *C. glabrata* strains to CF. Susceptible

strains identified in the primary robotic screenings were subjected to IC_{50} determination. Overnight cultures were grown to OD_{600} of 1.0 and a microdilution assay was carried out in YPD to determine IC_{50} as described in Materials & Methods. The optical density (OD) of each well was determined at 600 nm on a microplate reader after 24h and 48h of incubation at 30°C. Each strain was tested in triplicates and mean values normalized to the untreated control were plotted against the antifungal concentration. The IC_{50} was calculated by nonlinear regression (curve fit), using GraphPadPrism. Shown are data of 48h measurement. Bars denote standard deviations. (B) Confirmation of CF sensitivity on plates. Strains were spotted in serial dilutions on synthetic medium supplemented with 120ng/ml caspofungin (CF) and growth was monitored over 3 days at 30°C. (C) Congo Red (CR), heat and Calcofluor White (CW) sensitivity on plates. Strains were spotted in serial dilutions on synthetic medium supplemented with 250 μ g/ml Congo Red (CR) or 50 μ g/ml CW and growth was monitored over 3 days at 30°C. For heat stress assay cells were grown at 42°C over three days.

Supplemental Tables

Table S1. Classification of functional gene categories. Genes were selected by their homology to *S. cerevisiae* based on SGD gene ontology annotations (www.yeastgenome.org). *C. glabrata* orthologues were identified using a BLAST approach. The three best-aligned hits for each gene were saved. The orthologues have been remapped using a tree-based approach applying the algorithm described in [47,50].

Table S2. Isogenic *C. glabrata* background strains used in this study. The triple auxotrophic strain HTL and isogenic single and double deletion strains were generated in the sequenced reference strain ATCC2001. Strain HTL was used as recipient strain for the generation of the deletion mutants in the strain library.

Table S3. Summary of auxotrophic *C. glabrata* deletion strains generated in the HTL background derived from the clinical isolate strain ATCC2001. Sheet 1: deletion strains + corresponding barcodes. Independent transformants of all generated gene deletion strains are listed with corresponding UP and DOWN tags, position in storage plates, number corresponding to the individual biological replicate (IBR#) for a targeted gene (e.g. the second of three independent replicates for CAGL0A01133g has IBR #2) and the nourseothricin marker used. All data can be searched online under: <http://funpath.cdl.univie.ac.at>. (Sheet 2: barcode sequences only). Bar-codes used as unique genomic tags in *C. glabrata* deletion strains. 2 x 96 upstream and downstream barcodes were used for every set of 96 gene deletion strains. These can be amplified from constant regions (U1 + U2; D1 + D2) identical in every deletion strain. Strains labeled with BM or BG carry individual barcodes and were made in the histidine auxotrophic strain derived from ATCC2001. The reference strain in the HTL background carries a unique barcode not used for any other strain. Barcode sequences

were adopted from the systematic *S. cerevisiae* gene deletion project (http://www-sequence.stanford.edu/group/yeast_deletion_project/deletions3.html;))

Table S4. Fitness raw data of *C. glabrata* deletion with strong variations in relative fitness. Deletions displaying strong variations between independent mutants in the same gene or independent cultures, identifying 57 strains that were excluded from fitness analysis due to a standard deviation of more than 0.1, or an absolute difference in fitness of more than 0.1 between two biological replicates.

Table S5. Fitness raw data of *C. glabrata* deletion mutants. The table shows the raw data for fitness analysis, including fitness and standard deviation (SD). The orange and red color-coding (> 3 SD) and red ($>2<3$ SD) indicates genes with deviations below and above the average fitness indices.

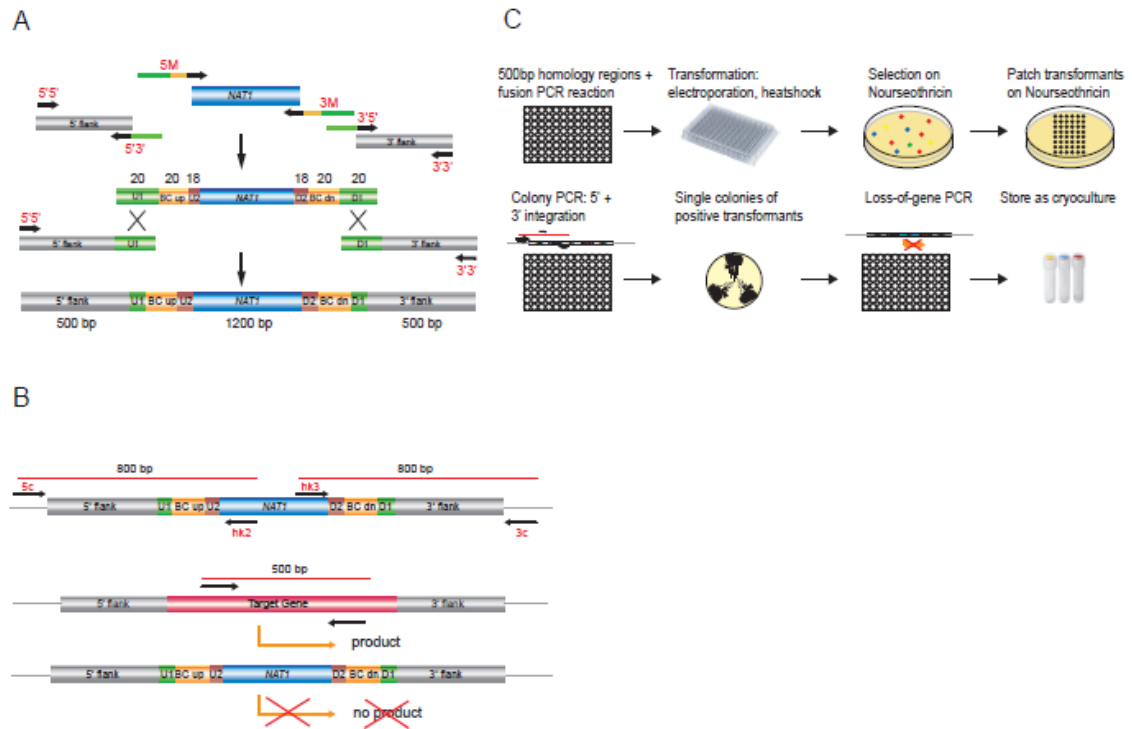
Table S6. Fitness distribution of *C. glabrata* knock-out mutants. The Table shows the distribution of fitness phenotypes. Strains with a standard deviation (SD) above 0.1 or an absolute difference in fitness of more than 0.1 between two biological replicates were excluded from detailed analysis. Classification was based on the number of standard deviations between the fitness of a single strain and the average fitness.

Table S7. Biofilm raw data - strains with strong variations in relative biofilm fitness. Some 158 deletions strains were excluded from biofilm analysis due to a standard deviation (SD) of more than 0.3 or an absolute difference of more than 0.5 between replicates.

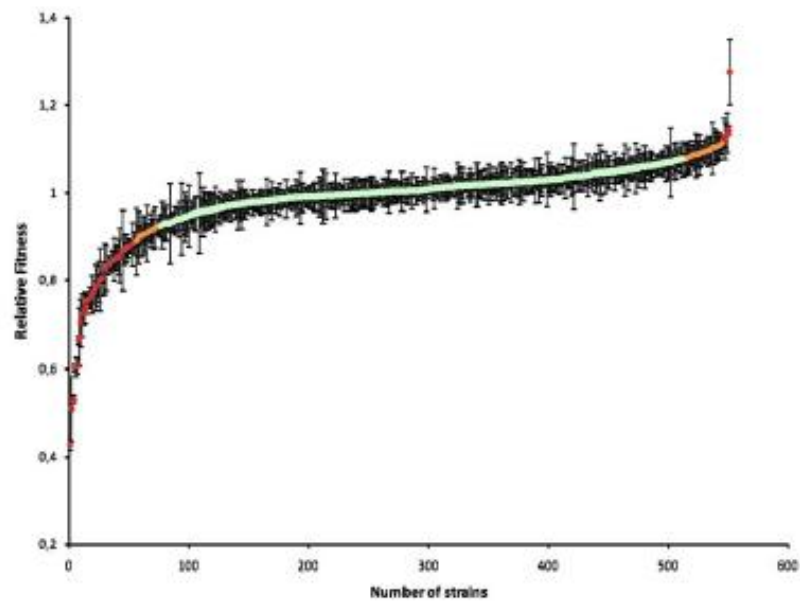
Table S8. Biomass quantification using fluorescein diacetate assay. The table shows the raw data for biofilm analysis, including fitness and standard deviation (SD).

Table S9. Biofilm fitness distribution of *C. glabrata* knock-out mutants. Summary of biofilm fitness phenotypes. Strains with a standard deviation (SD) above 0.3, or an absolute difference in biofilm fitness of more than 0.5 between replicates were excluded. Classification was based on the number of standard deviations between the fitness of a single strain and the average fitness.

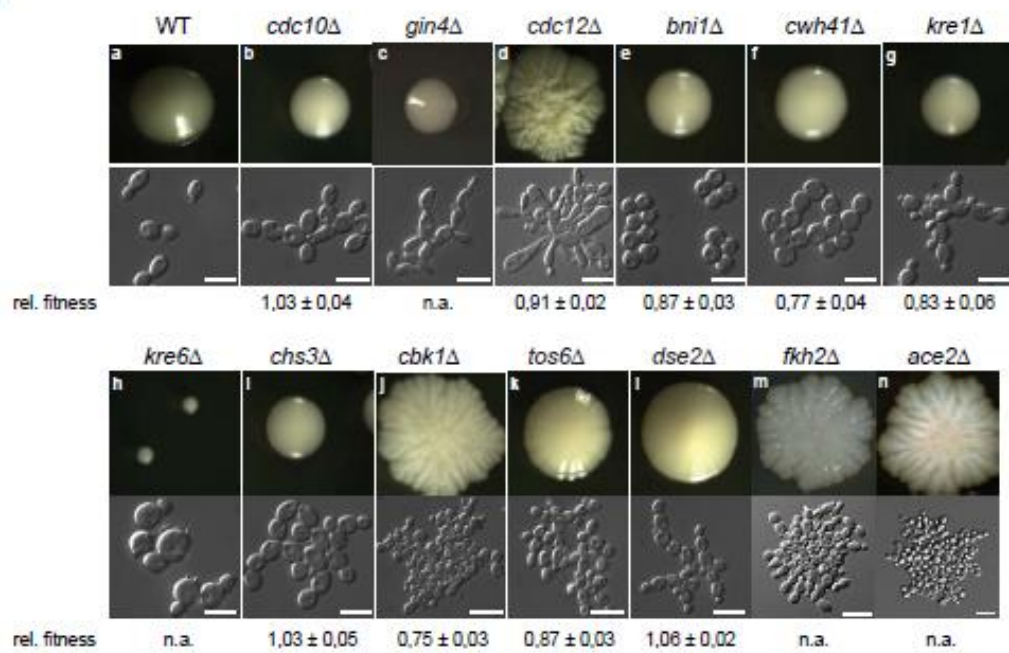
Schwarz Müller et al.; Figure 1 - TOP



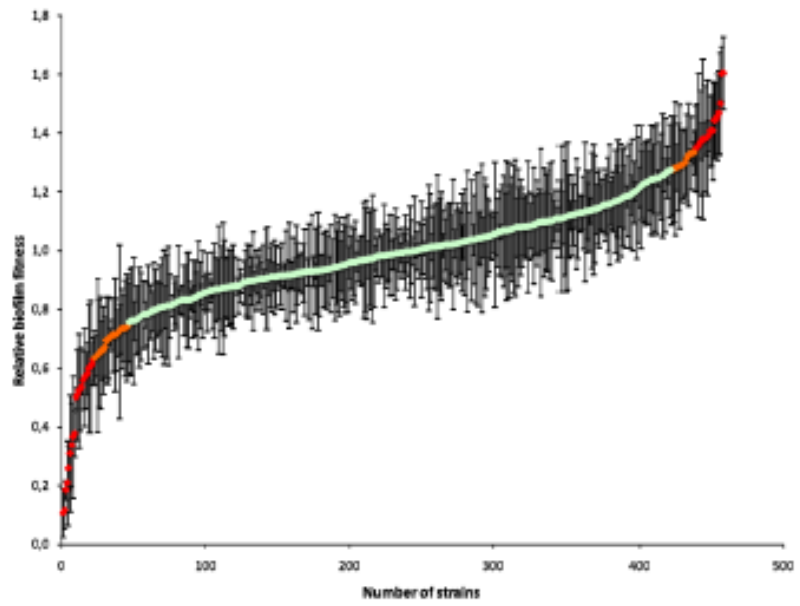
A

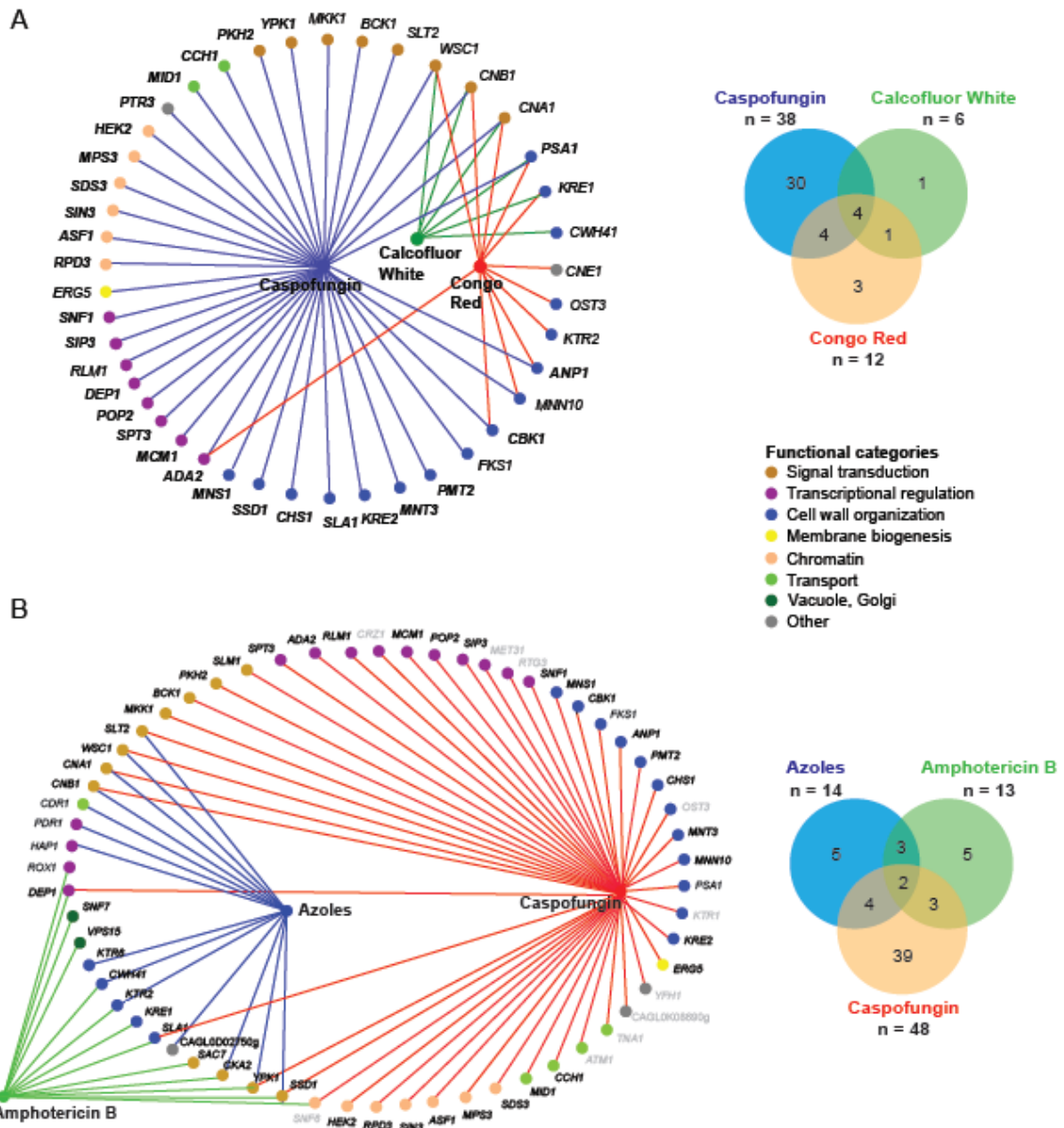


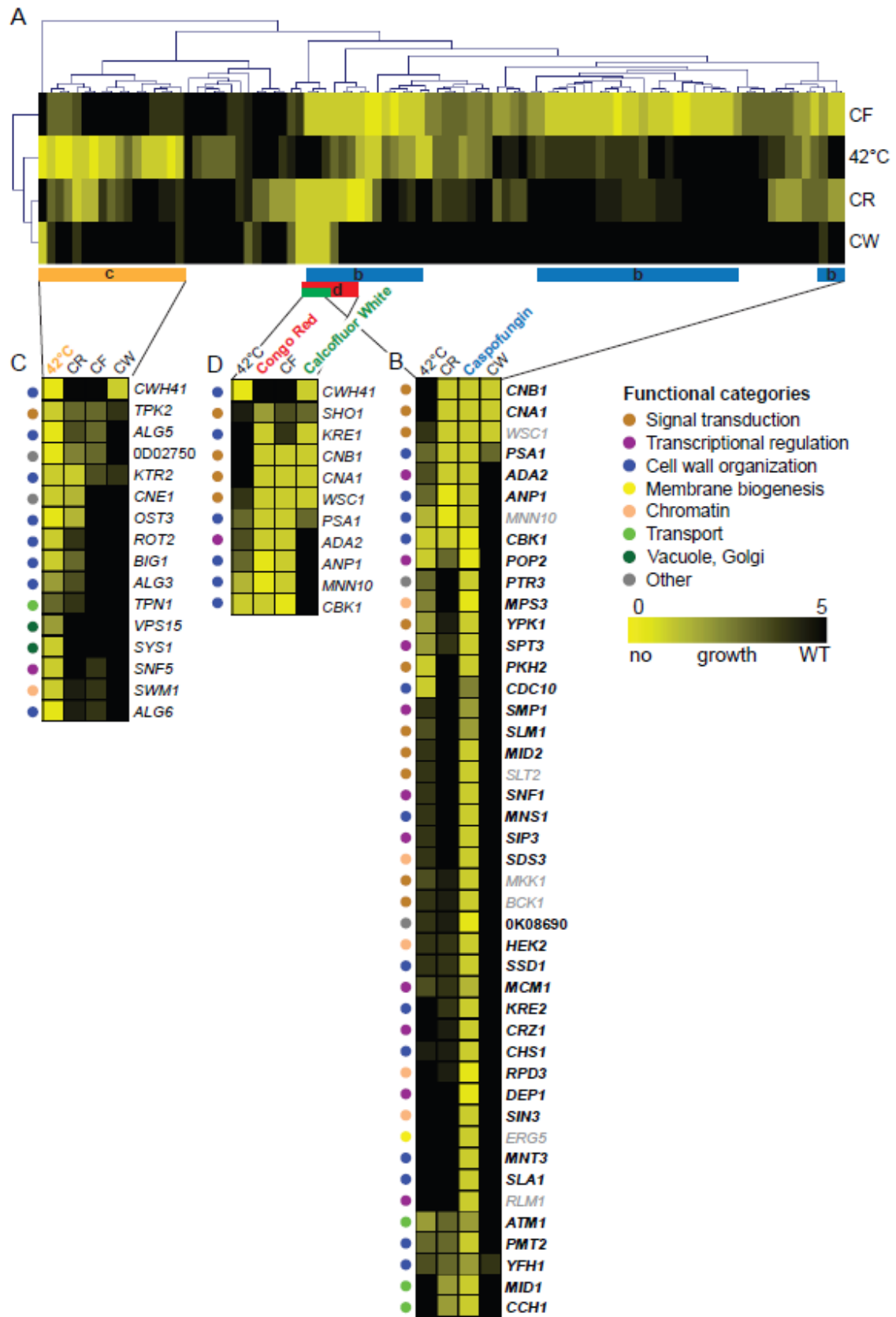
B



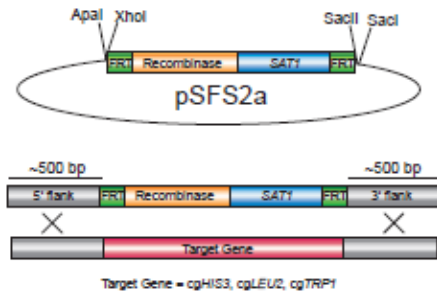
Schwarz Müller et al.; Figure 3 - TOP



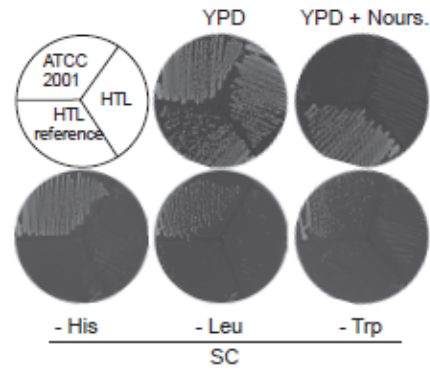




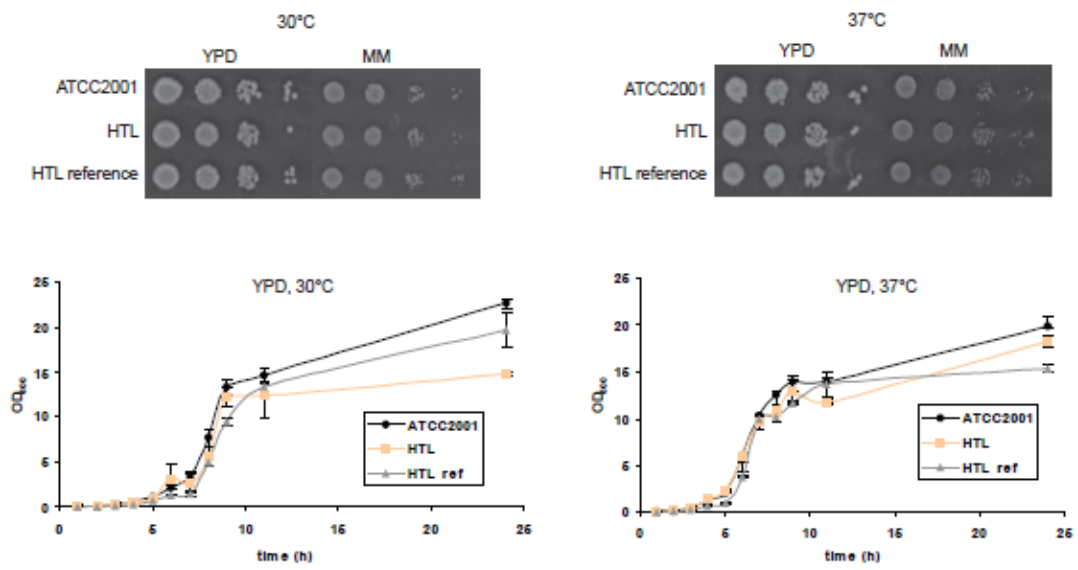
A



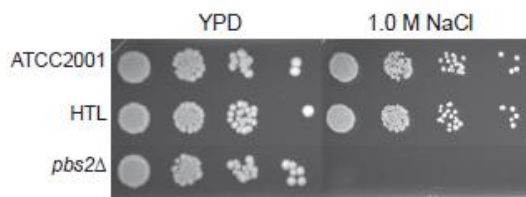
B



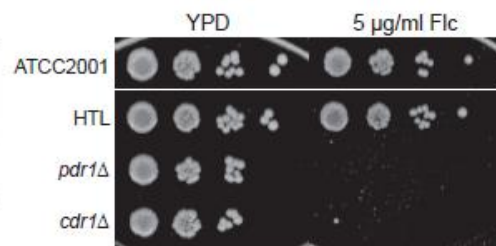
C



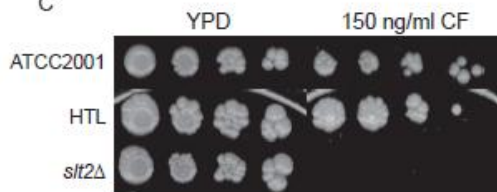
A



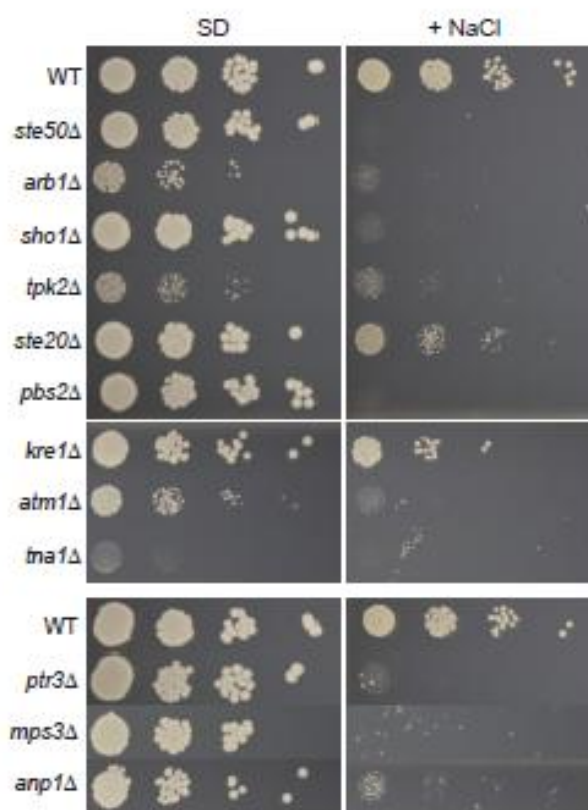
B



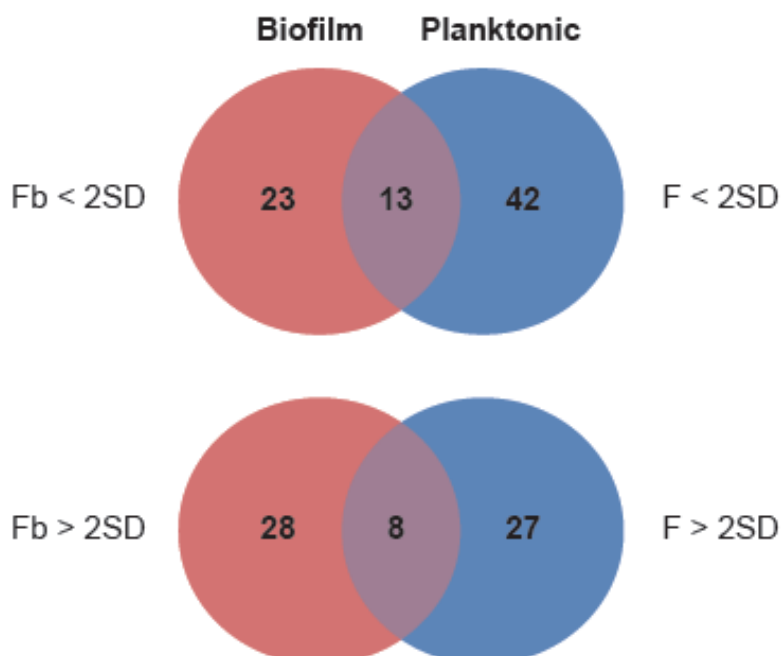
C

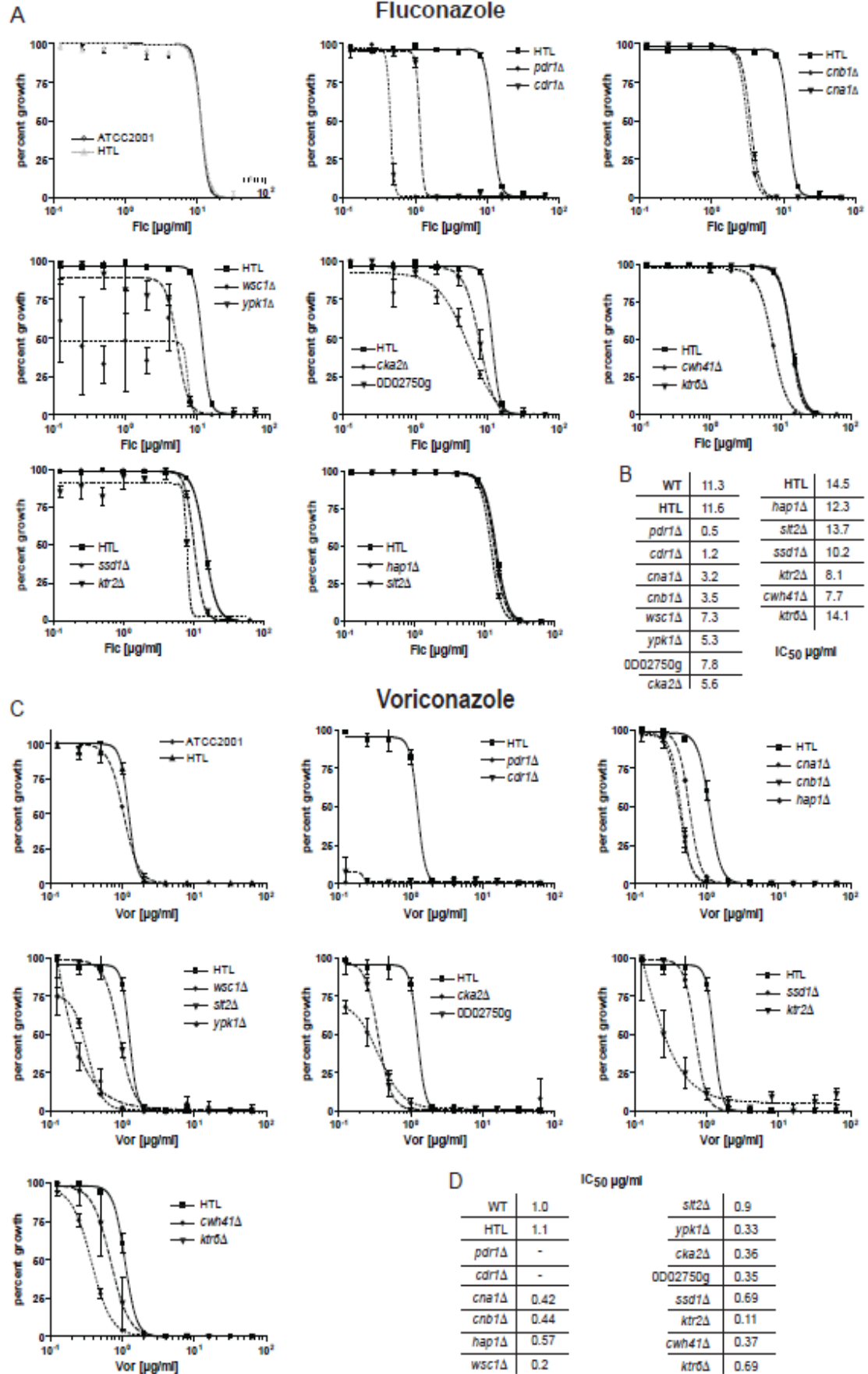


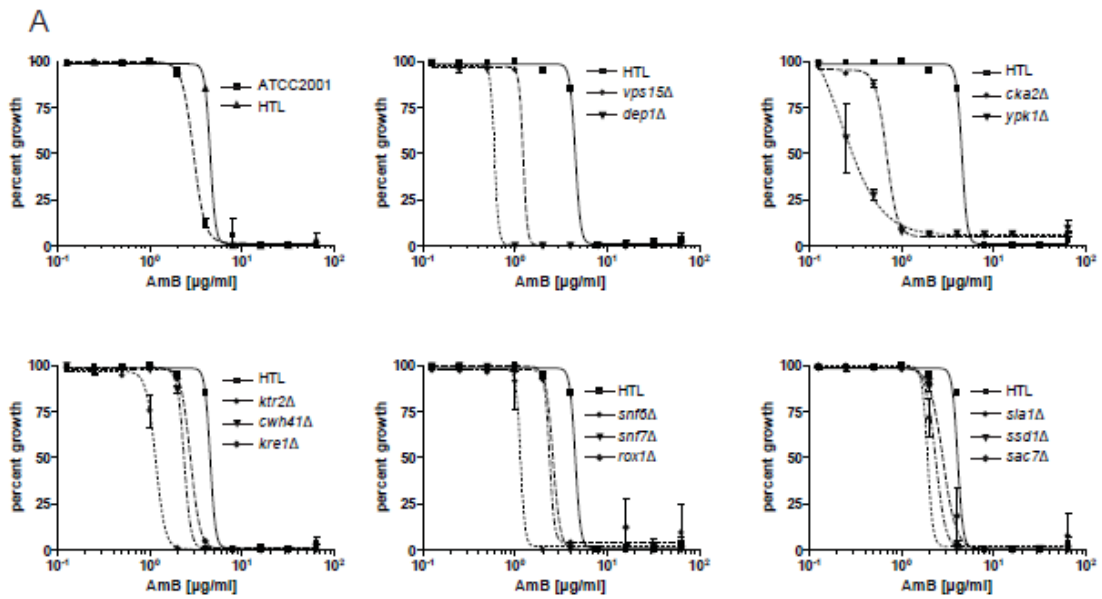
Schwarz Müller et al., Figure S3 - TOP



Schwarz Müller et al., Figure S4 - TOP

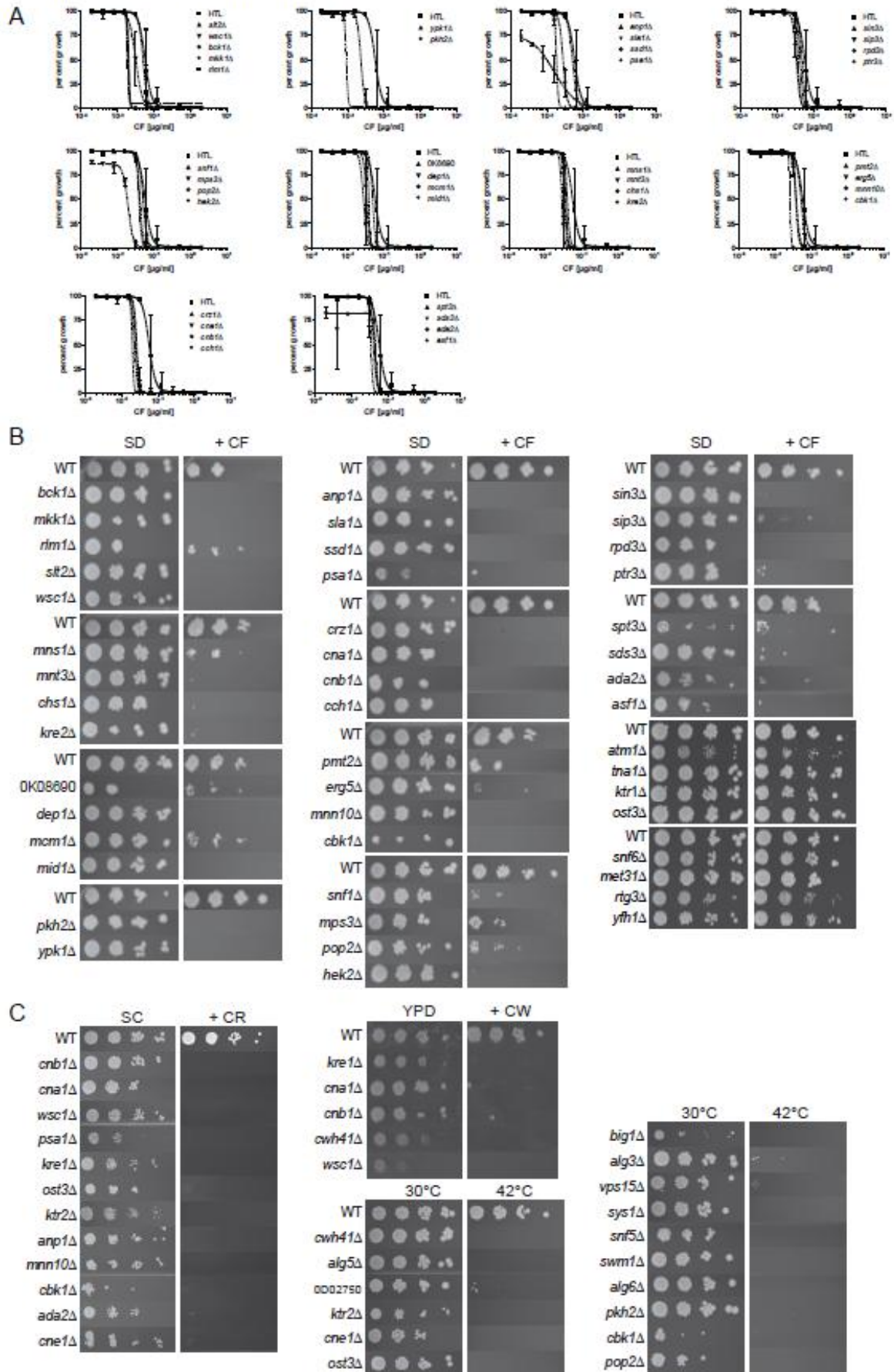






B

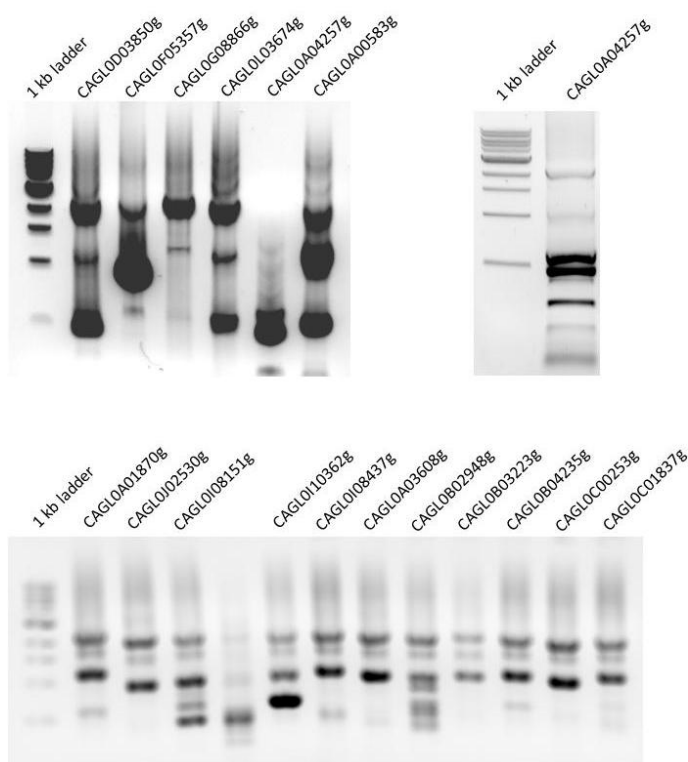
	IC ₅₀ µg/ml	IC ₅₀ µg/ml	IC ₅₀ µg/ml	IC ₅₀ µg/ml			
WT	3.0	<i>cka2Δ</i>	0.7	<i>kre1Δ</i>	2.8	<i>sla1Δ</i>	2.1
HTL	4.5	<i>ypk1Δ</i>	0.2	<i>snf6Δ</i>	1.2	<i>ssd1Δ</i>	2.6
<i>vps15Δ</i>	0.6	<i>ktr2Δ</i>	1.2	<i>snf7Δ</i>	2.6	<i>sac7Δ</i>	3.1
<i>dep1Δ</i>	1.2	<i>cwh41Δ</i>	2.4	<i>rox1Δ</i>	2.4		

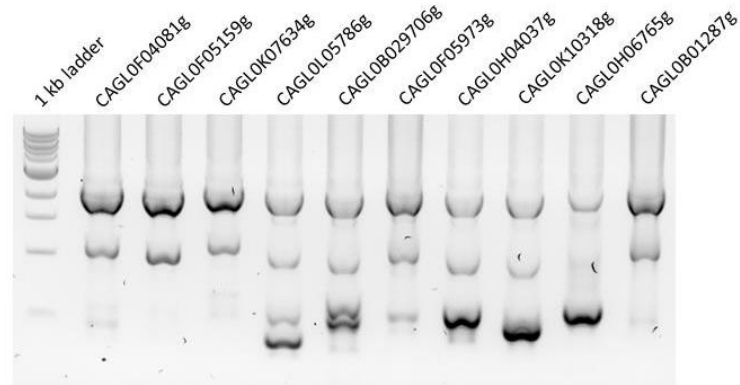
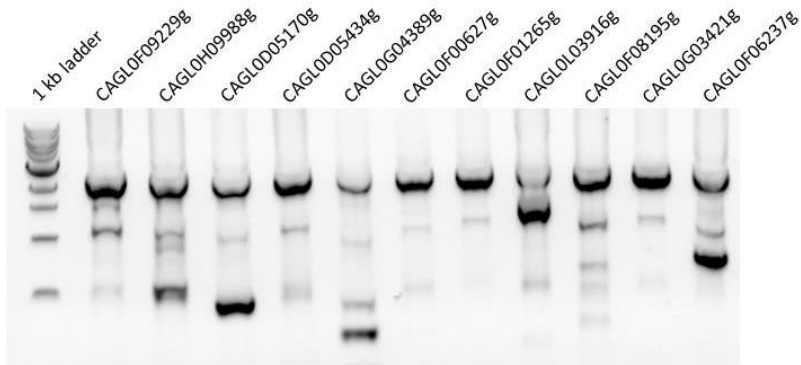
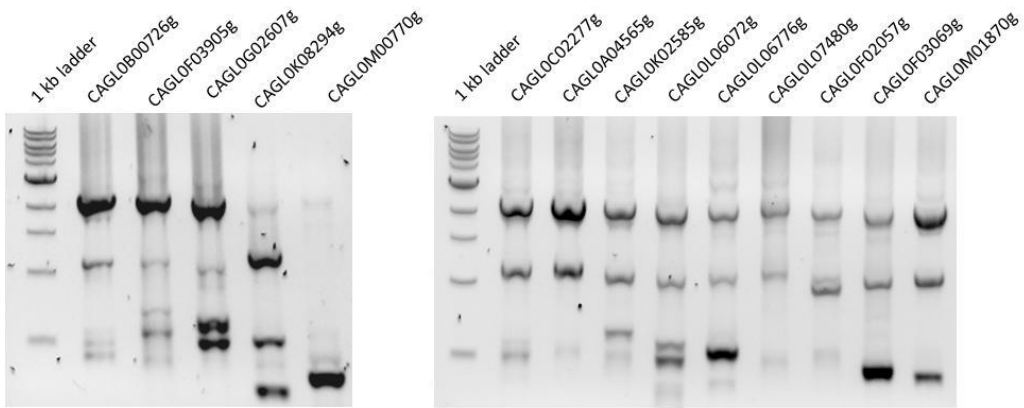


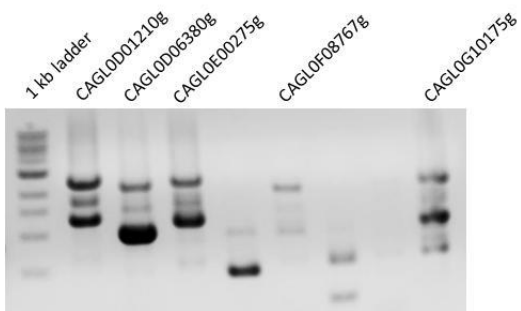
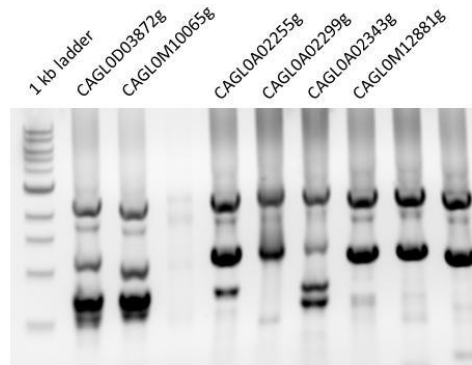
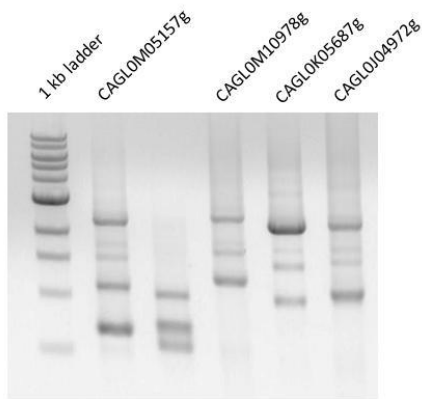
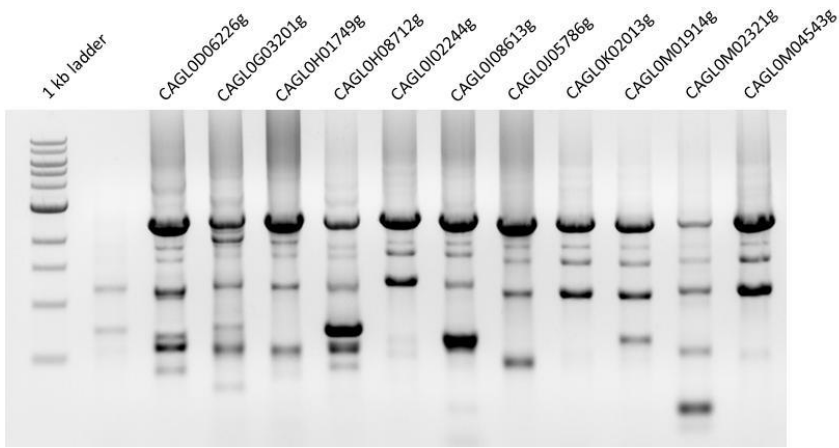
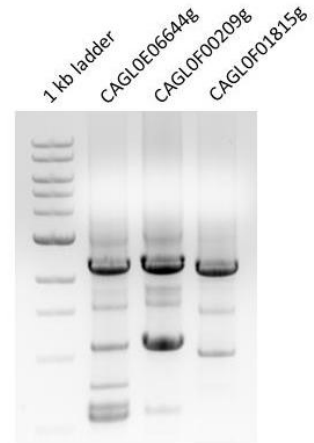
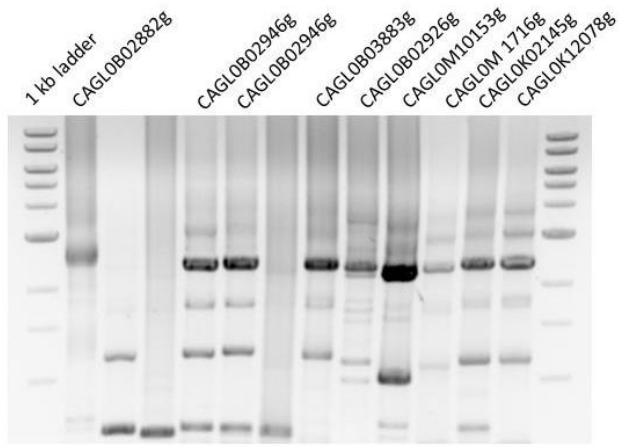
Appendix 14: Verification of fusion constructs and *C. glabrata* deletion mutants.

Verification of fusion constructs. ORF-specific -500-F and +500-R primers (Appendix 1 Table 2) were added to a PCR reaction permitting the fusion of the NAT^R cassette with homologous regions of ORF-specific 5' and 3' ends. Correct fusion produced a 2.3-2.4 kb amplification product, although several minor bands were also produced.

Figure 1: Verification of fusion constructs.







Verification of *C. glabrata* deletion mutants. Transformants (labelled numerically) were checked for the presence of the target ORF (“internal”) using ORF-specific primers int-F and int-R (Appendix 1 Table 3), yielding an amplification product in the parental strain (labelled C) and no product in correct transformants. Junction PCR checks were performed on transformants which passed the internal PCR check. For PCR amplification of the 5’ junction, primers -600-F (Appendix 1 Table 3) and NAT-5’-R (Appendix 1 Table 1) were used, yielding an amplification product of 1-1.3 kb in transformants where the fusion construct had integrated at the correct locus. For the 3’ junction, primers +600-R (Appendix 1 Table 3) and NAT-3’-F (Appendix 1 Table 1) were used, yielding a 0.9-1.2 kb amplification product in correct transformants.

Figure 2: Verification of *C. glabrata* Δ CAGL0A02299g. Three independent isolates (3, 7 and 14) were stored as glycerol stocks.

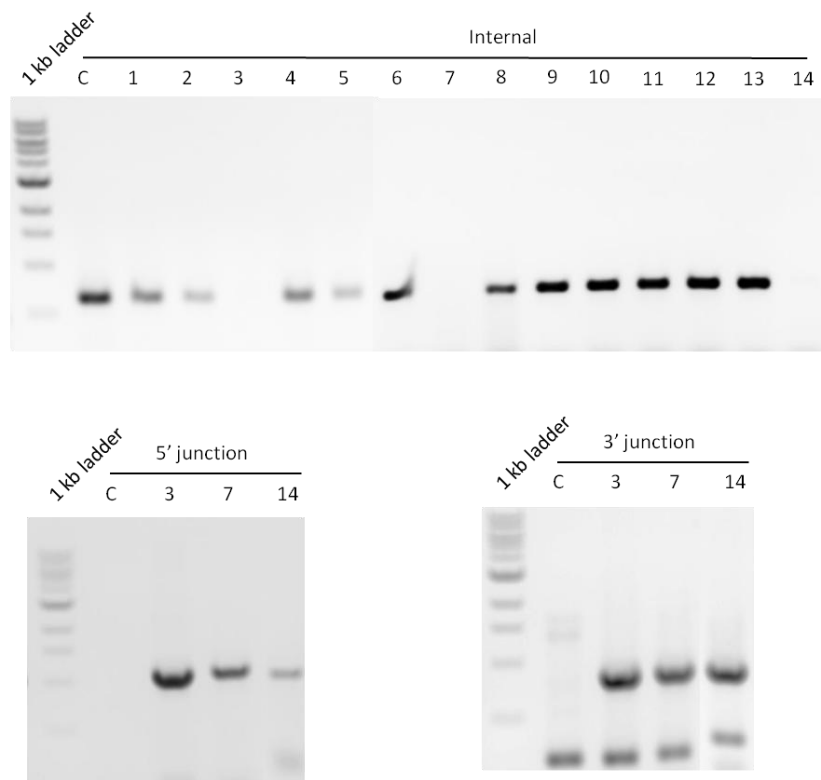


Figure 3: Verification of *C. glabrata* Δ CAGL0A02343g. Two independent isolates (3 and 13) were stored as glycerol stocks.

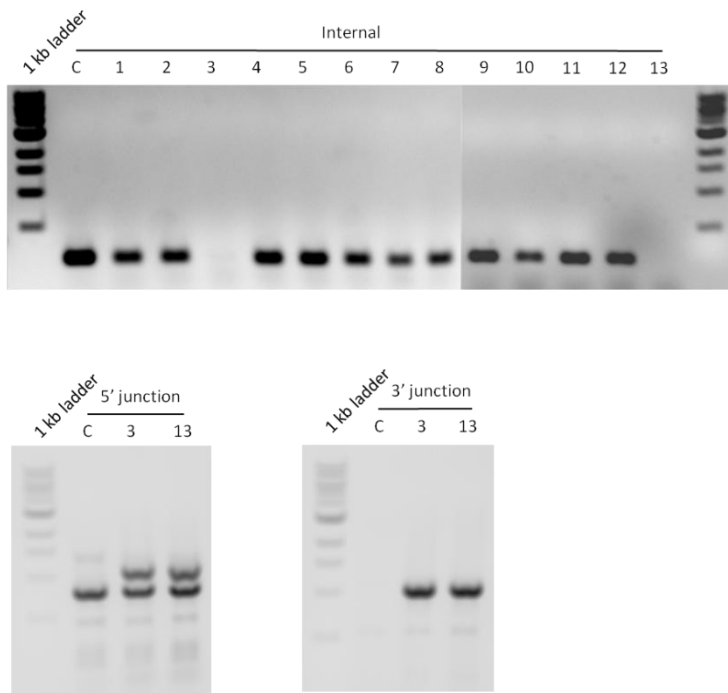


Figure 4: Verification of *C. glabrata* Δ CAGL0A04565g. One independent isolates (1) was stored as glycerol stocks.

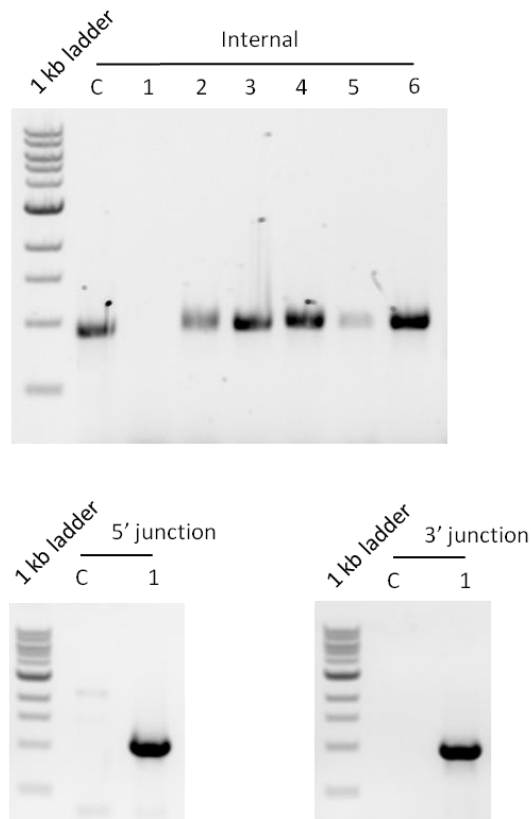


Figure 5: Verification of *C. glabrata* Δ CAGL0B00726g. Three independent isolates (1, 2 and 3) were stored as glycerol stocks.

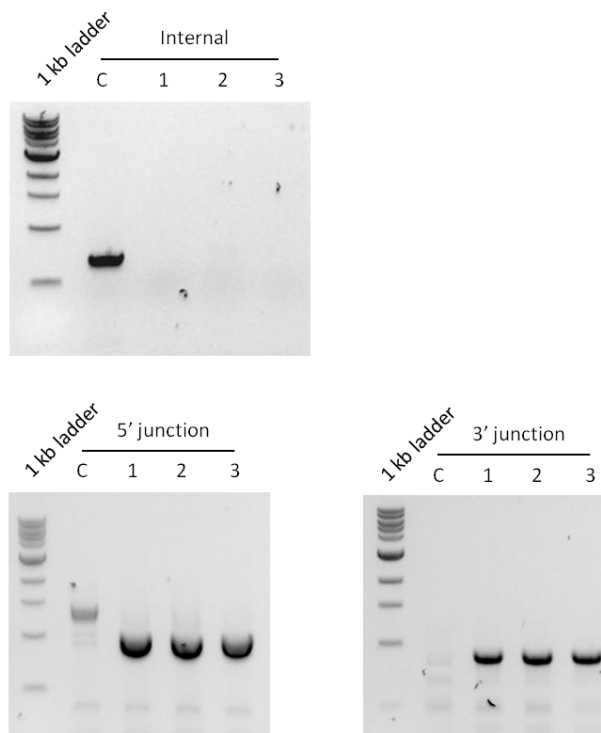


Figure 6: Verification of *C. glabrata* Δ CAGL0B02926g. One independent isolate (1) was stored as glycerol stocks.

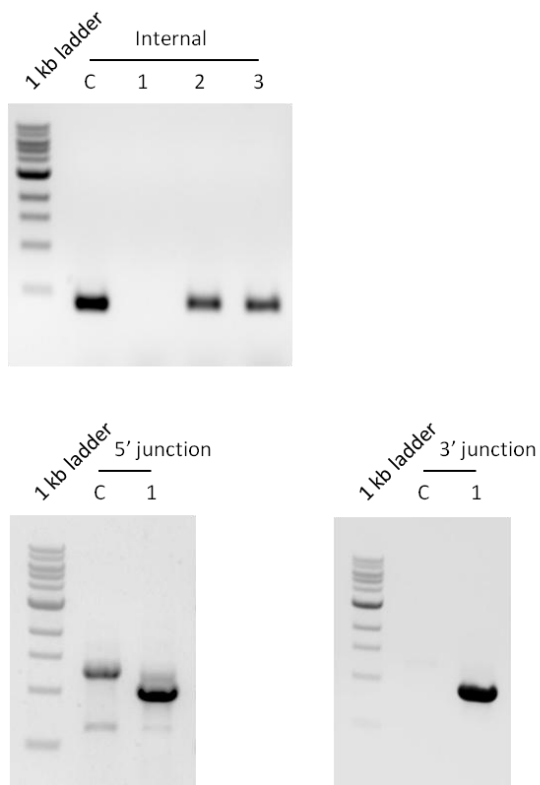


Figure 7: Verification of *C. glabrata* Δ CAGL0B02946g. Three independent isolates (4, 5 and 7) were stored as glycerol stocks.

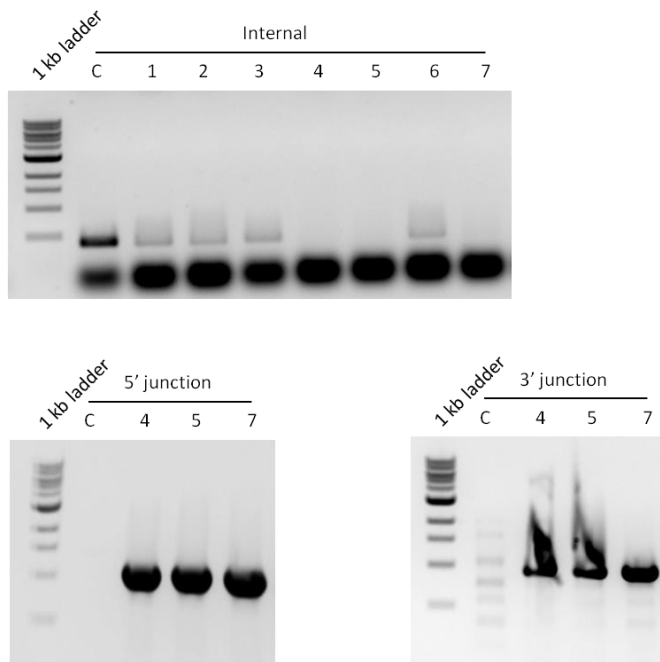


Figure 8: Verification of *C. glabrata* Δ CAGL0B02948g. Three independent isolates (1, 2 and 4) were stored as glycerol stocks.

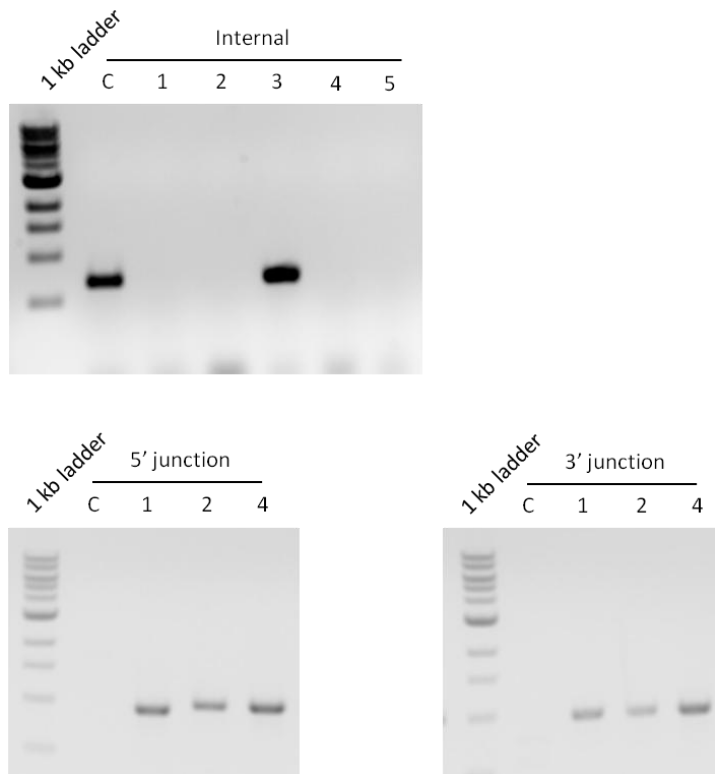


Figure 9: Verification of *C. glabrata* Δ CAGL0B02970g. One independent isolate (1) was stored as glycerol stocks.

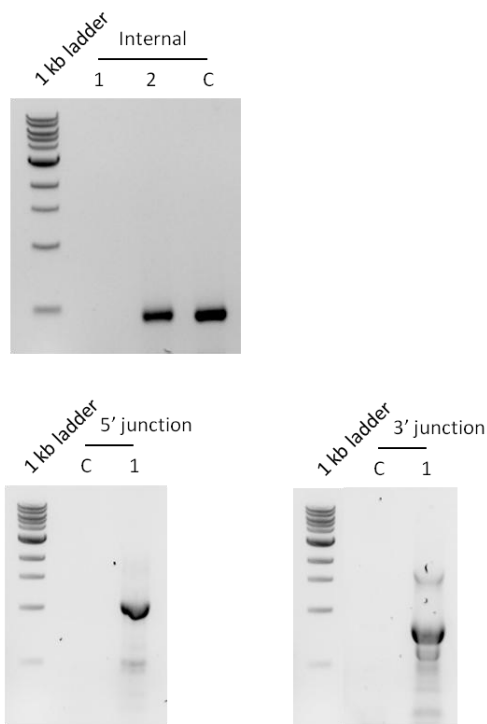


Figure 10: Verification of *C. glabrata* Δ CAGL0B03223g. Three independent isolates (7, 9 and 10) were stored as glycerol stocks.

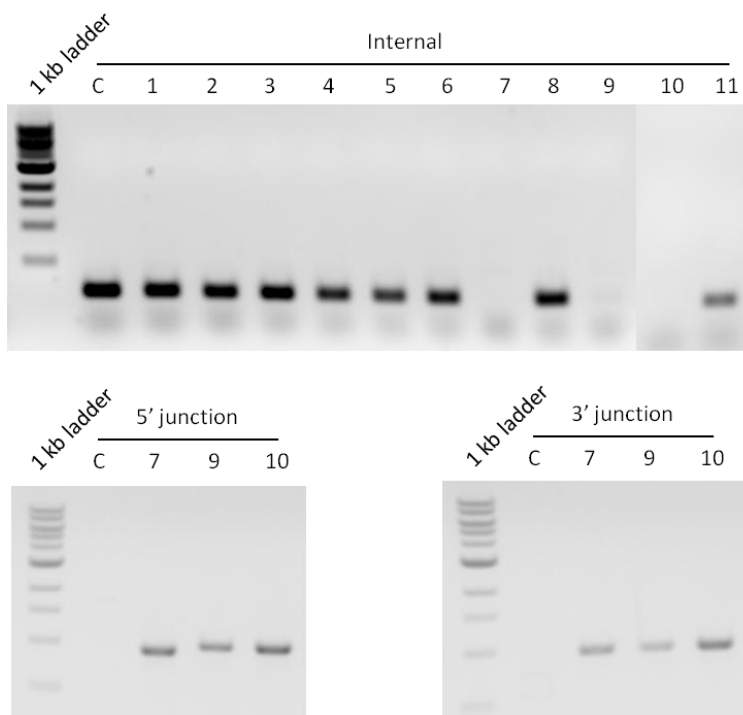


Figure 11: Verification of *C. glabrata* Δ CAGL0B03883g. Three independent isolates (2,7 and 13) were stored as glycerol stocks.

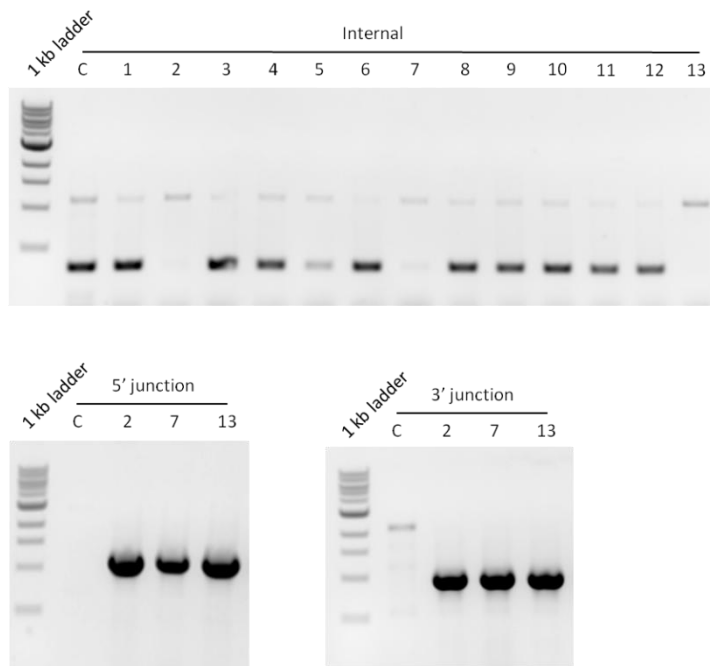


Figure 12: Verification of *C. glabrata* Δ CAGL0C00253g. Three independent isolates (1, 2 and 3) were stored as glycerol stocks.

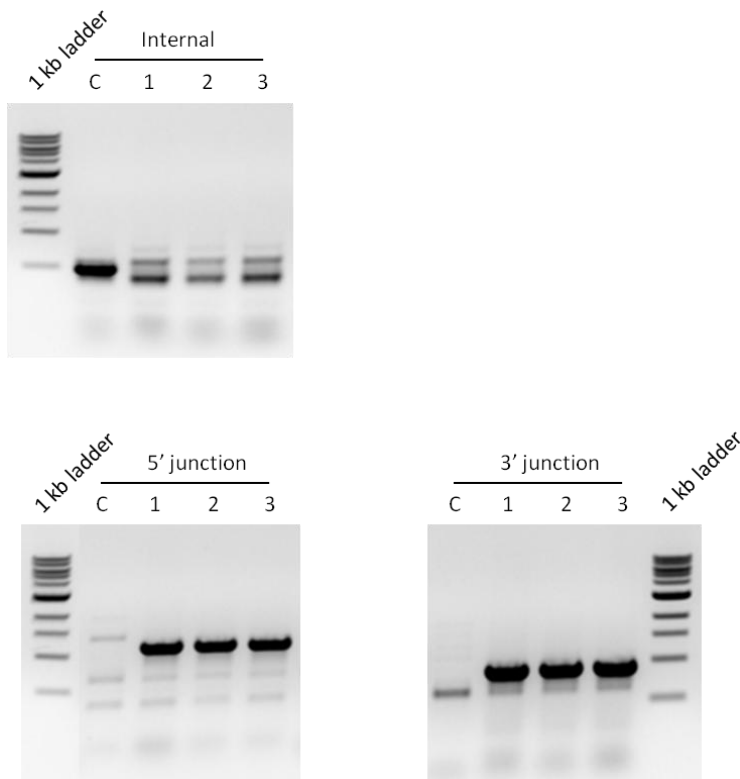


Figure 13: Verification of *C. glabrata* Δ CAGL0C01837g. Three independent isolates (1, 2 and 5) were stored as glycerol stocks.

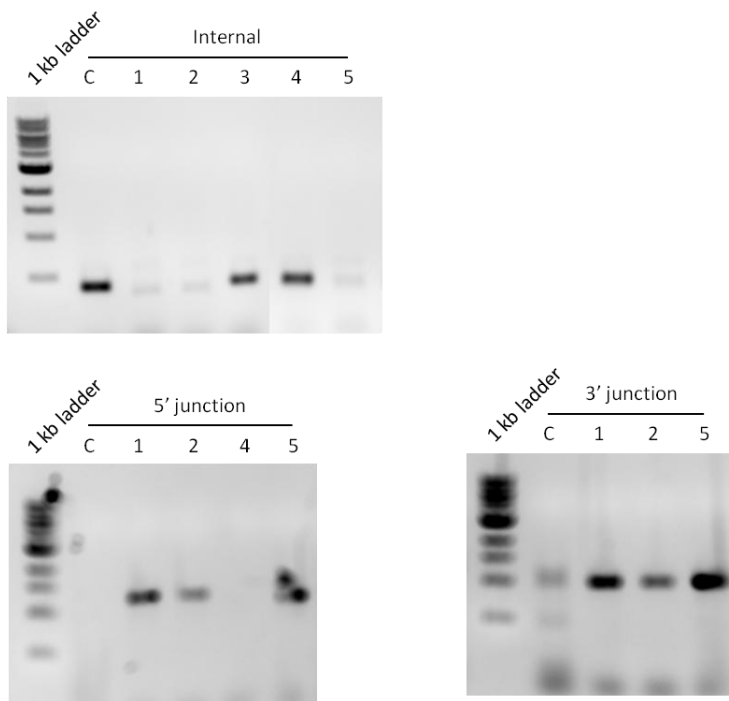


Figure 14: Verification of *C. glabrata* Δ CAGL0C04763g. Three independent isolates (1, 3 and 4) were stored as glycerol stocks.

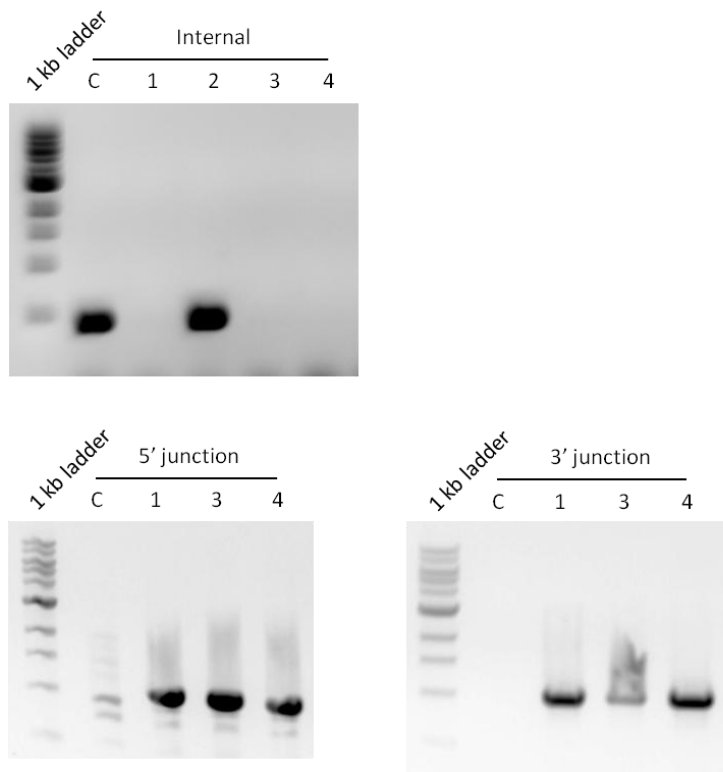


Figure 15: Verification of *C. glabrata* Δ CAGL0D00682g. Two independent isolates (1 and 3) were stored as glycerol stocks.

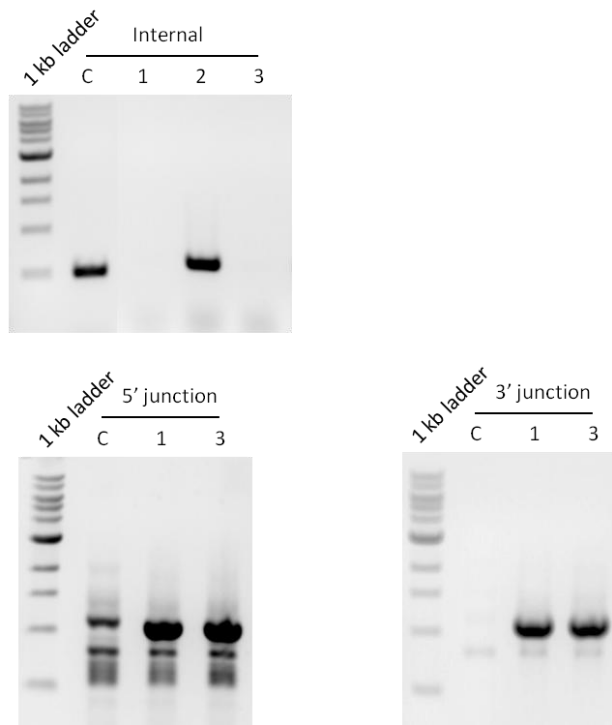


Figure 16: Verification of *C. glabrata* Δ CAGL0D01210g. Three independent isolates (2, 3 and 5) were stored as glycerol stocks.

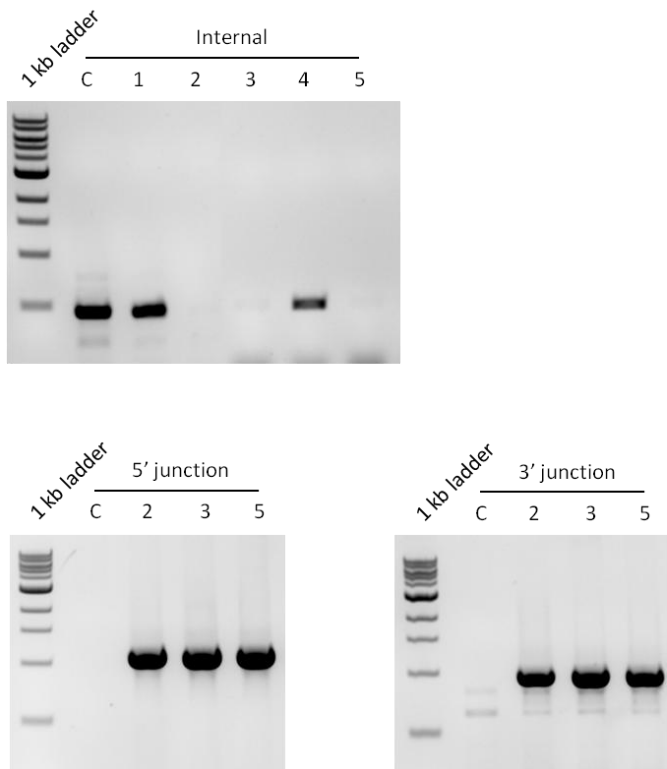


Figure 17: Verification of *C. glabrata* Δ CAGL0D03850g. Two independent isolates (3 and 4) were stored as glycerol stocks.

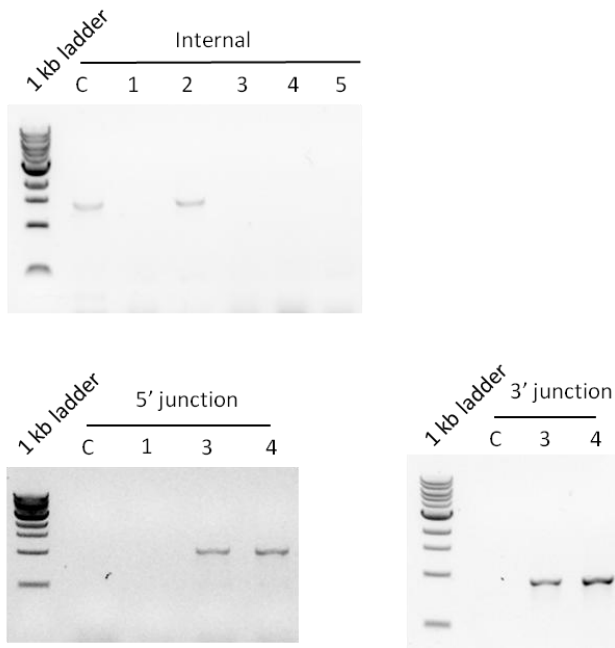


Figure 18: Verification of *C. glabrata* Δ CAGL0D03872g. Three independent isolates (6, 9 and 11) were stored as glycerol stocks.

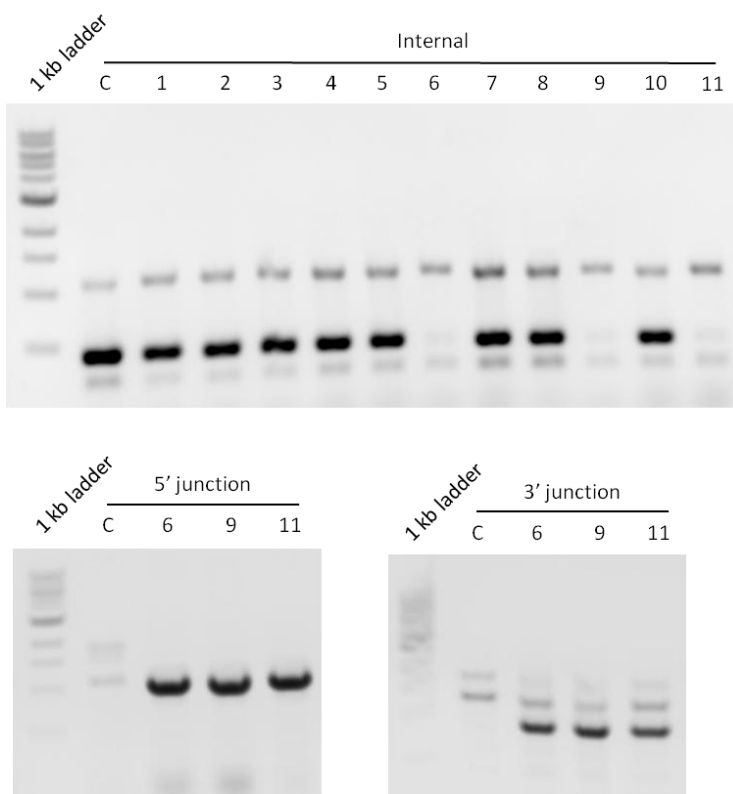


Figure 19: Verification of *C. glabrata* Δ CAGL0D05170g. Two independent isolates (1 and 4) were stored as glycerol stocks.

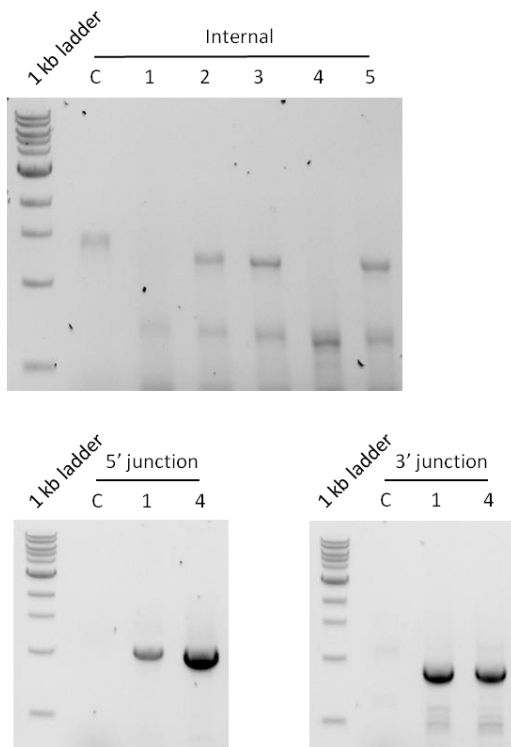


Figure 20: Verification of *C. glabrata* Δ CAGL0D05434g. Two independent isolates (1 and 4) were stored as glycerol stocks.

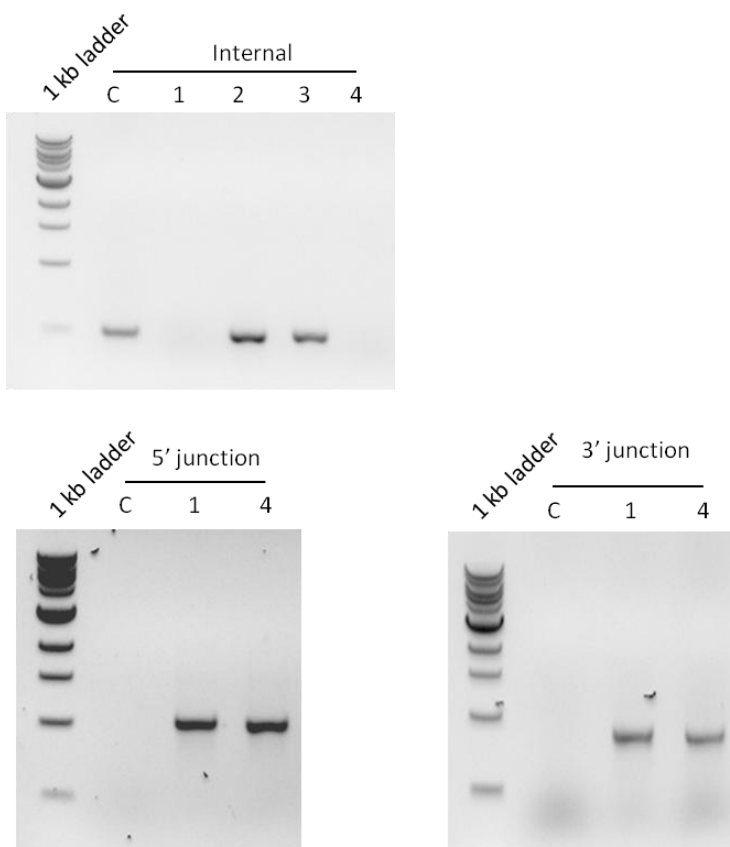


Figure 21: Verification of *C. glabrata* Δ CAGL0D06226g. Three independent isolates (3, 9 and 11) were stored as glycerol stocks.

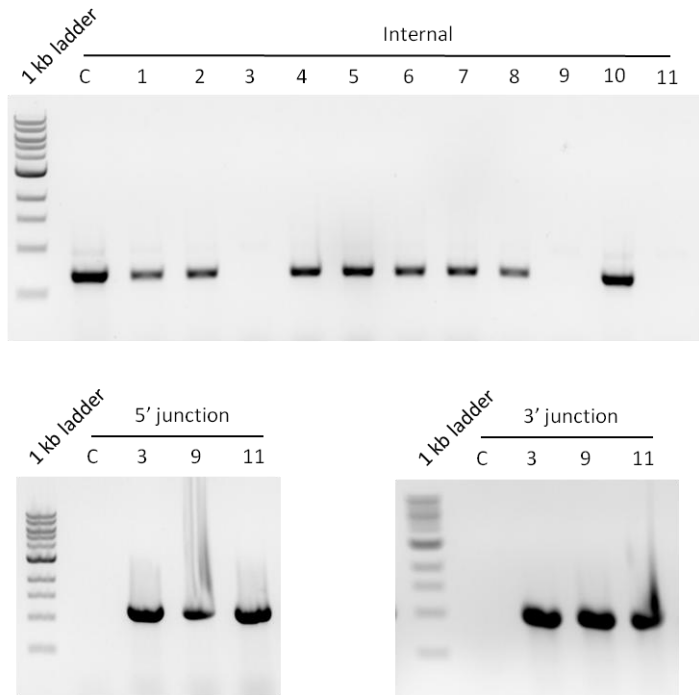


Figure 22: Verification of *C. glabrata* Δ CAGL0E00275g. One independent isolates (13) was stored as glycerol stocks.

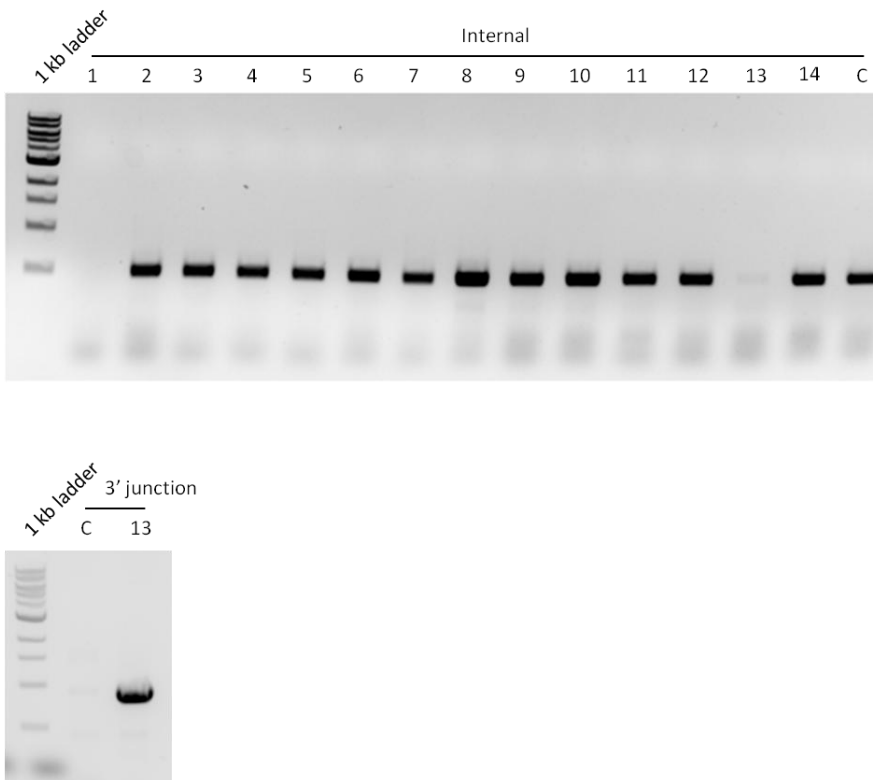


Figure 23: Verification of *C. glabrata* Δ CAGL0E06600g. Three independent isolates (1, 2 and 3) were stored as glycerol stocks.

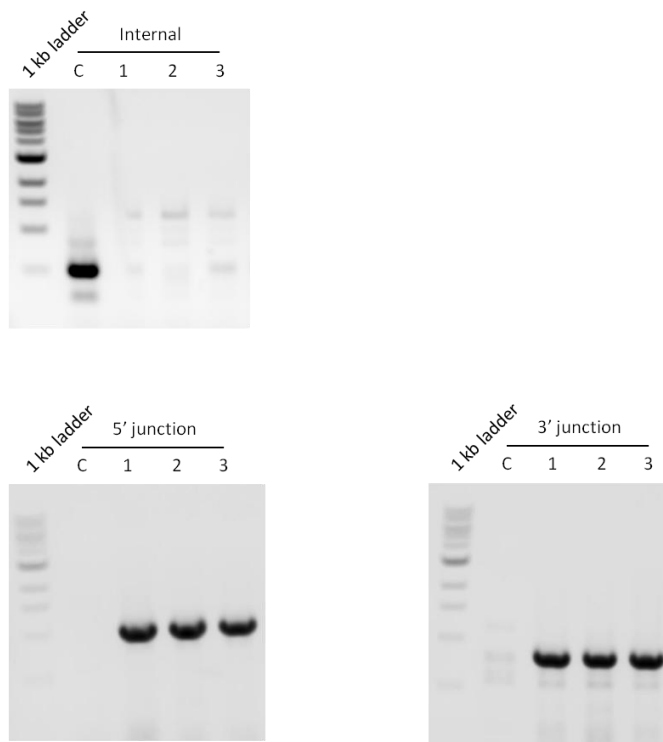


Figure 24: Verification of *C. glabrata* Δ CAGL0E06600g. Three independent isolates (2, 3 and 5) were stored as glycerol stocks.

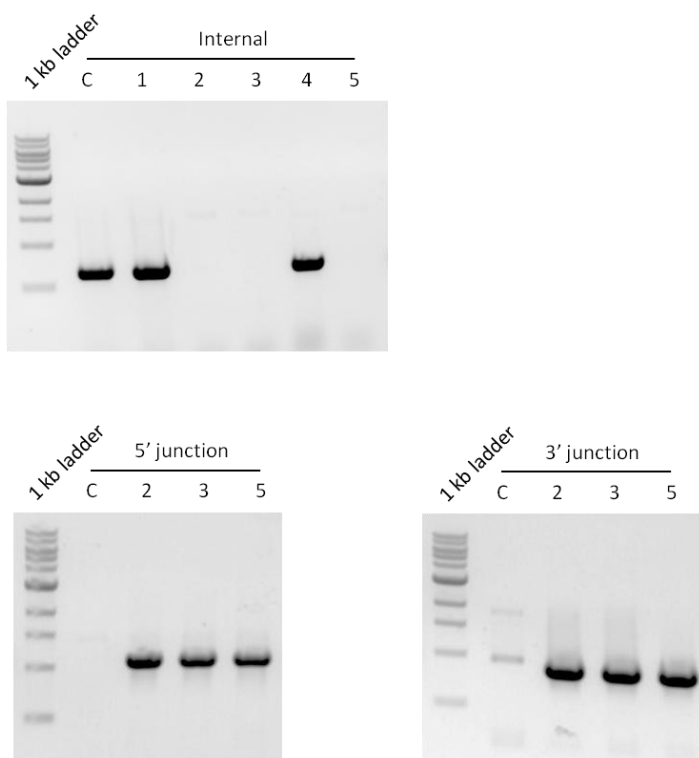


Figure 25: Verification of *C. glabrata* Δ CAGL0F01815g. Three independent isolates (4, 6 and 7) were stored as glycerol stocks.

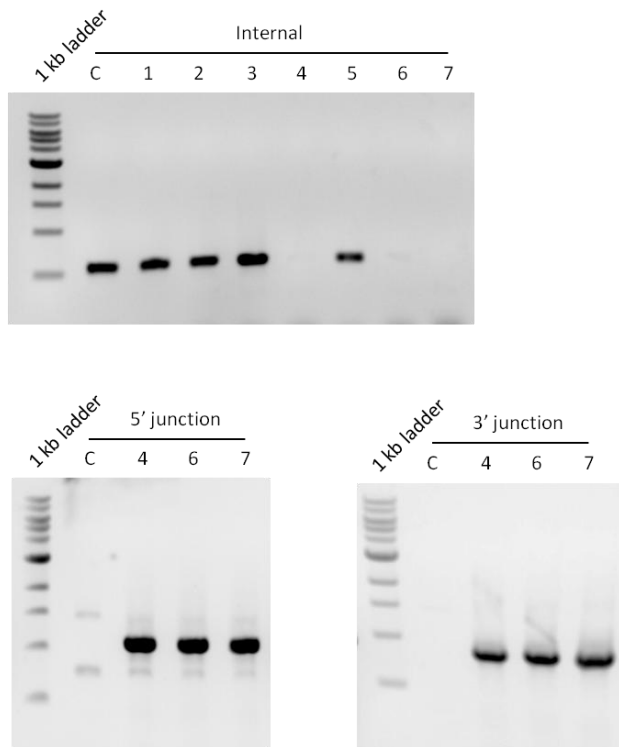


Figure 26: Verification of *C. glabrata* Δ CAGL0F03905g. Three independent isolates (1, 2 and 3) were stored as glycerol stocks.

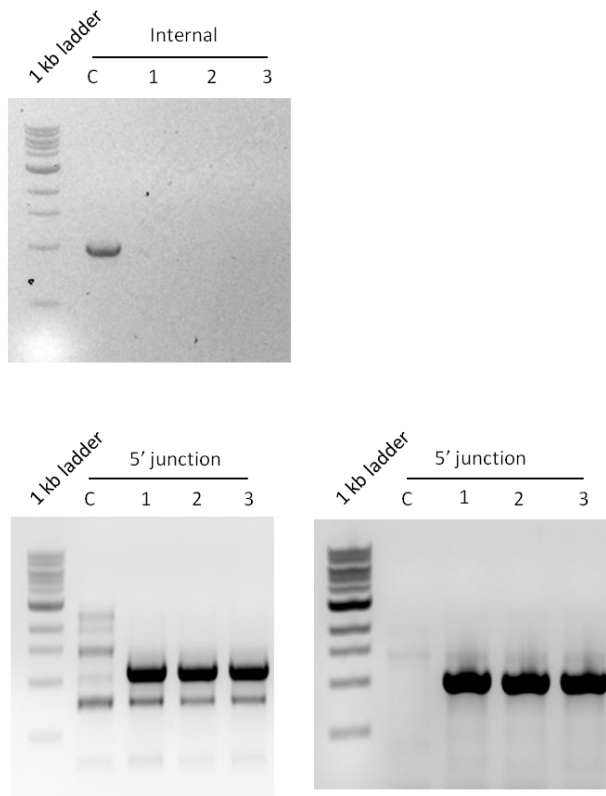


Figure 27: Verification of *C. glabrata* Δ CAGL0F04081g. One independent isolate (4) was stored as glycerol stocks.

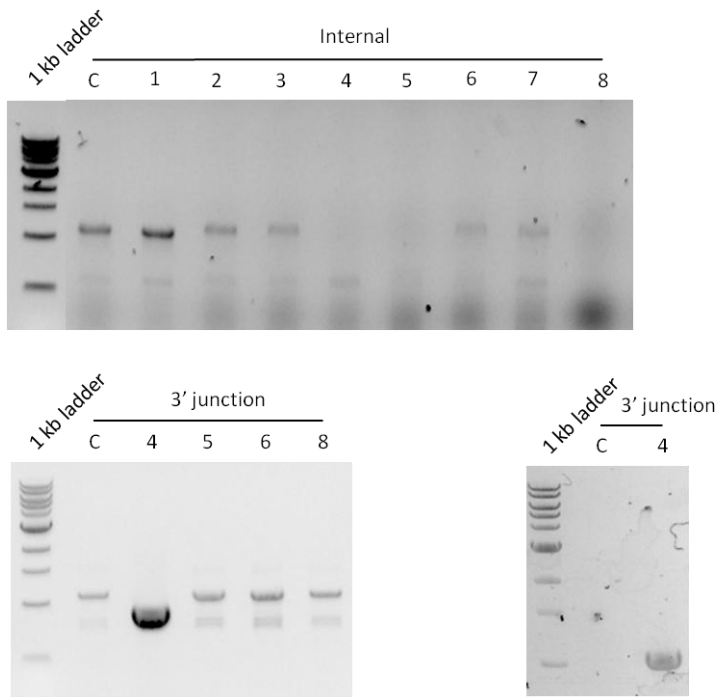


Figure 28: Verification of *C. glabrata* Δ CAGL0F05159g. Three independent isolates (5, 6 and 8) were stored as glycerol stocks.

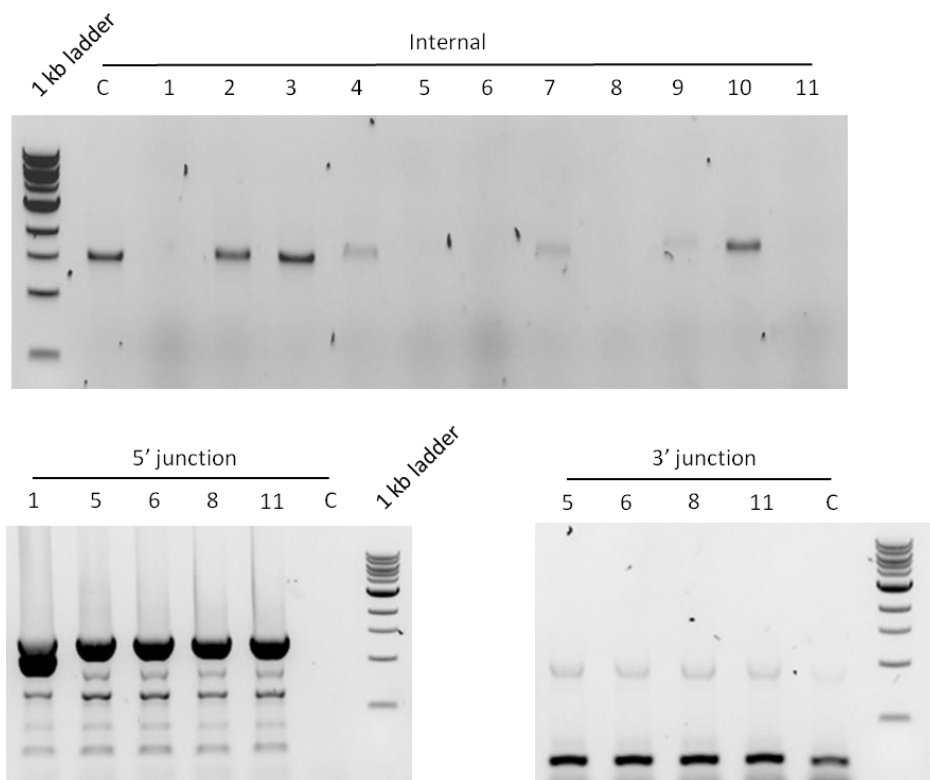


Figure 29: Verification of *C. glabrata* Δ CAGL0F05973g. One independent isolate (7) was stored as glycerol stocks.

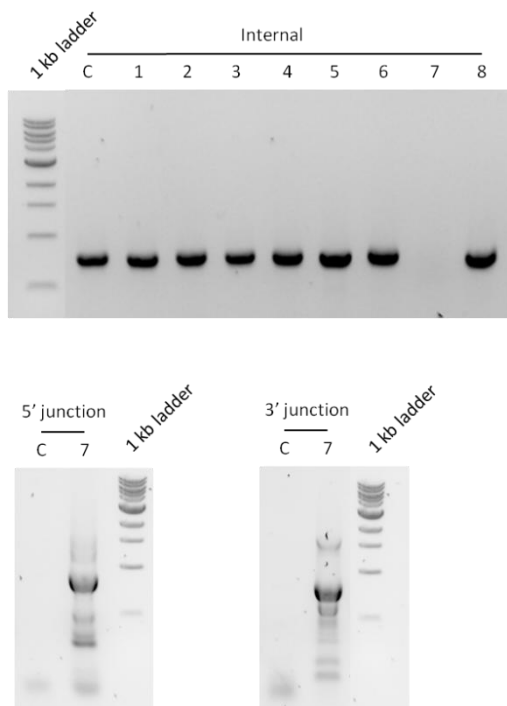


Figure 30: Verification of *C. glabrata* Δ CAGL0F06237g. Two independent isolates (13 and 15) were stored as glycerol stocks.

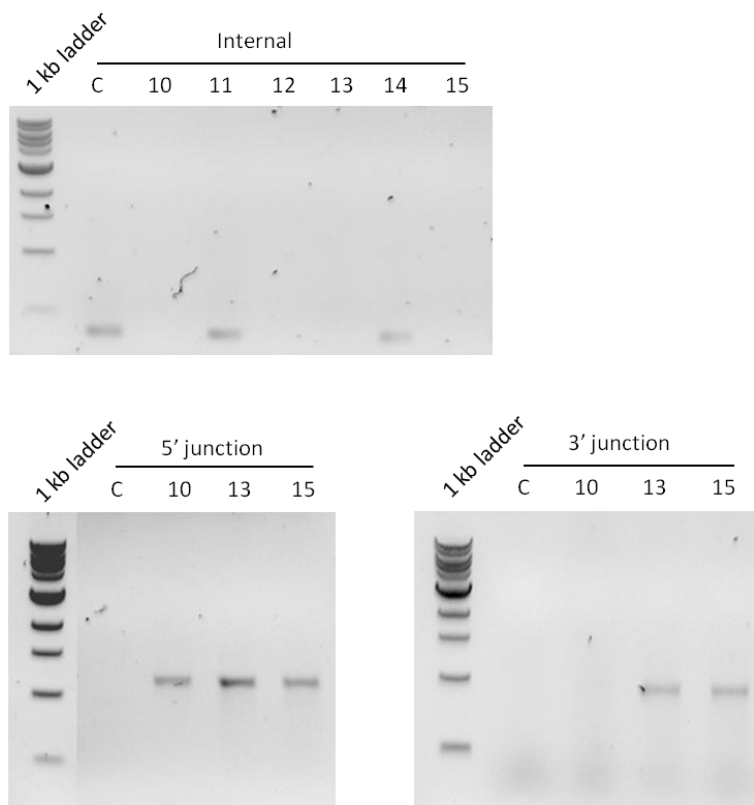


Figure 31: Verification of *C. glabrata* Δ CAGL0F08767g. Three independent isolates (1, 2 and 3) were stored as glycerol stocks.

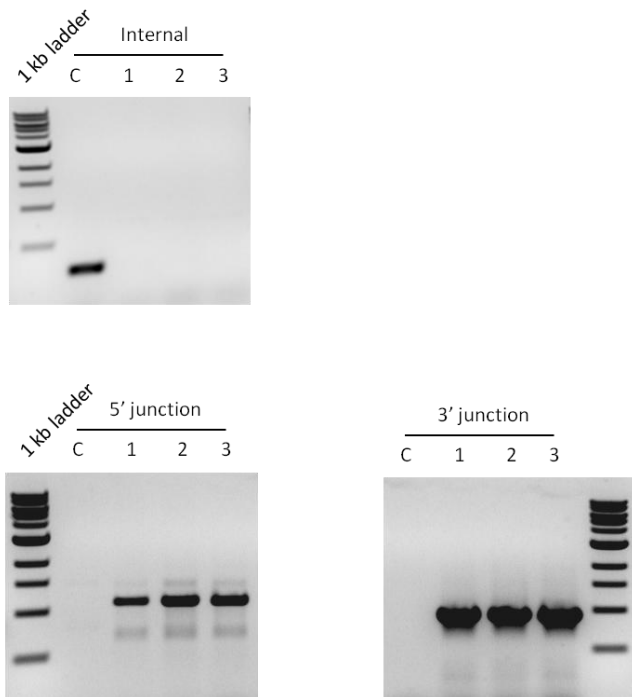


Figure 32: Verification of *C. glabrata* Δ CAGL0F09229g. Two independent isolates (2 and 3) were stored as glycerol stocks.

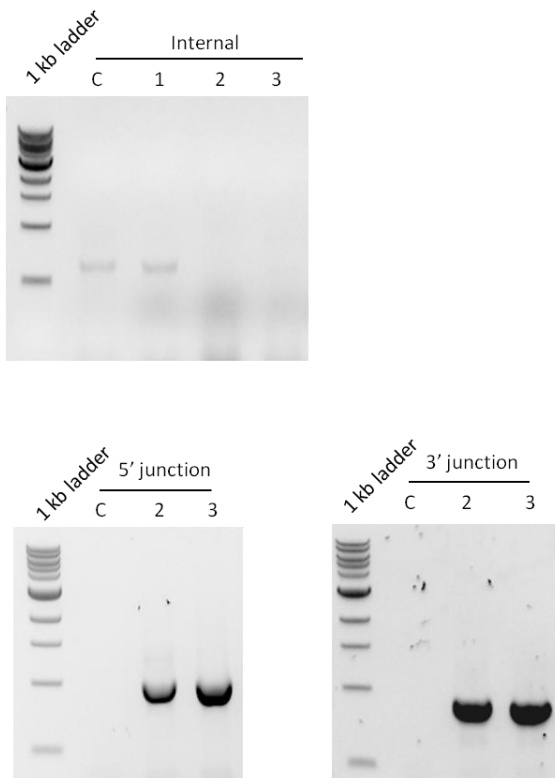


Figure 33: Verification of *C. glabrata* Δ CAGLOG02607g. One independent isolate (2) was stored as glycerol stocks.

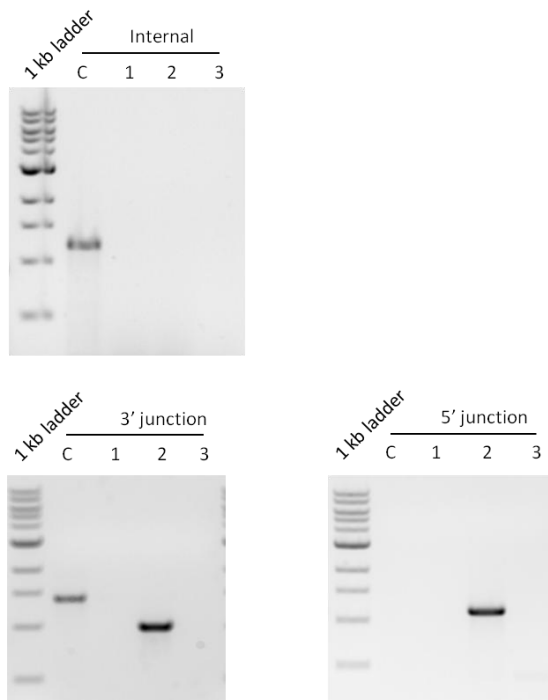


Figure 34: Verification of *C. glabrata* Δ CAGLOG03201g. Three independent isolates (2, 3 and 6) were stored as glycerol stocks.

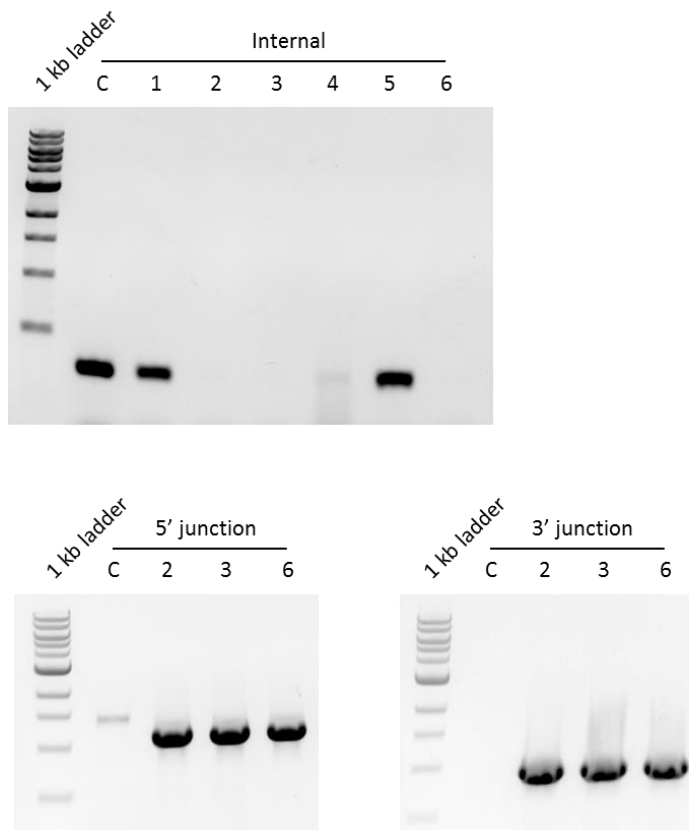


Figure 35: Verification of *C. glabrata* Δ CAGL0G04279g. Two independent isolates (1 and 2) were stored as glycerol stocks.

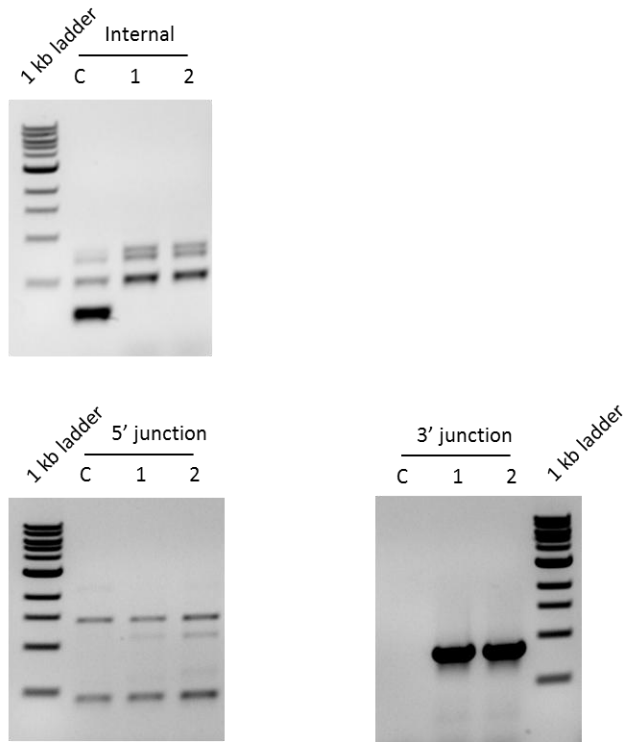


Figure 36: Verification of *C. glabrata* Δ CAGL0G05522g. Two independent isolates (1 and 2) were stored as glycerol stocks.

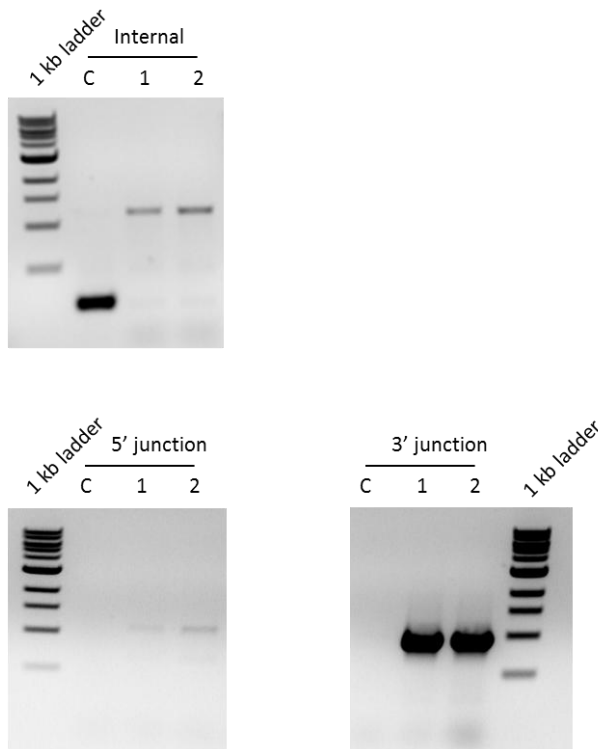


Figure 37: Verification of *C. glabrata* Δ CAGL0G08866g. Two independent isolates (4 and 8) were stored as glycerol stocks.

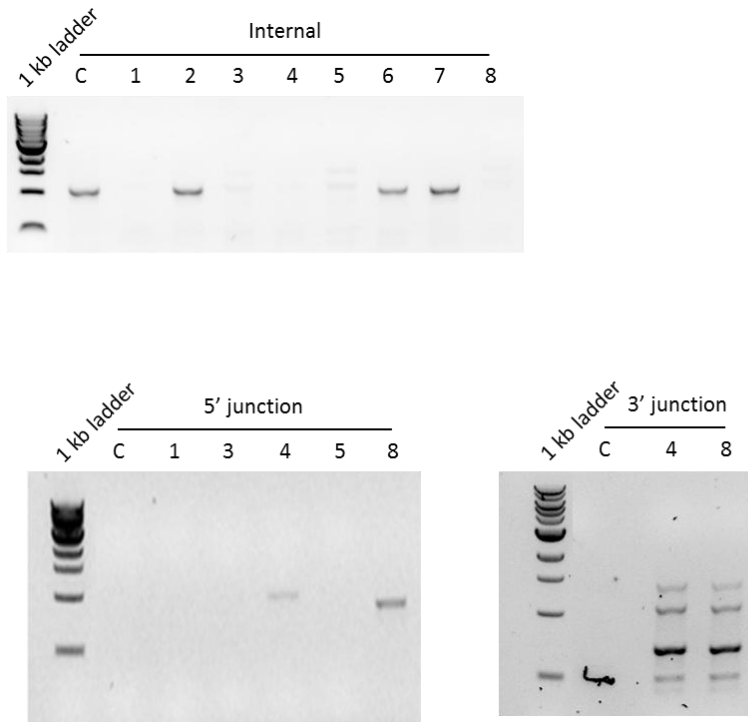


Figure 38: Verification of *C. glabrata* Δ CAGL0G10175g. Three independent isolates (1, 2 and 3) were stored as glycerol stocks.

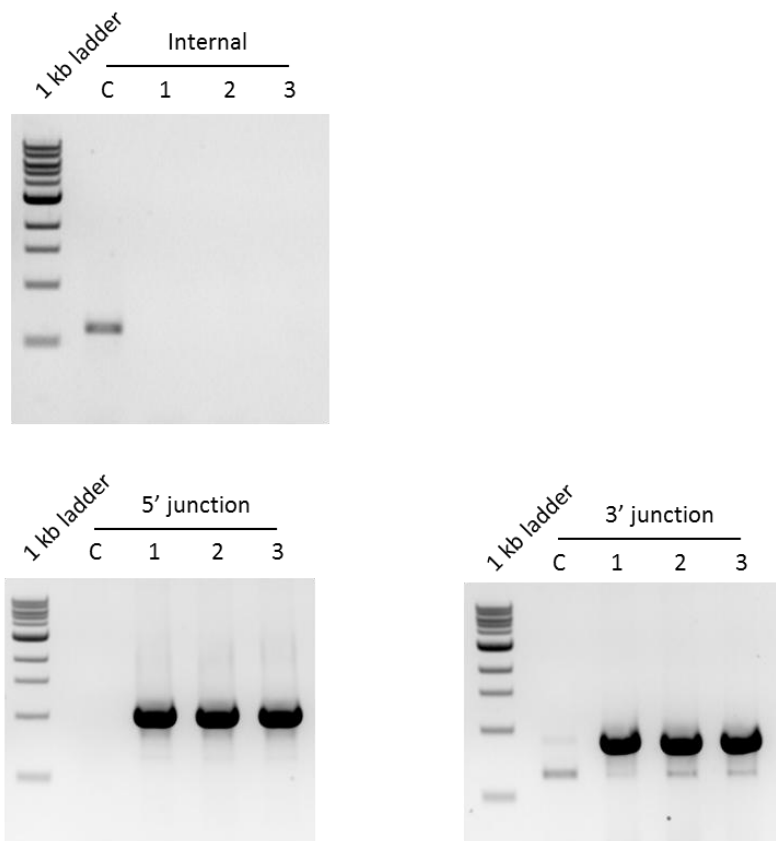


Figure 39: Verification of *C. glabrata* Δ CAGL0H01749g. Three independent isolates (2, 3 and 6) were stored as glycerol stocks.

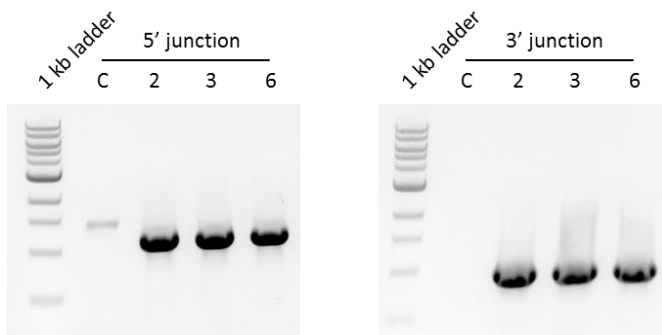
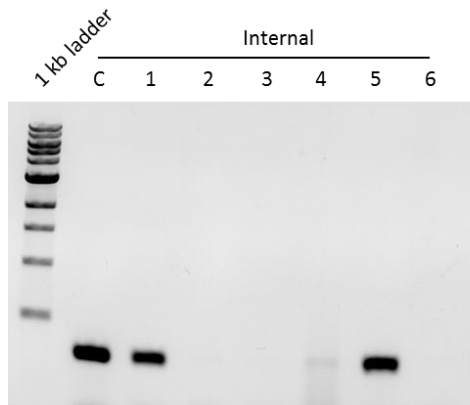


Figure 40: Verification of *C. glabrata* Δ CAGL0H06765g. Three independent isolates (1, 4 and 9) were stored as glycerol stocks.

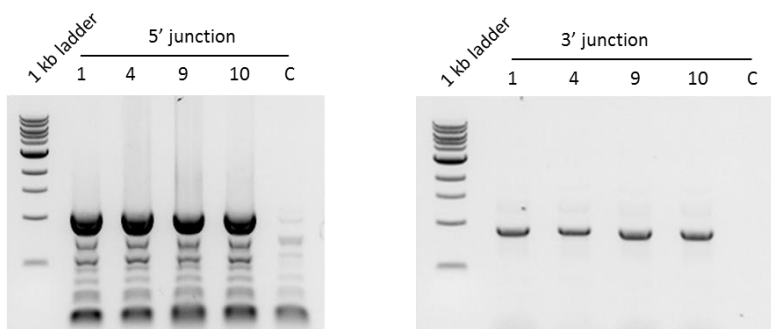
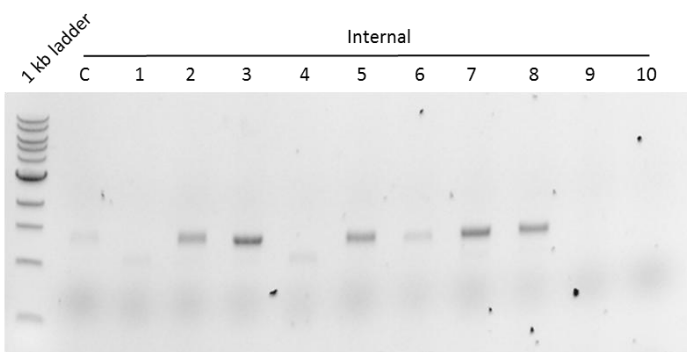


Figure 41: Verification of *C. glabrata* Δ CAGL0H08712g. Three independent isolates (3, 5 and 14) were stored as glycerol stocks.

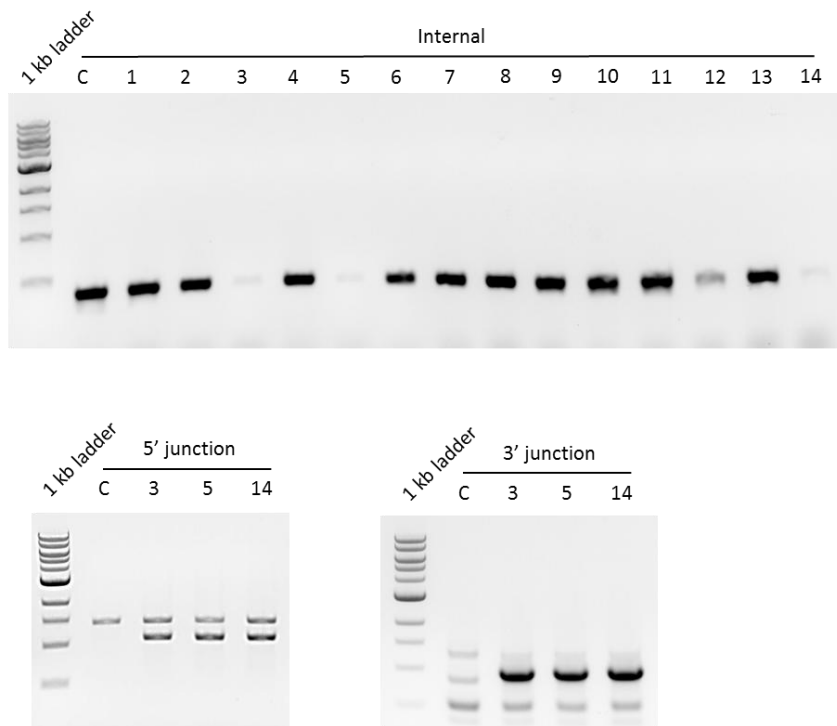


Figure 42: Verification of *C. glabrata* Δ CAGL0H09988g. Two independent isolates (1 and 6) were stored as glycerol stocks.

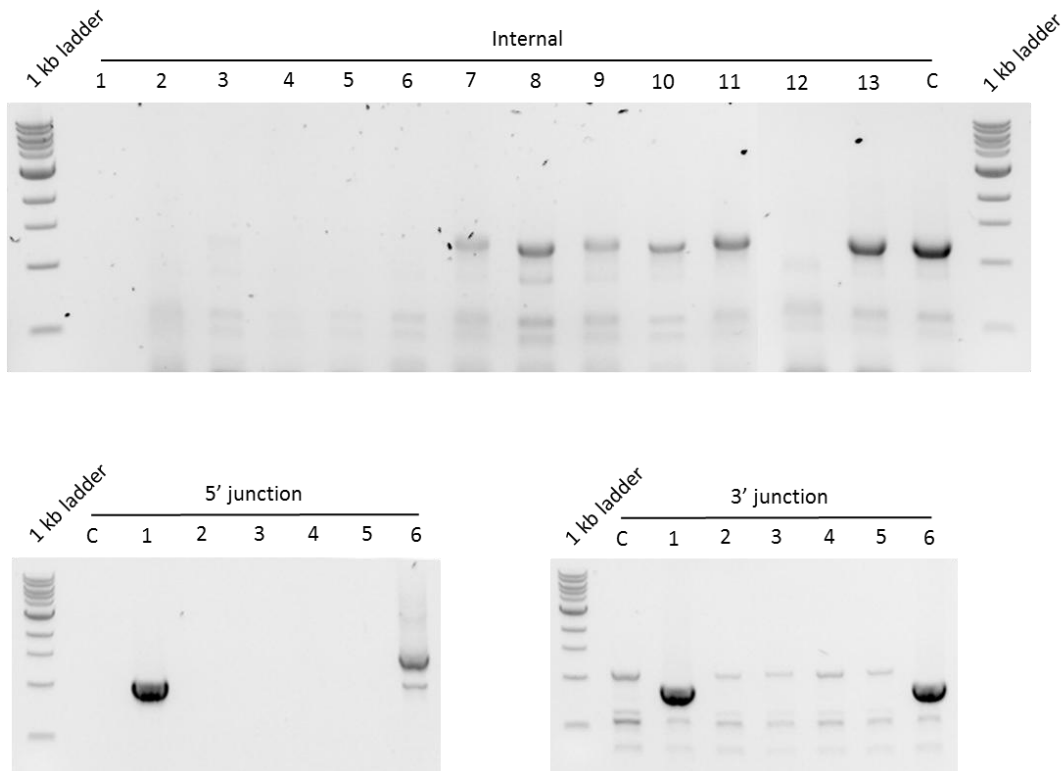


Figure 43: Verification of *C. glabrata* Δ CAGL0H10208g. Three independent isolates (1, 2 and 3) were stored as glycerol stocks.

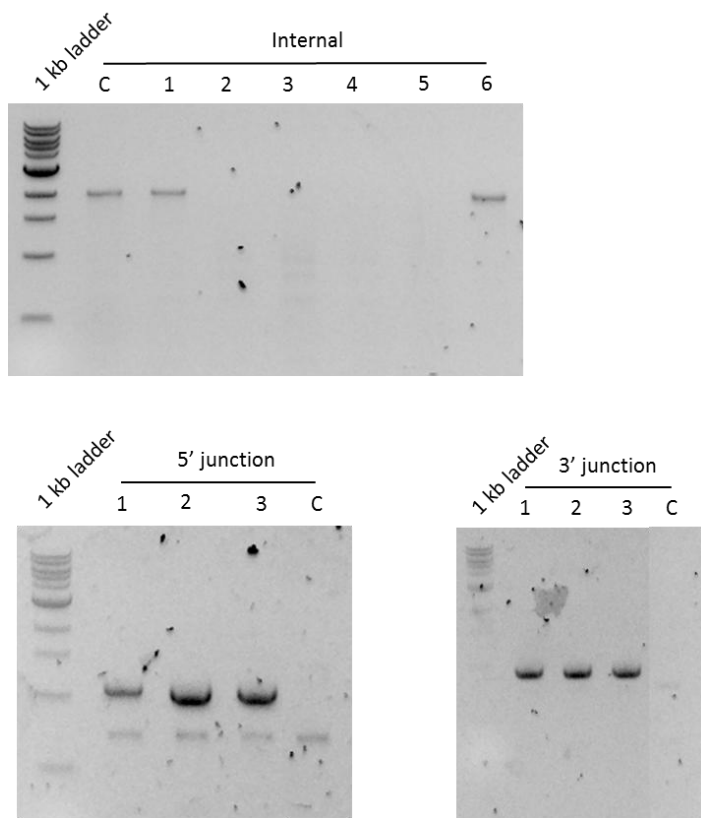


Figure 44: Verification of *C. glabrata* Δ CAGL0I02244g. Three independent isolates (2, 3 and 4) were stored as glycerol stocks.

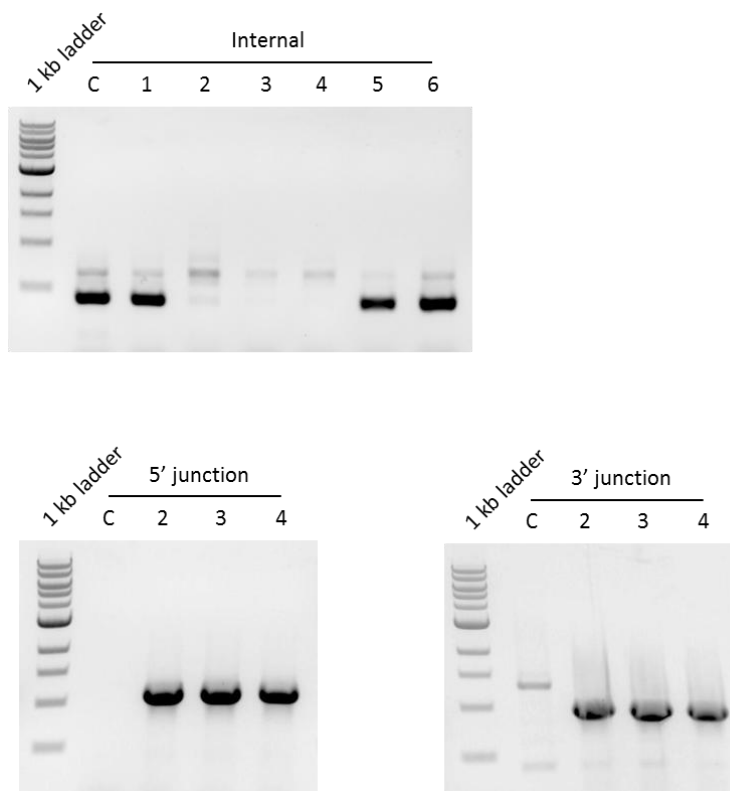


Figure 45: Verification of *C. glabrata* Δ CAGL0108437g. One independent isolate (5) was stored as glycerol stocks.

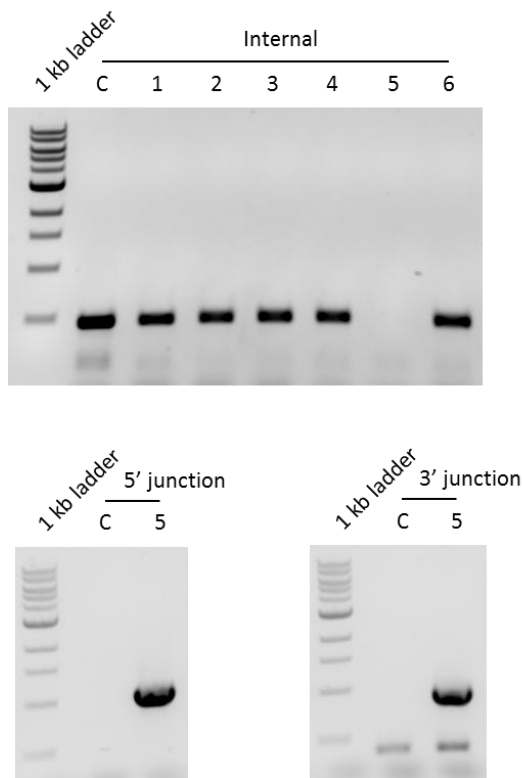


Figure 46: Verification of *C. glabrata* Δ CAGL0108613g. Three independent isolates (1, 2 and 4) were stored as glycerol stocks.

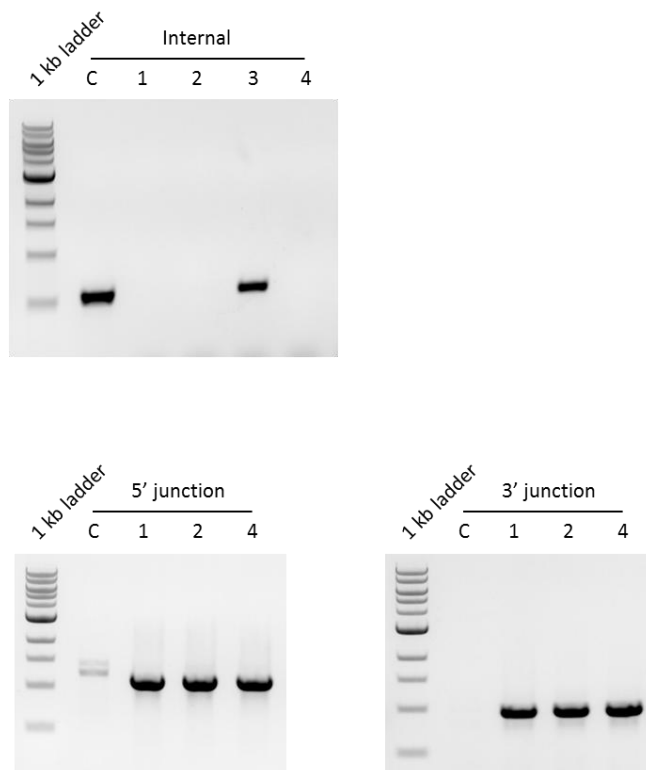


Figure 47: Verification of *C. glabrata* Δ CAGL0J05786g. Three independent isolates (1, 3 and 7) were stored as glycerol stocks.

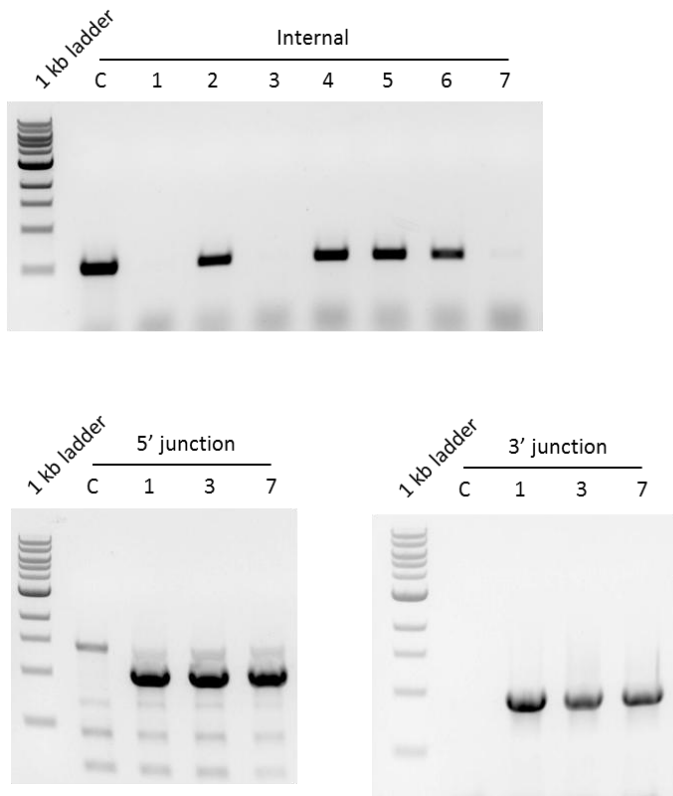


Figure 48: Verification of *C. glabrata* Δ CAGL0J05852g. Three independent isolates (1, 3 and 4) were stored as glycerol stocks.

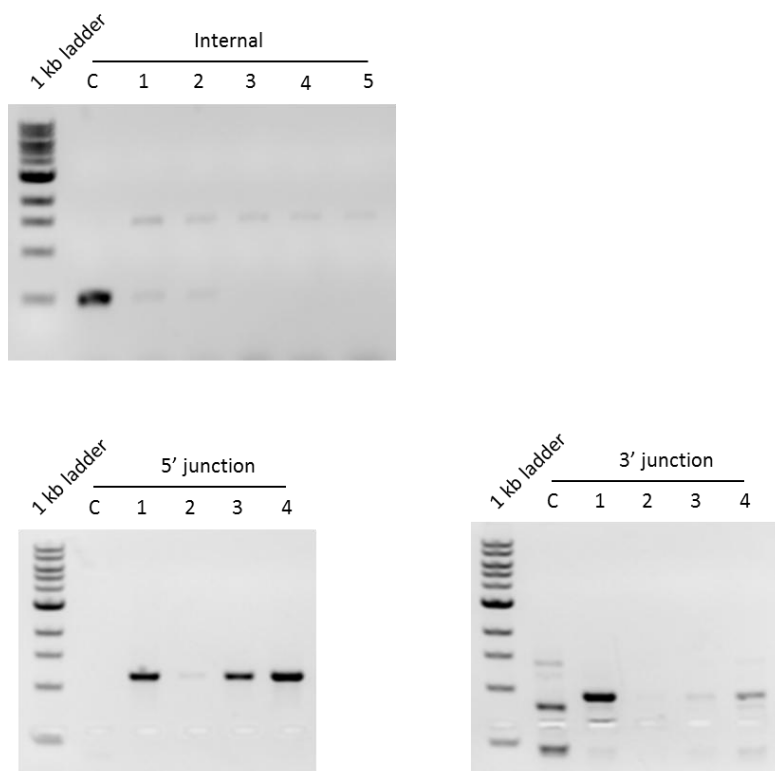


Figure 49: Verification of *C. glabrata* Δ CAGL0K02145g. Two independent isolates (1 and 13) were stored as glycerol stocks.

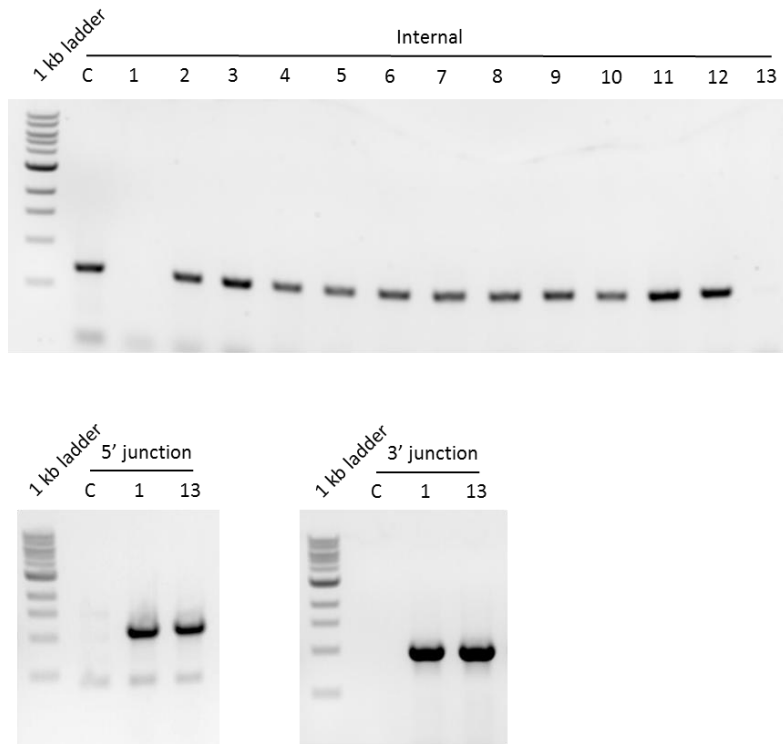


Figure 50: Verification of *C. glabrata* Δ CAGL0K05687g. Two independent isolates (2 and 9) were stored as glycerol stocks.

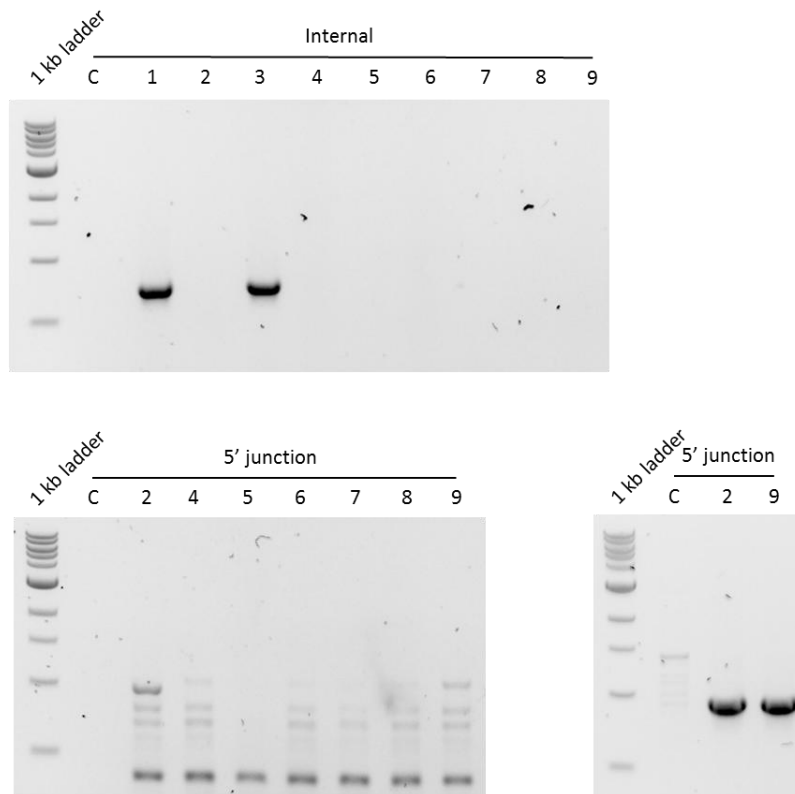


Figure 51: Verification of *C. glabrata* Δ CAGL0K07634g. One independent isolate (2) were stored as glycerol stocks.

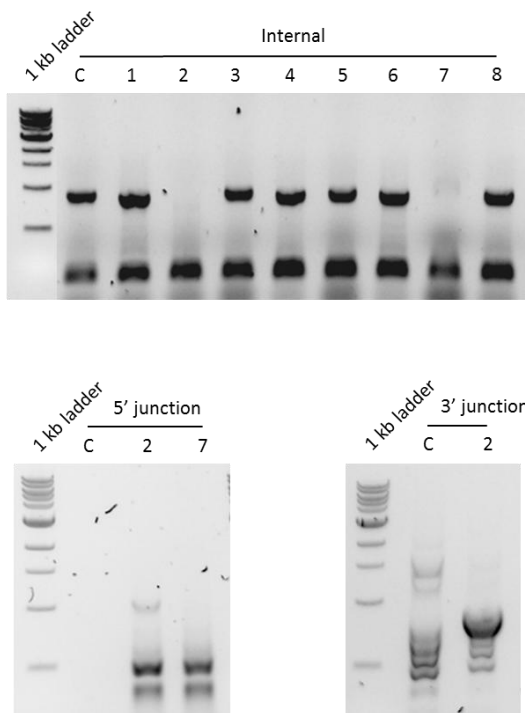


Figure 52: Verification of *C. glabrata* Δ CAGL0K10318g. Two independent isolates (3 and 11) were stored as glycerol stocks.

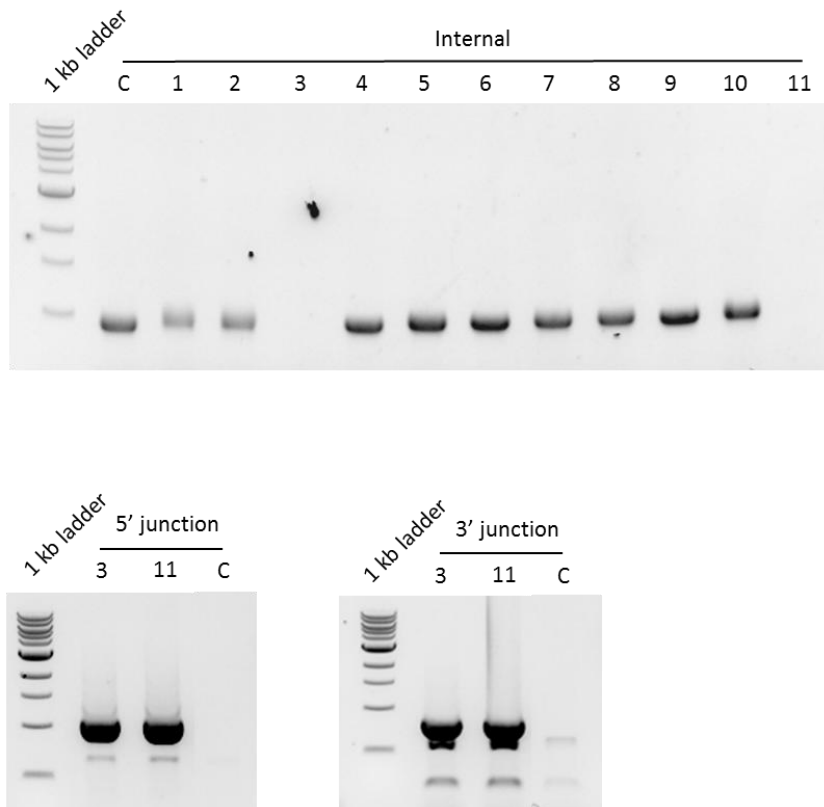


Figure 53: Verification of *C. glabrata* Δ CAGL0K11066g. Two independent isolates (5 and 9) were stored as glycerol stocks.

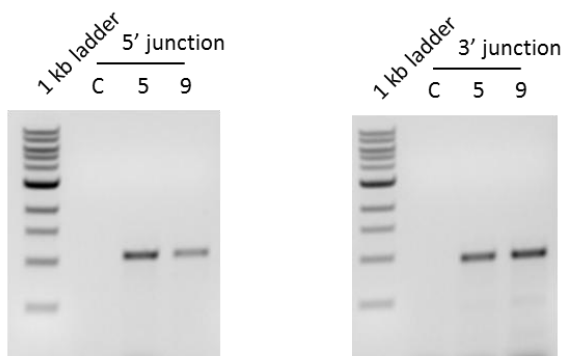
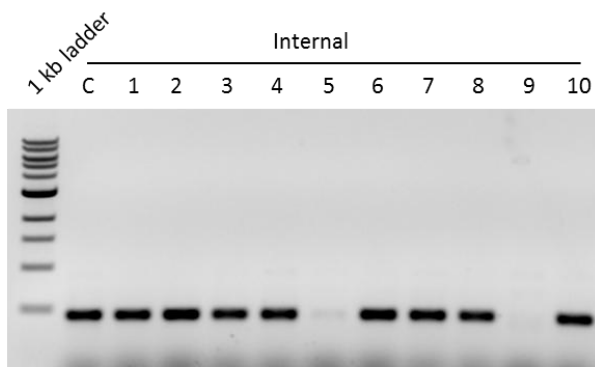


Figure 54: Verification of *C. glabrata* Δ CAGL0L03674g. Two independent isolates (2 and 4) were stored as glycerol stocks.

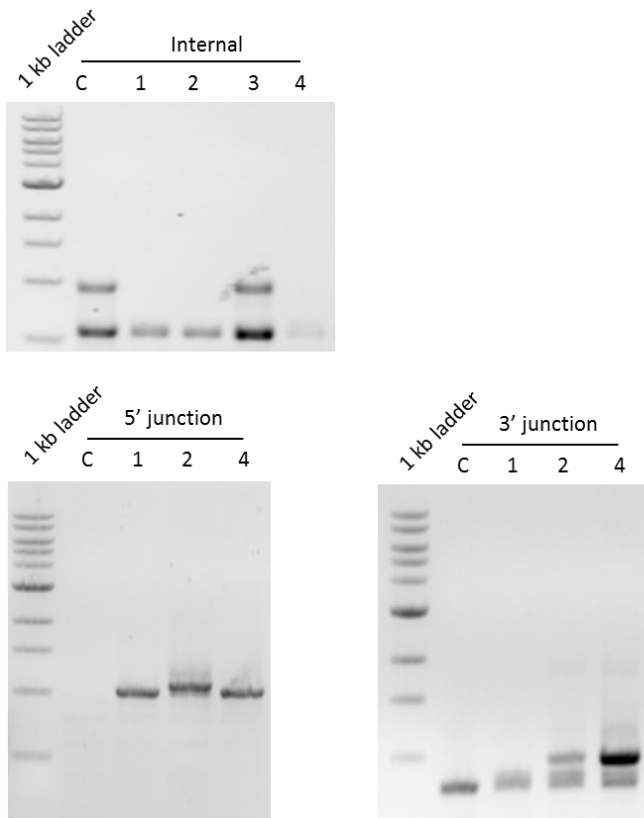


Figure 55: Verification of *C. glabrata* Δ CAGL0L06776g. Three independent isolates (2, 5 and 7) were stored as glycerol stocks.

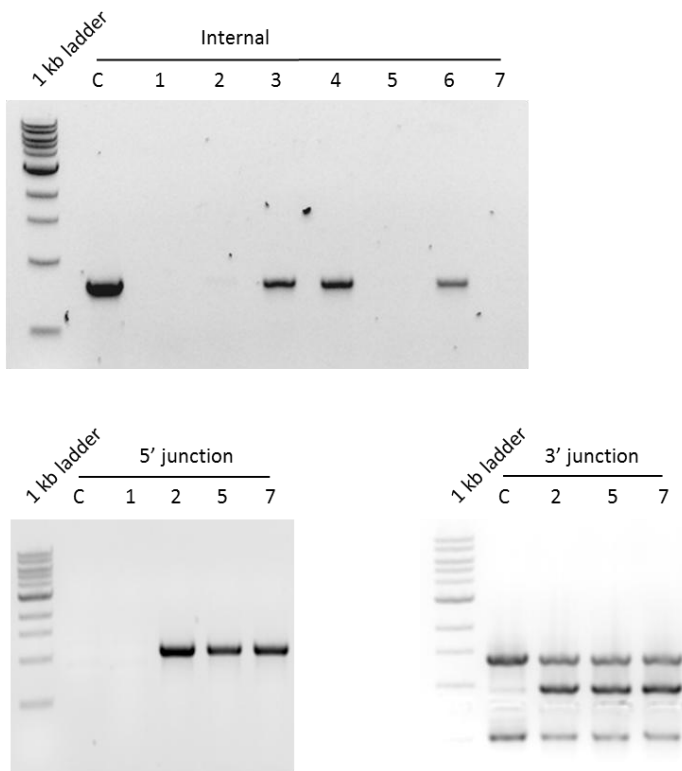


Figure 56: Verification of *C. glabrata* Δ CAGL0L07480g. Three independent isolates (2, 4 and 6) were stored as glycerol stocks.

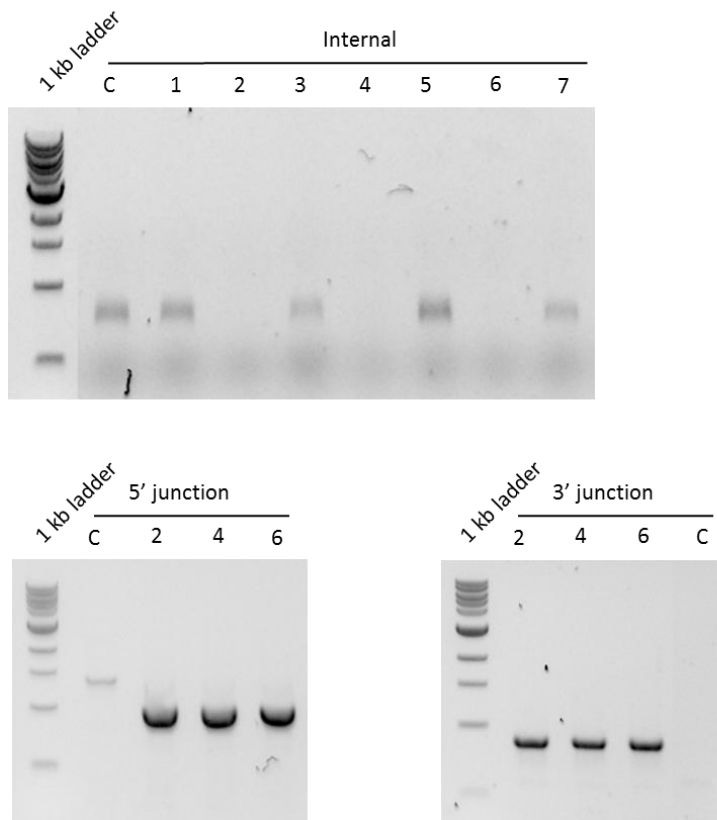


Figure 57: Verification of *C. glabrata* Δ CAGL0L09383g. Two independent isolates (1 and 3) were stored as glycerol stocks.

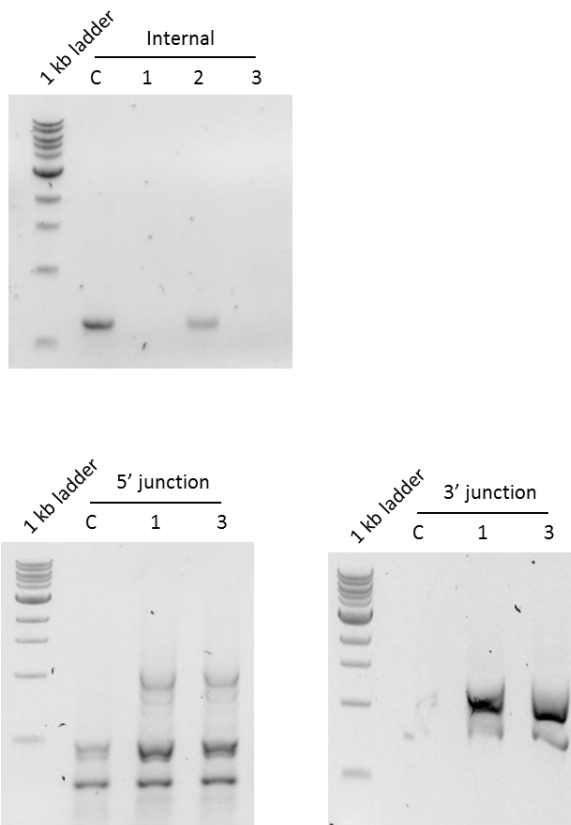


Figure 58: Verification of *C. glabrata* Δ CAGL0M01716g. Three independent isolates (3, 4 and 6) were stored as glycerol stocks.

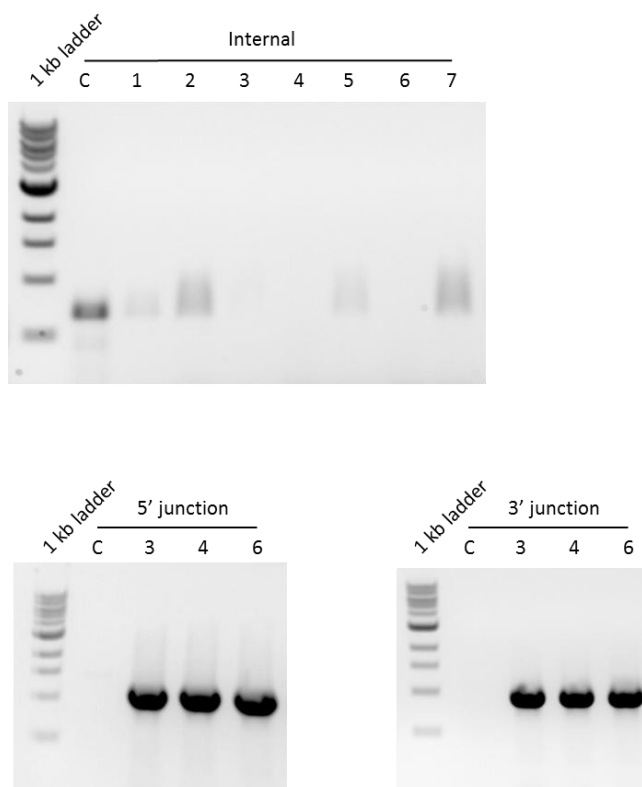


Figure 59: Verification of *C. glabrata* Δ CAGL0M01870g. One independent isolate (1) was stored as glycerol stocks.

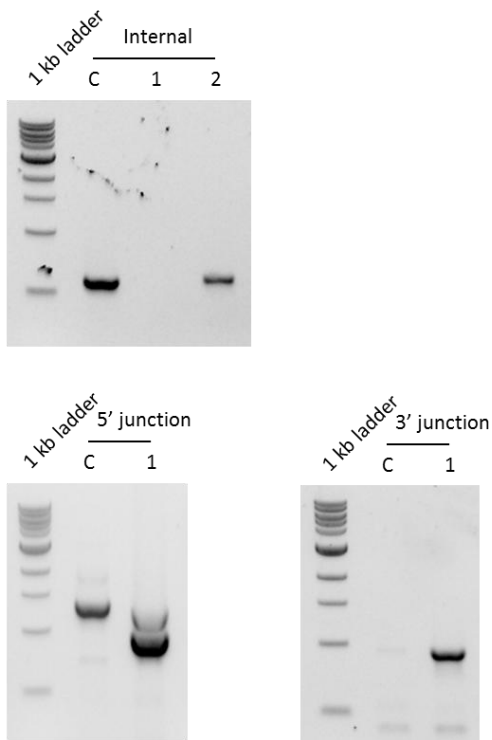


Figure 60: Verification of *C. glabrata* Δ CAGL0M01914g. One independent isolate (10) was stored as glycerol stocks.

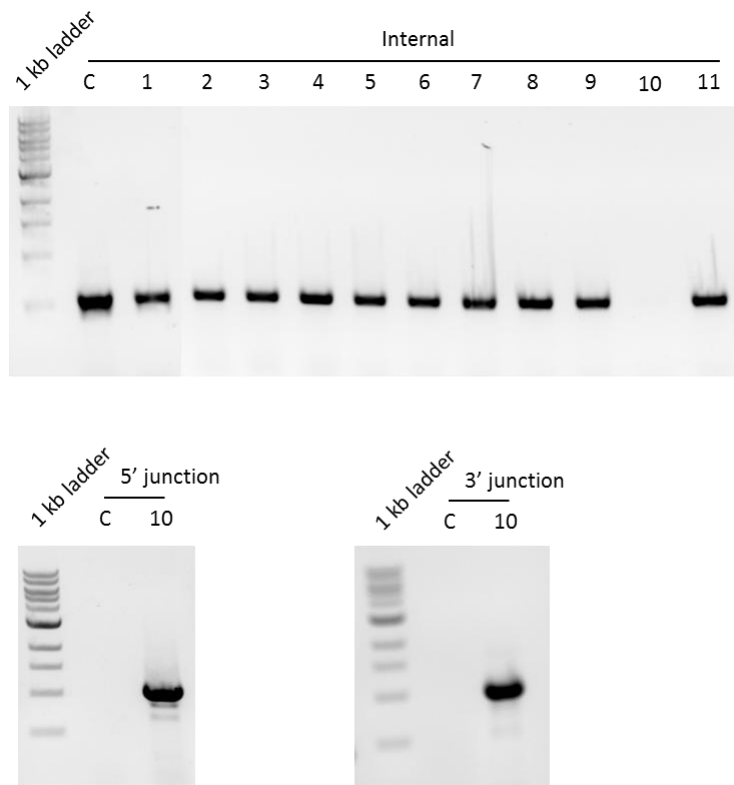


Figure 61: Verification of *C. glabrata* Δ CAGL0M02299g. One independent isolate (8) was stored as glycerol stocks.

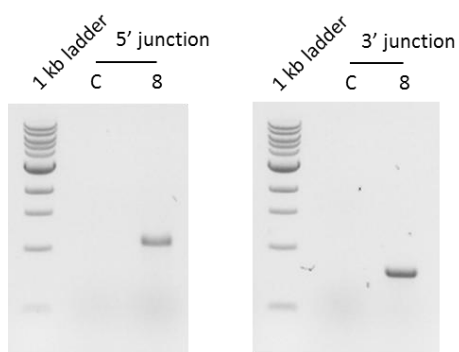
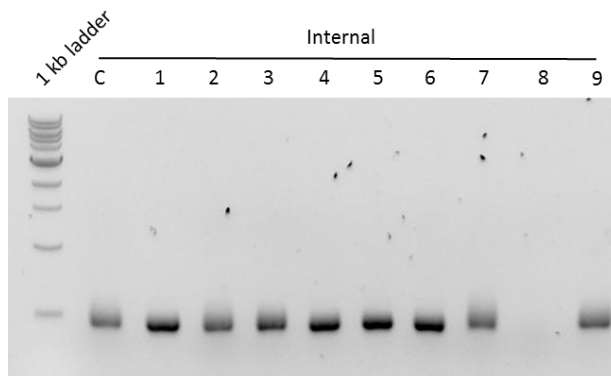


Figure 62: Verification of *C. glabrata* Δ CAGL0M02321g. Three independent isolates (2, 3 and 6) were stored as glycerol stocks.

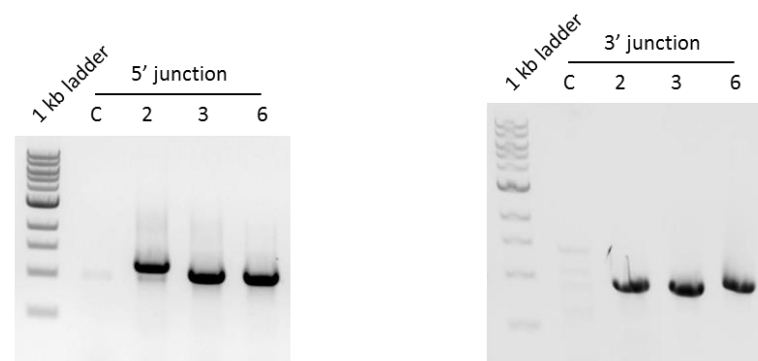
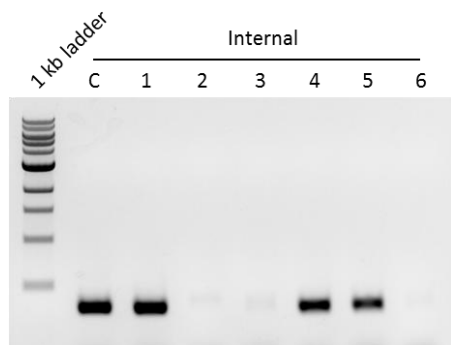


Figure 63: Verification of *C. glabrata* Δ CAGL0M05137g. Two independent isolates (2 and 5) were stored as glycerol stocks.

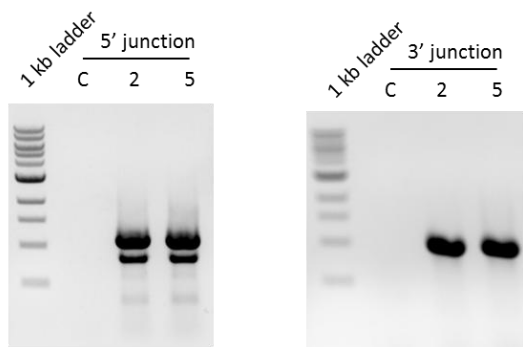
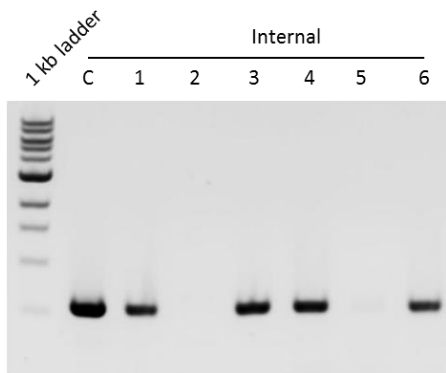


Figure 64: Verification of *C. glabrata* Δ CAGL0M10153g. One independent isolate (9) was stored as glycerol stocks.

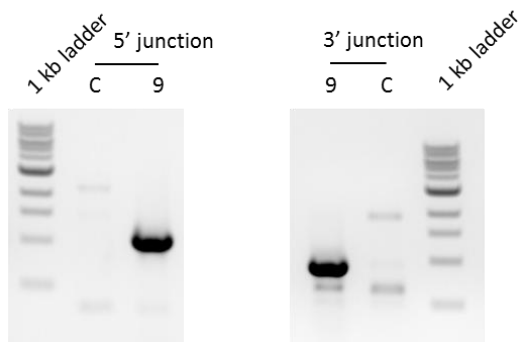
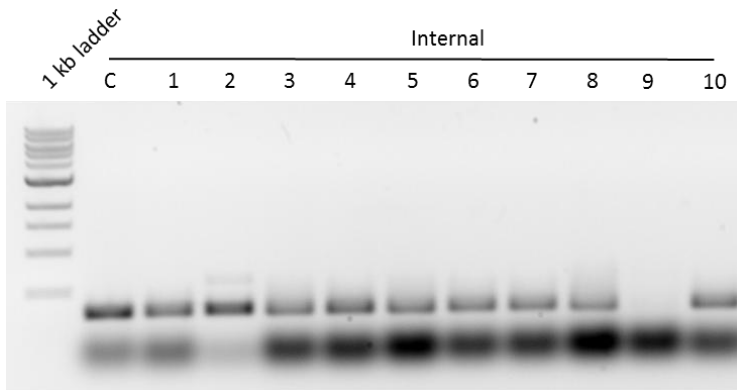


Figure 65: Verification of *C. glabrata* Δ CAGL0M10153g. One independent isolate (9) was stored as glycerol stocks.

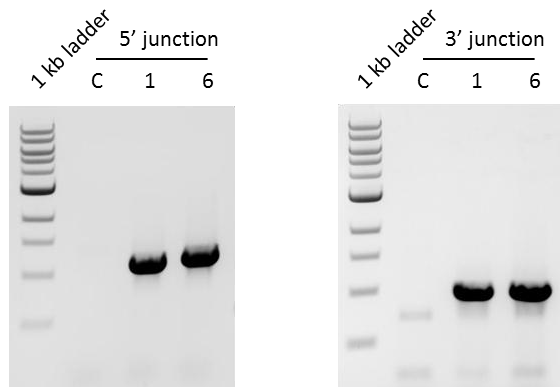
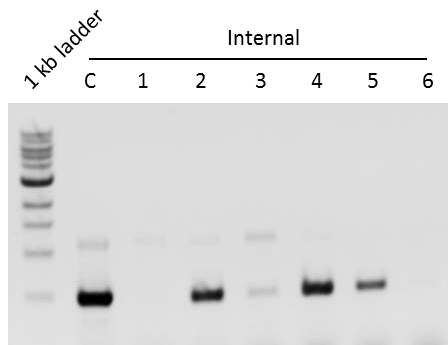
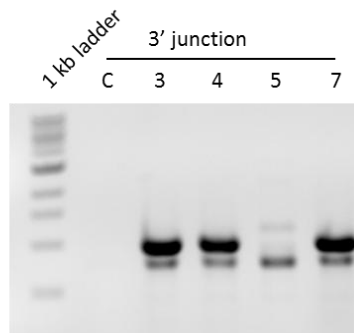
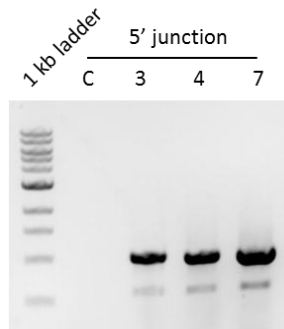
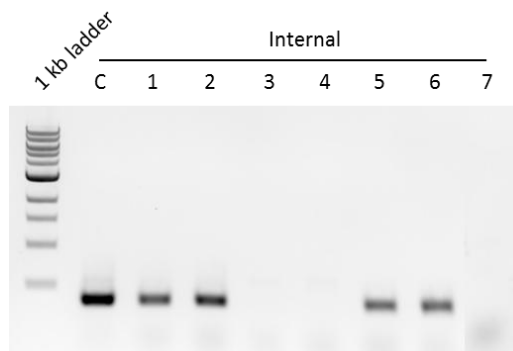
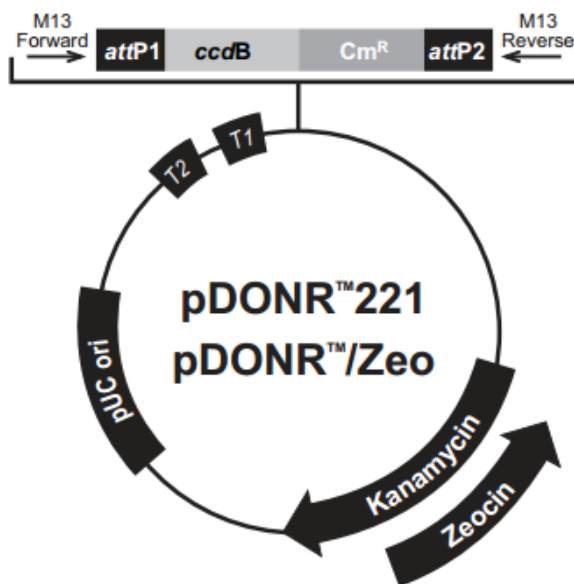


Figure 66: Verification of *C. glabrata* Δ CAGL0M04543g. Three independent isolates (3, 4 and 7) was stored as glycerol stocks.



Appendix 15: Plasmid maps of Gateway® vectors.

Figure 1: Plasmid map and features of ENTRY vector pENTR™221 (Life Technologies™).

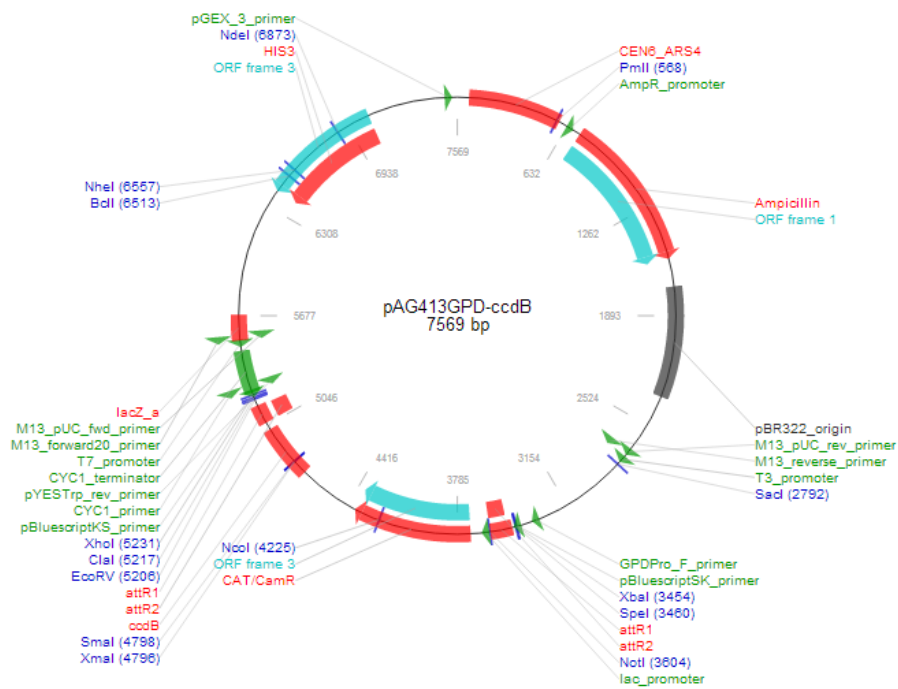


Comments for:

	pDONR™221 4761 nucleotides	pDONR™/Zeo 4291 nucleotides
<i>rrmB</i> T2 transcription termination sequence (c):	268-295	268-295
<i>rrmB</i> T1 transcription termination sequence (c):	427-470	427-470
M13 Forward (-20) priming site:	537-552	537-552
<i>attP1</i> :	570-801	570-801
<i>ccdB</i> gene (c):	1197-1502	1197-1502
Chloramphenicol resistance gene (c):	1825-2505	1847-2506
<i>attP2</i> (c):	2753-2984	2754-2985
M13 Reverse priming site:	3026-3042	3027-3043
Kanamycin resistance gene:	3155-3964	---
EM7 promoter (c):	---	3486-3552
Zeocin resistance gene (c):	---	3111-3485
pUC origin:	4085-4758	3615-4288

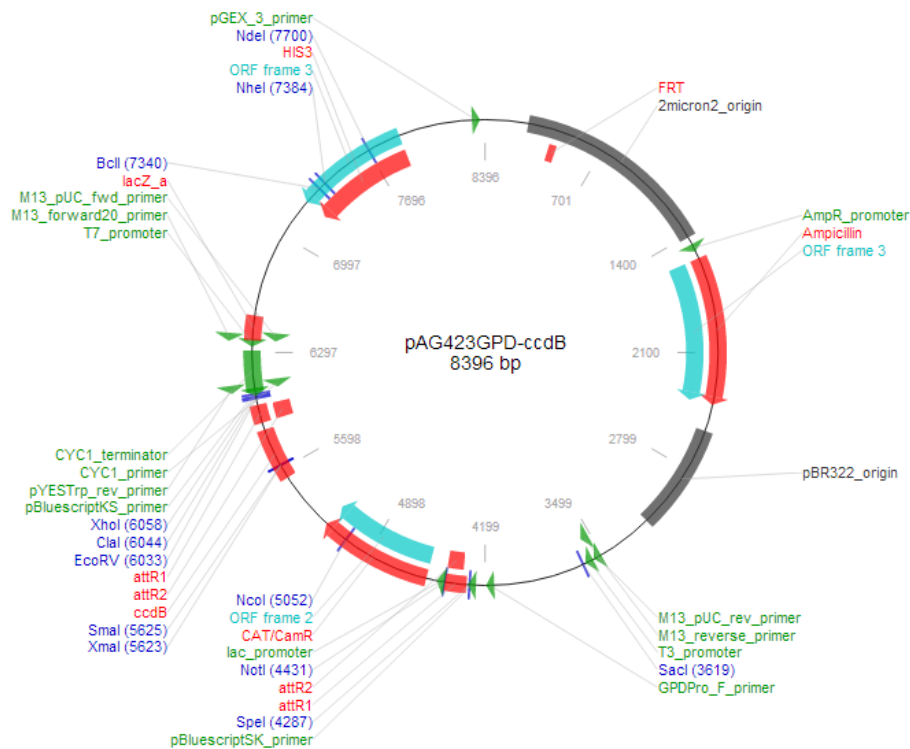
(c) = complementary strand

Figure 2: Plasmid map and features of destination vector pAG413GPD-ccdB (Addgene).



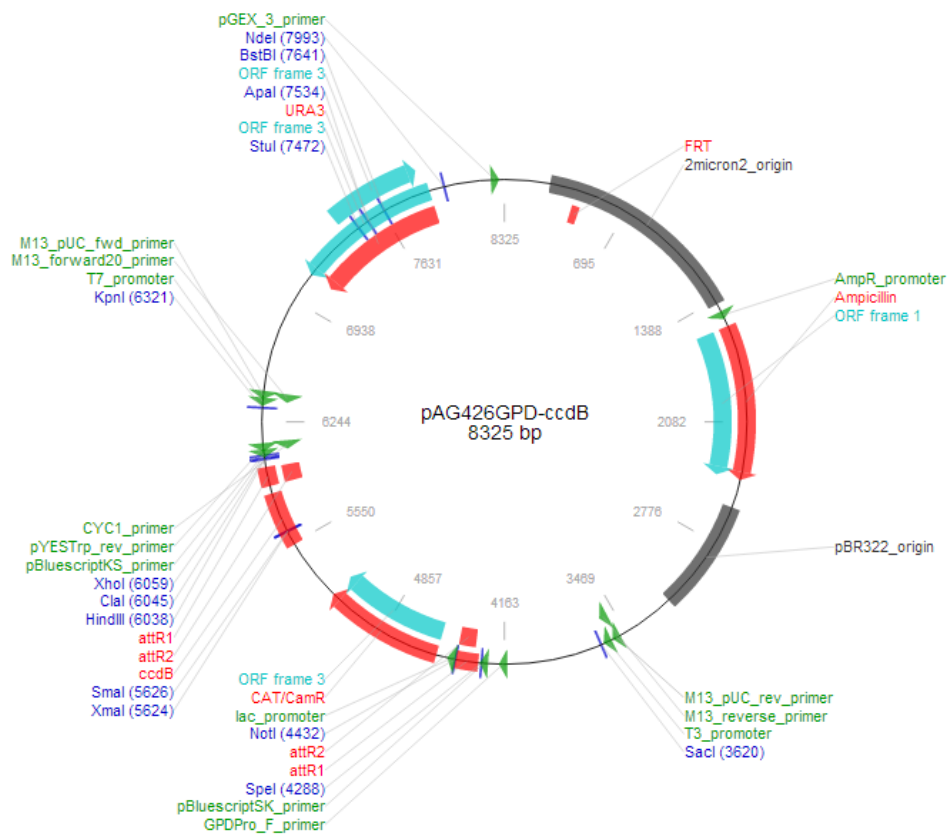
Feature Name	Start	End	ORF	Start	End
CEN6_ARS4	583	65	ORF frame 1	715	1575
AmpR_promoter	645	673	ORF frame 3	3711	4370
Ampicillin	715	1575	ORF frame 3	7066	6407
pBR322_origin	1730	2349			
M13_pUC_rev_primer	2701	2723	Enzyme Name	Cut	
M13_reverse_primer	2722	2740	PmlI	568	
T3_promoter	2757	2776	SacI	2792	
GPDPro_F_primer	3342	3365	XbaI	3454	
pBluescriptSK_primer	3454	3470	SpeI	3460	
attR1	3478	3602	NotI	3604	
attR2	3602	3502	NcoI	4225	
lac_promoter	3627	3650	SmaI	4798	
CAT/CamR	3711	4370	XmaI	4796	
ccdB	4715	5020	EcoRV	5206	
attR1	5168	5061	Clal	5217	
attR2	5061	5161	XhoI	5231	
pBluescriptKS_primer	5235	5219	BclI	6513	
CYC1_terminator	5244	5483	NheI	6557	
pYESTrp_rev_primer	5271	5253	NdeI	6873	
CYC1_primer	5271	5253			
T7_promoter	5521	5503			
M13_forward20_primer	5547	5531			
lacZ_a	5540	5683			
M13_pUC_fwd_primer	5562	5540			
HIS3	7066	6410			
pGEX_3_primer	7519	7541			

Figure 3: Plasmid map and features of destination vector pAG423GPD-ccdB (Addgene).



Feature Name	Start	End	ORF	Start	End
2micron2_origin	250	1410	ORF frame 3	1542	2402
FRT	400	447	ORF frame 2	4538	5197
AmpR_promoter	1472	1500	ORF frame 3	7893	7234
Ampicillin	1542	2402			
pBR322_origin	2557	3176	Enzyme Name	Cut	
M13_pUC_rev_primer	3528	3550	SacI	3619	
M13_reverse_primer	3549	3567	SpeI	4287	
T3_promoter	3584	3603	NotI	4431	
GPDPro_F_primer	4169	4192	NcoI	5052	
pBluescriptSK_primer	4281	4297	SmaI	5625	
attR1	4305	4429	XmaI	5623	
attR2	4429	4329	EcoRV	6033	
lac_promoter	4454	4477	ClaI	6044	
CAT/CamR	4538	5197	XhoI	6058	
ccdB	5542	5847	BclI	7340	
attR1	5995	5888	NheI	7384	
attR2	5888	5988	NdeI	7700	
pBluescriptKS_primer	6062	6046			
CYC1_terminator	6071	6310			
CYC1_primer	6098	6080			
pYESTrp_rev_primer	6098	6080			
T7_promoter	6348	6330			
M13_forward20_primer	6374	6358			
lacZ_a	6367	6510			
M13_pUC_fwd_primer	6389	6367			
HIS3	7893	7237			
pGEX_3_primer	8346	8368			

Figure 5: Plasmid map and features of destination vector pAG426GPD-ccdB (Addgene).



Feature Name	Start	End	ORF	Start	End
2micron2_origin	251	1411	ORF frame 1	1543	2403
FRT	401	448	ORF frame 3	4539	5198
AmpR_promoter	1473	1501	ORF frame 3	7909	7106
Ampicillin	1543	2403	ORF frame 3	7398	7874
pBR322_origin	2558	3177			
M13_pUC_rev_primer	3529	3551	Enzyme Name	Cut	
M13_reverse_primer	3550	3568	SacI	3620	
T3_promoter	3585	3604	SpeI	4288	
GPDPro_F_primer	4170	4193	NotI	4432	
pBluescriptSK_primer	4282	4298	Smal	5626	
attR1	4306	4430	XmaI	5624	
attR2	4430	4330	HindIII	6038	
lac_promoter	4455	4478	Clal	6045	
CAT/CamR	4539	5198	XhoI	6059	
ccdB	5543	5848	KpnI	6321	
attR1	5996	5889	Stul	7472	
attR2	5889	5989	Apal	7534	
pBluescriptKS_primer	6063	6047	BstBI	7641	
pYESTrp_rev_primer	6099	6081	NdeI	7993	
CYC1_primer	6099	6081			
T7_promoter	6349	6331			
M13_forward20_primer	6375	6359			
M13_pUC_fwd_primer	6390	6368			
URA3	7909	7109			
pGEX_3_primer	8275	8297			

References

Ahmad, K. M., Ishchuk, O. P., Hellborg, L., Jørgensen, G., Skvarc, M., Stenderup, J., Jørck-Ramberg, D., Polakova, S. & Piškur, J. (2013) Small chromosomes among Danish *Candida glabrata* isolates originated through different mechanisms. *Antonie van Leeuwenhoek*, DOI 10.1007/s10482-013-9931-3.

Albarouki, E. & Deising, H. B. (2013) Infection Structure-Specific Reductive Iron Assimilation is Required for Cell Wall Integrity and Full Virulence of the Maize Pathogen *Colletotrichum graminicola*. *Molecular Plant Microbe Interactions*, **26**: 695-708.

Alexander, B. D., Johnson, M. D., Pfeiffer, C. D., Jiménez-Ortigosa, C., Catania, J., Booker, R., Castanheira, M., Messer, S. A., Perlin, D. S. & Pfaller, M. A. (2013) Increasing Echinocandin Resistance in *Candida glabrata*: Clinical Failure Correlates With Presence of *FKS* Mutations and Elevated Minimum Inhibitory Concentrations. *Clinical Infectious Diseases*, **56**: 1724-1732.

Almirante, B., Rodríguez, D., Park, B. J., Cuenca-Estrella, M., Planes, A. M., Almela, M., Mensa, J., Sanchez, F., Ayats, J., Gimenez, M., Saballs, P., Fridkin, S. K., Morgan, J., Rodriguez-Tudela, J. L., Warnock, D. W., Pahissa, A. and the Barcelona Candidemia Project Study Group (2005) Epidemiology and Predictors of Mortality in Cases of *Candida* bloodstream infection: Results from Population-Based Surveillance, Barcelona, Spain, from 2002-2003. *Journal of Clinical Microbiology*, **43**: 1829-1835.

Alvino, G. M., Collingwood, D., Murphy, J. M., Delrow, J., Brewer, B. J. & Raghuraman, M. K. (2007) Replication in Hydroxyurea: It's a Matter of Time. *Molecular and Cellular Biology*, **27**: 6396-6406.

Anderson, J. B. (2005) Evolution of Antifungal-Drug Resistance: Mechanisms and Pathogen Fitness. *Nature Reviews Microbiology*, **3**: 547-556.

Andrusiak, K., Piotrowski, J. S. & Boone, C. (2012) Chemical-genomic profiling: Systematic analysis of the cellular targets of bioactive molecules. *Bioorganic & Medicinal Chemistry*, **20**: 1952-1960.

Angus-Hill, M. L., Schlichter, A., Roberts, D., Erdjument-Bromage, H., Tempst, P. & Cairns, B. R. (2001) A Rsc3/Rsc30 Zinc Cluster Dimer Reveals Novel Roles for the Chromatin Remodeler RSC in Gene Expression and Cell Cycle Control. *Molecular Cell*, **7**: 741-751.

Antão, E. M., Ewers, C., Gürlebeck, D., Preisinger, R., Homeier, T., Li, G. & Wieler, L. H. (2009) Signature-Tagged Mutagenesis in a Chicken Infection Model Leads to the Identification of a Novel Avian Pathogenic *Escherichia coli* Fimbrial Adhesin. *PLoS ONE*, **4**: e7796. doi:10.1371/journal.pone.0007796

Avery, S. V. (2001) Metal toxicity in yeasts and the role of oxidative stress. *Advances in Applied Microbiology*, **49**: 111-142.

Azie, N., Neofytos, D., Pfaller, M., Meier-Kriesche, H., Quan, S. & Horn, D. (2012) The PATH (Prospective Antifungal Therapy) Alliance® registry and invasive fungal infections: update 2012. *Diagnostic Microbiology and Infectious Disease*, **73**: 293-300.

Bairwa, G. & Kaur, R. (2011) A Novel Role for a Glycosylphosphatidylinositol-anchored aspartyl protease, CgYps1, in the regulation of pH homeostasis in *Candida glabrata*. *Molecular Microbiology*, **79**: 900-913.

Balashov, S. V., Park, S. & Perlin, D. S. (2006) Assessing Resistance to the Echinocandin Antifungal Drug Caspofungin in *Candida albicans* by Profiling Mutations in *FKS1*. *Antimicrobial Agents and Chemotherapy*, **50**: 2058-2063.

Bianconi, I., Milani, A., Cigana, C., Paroni, M., Levesque, R. C., Bertoni, G. & Bragonzi, A. (2011) Positive Signature-Tagged Mutagenesis in *Pseudomonas aeruginosa*: Tracking Patho-Adaptive Mutations Promoting Airways Chronic Infection. *PLoS Pathogens*, **7**: e1001270. doi:10.1371/journal.ppat.1001270.

Bivi, N., Romanello, M., Harrison, R., Clarke, I., Hoyle, D. C., Moro, L., Ortolani, F., Bonetti, A., Quadrifoglio, F., Tell, G., Delneri, D. (2009) Identification of secondary targets of N-containing bisphosphonates in mammalian cells via parallel competition analysis of the barcoded yeast deletion collection. *Genome Biology*, **10**: R93.

Blumenthal, A., Trujillo, C., Ehrt, S. & Schnappinger, D. (2010) Simultaneous Analysis of Multiple Mycobacterium tuberculosis Knockdown Mutants In Vitro and In Vivo. *PLoS ONE*, **5**: e15667. doi:10.1371/journal.pone.0015667.

Bouchara, J. P., Zouhair, R., Le Boudouil, S., Filmon, R., CHabasse, D., Hallet, J. N. & Defontaine, A. (2000) *In-Vivo* Selection of an azole-resistant petite mutant of *Candida glabrata*. *Journal of Medical Microbiology*, **49**, 977-984.

Braun, B., Kadosh, D. & Johnson, A. D. (2001) *NRG1*, a repressor of filamentous growth in *C. albicans*, is down-regulated during filament induction. *The EMBO Journal*, **20**: 4753-4761.

Brennan, M., Thomas, D. Y., Whiteway, M. & Kavanagh, K. (2002) Correlation between virulence of *Candida albicans* mutants in mice and *Galleria mellonella* larvae. *FEMS Immunology & Medical Microbiology*, **34**: 153-157.

Brieland, J., Essig, D., Jackson, C., Frank, D., Loebenberg, D., Menzel, F., Arnold, B., DiDomenico, B. & Hare, R. (2001) Comparison of Pathogenesis and Host Immune Responses to *Candida glabrata* and *Candida albicans* in Systemically Infected Immunocompetent Mice. *Infection and Immunity*, **68**: 5046-5055.

Brockert, P. J., Lachke, S. A., Srikantha, T., Pujol, C., Galask, R. & Soll, D. R. (2003) Phenotypic Switching and Mating Type Switching of *Candida glabrata* at sites of colonisation. *Infection and Immunity*, **71**, 7109-7118.

Brown, J. S., Aufauvre-Brown, A., Brown, J., Jennings, J. M., Arst Jr, H. A. & Holden, D. (2000) Signature-tagged and directed mutagenesis identify PABA synthetase as essential for *Spergillus fumigatus* pathogenicity. *Molecular Microbiology*, **36**: 1371-1380.

Brown, G. D., Denning, D. W. & Levitz, S. M. (2012) Tackling human fungal infections. *Science*, **336**: 647.

Brown, A. J. P., Haynes, K. & Quinn, J. (2009) Nitrosative and oxidative stress response in fungal pathogenicity. *Current Opinion in Microbiology*, **12**, 384-391.

Brown, J. C. S. & Madhani, H. D. (2012) Approaching the Functional Annotation of Fungal Virulence Factors Using Cross-Species Genetic Interaction Profiling. *PLoS Genetics*, 8(12): e1003168. doi:10.1371/journal.pgen.1003168.

Brun, S., Aubry, C., Lima, O., Filmon, R., Bergès, T., Chabasse, D. & Bouchara, J. (2003) Relationships between Respiration and Susceptibility to Azole Antifungals in *Candida glabrata*. *Antimicrobial Agents and Chemotherapy*, **47**: 847-853.

Brunke, S. & Hube, B. (2013) Two unlike cousins: *Candida albicans* and *C. glabrata* infection strategies. *Cellular Microbiology*, doi: 10.1111/cmi.12091.

Butler, G., Kenny, C., Fagan, A., Kurieschko, C., Gaillardin, C. & Wolfe, K. H. (2004) Evolution of the *MAT* locus and its Ho endonuclease in yeast species. *PNAS*, **101**: 1632-1637.

Bulawa, C. E., Miller, D. W., Henry, L. K. & Becker, J. M. (1995) Attenuated virulence of chitin-deficient mutants of *Candida albicans*. *PNAS*, **92**: 10570-10574.

Butler, G., Rasmussen, M. D., Lin, M. F., Santos, M. A., Sakthikumar, S., Munro, C. A., Rheinbay, E., Grabherr, M., Forche, A., Reedy, J. L., Agrafioti, I., Arnaud, M. B., Bates, S., Brown, A. J. P., Brunke, S., Costanzo, M. C., Fitzpatrick, D. A., de Groot, P. W. J., Harris, D., Hoyer, L. L., Hube, B., Klis, F. M., Kodira, C., Lennard, N., Logue, M. E., Martin, R., Neiman, A. M., Nikolaou, E., Quail, M. A., Quinn, J., Santos, M. C., Schmitzberger, F. F., Sherlock, G., Shah, P., Silverstein, K. A. T., Skrzypek, M. S., Soll, D., Staggs, R., Stansfield, I., Stumpf, M. P. H., Sudberry, P. E., Srikantha, T., Zeng, Q., Berman, J., Berriman, M., Heitman, J., Gow, N. A. R., Lorenz, M. C. Birren, B. W., Kellis, M. & Cuomo, C. A. (2009) Evolution of pathogenicity and sexual reproduction in eight *Candida* genomes. *Nature*, **459**: 657 – 662.

Butler, G. (2010) Fungal Sex and Pathogenesis. *Clinical Microbiology Reviews*, **23**, 140-159.

Byrne, K. P. & Wolfe, K. H. (2005) The Yeast Gene Order Browser: Combining curated homology and syntenic context reveals gene fate in polyploidy species. *Genome Research*, **15**: 1456-1461.

Calcagno, A., Bignell, E., Rogers, T. R., Canedo, M., Mühlischlegel, F. A. & Haynes, K. (2004) *Candida glabrata* Ste20 is involved in maintaining cell wall integrity and adaptation to hypertonic stress, and is required for wild-type levels of virulence. *Yeast*, **21**: 557-568.

Calcagno, A., Bignell, E., Warn, P., Jones, M. D., Denning, D. W., Mühlischleel, F. A., Rogers, T. R. & Haynes, K. (2003) *Candida glabrata* STE12 is required for wild-type levels of virulence and nitrogen starvation induced filamentation. *Molecular Microbiology*, **50**, 1309-1318.

Castaño, I., Pan, S., Zupancic, M., Hennequin, C., Dujon, B. & Cormack, B. P. (2005) Telomere length control and transcriptional regulation of subtelomeric adhesins in *Candida glabrata*. *Molecular Microbiology*, **55**: 1246-1258.

Caudle, K. E., Barker, K. S., Wiederhold, N. P., Xu, L., Homayouni, R. & Rogers, P. D. (2011) Genomwide Expression Profile Analysis of *Candida glabrata* Pdr1 Regulon. *Eukaryotic Cell*, **10**: 373-383.

Chen, C., Pande, K., French, S. D., Tuch, B. B., Noble, S. M. (2011) An Iron Homeostasis Regulatory Circuit with Reciprocal Roles in *Candida albicans* Commensalism and Pathogenesis. *Cell Host and Microbe*, **10**: 118-135.

Copping, V. M. S., Barelle, C. J., Hube, B., Gow, N. A. R., Brown, A. J. P. & Odds, F. C. (2005) Exposure to *Candida albicans* to antifungal agents affects expression of *SAP2* and *SAP9* secreted proteinase genes. *Journal of Antimicrobial Chemotherapy*, **55**: 645-654.

Córcoles-Sáez, I., Ballester-Thomas, L., de la Torre-Ruiz, M. A., Prieto, J. A. & Randez-Gil, F. (2012) Low temperature highlights the functional role of the cell wall integrity pathway in the regulation of growth in *Saccharomyces cerevisiae*, **446**: 477-88.

Cormack, B. P., Ghori, N. & Falkow, S. (1999) An Adhesin of the Yeast Pathogen *Candida glabrata* Mediating Adherence to Human Epithelial Cells. *Science*, **285**: 578-582.

Costa, C., Pires, C., Cabrito, T. R., Renaudin, A., Ohno, M., Chibana, H., Sá-Correia, I. & Teixeira, M. C. (2013) *Candida glabrata* drug:H⁺ antiporter CgQdr2 (ORF *CAGLOG08624g*) confers imidazole drug resistance, being activated by the CgPdr1 transcription factor. *Antimicrobial Agents and Chemotherapy*, **57**: 3159-3167.

Costanzo, M., Baryshnikova, A., Bellay, J., Kim, Y., Spear, E. D., Sevier, C. S., Ding, H., Koh, J. L. Y., Toufighi, K., Mostafavi, S., Prinz, J., Onge, R. P. S., VanderSluis, B., Makhnevych, T., Vizeacoumar, F. J., Alizadeh, S., Bahr, S., Brost, R. L., Chen, Y., Cokol, M., Deshpande, R., Li, Z., Lin, Z., Liang, W., Marback, M., Paw, J., San Luis, B., Shuteriqi, E., Ton, A. H.Y., van Dyk, N., Wallace, I. M., Whitney, J. A., Weirauch, M. T., Zhong, G., Zhu, H., Houry, W. A., Brudno, M., Ragibizadeh, S., Papp, B., Pál, C., Roth, F. P., Giaever, ., Nislow, C., Troyanskaya, O. G., Bussey, H., Bader, G. D., Gingras, A., Morris, Q. D., Kim, P. M., Kaiser, C. A., Myers, C. L., Andrews, B. J. & Boone, C. (2010) The Genetic Landscape of a Cell. *Science*, **327**: 425-431.

Cotter, G., Doyle, S. & Kavanagh, K. (2000) Development of an insect model for the in vivo pathogenicity testing of yeast. *FEMS Immunology & Medical Microbiology*, **27**: 163-169.

- Cox, J. S., Chen, B., McNeill, M., Jacobs Jr., W. R. (1999) Complex lipid determines tissue-specific replication of *Mycobacterium tuberculosis* in mice. *Nature*, **402**: 79-83.
- Craig, D. W., Pearson, J. V., Szelinger, S., Sekar, A., Redman, M., Corneveaux, J. J., Pawlowski, T. L., Laub, T., Nunn, G., Stephan, D. A., Homer, N. & Huentelman, M. J. (2008) Identification of genetic variants using bar-coded multiplexed sequencing. *Nature Methods*, **5**: 887-893.
- Cramer, K. L., Gerrald, Q. D., Nichols, C. B., Price, M. S. & Alspaugh, J. A. (2006) Transcription Factor Nrg1 Mediates Capsule Formation, Stress Response, and Pathogenesis in *Cryptococcus neoformans*. *Eukaryotic Cell*, **5**: 1147-1156.
- Csank, C. & Haynes, K. (2000) *Candida glabrata* displays pseudohyphal growth. *FEMS Microbiology Letters*, **189**: 115-120.
- Cuéllar-Cruz, M., Briones-Martin-del-Campo, M., Cañas-Villamar, I., Montalvo-Arredondo, J., Riego-Ruiz, L., Castaño, I., De Las Peñas, A. (2008) High Resistance to Oxidative Stress in the Fungal Pathogen *Candida glabrata* is Mediated by a Single Catalase, Cta1p, and is controlled by the Transcription Factors Yap1p, Skn7p, Msn2p, and Msn4p. *Eukaryotic Cell*, **7**, 814-825.
- Czaja, W., Miller, K. Y. & Miller, B. L. (2011) Complex Mechanisms Regulate Developmental Expression of the *matA* (HMG) Mating Type Gene in Homothallic *Aspergillus nidulans*. *Genetics*, **189**: 795-808.
- Dalle, F., Wachtler, B., L'Ollivier, C., Holland, G., Bannert, N., Wilson, D., Labruère, C., Bonnin, A. & Hube, B. (2010) Cellular interactions of *Candida albicans* with human oral epithelial cells and enterocytes. *Cellular Microbiology*, **12**: 248-271.
- Davierwala, A. P., Haynes, J., Li, Z., Brost, R. L., Robinson, M. D., Yu, L., Mnaimneh, S., Ding, H., Zhu, H., Chen, Y., Cheng, X., Brown, G. W., Boone, C., Andrews, B. J. & Hughes, T. R. (2005) The synthetic genetic interaction spectrum of essential genes. *Nature Genetics*, **37**: 1147-1152.
- Delneri, D. (2010) Barcode technology in yeast: application to pharmacogenomics. *FEMS Yeast Research*, **10**: 1083-1089.
- Denning, D. W. (2002) Echinocandins: a new class of antifungal. *Journal of Antimicrobial Chemotherapy*, **49**: 889-891.
- Desai, C., Mavrianos, J. & Chauhan, N. (2011) *Candida glabrata* Pwp7p and Aed1p are required for adherence to human endothelial cells. *FEMS Yeast Research*, **11**: 595-601.
- Deutschbauer, A. M., Williams, R. M., Chu, A. M. & Davis, R. W. (2002) Parallel phenotypic analysis of sporulation and postgermination growth in *Saccharomyces cerevisiae*. *PNAS*, **99**: 15530-15535.

Dixon, S. J., Costanzo, M., Baryshnikove, A., Andrews, B. & Boone, C. (2009) Systematic mapping of Genetic Interaction Networks. *Annual Reviews Genetics*, **43**: 601-625.

Dixon, S. J., Fedyszyn, Y., Koh, J. L. Y., Prasad, K., Chahwan, C., Chua, G., Toufighi, K., Baryshnikova, A., Hayles, J., Hoe, K., Klim, D., Park, H., Myers, C. L., Pandey, A., Durocher, D., Andrews, B. J. & Boone, C. (2008) Significant conservation of synthetic lethal genetic interaction networks between distantly related eukaryotes. *PNAS*, **105**: 16653-16658.

Doedt, T., Krishnamurthy, S., Bockmühl D. P., Tebarth, B., Stempel, C., Russel, C. L., Brown, A. J. P. & Ernst, J. F. (2004) APSES Proteins Regulate Morphogenesis and Metabolism in *Candida albicans*. *Molecular Biology of the Cell*, **15**: 3167-3180.

Domergue, R., Castaño, I., De Las Peñas, A., Zupancic, M., Lockett, V., Hebel, J. R., Johnson, D. & Cormack, B. P. (2005) Nicotinic Acid Limitation Regulates Silencing of *Candida* Adhesins During UTI. *Science*, **308**: 866-870.

Donini, M., Zenaro, E., Tamassia, N. & Dusi Dr, S. (2007) NADPH oxidase of human dendritic cells: Role in *Candida albicans* killing and regulation by interferons, dectin-1 and CD206. *European Journal of Immunology*, **37**, 1194-1203.

Dujon, B., Sherman, D., Fischer, G., Durrens, P., Casaregola, S., Lafontaine, I., de Montigny, J., Marck, C., Neuvéglise, C., Talla, E., Goffard, N., Frangeul, L., Aigle, M., Anthouard, V., Babour, A., Barbe, V., Barnay, S., Blanchin, S., Beckerich, J., Beyne, E., Bleykasten, C., Boisramé, A., Boyer, J., Cattolico, L., Confanioleri, F., de Daruvar, A., Despons, L., Fabre, E., Fairhead, C., Ferry-Dumazet, H., Groppi, A., Hantraye, F., Hennequin, C., Jaunlaux, N., Joyet, P., Kachouri, R., Kerrest, A., Koszul, R., Lemaire, M., Lesur, I., Ma, L., Muller, H., Nicaud, J., Nikolski, m., Oztas, S., Ozler-Kalogeropoulos, O., Pellenz, S., Potier, S., Richard, G., Straub, M., Suleau, A., Swennen, D., Tekaiia, F., Wésolowski-Louvel, M., Westhof, E., Wirthe, B., Zeniou-Meyer, M., Zivanovic, I., Bolotin-Fukuhara, M., Thierry, A., Bouchier, C., Caudron, B., Scarpelli, C., Gaillardin, C., Weissenbach, J., Winker, P. & Souciet, J. (2004) Genome Evolution in Yeasts. *Nature*, **430**: 35-44.

Dujon, B. (2010) Yeast evolutionary genomics. *Nature Reviews Genetics*, **11**: 512-524.

Duraisingh, M. T., Voss, T. S., Marty, A. J., Duffy, M. F., Good, R. T., Thompson, J. K., Freitas-Junior, L. H., Scherf, A., Crabb, B. S. & Cowman, A. F. (2006) Heterochromatin Silencing and Locus Repositioning Linked to Regulation of Virulence Genes in *Plasmodium falciparum*. *Cell*, **121**: 13-24.

Eichhorn, H., Lessing, F., Winterberg, B., Schirawski, J., Kämper, J., Müller, P. & Kahmann, R. (2006) A Ferroxidation/Permeation Iron Uptake System is Required for Virulence in *Ustilago Maydis*. *The Plant Cell*, **18**: 3332-3345.

El-Kirat-Chatel, S., Beaussart, A., Alsteens, D., Sarazin, A., Jouault, T. & Dufrénet, Y. F. (2013) Single-molecule analysis of the major glycopolymers of

pathogenic and non-pathogenic yeast cells. *Nanoscale*, DOI: 10.1039/c3nr00813d.

Elahi, S., Pang, G., Ashman, R. B. & Clancy, R. (2001) Nitric oxide-enhanced resistance to oral candidiasis. *Immunology*, **104**, 447-454.

Enjalbert, B., Smith, D. A., Cornell, M. J., Alam, I., Nicholls, S., Brown, A. J. P. & Quinn, J. (2006) Role of the Hog1 Stress-activated Protein Kinase in the Global Transcriptional Response to Stress in the Fungal Pathogen *Candida albicans*. *Molecular Biology of the Cell*, **17**: 1018-1032.

Fabre, E., Muller, H., Therizols, P., Lafontaine, I., Dujon, B. & Fairhead, C. (2005) Comparative Genomics in Hemiascomycete Yeasts: Evolution of Sex, Silencing, and Subtelomeres. *Molecular Biology and Evolution*, **22**: 856-873.

Fàbrega, A. & Vila, J. (2013) *Salmonella enteric* Serovar Typhimurium Skills To Succeed in the Host: Virulence and Regulation. *Clinical Microbiology Reviews*, **26**: 308-341.

Fabrizio, P., Hoon, S., Shamalnasab, M., Galbani, A., Wei, M., Giaever, G., Nislow, C & Longo, V. D. (2010) Genome-Wide Screen in *Saccharomyces cerevisiae* Identifies Vacuolar Protein Sorting, Autophagy, Biosynthetic, and tRNA Methylation Genes Involved in Life Span Regulation. *PLoS Genetics*, **6**(7): e1001024. doi:10.1371/journal.pgen.1001024

Fang, F. (2004) Antimicrobial Reactive Oxygen and Nitrogen Species: Concepts and Controversies. *Nature Reviews Microbiology*, **2**: 820-832.

Ferrari, S., Ischer, F., Calabrese, D., Posteraro, B., Sanguinetti, M., Fadda, G., Rohde, B., Bauser, C., Bader, O. & Sanglard, D. (2009) Gain of Function Mutations in *CgPDR1* of *Candida glabrata* Not Only Mediate Antifungal Resistance But Also Enhance Virulence. *PLoS Pathogens*, **5**(1): e1000268. doi:10.1371/journal.ppat.1000268.

Ferrari, S., Sanguinetti, M., Torelli, R., Posteraro, B. & Sanglard, D. (2011) Contribution of *CgPDR1*-Regulated Genes in Enhanced Virulence of Azole-Resistant *Candida glabrata*. *PLoS One*, **6**(3): e17589. doi:10.1371/journal.pone.0017589. (A)

Ferrari, S., Sanguinetti, M., De Bernardis, F., Torelli, R., Posteraro, B., Vandeputte, P. & Sanglard, D. (2011) Loss of Mitochondrial Functions Associated with Azole Resistance in *Candida glabrata* Results in Enhanced Virulence in Mice. *Antimicrobial Agents and Chemotherapy*, **55**: 1852 – 1860. (B)

Fidel Jr., P. L., Vazquez, J. A. & Sobel, J. D. (1999) *Candida glabrata*: Review of Epidemiology, Pathogenesis, and Clinical Disease with Comparison to *C. albicans*. *Clinical Microbiology Reviews*, **12**: 80-96.

Fischbach, M. A., Lin, H., Liu, D. R., Walsh, C. T. (2006) How pathogenic bacteria evade mammalian sabotage in the battle for iron. *Nature Chemical Biology*, **2**: 132-138.

Fisher, M. C., Henk, D. A., Briggs, C. J., Brownstein, J. S., Madoff, L. C., McCraw, S. L. & Gurr, S. J. (2012) Emerging fungal threats to animal, plant and ecosystem health. *Nature*, **484**: 186-194.

Fitzpatrick, D. A., Logue, M. E. & Butler, G. (2008) Evidence of a recent interkingdom horizontal gene transfer between bacteria and *Candida parapsilosis*. *BMC Evolutionary Biology*, **8**: 181-196.

Forche, A., Alby, K., Schaefer, D., Johnson, A. D., Berman, J. & Bennett, R. J. (2008) The Parasexual Cycle in *Candida albicans* Provides an Alternative Pathway to Meiosis for the Formation of Recombinant Strains. *PLoS Biology*, **6**(5): e110. doi:10.1371/journal.pbio.0060110.

Foury, F. (1997) Human genetic diseases: a cross-talk between man and yeast. *Gene*, **195**: 1-10.

Fox, C. A. & McConnell, K. H. (2005) Toward Biochemical Understanding of a Transcriptionally Silenced Chromosomal Domain in *Saccharomyces cerevisiae*. *Journal of Biological Chemistry*, **280**: 8629-8632.

Francolini, I. & Donelli, G. (2010) Prevention and control of biofilm-based medical-device-related infections. *FEMS Immunology & Medical Microbiology*, **59**: 227-238.

Frieman, M. B., McCaffery, J. M. & Cormack, B. P. (2002) Modular domain structure in the *Candida glabrata* adhesion Epa1p, a β 1,6 glucan-cross-linked cell wall protein. *Molecular Microbiology*, **2**: 479-492.

Fu, Y., Phan, Q. T., Luo, G., Solis, N. V., Cormack, B. P., Edwards, J. E. Jr., Ibrahim, A. S. & Fuller, S. G. (2013) Investigation of the Function of *Candida albicans* Als3 by Heterologous Expression in *Candida glabrata*. *Infection and Immunity*, **8**: 2528-2535.

Fukuda, Y., Tsai, H. F., Myers, T. G. & Bennett, J. E. (2013) Transcriptional profiling of *Candida glabrata* during phagocytosis by neutrophils and in the infected mouse spleen. *Infection and Immunity*, **81**: 1325-1333.

Garcia-Effron, G., Katiyar, S. K., Park, S., Edlind, T. D. & Perlin, D. S. (2008) A Naturally Occurring Proline-to-Alanine Amino Acid Change in Fsk1p in *Candida parapsilosis*, *Candida orthosilopsis*, and *Candida methapsilosis* Accounts for Reduced Echinocandin Susceptibility. *Antimicrobial Agents and Chemotherapy*, **52**: 2305-2312.

Garcia-Vallvé, S., Romeu, A. & Palau, J. (2000) Horizontal Gene Transfer of Glycosyl Hydrolases of the Rumen Fungi. *Molecular Biology and Evolution*, **17**:352-361.

Giaever, G., Chu, A. M., Ni, L., Connelly, C., Riles, L., Véronneau, S., Dow, S., Lucau-Danila, A., Anderson, K., André, B., Arkin, A. P., Astromoff, A., El Bakkoury, M., Bangham, R., Benito, R., Brachat, S., Companaro, S., Curtiss, M., Davis, K., Deutschbauer, A., Entian, K., Flaherty, P., Foury, F., Garfinkel, D. J., Gerstein, M., Gotte, D., Güldener, U., Hegemann, J. H., Hempel, S., Herman, Z., Jaramillo, D. F., Kelly, D. E., Kelly, S. L., Kötter, P., LaBonte, D.,

Lamb, D. C., Lan, N., Liang, H., Liao, H., Liu, L., Luo, C., Lussier, M., Mao, R., Menard, P., Ooi, S. L., Revuetta, J. L., Roberts, C. J., Rose, M., Ross-Macdonald, P., Scherens, B., Schimmack, G., Shafer, B., Shoemaker, D. D., Sookhai-Mahedeo, S., Storms, R. K., Strathern, J. N., Valle, G., Voet, M., Volckaert, G., Wang, C., Ward, T. R., Wilhelmy, J., Winzeler, E. A., Yang, Y., Yen, G., Youngman, E., Yu, K., Bussey, H., Boeke, J. D., Snyder, M., Philippsen, P., Davis, R. W. & Johnston, M. F. (2002) Functional Profiling of the *Saccharomyces cerevisiae* genome. *Nature*, **418**: 387-391.

Giaever, G., Shoemaker, D. D., Jones, T. W., Liang, H., Winzeler, E. A., Astromoff, A. & Davis, R. (1999) Genomic profiling of drug sensitivities via induced haploinsufficiency. *Nature Genetics*, **21**: 278-283.

Gallegos-García, V., Pan, S., Juárez-Cepeda, J., Ramírez-Zavaleta, C. Y., Martín-del-Campo, M. B., Martínez-Jiménez, V., Castaño, I., Cormack, B. & De Las Peñas, A. (2012) A Novel Downstream Regulatory Element Cooperates with the Silencing Machinery to Repress *EPA1* Expression in *Candida glabrata*. *Genetics*, **190**: 1285-1297.

Gelperin, D. M., White, M. A., Wilkinson, M. L., Kon, Y., Kung, L. A., Wise, K. J., Lopez-Hoyo, N. L., Jiang, L. J., Piccirillo, S., Yu, H., Gerstein, M., Dumont, M. E., Phizicky, E. M., Snyder, M. & Grayhack, E. J. (2005) Biochemical and genetic analysis of the yeast proteome with a movable ORF collection. *Genes & Development*, **19**, 2816-2826.

Ghaemmaghami, S., Huh, W., Bower, K., Howson, R. W., Belle, A., Dephoure, N., O'Shea, E. K. & Weissman, J. S. (2003) Global analysis of protein expression in yeast. *Nature*, **425**: 737-741.

Glittenberg, M. T., Kounatidis, I., Christensen, D., Kostov, M., Kimber, S., Roberts, I. & Ligoxygakis, P. (2011) Pathogen and host factors are needed to provoke a systemic host response to gastrointestinal infection of *Drosophila* larvae by *Candida albicans*. *Disease Models & Mechanisms*, **4**: 515-525.

Glittenberg, M. T., Silas, S., MacCallum, D. M., Gow, N. A. R. & Ligoxygakis, P. (2011) Wild-type *Drosophila melanogaster* as an alternative model system for investigating the pathogenicity of *Candida albicans*. *Disease Models & Mechanisms*, **4**: 504-514.

Gonzalez, M. D., Lichtensteiger, C. A. & Vimr, E. R. (2001) Adaptation of the signature-tagged mutagenesis to *Escherichia coli* K1 and the infant-rat model of invasive disease. *FEMS Microbiology Letters*, **198**: 125-128.

Gow, N. A. R., Brown, A. J. P. & Odds, F. C. (2002) Fungal morphogenesis and host invasion. *Current opinion in Microbiology*, **5**: 366-371.

Gow, N. A. R., van de Veerdonk, F. L., Brown, A. J. P. & Netea, M. G. (2012) *Candida albicans* morphogenesis and host defence: discriminating invasion from colonization. *Nature Reviews Microbiology*, **10**: 112-122.

de Groot, P. W. J., Kraneveld, E. A., Yin, Q. Y., Dekker, H. L., Groß, U., Crielaard, W. & de Koster, C. G. (2008) The Cell Wall of the Human Pathogen

- Candida glabrata*: Differential Incorporation of Novel Adhesion-Like Wall Proteins. *Eukaryotic Cell*, **7**, 1951-1964.
- Gu, Z., Steinmetz, L. M., Gu, X., Scharfe, C., Davis, R. W. & Li, W. (2003) Role of duplicate genes in genetic robustness against null mutations. *Nature*, **421**: 63-66.
- Guindon, S., Dufayard, J., Lefort, V., Anisimova, M., Hordijk, W. & Gascuel, O. (2010) New Algorithms and Methods to Estimate Maximum-Likelihood Phylogenies: Assessing the Performance of PhyML 3.0. *Systematic Biology*, **59**: 307-321.
- Gutiérrez-Escobedo, G., Orta-Zavalza, E., Castaño, I. & De Las Peñas, A. (2013) Role of glutathione in the oxidative stress response in the fungal pathogen *Candida glabrata*. *Current Genetics*, DOI 10.1007/s00294-013-0390-1.
- Haas, H. (2003) Molecular genetics of fungal siderophore biosynthesis and uptake: the role of siderophores in iron uptake and storage. *Applied Microbiology & Biotechnology*, **62**: 316-330.
- Haber, J. E. (2000) Partners and pathways: repairing a double-strand break. *Trends in Genetics*, **16**: 259-264.
- Hall, R. A., Bates, S., Lenardon, M. D., MacCallum, D. M., Wagener, J., Lowman, D. W., Kruppa, M. D., Williams, D. L., Odds, F. C., Brown, A. J. P. & Gow, N. A. R. (2013) The Mnn2 Mannosyltransferase Family Modulates Mannoprotein Fibril Length, Immune Recognition and Virulence of *Candida albicans*. *PLoS Pathogens*, 9(4): e1003276doi:10.1371/journal.ppat.1003276
- Halliwell, S. C., Smith, M. C. A., Muston, P., Holland, S. L. & Avery, S. V. (2012) Heterogeneous Expression of the Virulence-Related Adhesin Epa1 between Individual Cells and Strains of the Pathogen *Candida glabrata*. *Eukaryotic Cell*, **11**: 141-150.
- Hampsey, M. (1997) A Review of Phenotypes in *Saccharomyces cerevisiae*. *Yeast*, **13**: 1099-1133.
- Hanway, D., Chin, J. K., Xia, G., Oshiro, G., Winzeler, E. & Romesberg, F. E. (2002) Previously uncharacterised genes in the UV- and MMS-induced DNA damage response in yeast. *PNAS*, **99**: 10605-10610.
- Hawksworth, D. L. (2001) The magnitude of fungal diversity: the 1.5 million species estimate revisited. *Mycological Research*, **105**: 1422-1432.
- Hensel, M., Shea, J. E., Gleeson, C., Jones, M. D., Dalton, E. & Holden, D. W. (1995) Simultaneous Identification of Bacterial Virulence Genes by Negative Selection. *Science*, **269**: 400-403.
- Hickman, M. A., Zeng, G., Forche, A., Hirakawa, M. P., Abbey, D., Harrison, B. D., Wang, Y., Su, C., Bennett, R. J., Wang, Y. & Berman, J. (2013) The 'obligate diploid' *Candida albicans* forms mating-competent haploids. *Nature*, doi:10.1038/nature11865.

- Hillenmeyer, M. E., Ericson, E., Davis, R. W., Nislow, C., Koller, D. & Giaever, G. (2010) Systematic analysis of genome-wide fitness data in yeast reveals novel gene function and drug action. *Genome Biology*, **11**: R30.
- Ho, C. H., Magtanong, L., Barker, S. L., Gresham, D., Nishimura, S., Natarajan, P., Koh, J. L. Y., Porter, J., Gray, C. A., Andersen, R. J., Giaever, G., Nislow, C., Andrews, B., Botstein, D., Graham, T. R., Yoshida, M. & Boone, C. (2009) A molecular barcoded yeast ORF library enables mode-of-action analysis of bioactive compounds. *Nature Biotechnology*, **27**: 369-377.
- Ho, C. H., Piotrowski, J., Dixon, S. J., Baryshnikova, A., Costanzo, M. & Boone, C. (2011) Combining functional genomics and chemical biology to identify targets of bioactive compounds. *Current Opinion in Chemical Biology*, **15**: 66-78.
- Homann, O. R., Dea, J., Noble, S. M. & Johnson, A. D. (2009) A Phenotypic Profile of the *Candida albicans* Regulatory Network. *PLoS Genetics*, **5**: doi:10.1371/journal.pgen.1000783.
- Hood, M. I. & Skaar, E. P. (2012) Nutritional immunity: transition metals at the pathogen-host interface. *Nature Reviews Microbiology*, **10**: 525-537.
- Horn, D. & Barry, J. D. (2005) The central roles of telomeres and subtelomeres in antigenic variation in African trypanosomes. *Chromosome Research*, **13**: 525-533.
- Horn, D. L., Neofytos, D., Anaissie, E. J., Fishman, J. A., Steinbach, W. J., Olyaei, A. J., Marr, K. A., Pfaller, M. A., Chang, C. & Webster, K. M. (2009) Epidemiology and Outcomes of Candidemia in 2019 Patients: Data from the Prospective Antifungal Therapy Alliance Registry. *Clinical Infectious Diseases*, **48**: 1695-1703.
- Horn, T., Sandmann, T., Fischer, B., Axelsson, E., Huber, W. & Boutros, M. (2011) Mapping of signalling networks through synthetic genetic interaction analysis by RNAi. *Nature Methods*, **8**: 341-346.
- Hosiner, D., Lempiäinen, H., Reiter, W., Urban, J., Loewith, R., Ammerer, G., Schweyen, R., Shore, D. & Schüller, C. (2009) Arsenic Toxicity to *Saccharomyces cerevisiae* Is a Consequence of Inhibition of the TORC1 Kinase Combined with Chronic Stress Response. *Molecular Biology of the Cell*, **20**: 1048-1057.
- Hosogaya, N., Miyazaki, T., Nagi, M., Tanabe, K., Minematsu, A., Nagayoshi, Y., Yamauchi, S., Nakamura, S., Imamura, Y., Izumikawa, K., Kakeya, H., Yanagihara, K., Miyazaki, Y., Kugiyama, K. & Kohno, S. (2013) The heme-binding protein Dap1 links iron homeostasis to azole resistance via the P450 protein Erg11 in *Candida glabrata*. *FEMS Yeast Research*, DOI: 10.1111/1567-1364.12043.
- Hughes, T. R., Roberts, C. J., Dai, H., Jones, A. R., Meyer, M. R., Slade, D., Burchard, J., Dow, S., Ward, T. R., Kidd, M. J., Friend, S. H. & Marton, M. J. (2000) Widespread aneuploidy revealed by DNA microarray expression profiling. *Nature Genetics*, **25**: 333-337.

Hwang, C., Oh, J., Huh, W., Yim, H., Kang, S. (2003) Ssn6, an important factor of morphological conversion and virulence in *Candida albicans*. *Molecular Microbiology*, **47**: 1029-1043.

Ibata-Ombetta, S., Idziorek, T., Trinel, P., Poulain, D. & Jouault, T. (2003) *Candida albicans* Phospholipomannan Promotes Survival of Phagocytosed Yeasts through Modulation of Bad Phosphorylation and Macrophage Apoptosis. *Journal of Biological Chemistry*, **278**: 13086-13093.

Idnurm, A., Walkton, F. J., Floyd, A., Reedy, J. L. & Heitman, J. (2009) Identification of *ENA1* as a Virulence Gene of the Human Pathogenic Fungus *Cryptococcus neoformans* through Signature-Tagged Insertional Mutagenesis. *Eukaryotic Cell*, **8**: 315-326.

Iraqui, I., Garcia-Sanchez, S., Aubert, S., Dromer, F., Ghigo, J. M., d'Enfert, C., Janbon, G. (2005) The Yak1p kinase controls expression of adhesions and biofilm formation in *Candida glabrata* in a Sir4p-dependent pathway. *Molecular Microbiology*, **55**: 1259-71.

Iyer, V. R., Horak, C. E., Scafe, C. S., Botstein, D., Snyder, M. & Brown, P. O. (2001) Genomic binding sites of the yeast cell-cycle transcription factors SBF and MBF. *Nature*, **409**: 533-538.

Jacobsen, I. D., Brunke, S., Seider, K., Schwarzmüller, T., Firon, A., d'Enfert, C., Kuchler, K. & Hube, B. (2010) *Candida glabrata* Persistence in Mice Does Not Depend on Host Immunosuppression and Is Unaffected by Fungal Amino Acid Auxotrophy. *Infection and Immunity*, **78**: 1066-1077.

Jacobsen, I. D., Große, K., Berndt, A. & Hube, B. (2011) Pathogenesis of *Candida albicans* Infections in the Alternative Chorio-Allantoic Membrane Chicken Embryo Model Resembles Systemic Murine Infections. *PLoS One*, **6**: e19741. doi:10.1371/journal.pone.0019741

Jandric, Z. & Schüller, C. (2011) Stress response in *Candida glabrata*: pieces of a fragmented picture. *Future Microbiology*, **6**, 1475-1484.

Ju, J. Y., Polhamus, C., Marr, K. A., Holland, S. M. & Bennett, J. E. (2002) Efficacies of Fluconazole, Caspofungin and Amphotericin B in *Candida glabrata*-Infected p47^{phox}^{-/-} Knockout Mice. *Antimicrobial Agents and Chemotherapy*, **46**: 1240-1245.

Kadosh, D. & Johnson, A. D. (2005) Induction of the *Candida albicans* Filamentous Growth Program by Relief of Transcriptional Repression: A Genome-Wide Analysis. *Molecular Biology of the Cell*, **16**: 2903-2912.

Kahn, J. N., Garcia-Effron, G., Hsu, M., Park, S., Marr, K. A. & Perlin, D. S. (2007) Acquired Echinocandin Resistance in a *Candida krusei* Isolate Due to Modification of Glucan Synthase. *Antimicrobial Agents and Chemotherapy*, **51**: 1876-1878.

Kaloriti, D., Tillmann, A., Cook, E., Jacobsen, M., You, T., Lenardon, M., Ames, L., Barahona, M., Chandrasekaran, K., Coghill, G., Goodman, D., Gow, N. A. R., Grebogi, C., Ho, H., Ingram, P., McDonagh, A., de Moura, A. P. S., Pang,

W., Puttnam, M., Radmaneshfar, E., Romano, M. C., Silk, D., Stark, J., Stumpf, M., Thiel, M., Thorne, T., Usher, J., Yin, Z., Haynes, K. & Brown, A. J. P. (2012) Combinatorial stresses kill pathogenic *Candida* species. *Medical Mycology*, **50**: 699-709.

Kassir, Y., Adir, N., Boger-Nadjar, E., Raviv, N. G., Rubin-Bejerano, I., Sagee, S. & Shenhar, G. (2003) Transcriptional regulation of meiosis in budding yeast

Katiyar, S. K., Alastruey-Izquierdo, A., Healey, K. R., Johnson, M. E., Perlin, D. S. & Edlind, T. D. (2012) Fks1 and Fks2 Are Functionally Redundant but Differentially Regulated in *Candida glabrata*: Implications for Echinocandin Resistance. *Antimicrobial Agents and Chemotherapy*, **56**, 6304-6309.

Kaur, R., Domergue, R., Zupancic, M. L. & Cormack, B. P. (2005) A yeast by any other name: *Candida glabrata* and its interaction with the host. *Current Opinion in Microbiology*, **8**: 378-384.

Kaur, R., Ma, B. & Cormack, B. P. (2007) A family of glycosylphosphatidylinositol-linked aspartyl proteases is required for virulence of *C. glabrata*. *PNAS*, **104**, 7628-7633.

Keane, T. M., Creevey, C. J., Pentony, M. M., Naughton, T. J. & McInerney, J. O. (2006) Assessment of methods for amino acid matrix selection and their use on empirical data shows that ad hoc assumptions for choice of matrix are not justified. *BMC Evolutionary Biology*, **6**: 29-46.

Kellis, M., Birren, B. W. & Lander, E. S. (2004) Proof of evolutionary analysis of ancient genome duplication in the yeast *Saccharomyces cerevisiae*. *Nature*, **428**, 617-624.

Keppler-Ross, S., Douglas, L., Konopka, J. B. & Dean, N. (2010) Recognition of Yeast by Murine Macrophages Requires Mannan but not Glucan. *Eukaryotic Cell*, **9**: 1776-1787.

Klis, F. M., Sosinska, G. J., de Groot, P. W. J. & Brul, S. (2009) Covalently linked cell wall proteins of *Candida albicans* and their role in fitness and virulence. *FEMS Yeast Research*, **9**: 1013-1028.

Klotz, S. A., Chasin, B. S., Powell, B., Gaur, N. K. & Lipke, P. N. (2007) Polymicrobial bloodstream infections involving *Candida* species: analysis of patients and review of the literature. *Diagnostic Microbiology and Infectious Disease*, **59**: 401-406.

Koh, J. L. Y., Ding, H., Costanzo, M., Baryshnikova, A., Toufighi, K., Bader, G. D., Myers, C. L., Andrews, B. J. & Boone, C. (2010) DRYGIN: a database of quantitative genetic interaction networks in yeast. *Nucleic Acids Research*, **38**: D502-D507.

Kounatidis, I. & Ligoxygakis, P. (2012) *Drosophila* as a model system to unravel the layers of innate immunity to infection. *Open Biology*, **2**: **doi:10.1098/rsob.120075**.

- Kraneveld, E. A., de Soet, J. J., Deng, D. M., Dekker, H. L., de Koster, C. G., Klis, F. M., Crielaard, W. & de Groot, P. W. J. (2011) Identification and Differential Gene Expression of Adhesin-Like Wall Proteins in *Candida glabrata* Biofilms. *Mycopathologica*, **172**: 415-427.
- Kuchin, S., Vyas, V. K. & Carlson, M. (2002) Snf1 Protein Kinase and the Repressors Nrg1 and Nrg2 Regulate *FLO11*, Haploid Invasive Growth, and Diploid Pseudohyphal Differentiation. *Molecular and Cellular Biology*, **22**: 3994-4000.
- Kuhn, D. M. & Vyas, V. K. (2012) The *Candida glabrata* adhesion Epa1p causes adhesion, phagocytosis, and cytokine secretion by innate immune cells. *FEMS Yeast Research*, **12**, 398-414.
- Kumar, A., Agarwal, S., Heyman, J. A., Matson, S., Heidtman, M., Piccirillo, S., Umansky, L., Drawid, A., Jansen, R., Liu, Y., Cheung, K., Miller, P., Gerstein, M., Roeder, G. S. & Snyder, M. (2002) Subcellular localization of the yeast proteome. *Genes & Development*, **16**: 707-719.
- Kurischko, C., Schilhabel, M. B., Kunze, I. & Franzl, E. (1999) The *MATA* locus of the dimorphic yeast *Yarrowia lipolytica* consists of two divergently orientated genes. *Molecular and General Genetics*, **262**: 180-188.
- Lachke, S. A., Srikantha, T., Tsai, L. K., Daniels, K. & Soll, D. R. (2000) Phenotypic Switching in *Candida glabrata* Involves Phase-Specific Regulation of the Metallothionein Gene *MT-II* and the Newly Discovered Hemolysin Gene *HLP*. *Infection and Immunity*, **68**: 884-895.
- Lachke, S. A., Joly, S., Daniels, K. & Soll, D. R. (2002) Phenotypic switching and filamentation in *Candida glabrata*. *Microbiology*, **148**: 2661-2674.
- Lan, C., Newport, G., Murillo, L. A., Jones, T., Scherer, S., Davis, R. W. & Agabian, N. (2002) Metabolic specialization associated with phenotypic switching in *Candida albicans*. *PNAS*, **99**, 14907 – 14912.
- Lehner, B., Crombie, C., Tischler, J., Fortunato, A. & Fraser, A. G. (2006) Systematic mapping of genetic interactions in *Caenorhabditis elegans* identifies common modifiers of diverse signalling pathways. *Nature Genetics*, **38**: 896-903.
- Levin, D. E. (2005) Cell Wall Integrity Signalling in *Saccharomyces cerevisiae*. *Microbiology and Molecular Biology Reviews*, **69**: 262-291.
- Levitz, S. M. (2010) Innate Recognition of Fungal Cell Walls. *PLoS Pathogens*, **6**(4): e1000758. doi:10.1371/journal.ppat.1000758.
- Li, L. & Dongari-Bagtzoglou, A. (2009) Epithelial GM-CSF Induction by *Candida glabrata*. *Journal of Dental Research*, **88**: 746-751.
- Lin, C., Kabrawala, S., Fox, E. P., Nobile, C. J., Johnson, A. D. & Bennett, R. J. (2013) Genetic Control of Conventional and Pheromone-Stimulated Biofilm Formation in *Candida albicans*. *PLoS Pathogens*, **9**(4): e1003305. doi:10.1371/journal.ppat.1003305.

- Lin, H., Li, L., Jia, X., Ward, D. M. & Kaplan, J. (2011) Genetic and Biochemical Analysis of High Iron Toxicity in Yeast. *Journal of Biological Chemistry*, **286**: 3851-3862.
- Lin, J., Lin, C., Lai, C., Yang, Y., Chen, H., Weng, H., Hsieh, L., Kuo, Y., Lauderdale, T., Tseng, F., Lin, H. & Lo, H. (2012) Predisposing factors for oropharyngeal colonization of yeasts in human immunodeficiency virus-infected patients: A prospective cross-sectional study. *Journal of Microbiology, Immunology and Infection*, **46**: 129-135.
- Litwin, I., Bocer, T., Dziadkowiec, D. & Wysocki, R. (2013) Oxidative Stress and Replication-Independent DNA Breakage Induced by Arsenic in *Saccharomyces cerevisiae*. *PLoS Genetics*, **9**: e1003640. doi:10.1371/journal.pgen.1003640.
- Liu, O. W., Chun, C. D., Chow, E. D., Chen, C., Madhani, H. D. & Noble, S. M. (2008) Systematic Genetic Analysis of Virulence in the Human Fungal Pathogen *Cryptococcus neoformans*. *Cell*, **135**: 174-188.
- López-Mirabal, H. R. & Winther, J. R. (2008) Redox characteristics of the eukaryotic cytosol. *Biochimica et Biophysica Acta*, **4**: 629-640.
- Lorenz, M. C., Bender, J. A. & Fink, G. R. (2004) Transcriptional Response of *Candida albicans* upon Internalization by Macrophages. *Eukaryotic Cell*, **3**: 1076–1087.
- Lorenz, M. C. & Fink, G. R. (2001) The glyoxylate cycle is required for fungal virulence. *Nature*, **412**: 83-86.
- Ma, B., Pan, S., Domergue, R., Rigby, T., Whiteway, M., Johnson, D. & Cormack, B. P. (2009) High-Affinity Transporters for NAD⁺ Precursors in *Candida glabrata* Are Regulated by Hst1 and Induced in Response to Niacin Limitation. *Molecular and Cellular Biology*, **29**: 4067-4079.
- Ma, J., Bharucha, N., Dobry, C. J., Frisch, R. L., Lawson, S. & Kumar, A. (2008) Localization of autophagy-related proteins in yeast using a versatile plasmid-based resource of fluorescent protein fusions. *Autophagy*, **4**: 792-800.
- MacCallum, D. M., Castillo, L., Brown, A. J. P., Gow, N. A. R. & Odds, F. C. (2009) Early-Expressed Chemokines Predict Kidney Immunopathology in Experimental Disseminated *Candida albicans* Infections. *PLoS ONE* **4**(7): e6420. doi:10.1371/journal.pone.0006420
- Maestre-Reyna, M., Diderrich, R., Veelders, M. S., Eulenburg, G., Kalugin, V., Brückner, S., Keller, P., Rupp, S., Mösch, H. & Essen, L. (2012) Structural basis for promiscuity and specificity during *Candida glabrata* invasion of host epithelia. *PNAS*, **109**: 16864-16869.
- Magadum, S., Banerjee, U., Murugan, P., Gangapur, D. & Ravikesavan, R. (2013) Gene duplication as a major force in evolution. *Journal of Genetics*, **92**: 155–161.
- Marcet-Houben & Gabaldón, (2010) Acquisition of prokaryotic genes by fungal genomes. *Trends in Genetics*, **26**: 5-8.

Marchler-Bauer, A., Lu, S., Anderson, J. B., Chitsaz, F., Derbyshire, M. K., DeWeese-Scott, C., Fong, J. H., Geer, L. Y., Geer, R. C., Gonzales, N. R., Gwadz, M., Hurwitz, D. I., Jackson, J. D., Ke, Z., Lanczycki, C. J., Lu, F., Marchler, G. H., Mullokandov, M., Omelchenko, M. V., Robertson, C. L., Song, J. S., Thanki, N., Yamashita, R. A., Zhang, D., Zhang, N., Zheng, C. & Bryant, S. H. (2011) CDD: a Conserved Domain Database for the Functional Annotation of Proteins. *Nucleic Acids Research*, **39**: 225-229.

Martínez, P. & Ljungdahl, P. O. (2004) An ER packaging chaperone determines the amino acid uptake capacity and virulence of *Candida albicans*. *Molecular Microbiology*, **51**: 371-384.

Mazurkiewicz, P., Tang, C. T., Boone, C. & Holden, D. W. (2006) Signature-tagged mutagenesis: barcoding mutants for genome-wide screens. *Nature Reviews Genetics*, **7**: 929-939.

McDonagh, A., Fedorova, N. D., Crabtree, J., Yu, Y., Kim, S., Chen, D., Loss, O., Cairns, T., Goldman, G., Armstrong-James, D., Haynes, K., Haas, H., Schretti, M., May, G., Nierman, W. C. & Bignell, E. (2008) Sub-Telomere Directed Gene Expression during Initiation of Invasive Aspergillosis. *PLoS Pathogens*, **4**(9): e1000154. doi:10.1371/journal.ppat.1000154

McKenzie, C. G. J., Koser, U., Lewis, L. E., Bain, J. M., Mora-Montes, H. M., Barker, R. N., Gow, N. A. R. & Erwig, L. P. (2010) Contribution of *Candida albicans* Cell Wall Components to Recognition by and Escape from Murine Macrophages. *Infection and Immunity*, **78**: 1650-1658.

Merlini, L., Dudin, O. & Martin, S. G. (2013) Mate and fuse: how yeast cells do it. *Open Biology*, **3**: doi:10.1098/rsob.130008

Miramón, P., Kasper, L. & Hube, B. (2013) Thriving within the host: *Candida* spp. Interactions with phagocytic cells. *Medical Microbiology and Immunology*, doi 10.1007/s00430-013-0288-z

Mitchell, K. F., Taff, H. T., Cuevas, M. A., Reinicke, E. L., Sanchez, H. & Andes, D. R. (2013) Role of matrix β -1,3 glucan in antifungal resistance of non-*albicans* *Candida* biofilms. *Antimicrobial Agents and Chemotherapy*, **57**: 1918-1920.

Moran, G. P., Coleman, D. C. & Sullivan, D. J. (2011) Comparative Genomics and the Evolution of Pathogenicity in Human Pathogenic Fungi. *Eukaryotic Cell*, **10**: 34-42.

Muller, H., Hennequin, C., Gallaud, J., Dujon, B. & Fairhead, C. (2008) The Asexual Yeast *Candida glabrata* Maintains Distinct α and α Haploid Mating Types. *Eukaryotic Cell*, **7**: 848-858.

Miyazaki, T., Izumikawa, K., Yamauchi, S., Inamine, T., Nagayoshi, Y., Saijo, T., Seki, M., Kakeya, H., Yamamoto, Y., Yanagihara, K., Miyazaki, Y., Yasuoka, A. & Kohno, S. (2011) The glycosylphosphatidylinositol-linked aspartyl protease Yps1 is transcriptionally regulated by the calcineurin-Crz1 and Sit2 MAPK pathways in *Candida glabrata*. *FEMS Yeast Research*, **11**, 449-456.

- Murakami, H. & Keeney, S. (2008) Regulating the formation of DNA double-strand breaks in meiosis. *Genes & Development*, **22**: 286-292.
- Nairz, M., Schroll, A., Sonnweber, T. & Weiss, G. (2010) The struggle for iron - a metal at the host-pathogen interface. *Cellular Microbiology*, **12**: 1691-1702.
- Navarre, W. W. & Zychlinsky, A. (2000) Pathogen-induced apoptosis of macrophages: a common end for different pathogenic strategies. *Cellular Microbiology*, **2**: 265-273.
- Neiman, A. M. (2011) Sporulation in the Budding Yeast *Saccharomyces cerevisiae*. *Genetics*, **189**: 737-765.
- Nelson, R. T., Hua, J., Pryor, B. & Lodge, J. K. (2001) Identification of Virulence Mutants of the Fungal Pathogen *Cryptococcus neoformans* Using Signature-Tagged Mutagenesis. *Genetics*, **157**: 935-947.
- Netea, M. G., Brown, G. D., Kullberg, B. J. & Gow, N. A. R. (2008) An Integrated model of the recognition of *Candida albicans* by the innate immune system. *Nature Reviews Microbiology*, **6**: 67-78.
- Nevitt, T. & Thiele, D. J. (2011) Host Iron Withholding Demands Siderophore Utilization for *Candida glabrata* to Survive Macrophage Killing. *PLoS Pathogens*, **7**(3):e1001322. doi:10.1371/journal.ppat.1001322.
- Nobile, C. J., Fox, E. P., Nett, J. E., Sorrells, T. R., Mitrovitch, Q. M., Hernday, A. D., Tuch, B., Andes, D. R. & Johnson, A. D. (2012) A Recently Evolved Transcriptional Network Controls Biofilm Development in *Candida albicans*. *Cell*, **148**: 126-138.
- Noble, S. M., French, S., Kohn, L. A., Chen, V. & Johnson, A. D. (2010) Systematic screens of a *Candida albicans* homozygous deletion library decouple morphogenetic switching and pathogenicity. *Nature Genetics*, **42**: 590-598.
- Noble, J. A., Tsai, H., Suffis, S. D., Su, Q., Myers, T. G. & Bennett, J. E. (2013) *STB5* Is a Negative Regulator of Azole Resistance in *Candida glabrata*. *Antimicrobial Agents and Chemotherapy*, **57**, 959-967.
- O'Gorman, C. M., Fuller, H. T. & Dyer, P. S. (2009) Discovery of a sexual cycle in the opportunistic fungal pathogen *Aspergillus fumigatus*. *Nature*, **457**: 471-475.
- Oh, J., Fung, E., Schlect, U., Davis, R. W., Giaever, G., Onge, R. P. S., Deutschbauer, A. & Nislow, C. (2010) Gene Annotation and Drug Target Discovery in *Candida albicans* with a Tagged Transposon Mutant Collection. *PLoS Pathogens*, **6**(10): e1001140. doi:10.1371/journal.ppat.1001140.
- Orkwis, B. R., Davies, D. L., Kerwin, C. L., Sanglard, D. & Wykoff, D. D. (2010) Novel Acid Phosphatase in *Candida glabrata* Suggests Selective Pressure and Niche Specialization in the Phosphate Signal Transduction Pathway. *Genetics*, **185**: 885-895.

- Orta-Zavalza, E., Guerrero-Serrano, G., Gutiérrez-Escobedo, G., Cañas-Villamar, I., Juárez-Cepeda, J., Castaño, I. & De Las Peñas, A. (2013) Local silencing controls the oxidative stress response and the multidrug resistance in *Candida glabrata*. *Molecular Microbiology*, **88**: 1135-1148.
- Palmer, G. E., Askew, D. S. & Williamson, P. R. (2008) The diverse roles of autophagy in medically important fungi. *Autophagy*, **4**: 982-988.
- Paoletti, M., Rydholm, C., Schwler, E. U., Anderson, M. J., Szakacs, G., Lutzoni, F., Debeaupuis, J., Latgé, J., Denning, D. W. & Dyer, P. S. (2005) Evidence for Sexuality in the Opportunistic Fungal Pathogen *Aspergillus fumigatus*. *Current Biology*, **15**: 1242-1248.
- Parsons, A. B., Brost, R. L., Ding, H., Li, Z., Zhang, C., Sheikh, B., Brown, G. W., Kane, P. M., Hughes, T. R. & Boone, C. (2004) Integration of chemical genetic and genetic interaction data links bioactive compounds to cellular target pathways. *Nature Biotechnology*, **22**: 62-69.
- van Pel, D. M., Barrett, I. J., Shimizu, Y., Sajesh, B. V., Guppy, B. J., Pfeifer, T., McManus, K. J. & Heiter, P. (2013) An Evolutionarily Conserved Synthetic Lethal Interaction Network Identifies FEN1 as a Broad-Spectrum Target for Anticancer Therapeutic Development. *PLoS Genetics*, **9**(1): e1003254. doi:10.1371/journal.pgen.1003254.
- Pelz, R. K., Lipsett, P. A., Swoboda, S. M., Diener-West, M., Powe, N. R., Brower, R. G., Perl, T. M., Hammond, J. M. & Hendrix, C. W. (2008) *Candida* Infections: Outcome and Attributable ICU Costs in Critically Ill Patients. *Journal of Intensive Care Medicine*, **15**: 255-261.
- De Las Peñas, A., Pan, S., Castaño, I., Alder, J., Cregg, R. & Cormack, B. P. (2003) Virulence-related surface glycoproteins in the yeast pathogen *Candida glabrata* are encoded in subtelomeric clusters and subject to *RAP1*- and *SIR*-dependent transcriptional silencing. *Genes & Development*, **17**: 2245-2258.
- Phan, Q. T., Myers, C. L., Fu, Y., Sheppard, D. C., Yeaman, M. R., Welch, W. H., Ibrahim, A. S., Edwards Jr., J. E. & Filler, S. G. (2007) Als3 Is a *Candida albicans* Incasin That Binds to Cadherins and Induces Endocytosis by Host Cells. *PLoS Biology*, **5**(3): e64. doi:10.1371/journal.pbio.0050064.
- Pierce, S. E., Davis, R. W., Nislow, C. & Giaever, G. (2007) Genome-wide analysis of barcoded *Saccharomyces cerevisiae* gene-deletion mutants in pooled cultures. *Nature Protocols*, **2**: 2958-2974.
- Poláková, S., Blume, C., Zárate, J., Á., Mentel, M., Jørck-Ramberg, D., Stenderup, J. & Piškur, J. (2009) Formation of new chromosomes as a virulence mechanism in yeast *Candida glabrata*. *PNAS*, **106**: 2688-2693.
- Pfaller, M. A., Castanheira, M., Lockhart, S. R., Ahlquist, A. M., Messer, S. A. & Jones, R. N. (2012) Frequency of Decreased Susceptibility and Resistance to Echinocandins among Fluconazole-Resistant Bloodstream Isolates of *Candida glabrata*. *Journal of Clinical Microbiology*, **50**: 1199-1203.

- Pfaller, M. A. & Diekema, D. J. (2007) Epidemiology of Invasive Candidiasis: a Persistent Public Health problem. *Clinical Microbiology Reviews*, **20**: 133-163.
- Pfaller, M., Neofytos, D., Diekema, D., Azie, N., Meier-Kriesche, H., Quan, S. & Horn, D. (2012) Epidemiology and outcomes of candidemia in 3648 patients data from the Prospective Antifungal Therapy (PATH Alliance®) registry, 2004-2008. *Diagnostic Microbiology and Infectious disease*, **74**: 323-331.
- Quezada, G., Koshkina, N. V., Zweidler-McKay, P., Zhou, Z., Kontoyiannis, D. P. & Kleinerman, E. S. (2007) Intranasal Granulocyte-Macrophage Colony-Stimulating Factor Reduces the *Aspergillus* Burden in an Immunosuppressed Murine Model of Pulmonary Aspergillosis. *Antimicrobial Agents and Chemotherapy*, **52**: 716-718.
- Quintin, J., Asmar, J., Matskevich, A. A., Larage, M. C. & Ferrandon, D. (2013) The Drosophila Toll pathway controls but does not clear *Candida glabrata* infections. *Journal of Immunology*, **190**: 2818-2827.
- Ragsdale, S. W. (2006) Metals and Their Scaffolds To Promote Difficult Enzymatic Reactions. *Chemical Reviews*, **106**: 3317-3337.
- Rai, M. N., Balusu, S., Gorityala, N., Dandu, L. & Kaur, R. (2012) Functional Genomic Analysis of *Candida glabrata*-Macrophage Interaction: Role of Chromatin Remodelling in Virulence. *PLoS Pathogens*, **8**(8): e1002863. doi:10.1371/journal.ppat.1002863.
- Ram, A. F. J. & Klis, F. M. (2006) Identification of fungal cell wall mutants using susceptibility assays based on Calcofluor white and Congo red. *Nature Protocols*, **1**: 2253-2256.
- Rentz, A. M., Halpern, M. T. & Bowden, R. (1998) The Impact of Candidemia on length of Hospital Stay, Outcome, and Overall Cost of Illness. *Clinical Infectious Diseases*, **27**: 781-788.
- Riera, M., Mogensen, E., d'Enfert, C. & Janbon, G. (2012) New regulators of biofilm development in *Candida glabrata*. *Research in Microbiology*, **163**: 297-307.
- Robinson, M. D., Grigull, J., Mohammad, N. & Hughes, T. R. (2002) FunSpec: a web-based cluster interpreter for yeast. *BMC Bioinformatics*, **3**: 35-40.
- Roetzer, A., Gratz, N., Kovarik, P. & Schüller, C. (2010) Autophagy supports *Candida glabrata* survival during phagocytosis. *Cellular Microbiology*, **12**, 199-216.
- Roetzer, A., Klopff, E., Gratz, N., Marcet-Houben, M., Hiller, E., Rupp, S., Gabaldón, T., Kovarik, P. & Schüller, C. (2011) Regulation of *Candida glabrata* oxidative stress resistance is adapted to host environment. *FEBS Letters*, **585**, 319-327.
- Roguev, A., Talbot, D., Negri, G. L., Shales, M., Cagney, G., Bandyopadhyay, S., Panning, B. & Krogan, N. J. (2013) Quantitative genetic-interaction mapping in mammalian cells. *Nature Methods*, **10**: 432-437.

Roguev, A., Wiren, M., Weissman, J. S. & Krogan, N. J. (2007) High-throughput genetic interaction mapping in the fission yeast *Schizosaccharomyces pombe*. *Nature Methods*, **4**: 861-866.

Rui, O. & Hahn, M. (2007) The *Botrytis cinerea* hexokinase, Hxk1, but not the glucokinase, Glk1, is required for normal growth and sugar metabolism, and for pathogenicity on fruits. *Microbiology*, **153**: 2791-2802.

Ryan, C. J., Roguev, A., Patrick, K., Xu, J., Jahari, H., Tong, Z., Beltrao, P., Shales, M., Qu, H., Collins, S. R., Kliegman, J. I., Jiang, L., Kuo, D., Tosti, E., Kim, H., Edelman, W., Keogh, M., Greene, D., Tang, C., Cunningham, P., Shokat, K. M., Cagney, G., Svensson, J. P., Guthrie, C., Espenshade, P. J., Ideker, T. & Krogan, N. J. (2012) Hierarchical Modularity and the Evolution of Genetic Interactomes across Species. *Molecular Cell*, **46**: 691-704.

Saijo, T., Miyazaki, T., Izumikawa, K., Mihara, T., Takazono, T., Kosai, K., Imamura, Y., Seki, M., Takeya, H., Yamamoto, Y., Yanagihara, K. & Kohno, S. (2010) Skn7p Is Involved in Oxidative Stress Response and Virulence of *Candida glabrata*. *Mycopathologia*, **169**, 81-90.

Sanglard, D., Ischer, F. & Bille, J. (2001) Role of ATP-Binding-Cassette Transporter Genes in High-Frequency Acquisition of Resistance to Azole Antifungals in *Candida glabrata*. *Antimicrobial Agents and Chemotherapy*. **45**, 1174-1183.

Sanglard, D., Ischer, F., Calabrese, D., Majcherczyk, P. A. & Bille, J. (1999) The ATP Binding Cassette Transporter Gene *CgCDR1* from *Candida glabrata* Is Involved in the Resistance of Clinical Isolates to Azole Antifungal Agents. *Antimicrobial Agents and Chemotherapy*, **43**: 2753-2765.

Santangelo, G. M. (2006) Glucose Signalling in *Saccharomyces cerevisiae*. *Microbiology and Molecular Biology Reviews*, **70**: 253-282.

Dos Santos, S. C. & Sá-Correia (2011) A genome-wide screen identifies yeast genes required for protection against or enhanced cytotoxicity of the antimalarial drug quinine. *Molecular Genetics & Genomics*, **286**: 333-346.

Santos, M. A. S. & Tuite, M. F. (1995) The CUG codon is decoded *in vivo* as serine and not leucine in *Candida albicans*. *Nucleic acids research*, **23**, 1481-1486.

Saville, S. P., Lazzell, A. L., Chaturvedi, A. K., Monteagudo, C. & Lopez-Ribot, J. L. (2009) Efficacy of a Genetically Engineered *Candida albicans tet-NRG1* Strain as an Experimental Live Attenuated Vaccine Against Hematogenously Disseminated Candidiasis. *Clinical & Vaccine Immunology*, **16**: 430-432.

Schrettl, M., Bignell, E., Kragl, C., Joehchl, C., Rogers, T., Arst Jr., H. N., Haynes, K. & Haas, H. (2004) Siderophore Biosynthesis but not Reductive Iron Assimilation is Essential for *Aspergillus fumigatus* virulence. *Journal of Experimental Medicine*, **200**: 1213-1219.

Seider, K., Brunke, S., Schild, L., Jablonowski, N., Wilson, D., Majer, O., Barz, D., Haas, A., Kuchler, K., Schaller, M. & Hube, B. (2011) The Facultative

Intracellular Pathogen *Candida glabrata* Subverts Macrophage Cytokine Production and Phagolysosome Maturation. *Journal of Immunology*, **187**: 3072-3086.

Senevirante, C. J., Wang, Y., Jin, L., Abiko, Y. & Samaranayake, L. P. (2010) Proteomics of drug resistance in *Candida glabrata*. *Proteomics*, **10**: 1444-1454.

Sherman, D., Durrens, P., Beyne, E., Nikolski, M. & Societ J. (2004) Génolevures: comparative genomics and molecular evolution of hemiascomycetous yeasts. *Nucleic Acids Research*, **32**: 315-318.

Sherman, D. J., Martin, T., Nikolski, M., Cayla, C., Souciet, J. & Durrens, P. (2009) Génolevures: protein families and synteny among complete hemiascomycetous yeast proteomes and genomes. *Nucleic Acids Research*, **37**: 550-554.

Shim, E. Y., Ma, J., Oum, J., Yanez, Y. & Lee, S. E. (2005) The Yeast Chromatin Remodeler RSC Complex Facilitates End Joining Repair of DNA Double-Strand Breaks. *Molecular and Cellular Biology*, **25**: 3934-3944.

Shin, J. H., CHae, M. J., Song, J. W., Jung, S., Cho, D., Kee, S. J., Kim, S. H., Shin, M. G., Suh, S. P. & Ryang, D. W. (2007) Changes in Karyotype and Azole Susceptibility of Sequential Bloodstream Isolates from Patients with *Candida glabrata* Candidemia. *Journal of Clinical Microbiology*, **45**: 2385-2391.

Shiu, P. K. T. & Glass, N. L. (2000) Cell and nuclear recognition mechanisms mediated by mating type filamentous ascomycetes. *Current Opinion in Microbiology*, **3**: 183-188.

Sifuentes-Orsornio, J., Corzo-Léon, D. E. & Ponce-de-León, L. A. (2012) Epidemiology of Invasive Fungal Infections in Latin America. *Current Fungal Infections in Latin America*, **6**: 23-34.

Silva, S., Henriques, M., Martins, A., Oliveira, R., Williams, D. & Azeredo, J. (2009) Biofilms of non-*Candida albicans* *Candida* species: quantification, structure and matrix composition. *Medical Mycology*, **47**: 681-689.

Silva, S., Henriques, M., Oliveira, R., Azeredo, J., Malic, S., Hooper, S. J., Williams, D. W. (2009) Characterisation of *Candida parapsilosis* infection of an *in vitro* reconstituted human oral epithelium. *European Journal of Oral Sciences*. **117**: 669-675. B

Silva, S., Negri, M., Henriques, M., Oliveira, R., Williams, D. W. & Azeredo, J. (2011) Adherence and biofilm formation of non-*Candida albicans* *Candida* species. *Trends in Microbiology*, **19**: 241-247. A

Silva, S., Henriques, M., Hayes, A., Oliveira, R., Azeredo, J. & Williams, D. W. (2011) *Candida glabrata* and *Candida albicans* co-infection of an *in vitro* oral epithelium. *Journal of Oral Pathology & Medicine*, **40**: 421-427. B

Silva, S., Hooper, S. J., Henriques, M., Oliveira, R., Azeredo, J. & Williams, D. W. (2011) The role of secreted aspartyl proteinases in *Candida tropicalis* invasion and damage of oral mucosa. *Mycology*, **17**: 264-272.

Singh-Babak, S. D., Babak, T., Diezmann, S., Hill, J. A., Xie, J. L., Chen, Y., Poutanen, S. M., Rennie, R. P., Heitman, J. & Cowen, L. E. (2012) Global Analysis of the Evolution and Mechanism of Echinocandin Resistance in *Candida glabrata*. *PLoS Pathogens*, **8**: e1002718. doi:10.1371/journal.ppat.1002718.

Smith, A. M., Heisler, L. E., St. Onge, R. P., Farias-Hesson, E., Wallace, I. A., Bodeau, J., Harris, A. N., Perry, K. M., Giaever, G., Pourmand, N. & Nislow, C. (2010) Highly-multiplexed barcode sequencing: an efficient method for parallel analysis of pooled samples. *Nucleic Acids Research*, **38**: e142.

Soares, E. V. (2011) Flocculation in *Saccharomyces cerevisiae*: a review. *Journal of Applied Microbiology*, **110**: 1-18.

Sopko, R., Huang, D., Preston, N., Chua, G., Papp, B., Kafadar, K., Snyder, M., Oliver, S. G., Cyert, M., Hughes, T. R., Boone, C. & Andrews, B. (2006) Mapping Pathways and Phenotypes by Systematic Gene Overexpression. *Molecular Cell*, **21**: 319-330.

Souciet, J., Aigle, M., Artiguenave, F., Blandin, G., Bolotin-Fukuhara, M., Bon, E., Brottier, P., Casaregola, S., de Montigny, J., Dujon, B., Durrens, P., Gaillardin, C., Lépingle, A., Llorente, B., Malpertuy, A., Neuvéglise, C., Ozier-Kalogéropoulos, O., Potier, S., Saurin, W., Tekaiia, F., Toffano-Nioche, C., Wésolowski-Louvel, M., Wincker, P. & Weissenbach, J. (2000) Genomic Exploration of the Hemiascomycetous Yeasts: 1. A set of yeast species for molecular evolution studies. *FEBS Letters*, **287**: 3-12.

Srikantha, T., Lachke, S. A. & Soll, D. R. (2003) Three Mating Type-Like Loci in *Candida glabrata*. *Eukaryotic Cell*, **2**: 328-340.

Srikantha, T., Zhao, R., Daniels, K., Radke, J. & Soll, D. R. (2005) Phenotypic Switching in *Candida glabrata* Accompanied by changes in Expression of Genes with Deduced Functions on Copper Detoxification and Stress. *Eukaryotic Cell*, **4**, 1434-1445.

Srikantha, T., Daniels, K. J., Wu, W., Lockhart, S. R., Yi, S., Sahni, N., Ma, N. & Soll, D. R. (2008) Dark brown is the more virulent of the switch phenotypes of *Candida glabrata*. *Microbiology*, **154**: 3309-3318.

Staib, P. & Morschhäuser, M. (2005) Differential expression of the *NRG1* repressor controls species-specific regulation of chlamydospore development in *Candida albicans* and *Candida dubliniensis*. *Molecular Microbiology*, **55**: 637-652.

Steinmetz, L. M., Scharfe, C., Deutschbauer, A. M., Mokranjic, D., Herman, Z. S., Jones, T., Chu, A. M., Giaever, G., Prokisch, H., Oefner, P. J. & Davis, R. W. (2002) Systematic screen for human disease genes in yeast. *Nature genetics*, **31**: 400-404.

Štros, M. (2010) HMGB proteins: Interactions with DNA and chromatin. *Biochimica et Biophysica Acta*, **1799**: 101-113.

Štros, M., Launholt, D. & Grasser, K. D. (2007) The HMG-box: a versatile protein domain occurring in a wide variety of DNA-binding proteins. *Cellular and Molecular Life Sciences*, **64**: 2590-2606.

Sudbery, P. E. (2011) Growth of *Candida albicans* hyphae. *Nature Reviews Microbiology*, **9**: 737-748.

Sun, J. N., Solis, N. V., Phan, Q. T., Bajwa, J. S., Kashleva, H., Thompson, A., Liu, Y., Dongari-Bagtzoglou, A., Edgerton, M. & Filler, S. G. (2010) *PLoS Pathogens*, 6(11): e1001181. doi:10.1371/journal.ppat.1001181

Talbert, P. B. & Henikoff, S. (2006) Spreading of silent chromatin: inaction at a distance. *Nature Reviews Genetics*, **7**: 793-803.

Tati, S., Jang, W. S., Li, R., Kumar, R., Puri, S., Edgerton, M. (2013) Histatin 5 Resistance of *Candida glabrata* Can Be Reversed by Insertion of *Candida albicans* Polyamine Transporter-Encoding Genes *DUR3* and *DUR31*. *PLoS ONE*, 8(4): e61480. doi:10.1371/journal.pone.0061480.

Tercero, J. A. & Diffley, J. F. X. (2001) Regulation of DNA replication fork progression through damaged DNA by the Mec1/Rad53 checkpoint. *Nature*, **412**: 553-557.

Thakur, J. K., Arthanari, H., Yang, F., Pan, S., Fan, X., Breger, J., Frueh, D. P., Gulshan, K., Li, D. K., Mylonakis, E., Struhl, K., Moye-Rowley, W. S., Cormack, B. P., Wagner, G. & Näär, A. M. (2008) A nuclear receptor-like pathway regulating multidrug resistance in fungi. *Nature*, **452**: 604-609.

Thorsen, M., Jacobsen, T., Vooijs, R., Navarrete, C., Blik, T., Schat, H. & Tamás, M. J. (2012) Glutathione serves an extracellular defence function to decrease arsenite accumulation and toxicity in yeast. *Molecular Microbiology*, **84**: 1177-1188.

Tong, A. & Boone, C. (2005) Synthetic Genetic Array (SGA) Analysis in *Saccharomyces cerevisiae*. *Yeast Protocols, Second Edition. Methods in Molecular Biology*, **313**: 171-192.

Tong, A. H. Y., Evangelista, M., Parsons, A. B., Xu, H., Bager, G. D., Pagé, N., Robinson, M., Raghibizadeh, S., Hogue, C. W. V., Bussey, H., Andrews, B., Tyers, M., Boone, C. (2001) Systematic Genetic Analysis with Ordered Arrays of Yeast Deletion Mutants. *Science*, **294**: 2364-2368.

Tong, A. H. Y., Lesage, G., Bader, G. D., Ding, H., Xu, H., Xin, X., Young, J., Berriz, G. F., Brost, R. L., Chang, M., Chen, Y., Cheng, X., Chua, G., Friesen, H., Goldberg, D. S., Haynes, J., Humphries, C., He, G., Hussein, S., Ke, L., Krogan, N., Li, Z., Levinson, J., Lu, H., Ménard, P., Munyana, C., Parsons, A. B., Ryan, O., Tonikian, R., Roberts, T., Sdicu, A., Shapiro, J., Sheikh, B., Suter, B., Wong, S. L., Zhang, L. V., Zhu, H., Burd, C. G., Munro, S., Sander, C., Rine, J., Greenblatt, J., Peter, M., Bretscher, A., Bell, G., Roth, F. P., Brown, G. W., Andrews, B., Bussey, H. & Boone, C. (2004) Global Mapping of the Yeast Genetic Interaction Network. *Science*, **303**: 808-813.

Torelli, R., Posteraro, B., Ferrari, S., La Sorda, M., Fadda, G., Sanglard, D. & Sanguinetti, M. (2008) The ATP-binding cassette transporter-encoding gene *CgSNQ2* is contributing to the *CgPDR1*-dependent azole resistance of *Candida glabrata*. *Molecular Microbiology*, **68**: 186-201.

Troppens, D. M., Dmitriev, R. I., Papkovsky, D. B., O'Gara, F. & Morrissey, J. P. (2013) Genome-wide investigation of cellular targets and mode of action of the antifungal bacterial metabolite 2,4-diacetylphloroglucinol in *Saccharomyces cerevisiae*. *FEMS Yeast Research*, **13**: 322-334.

Tsai, H., Krol, A. A., Sarti, K. E. & Bennett, J. E. (2006) *Candida glabrata PDR1*, a Transcriptional Regulator of a Pleiotropic Drug Resistance Network, Mediates Azole Resistance in Clinical Isolates and Petite Mutants. *Antimicrobial Agents and Chemotherapy*, **50**: 1384-1392.

Tsong, A. E., Miller, M. G., Raisner, R. M. & Johnson, A. D. (2003) Evolution of a Combinatorial Transcriptional Circuit: A Case Study in Yeasts. *Cell*, **115**: 389-399.

Typas, A., Nichols, R. J., Siegele, D. A., Shales, M., Collins, S., Lim, B., Braberg, H., Yamamoto, N., Tikeuchi, R., Wanner, B. L., Mori, H., Weissman, J. S., Krogan, N. & Gross, C. A. (2008) A tool-kit for high-throughput, quantitative analyses of genetic interactions in *E. coli*. *Nature Methods*, **5**: 781-787.

Tzung, K., Williams, R. M., Scherer, S., Federspiel, N., Jones, T., Hansen, N., Bivolarevic, V., Huiznar, L., Komp, C., Surzycki, R., Tamse, R., Davis, R. W. & Agabian, N. (2001) Genomic evidence for a complete sexual cycle in *Candida albicans*. *PNAS*, **98**: 3249 – 3253.

Uhl, M. A., Biery, M., Craig, N. & Johnson, A. D. (2003) Haploinsufficiency-based large-scale forward genetic analysis of filamentous growth in the diploid human fungal pathogen *C. albicans*. *The EMBO Journal*, **22**: 2668-2678.

Uo, T., Yoshimura, T., Tanaka, N., Takegawa, K. & Esaki, N. (2001) Functional Characterisation of Alanine Racemase from *Schizosaccharomyces pombe*: a Eucaryotic Counterpart to Bacterial Alanine Racemase. *Journal of Bacteriology*, **183**: 2226-2233.

Urban, C. F., Ermert, D., Schmid, M., Abu-Abed, U., Goosmann, C., Nacken, W., Brinkmann, V., Jungblut, P. R. & Zychlinsky, A. (2009) Neutrophil Extracellular Traps Contain Calprotectin, a Cytosolic Protein Complex Involved in Host Defense against *Candida albicans*. *PLoS Pathogens*, **5**(10): e1000639. doi:10.1371/journal.ppat.1000639.

Vale-Silva, L., Ischer, F., LeibundGut-Landmann, S. & Sanglard, D. (2013) Gain of function mutations in *CgPDR1*, a regulator of antifungal drug resistance in *Candida glabrata*, control adherence to host cells. *Infection and Immunity*, **81**: 1709-1720.

Vermitsky, J. & Edlind, T. D. (2004) Azole Resistance in *Candida glabrata*: Coordinate Upregulation of Multidrug Transporters and Evidence for a Pdr1-Like Transcription Factor. *Antimicrobial Agents and Chemotherapy*, **48**: 3773-3781.

- Verstrepen, K. J. & Klis, F. M. (2006) Flocculation, adhesion and biofilm formation in yeasts. *Molecular Microbiology*, **60**: 5-15.
- Vieira, O. V., Botelho, R. J. & Grinstein, S. (2002) Phagosome maturation: aging gracefully. *Biochemical Journal*, **366**: 689 – 704.
- Vizeacoumar, F. J., van Dyk, N., Vizeacoumar, F. S., Cheung, V., Li, J., Sydorsky, Y., Case, N., Li, Z., Datti, A., Nislow, C., Raught, B., Zhang, Z., Frey, B., Bloom, K., Boone, C. & Andrews, B. J. (2010) Integrating high-throughput genetic interaction mapping and high-content screening to explore yeast spindle morphogenesis. *Journal of Cell Biology*, **188**: 69-81.
- Vyas, V. K., Berkey, C. D., Miyao, T. & Carlson, M. (2005) Repressors Nrg1 and Nrg2 Regulate a Set of Stress-Responsive Genes in *Saccharomyces cerevisiae*. *Eukaryotic Cell*, **4**: 1882-1891.
- Wächtler, B., Citiulo, F., Jablonowski, N., Förster, S., Dalle, F., Schaller, M., Wilson, D. & Hube, B. (2012) *Candida albicans*-Epithelial Interactions: Dissecting the Roles of Active Penetration, Induced Endocytosis and Host Factors on the Infection Process. *PLoS ONE*, **7**(5): e36952. doi:10.1371/journal.pone.0036952.
- Walker, L. A., Gow, N. A. R. & Munro, C. A. (2010) Fungal echinocandin resistance. *Fungal Genetics and Biology*, **47**: 117-126.
- Walker, L. A., Gow, N. A. R. & Munro, C. A. (2013) Elevated Chitin Content Reduces the Susceptibility of *Candida* Species to Caspofungin. *Antimicrobial Agents and Chemotherapy*, **57**: 146-154.
- Walker, L. A., Munro, C. A., de Bruijn, I., Lenardon, M., McKinnon, A. & Gow, N. A. R. (2008) Stimulation of Chitin Synthesis Rescues *Candida albicans* from Echinocandins. *PLoS Pathogens* **4**(4): e1000040. doi:10.1371/journal.ppat.1000040.
- Wang, L. & Ligoxygakis, P. (2006) Pathogen recognition and signalling in the *Drosophila* innate immune response. *Immunobiology*, **211**: 251-261.
- Weig, M., Jänsch, L., Groß, U., De Koster, G. G., Klis, F. M. & De Groot, P. W. J. (2004) Systematic identification *in silico* of covalently bound cell wall proteins and analysis of protein-polysaccharide linkages of the human pathogen *Candida glabrata*. *Microbiology*, **150**: 3129-3144.
- Wheeler, R. T., Kombe, D., Agarwala, S. D. & Fink, G. R. (2008) Dynamic, Morphotype-Specific *Candida albicans* β -Glucan Exposure during Infection and Drug Treatment. *PLoS Pathogens*, **4**: doi:10.1371/journal.ppat.1000227.
- White, M. A., Riles, L. & Cohen, B. A. (2009) A Systematic Screen for Transcriptional Regulators of the Yeast Cell Cycle. *Genetics*, **181**: 435-446.
- Winzeler, E. A., Shoemaker, D. D., Astromoff, A., Liang, H., Anderson, K., Andre, B., Bangham, R., Benito, R., Boeke, J. D., Bussey, H., Chu, A. M., Connelle, C., Davis, K., Dietrich, F., Dow, S. W., Bakkpury, M. E., Foury, F., Friend, S. H., Gentalen, E., Giaever, G., Hegemann, J. H., Jones, T., Laub, M.,

Liao, H., Liebundguth, N., Lockhart, D. J., Lucau-Danilla, A., Lussier, M., M'Rabet, N., Menard, P., Mittmann, M., Pai, C., Rebischung, C., Revuelta, J. L., Riles, L., Roberts, C. J., Ross-MacDonald, P., Scherens, B., Snyder, M., Sooghai-Mahadeo, S., Storms, R. K., Vééonneau, S., Voet, M., Volkaert, G., Ward, T. R., Wysocki, R., Yen, G. S., Yu, K., Zimmermann, K., Philippsen, P., Johnstons, M. & Davis, R. W. (1999) Functional Characterisation of the *S. cerevisiae* Genome by Gene Deletion and Parallel Analysis. *Science*, **6**: 901-906.

Wisplinghoff, H., Bischoff, T., Tallent, S. M., Seifert, H., Wenzel, R. P. & Edmond, M. B. (2004) Nosocomial Bloodstream infections in US Hospitals: Analysis of 24,179 Cases from a Propective Nationwide Surveillance Study. *Clinical Infectious Diseases*, **39**, 309-317.

Wong, S., Fares, M. A., Zimmermann, W., Butler, G. & Wolfe, K. H. (2003) Evidence from comparative genomics for a complete sexual cycle in the 'asexual' pathogenic yeast *Candida glabrata*. *Genome Biology*, **4**: R10.

Wuster, A. & Babu, M. M. (2008) Chemogenomics and Biotechnology. *Trends in Biotechnology*, **26**: 252-258.

Wysocki, R. & Tamás, M. J. (2010) How *Saccharomyces cerevisiae* copes with toxic metals and metalloids. *FEMS Microbiology Reviews*, **34**: 925-951.

Xu, D., Jiang, B., Ketela, T., Lemieux, S., Veillette, K., Martel, N., Davison, J., Sillaots, S., Trosok, S., Bachewich, C., Bussey, H., Youngman, P. & Roemer, T. (2007) Genome-Wide Fitness Test and Mechanism-of-Action Studies of Inhibitory Compounds in *Candida albicans*. *PLoS Pathogens*, e92. doi:10.1371/journal.ppat.0030092.

Xu, N., Cheng, X., Yu, Q., Qian, K., Ding, X., Liu, R., Zhang, B., Xing, L. & Li, M. (2013) Aft2, a Novel Transcription Regulator, Is Required for Iron Metabolism, Oxidative Stress, Surface Adhesion and Hyphal Development in *Candida albicans*. *PLoS ONE*, 8(4): e62367. doi:10.1371/journal.pone.0062367.

Yadav, A. K., Desai, P. R., Rai, M. N., Kaur, R., Ganesan, K. & Bachhawat, A. K. (2011) Glutathione biosynthesis in the yeast pathogens *Candida glabrata* and *Candida albicans*: essential in *C. glabrata*, and essential for virulence in *C. albicans*. *Microbiology*, **157**: 484-495.

Yan, Z., Costanzo, M., Heisler, L. E., Paw, J., Kaper, F., Andrews, B. J., Boone, C., Giaever, G. & Nislow, C. (2008) Yeast Barcoders: a chemogenomic application of a universal donor strain collection carrying bar-code identifiers. *Nature Methods*, **5**: 719-725.

Yan, L., Zhang, J., Li, M., Cao, Y., Xu, Z., Cao, Y., Gao, P., Wang, Y. & Jiang, Y. (2008) DNA microarray analysis of fluconazole resistance in a laboratory *Candida albicans* strain. *Acta Biochimica et Biophysica Sinica*, **40**: 1048-1060. (B)

Yoshimura, T. & Esaki, N. (2003) Amino Acid Racemases: Functions and Mechanisms. *Journal of Bioscience and Bioengineering*, **96**: 103-109.

Yu, S., Qin, W., Zhuang, G., Zhang, X., Chen, G. & Liu, W. (2009) Monitoring Oxidative Stress and DNA Damage Induced by Heavy Metals in Yeast Expressing a Redox-Sensitive Green Fluorescent Protein. *Current Microbiology*, **58**: 504-510.

Zakrzewska, A., Boorsma, A., Delneri, D., Brul, S., Oliver, S. G. & Klis, F. M. (2007) Cellular Processes and Pathways That Protect *Saccharomyces cerevisiae* Cells against the Plasma Membrane-Perturbing Compound Chitosan. *Eukaryotic Cell*, **6**: 600-608.

Zhu, W. & Filler, S. G. (2010) Interactions of *Candida albicans* with epithelial cells. *Cellular Microbiology*, **12**: 273-282.

Zupancic, M. L., Frieman, M., Smith, D., Alvarez, R. A., Cummings, R. D. & Cormack, B. P. (2008) Glycan microarray analysis of *Candida glabrata* adhesion ligand specificity. *Molecular Microbiology*, **68**: 547-559.